Supplementary Information for

Effect of Local Heterogeneities on Single-Layer DNA-Directed Protein Lattices Through Non-Averaged Single-Molecule 3D Structure Determination

Jianfang Liu[1,*], Shih-Ting Wang[2], Meng Zhang[1], Zijian Hu[1,3], Hao Wu[3], Oleg Gang[2,4,5,*] and Gang Ren[1,*]

[1] The Molecular Foundry, Lawrence Berkeley National Laboratory, Berkeley, CA, 94720, USA;
[2] Center for Functional Nanomaterials, Brookhaven National Laboratory, Upton, NY, 11973, USA;
[3] College of Artificial Intelligence, Beijing Normal University, Beijing, China;
[4] Department of Chemical Engineering, Columbia University, New York City, NY, 10027, USA;
[5] Department of Applied Physics and Applied Mathematics, Columbia University, New York City, NY, 10027, USA.

[*]Corresponding Author
Gang Ren, E-mail: gren@lbl.gov; Jianfang Liu, E-mail: jianfangliu@lbl.gov; Oleg Gang, E-mail: og2226@columbia.edu

Supplementary Videos:

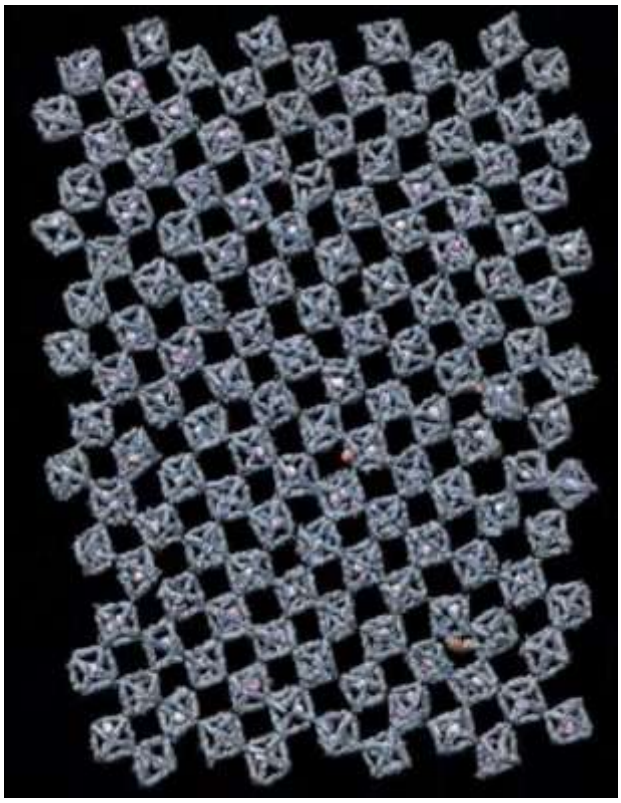

Supplementary Video 1: Analysis of 3D reconstruction of a low-ordered 2D lattice of DNA-origami octahedral cages loaded with 100% ferritin. This video illustrates the cryo-ET and IPET 3D reconstruction process of DNA origami 2D lattices fully loaded with ferritin. It showcases the detailed steps involved in obtaining the final 3D model and performing the distortion analysis of the lattice.

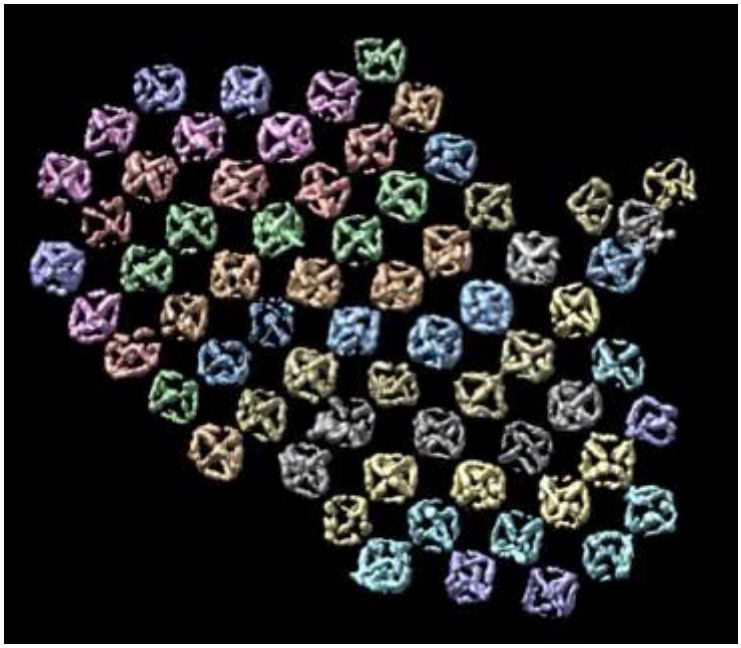

Supplementary Video 2: Analysis of 3D reconstruction of a low-ordered 2D lattice of DNA-origami octahedral cages loaded with 70% ferritin. This video illustrates the cryo-ET and IPET 3D reconstruction process of DNA origami 2D lattices fully loaded with ferritin. It showcases the detailed steps involved in obtaining the final 3D model and performing the distortion analysis of the lattice.

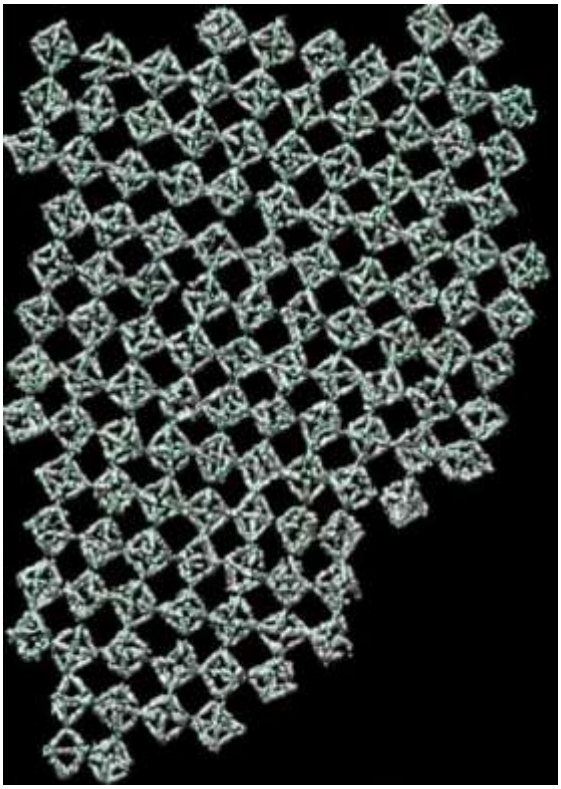

Supplementary Video 3: Analysis of 3D reconstruction of a low-ordered 2D lattice of DNA-origami octahedral cages without ferritin loading. This video illustrates the cryo-ET and IPET 3D reconstruction process of DNA origami 2D lattices without ferritin loading. It showcases the detailed steps involved in obtaining the final 3D model and performing the distortion analysis of the lattice.

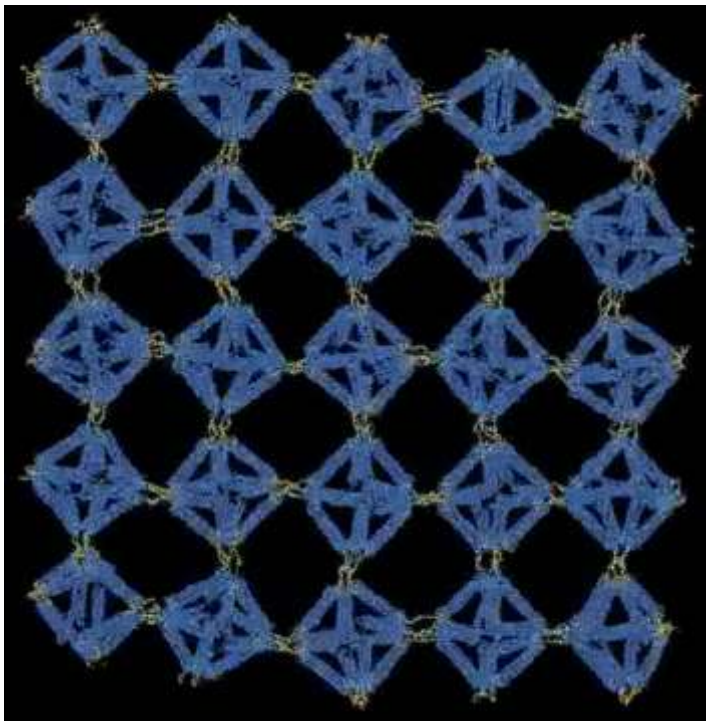

Supplementary Video 4: MD simulations of a 5x5 lattice of DNA-origami octahedral cages without ferritin loading. This video illustrates the MD simulation process of 5 x 5 unit-cell formed DNA origami 2D lattices without ferritin loading.

Supplementary Table 1. The parameters of IPET 3D reconstructions of the unit-cell particles

Part. ID	Sample	EMDB ID	TEM, camera, CDS mode	Mag. and Å/pix (Å)	Dose rate ($e^{-}Å^{-2}s^{-1}$)	Exp. time (s)	Total dose ($e^{-}Å^{-2}$)	Angle range; step	Contour levels	Resolutions (Å)			Ferritin #	Figure #
										Map-map FSC @0.5	Map-map FSC @0.143	Map-model FSC@0.5		
1	100% load	46070	Krios G2, K3, Yes	53Kx, 1.46 Å	3.0	2.2	231	-51° to +51°; 3°	0.6/1.0	64	20	82	1	S9
2	100% load	46071	Krios G2, K3, Yes	53Kx, 1.46 Å	3.0	2.2	231	-51° to +51°; 3°	0.6/1.0	77	19	75	1	S10
3	100% load	46072	Krios G2, K3, Yes	53Kx, 1.46 Å	3.0	2.2	231	-51° to +51°; 3°	0.6/1.0	70	20	90	2	S11
4	100% load	46073	Krios G2, K3, Yes	53Kx, 1.46 Å	3.0	2.2	231	-51° to +51°; 3°	0.6/1.0	72	20	83	1	S12
5	100% load	46074	Krios G2, K3, Yes	53Kx, 1.46 Å	3.0	2.2	231	-51° to +51°; 3°	0.6/1.0	74	19	73	2	S13
6	100% load	46075	Krios G2, K3, No	53Kx, 1.46 Å	6.0	1.0	210	-51° to +51°; 3°	0.6/1.0	75	28	88	1	S14
7	100% load	46076	Krios G2, K3, No	53Kx, 1.46 Å	6.0	1.0	210	-51° to +51°; 3°	0.6/1.0	89	29	82	1	S15
8	100% load	46077	Krios G2, K3, No	53Kx, 1.46 Å	6.0	1.0	210	-51° to +51°; 3°	0.6/1.0	88	31	80	1	S16
9	100% load	46078	Krios G2, K3, No	53Kx, 1.46 Å	6.0	1.0	210	-51° to +51°; 3°	0.6/1.0	69	28	350	1	S17
10	100% load	46079	Krios G2, K3, No	53Kx, 1.46 Å	6.0	1.0	210	-51° to +51°; 3°	0.6/1.0	85	30	78	1	S18
11	100% load	46080	Krios G2, K3, No	53Kx, 1.46 Å	6.0	1.0	210	-51° to +51°; 3°	0.6/1.0	80	30	76	1	S19
12	100% load	46081	Krios G2, K3, No	53Kx, 1.46 Å	6.0	1.0	210	-51° to +51°; 3°	0.6/1.0	252	63	79	1	S20
13	100% load	46082	Krios G2, K3, No	53Kx, 1.46 Å	6.0	1.0	210	-51° to +51°; 3°	0.6/1.0	71	28	302	1	S21
14	100% load	46083	Krios G2, K3, No	53Kx, 1.46 Å	6.0	1.0	210	-51° to +51°; 3°	0.6/1.0	76	29	91	1	S22
15	100% load	46084	Krios G2, K3, No	53Kx, 1.46 Å	6.0	1.0	210	-51° to +51°; 3°	0.6/1.0	36	29	233	2	S23
16	100% load	46085	Krios G2, K3, No	53Kx, 1.46 Å	6.0	1.0	210	-51° to +51°; 3°	0.6/1.0	83	27	103	1	S24
17	100% load	46086	Krios G2, K3, No	53Kx, 1.46 Å	6.0	1.0	210	-51° to +51°; 3°	0.6/1.0	83	29	280	1	S25
18	100% load	46087	Krios G2, K3, No	53Kx, 1.46 Å	6.0	1.0	210	-51° to +51°; 3°	0.6/1.0	74	30	262	2	S26
19	100% load	46088	Krios G2, K3, No	53Kx, 1.46 Å	6.0	1.0	210	-51° to +51°; 3°	0.6/1.0	80	30	260	1	S27
20	100% load	46089	Krios G2, K3, No	53Kx, 1.46 Å	6.0	1.0	210	-51° to +51°; 3°	0.6/1.0	80	30	253	1	S28
21	100% load	46090	Krios G2, K3, No	53Kx, 1.46 Å	6.0	1.0	210	-51° to +51°; 3°	0.6/1.0	88	68	80	1	S29
22	100% load	46091	Krios G2, K3, No	53Kx, 1.46 Å	6.0	1.0	210	-51° to +51°; 3°	0.6/1.0	74	28	75	1	S30
23	100% load	46092	Krios G2, K3, No	53Kx, 1.46 Å	6.0	1.0	210	-51° to +51°; 3°	0.6/1.0	84	29	75	1	S31
24	100% load	46093	Krios G2, K3, No	53Kx, 1.46 Å	6.0	1.0	210	-51° to +51°; 3°	0.6/1.0	76	29	77	1	S32
25	100% load	46094	Krios G2, K3, No	53Kx, 1.46 Å	6.0	1.0	210	-51° to +51°; 3°	0.6/1.0	75	27	128	1	S33
26	100% load	46095	Krios G2, K3, No	53Kx, 1.46 Å	6.0	1.0	210	-51° to +51°; 3°	0.6/1.0	71	29	100	2	S34
27	100% load	46096	Krios G2, K3, No	53Kx, 1.46 Å	6.0	1.0	210	-51° to +51°; 3°	0.6/1.0	71	29	107	2	S35
28	100% load	46097	Krios G2, K3, No	53Kx, 1.46 Å	6.0	1.0	210	-51° to +51°; 3°	0.6/1.0	71	29	67	1	S36
29	100% load	46098	Krios G2, K3, No	53Kx, 1.46 Å	6.0	1.0	210	-51° to +51°; 3°	0.6/1.0	82	69	90	1	S37
30	100% load	46099	Krios G2, K3, No	53Kx, 1.46 Å	6.0	1.0	210	-51° to +51°; 3°	0.6/1.0	75	30	127	2	S38
31	100% load	46100	Krios G2, K3, No	53Kx, 1.46 Å	6.0	1.0	210	-51° to +51°; 3°	0.6/1.0	47	27	125	1	S39
32	100% load	46101	Krios G2, K3, No	53Kx, 1.46 Å	6.0	1.0	210	-51° to +51°; 3°	0.6/1.0	37	28	117	3	S40
33	100% load	46102	Krios G2, K3, No	53Kx, 1.46 Å	6.0	1.0	210	-51° to +51°; 3°	0.6/1.0	36	27	125	2	S41
34	100% load	46103	Krios G2, K3, No	53Kx, 1.46 Å	6.0	1.0	210	-51° to +51°; 3°	0.6/1.0	72	28	110	2	S42
35	100% load	46104	Krios G2, K3, No	53Kx, 1.46 Å	6.0	1.0	210	-51° to +51°; 3°	0.6/1.0	72	32	80	0	S43
36	100% load	46105	Krios G2, K3, No	53Kx, 1.46 Å	6.0	1.0	210	-51° to +51°; 3°	0.6/1.0	72	28	79	1	S44
37	100% load	46106	Krios G2, K3, No	53Kx, 1.46 Å	6.0	1.0	210	-51° to +51°; 3°	0.6/1.0	75	29	92	1	S45
38	100% load	46107	Krios G2, K3, No	53Kx, 1.46 Å	6.0	1.0	210	-51° to +51°; 3°	0.6/1.0	72	29	156	2	S46
39	100% load	46108	Krios G2, K3, No	53Kx, 1.46 Å	6.0	1.0	210	-51° to +51°; 3°	0.6/1.0	72	29	86	1	S47
40	100% load	46109	Krios G2, K3, No	53Kx, 1.46 Å	6.0	1.0	210	-51° to +51°; 3°	0.6/1.0	84	28	88	1	S48
41	100% load	46110	Krios G2, K3, No	53Kx, 1.46 Å	6.0	1.0	210	-51° to +51°; 3°	0.6/1.0	81	40	81	1	S49
42	100% load	46111	Krios G2, K3, No	53Kx, 1.46 Å	6.0	1.0	210	-51° to +51°; 3°	0.6/1.0	78	31	77	2	S50
43	100% load	46112	Krios G2, K3, No	53Kx, 1.46 Å	6.0	1.0	210	-51° to +51°; 3°	0.6/1.0	86	27	83	1	S51
44	100% load	46113	Krios G2, K3, No	53Kx, 1.46 Å	6.0	1.0	210	-51° to +51°; 3°	0.6/1.0	76	32	86	2	S52
45	100% load	46114	Krios G2, K3, No	53Kx, 1.46 Å	6.0	1.0	210	-51° to +51°; 3°	0.6/1.0	75	29	92	2	S53
46	100% load	46115	Krios G2, K3, No	53Kx, 1.46 Å	6.0	1.0	210	-51° to +51°; 3°	0.6/1.0	47	30	89	1	S54

47	100% load	46116	Krios G2, K3, No	53Kx, 1.46 Å	6.0	1.0	210	-51° to +51°; 3°	0.6/1.0	66	29	91	1	S55
48	100% load	46117	Krios G2, K3, No	53Kx, 1.46 Å	6.0	1.0	210	-51° to +51°; 3°	0.6/1.0	64	28	272	1	S56
49	100% load	46118	Krios G2, K3, No	53Kx, 1.46 Å	6.0	1.0	210	-51° to +51°; 3°	0.6/1.0	82	30	73	1	S57
50	100% load	46119	Krios G2, K3, No	53Kx, 1.46 Å	6.0	1.0	210	-51° to +51°; 3°	0.6/1.0	69	29	74	1	S58
51	100% load	46120	Krios G2, K3, No	53Kx, 1.46 Å	6.0	1.0	210	-51° to +51°; 3°	0.6/1.0	63	28	91	1	S59
52	100% load	46121	Krios G2, K3, No	53Kx, 1.46 Å	6.0	1.0	210	-51° to +51°; 3°	0.6/1.0	120	30	267	1	S60
53	100% load	46122	Krios G2, K3, No	53Kx, 1.46 Å	6.0	1.0	210	-51° to +51°; 3°	0.6/1.0	76	31	74	1	S61
54	100% load	46123	Krios G2, K3, No	53Kx, 1.46 Å	6.0	1.0	210	-51° to +51°; 3°	0.6/1.0	78	30	152	2	S62
55	100% load	46124	Krios G2, K3, No	53Kx, 1.46 Å	6.0	1.0	210	-51° to +51°; 3°	0.6/1.0	80	29	76	1	S63
56	100% load	46125	Krios G2, K3, No	53Kx, 1.46 Å	6.0	1.0	210	-51° to +51°; 3°	0.6/1.0	81	29	84	2	S64
57	100% load	46126	Krios G2, K3, No	53Kx, 1.46 Å	6.0	1.0	210	-51° to +51°; 3°	0.6/1.0	78	30	77	1	S65
58	100% load	46127	Krios G2, K3, No	53Kx, 1.46 Å	6.0	1.0	210	-51° to +51°; 3°	0.6/1.0	70	29	79	1	S66
59	100% load	46128	Krios G2, K3, No	53Kx, 1.46 Å	6.0	1.0	210	-51° to +51°; 3°	0.6/1.0	75	30	260	1	S67
60	100% load	46129	Krios G2, K3, No	53Kx, 1.46 Å	6.0	1.0	210	-51° to +51°; 3°	0.6/1.0	65	29	195	1	S68
61	100% load	46130	Krios G2, K3, No	53Kx, 1.46 Å	6.0	1.0	210	-51° to +51°; 3°	0.6/1.0	86	29	82	2	S69
62	100% load	46131	Krios G2, K3, No	53Kx, 1.46 Å	6.0	1.0	210	-51° to +51°; 3°	0.6/1.0	67	29	139	2	S70
63	100% load	46132	Krios G2, K3, No	53Kx, 1.46 Å	6.0	1.0	210	-51° to +51°; 3°	0.6/1.0	72	29	82	1	S71
64	100% load	46133	Krios G2, K3, No	53Kx, 1.46 Å	6.0	1.0	210	-51° to +51°; 3°	0.6/1.0	94	30	90	1	S72
65	100% load	46134	Krios G2, K3, No	53Kx, 1.46 Å	6.0	1.0	210	-51° to +51°; 3°	0.6/1.0	73	30	292	1	S73
66	100% load	46135	Krios G2, K3, No	53Kx, 1.46 Å	6.0	1.0	210	-51° to +51°; 3°	0.6/1.0	79	29	88	1	S74
67	100% load	46136	Krios G2, K3, No	53Kx, 1.46 Å	6.0	1.0	210	-51° to +51°; 3°	0.6/1.0	63	30	136	2	S75
68	100% load	46137	Krios G2, K3, No	53Kx, 1.46 Å	6.0	1.0	210	-51° to +51°; 3°	0.6/1.0	78	29	81	1	S76
69	100% load	46138	Krios G2, K3, No	53Kx, 1.46 Å	6.0	1.0	210	-51° to +51°; 3°	0.6/1.0	61	29	252	1	S77
70	100% load	46139	Krios G2, K3, No	53Kx, 1.46 Å	6.0	1.0	210	-51° to +51°; 3°	0.6/1.0	73	30	82	1	S78
71	100% load	46140	Krios G2, K3, No	53Kx, 1.46 Å	6.0	1.0	210	-51° to +51°; 3°	0.6/1.0	73	29	89	1	S79
72	100% load	46141	Krios G2, K3, No	53Kx, 1.46 Å	6.0	1.0	210	-51° to +51°; 3°	0.6/1.0	78	30	76	1	S80
73	100% load	46142	Krios G2, K3, No	53Kx, 1.46 Å	6.0	1.0	210	-51° to +51°; 3°	0.6/1.0	72	27	90	1	S81
74	100% load	46143	Krios G2, K3, No	53Kx, 1.46 Å	6.0	1.0	210	-51° to +51°; 3°	0.6/1.0	84	29	72	1	S82
75	100% load	46144	Krios G2, K3, No	53Kx, 1.46 Å	6.0	1.0	210	-51° to +51°; 3°	0.6/1.0	79	30	92	2	S83
76	100% load	46145	Krios G2, K3, No	53Kx, 1.46 Å	6.0	1.0	210	-51° to +51°; 3°	0.6/1.0	81	30	78	1	S84
77	100% load	46146	Krios G2, K3, No	53Kx, 1.46 Å	6.0	1.0	210	-51° to +51°; 3°	0.6/1.0	92	68	82	1	S85
78	100% load	46147	Krios G2, K3, No	53Kx, 1.46 Å	6.0	1.0	210	-51° to +51°; 3°	0.6/1.0	72	30	74	2	S86
79	100% load	46148	Krios G2, K3, No	53Kx, 1.46 Å	6.0	1.0	210	-51° to +51°; 3°	0.6/1.0	73	30	84	1	S87
80	100% load	46149	Krios G2, K3, No	53Kx, 1.46 Å	6.0	1.0	210	-51° to +51°; 3°	0.6/1.0	76	30	320	1	S88
81	100% load	46150	Krios G2, K3, No	53Kx, 1.46 Å	6.0	1.0	210	-51° to +51°; 3°	0.6/1.0	73	29	256	1	S89
82	100% load	46151	Krios G2, K3, No	53Kx, 1.46 Å	6.0	1.0	210	-51° to +51°; 3°	0.6/1.0	69	31	97	2	S90
83	100% load	46152	Krios G2, K3, No	53Kx, 1.46 Å	6.0	1.0	210	-51° to +51°; 3°	0.6/1.0	68	29	70	1	S91
84	100% load	46153	Krios G2, K3, No	53Kx, 1.46 Å	6.0	1.0	210	-51° to +51°; 3°	0.6/1.0	75	28	91	1	S92
85	100% load	46154	Krios G2, K3, No	53Kx, 1.46 Å	6.0	1.0	210	-51° to +51°; 3°	0.6/1.0	71	30	101	1	S93
86	100% load	46155	Krios G2, K3, No	53Kx, 1.46 Å	6.0	1.0	210	-51° to +51°; 3°	0.6/1.0	75	31	78	1	S94
87	100% load	46156	Krios G2, K3, No	53Kx, 1.46 Å	6.0	1.0	210	-51° to +51°; 3°	0.6/1.0	40	29	134	1	S95
88	100% load	46157	Krios G2, K3, No	53Kx, 1.46 Å	6.0	1.0	210	-51° to +51°; 3°	0.6/1.0	70	31	247	2	S96
89	100% load	46158	Krios G2, K3, No	53Kx, 1.46 Å	6.0	1.0	210	-51° to +51°; 3°	0.6/1.0	66	30	307	1	S97
90	100% load	46159	Krios G2, K3, No	53Kx, 1.46 Å	6.0	1.0	210	-51° to +51°; 3°	0.6/1.0	86	30	97	1	S98
91	100% load	46160	Krios G2, K3, No	53Kx, 1.46 Å	6.0	1.0	210	-51° to +51°; 3°	0.6/1.0	69	29	108	1	S99
92	100% load	46161	Krios G2, K3, No	53Kx, 1.46 Å	6.0	1.0	210	-51° to +51°; 3°	0.6/1.0	79	28	80	1	S100
93	100% load	46162	Krios G2, K3, No	53Kx, 1.46 Å	6.0	1.0	210	-51° to +51°; 3°	0.6/1.0	38	28	276	2	S101
94	100% load	46163	Krios G2, K3, No	53Kx, 1.46 Å	6.0	1.0	210	-51° to +51°; 3°	0.6/1.0	82	30	95	1	S102
95	100% load	46164	Krios G2, K3, No	53Kx, 1.46 Å	6.0	1.0	210	-51° to +51°; 3°	0.6/1.0	71	30	104	1	S103
96	100% load	46165	Krios G2, K3, No	53Kx, 1.46 Å	6.0	1.0	210	-51° to +51°; 3°	0.6/1.0	78	28	110	1	S104
97	100% load	46166	Krios G2, K3, No	53Kx, 1.46 Å	6.0	1.0	210	-51° to +51°; 3°	0.6/1.0	77	31	77	1	S105

98	100% load	46167	Krios G2, K3, No	53Kx, 1.46 Å	6.0	1.0	210	-51° to +51°; 3°	0.6/1.0	87	30	87	1	S106
99	100% load	46168	Krios G2, K3, No	53Kx, 1.46 Å	6.0	1.0	210	-51° to +51°; 3°	0.6/1.0	72	29	94	1	S107
100	100% load	46169	Krios G2, K3, No	53Kx, 1.46 Å	6.0	1.0	210	-51° to +51°; 3°	0.6/1.0	70	30	74	1	S108
101	100% load	46170	Krios G2, K3, No	53Kx, 1.46 Å	6.0	1.0	210	-51° to +51°; 3°	0.6/1.0	74	30	83	1	S109
102	100% load	46171	Krios G2, K3, No	53Kx, 1.46 Å	6.0	1.0	210	-51° to +51°; 3°	0.6/1.0	70	29	134	1	S110
103	100% load	46172	Krios G2, K3, No	53Kx, 1.46 Å	6.0	1.0	210	-51° to +51°; 3°	0.6/1.0	81	27	78	1	S111
104	100% load	46173	Krios G2, K3, No	53Kx, 1.46 Å	6.0	1.0	210	-51° to +51°; 3°	0.6/1.0	72	31	74	1	S112
105	100% load	46174	Krios G2, K3, No	53Kx, 1.46 Å	6.0	1.0	210	-51° to +51°; 3°	0.6/1.0	68	29	82	1	S113
106	100% load	46175	Krios G2, K3, No	53Kx, 1.46 Å	6.0	1.0	210	-51° to +51°; 3°	0.6/1.0	72	29	102	1	S114
107	100% load	46176	Krios G2, K3, No	53Kx, 1.46 Å	6.0	1.0	210	-51° to +51°; 3°	0.6/1.0	60	28	146	3	S115
108	100% load	46177	Krios G2, K3, No	53Kx, 1.46 Å	6.0	1.0	210	-51° to +51°; 3°	0.6/1.0	64	29	116	2	S116
109	100% load	46178	Krios G2, K3, No	53Kx, 1.46 Å	6.0	1.0	210	-51° to +51°; 3°	0.6/1.0	85	31	85	1	S117
110	100% load	46179	Krios G2, K3, No	53Kx, 1.46 Å	6.0	1.0	210	-51° to +51°; 3°	0.6/1.0	86	29	85	1	S118
111	100% load	46180	Krios G2, K3, No	53Kx, 1.46 Å	6.0	1.0	210	-51° to +51°; 3°	0.6/1.0	76	28	314	2	S119
112	100% load	46181	Krios G2, K3, No	53Kx, 1.46 Å	6.0	1.0	210	-51° to +51°; 3°	0.6/1.0	87	31	77	1	S120
113	100% load	46182	Krios G2, K3, No	53Kx, 1.46 Å	6.0	1.0	210	-51° to +51°; 3°	0.6/1.0	76	30	302	1	S121
114	100% load	46183	Krios G2, K3, No	53Kx, 1.46 Å	6.0	1.0	210	-51° to +51°; 3°	0.6/1.0	82	31	82	1	S122
115	100% load	46184	Krios G2, K3, No	53Kx, 1.46 Å	6.0	1.0	210	-51° to +51°; 3°	0.6/1.0	72	29	81	1	S123
116	100% load	46185	Krios G2, K3, No	53Kx, 1.46 Å	6.0	1.0	210	-51° to +51°; 3°	0.6/1.0	75	29	85	1	S124
117	100% load	46186	Krios G2, K3, No	53Kx, 1.46 Å	6.0	1.0	210	-51° to +51°; 3°	0.6/1.0	73	29	77	1	S125
118	100% load	46187	Krios G2, K3, No	53Kx, 1.46 Å	6.0	1.0	210	-51° to +51°; 3°	0.6/1.0	73	31	87	1	S126
119	100% load	46188	Krios G2, K3, No	53Kx, 1.46 Å	6.0	1.0	210	-51° to +51°; 3°	0.6/1.0	71	29	88	1	S127
120	100% load	46189	Krios G2, K3, No	53Kx, 1.46 Å	6.0	1.0	210	-51° to +51°; 3°	0.6/1.0	68	29	78	1	S128
121	100% load	46190	Krios G2, K3, No	53Kx, 1.46 Å	6.0	1.0	210	-51° to +51°; 3°	0.6/1.0	94	30	76	2	S129
122	100% load	46191	Krios G2, K3, No	53Kx, 1.46 Å	6.0	1.0	210	-51° to +51°; 3°	0.6/1.0	73	29	74	1	S130
123	100% load	46192	Krios G2, K3, No	53Kx, 1.46 Å	6.0	1.0	210	-51° to +51°; 3°	0.6/1.0	53	29	104	1	S131
124	100% load	46193	Krios G2, K3, No	53Kx, 1.46 Å	6.0	1.0	210	-51° to +51°; 3°	0.6/1.0	78	29	100	1	S132
125	100% load	46194	Krios G2, K3, No	53Kx, 1.46 Å	6.0	1.0	210	-51° to +51°; 3°	0.6/1.0	71	31	150	2	S133
126	100% load	46195	Krios G2, K3, No	53Kx, 1.46 Å	6.0	1.0	210	-51° to +51°; 3°	0.6/1.0	85	28	84	1	S134
127	100% load	46196	Krios G2, K3, No	53Kx, 1.46 Å	6.0	1.0	210	-51° to +51°; 3°	0.6/1.0	81	29	87	1	S135
128	100% load	46197	Krios G2, K3, No	53Kx, 1.46 Å	6.0	1.0	210	-51° to +51°; 3°	0.6/1.0	78	30	89	1	S136
129	100% load	46198	Krios G2, K3, No	53Kx, 1.46 Å	6.0	1.0	210	-51° to +51°; 3°	0.6/1.0	98	30	75	2	S137
130	100% load	46199	Krios G2, K3, No	53Kx, 1.46 Å	6.0	1.0	210	-51° to +51°; 3°	0.6/1.0	80	28	89	1	S138
131	100% load	46200	Krios G2, K3, No	53Kx, 1.46 Å	6.0	1.0	210	-51° to +51°; 3°	0.6/1.0	73	28	98	1	S139
132	100% load	46201	Krios G2, K3, No	53Kx, 1.46 Å	6.0	1.0	210	-51° to +51°; 3°	0.6/1.0	61	29	135	2	S140
133	100% load	46202	Krios G2, K3, No	53Kx, 1.46 Å	6.0	1.0	210	-51° to +51°; 3°	0.6/1.0	72	29	74	1	S141
134	100% load	46203	Krios G2, K3, No	53Kx, 1.46 Å	6.0	1.0	210	-51° to +51°; 3°	0.6/1.0	79	30	76	1	S142
135	100% load	46204	Krios G2, K3, No	53Kx, 1.46 Å	6.0	1.0	210	-51° to +51°; 3°	0.6/1.0	73	29	73	2	S143
136	100% load	46205	Krios G2, K3, No	53Kx, 1.46 Å	6.0	1.0	210	-51° to +51°; 3°	0.6/1.0	81	29	105	1	S144
137	100% load	46206	Krios G2, K3, No	53Kx, 1.46 Å	6.0	1.0	210	-51° to +51°; 3°	0.6/1.0	88	30	90	1	S145
138	100% load	46207	Krios G2, K3, No	53Kx, 1.46 Å	6.0	1.0	210	-51° to +51°; 3°	0.6/1.0	83	31	80	1	S146
139	100% load	46208	Krios G2, K3, No	53Kx, 1.46 Å	6.0	1.0	210	-51° to +51°; 3°	0.6/1.0	79	32	87	1	S147
140	100% load	46209	Krios G2, K3, No	53Kx, 1.46 Å	6.0	1.0	210	-51° to +51°; 3°	0.6/1.0	87	31	78	1	S148
141	100% load	46210	Krios G2, K3, No	53Kx, 1.46 Å	6.0	1.0	210	-51° to +51°; 3°	0.6/1.0	72	29	71	1	S149
142	100% load	46211	Krios G2, K3, No	53Kx, 1.46 Å	6.0	1.0	210	-51° to +51°; 3°	0.6/1.0	74	32	80	1	S150
143	100% load	46212	Krios G2, K3, No	53Kx, 1.46 Å	6.0	1.0	210	-51° to +51°; 3°	0.6/1.0	78	29	79	1	S151
144	100% load	46213	Krios G2, K3, No	53Kx, 1.46 Å	6.0	1.0	210	-51° to +51°; 3°	0.6/1.0	80	31	80	1	S152
145	100% load	46214	Krios G2, K3, No	53Kx, 1.46 Å	6.0	1.0	210	-51° to +51°; 3°	0.6/1.0	77	29	81	1	S153
Part. ID	**Sample**	**EMDB ID**	**TEM, camera, CDS mode**	**Mag. and Apix (Å)**	**Dose rate ($e^{-}Å^{-2}s^{-1}$)**	**Exp. time (s)**	**Total dose ($e^{-}Å^{-2}$)**	**Angle range; step**	**Contour levels**	**Map-map FSC @0.5**	**Map-map FSC @0.143**	**Map-model FSC @0.5**	**Ferritin #**	**Figure #**

146	70% load	46215	Zeiss 120, CCD, No	80Kx, 1.48Å	-	1.0	66	-48° to +48°; 3°	0.7/1.3	72	64	77	1	S154
147	70% load	46216	Zeiss 120, CCD, No	80Kx, 1.48Å	-	1.0	66	-48° to +48°; 3°	0.7/1.3	74	62	82	1	S155
148	70% load	46217	Zeiss 120, CCD, No	80Kx, 1.48Å	-	1.0	66	-48° to +48°; 3°	0.7/1.3	76	60	81	1	S156
149	70% load	46218	Zeiss 120, CCD, No	80Kx, 1.48Å	-	1.0	66	-48° to +48°; 3°	0.7/1.3	75	60	81	1	S157
150	70% load	46219	Zeiss 120, CCD, No	80Kx, 1.48Å	-	1.0	66	-48° to +48°; 3°	0.7/1.3	77	65	74	1	S158
151	70% load	46220	Zeiss 120, CCD, No	80Kx, 1.48Å	-	1.0	66	-48° to +48°; 3°	0.7/1.3	76	65	78	0	S159
152	70% load	46221	Zeiss 120, CCD, No	80Kx, 1.48Å	-	1.0	66	-48° to +48°; 3°	0.7/1.3	78	60	83	2	S160
153	70% load	46222	Zeiss 120, CCD, No	80Kx, 1.48Å	-	1.0	66	-48° to +48°; 3°	0.7/1.3	78	63	277	1	S161
154	70% load	46223	Zeiss 120, CCD, No	80Kx, 1.48Å	-	1.0	66	-48° to +48°; 3°	0.7/1.3	75	60	75	0	S162
155	70% load	46224	Zeiss 120, CCD, No	80Kx, 1.48Å	-	1.0	66	-48° to +48°; 3°	0.7/1.3	74	63	94	1	S163
156	70% load	46225	Zeiss 120, CCD, No	80Kx, 1.48Å	-	1.0	66	-48° to +48°; 3°	0.7/1.3	78	64	73	0	S164
157	70% load	46226	Zeiss 120, CCD, No	80Kx, 1.48Å	-	1.0	66	-48° to +48°; 3°	0.7/1.3	76	65	85	1	S165
158	70% load	46227	Zeiss 120, CCD, No	80Kx, 1.48Å	-	1.0	66	-48° to +48°; 3°	0.7/1.3	75	66	89	1	S166
159	70% load	46228	Zeiss 120, CCD, No	80Kx, 1.48Å	-	1.0	66	-48° to +48°; 3°	0.7/1.3	73	62	75	1	S167
160	70% load	46229	Zeiss 120, CCD, No	80Kx, 1.48Å	-	1.0	66	-48° to +48°; 3°	0.7/1.3	75	64	71	1	S168
161	70% load	46230	Zeiss 120, CCD, No	80Kx, 1.48Å	-	1.0	66	-48° to +48°; 3°	0.7/1.3	72	57	84	1	S169
162	70% load	46231	Zeiss 120, CCD, No	80Kx, 1.48Å	-	1.0	66	-48° to +48°; 3°	0.7/1.3	77	61	91	1	S170
163	70% load	46232	Zeiss 120, CCD, No	80Kx, 1.48Å	-	1.0	66	-48° to +48°; 3°	0.7/1.3	77	63	74	1	S171
164	70% load	46233	Zeiss 120, CCD, No	80Kx, 1.48Å	-	1.0	66	-48° to +48°; 3°	0.7/1.3	78	64	81	1	S172
165	70% load	46234	Zeiss 120, CCD, No	80Kx, 1.48Å	-	1.0	66	-48° to +48°; 3°	0.7/1.3	71	55	80	1	S173
166	70% load	46235	Zeiss 120, CCD, No	80Kx, 1.48Å	-	1.0	66	-48° to +48°; 3°	0.7/1.3	75	62	77	1	S174
167	70% load	46236	Zeiss 120, CCD, No	80Kx, 1.48Å	-	1.0	66	-48° to +48°; 3°	0.7/1.3	79	62	81	1	S175
168	70% load	46237	Zeiss 120, CCD, No	80Kx, 1.48Å	-	1.0	66	-48° to +48°; 3°	0.7/1.3	74	64	75	1	S176
169	70% load	46238	Zeiss 120, CCD, No	80Kx, 1.48Å	-	1.0	66	-48° to +48°; 3°	0.7/1.3	75	57	81	1	S177
170	70% load	46239	Zeiss 120, CCD, No	80Kx, 1.48Å	-	1.0	66	-48° to +48°; 3°	0.7/1.3	80	67	79	0	S178
171	70% load	46240	Zeiss 120, CCD, No	80Kx, 1.48Å	-	1.0	66	-48° to +48°; 3°	0.7/1.3	78	69	93	1	S179
172	70% load	46241	Zeiss 120, CCD, No	80Kx, 1.48Å	-	1.0	66	-48° to +48°; 3°	0.7/1.3	81	59	82	0	S180
173	70% load	46242	Zeiss 120, CCD, No	80Kx, 1.48Å	-	1.0	66	-48° to +48°; 3°	0.7/1.3	82	65	80	1	S181
174	70% load	46243	Zeiss 120, CCD, No	80Kx, 1.48Å	-	1.0	66	-48° to +48°; 3°	0.7/1.3	83	70	73	1	S182
175	70% load	46244	Zeiss 120, CCD, No	80Kx, 1.48Å	-	1.0	66	-48° to +48°; 3°	0.7/1.3	77	68	89	1	S183
176	70% load	46245	Zeiss 120, CCD, No	80Kx, 1.48Å	-	1.0	66	-48° to +48°; 3°	0.7/1.3	75	61	157	1	S184
177	70% load	46246	Zeiss 120, CCD, No	80Kx, 1.48Å	-	1.0	66	-48° to +48°; 3°	0.7/1.3	79	67	77	1	S185
178	70% load	46247	Zeiss 120, CCD, No	80Kx, 1.48Å	-	1.0	66	-48° to +48°; 3°	0.7/1.3	77	66	75	0	S186
179	70% load	46248	Zeiss 120, CCD, No	80Kx, 1.48Å	-	1.0	66	-48° to +48°; 3°	0.7/1.3	75	64	85	1	S187
180	70% load	46249	Zeiss 120, CCD, No	80Kx, 1.48Å	-	1.0	66	-48° to +48°; 3°	0.7/1.3	79	65	79	0	S188
181	70% load	46250	Zeiss 120, CCD, No	80Kx, 1.48Å	-	1.0	66	-48° to +48°; 3°	0.7/1.3	79	64	82	1	S189
182	70% load	46251	Zeiss 120, CCD, No	80Kx, 1.48Å	-	1.0	66	-48° to +48°; 3°	0.7/1.3	76	65	80	1	S190
183	70% load	46252	Zeiss 120, CCD, No	80Kx, 1.48Å	-	1.0	66	-48° to +48°; 3°	0.7/1.3	81	64	79	1	S191
184	70% load	46253	Zeiss 120, CCD, No	80Kx, 1.48Å	-	1.0	66	-48° to +48°; 3°	0.7/1.3	77	66	73	1	S192
185	70% load	46254	Zeiss 120, CCD, No	80Kx, 1.48Å	-	1.0	66	-48° to +48°; 3°	0.7/1.3	75	63	82	1	S193
186	70% load	46255	Zeiss 120, CCD, No	80Kx, 1.48Å	-	1.0	66	-48° to +48°; 3°	0.7/1.3	74	63	73	1	S194
187	70% load	46256	Zeiss 120, CCD, No	80Kx, 1.48Å	-	1.0	66	-48° to +48°; 3°	0.7/1.3	79	65	79	1	S195
188	70% load	46257	Zeiss 120, CCD, No	80Kx, 1.48Å	-	1.0	66	-48° to +48°; 3°	0.7/1.3	79	56	75	1	S196
189	70% load	46258	Zeiss 120, CCD, No	80Kx, 1.48Å	-	1.0	66	-48° to +48°; 3°	0.7/1.3	74	65	128	1	S197
190	70% load	46259	Zeiss 120, CCD, No	80Kx, 1.48Å	-	1.0	66	-48° to +48°; 3°	0.7/1.3	70	46	133	2	S198
191	70% load	46260	Zeiss 120, CCD, No	80Kx, 1.48Å	-	1.0	66	-48° to +48°; 3°	0.7/1.3	75	62	78	1	S199
192	70% load	46261	Zeiss 120, CCD, No	80Kx, 1.48Å	-	1.0	66	-48° to +48°; 3°	0.7/1.3	78	56	81	2	S200
193	70% load	46262	Zeiss 120, CCD, No	80Kx, 1.48Å	-	1.0	66	-48° to +48°; 3°	0.7/1.3	79	62	77	0	S201
194	70% load	46263	Zeiss 120, CCD, No	80Kx, 1.48Å	-	1.0	66	-48° to +48°; 3°	0.7/1.3	76	62	87	1	S202
195	70% load	46264	Zeiss 120, CCD, No	80Kx, 1.48Å	-	1.0	66	-48° to +48°; 3°	0.7/1.3	73	62	84	1	S203
196	70% load	46265	Zeiss 120, CCD, No	80Kx, 1.48Å	-	1.0	66	-48° to +48°; 3°	0.7/1.3	75	63	81	1	S204

197	70% load	46266	Zeiss 120, CCD, No	80Kx, 1.48Å	-	1.0	66	-48° to +48°; 3°	0.7/1.3	78	63	76	1	S205
198	70% load	46267	Zeiss 120, CCD, No	80Kx, 1.48Å	-	1.0	66	-48° to +48°; 3°	0.7/1.3	76	67	84	1	S206
199	70% load	46268	Zeiss 120, CCD, No	80Kx, 1.48Å	-	1.0	66	-48° to +48°; 3°	0.7/1.3	73	54	82	0	S207
200	70% load	46269	Zeiss 120, CCD, No	80Kx, 1.48Å	-	1.0	66	-48° to +48°; 3°	0.7/1.3	75	57	98	1	S208
201	70% load	46270	Zeiss 120, CCD, No	80Kx, 1.48Å	-	1.0	66	-48° to +48°; 3°	0.7/1.3	75	64	92	1	S209
202	70% load	46271	Zeiss 120, CCD, No	80Kx, 1.48Å	-	1.0	66	-48° to +48°; 3°	0.7/1.3	77	58	82	0	S210
203	70% load	46272	Zeiss 120, CCD, No	80Kx, 1.48Å	-	1.0	66	-48° to +48°; 3°	0.7/1.3	78	64	80	1	S211
204	70% load	46273	Zeiss 120, CCD, No	80Kx, 1.48Å	-	1.0	66	-48° to +48°; 3°	0.7/1.3	78	57	78	1	S212
205	70% load	46274	Zeiss 120, CCD, No	80Kx, 1.48Å	-	1.0	66	-48° to +48°; 3°	0.7/1.3	77	56	78	1	S213
206	70% load	46275	Zeiss 120, CCD, No	80Kx, 1.48Å	-	1.0	66	-48° to +48°; 3°	0.7/1.3	74	61	76	1	S214
207	70% load	46276	Zeiss 120, CCD, No	80Kx, 1.48Å	-	1.0	66	-48° to +48°; 3°	0.7/1.3	78	64	77	1	S215
208	70% load	46277	Zeiss 120, CCD, No	80Kx, 1.48Å	-	1.0	66	-48° to +48°; 3°	0.7/1.3	77	63	82	1	S216
209	70% load	46278	Zeiss 120, CCD, No	80Kx, 1.48Å	-	1.0	66	-48° to +48°; 3°	0.7/1.3	75	66	76	0	S217
210	70% load	46279	Zeiss 120, CCD, No	80Kx, 1.48Å	-	1.0	66	-48° to +48°; 3°	0.7/1.3	74	59	80	0	S218
211	70% load	46280	Zeiss 120, CCD, No	80Kx, 1.48Å	-	1.0	66	-48° to +48°; 3°	0.7/1.3	88	62	82	1	S219
212	70% load	46281	Zeiss 120, CCD, No	80Kx, 1.48Å	-	1.0	66	-48° to +48°; 3°	0.7/1.3	85	64	91	1	S220
213	70% load	46282	Zeiss 120, CCD, No	80Kx, 1.48Å	-	1.0	66	-48° to +48°; 3°	0.7/1.3	81	53	141	1	S221
214	70% load	46283	Zeiss 120, CCD, No	80Kx, 1.48Å	-	1.0	66	-48° to +48°; 3°	0.7/1.3	81	69	77	1	S222
215	70% load	46284	Zeiss 120, CCD, No	80Kx, 1.48Å	-	1.0	66	-48° to +48°; 3°	0.7/1.3	78	67	79	1	S223
Part. ID	**Sample**	**EMDB ID**	**TEM, camera, CDS mode**	**Mag. and Apix (Å)**	**Dose rate ($e^{-}Å^{-2}s^{-1}$)**	**Exp. time (s)**	**Total dose ($e^{-}Å^{-2}$)**	**Angle range; step**	**Contour levels**	**Map-map FSC @0.5**	**Map-map FSC @0.143**	**Map-model FSC @0.5**	**Ferritin #**	**Figure #**
216	0% load	46285	Krios G2, K3, No	53Kx, 1.46 Å	6.0	1.0	210	-51° to +51°; 3°	0.6/1.0	69	28	79	0	S224
217	0% load	46286	Krios G2, K3, No	53Kx, 1.46 Å	6.0	1.0	210	-51° to +51°; 3°	0.6/1.0	73	27	73	0	S225
218	0% load	46287	Krios G2, K3, No	53Kx, 1.46 Å	6.0	1.0	210	-51° to +51°; 3°	0.6/1.0	72	27	84	0	S226
219	0% load	46288	Krios G2, K3, No	53Kx, 1.46 Å	6.0	1.0	210	-51° to +51°; 3°	0.6/1.0	79	29	77	0	S227
220	0% load	46289	Krios G2, K3, No	53Kx, 1.46 Å	6.0	1.0	210	-51° to +51°; 3°	0.6/1.0	74	27	79	0	S228
221	0% load	46290	Krios G2, K3, No	53Kx, 1.46 Å	6.0	1.0	210	-51° to +51°; 3°	0.6/1.0	74	26	75	0	S229
222	0% load	46291	Krios G2, K3, No	53Kx, 1.46 Å	6.0	1.0	210	-51° to +51°; 3°	0.6/1.0	69	28	77	0	S230
223	0% load	46292	Krios G2, K3, No	53Kx, 1.46 Å	6.0	1.0	210	-51° to +51°; 3°	0.6/1.0	73	25	78	0	S231
224	0% load	46293	Krios G2, K3, No	53Kx, 1.46 Å	6.0	1.0	210	-51° to +51°; 3°	0.6/1.0	97	75	74	0	S232
225	0% load	46294	Krios G2, K3, No	53Kx, 1.46 Å	6.0	1.0	210	-51° to +51°; 3°	0.6/1.0	82	32	76	0	S233
226	0% load	46295	Krios G2, K3, No	53Kx, 1.46 Å	6.0	1.0	210	-51° to +51°; 3°	0.6/1.0	84	28	79	0	S234
227	0% load	46296	Krios G2, K3, No	53Kx, 1.46 Å	6.0	1.0	210	-51° to +51°; 3°	0.6/1.0	77	27	76	0	S235
228	0% load	46297	Krios G2, K3, No	53Kx, 1.46 Å	6.0	1.0	210	-51° to +51°; 3°	0.6/1.0	72	25	75	0	S236
229	0% load	46298	Krios G2, K3, No	53Kx, 1.46 Å	6.0	1.0	210	-51° to +51°; 3°	0.6/1.0	73	25	81	0	S237
230	0% load	46299	Krios G2, K3, No	53Kx, 1.46 Å	6.0	1.0	210	-51° to +51°; 3°	0.6/1.0	75	27	76	0	S238
231	0% load	46300	Krios G2, K3, No	53Kx, 1.46 Å	6.0	1.0	210	-51° to +51°; 3°	0.6/1.0	72	27	76	0	S239
232	0% load	46301	Krios G2, K3, No	53Kx, 1.46 Å	6.0	1.0	210	-51° to +51°; 3°	0.6/1.0	69	29	75	0	S240
233	0% load	46302	Krios G2, K3, No	53Kx, 1.46 Å	6.0	1.0	210	-51° to +51°; 3°	0.6/1.0	74	27	77	0	S241
234	0% load	46303	Krios G2, K3, No	53Kx, 1.46 Å	6.0	1.0	210	-51° to +51°; 3°	0.6/1.0	78	27	79	0	S242
235	0% load	46304	Krios G2, K3, No	53Kx, 1.46 Å	6.0	1.0	210	-51° to +51°; 3°	0.6/1.0	78	27	79	0	S243
236	0% load	46305	Krios G2, K3, No	53Kx, 1.46 Å	6.0	1.0	210	-51° to +51°; 3°	0.6/1.0	74	28	75	0	S244
237	0% load	46306	Krios G2, K3, No	53Kx, 1.46 Å	6.0	1.0	210	-51° to +51°; 3°	0.6/1.0	72	26	77	0	S245
238	0% load	46307	Krios G2, K3, No	53Kx, 1.46 Å	6.0	1.0	210	-51° to +51°; 3°	0.6/1.0	77	28	76	0	S246
239	0% load	46308	Krios G2, K3, No	53Kx, 1.46 Å	6.0	1.0	210	-51° to +51°; 3°	0.6/1.0	80	29	77	0	S247
240	0% load	46309	Krios G2, K3, No	53Kx, 1.46 Å	6.0	1.0	210	-51° to +51°; 3°	0.6/1.0	78	28	76	0	S248
241	0% load	46310	Krios G2, K3, No	53Kx, 1.46 Å	6.0	1.0	210	-51° to +51°; 3°	0.6/1.0	75	28	74	0	S249
242	0% load	46311	Krios G2, K3, No	53Kx, 1.46 Å	6.0	1.0	210	-51° to +51°; 3°	0.6/1.0	72	28	82	0	S250
243	0% load	46312	Krios G2, K3, No	53Kx, 1.46 Å	6.0	1.0	210	-51° to +51°; 3°	0.6/1.0	69	27	80	0	S251
244	0% load	46313	Krios G2, K3, No	53Kx, 1.46 Å	6.0	1.0	210	-51° to +51°; 3°	0.6/1.0	75	27	80	0	S252

245	0% load	46314	Krios G2, K3, No	53Kx, 1.46 Å	6.0	1.0	210	-51° to +51°; 3°	0.6/1.0	93	70	86	0	S253
246	0% load	46315	Krios G2, K3, No	53Kx, 1.46 Å	6.0	1.0	210	-51° to +51°; 3°	0.6/1.0	77	28	77	0	S254
247	0% load	46316	Krios G2, K3, No	53Kx, 1.46 Å	6.0	1.0	210	-51° to +51°; 3°	0.6/1.0	75	29	72	0	S255
248	0% load	46317	Krios G2, K3, No	53Kx, 1.46 Å	6.0	1.0	210	-51° to +51°; 3°	0.6/1.0	74	27	74	0	S256
249	0% load	46318	Krios G2, K3, No	53Kx, 1.46 Å	6.0	1.0	210	-51° to +51°; 3°	0.6/1.0	77	26	75	0	S257
250	0% load	46319	Krios G2, K3, No	53Kx, 1.46 Å	6.0	1.0	210	-51° to +51°; 3°	0.6/1.0	83	28	79	0	S258
251	0% load	46320	Krios G2, K3, No	53Kx, 1.46 Å	6.0	1.0	210	-51° to +51°; 3°	0.6/1.0	81	28	74	0	S259
252	0% load	46321	Krios G2, K3, No	53Kx, 1.46 Å	6.0	1.0	210	-51° to +51°; 3°	0.6/1.0	83	27	75	0	S260
253	0% load	46322	Krios G2, K3, No	53Kx, 1.46 Å	6.0	1.0	210	-51° to +51°; 3°	0.6/1.0	77	27	78	0	S261
254	0% load	46323	Krios G2, K3, No	53Kx, 1.46 Å	6.0	1.0	210	-51° to +51°; 3°	0.6/1.0	77	28	79	0	S262
255	0% load	46324	Krios G2, K3, No	53Kx, 1.46 Å	6.0	1.0	210	-51° to +51°; 3°	0.6/1.0	93	63	84	0	S263
256	0% load	46325	Krios G2, K3, No	53Kx, 1.46 Å	6.0	1.0	210	-51° to +51°; 3°	0.6/1.0	77	29	82	0	S264
257	0% load	46326	Krios G2, K3, No	53Kx, 1.46 Å	6.0	1.0	210	-51° to +51°; 3°	0.6/1.0	77	30	76	0	S265
258	0% load	46327	Krios G2, K3, No	53Kx, 1.46 Å	6.0	1.0	210	-51° to +51°; 3°	0.6/1.0	73	26	74	0	S266
259	0% load	46328	Krios G2, K3, No	53Kx, 1.46 Å	6.0	1.0	210	-51° to +51°; 3°	0.6/1.0	72	27	77	0	S267
260	0% load	46329	Krios G2, K3, No	53Kx, 1.46 Å	6.0	1.0	210	-51° to +51°; 3°	0.6/1.0	76	27	79	0	S268
261	0% load	46330	Krios G2, K3, No	53Kx, 1.46 Å	6.0	1.0	210	-51° to +51°; 3°	0.6/1.0	75	27	78	0	S269
262	0% load	46331	Krios G2, K3, No	53Kx, 1.46 Å	6.0	1.0	210	-51° to +51°; 3°	0.6/1.0	73	27	78	0	S270
263	0% load	46332	Krios G2, K3, No	53Kx, 1.46 Å	6.0	1.0	210	-51° to +51°; 3°	0.6/1.0	72	27	78	0	S271
264	0% load	46333	Krios G2, K3, No	53Kx, 1.46 Å	6.0	1.0	210	-51° to +51°; 3°	0.6/1.0	85	29	76	0	S272
265	0% load	46334	Krios G2, K3, No	53Kx, 1.46 Å	6.0	1.0	210	-51° to +51°; 3°	0.6/1.0	71	27	78	0	S273
266	0% load	46335	Krios G2, K3, No	53Kx, 1.46 Å	6.0	1.0	210	-51° to +51°; 3°	0.6/1.0	75	27	77	0	S274
267	0% load	46336	Krios G2, K3, No	53Kx, 1.46 Å	6.0	1.0	210	-51° to +51°; 3°	0.6/1.0	78	27	79	0	S275
268	0% load	46337	Krios G2, K3, No	53Kx, 1.46 Å	6.0	1.0	210	-51° to +51°; 3°	0.6/1.0	77	27	77	0	S276
269	0% load	46338	Krios G2, K3, No	53Kx, 1.46 Å	6.0	1.0	210	-51° to +51°; 3°	0.6/1.0	73	28	80	0	S277
270	0% load	46339	Krios G2, K3, No	53Kx, 1.46 Å	6.0	1.0	210	-51° to +51°; 3°	0.6/1.0	72	26	78	0	S278
271	0% load	46340	Krios G2, K3, No	53Kx, 1.46 Å	6.0	1.0	210	-51° to +51°; 3°	0.6/1.0	70	28	74	0	S279
272	0% load	46341	Krios G2, K3, No	53Kx, 1.46 Å	6.0	1.0	210	-51° to +51°; 3°	0.6/1.0	80	29	80	0	S280
273	0% load	46342	Krios G2, K3, No	53Kx, 1.46 Å	6.0	1.0	210	-51° to +51°; 3°	0.6/1.0	77	26	74	0	S281
274	0% load	46343	Krios G2, K3, No	53Kx, 1.46 Å	6.0	1.0	210	-51° to +51°; 3°	0.6/1.0	78	26	76	0	S282
275	0% load	46344	Krios G2, K3, No	53Kx, 1.46 Å	6.0	1.0	210	-51° to +51°; 3°	0.6/1.0	77	27	76	0	S283
276	0% load	46345	Krios G2, K3, No	53Kx, 1.46 Å	6.0	1.0	210	-51° to +51°; 3°	0.6/1.0	74	29	73	0	S284
277	0% load	46346	Krios G2, K3, No	53Kx, 1.46 Å	6.0	1.0	210	-51° to +51°; 3°	0.6/1.0	70	27	74	0	S285
278	0% load	46347	Krios G2, K3, No	53Kx, 1.46 Å	6.0	1.0	210	-51° to +51°; 3°	0.6/1.0	71	28	77	0	S286
279	0% load	46348	Krios G2, K3, No	53Kx, 1.46 Å	6.0	1.0	210	-51° to +51°; 3°	0.6/1.0	79	27	79	0	S287
280	0% load	46349	Krios G2, K3, No	53Kx, 1.46 Å	6.0	1.0	210	-51° to +51°; 3°	0.6/1.0	78	29	82	0	S288
281	0% load	46350	Krios G2, K3, No	53Kx, 1.46 Å	6.0	1.0	210	-51° to +51°; 3°	0.6/1.0	72	27	82	0	S289
282	0% load	46351	Krios G2, K3, No	53Kx, 1.46 Å	6.0	1.0	210	-51° to +51°; 3°	0.6/1.0	63	27	77	0	S290
283	0% load	46352	Krios G2, K3, No	53Kx, 1.46 Å	6.0	1.0	210	-51° to +51°; 3°	0.6/1.0	66	27	73	0	S291
284	0% load	46353	Krios G2, K3, No	53Kx, 1.46 Å	6.0	1.0	210	-51° to +51°; 3°	0.6/1.0	77	29	73	0	S292
285	0% load	46354	Krios G2, K3, No	53Kx, 1.46 Å	6.0	1.0	210	-51° to +51°; 3°	0.6/1.0	84	25	78	0	S293
286	0% load	46355	Krios G2, K3, No	53Kx, 1.46 Å	6.0	1.0	210	-51° to +51°; 3°	0.6/1.0	86	29	83	0	S294
287	0% load	46356	Krios G2, K3, No	53Kx, 1.46 Å	6.0	1.0	210	-51° to +51°; 3°	0.6/1.0	72	28	75	0	S295
288	0% load	46357	Krios G2, K3, No	53Kx, 1.46 Å	6.0	1.0	210	-51° to +51°; 3°	0.6/1.0	79	28	76	0	S296
289	0% load	46358	Krios G2, K3, No	53Kx, 1.46 Å	6.0	1.0	210	-51° to +51°; 3°	0.6/1.0	80	27	79	0	S297
290	0% load	46359	Krios G2, K3, No	53Kx, 1.46 Å	6.0	1.0	210	-51° to +51°; 3°	0.6/1.0	84	26	79	0	S298
291	0% load	46360	Krios G2, K3, No	53Kx, 1.46 Å	6.0	1.0	210	-51° to +51°; 3°	0.6/1.0	79	27	76	0	S299
292	0% load	46361	Krios G2, K3, No	53Kx, 1.46 Å	6.0	1.0	210	-51° to +51°; 3°	0.6/1.0	69	27	74	0	S300
293	0% load	46362	Krios G2, K3, No	53Kx, 1.46 Å	6.0	1.0	210	-51° to +51°; 3°	0.6/1.0	80	28	83	0	S301
294	0% load	46363	Krios G2, K3, No	53Kx, 1.46 Å	6.0	1.0	210	-51° to +51°; 3°	0.6/1.0	76	29	80	0	S302
295	0% load	46364	Krios G2, K3, No	53Kx, 1.46 Å	6.0	1.0	210	-51° to +51°; 3°	0.6/1.0	89	76	87	0	S303

296	0% load	46365	Krios G2, K3, No	53Kx, 1.46 Å	6.0	1.0	210	-51° to +51°; 3°	0.6/1.0	69	33	83	0	S304
297	0% load	46366	Krios G2, K3, No	53Kx, 1.46 Å	6.0	1.0	210	-51° to +51°; 3°	0.6/1.0	78	29	76	0	S305
298	0% load	46367	Krios G2, K3, No	53Kx, 1.46 Å	6.0	1.0	210	-51° to +51°; 3°	0.6/1.0	72	26	79	0	S306
299	0% load	46368	Krios G2, K3, No	53Kx, 1.46 Å	6.0	1.0	210	-51° to +51°; 3°	0.6/1.0	61	27	75	0	S307
300	0% load	46369	Krios G2, K3, No	53Kx, 1.46 Å	6.0	1.0	210	-51° to +51°; 3°	0.6/1.0	73	28	80	0	S308
301	0% load	46370	Krios G2, K3, No	53Kx, 1.46 Å	6.0	1.0	210	-51° to +51°; 3°	0.6/1.0	71	26	74	0	S309
302	0% load	46371	Krios G2, K3, No	53Kx, 1.46 Å	6.0	1.0	210	-51° to +51°; 3°	0.6/1.0	81	28	76	0	S310
303	0% load	46372	Krios G2, K3, No	53Kx, 1.46 Å	6.0	1.0	210	-51° to +51°; 3°	0.6/1.0	71	29	79	0	S311
304	0% load	46373	Krios G2, K3, No	53Kx, 1.46 Å	6.0	1.0	210	-51° to +51°; 3°	0.6/1.0	86	34	82	0	S312
305	0% load	46374	Krios G2, K3, No	53Kx, 1.46 Å	6.0	1.0	210	-51° to +51°; 3°	0.6/1.0	75	26	75	0	S313
306	0% load	46375	Krios G2, K3, No	53Kx, 1.46 Å	6.0	1.0	210	-51° to +51°; 3°	0.6/1.0	71	28	74	0	S314
307	0% load	46376	Krios G2, K3, No	53Kx, 1.46 Å	6.0	1.0	210	-51° to +51°; 3°	0.6/1.0	78	26	74	0	S315
308	0% load	46377	Krios G2, K3, No	53Kx, 1.46 Å	6.0	1.0	210	-51° to +51°; 3°	0.6/1.0	78	29	78	0	S316
309	0% load	46378	Krios G2, K3, No	53Kx, 1.46 Å	6.0	1.0	210	-51° to +51°; 3°	0.6/1.0	73	27	73	0	S317
310	0% load	46379	Krios G2, K3, No	53Kx, 1.46 Å	6.0	1.0	210	-51° to +51°; 3°	0.6/1.0	69	30	81	0	S318
311	0% load	46380	Krios G2, K3, No	53Kx, 1.46 Å	6.0	1.0	210	-51° to +51°; 3°	0.6/1.0	72	27	74	0	S319
312	0% load	46381	Krios G2, K3, No	53Kx, 1.46 Å	6.0	1.0	210	-51° to +51°; 3°	0.6/1.0	91	28	77	0	S320
313	0% load	46382	Krios G2, K3, No	53Kx, 1.46 Å	6.0	1.0	210	-51° to +51°; 3°	0.6/1.0	77	26	74	0	S321
314	0% load	46383	Krios G2, K3, No	53Kx, 1.46 Å	6.0	1.0	210	-51° to +51°; 3°	0.6/1.0	73	63	77	0	S322
315	0% load	46384	Krios G2, K3, No	53Kx, 1.46 Å	6.0	1.0	210	-51° to +51°; 3°	0.6/1.0	74	27	77	0	S323
316	0% load	46385	Krios G2, K3, No	53Kx, 1.46 Å	6.0	1.0	210	-51° to +51°; 3°	0.6/1.0	76	30	74	0	S324
317	0% load	46386	Krios G2, K3, No	53Kx, 1.46 Å	6.0	1.0	210	-51° to +51°; 3°	0.6/1.0	73	26	77	0	S325
318	0% load	46387	Krios G2, K3, No	53Kx, 1.46 Å	6.0	1.0	210	-51° to +51°; 3°	0.6/1.0	71	29	78	0	S326
319	0% load	46388	Krios G2, K3, No	53Kx, 1.46 Å	6.0	1.0	210	-51° to +51°; 3°	0.6/1.0	109	73	76	0	S327
320	0% load	46389	Krios G2, K3, No	53Kx, 1.46 Å	6.0	1.0	210	-51° to +51°; 3°	0.6/1.0	69	28	73	0	S328
321	0% load	46390	Krios G2, K3, No	53Kx, 1.46 Å	6.0	1.0	210	-51° to +51°; 3°	0.6/1.0	79	27	78	0	S329
322	0% load	46391	Krios G2, K3, No	53Kx, 1.46 Å	6.0	1.0	210	-51° to +51°; 3°	0.6/1.0	78	28	80	0	S330
323	0% load	46392	Krios G2, K3, No	53Kx, 1.46 Å	6.0	1.0	210	-51° to +51°; 3°	0.6/1.0	77	28	72	0	S331
324	0% load	46393	Krios G2, K3, No	53Kx, 1.46 Å	6.0	1.0	210	-51° to +51°; 3°	0.6/1.0	81	26	78	0	S332
325	0% load	46394	Krios G2, K3, No	53Kx, 1.46 Å	6.0	1.0	210	-51° to +51°; 3°	0.6/1.0	83	69	76	0	S333
326	0% load	46395	Krios G2, K3, No	53Kx, 1.46 Å	6.0	1.0	210	-51° to +51°; 3°	0.6/1.0	95	30	83	0	S334
327	0% load	46396	Krios G2, K3, No	53Kx, 1.46 Å	6.0	1.0	210	-51° to +51°; 3°	0.6/1.0	70	28	74	0	S335
328	0% load	46397	Krios G2, K3, No	53Kx, 1.46 Å	6.0	1.0	210	-51° to +51°; 3°	0.6/1.0	76	27	75	0	S336
329	0% load	46398	Krios G2, K3, No	53Kx, 1.46 Å	6.0	1.0	210	-51° to +51°; 3°	0.6/1.0	78	27	79	0	S337
330	0% load	46399	Krios G2, K3, No	53Kx, 1.46 Å	6.0	1.0	210	-51° to +51°; 3°	0.6/1.0	73	27	76	0	S338
331	0% load	46400	Krios G2, K3, No	53Kx, 1.46 Å	6.0	1.0	210	-51° to +51°; 3°	0.6/1.0	77	27	74	0	S339
332	0% load	46401	Krios G2, K3, No	53Kx, 1.46 Å	6.0	1.0	210	-51° to +51°; 3°	0.6/1.0	77	29	75	0	S340
333	0% load	46402	Krios G2, K3, No	53Kx, 1.46 Å	6.0	1.0	210	-51° to +51°; 3°	0.6/1.0	72	27	79	0	S341
334	0% load	46403	Krios G2, K3, No	53Kx, 1.46 Å	6.0	1.0	210	-51° to +51°; 3°	0.6/1.0	73	28	74	0	S342
335	0% load	46404	Krios G2, K3, No	53Kx, 1.46 Å	6.0	1.0	210	-51° to +51°; 3°	0.6/1.0	72	27	71	0	S343
336	0% load	46405	Krios G2, K3, No	53Kx, 1.46 Å	6.0	1.0	210	-51° to +51°; 3°	0.6/1.0	98	28	73	0	S344
337	0% load	46406	Krios G2, K3, No	53Kx, 1.46 Å	6.0	1.0	210	-51° to +51°; 3°	0.6/1.0	68	26	77	0	S345
Part. ID	**Sample**	**EMDB ID**	**TEM, camera, CDS mode**	**Mag. and Apix (Å)**	**Dose rate ($e^{-}Å^{-2}s^{-1}$)**	**Exp. time (s)**	**Total dose ($e^{-}Å^{-2}$)**	**Angle range; step**	**Contour levels**	**Map-map FSC @0.5**	**Map-map FSC @0.143**	**Map-model FSC @0.5**	**Ferritin #**	**Figure #**

EMDB stands for Electron Microscopy Data Bank, https://www.ebi.ac.uk/pdbe/emdb/. Krios G2 refers to the FEI Titan Krios TEM. Zeiss 120 refers to the Zeiss Libra 120 Plus TEM. K3 refers to the Gatan K3 Direct Detector. CCD refers to the Gatan UltraScan 4000 4Kx4K charged-coupled device. CDS stands for correlated-double sampling mode.

Supplementary Figures:

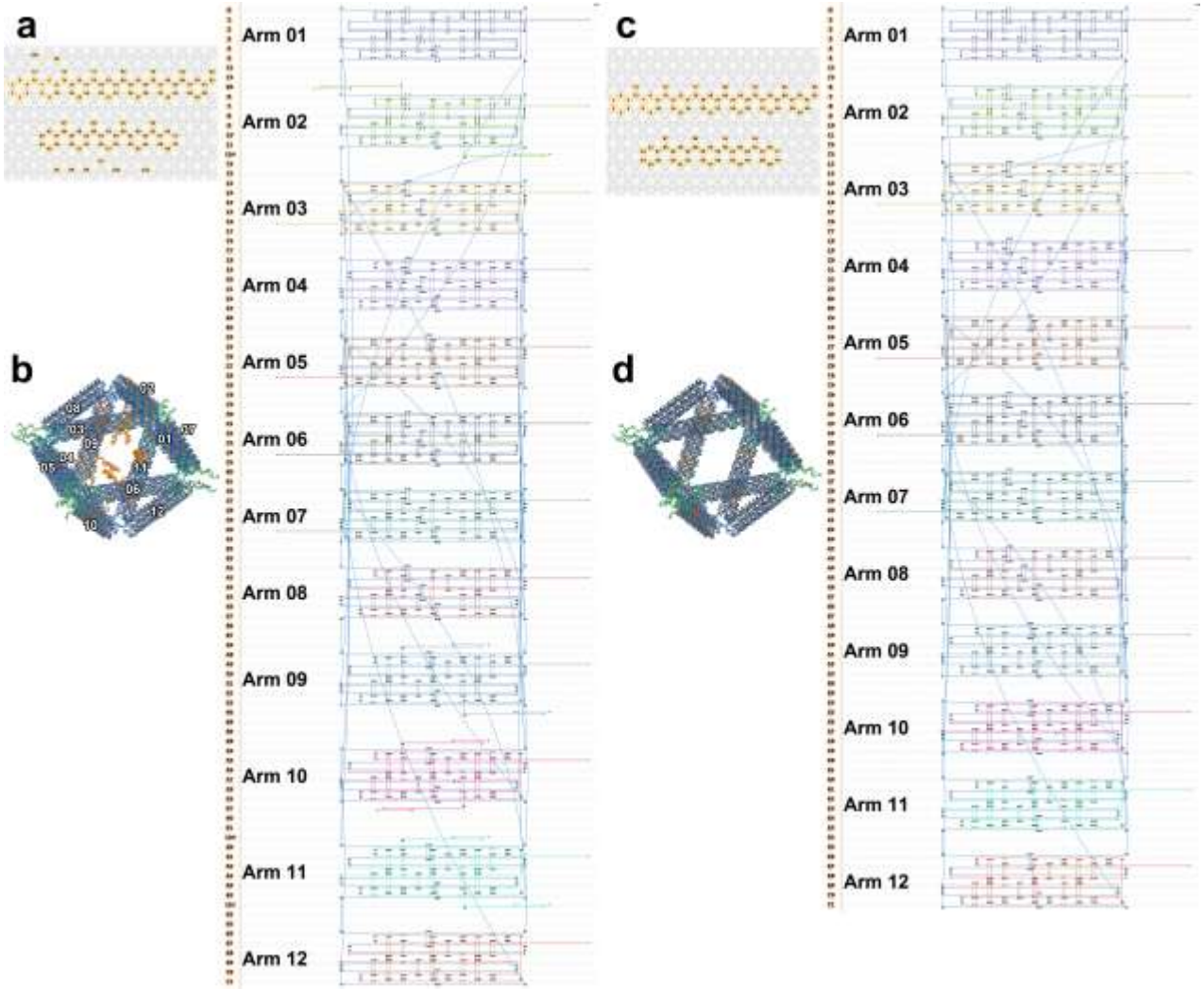

Supplementary Fig. 1: Secondary structure of DNA origami octahedral cage with and without a linker for ferritin. **a,** Secondary structure of the DNA origami octahedral cage with ferritin linkers. **b,** Secondary structure of the DNA origami octahedral cage without ferritin linkers.

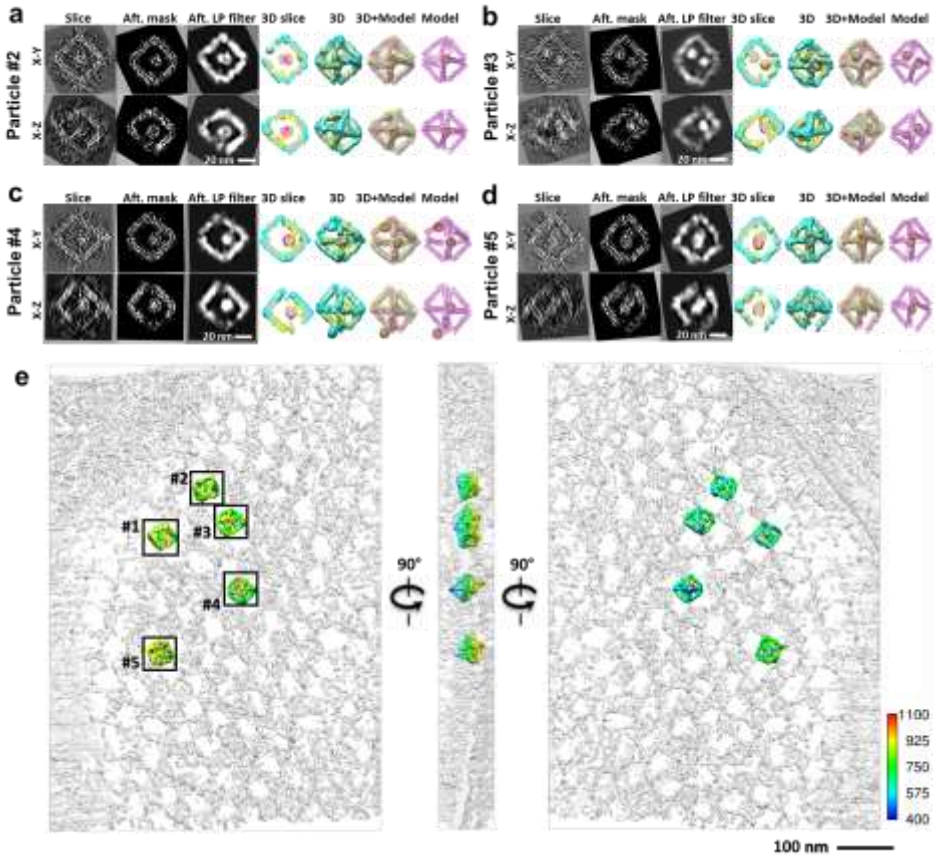

Supplementary Fig. 2: Examples of IPET 3D reconstruction intermediate for four representative unit-cell particle in a 2D lattice with 100% ferritin loading. **a**, Perpendicular cross-sections of an IPET 3D reconstruction for the unit-cell particle #38. The first four images (left) show the reconstruction stages: before and after applying a soft-boundary mask, following low-pass filtering, and the 3D view of the cross-section in the final reconstruction. These are compared with the next three columns (right), which display the 3D map, the superimposed fitting model, and the final fitted model. **b-d**, Examples of IPET 3D reconstructions for three additional particles (#46, #65, and #101), analyzed using the same methodology as in a. **e**, Three views of the low-resolution 3D map of the entire 2D lattice reconstructed by IMOD, with five IPET 3D density maps from five individual unit-cell particles superimposed. The color scheme represents depth, enhancing visualization of structural features.

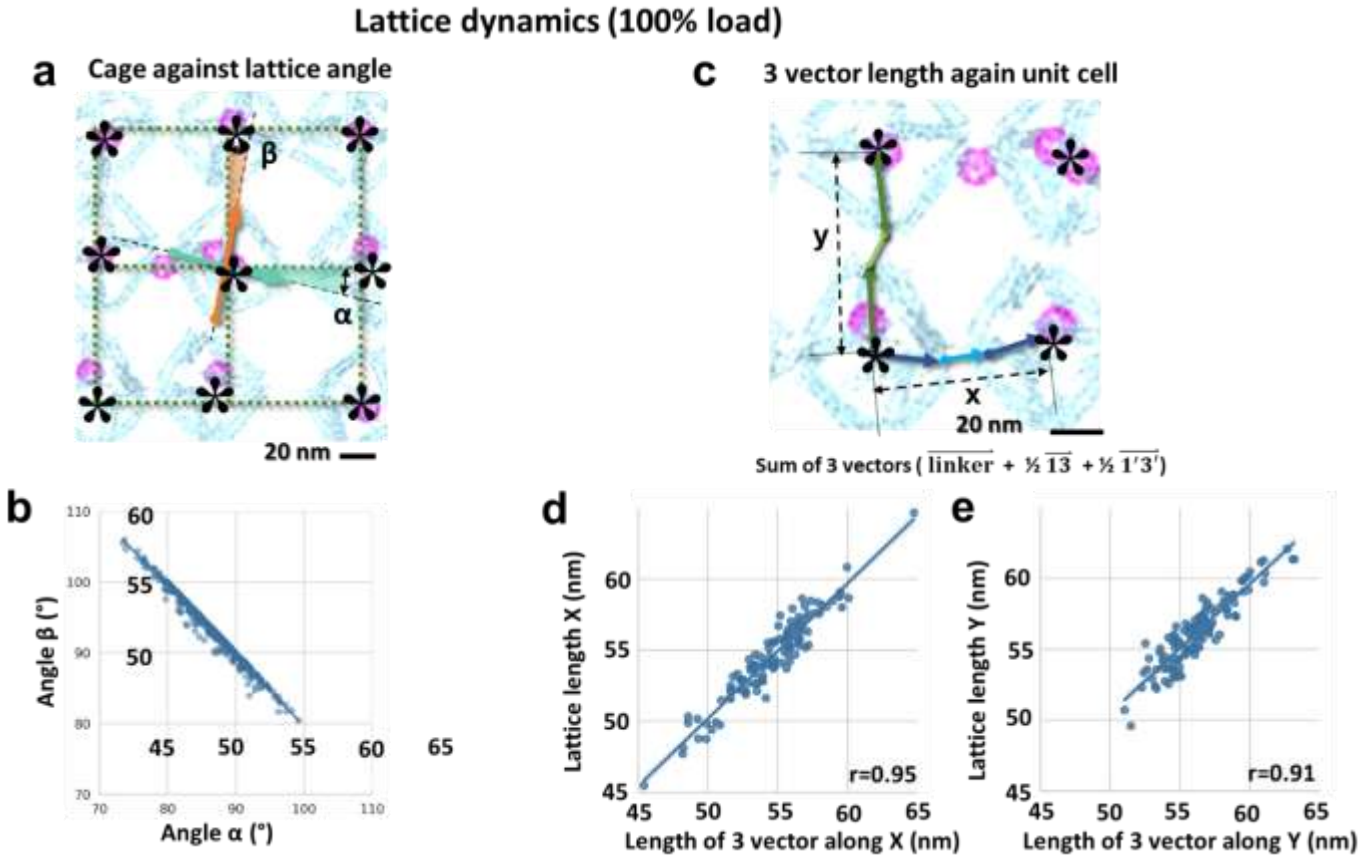

Supplementary Fig. 3: Statistical analysis of structural variability in unit-cell particles relative to their formed lattice (100% ferritin loading). a, Schematic representation of the measurement of the unit-cell angle relative to the lattice. This angle is defined as the direction from vertex to vertex along the diagonal within the unit-cell in-plane quadrilateral formed by the 4 HBs, compared to the lattice-averaged direction along the X and Y axes, respectively. **b,** Correlation analysis the angles along X-axis versus the Y-axis. **c**, Schematic illustration of the measurement of the center-to-center distances between two adjunct unit-cell particles, as well as the combined distances of the vectors. These vectors are composed of two halves of the adjacent unit-cell particle sizes plus their linker, measured along the X and Y axes, respectively. **d,e**, Correlation analyses of the center-to-center distances and the combined distances of the three vectors along the X-axis and Y-axis, respectively.

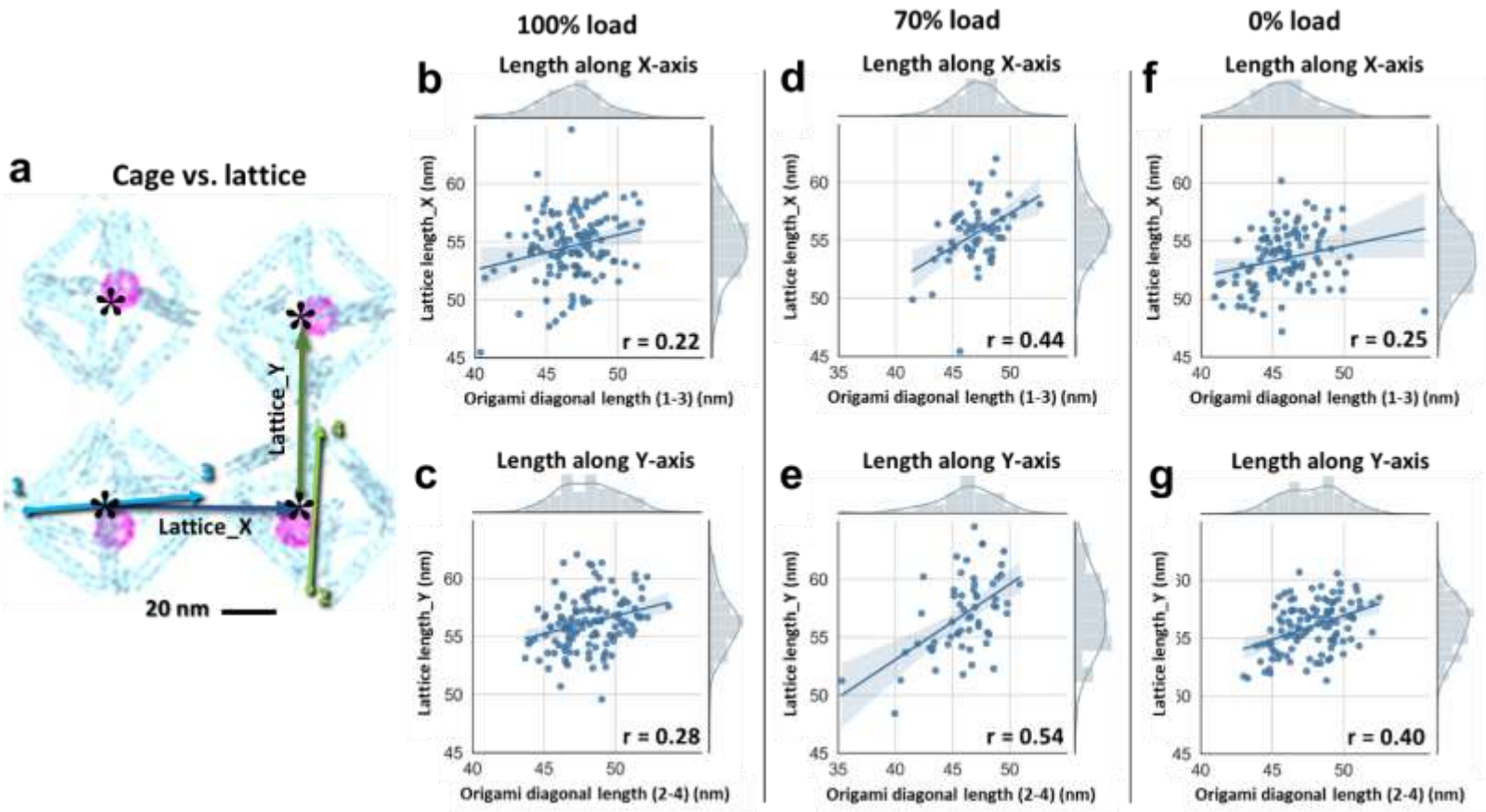

Supplementary Fig. 4: Correlation analysis between unit-cell particle size and lattice lengths. a, Schematic illustration of unit-cell particle size and lattice length measurements. The particle size is determined by the vertex-to-vertex distances along two diagonal directions within the in-plane quadrilateral formed by the 4 HBs of a unit-cell particle. The lattice length is measured as the distance between the centers of two adjacent unit-cell particles. **b,c**, Histograms of particle sizes and lattice lengths within a lattice with 100% ferritin loading, along with correlation analyses between particle sizes and lattice lengths along the X- and Y-axes, respectively. **d, e,** Equivalent analyses performed on a lattice with 70% ferritin loading. **f, g,** Equivalent analyses performed on a lattice with 0% ferritin loading.

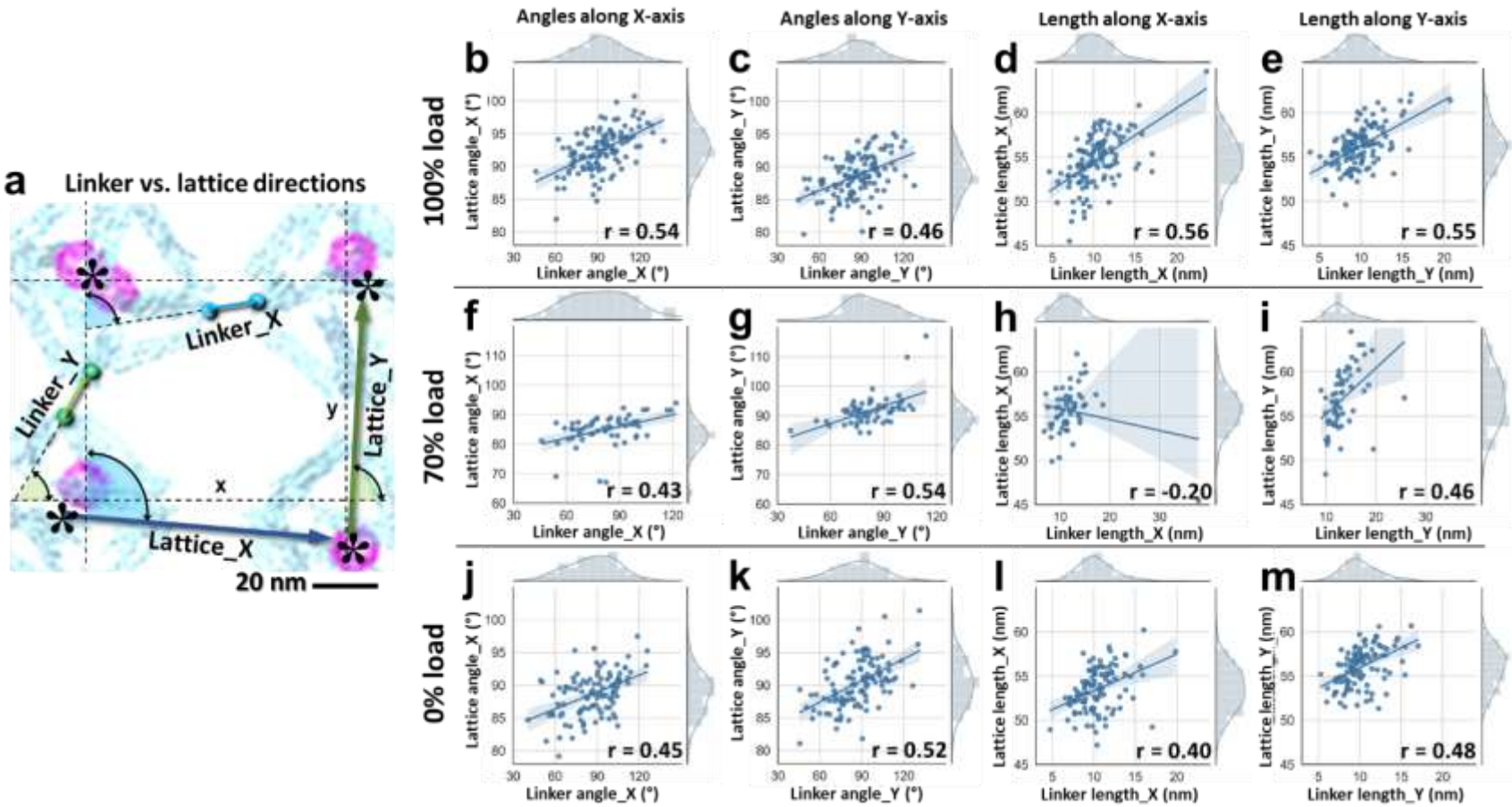

Supplementary Fig. 5: Correlation analysis between linker angle and length versus lattice angles and lengths. a, Schematic illustration of the measurements. The linker angle and length are determined between the closest vertices of two adjacent unit-cell particles relative to the averaged lattice direction. The lattice angle and length are measured between the centers of two adjacent unit-cell particles. **b,c**, Histograms of linker angles and lattice angles along the X- and Y-axes within the 100% ferritin-loaded 2D lattice, along with correlation analyses between these angles along the X- and Y-axes, respectively. **d,e**, Histograms of linker lengths and lattice lengths along the X- and Y-axes within the 100% ferritin-loaded 2D lattice, along with correlation analyses between these lengths along the X- and Y-axes, respectively. **f-i,** Equivalent analyses performed on a lattice with 70% ferritin loading. **j-m,** Equivalent analyses performed on a lattice with 0% ferritin loading.

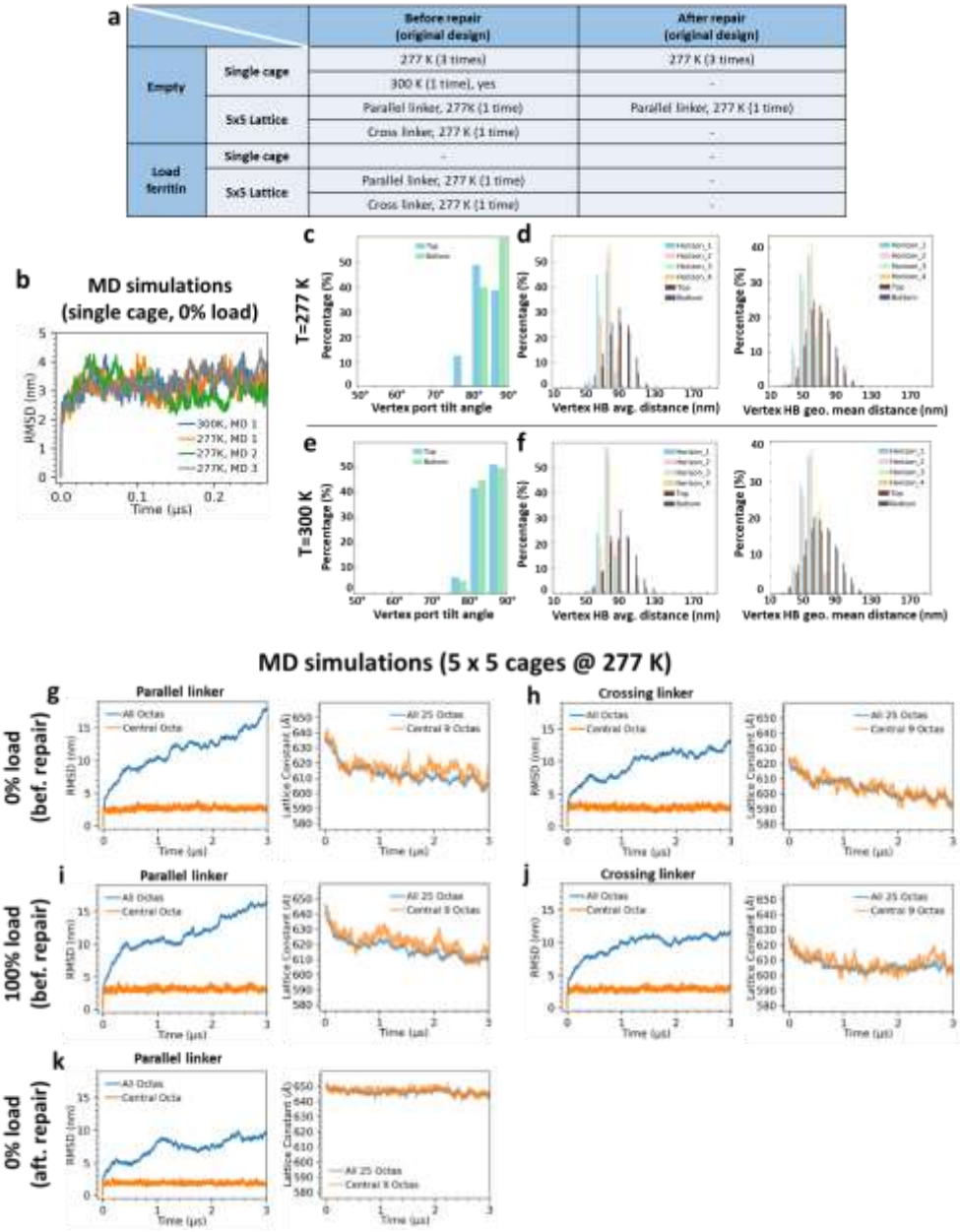

Supplementary Fig. 6: MD simulation of DNA origami unit-cell particles and their 2D lattices. a, Overview of MD simulation performance under various conditions. **b**, RMSD of a single unit-cell (a cage) over 0.25 μs at different temperatures. **c**, Distribution of the top and bottom vertex angles relative to the lattice plane under a temperature of 277 K. **d**, Distribution of pore sizes analyzed using two averaging methods. e,f, A similar MD simulation under a temperature of 300 K. **g**, MD simulation of a 5×5 2D lattice of unit-cell particles without repair or ferritin loading, using parallel linkers for a 3 μs simulation. Both RMSD and lattice lengths are analyzed. **h**, MD simulation of the above 5x5 2D lattice under crossing linker conditions. **i,j**, MD simulations of the above 2D lattice with 100% ferritin loading. **k**, MD simulation of the repaired 2D lattice under the parallel linker condition.

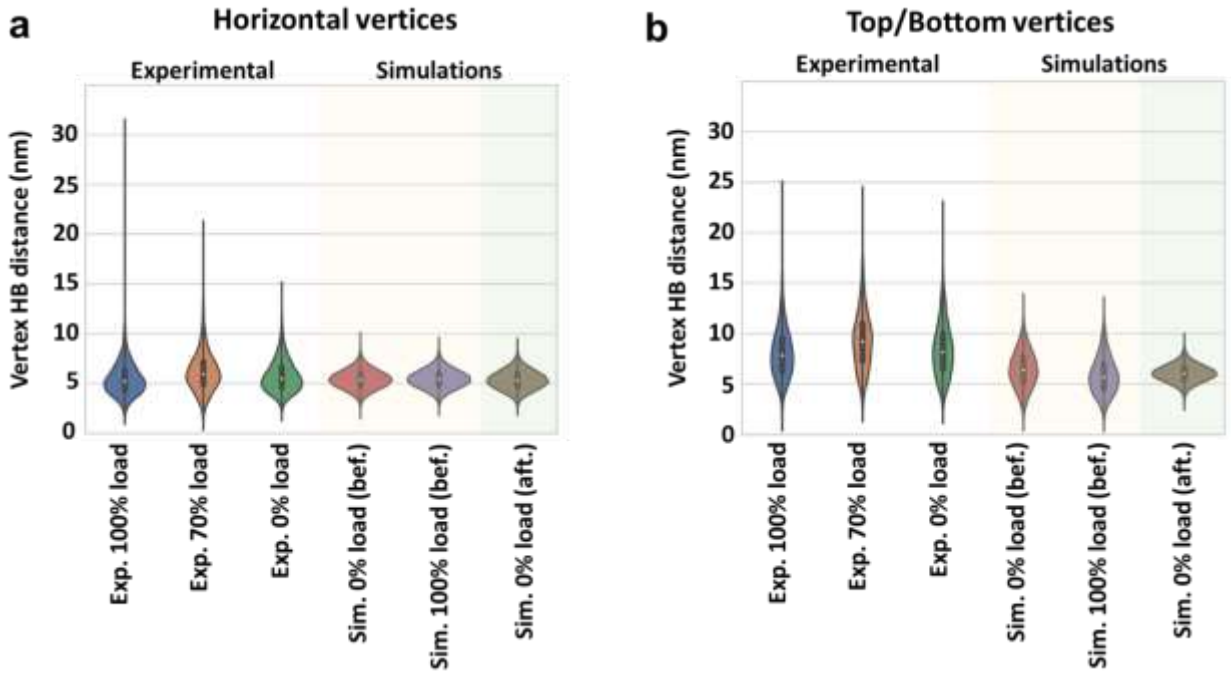

Supplementary Fig. 7: Analysis of pore size variability under different experimental and MD simulations conditions. a, Comparison of pore size distributions, measured as the average distances among the four distal ends of helical bundles at each vertex, along the lattice plane. **b**, Comparison of pore size distributions above and below the lattice plane.

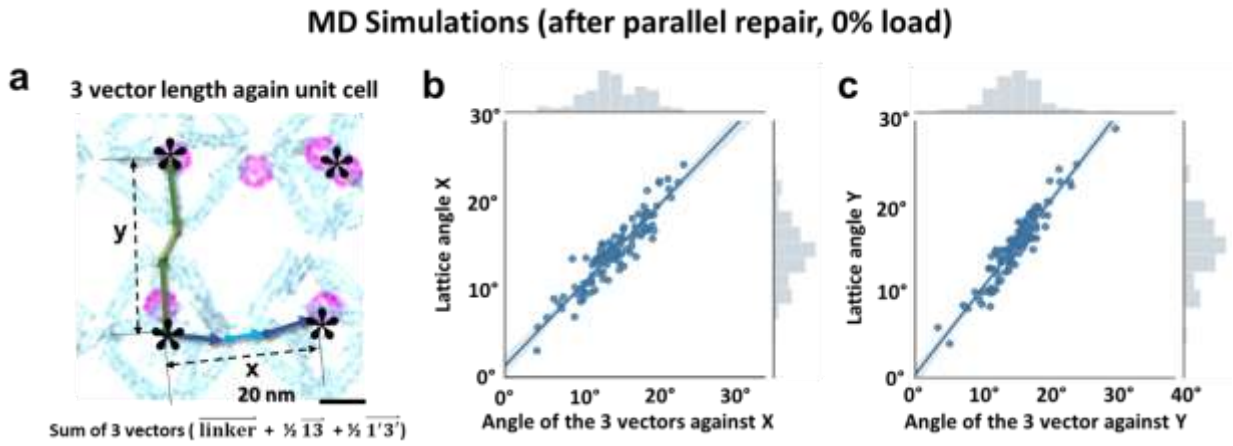

Supplementary Fig. 8: Analysis of structural variability in repaired unit-cell particles relative to their simulated lattice formation. a, A schematic representation of the measurement process for center-to-center distances between adjacent unit-cell particles, as well as the combined distances of their associated vectors. These vectors consist of the sum of two halves of the adjacent unit-cell particle sizes and their linker, measured along the X and Y axes, respectively. **b,c**, Correlation analyses of the center-to-center distances and combined vector distances along the X-axis and Y-axis, respectively.

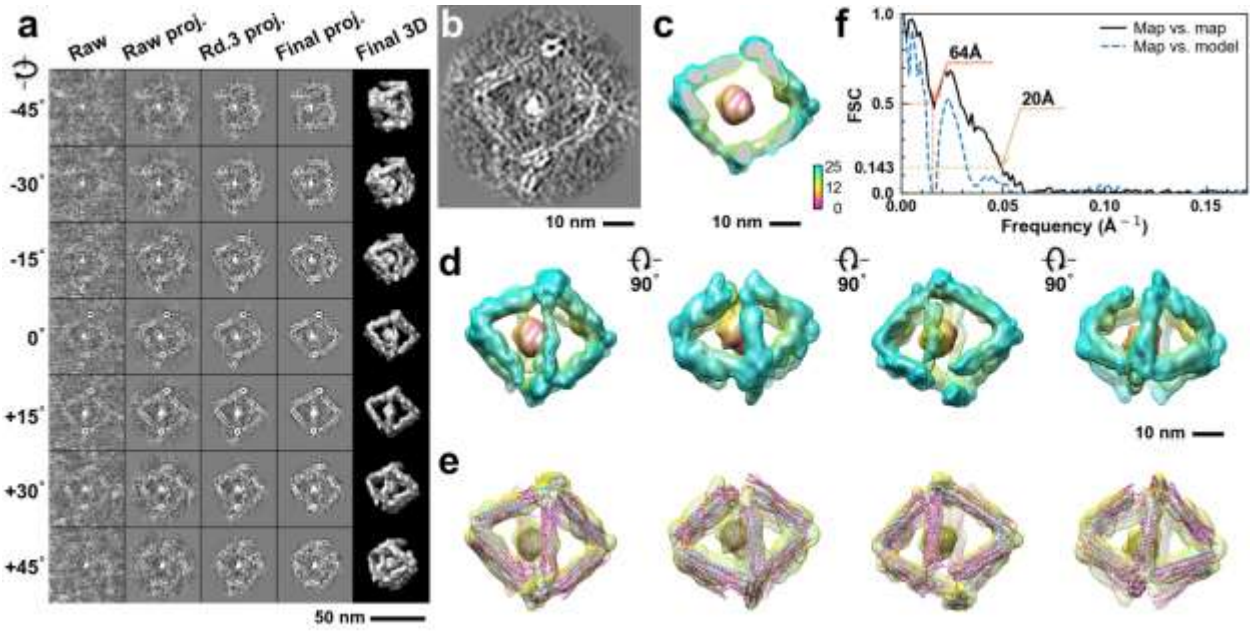

Supplementary Fig. 9: IPET 3D reconstruction and model fitting of an individual unit-cell particle (Index: 001) within a 2D lattice with 100% ferritin loading. a, Seven representative tilt images of a single unit-cell particle are shown in the first column (from left). The tilt images are aligned to a common center using IPET through iterative refinement. The projections of the raw, intermediate, and final 3D reconstruction at the corresponding angles are displayed in the subsequent four columns. **b**, A central cross-section (~23 nm thick) of the final reconstruction before masking is applied. **c**, 3D views of the central cross-section. **d**, Final 3D density map of this particle, viewed from four perpendicular directions. **e**, Final 3D reconstruction superimposed with the fitted model, viewed from four perpendicular directions. **f**, FSC analyses of the final map resolution using two methods: map-map FSC, where each map is reconstructed from one half of the images (even vs. odd tilt angle indices), and map-model FSC, where the model map is generated from the fitted model. Resolution assessments are provided based on tilt-based map-map and map-model FSC analyses at thresholds of FSC=0.5 and 0.143, respectively.

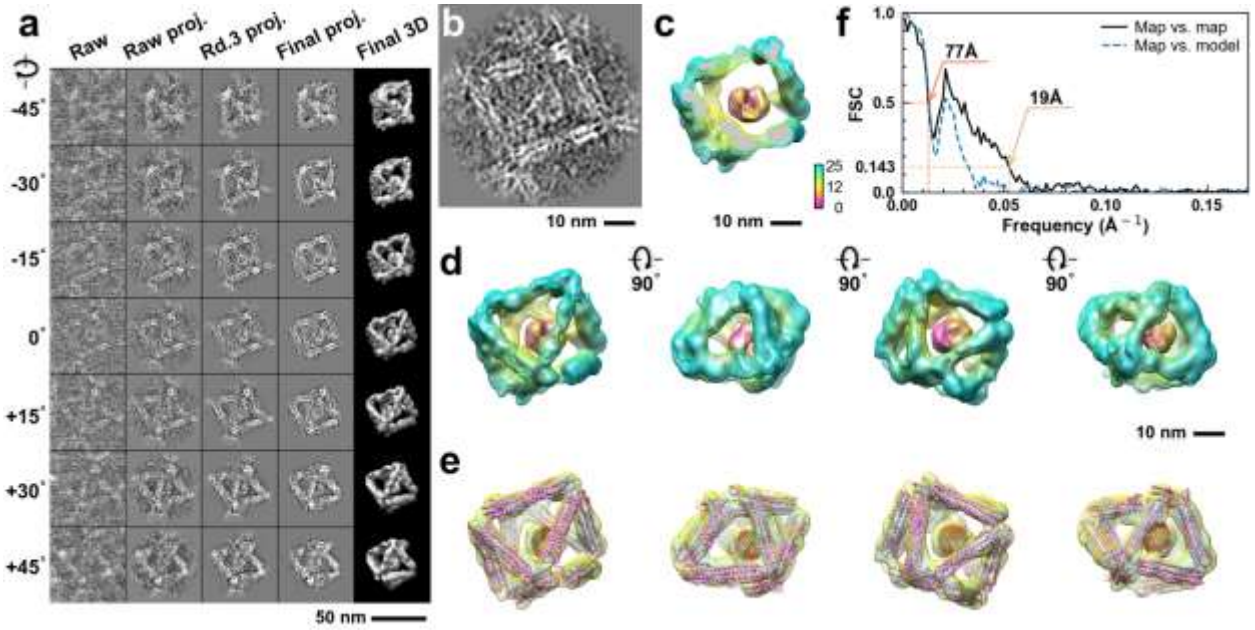

Supplementary Fig. 10: IPET 3D reconstruction and model fitting of an individual unit-cell particle (Index: 002) within a 2D lattice with 100% ferritin loading. a, Seven representative tilt images of a single unit-cell particle are shown in the first column (from left). The tilt images are aligned to a common center using IPET through iterative refinement. The projections of the raw, intermediate, and final 3D reconstruction at the corresponding angles are displayed in the subsequent four columns. **b**, A central cross-section (~23 nm thick) of the final reconstruction before masking is applied. **c**, 3D views of the central cross-section. **d**, Final 3D density map of this particle, viewed from four perpendicular directions. **e**, Final 3D reconstruction superimposed with the fitted model, viewed from four perpendicular directions. **f**, FSC analyses of the final map resolution using two methods: map-map FSC, where each map is reconstructed from one half of the images (even vs. odd tilt angle indices), and map-model FSC, where the model map is generated from the fitted model. Resolution assessments are provided based on tilt-based map-map and map-model FSC analyses at thresholds of FSC=0.5 and 0.143, respectively.

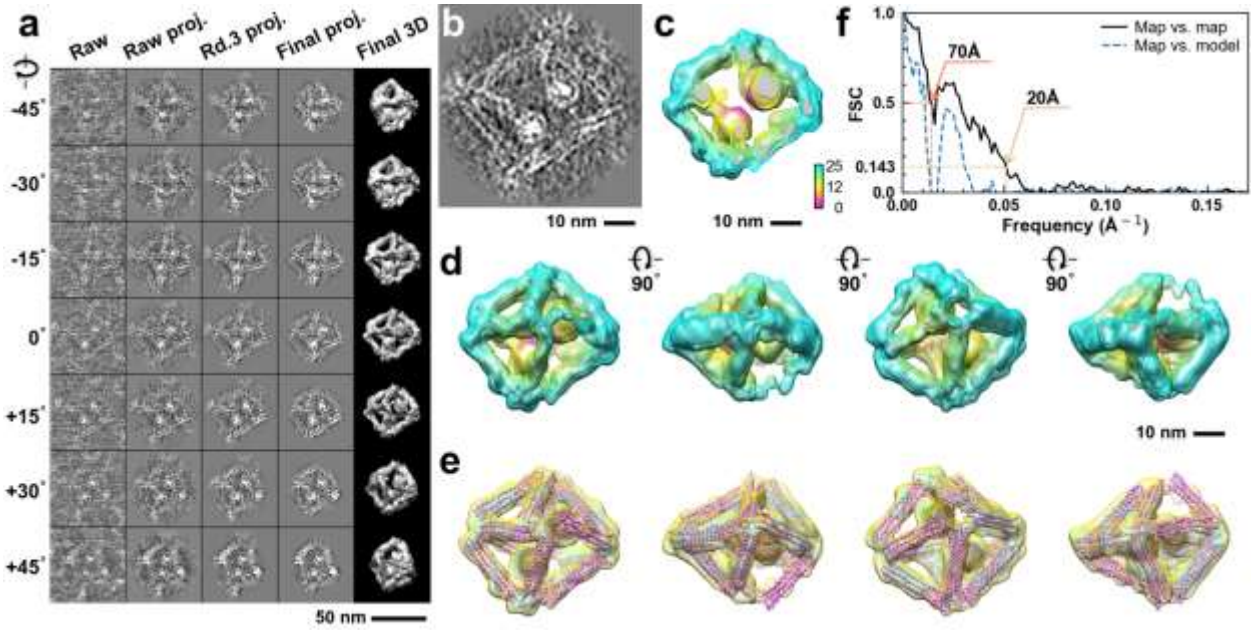

Supplementary Fig. 11: IPET 3D reconstruction and model fitting of an individual unit-cell particle (Index: 003) within a 2D lattice with 100% ferritin loading. a, Seven representative tilt images of a single unit-cell particle are shown in the first column (from left). The tilt images are aligned to a common center using IPET through iterative refinement. The projections of the raw, intermediate, and final 3D reconstruction at the corresponding angles are displayed in the subsequent four columns. **b**, A central cross-section (~23 nm thick) of the final reconstruction before masking is applied. **c**, 3D views of the central cross-section. **d**, Final 3D density map of this particle, viewed from four perpendicular directions. **e**, Final 3D reconstruction superimposed with the fitted model, viewed from four perpendicular directions. **f**, FSC analyses of the final map resolution using two methods: map-map FSC, where each map is reconstructed from one half of the images (even vs. odd tilt angle indices), and map-model FSC, where the model map is generated from the fitted model. Resolution assessments are provided based on tilt-based map-map and map-model FSC analyses at thresholds of FSC=0.5 and 0.143, respectively.

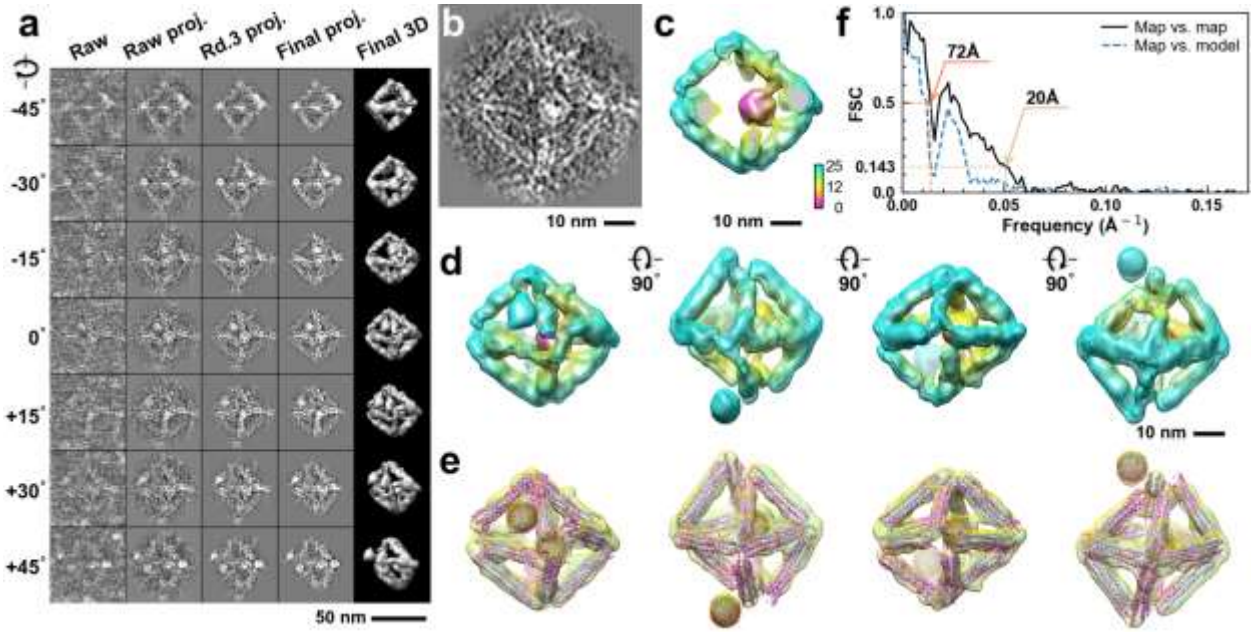

Supplementary Fig. 12: IPET 3D reconstruction and model fitting of an individual unit-cell particle (Index: 004) within a 2D lattice with 100% ferritin loading. a, Seven representative tilt images of a single unit-cell particle are shown in the first column (from left). The tilt images are aligned to a common center using IPET through iterative refinement. The projections of the raw, intermediate, and final 3D reconstruction at the corresponding angles are displayed in the subsequent four columns. **b**, A central cross-section (~23 nm thick) of the final reconstruction before masking is applied. **c**, 3D views of the central cross-section. **d**, Final 3D density map of this particle, viewed from four perpendicular directions. **e**, Final 3D reconstruction superimposed with the fitted model, viewed from four perpendicular directions. **f**, FSC analyses of the final map resolution using two methods: map-map FSC, where each map is reconstructed from one half of the images (even vs. odd tilt angle indices), and map-model FSC, where the model map is generated from the fitted model. Resolution assessments are provided based on tilt-based map-map and map-model FSC analyses at thresholds of FSC=0.5 and 0.143, respectively.

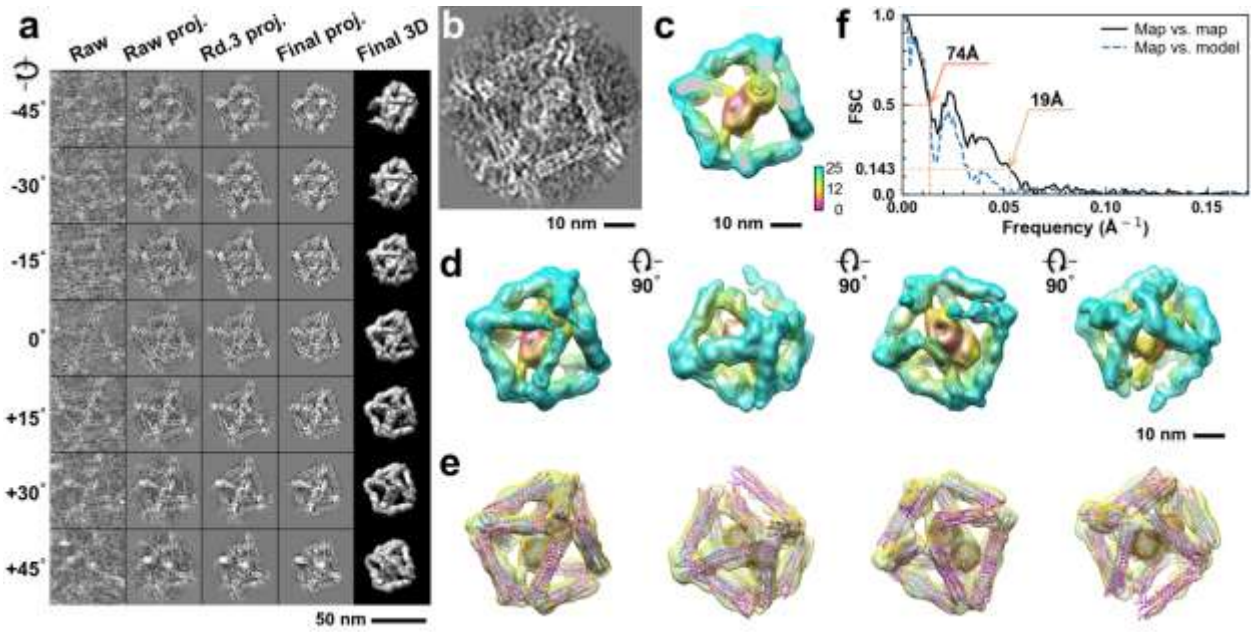

Supplementary Fig. 13: IPET 3D reconstruction and model fitting of an individual unit-cell particle (Index: 005) within a 2D lattice with 100% ferritin loading. a, Seven representative tilt images of a single unit-cell particle are shown in the first column (from left). The tilt images are aligned to a common center using IPET through iterative refinement. The projections of the raw, intermediate, and final 3D reconstruction at the corresponding angles are displayed in the subsequent four columns. **b**, A central cross-section (~23 nm thick) of the final reconstruction before masking is applied. **c**, 3D views of the central cross-section. **d**, Final 3D density map of this particle, viewed from four perpendicular directions. **e**, Final 3D reconstruction superimposed with the fitted model, viewed from four perpendicular directions. **f**, FSC analyses of the final map resolution using two methods: map-map FSC, where each map is reconstructed from one half of the images (even vs. odd tilt angle indices), and map-model FSC, where the model map is generated from the fitted model. Resolution assessments are provided based on tilt-based map-map and map-model FSC analyses at thresholds of FSC=0.5 and 0.143, respectively.

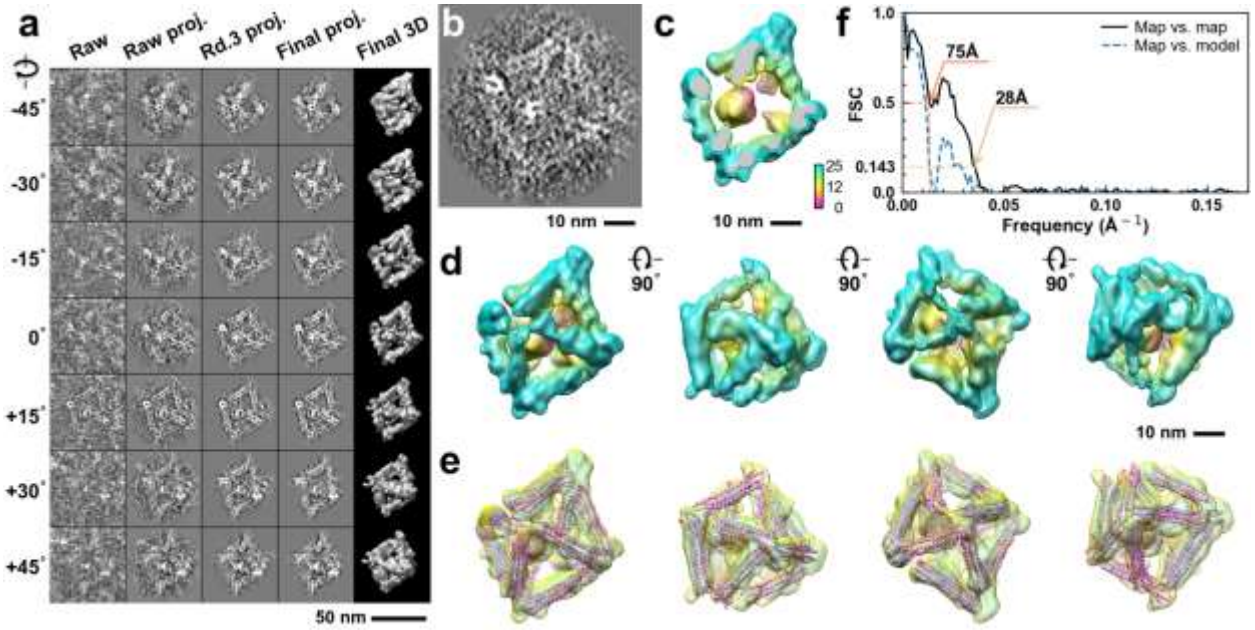

Supplementary Fig. 14: IPET 3D reconstruction and model fitting of an individual unit-cell particle (Index: 006) within a 2D lattice with 100% ferritin loading. a, Seven representative tilt images of a single unit-cell particle are shown in the first column (from left). The tilt images are aligned to a common center using IPET through iterative refinement. The projections of the raw, intermediate, and final 3D reconstruction at the corresponding angles are displayed in the subsequent four columns. **b**, A central cross-section (~23 nm thick) of the final reconstruction before masking is applied. **c**, 3D views of the central cross-section. **d**, Final 3D density map of this particle, viewed from four perpendicular directions. **e**, Final 3D reconstruction superimposed with the fitted model, viewed from four perpendicular directions. **f**, FSC analyses of the final map resolution using two methods: map-map FSC, where each map is reconstructed from one half of the images (even vs. odd tilt angle indices), and map-model FSC, where the model map is generated from the fitted model. Resolution assessments are provided based on tilt-based map-map and map-model FSC analyses at thresholds of FSC=0.5 and 0.143, respectively.

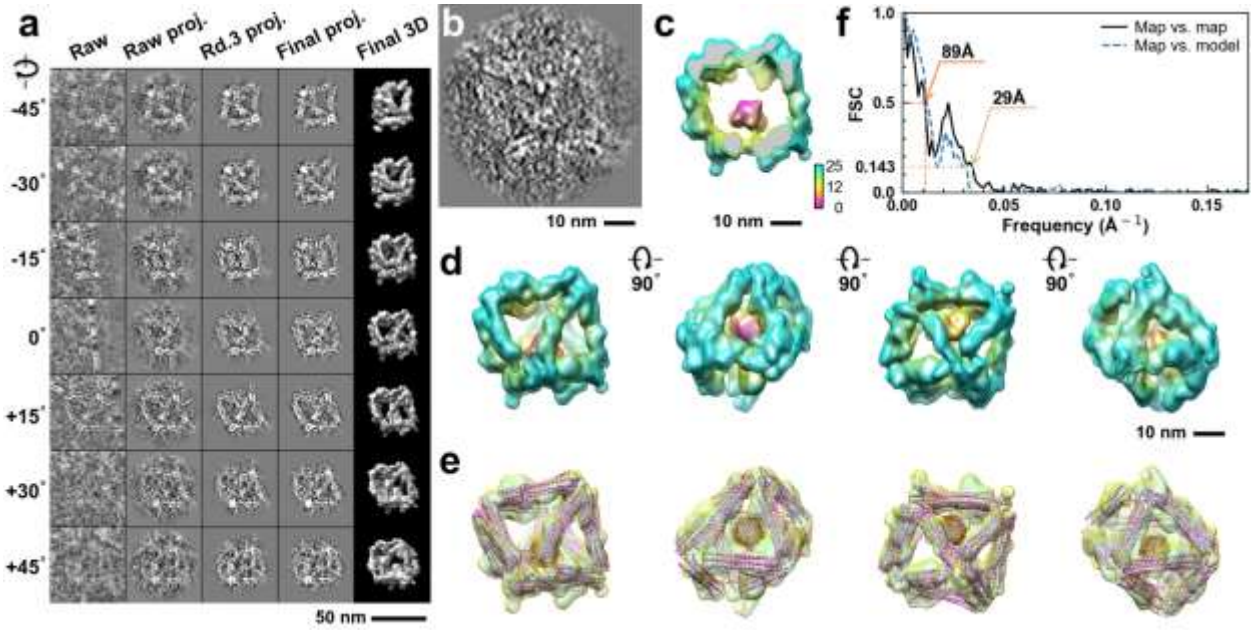

Supplementary Fig. 15: IPET 3D reconstruction and model fitting of an individual unit-cell particle (Index: 007) within a 2D lattice with 100% ferritin loading. a, Seven representative tilt images of a single unit-cell particle are shown in the first column (from left). The tilt images are aligned to a common center using IPET through iterative refinement. The projections of the raw, intermediate, and final 3D reconstruction at the corresponding angles are displayed in the subsequent four columns. **b**, A central cross-section (~23 nm thick) of the final reconstruction before masking is applied. **c**, 3D views of the central cross-section. **d**, Final 3D density map of this particle, viewed from four perpendicular directions. **e**, Final 3D reconstruction superimposed with the fitted model, viewed from four perpendicular directions. **f**, FSC analyses of the final map resolution using two methods: map-map FSC, where each map is reconstructed from one half of the images (even vs. odd tilt angle indices), and map-model FSC, where the model map is generated from the fitted model. Resolution assessments are provided based on tilt-based map-map and map-model FSC analyses at thresholds of FSC=0.5 and 0.143, respectively.

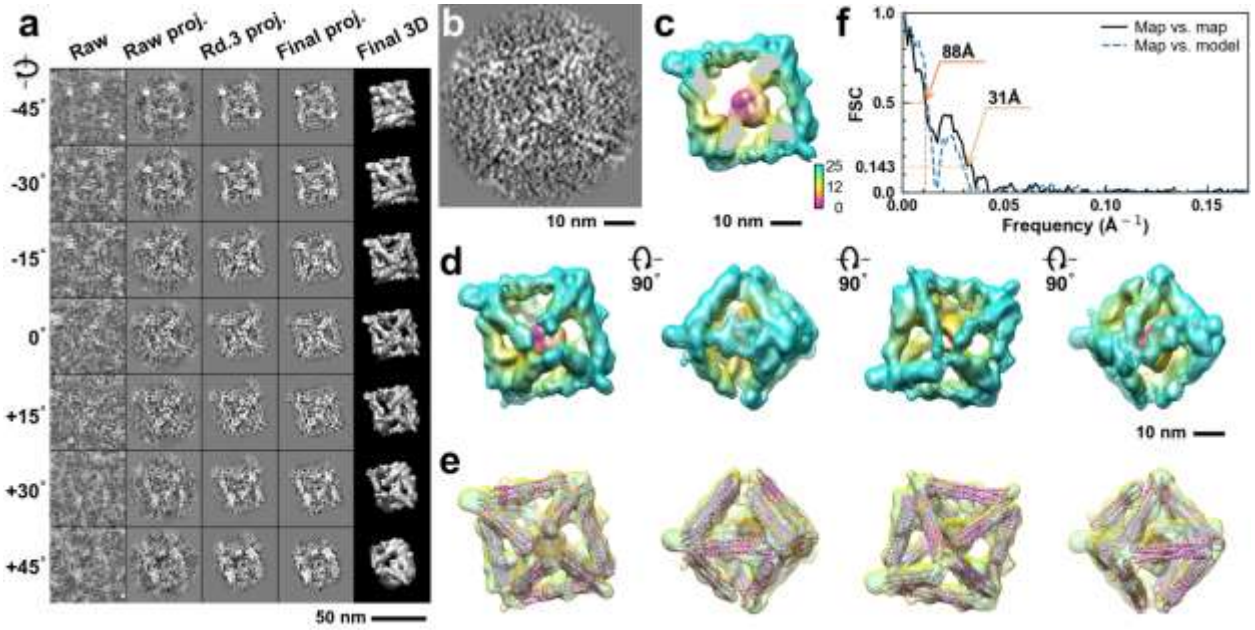

Supplementary Fig. 16: IPET 3D reconstruction and model fitting of an individual unit-cell particle (Index: 008) within a 2D lattice with 100% ferritin loading. a, Seven representative tilt images of a single unit-cell particle are shown in the first column (from left). The tilt images are aligned to a common center using IPET through iterative refinement. The projections of the raw, intermediate, and final 3D reconstruction at the corresponding angles are displayed in the subsequent four columns. **b**, A central cross-section (~23 nm thick) of the final reconstruction before masking is applied. **c**, 3D views of the central cross-section. **d**, Final 3D density map of this particle, viewed from four perpendicular directions. **e**, Final 3D reconstruction superimposed with the fitted model, viewed from four perpendicular directions. **f**, FSC analyses of the final map resolution using two methods: map-map FSC, where each map is reconstructed from one half of the images (even vs. odd tilt angle indices), and map-model FSC, where the model map is generated from the fitted model. Resolution assessments are provided based on tilt-based map-map and map-model FSC analyses at thresholds of FSC=0.5 and 0.143, respectively.

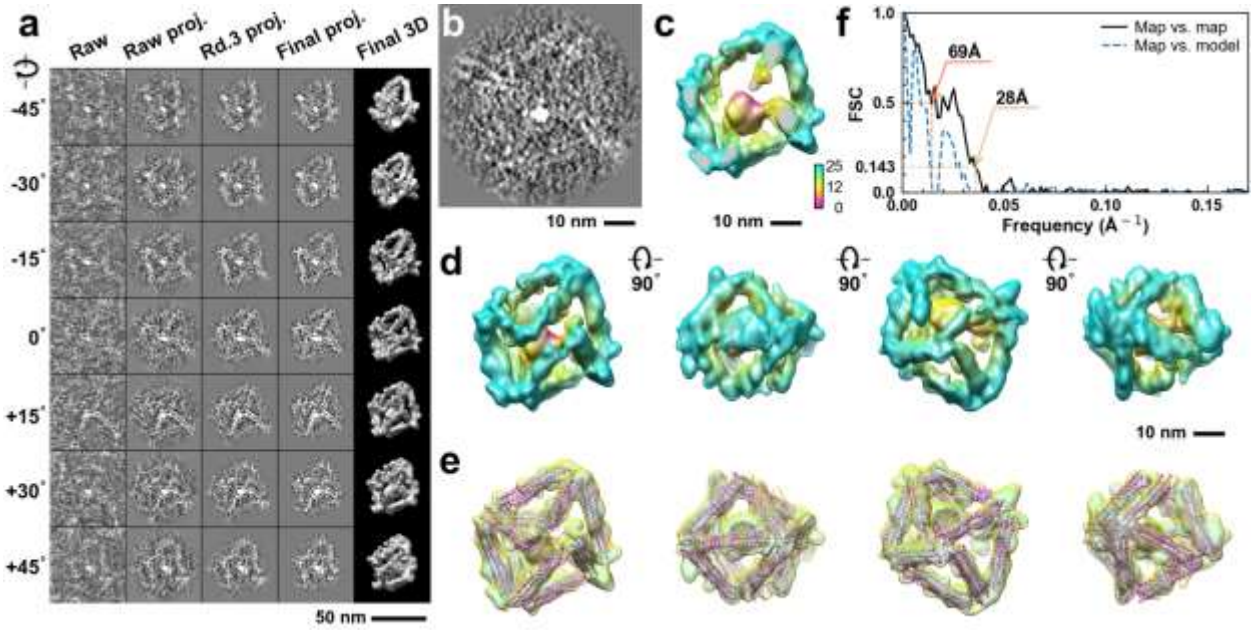

Supplementary Fig. 17: IPET 3D reconstruction and model fitting of an individual unit-cell particle (Index: 009) within a 2D lattice with 100% ferritin loading. a, Seven representative tilt images of a single unit-cell particle are shown in the first column (from left). The tilt images are aligned to a common center using IPET through iterative refinement. The projections of the raw, intermediate, and final 3D reconstruction at the corresponding angles are displayed in the subsequent four columns. **b**, A central cross-section (~23 nm thick) of the final reconstruction before masking is applied. **c**, 3D views of the central cross-section. **d**, Final 3D density map of this particle, viewed from four perpendicular directions. **e**, Final 3D reconstruction superimposed with the fitted model, viewed from four perpendicular directions. **f**, FSC analyses of the final map resolution using two methods: map-map FSC, where each map is reconstructed from one half of the images (even vs. odd tilt angle indices), and map-model FSC, where the model map is generated from the fitted model. Resolution assessments are provided based on tilt-based map-map and map-model FSC analyses at thresholds of FSC=0.5 and 0.143, respectively.

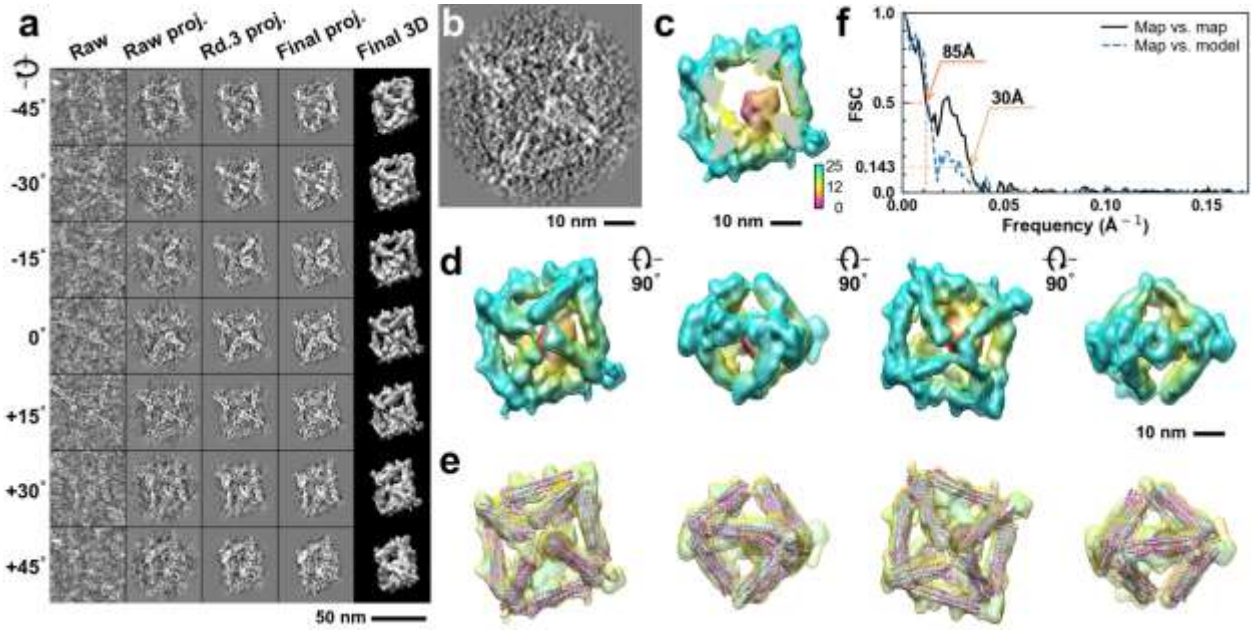

Supplementary Fig. 18: IPET 3D reconstruction and model fitting of an individual unit-cell particle (Index: 010) within a 2D lattice with 100% ferritin loading. a, Seven representative tilt images of a single unit-cell particle are shown in the first column (from left). The tilt images are aligned to a common center using IPET through iterative refinement. The projections of the raw, intermediate, and final 3D reconstruction at the corresponding angles are displayed in the subsequent four columns. **b**, A central cross-section (~23 nm thick) of the final reconstruction before masking is applied. **c**, 3D views of the central cross-section. **d**, Final 3D density map of this particle, viewed from four perpendicular directions. **e**, Final 3D reconstruction superimposed with the fitted model, viewed from four perpendicular directions. **f**, FSC analyses of the final map resolution using two methods: map-map FSC, where each map is reconstructed from one half of the images (even vs. odd tilt angle indices), and map-model FSC, where the model map is generated from the fitted model. Resolution assessments are provided based on tilt-based map-map and map-model FSC analyses at thresholds of FSC=0.5 and 0.143, respectively.

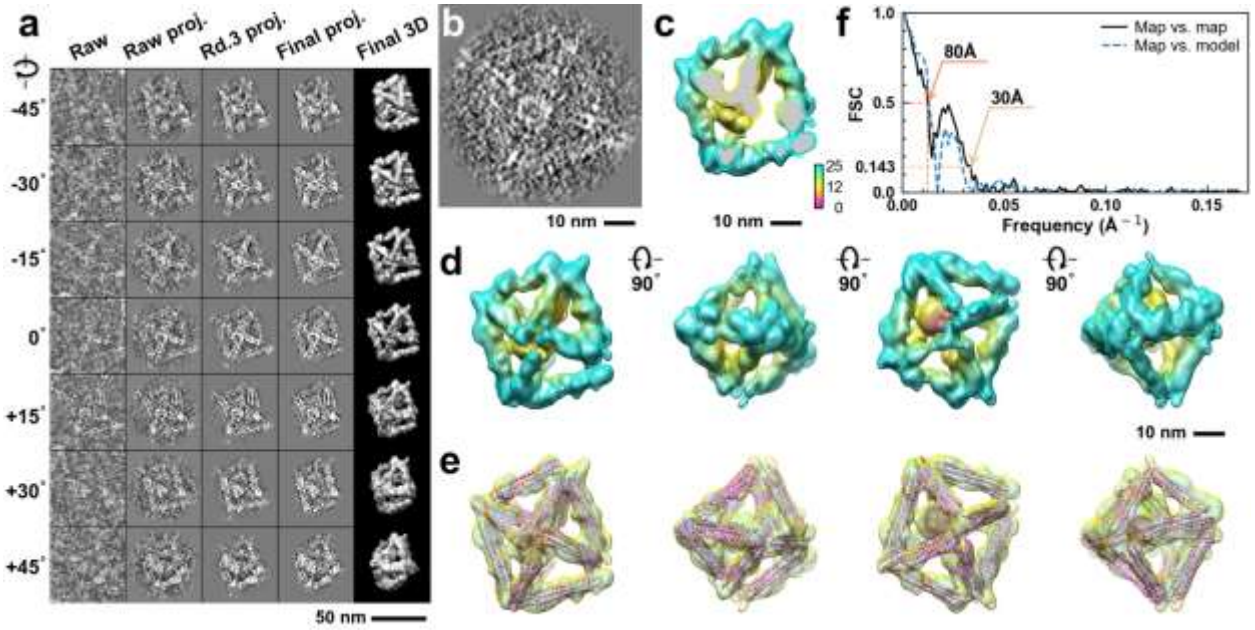

Supplementary Fig. 19: IPET 3D reconstruction and model fitting of an individual unit-cell particle (Index: 011) within a 2D lattice with 100% ferritin loading. a, Seven representative tilt images of a single unit-cell particle are shown in the first column (from left). The tilt images are aligned to a common center using IPET through iterative refinement. The projections of the raw, intermediate, and final 3D reconstruction at the corresponding angles are displayed in the subsequent four columns. **b**, A central cross-section (~23 nm thick) of the final reconstruction before masking is applied. **c**, 3D views of the central cross-section. **d**, Final 3D density map of this particle, viewed from four perpendicular directions. **e**, Final 3D reconstruction superimposed with the fitted model, viewed from four perpendicular directions. **f**, FSC analyses of the final map resolution using two methods: map-map FSC, where each map is reconstructed from one half of the images (even vs. odd tilt angle indices), and map-model FSC, where the model map is generated from the fitted model. Resolution assessments are provided based on tilt-based map-map and map-model FSC analyses at thresholds of FSC=0.5 and 0.143, respectively.

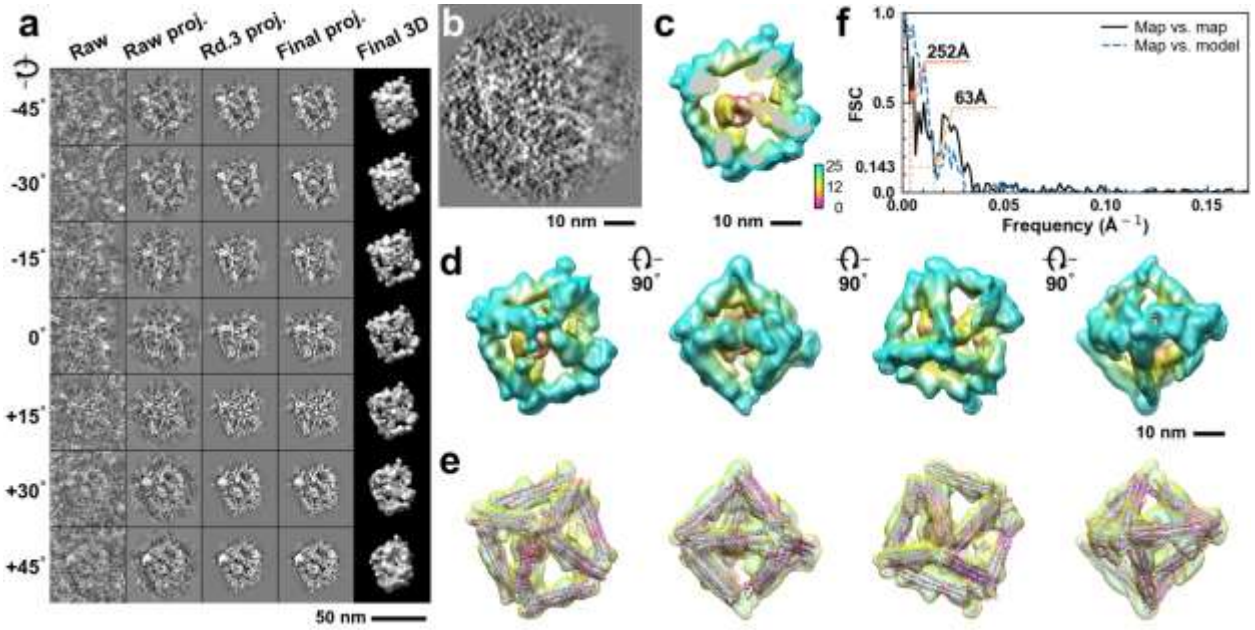

Supplementary Fig. 20: IPET 3D reconstruction and model fitting of an individual unit-cell particle (Index: 012) within a 2D lattice with 100% ferritin loading. a, Seven representative tilt images of a single unit-cell particle are shown in the first column (from left). The tilt images are aligned to a common center using IPET through iterative refinement. The projections of the raw, intermediate, and final 3D reconstruction at the corresponding angles are displayed in the subsequent four columns. **b**, A central cross-section (~23 nm thick) of the final reconstruction before masking is applied. **c**, 3D views of the central cross-section. **d**, Final 3D density map of this particle, viewed from four perpendicular directions. **e**, Final 3D reconstruction superimposed with the fitted model, viewed from four perpendicular directions. **f**, FSC analyses of the final map resolution using two methods: map-map FSC, where each map is reconstructed from one half of the images (even vs. odd tilt angle indices), and map-model FSC, where the model map is generated from the fitted model. Resolution assessments are provided based on tilt-based map-map and map-model FSC analyses at thresholds of FSC=0.5 and 0.143, respectively.

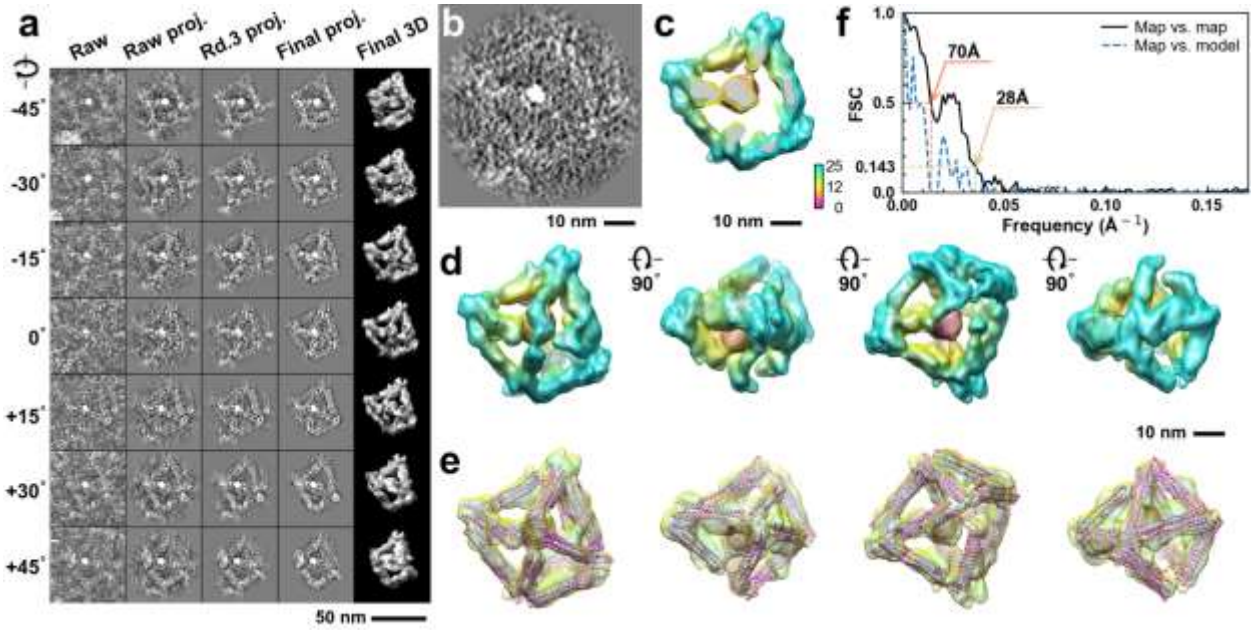

Supplementary Fig. 21: IPET 3D reconstruction and model fitting of an individual unit-cell particle (Index: 013) within a 2D lattice with 100% ferritin loading. a, Seven representative tilt images of a single unit-cell particle are shown in the first column (from left). The tilt images are aligned to a common center using IPET through iterative refinement. The projections of the raw, intermediate, and final 3D reconstruction at the corresponding angles are displayed in the subsequent four columns. **b**, A central cross-section (~23 nm thick) of the final reconstruction before masking is applied. **c**, 3D views of the central cross-section. **d**, Final 3D density map of this particle, viewed from four perpendicular directions. **e**, Final 3D reconstruction superimposed with the fitted model, viewed from four perpendicular directions. **f**, FSC analyses of the final map resolution using two methods: map-map FSC, where each map is reconstructed from one half of the images (even vs. odd tilt angle indices), and map-model FSC, where the model map is generated from the fitted model. Resolution assessments are provided based on tilt-based map-map and map-model FSC analyses at thresholds of FSC=0.5 and 0.143, respectively.

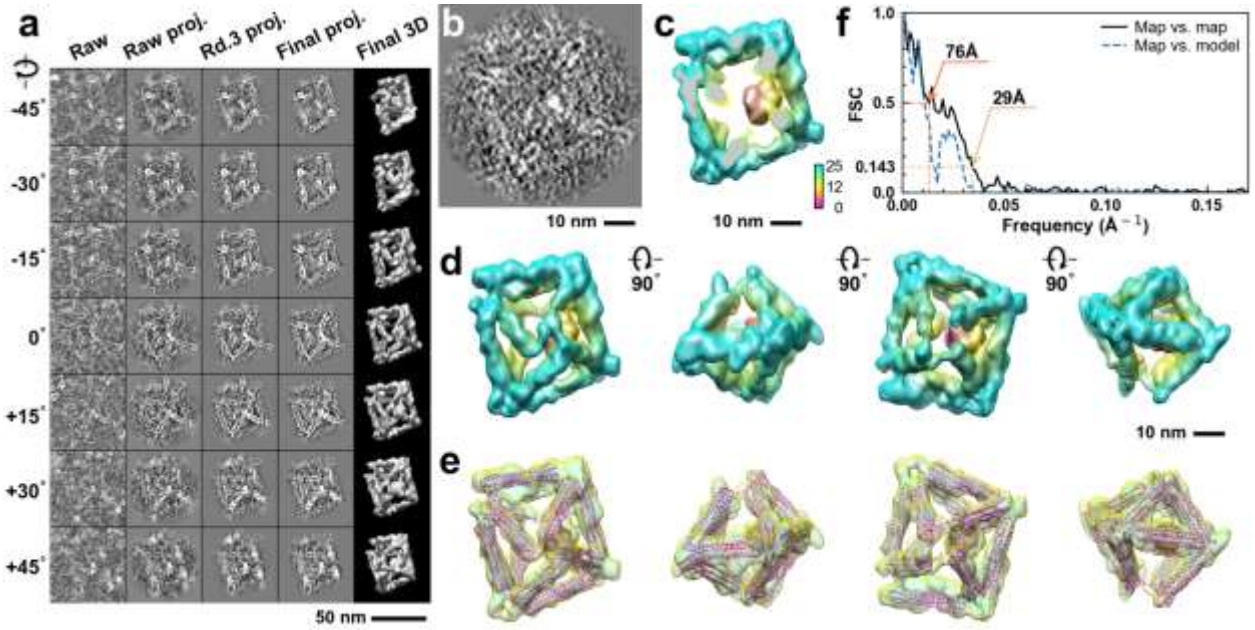

Supplementary Fig. 22: IPET 3D reconstruction and model fitting of an individual unit-cell particle (Index: 014) within a 2D lattice with 100% ferritin loading. a, Seven representative tilt images of a single unit-cell particle are shown in the first column (from left). The tilt images are aligned to a common center using IPET through iterative refinement. The projections of the raw, intermediate, and final 3D reconstruction at the corresponding angles are displayed in the subsequent four columns. **b**, A central cross-section (~23 nm thick) of the final reconstruction before masking is applied. **c**, 3D views of the central cross-section. **d**, Final 3D density map of this particle, viewed from four perpendicular directions. **e**, Final 3D reconstruction superimposed with the fitted model, viewed from four perpendicular directions. **f**, FSC analyses of the final map resolution using two methods: map-map FSC, where each map is reconstructed from one half of the images (even vs. odd tilt angle indices), and map-model FSC, where the model map is generated from the fitted model. Resolution assessments are provided based on tilt-based map-map and map-model FSC analyses at thresholds of FSC=0.5 and 0.143, respectively.

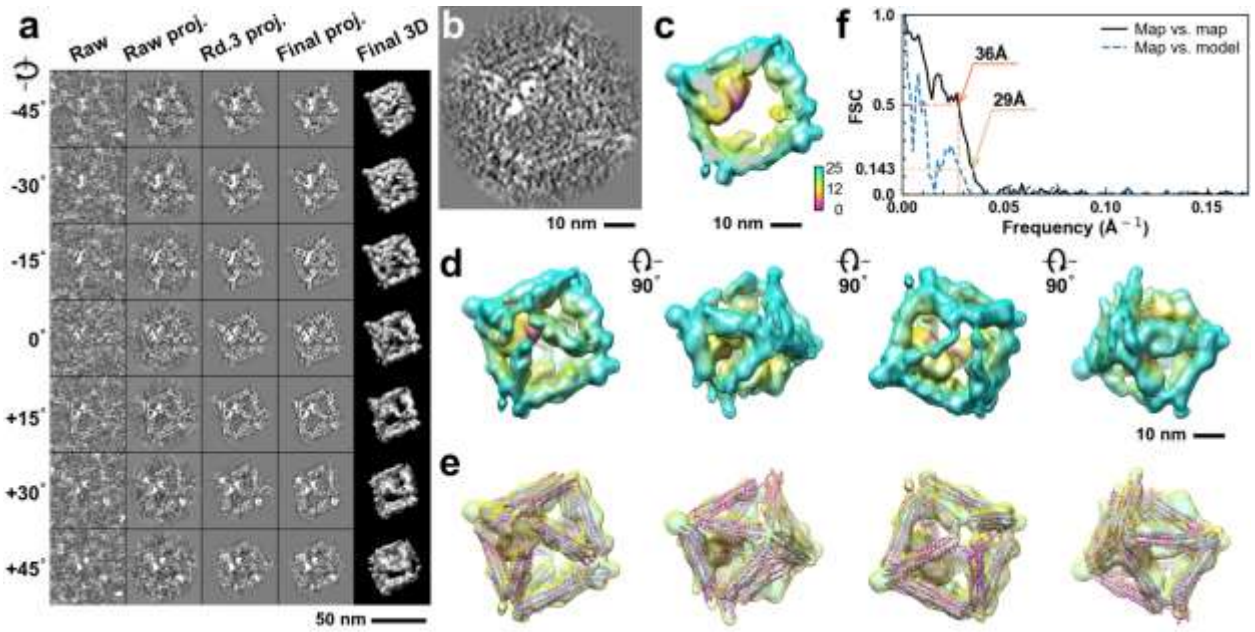

Supplementary Fig. 23: IPET 3D reconstruction and model fitting of an individual unit-cell particle (Index: 015) within a 2D lattice with 100% ferritin loading. a, Seven representative tilt images of a single unit-cell particle are shown in the first column (from left). The tilt images are aligned to a common center using IPET through iterative refinement. The projections of the raw, intermediate, and final 3D reconstruction at the corresponding angles are displayed in the subsequent four columns. **b**, A central cross-section (~23 nm thick) of the final reconstruction before masking is applied. **c**, 3D views of the central cross-section. **d**, Final 3D density map of this particle, viewed from four perpendicular directions. **e**, Final 3D reconstruction superimposed with the fitted model, viewed from four perpendicular directions. **f**, FSC analyses of the final map resolution using two methods: map-map FSC, where each map is reconstructed from one half of the images (even vs. odd tilt angle indices), and map-model FSC, where the model map is generated from the fitted model. Resolution assessments are provided based on tilt-based map-map and map-model FSC analyses at thresholds of FSC=0.5 and 0.143, respectively.

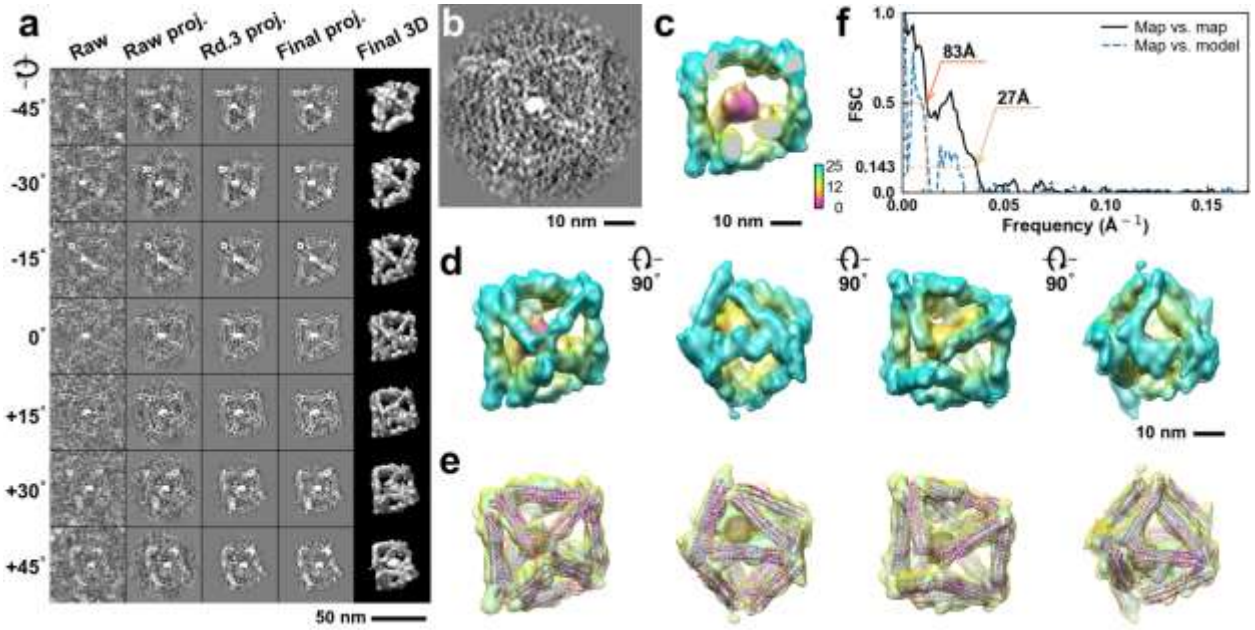

Supplementary Fig. 24: IPET 3D reconstruction and model fitting of an individual unit-cell particle (Index: 016) within a 2D lattice with 100% ferritin loading. a, Seven representative tilt images of a single unit-cell particle are shown in the first column (from left). The tilt images are aligned to a common center using IPET through iterative refinement. The projections of the raw, intermediate, and final 3D reconstruction at the corresponding angles are displayed in the subsequent four columns. **b**, A central cross-section (~23 nm thick) of the final reconstruction before masking is applied. **c**, 3D views of the central cross-section. **d**, Final 3D density map of this particle, viewed from four perpendicular directions. **e**, Final 3D reconstruction superimposed with the fitted model, viewed from four perpendicular directions. **f**, FSC analyses of the final map resolution using two methods: map-map FSC, where each map is reconstructed from one half of the images (even vs. odd tilt angle indices), and map-model FSC, where the model map is generated from the fitted model. Resolution assessments are provided based on tilt-based map-map and map-model FSC analyses at thresholds of FSC=0.5 and 0.143, respectively.

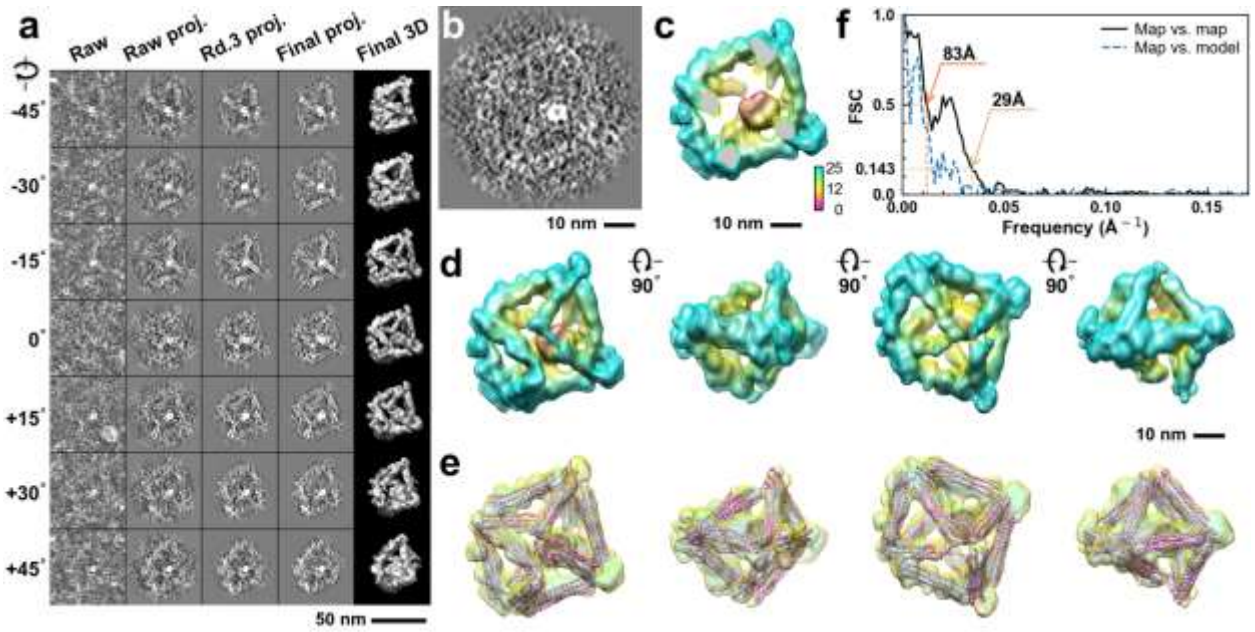

Supplementary Fig. 25: IPET 3D reconstruction and model fitting of an individual unit-cell particle (Index: 017) within a 2D lattice with 100% ferritin loading. a, Seven representative tilt images of a single unit-cell particle are shown in the first column (from left). The tilt images are aligned to a common center using IPET through iterative refinement. The projections of the raw, intermediate, and final 3D reconstruction at the corresponding angles are displayed in the subsequent four columns. **b**, A central cross-section (~23 nm thick) of the final reconstruction before masking is applied. **c**, 3D views of the central cross-section. **d**, Final 3D density map of this particle, viewed from four perpendicular directions. **e**, Final 3D reconstruction superimposed with the fitted model, viewed from four perpendicular directions. **f**, FSC analyses of the final map resolution using two methods: map-map FSC, where each map is reconstructed from one half of the images (even vs. odd tilt angle indices), and map-model FSC, where the model map is generated from the fitted model. Resolution assessments are provided based on tilt-based map-map and map-model FSC analyses at thresholds of FSC=0.5 and 0.143, respectively.

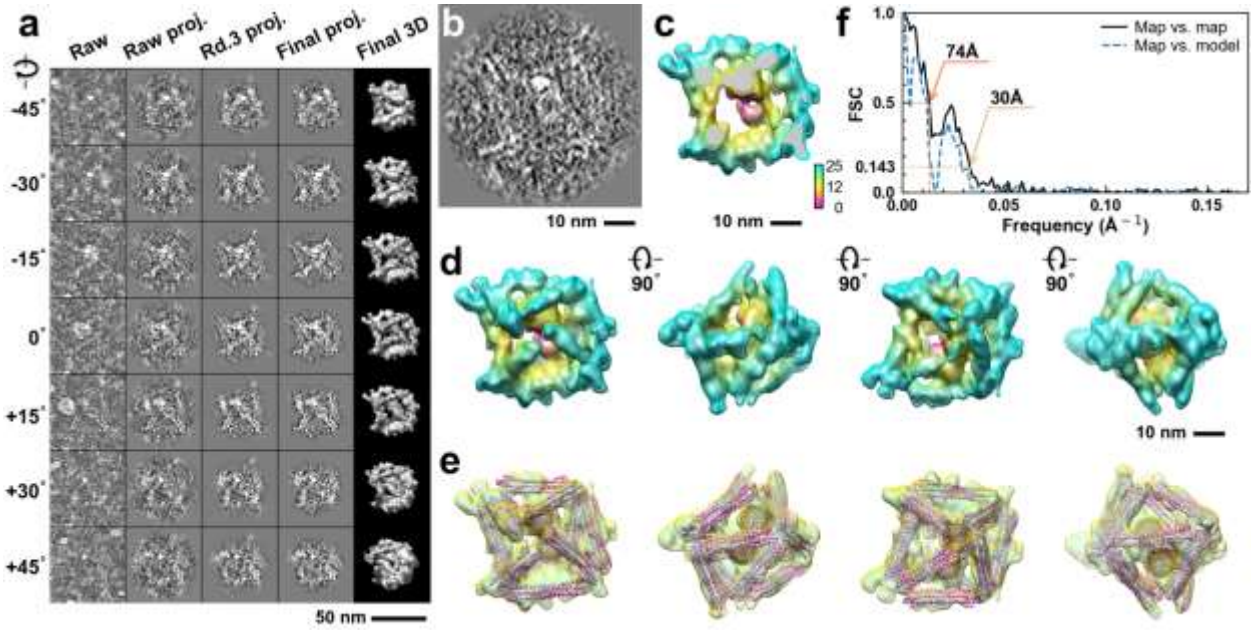

Supplementary Fig. 26: IPET 3D reconstruction and model fitting of an individual unit-cell particle (Index: 018) within a 2D lattice with 100% ferritin loading. a, Seven representative tilt images of a single unit-cell particle are shown in the first column (from left). The tilt images are aligned to a common center using IPET through iterative refinement. The projections of the raw, intermediate, and final 3D reconstruction at the corresponding angles are displayed in the subsequent four columns. **b**, A central cross-section (~23 nm thick) of the final reconstruction before masking is applied. **c**, 3D views of the central cross-section. **d**, Final 3D density map of this particle, viewed from four perpendicular directions. **e**, Final 3D reconstruction superimposed with the fitted model, viewed from four perpendicular directions. **f**, FSC analyses of the final map resolution using two methods: map-map FSC, where each map is reconstructed from one half of the images (even vs. odd tilt angle indices), and map-model FSC, where the model map is generated from the fitted model. Resolution assessments are provided based on tilt-based map-map and map-model FSC analyses at thresholds of FSC=0.5 and 0.143, respectively.

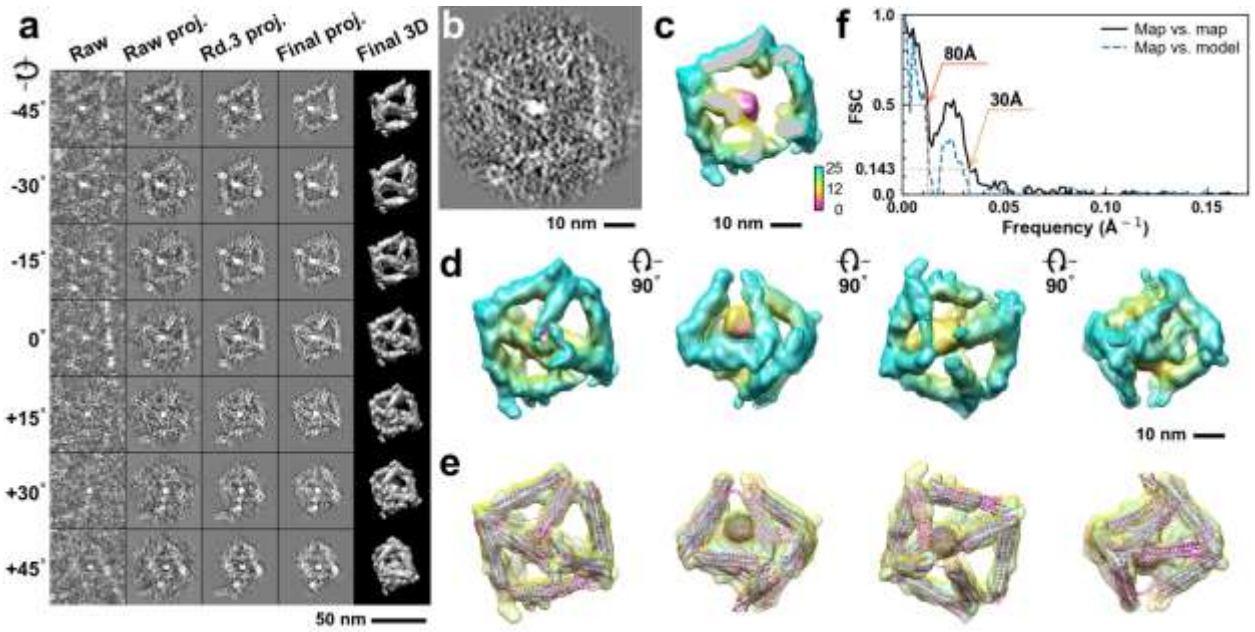

Supplementary Fig. 27: IPET 3D reconstruction and model fitting of an individual unit-cell particle (Index: 019) within a 2D lattice with 100% ferritin loading. a, Seven representative tilt images of a single unit-cell particle are shown in the first column (from left). The tilt images are aligned to a common center using IPET through iterative refinement. The projections of the raw, intermediate, and final 3D reconstruction at the corresponding angles are displayed in the subsequent four columns. **b**, A central cross-section (~23 nm thick) of the final reconstruction before masking is applied. **c**, 3D views of the central cross-section. **d**, Final 3D density map of this particle, viewed from four perpendicular directions. **e**, Final 3D reconstruction superimposed with the fitted model, viewed from four perpendicular directions. **f**, FSC analyses of the final map resolution using two methods: map-map FSC, where each map is reconstructed from one half of the images (even vs. odd tilt angle indices), and map-model FSC, where the model map is generated from the fitted model. Resolution assessments are provided based on tilt-based map-map and map-model FSC analyses at thresholds of FSC=0.5 and 0.143, respectively.

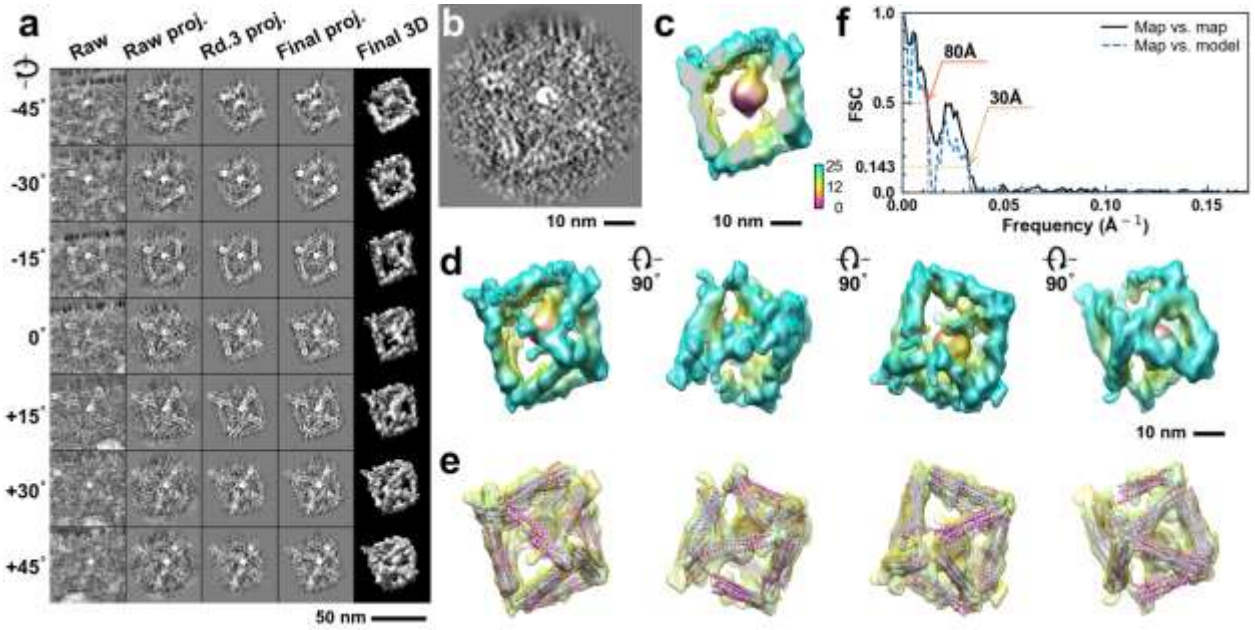

Supplementary Fig. 28: IPET 3D reconstruction and model fitting of an individual unit-cell particle (Index: 020) within a 2D lattice with 100% ferritin loading. a, Seven representative tilt images of a single unit-cell particle are shown in the first column (from left). The tilt images are aligned to a common center using IPET through iterative refinement. The projections of the raw, intermediate, and final 3D reconstruction at the corresponding angles are displayed in the subsequent four columns. **b**, A central cross-section (~23 nm thick) of the final reconstruction before masking is applied. **c**, 3D views of the central cross-section. **d**, Final 3D density map of this particle, viewed from four perpendicular directions. **e**, Final 3D reconstruction superimposed with the fitted model, viewed from four perpendicular directions. **f**, FSC analyses of the final map resolution using two methods: map-map FSC, where each map is reconstructed from one half of the images (even vs. odd tilt angle indices), and map-model FSC, where the model map is generated from the fitted model. Resolution assessments are provided based on tilt-based map-map and map-model FSC analyses at thresholds of FSC=0.5 and 0.143, respectively.

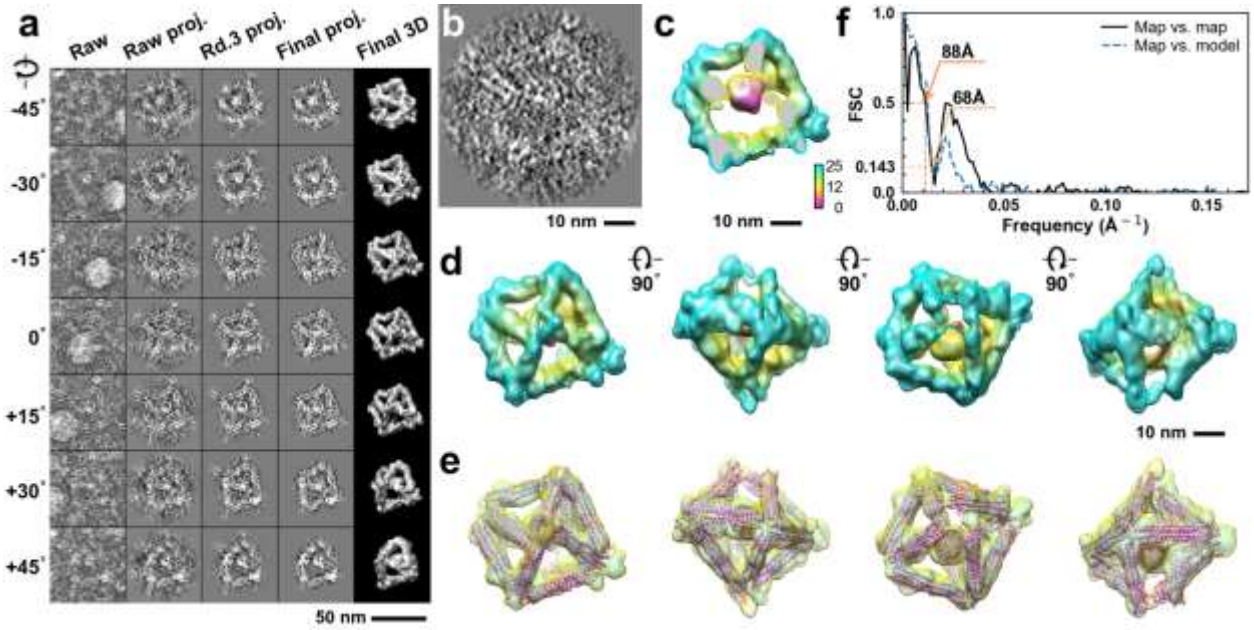

Supplementary Fig. 29: IPET 3D reconstruction and model fitting of an individual unit-cell particle (Index: 021) within a 2D lattice with 100% ferritin loading. a, Seven representative tilt images of a single unit-cell particle are shown in the first column (from left). The tilt images are aligned to a common center using IPET through iterative refinement. The projections of the raw, intermediate, and final 3D reconstruction at the corresponding angles are displayed in the subsequent four columns. **b**, A central cross-section (~23 nm thick) of the final reconstruction before masking is applied. **c**, 3D views of the central cross-section. **d**, Final 3D density map of this particle, viewed from four perpendicular directions. **e**, Final 3D reconstruction superimposed with the fitted model, viewed from four perpendicular directions. **f**, FSC analyses of the final map resolution using two methods: map-map FSC, where each map is reconstructed from one half of the images (even vs. odd tilt angle indices), and map-model FSC, where the model map is generated from the fitted model. Resolution assessments are provided based on tilt-based map-map and map-model FSC analyses at thresholds of FSC=0.5 and 0.143, respectively.

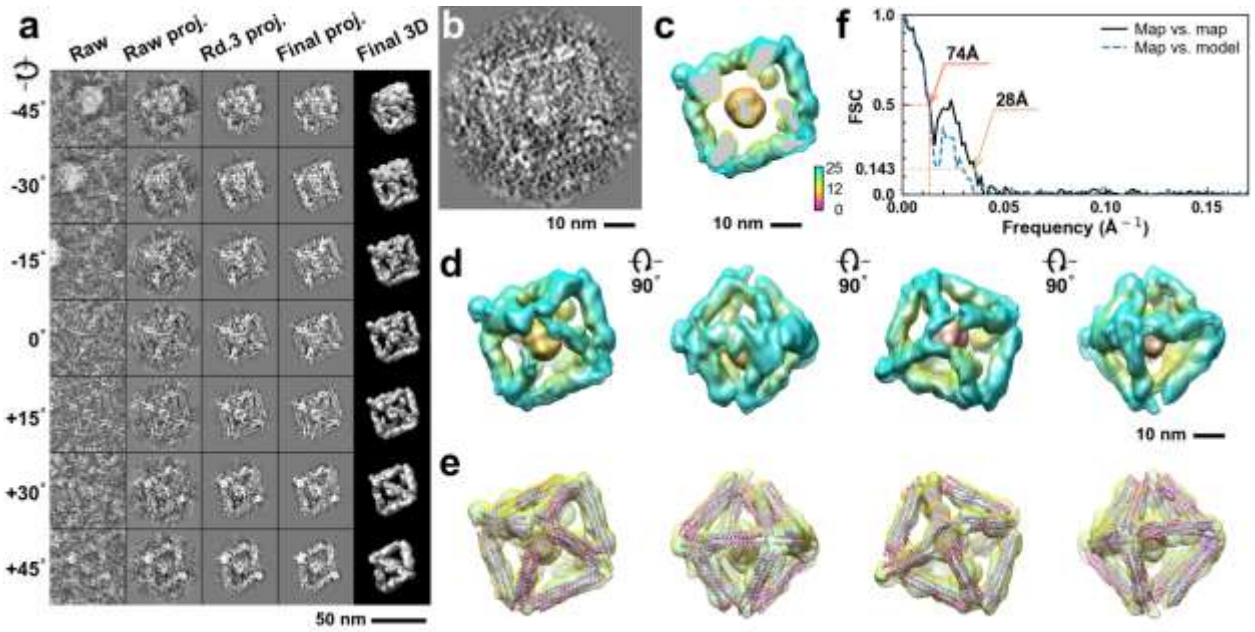

Supplementary Fig. 30: IPET 3D reconstruction and model fitting of an individual unit-cell particle (Index: 022) within a 2D lattice with 100% ferritin loading. a, Seven representative tilt images of a single unit-cell particle are shown in the first column (from left). The tilt images are aligned to a common center using IPET through iterative refinement. The projections of the raw, intermediate, and final 3D reconstruction at the corresponding angles are displayed in the subsequent four columns. **b**, A central cross-section (~23 nm thick) of the final reconstruction before masking is applied. **c**, 3D views of the central cross-section. **d**, Final 3D density map of this particle, viewed from four perpendicular directions. **e**, Final 3D reconstruction superimposed with the fitted model, viewed from four perpendicular directions. **f**, FSC analyses of the final map resolution using two methods: map-map FSC, where each map is reconstructed from one half of the images (even vs. odd tilt angle indices), and map-model FSC, where the model map is generated from the fitted model. Resolution assessments are provided based on tilt-based map-map and map-model FSC analyses at thresholds of FSC=0.5 and 0.143, respectively.

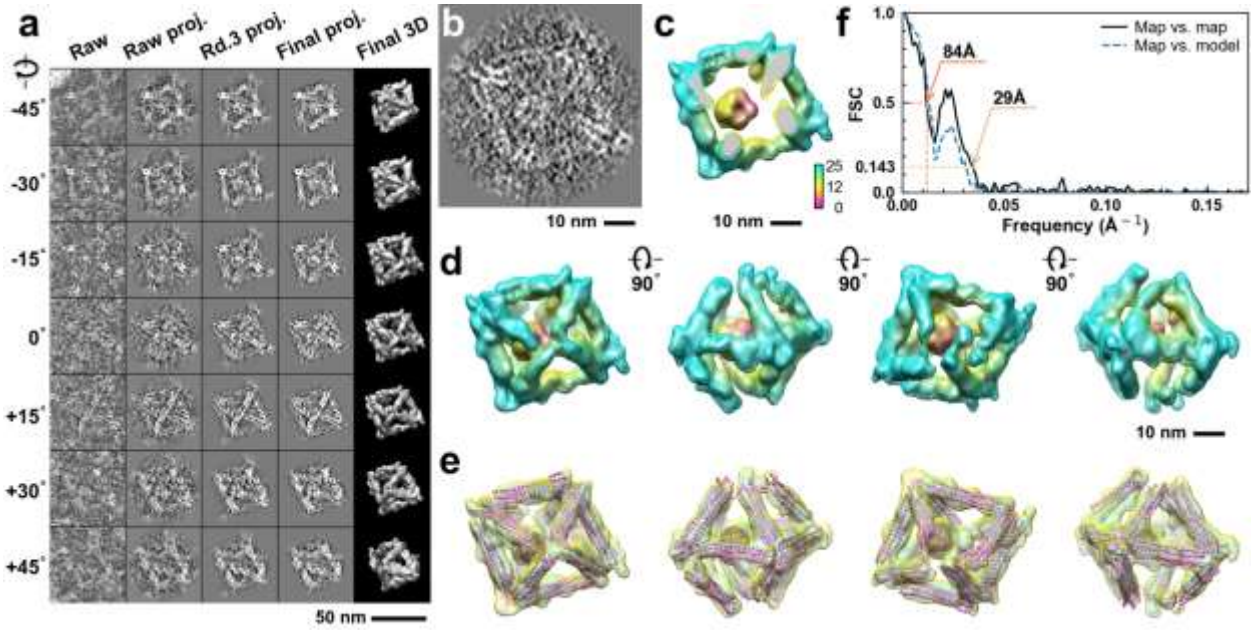

Supplementary Fig. 31: IPET 3D reconstruction and model fitting of an individual unit-cell particle (Index: 023) within a 2D lattice with 100% ferritin loading. a, Seven representative tilt images of a single unit-cell particle are shown in the first column (from left). The tilt images are aligned to a common center using IPET through iterative refinement. The projections of the raw, intermediate, and final 3D reconstruction at the corresponding angles are displayed in the subsequent four columns. **b**, A central cross-section (~23 nm thick) of the final reconstruction before masking is applied. **c**, 3D views of the central cross-section. **d**, Final 3D density map of this particle, viewed from four perpendicular directions. **e**, Final 3D reconstruction superimposed with the fitted model, viewed from four perpendicular directions. **f**, FSC analyses of the final map resolution using two methods: map-map FSC, where each map is reconstructed from one half of the images (even vs. odd tilt angle indices), and map-model FSC, where the model map is generated from the fitted model. Resolution assessments are provided based on tilt-based map-map and map-model FSC analyses at thresholds of FSC=0.5 and 0.143, respectively.

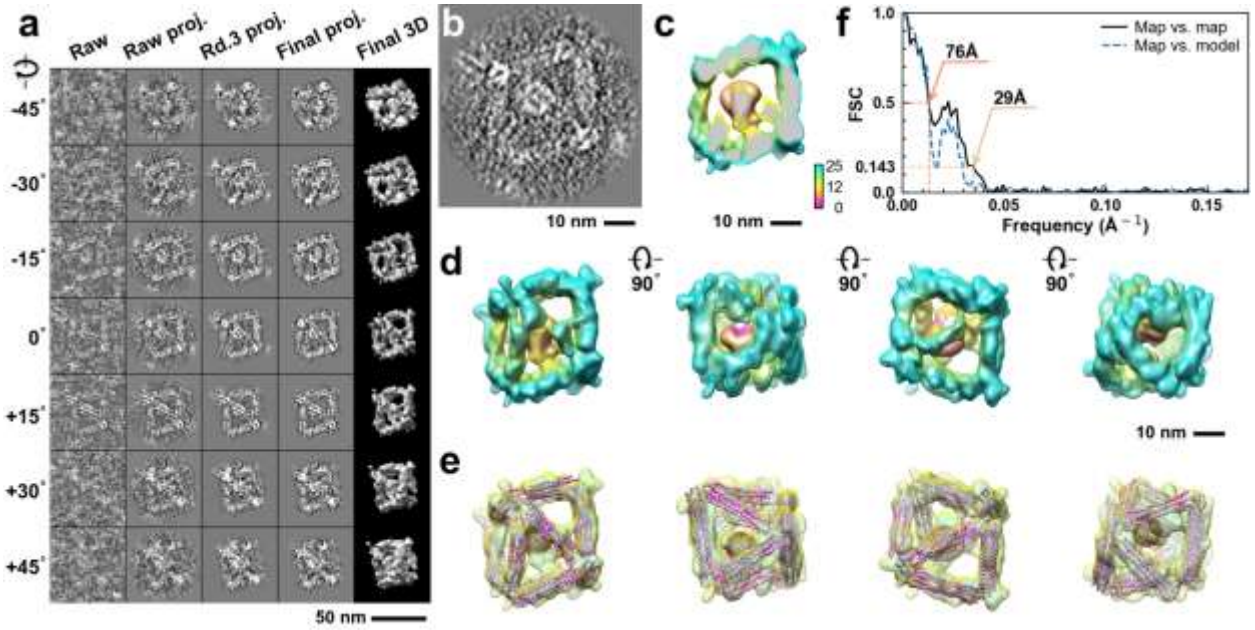

Supplementary Fig. 32: IPET 3D reconstruction and model fitting of an individual unit-cell particle (Index: 024) within a 2D lattice with 100% ferritin loading. a, Seven representative tilt images of a single unit-cell particle are shown in the first column (from left). The tilt images are aligned to a common center using IPET through iterative refinement. The projections of the raw, intermediate, and final 3D reconstruction at the corresponding angles are displayed in the subsequent four columns. **b**, A central cross-section (~23 nm thick) of the final reconstruction before masking is applied. **c**, 3D views of the central cross-section. **d**, Final 3D density map of this particle, viewed from four perpendicular directions. **e**, Final 3D reconstruction superimposed with the fitted model, viewed from four perpendicular directions. **f**, FSC analyses of the final map resolution using two methods: map-map FSC, where each map is reconstructed from one half of the images (even vs. odd tilt angle indices), and map-model FSC, where the model map is generated from the fitted model. Resolution assessments are provided based on tilt-based map-map and map-model FSC analyses at thresholds of FSC=0.5 and 0.143, respectively.

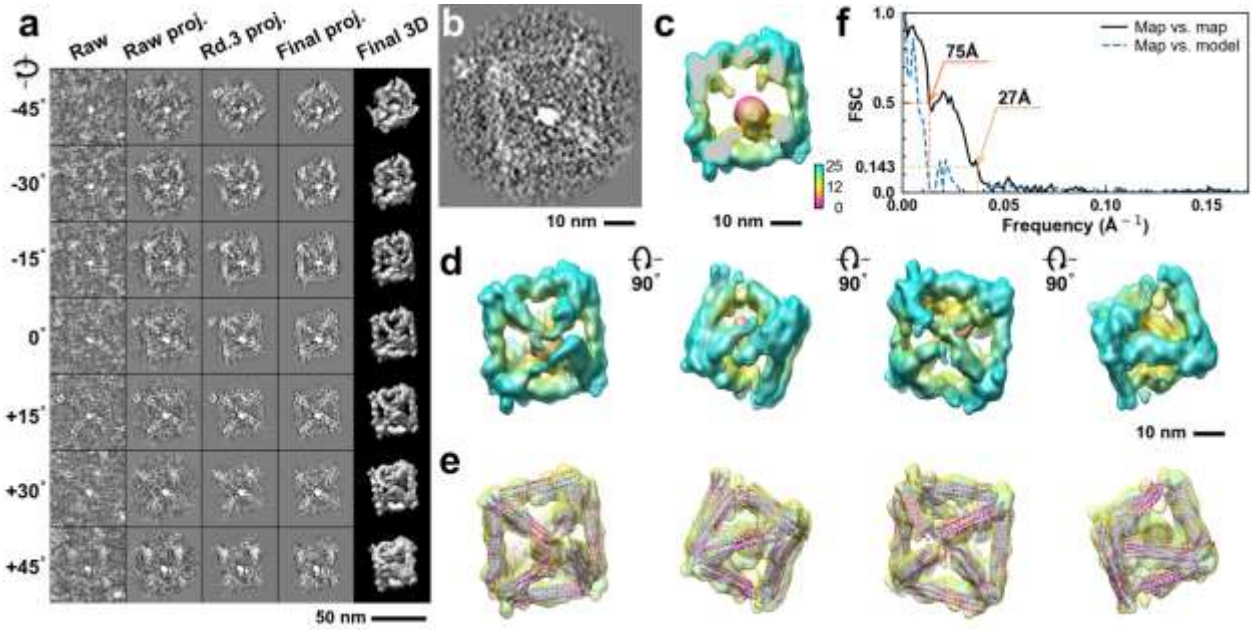

Supplementary Fig. 33: IPET 3D reconstruction and model fitting of an individual unit-cell particle (Index: 025) within a 2D lattice with 100% ferritin loading. a, Seven representative tilt images of a single unit-cell particle are shown in the first column (from left). The tilt images are aligned to a common center using IPET through iterative refinement. The projections of the raw, intermediate, and final 3D reconstruction at the corresponding angles are displayed in the subsequent four columns. **b**, A central cross-section (~23 nm thick) of the final reconstruction before masking is applied. **c**, 3D views of the central cross-section. **d**, Final 3D density map of this particle, viewed from four perpendicular directions. **e**, Final 3D reconstruction superimposed with the fitted model, viewed from four perpendicular directions. **f**, FSC analyses of the final map resolution using two methods: map-map FSC, where each map is reconstructed from one half of the images (even vs. odd tilt angle indices), and map-model FSC, where the model map is generated from the fitted model. Resolution assessments are provided based on tilt-based map-map and map-model FSC analyses at thresholds of FSC=0.5 and 0.143, respectively.

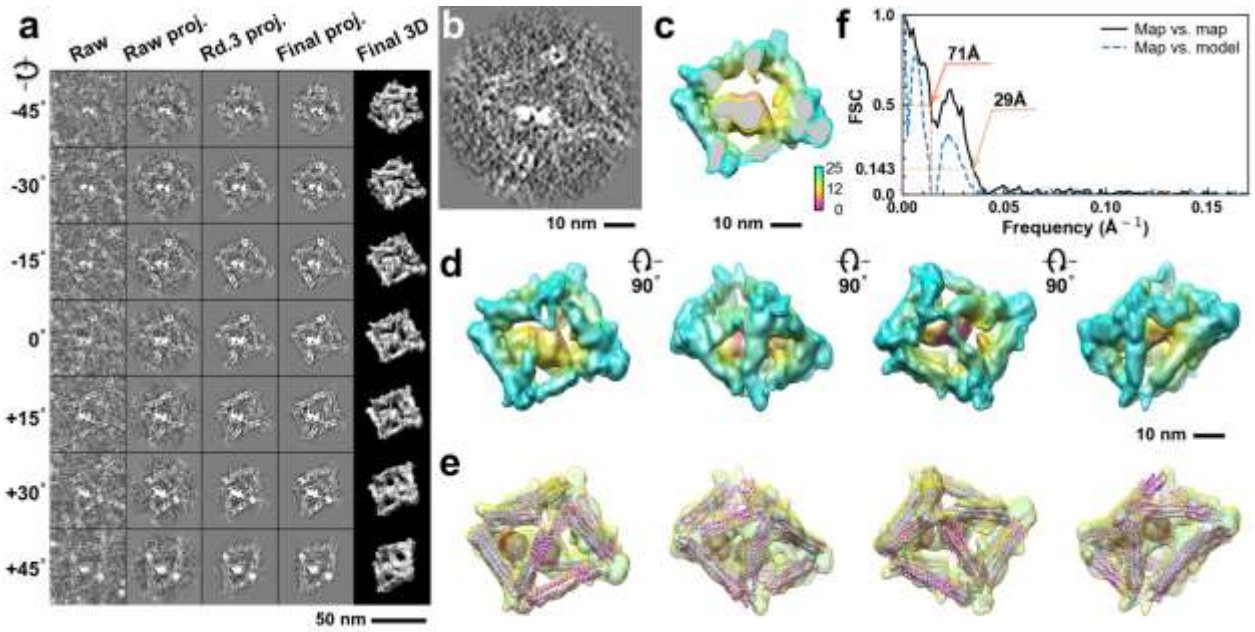

Supplementary Fig. 34: IPET 3D reconstruction and model fitting of an individual unit-cell particle (Index: 026) within a 2D lattice with 100% ferritin loading. a, Seven representative tilt images of a single unit-cell particle are shown in the first column (from left). The tilt images are aligned to a common center using IPET through iterative refinement. The projections of the raw, intermediate, and final 3D reconstruction at the corresponding angles are displayed in the subsequent four columns. **b**, A central cross-section (~23 nm thick) of the final reconstruction before masking is applied. **c**, 3D views of the central cross-section. **d**, Final 3D density map of this particle, viewed from four perpendicular directions. **e**, Final 3D reconstruction superimposed with the fitted model, viewed from four perpendicular directions. **f**, FSC analyses of the final map resolution using two methods: map-map FSC, where each map is reconstructed from one half of the images (even vs. odd tilt angle indices), and map-model FSC, where the model map is generated from the fitted model. Resolution assessments are provided based on tilt-based map-map and map-model FSC analyses at thresholds of FSC=0.5 and 0.143, respectively.

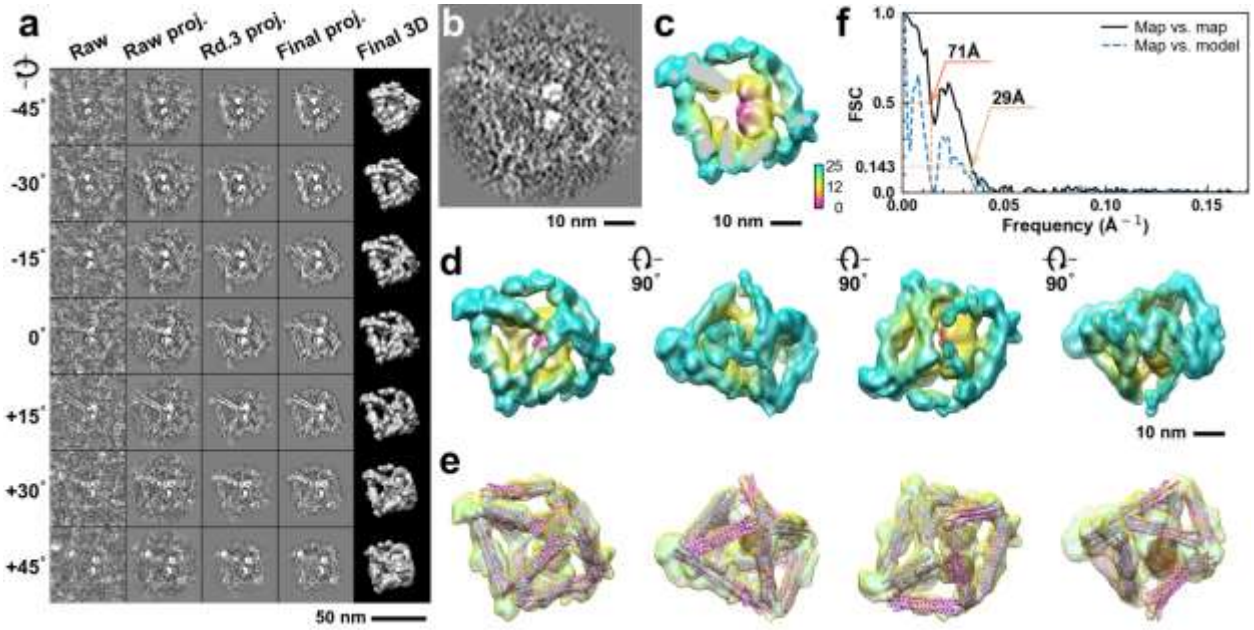

Supplementary Fig. 35: IPET 3D reconstruction and model fitting of an individual unit-cell particle (Index: 027) within a 2D lattice with 100% ferritin loading. a, Seven representative tilt images of a single unit-cell particle are shown in the first column (from left). The tilt images are aligned to a common center using IPET through iterative refinement. The projections of the raw, intermediate, and final 3D reconstruction at the corresponding angles are displayed in the subsequent four columns. **b**, A central cross-section (~23 nm thick) of the final reconstruction before masking is applied. **c**, 3D views of the central cross-section. **d**, Final 3D density map of this particle, viewed from four perpendicular directions. **e**, Final 3D reconstruction superimposed with the fitted model, viewed from four perpendicular directions. **f**, FSC analyses of the final map resolution using two methods: map-map FSC, where each map is reconstructed from one half of the images (even vs. odd tilt angle indices), and map-model FSC, where the model map is generated from the fitted model. Resolution assessments are provided based on tilt-based map-map and map-model FSC analyses at thresholds of FSC=0.5 and 0.143, respectively.

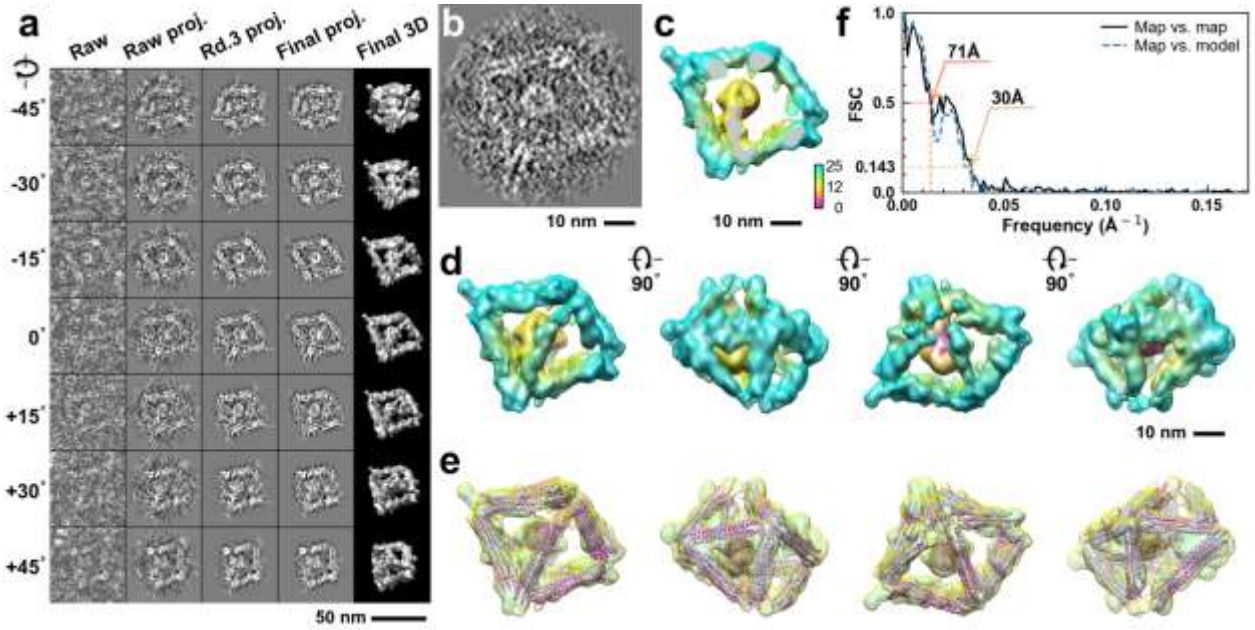

Supplementary Fig. 36: IPET 3D reconstruction and model fitting of an individual unit-cell particle (Index: 028) within a 2D lattice with 100% ferritin loading. a, Seven representative tilt images of a single unit-cell particle are shown in the first column (from left). The tilt images are aligned to a common center using IPET through iterative refinement. The projections of the raw, intermediate, and final 3D reconstruction at the corresponding angles are displayed in the subsequent four columns. **b**, A central cross-section (~23 nm thick) of the final reconstruction before masking is applied. **c**, 3D views of the central cross-section. **d**, Final 3D density map of this particle, viewed from four perpendicular directions. **e**, Final 3D reconstruction superimposed with the fitted model, viewed from four perpendicular directions. **f**, FSC analyses of the final map resolution using two methods: map-map FSC, where each map is reconstructed from one half of the images (even vs. odd tilt angle indices), and map-model FSC, where the model map is generated from the fitted model. Resolution assessments are provided based on tilt-based map-map and map-model FSC analyses at thresholds of FSC=0.5 and 0.143, respectively.

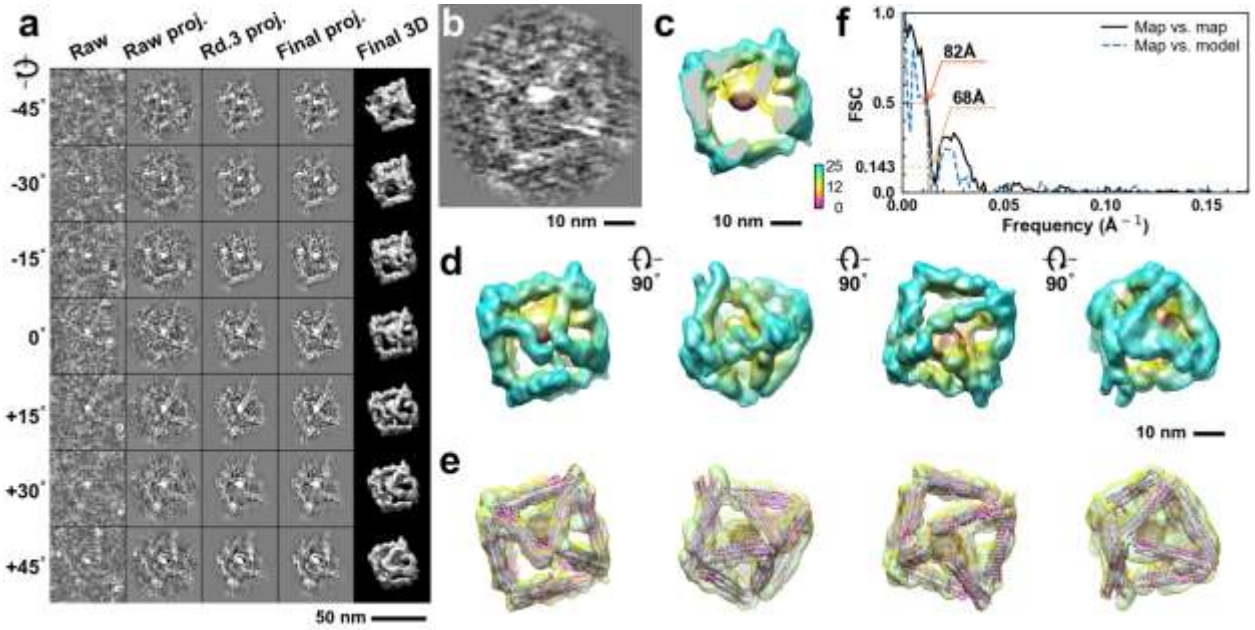

Supplementary Fig. 37: IPET 3D reconstruction and model fitting of an individual unit-cell particle (Index: 029) within a 2D lattice with 100% ferritin loading. a, Seven representative tilt images of a single unit-cell particle are shown in the first column (from left). The tilt images are aligned to a common center using IPET through iterative refinement. The projections of the raw, intermediate, and final 3D reconstruction at the corresponding angles are displayed in the subsequent four columns. **b**, A central cross-section (~23 nm thick) of the final reconstruction before masking is applied. **c**, 3D views of the central cross-section. **d**, Final 3D density map of this particle, viewed from four perpendicular directions. **e**, Final 3D reconstruction superimposed with the fitted model, viewed from four perpendicular directions. **f**, FSC analyses of the final map resolution using two methods: map-map FSC, where each map is reconstructed from one half of the images (even vs. odd tilt angle indices), and map-model FSC, where the model map is generated from the fitted model. Resolution assessments are provided based on tilt-based map-map and map-model FSC analyses at thresholds of FSC=0.5 and 0.143, respectively.

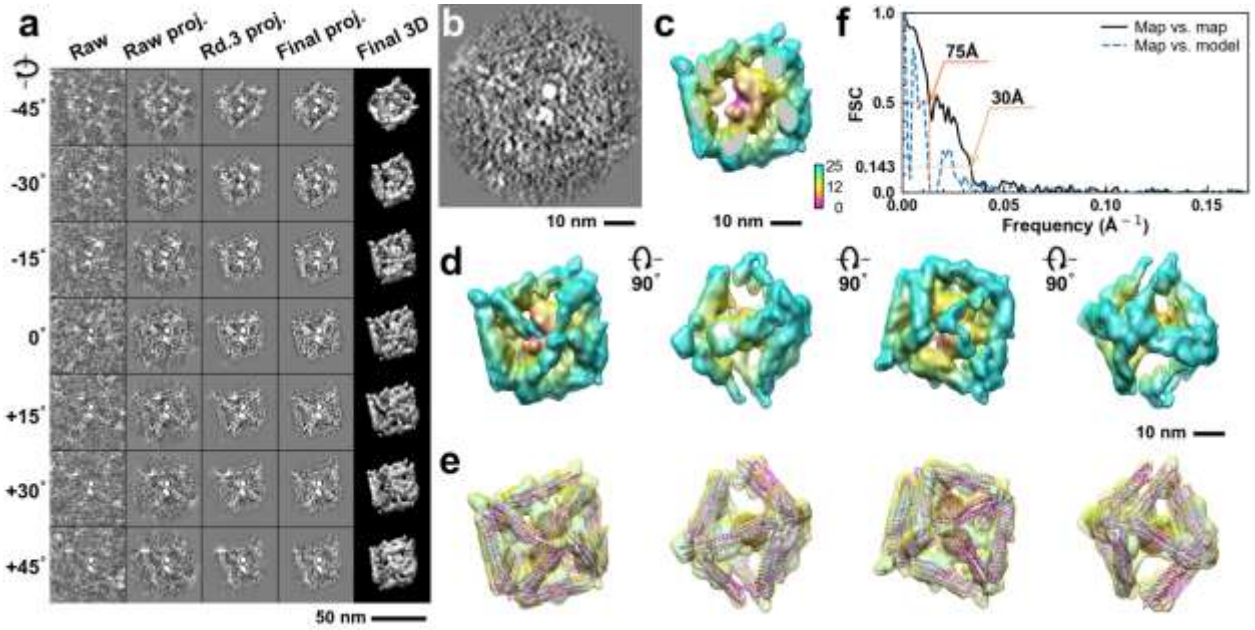

Supplementary Fig. 38: IPET 3D reconstruction and model fitting of an individual unit-cell particle (Index: 030) within a 2D lattice with 100% ferritin loading. a, Seven representative tilt images of a single unit-cell particle are shown in the first column (from left). The tilt images are aligned to a common center using IPET through iterative refinement. The projections of the raw, intermediate, and final 3D reconstruction at the corresponding angles are displayed in the subsequent four columns. **b**, A central cross-section (~23 nm thick) of the final reconstruction before masking is applied. **c**, 3D views of the central cross-section. **d**, Final 3D density map of this particle, viewed from four perpendicular directions. **e**, Final 3D reconstruction superimposed with the fitted model, viewed from four perpendicular directions. **f**, FSC analyses of the final map resolution using two methods: map-map FSC, where each map is reconstructed from one half of the images (even vs. odd tilt angle indices), and map-model FSC, where the model map is generated from the fitted model. Resolution assessments are provided based on tilt-based map-map and map-model FSC analyses at thresholds of FSC=0.5 and 0.143, respectively.

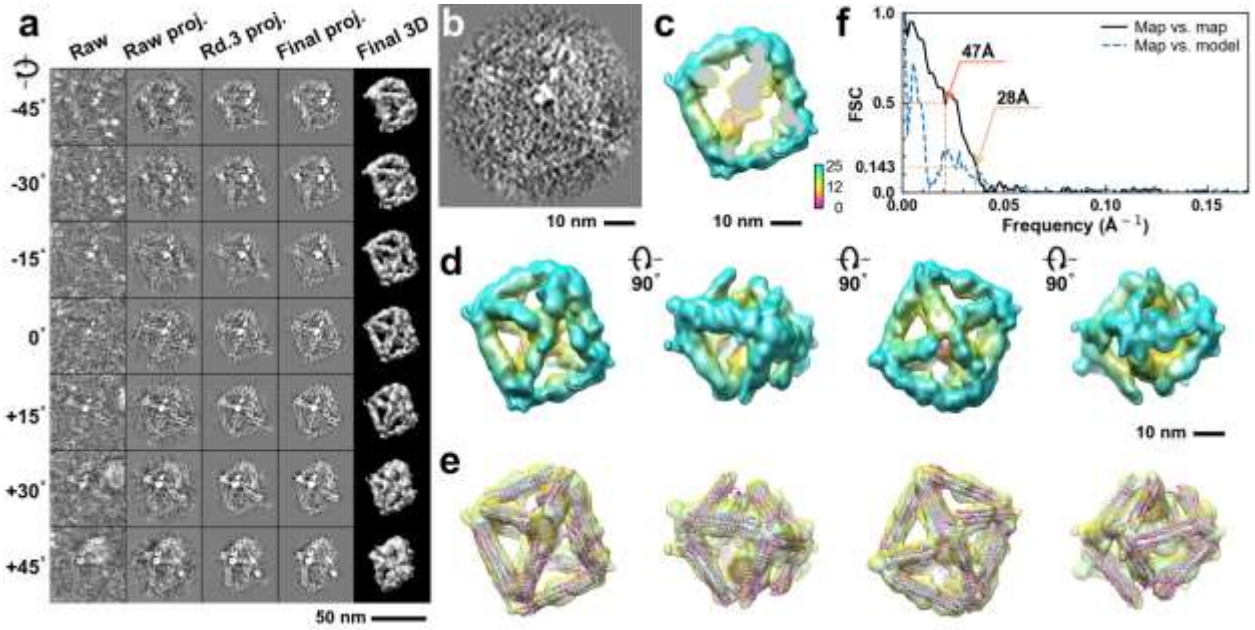

Supplementary Fig. 39: IPET 3D reconstruction and model fitting of an individual unit-cell particle (Index: 031) within a 2D lattice with 100% ferritin loading. a, Seven representative tilt images of a single unit-cell particle are shown in the first column (from left). The tilt images are aligned to a common center using IPET through iterative refinement. The projections of the raw, intermediate, and final 3D reconstruction at the corresponding angles are displayed in the subsequent four columns. **b**, A central cross-section (~23 nm thick) of the final reconstruction before masking is applied. **c**, 3D views of the central cross-section. **d**, Final 3D density map of this particle, viewed from four perpendicular directions. **e**, Final 3D reconstruction superimposed with the fitted model, viewed from four perpendicular directions. **f**, FSC analyses of the final map resolution using two methods: map-map FSC, where each map is reconstructed from one half of the images (even vs. odd tilt angle indices), and map-model FSC, where the model map is generated from the fitted model. Resolution assessments are provided based on tilt-based map-map and map-model FSC analyses at thresholds of FSC=0.5 and 0.143, respectively.

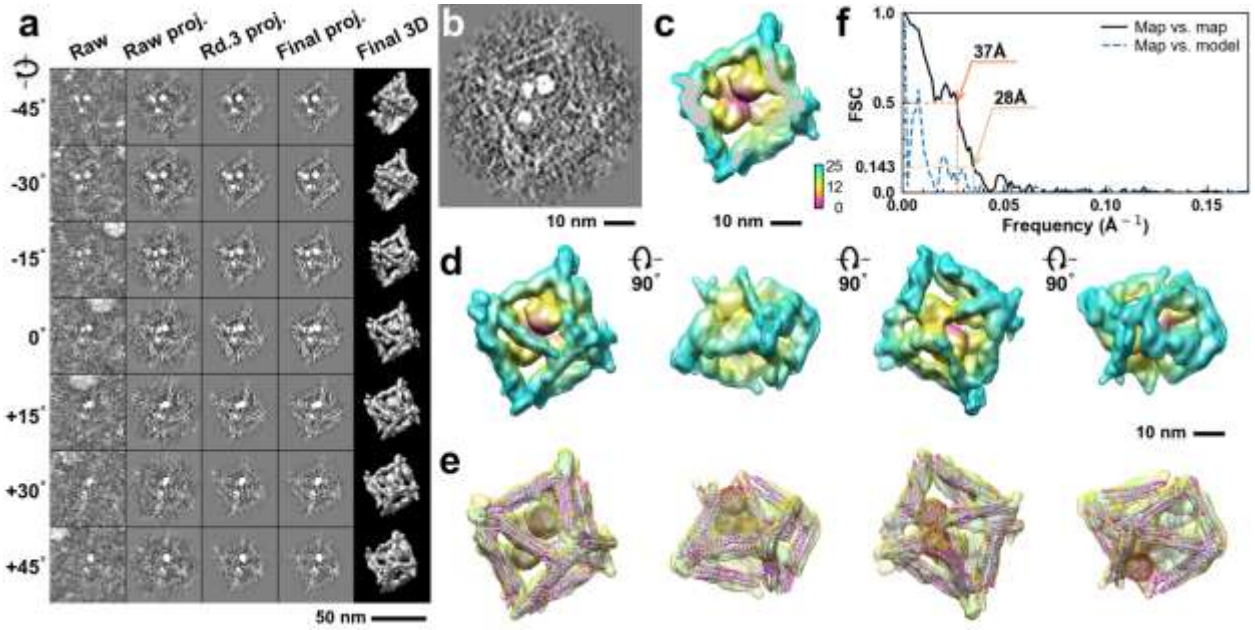

Supplementary Fig. 40: IPET 3D reconstruction and model fitting of an individual unit-cell particle (Index: 032) within a 2D lattice with 100% ferritin loading. a, Seven representative tilt images of a single unit-cell particle are shown in the first column (from left). The tilt images are aligned to a common center using IPET through iterative refinement. The projections of the raw, intermediate, and final 3D reconstruction at the corresponding angles are displayed in the subsequent four columns. **b**, A central cross-section (~23 nm thick) of the final reconstruction before masking is applied. **c**, 3D views of the central cross-section. **d**, Final 3D density map of this particle, viewed from four perpendicular directions. **e**, Final 3D reconstruction superimposed with the fitted model, viewed from four perpendicular directions. **f**, FSC analyses of the final map resolution using two methods: map-map FSC, where each map is reconstructed from one half of the images (even vs. odd tilt angle indices), and map-model FSC, where the model map is generated from the fitted model. Resolution assessments are provided based on tilt-based map-map and map-model FSC analyses at thresholds of FSC=0.5 and 0.143, respectively.

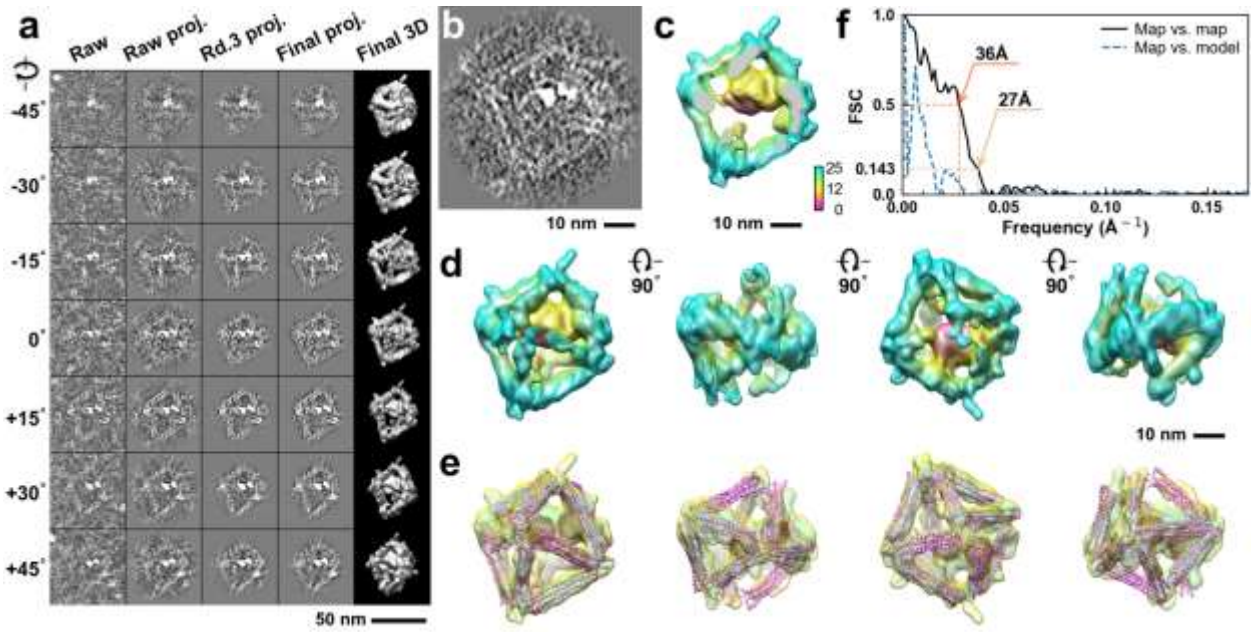

Supplementary Fig. 41: IPET 3D reconstruction and model fitting of an individual unit-cell particle (Index: 033) within a 2D lattice with 100% ferritin loading. a, Seven representative tilt images of a single unit-cell particle are shown in the first column (from left). The tilt images are aligned to a common center using IPET through iterative refinement. The projections of the raw, intermediate, and final 3D reconstruction at the corresponding angles are displayed in the subsequent four columns. **b**, A central cross-section (~23 nm thick) of the final reconstruction before masking is applied. **c**, 3D views of the central cross-section. **d**, Final 3D density map of this particle, viewed from four perpendicular directions. **e**, Final 3D reconstruction superimposed with the fitted model, viewed from four perpendicular directions. **f**, FSC analyses of the final map resolution using two methods: map-map FSC, where each map is reconstructed from one half of the images (even vs. odd tilt angle indices), and map-model FSC, where the model map is generated from the fitted model. Resolution assessments are provided based on tilt-based map-map and map-model FSC analyses at thresholds of FSC=0.5 and 0.143, respectively.

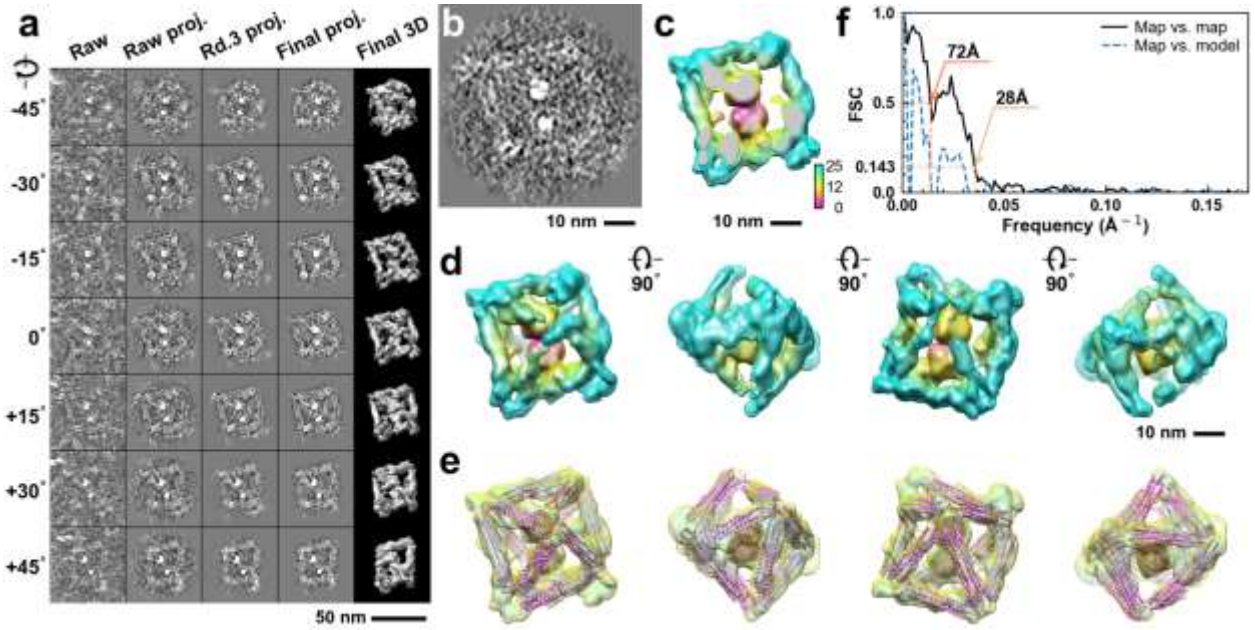

Supplementary Fig. 42: IPET 3D reconstruction and model fitting of an individual unit-cell particle (Index: 034) within a 2D lattice with 100% ferritin loading. a, Seven representative tilt images of a single unit-cell particle are shown in the first column (from left). The tilt images are aligned to a common center using IPET through iterative refinement. The projections of the raw, intermediate, and final 3D reconstruction at the corresponding angles are displayed in the subsequent four columns. **b**, A central cross-section (~23 nm thick) of the final reconstruction before masking is applied. **c**, 3D views of the central cross-section. **d**, Final 3D density map of this particle, viewed from four perpendicular directions. **e**, Final 3D reconstruction superimposed with the fitted model, viewed from four perpendicular directions. **f**, FSC analyses of the final map resolution using two methods: map-map FSC, where each map is reconstructed from one half of the images (even vs. odd tilt angle indices), and map-model FSC, where the model map is generated from the fitted model. Resolution assessments are provided based on tilt-based map-map and map-model FSC analyses at thresholds of FSC=0.5 and 0.143, respectively.

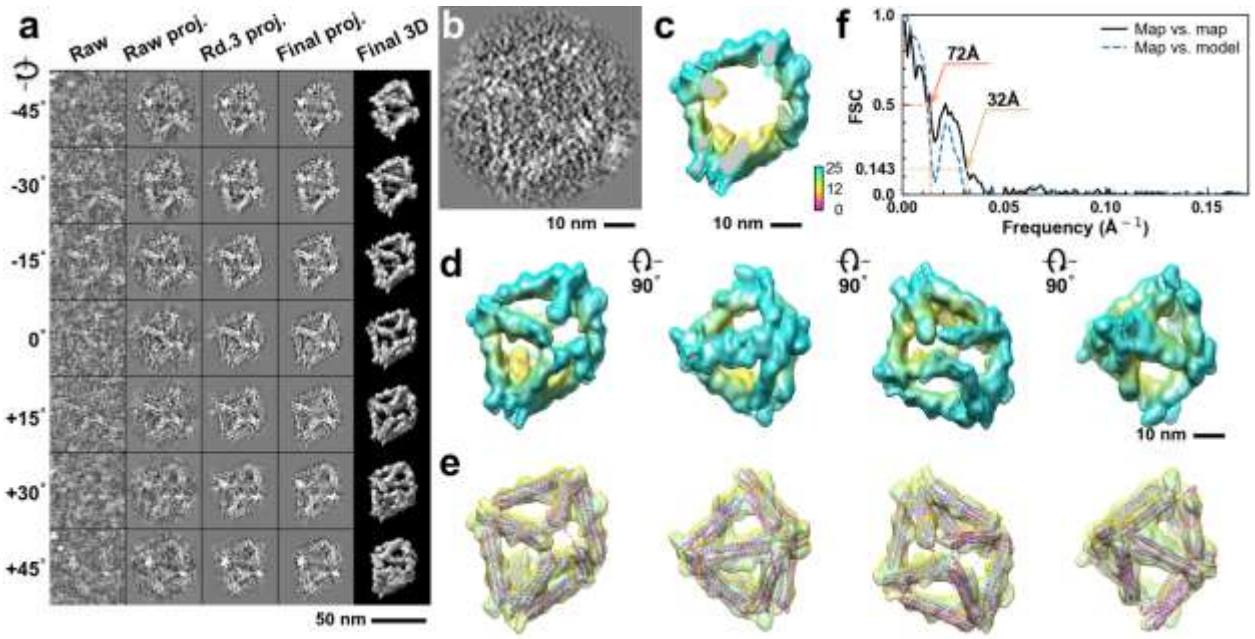

Supplementary Fig. 43: IPET 3D reconstruction and model fitting of an individual unit-cell particle (Index: 035) within a 2D lattice with 100% ferritin loading. a, Seven representative tilt images of a single unit-cell particle are shown in the first column (from left). The tilt images are aligned to a common center using IPET through iterative refinement. The projections of the raw, intermediate, and final 3D reconstruction at the corresponding angles are displayed in the subsequent four columns. **b**, A central cross-section (~23 nm thick) of the final reconstruction before masking is applied. **c**, 3D views of the central cross-section. **d**, Final 3D density map of this particle, viewed from four perpendicular directions. **e**, Final 3D reconstruction superimposed with the fitted model, viewed from four perpendicular directions. **f**, FSC analyses of the final map resolution using two methods: map-map FSC, where each map is reconstructed from one half of the images (even vs. odd tilt angle indices), and map-model FSC, where the model map is generated from the fitted model. Resolution assessments are provided based on tilt-based map-map and map-model FSC analyses at thresholds of FSC=0.5 and 0.143, respectively.

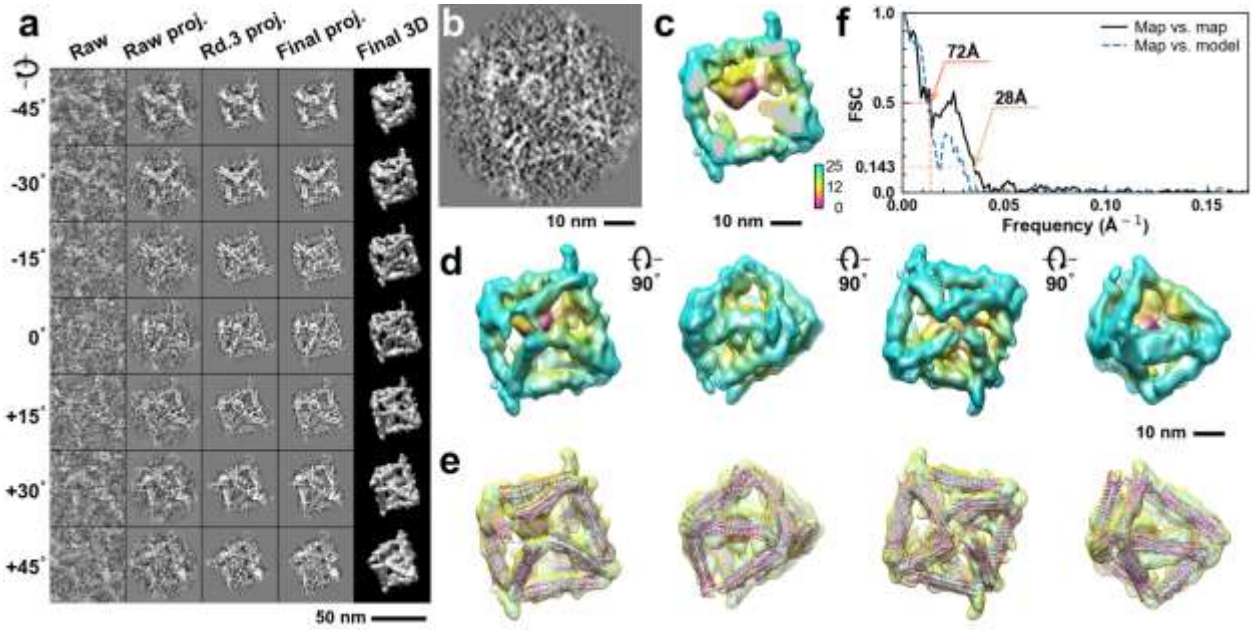

Supplementary Fig. 44: IPET 3D reconstruction and model fitting of an individual unit-cell particle (Index: 036) within a 2D lattice with 100% ferritin loading. a, Seven representative tilt images of a single unit-cell particle are shown in the first column (from left). The tilt images are aligned to a common center using IPET through iterative refinement. The projections of the raw, intermediate, and final 3D reconstruction at the corresponding angles are displayed in the subsequent four columns. **b**, A central cross-section (~23 nm thick) of the final reconstruction before masking is applied. **c**, 3D views of the central cross-section. **d**, Final 3D density map of this particle, viewed from four perpendicular directions. **e**, Final 3D reconstruction superimposed with the fitted model, viewed from four perpendicular directions. **f**, FSC analyses of the final map resolution using two methods: map-map FSC, where each map is reconstructed from one half of the images (even vs. odd tilt angle indices), and map-model FSC, where the model map is generated from the fitted model. Resolution assessments are provided based on tilt-based map-map and map-model FSC analyses at thresholds of FSC=0.5 and 0.143, respectively.

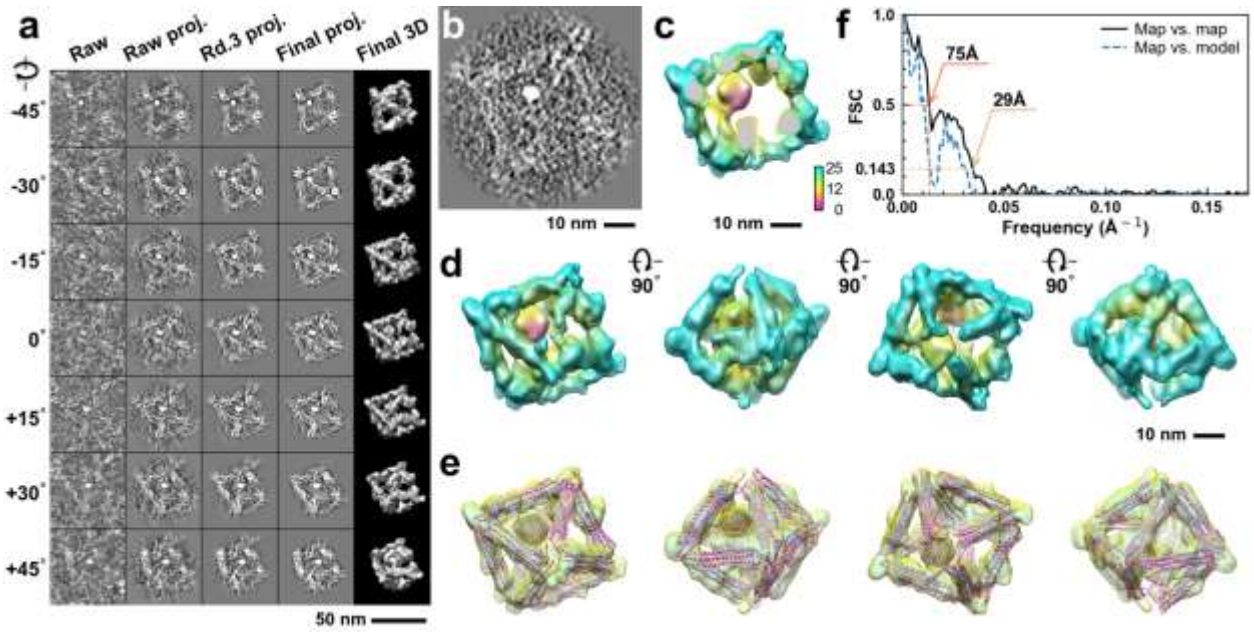

Supplementary Fig. 45: IPET 3D reconstruction and model fitting of an individual unit-cell particle (Index: 037) within a 2D lattice with 100% ferritin loading. a, Seven representative tilt images of a single unit-cell particle are shown in the first column (from left). The tilt images are aligned to a common center using IPET through iterative refinement. The projections of the raw, intermediate, and final 3D reconstruction at the corresponding angles are displayed in the subsequent four columns. **b**, A central cross-section (~23 nm thick) of the final reconstruction before masking is applied. **c**, 3D views of the central cross-section. **d**, Final 3D density map of this particle, viewed from four perpendicular directions. **e**, Final 3D reconstruction superimposed with the fitted model, viewed from four perpendicular directions. **f**, FSC analyses of the final map resolution using two methods: map-map FSC, where each map is reconstructed from one half of the images (even vs. odd tilt angle indices), and map-model FSC, where the model map is generated from the fitted model. Resolution assessments are provided based on tilt-based map-map and map-model FSC analyses at thresholds of FSC=0.5 and 0.143, respectively.

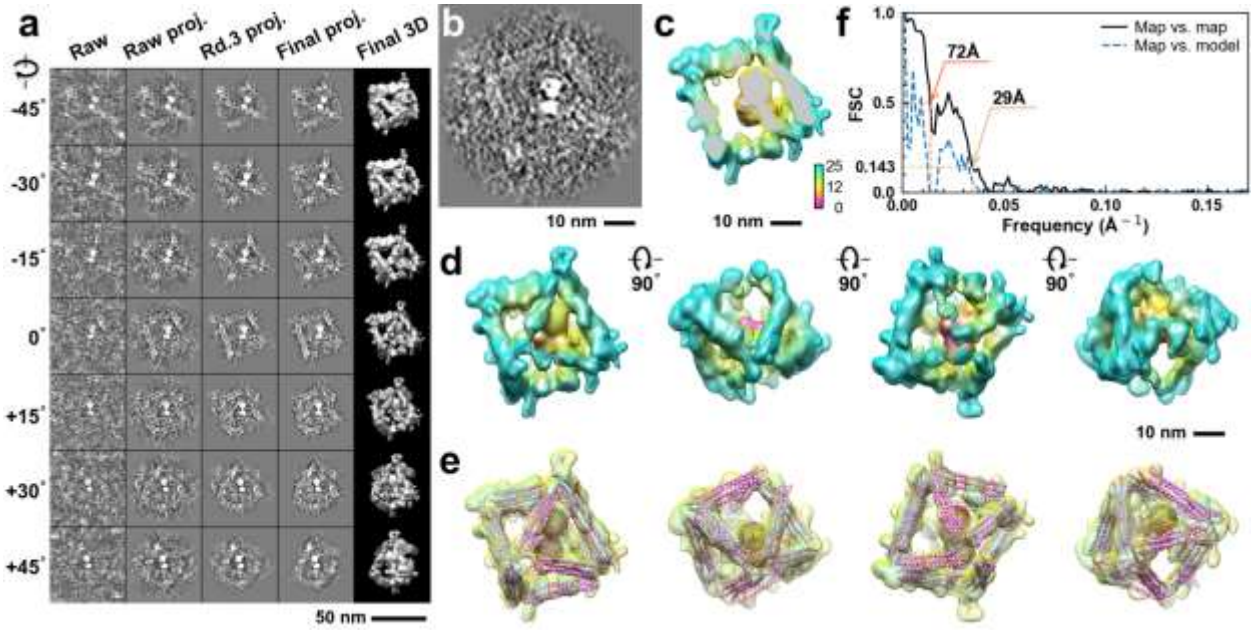

Supplementary Fig. 46: IPET 3D reconstruction and model fitting of an individual unit-cell particle (Index: 038) within a 2D lattice with 100% ferritin loading. a, Seven representative tilt images of a single unit-cell particle are shown in the first column (from left). The tilt images are aligned to a common center using IPET through iterative refinement. The projections of the raw, intermediate, and final 3D reconstruction at the corresponding angles are displayed in the subsequent four columns. **b**, A central cross-section (~23 nm thick) of the final reconstruction before masking is applied. **c**, 3D views of the central cross-section. **d**, Final 3D density map of this particle, viewed from four perpendicular directions. **e**, Final 3D reconstruction superimposed with the fitted model, viewed from four perpendicular directions. **f**, FSC analyses of the final map resolution using two methods: map-map FSC, where each map is reconstructed from one half of the images (even vs. odd tilt angle indices), and map-model FSC, where the model map is generated from the fitted model. Resolution assessments are provided based on tilt-based map-map and map-model FSC analyses at thresholds of FSC=0.5 and 0.143, respectively.

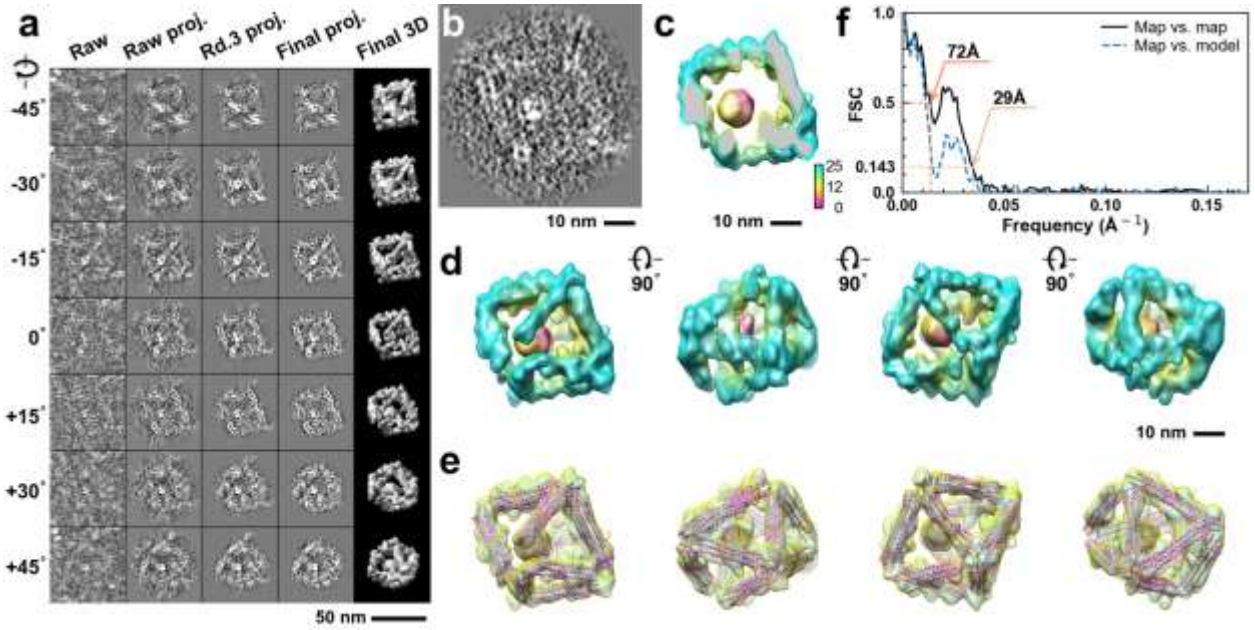

Supplementary Fig. 47: IPET 3D reconstruction and model fitting of an individual unit-cell particle (Index: 039) within a 2D lattice with 100% ferritin loading. a, Seven representative tilt images of a single unit-cell particle are shown in the first column (from left). The tilt images are aligned to a common center using IPET through iterative refinement. The projections of the raw, intermediate, and final 3D reconstruction at the corresponding angles are displayed in the subsequent four columns. **b**, A central cross-section (~23 nm thick) of the final reconstruction before masking is applied. **c**, 3D views of the central cross-section. **d**, Final 3D density map of this particle, viewed from four perpendicular directions. **e**, Final 3D reconstruction superimposed with the fitted model, viewed from four perpendicular directions. **f**, FSC analyses of the final map resolution using two methods: map-map FSC, where each map is reconstructed from one half of the images (even vs. odd tilt angle indices), and map-model FSC, where the model map is generated from the fitted model. Resolution assessments are provided based on tilt-based map-map and map-model FSC analyses at thresholds of FSC=0.5 and 0.143, respectively.

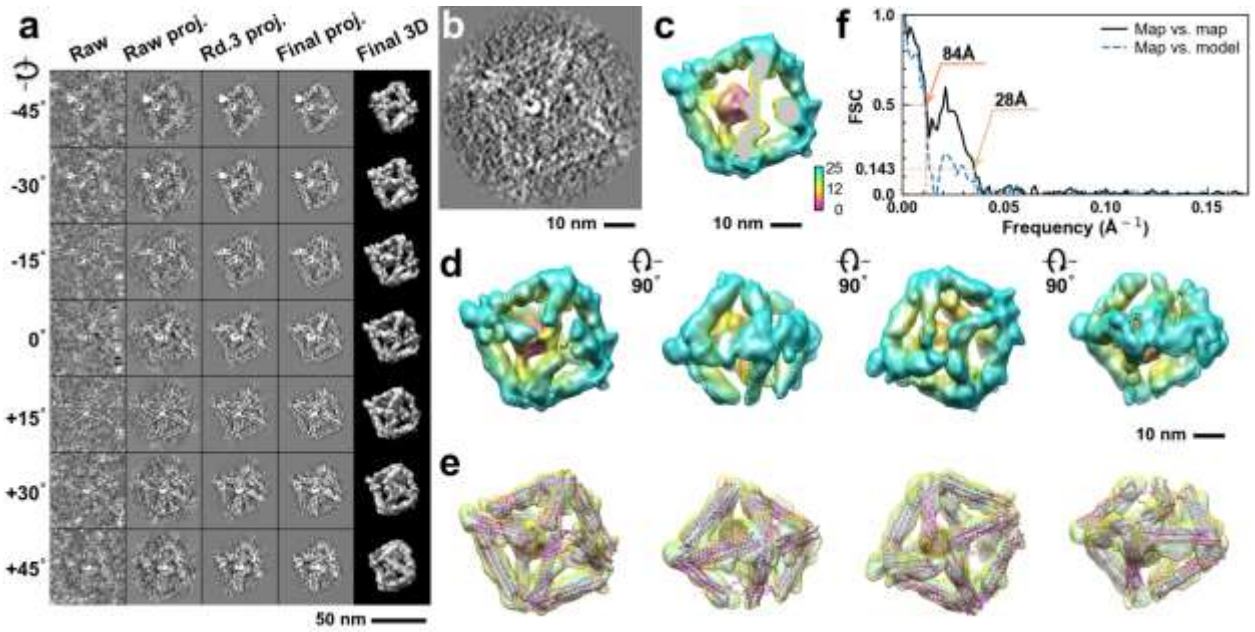

Supplementary Fig. 48: IPET 3D reconstruction and model fitting of an individual unit-cell particle (Index: 040) within a 2D lattice with 100% ferritin loading. a, Seven representative tilt images of a single unit-cell particle are shown in the first column (from left). The tilt images are aligned to a common center using IPET through iterative refinement. The projections of the raw, intermediate, and final 3D reconstruction at the corresponding angles are displayed in the subsequent four columns. **b**, A central cross-section (~23 nm thick) of the final reconstruction before masking is applied. **c**, 3D views of the central cross-section. **d**, Final 3D density map of this particle, viewed from four perpendicular directions. **e**, Final 3D reconstruction superimposed with the fitted model, viewed from four perpendicular directions. **f**, FSC analyses of the final map resolution using two methods: map-map FSC, where each map is reconstructed from one half of the images (even vs. odd tilt angle indices), and map-model FSC, where the model map is generated from the fitted model. Resolution assessments are provided based on tilt-based map-map and map-model FSC analyses at thresholds of FSC=0.5 and 0.143, respectively.

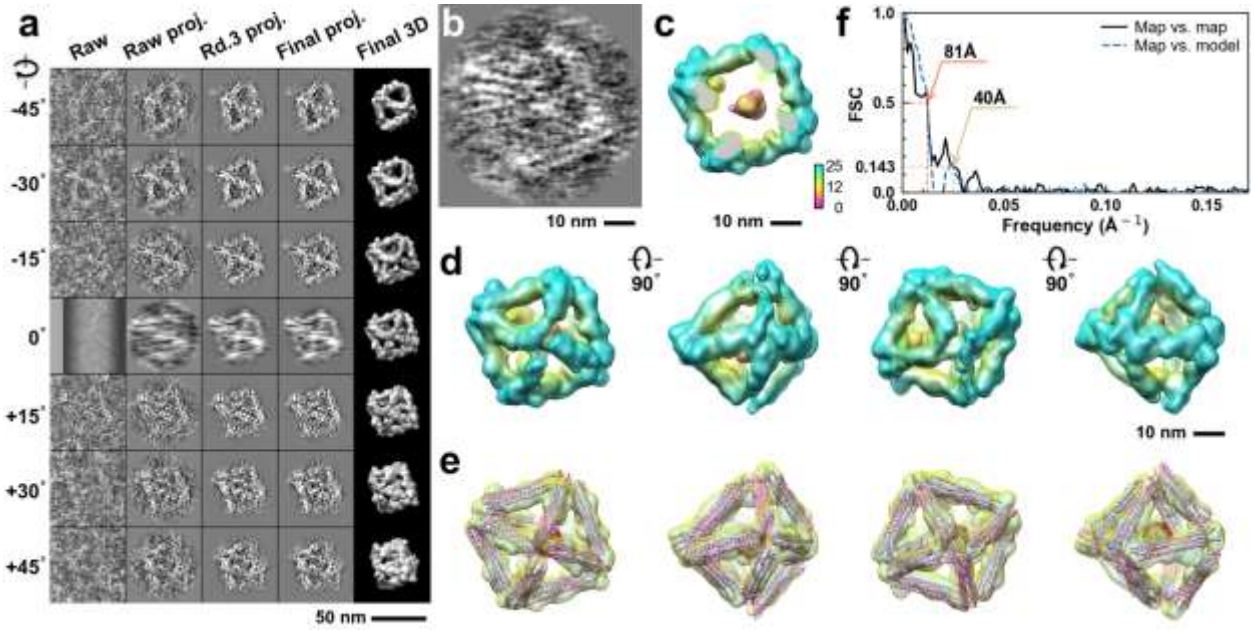

Supplementary Fig. 49: IPET 3D reconstruction and model fitting of an individual unit-cell particle (Index: 041) within a 2D lattice with 100% ferritin loading. a, Seven representative tilt images of a single unit-cell particle are shown in the first column (from left). The tilt images are aligned to a common center using IPET through iterative refinement. The projections of the raw, intermediate, and final 3D reconstruction at the corresponding angles are displayed in the subsequent four columns. **b**, A central cross-section (~23 nm thick) of the final reconstruction before masking is applied. **c**, 3D views of the central cross-section. **d**, Final 3D density map of this particle, viewed from four perpendicular directions. **e**, Final 3D reconstruction superimposed with the fitted model, viewed from four perpendicular directions. **f**, FSC analyses of the final map resolution using two methods: map-map FSC, where each map is reconstructed from one half of the images (even vs. odd tilt angle indices), and map-model FSC, where the model map is generated from the fitted model. Resolution assessments are provided based on tilt-based map-map and map-model FSC analyses at thresholds of FSC=0.5 and 0.143, respectively.

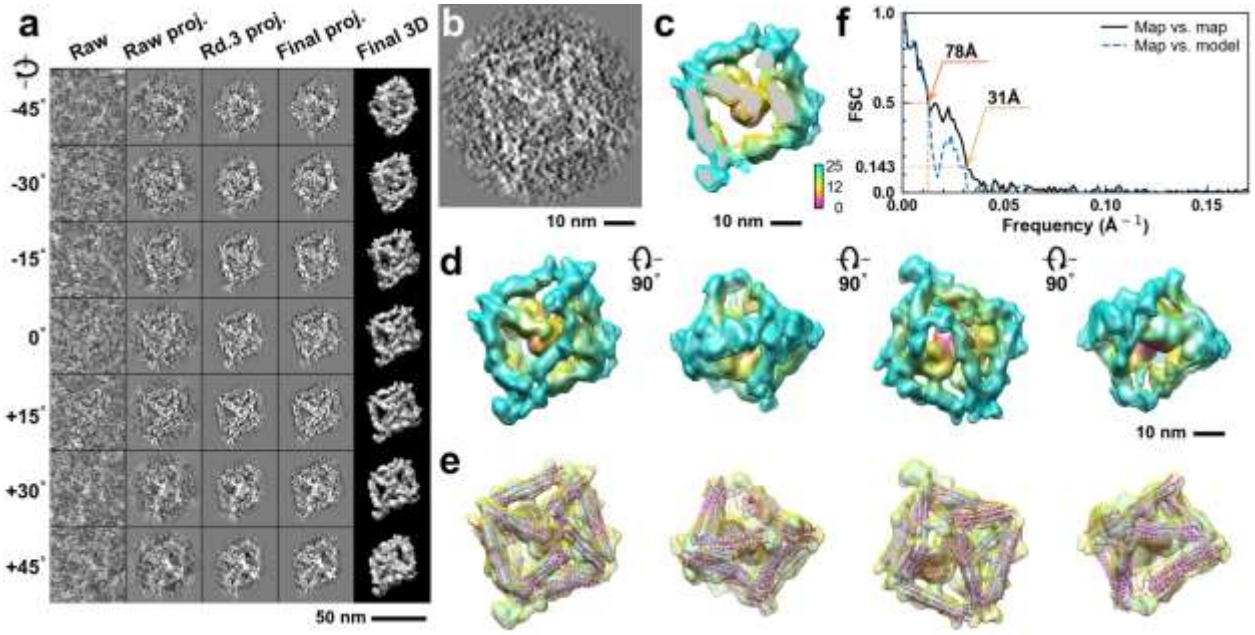

Supplementary Fig. 50: IPET 3D reconstruction and model fitting of an individual unit-cell particle (Index: 042) within a 2D lattice with 100% ferritin loading. a, Seven representative tilt images of a single unit-cell particle are shown in the first column (from left). The tilt images are aligned to a common center using IPET through iterative refinement. The projections of the raw, intermediate, and final 3D reconstruction at the corresponding angles are displayed in the subsequent four columns. **b**, A central cross-section (~23 nm thick) of the final reconstruction before masking is applied. **c**, 3D views of the central cross-section. **d**, Final 3D density map of this particle, viewed from four perpendicular directions. **e**, Final 3D reconstruction superimposed with the fitted model, viewed from four perpendicular directions. **f**, FSC analyses of the final map resolution using two methods: map-map FSC, where each map is reconstructed from one half of the images (even vs. odd tilt angle indices), and map-model FSC, where the model map is generated from the fitted model. Resolution assessments are provided based on tilt-based map-map and map-model FSC analyses at thresholds of FSC=0.5 and 0.143, respectively.

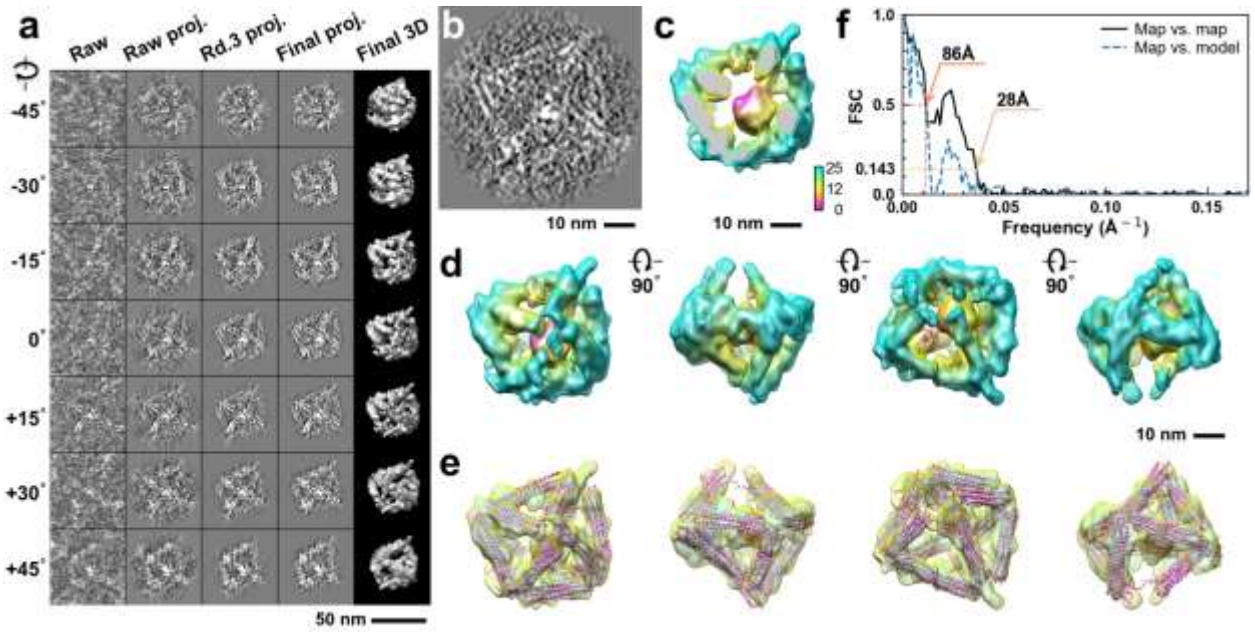

Supplementary Fig. 51: IPET 3D reconstruction and model fitting of an individual unit-cell particle (Index: 043) within a 2D lattice with 100% ferritin loading. a, Seven representative tilt images of a single unit-cell particle are shown in the first column (from left). The tilt images are aligned to a common center using IPET through iterative refinement. The projections of the raw, intermediate, and final 3D reconstruction at the corresponding angles are displayed in the subsequent four columns. **b**, A central cross-section (~23 nm thick) of the final reconstruction before masking is applied. **c**, 3D views of the central cross-section. **d**, Final 3D density map of this particle, viewed from four perpendicular directions. **e**, Final 3D reconstruction superimposed with the fitted model, viewed from four perpendicular directions. **f**, FSC analyses of the final map resolution using two methods: map-map FSC, where each map is reconstructed from one half of the images (even vs. odd tilt angle indices), and map-model FSC, where the model map is generated from the fitted model. Resolution assessments are provided based on tilt-based map-map and map-model FSC analyses at thresholds of FSC=0.5 and 0.143, respectively.

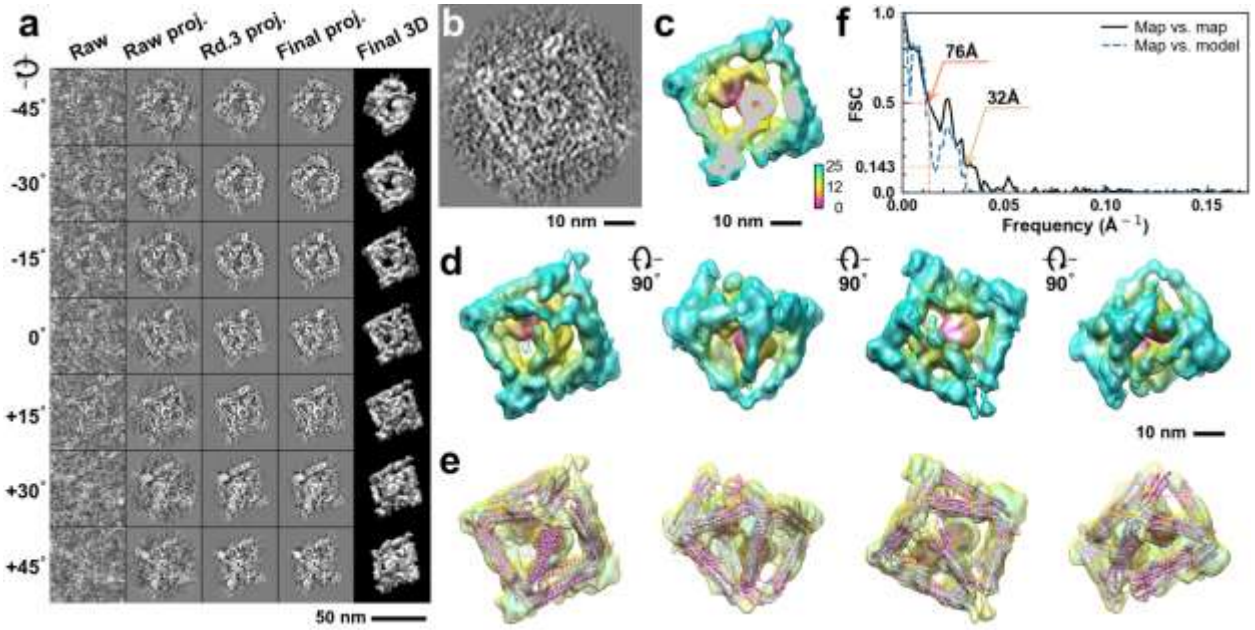

Supplementary Fig. 52: IPET 3D reconstruction and model fitting of an individual unit-cell particle (Index: 044) within a 2D lattice with 100% ferritin loading. a, Seven representative tilt images of a single unit-cell particle are shown in the first column (from left). The tilt images are aligned to a common center using IPET through iterative refinement. The projections of the raw, intermediate, and final 3D reconstruction at the corresponding angles are displayed in the subsequent four columns. **b**, A central cross-section (~23 nm thick) of the final reconstruction before masking is applied. **c**, 3D views of the central cross-section. **d**, Final 3D density map of this particle, viewed from four perpendicular directions. **e**, Final 3D reconstruction superimposed with the fitted model, viewed from four perpendicular directions. **f**, FSC analyses of the final map resolution using two methods: map-map FSC, where each map is reconstructed from one half of the images (even vs. odd tilt angle indices), and map-model FSC, where the model map is generated from the fitted model. Resolution assessments are provided based on tilt-based map-map and map-model FSC analyses at thresholds of FSC=0.5 and 0.143, respectively.

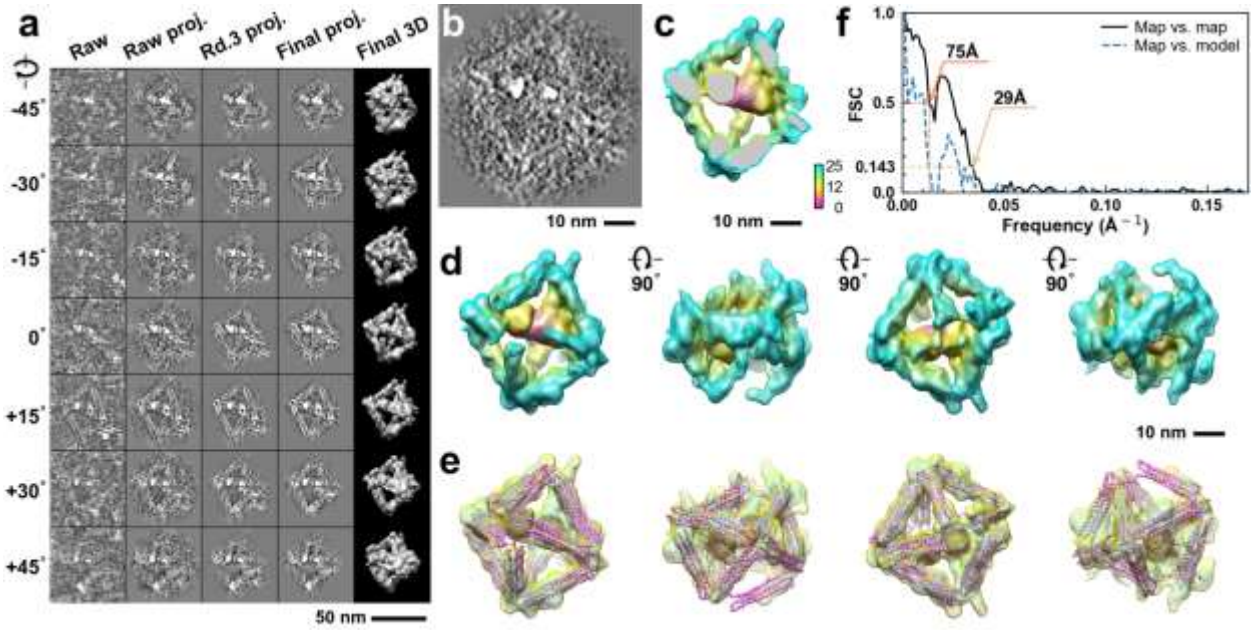

Supplementary Fig. 53: IPET 3D reconstruction and model fitting of an individual unit-cell particle (Index: 045) within a 2D lattice with 100% ferritin loading. a, Seven representative tilt images of a single unit-cell particle are shown in the first column (from left). The tilt images are aligned to a common center using IPET through iterative refinement. The projections of the raw, intermediate, and final 3D reconstruction at the corresponding angles are displayed in the subsequent four columns. **b**, A central cross-section (~23 nm thick) of the final reconstruction before masking is applied. **c**, 3D views of the central cross-section. **d**, Final 3D density map of this particle, viewed from four perpendicular directions. **e**, Final 3D reconstruction superimposed with the fitted model, viewed from four perpendicular directions. **f**, FSC analyses of the final map resolution using two methods: map-map FSC, where each map is reconstructed from one half of the images (even vs. odd tilt angle indices), and map-model FSC, where the model map is generated from the fitted model. Resolution assessments are provided based on tilt-based map-map and map-model FSC analyses at thresholds of FSC=0.5 and 0.143, respectively.

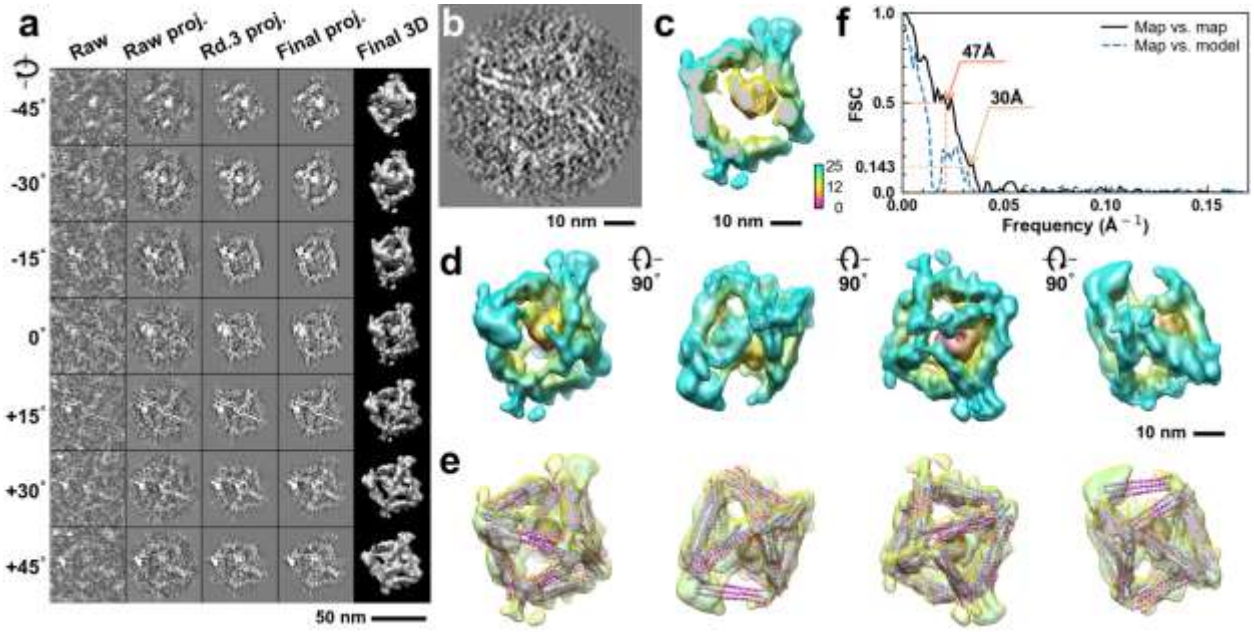

Supplementary Fig. 54: IPET 3D reconstruction and model fitting of an individual unit-cell particle (Index: 046) within a 2D lattice with 100% ferritin loading. a, Seven representative tilt images of a single unit-cell particle are shown in the first column (from left). The tilt images are aligned to a common center using IPET through iterative refinement. The projections of the raw, intermediate, and final 3D reconstruction at the corresponding angles are displayed in the subsequent four columns. **b**, A central cross-section (~23 nm thick) of the final reconstruction before masking is applied. **c**, 3D views of the central cross-section. **d**, Final 3D density map of this particle, viewed from four perpendicular directions. **e**, Final 3D reconstruction superimposed with the fitted model, viewed from four perpendicular directions. **f**, FSC analyses of the final map resolution using two methods: map-map FSC, where each map is reconstructed from one half of the images (even vs. odd tilt angle indices), and map-model FSC, where the model map is generated from the fitted model. Resolution assessments are provided based on tilt-based map-map and map-model FSC analyses at thresholds of FSC=0.5 and 0.143, respectively.

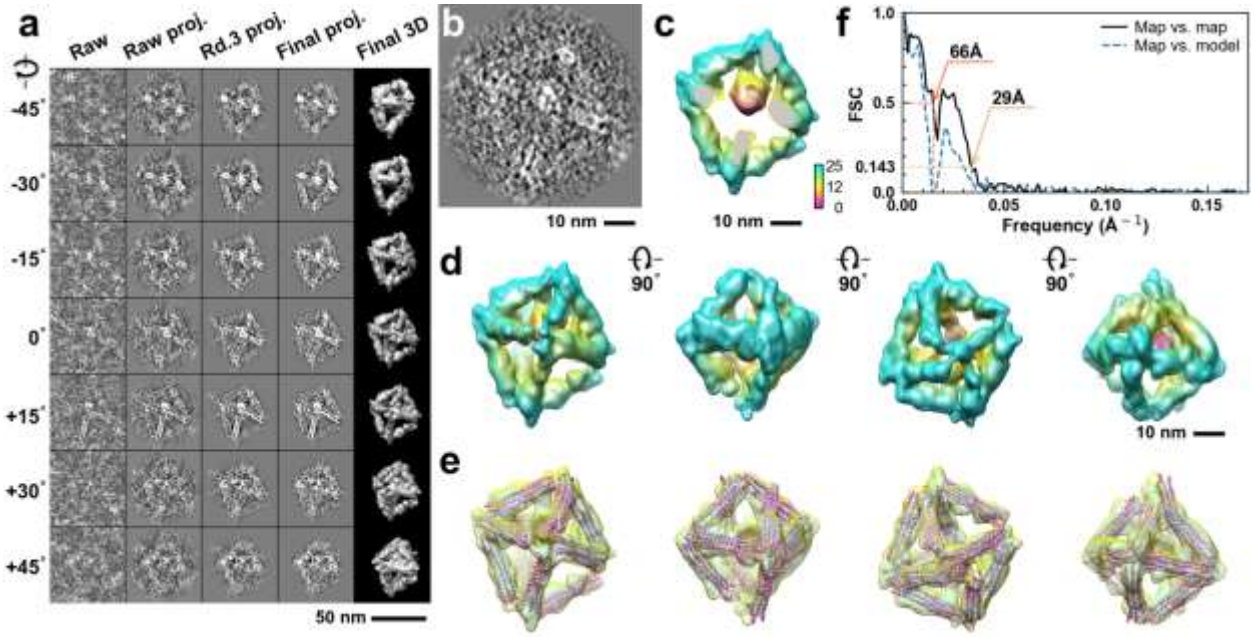

Supplementary Fig. 55: IPET 3D reconstruction and model fitting of an individual unit-cell particle (Index: 047) within a 2D lattice with 100% ferritin loading. a, Seven representative tilt images of a single unit-cell particle are shown in the first column (from left). The tilt images are aligned to a common center using IPET through iterative refinement. The projections of the raw, intermediate, and final 3D reconstruction at the corresponding angles are displayed in the subsequent four columns. **b**, A central cross-section (~23 nm thick) of the final reconstruction before masking is applied. **c**, 3D views of the central cross-section. **d**, Final 3D density map of this particle, viewed from four perpendicular directions. **e**, Final 3D reconstruction superimposed with the fitted model, viewed from four perpendicular directions. **f**, FSC analyses of the final map resolution using two methods: map-map FSC, where each map is reconstructed from one half of the images (even vs. odd tilt angle indices), and map-model FSC, where the model map is generated from the fitted model. Resolution assessments are provided based on tilt-based map-map and map-model FSC analyses at thresholds of FSC=0.5 and 0.143, respectively.

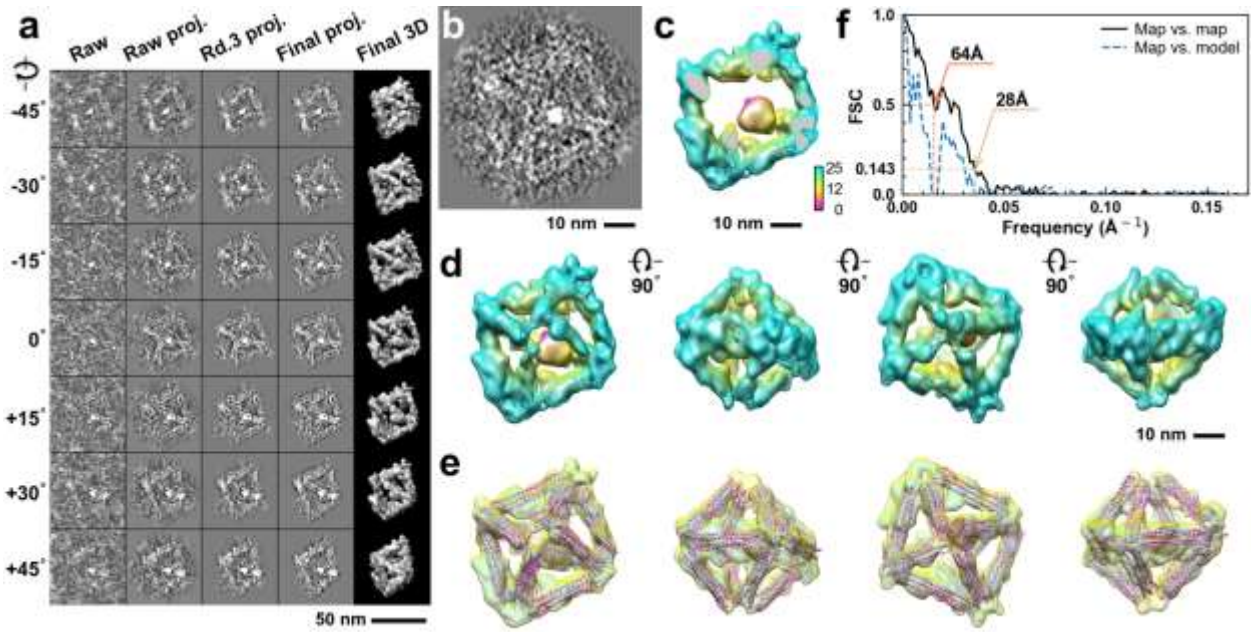

Supplementary Fig. 56: IPET 3D reconstruction and model fitting of an individual unit-cell particle (Index: 048) within a 2D lattice with 100% ferritin loading. a, Seven representative tilt images of a single unit-cell particle are shown in the first column (from left). The tilt images are aligned to a common center using IPET through iterative refinement. The projections of the raw, intermediate, and final 3D reconstruction at the corresponding angles are displayed in the subsequent four columns. **b**, A central cross-section (~23 nm thick) of the final reconstruction before masking is applied. **c**, 3D views of the central cross-section. **d**, Final 3D density map of this particle, viewed from four perpendicular directions. **e**, Final 3D reconstruction superimposed with the fitted model, viewed from four perpendicular directions. **f**, FSC analyses of the final map resolution using two methods: map-map FSC, where each map is reconstructed from one half of the images (even vs. odd tilt angle indices), and map-model FSC, where the model map is generated from the fitted model. Resolution assessments are provided based on tilt-based map-map and map-model FSC analyses at thresholds of FSC=0.5 and 0.143, respectively.

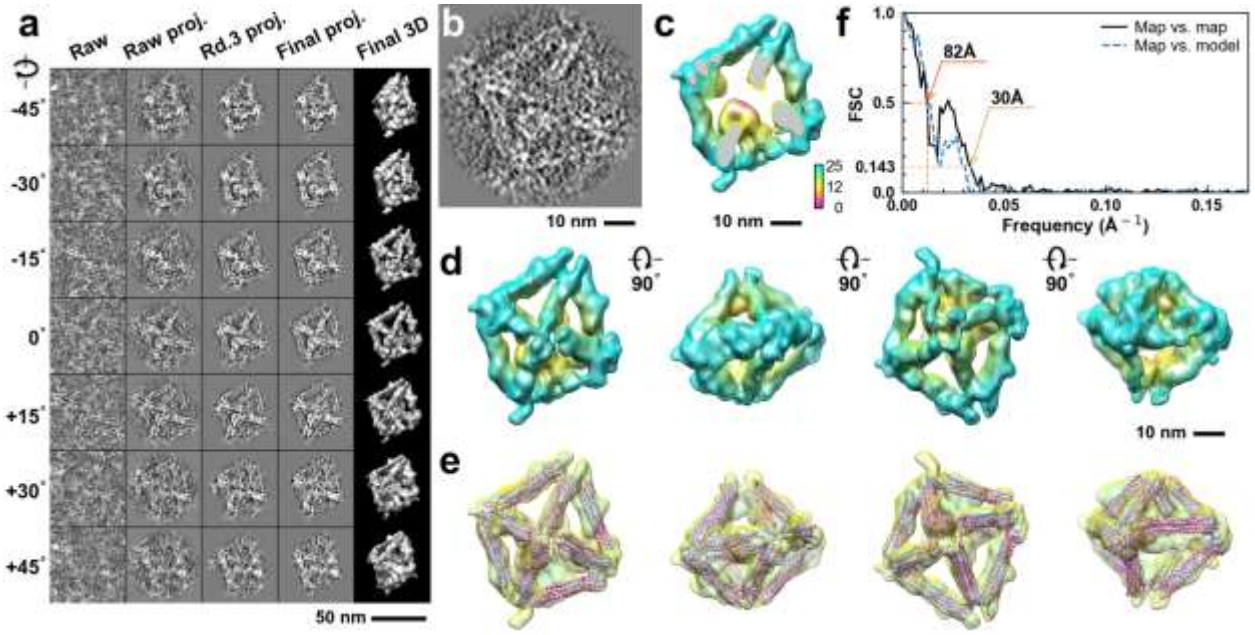

Supplementary Fig. 57: IPET 3D reconstruction and model fitting of an individual unit-cell particle (Index: 049) within a 2D lattice with 100% ferritin loading. a, Seven representative tilt images of a single unit-cell particle are shown in the first column (from left). The tilt images are aligned to a common center using IPET through iterative refinement. The projections of the raw, intermediate, and final 3D reconstruction at the corresponding angles are displayed in the subsequent four columns. **b**, A central cross-section (~23 nm thick) of the final reconstruction before masking is applied. **c**, 3D views of the central cross-section. **d**, Final 3D density map of this particle, viewed from four perpendicular directions. **e**, Final 3D reconstruction superimposed with the fitted model, viewed from four perpendicular directions. **f**, FSC analyses of the final map resolution using two methods: map-map FSC, where each map is reconstructed from one half of the images (even vs. odd tilt angle indices), and map-model FSC, where the model map is generated from the fitted model. Resolution assessments are provided based on tilt-based map-map and map-model FSC analyses at thresholds of FSC=0.5 and 0.143, respectively.

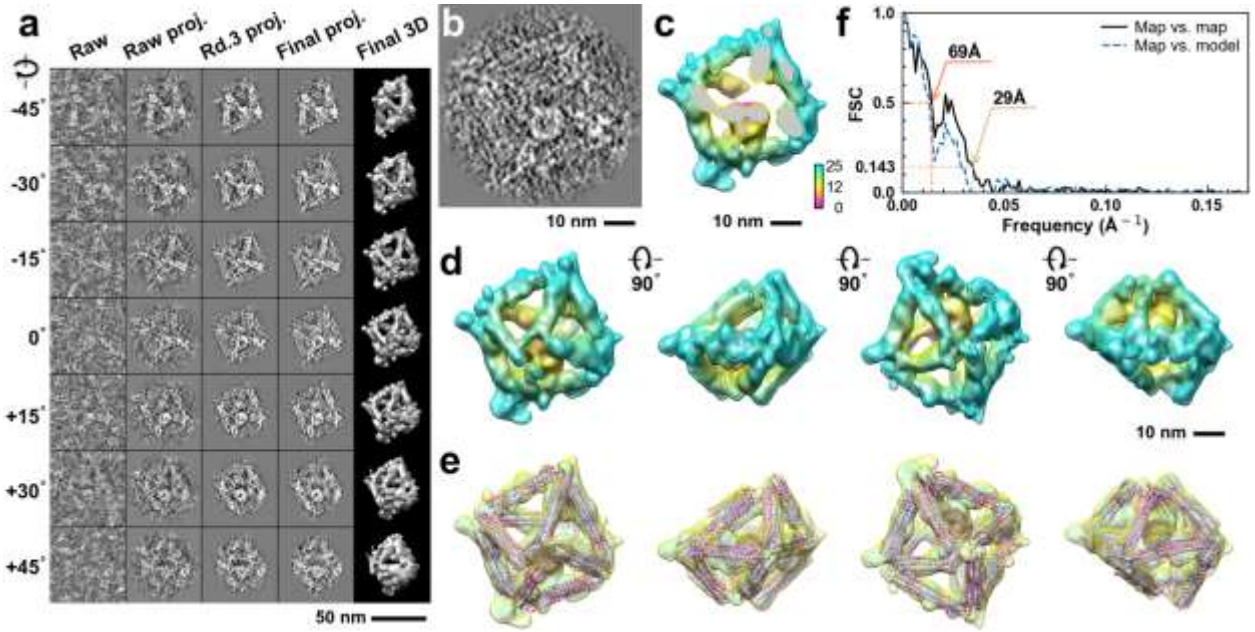

Supplementary Fig. 58: IPET 3D reconstruction and model fitting of an individual unit-cell particle (Index: 050) within a 2D lattice with 100% ferritin loading. a, Seven representative tilt images of a single unit-cell particle are shown in the first column (from left). The tilt images are aligned to a common center using IPET through iterative refinement. The projections of the raw, intermediate, and final 3D reconstruction at the corresponding angles are displayed in the subsequent four columns. **b**, A central cross-section (~23 nm thick) of the final reconstruction before masking is applied. **c**, 3D views of the central cross-section. **d**, Final 3D density map of this particle, viewed from four perpendicular directions. **e**, Final 3D reconstruction superimposed with the fitted model, viewed from four perpendicular directions. **f**, FSC analyses of the final map resolution using two methods: map-map FSC, where each map is reconstructed from one half of the images (even vs. odd tilt angle indices), and map-model FSC, where the model map is generated from the fitted model. Resolution assessments are provided based on tilt-based map-map and map-model FSC analyses at thresholds of FSC=0.5 and 0.143, respectively.

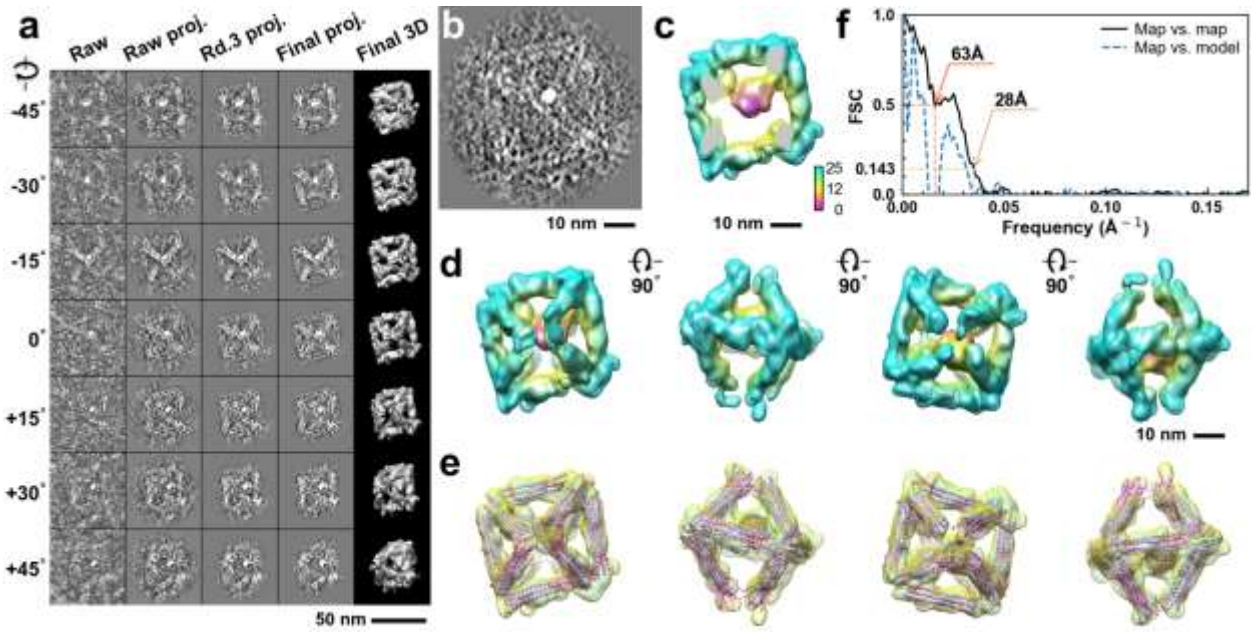

Supplementary Fig. 59: IPET 3D reconstruction and model fitting of an individual unit-cell particle (Index: 051) within a 2D lattice with 100% ferritin loading. a, Seven representative tilt images of a single unit-cell particle are shown in the first column (from left). The tilt images are aligned to a common center using IPET through iterative refinement. The projections of the raw, intermediate, and final 3D reconstruction at the corresponding angles are displayed in the subsequent four columns. **b**, A central cross-section (~23 nm thick) of the final reconstruction before masking is applied. **c**, 3D views of the central cross-section. **d**, Final 3D density map of this particle, viewed from four perpendicular directions. **e**, Final 3D reconstruction superimposed with the fitted model, viewed from four perpendicular directions. **f**, FSC analyses of the final map resolution using two methods: map-map FSC, where each map is reconstructed from one half of the images (even vs. odd tilt angle indices), and map-model FSC, where the model map is generated from the fitted model. Resolution assessments are provided based on tilt-based map-map and map-model FSC analyses at thresholds of FSC=0.5 and 0.143, respectively.

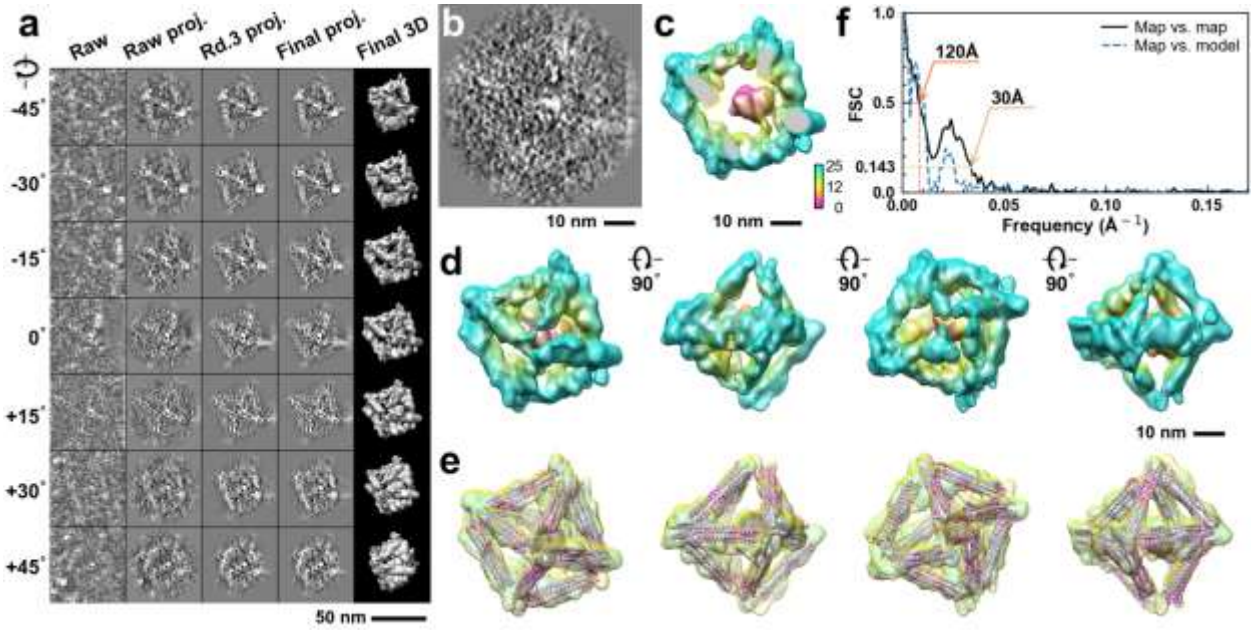

Supplementary Fig. 60: IPET 3D reconstruction and model fitting of an individual unit-cell particle (Index: 052) within a 2D lattice with 100% ferritin loading. a, Seven representative tilt images of a single unit-cell particle are shown in the first column (from left). The tilt images are aligned to a common center using IPET through iterative refinement. The projections of the raw, intermediate, and final 3D reconstruction at the corresponding angles are displayed in the subsequent four columns. **b**, A central cross-section (~23 nm thick) of the final reconstruction before masking is applied. **c**, 3D views of the central cross-section. **d**, Final 3D density map of this particle, viewed from four perpendicular directions. **e**, Final 3D reconstruction superimposed with the fitted model, viewed from four perpendicular directions. **f**, FSC analyses of the final map resolution using two methods: map-map FSC, where each map is reconstructed from one half of the images (even vs. odd tilt angle indices), and map-model FSC, where the model map is generated from the fitted model. Resolution assessments are provided based on tilt-based map-map and map-model FSC analyses at thresholds of FSC=0.5 and 0.143, respectively.

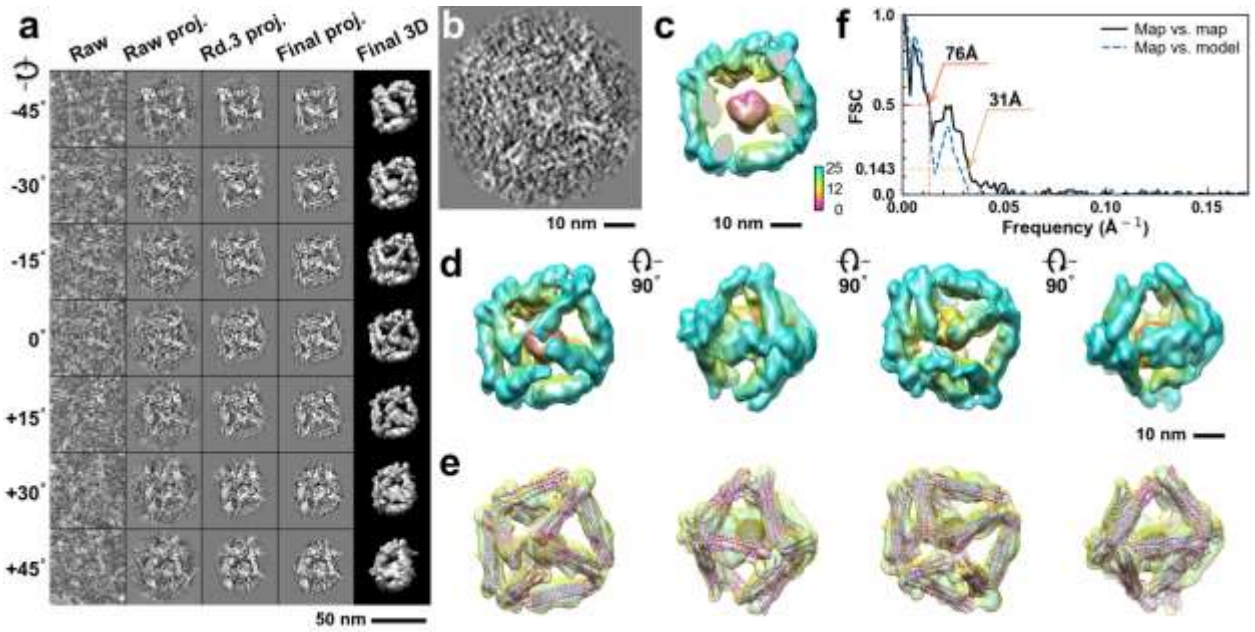

Supplementary Fig. 61: IPET 3D reconstruction and model fitting of an individual unit-cell particle (Index: 053) within a 2D lattice with 100% ferritin loading. a, Seven representative tilt images of a single unit-cell particle are shown in the first column (from left). The tilt images are aligned to a common center using IPET through iterative refinement. The projections of the raw, intermediate, and final 3D reconstruction at the corresponding angles are displayed in the subsequent four columns. **b**, A central cross-section (~23 nm thick) of the final reconstruction before masking is applied. **c**, 3D views of the central cross-section. **d**, Final 3D density map of this particle, viewed from four perpendicular directions. **e**, Final 3D reconstruction superimposed with the fitted model, viewed from four perpendicular directions. **f**, FSC analyses of the final map resolution using two methods: map-map FSC, where each map is reconstructed from one half of the images (even vs. odd tilt angle indices), and map-model FSC, where the model map is generated from the fitted model. Resolution assessments are provided based on tilt-based map-map and map-model FSC analyses at thresholds of FSC=0.5 and 0.143, respectively.

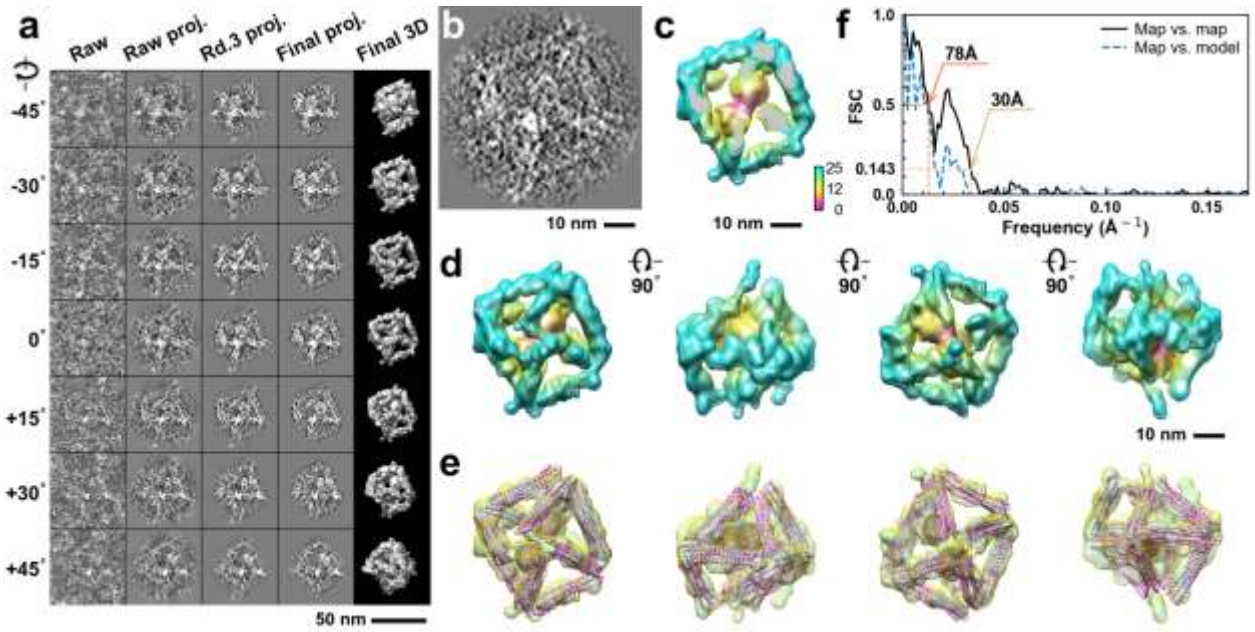

Supplementary Fig. 62: IPET 3D reconstruction and model fitting of an individual unit-cell particle (Index: 054) within a 2D lattice with 100% ferritin loading. a, Seven representative tilt images of a single unit-cell particle are shown in the first column (from left). The tilt images are aligned to a common center using IPET through iterative refinement. The projections of the raw, intermediate, and final 3D reconstruction at the corresponding angles are displayed in the subsequent four columns. **b**, A central cross-section (~23 nm thick) of the final reconstruction before masking is applied. **c**, 3D views of the central cross-section. **d**, Final 3D density map of this particle, viewed from four perpendicular directions. **e**, Final 3D reconstruction superimposed with the fitted model, viewed from four perpendicular directions. **f**, FSC analyses of the final map resolution using two methods: map-map FSC, where each map is reconstructed from one half of the images (even vs. odd tilt angle indices), and map-model FSC, where the model map is generated from the fitted model. Resolution assessments are provided based on tilt-based map-map and map-model FSC analyses at thresholds of FSC=0.5 and 0.143, respectively.

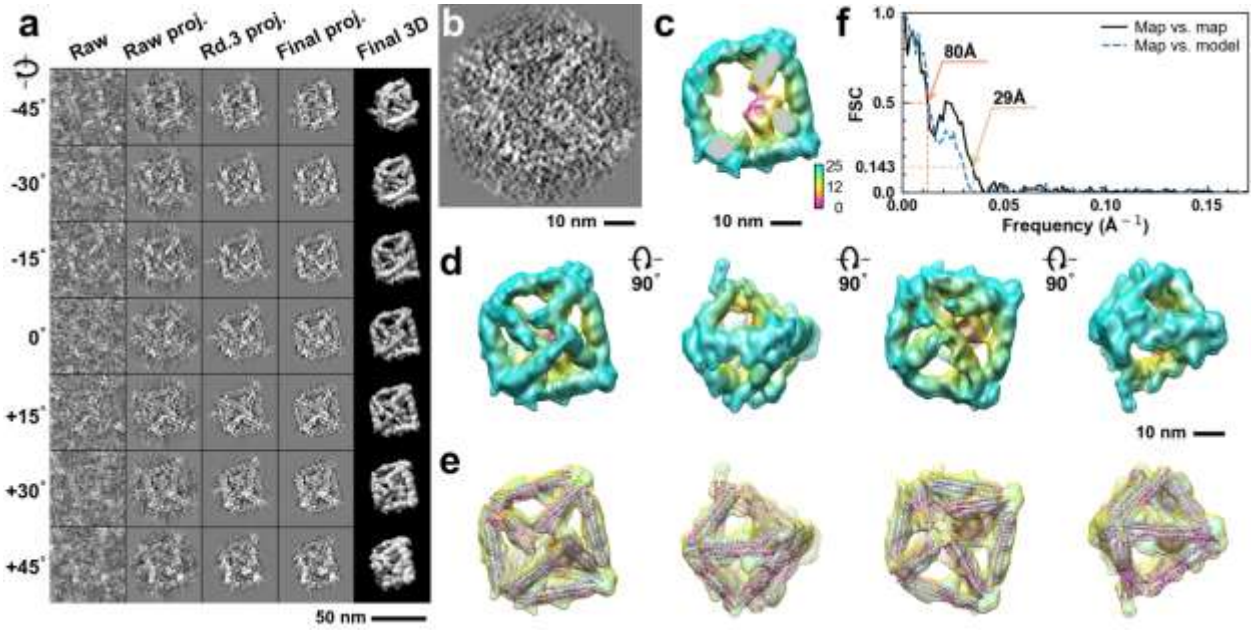

Supplementary Fig. 63: IPET 3D reconstruction and model fitting of an individual unit-cell particle (Index: 055) within a 2D lattice with 100% ferritin loading. a, Seven representative tilt images of a single unit-cell particle are shown in the first column (from left). The tilt images are aligned to a common center using IPET through iterative refinement. The projections of the raw, intermediate, and final 3D reconstruction at the corresponding angles are displayed in the subsequent four columns. **b**, A central cross-section (~23 nm thick) of the final reconstruction before masking is applied. **c**, 3D views of the central cross-section. **d**, Final 3D density map of this particle, viewed from four perpendicular directions. **e**, Final 3D reconstruction superimposed with the fitted model, viewed from four perpendicular directions. **f**, FSC analyses of the final map resolution using two methods: map-map FSC, where each map is reconstructed from one half of the images (even vs. odd tilt angle indices), and map-model FSC, where the model map is generated from the fitted model. Resolution assessments are provided based on tilt-based map-map and map-model FSC analyses at thresholds of FSC=0.5 and 0.143, respectively.

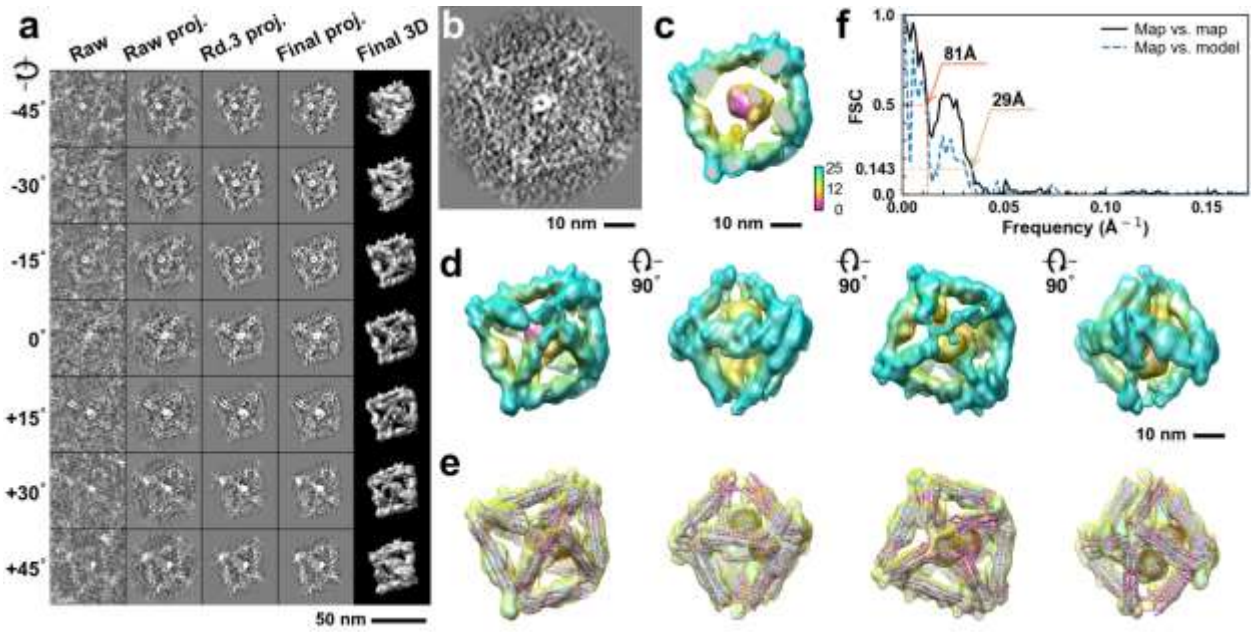

Supplementary Fig. 64: IPET 3D reconstruction and model fitting of an individual unit-cell particle (Index: 056) within a 2D lattice with 100% ferritin loading. a, Seven representative tilt images of a single unit-cell particle are shown in the first column (from left). The tilt images are aligned to a common center using IPET through iterative refinement. The projections of the raw, intermediate, and final 3D reconstruction at the corresponding angles are displayed in the subsequent four columns. **b**, A central cross-section (~23 nm thick) of the final reconstruction before masking is applied. **c**, 3D views of the central cross-section. **d**, Final 3D density map of this particle, viewed from four perpendicular directions. **e**, Final 3D reconstruction superimposed with the fitted model, viewed from four perpendicular directions. **f**, FSC analyses of the final map resolution using two methods: map-map FSC, where each map is reconstructed from one half of the images (even vs. odd tilt angle indices), and map-model FSC, where the model map is generated from the fitted model. Resolution assessments are provided based on tilt-based map-map and map-model FSC analyses at thresholds of FSC=0.5 and 0.143, respectively.

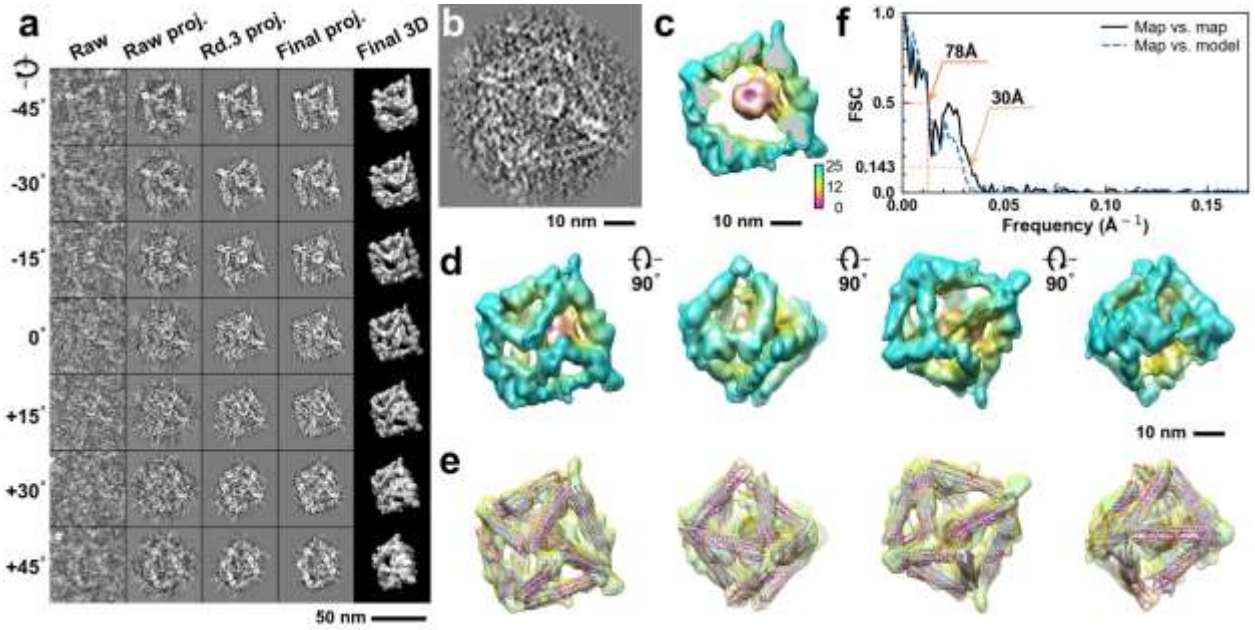

Supplementary Fig. 65: IPET 3D reconstruction and model fitting of an individual unit-cell particle (Index: 057) within a 2D lattice with 100% ferritin loading. a, Seven representative tilt images of a single unit-cell particle are shown in the first column (from left). The tilt images are aligned to a common center using IPET through iterative refinement. The projections of the raw, intermediate, and final 3D reconstruction at the corresponding angles are displayed in the subsequent four columns. **b**, A central cross-section (~23 nm thick) of the final reconstruction before masking is applied. **c**, 3D views of the central cross-section. **d**, Final 3D density map of this particle, viewed from four perpendicular directions. **e**, Final 3D reconstruction superimposed with the fitted model, viewed from four perpendicular directions. **f**, FSC analyses of the final map resolution using two methods: map-map FSC, where each map is reconstructed from one half of the images (even vs. odd tilt angle indices), and map-model FSC, where the model map is generated from the fitted model. Resolution assessments are provided based on tilt-based map-map and map-model FSC analyses at thresholds of FSC=0.5 and 0.143, respectively.

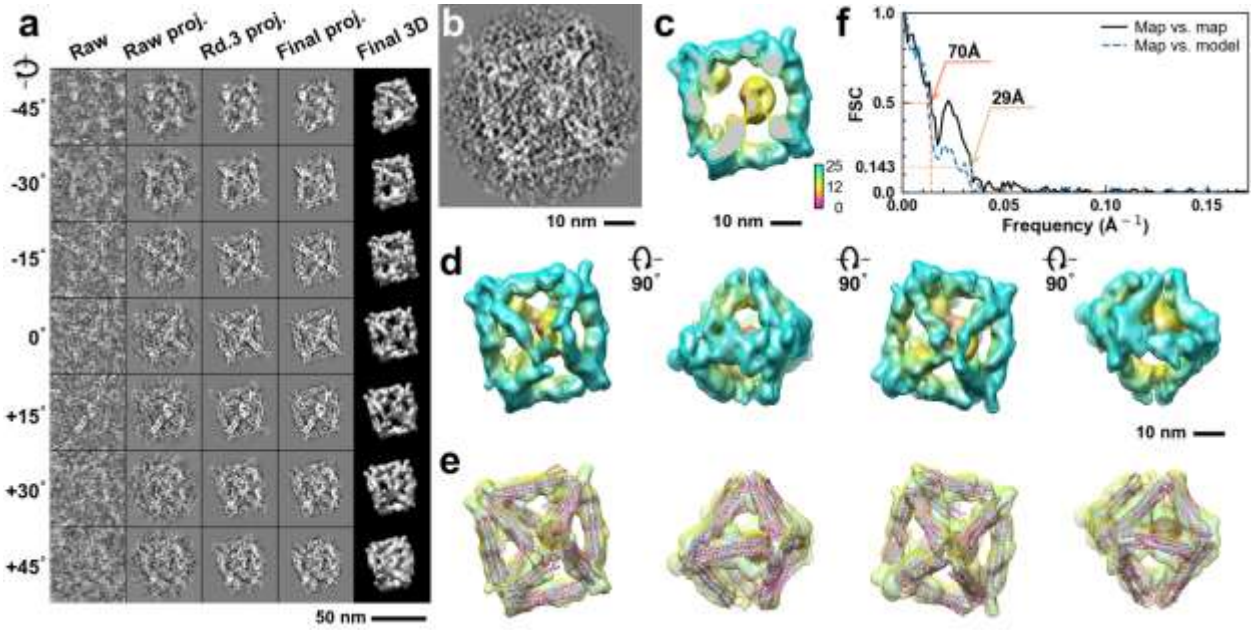

Supplementary Fig. 66: IPET 3D reconstruction and model fitting of an individual unit-cell particle (Index: 058) within a 2D lattice with 100% ferritin loading. a, Seven representative tilt images of a single unit-cell particle are shown in the first column (from left). The tilt images are aligned to a common center using IPET through iterative refinement. The projections of the raw, intermediate, and final 3D reconstruction at the corresponding angles are displayed in the subsequent four columns. **b**, A central cross-section (~23 nm thick) of the final reconstruction before masking is applied. **c**, 3D views of the central cross-section. **d**, Final 3D density map of this particle, viewed from four perpendicular directions. **e**, Final 3D reconstruction superimposed with the fitted model, viewed from four perpendicular directions. **f**, FSC analyses of the final map resolution using two methods: map-map FSC, where each map is reconstructed from one half of the images (even vs. odd tilt angle indices), and map-model FSC, where the model map is generated from the fitted model. Resolution assessments are provided based on tilt-based map-map and map-model FSC analyses at thresholds of FSC=0.5 and 0.143, respectively.

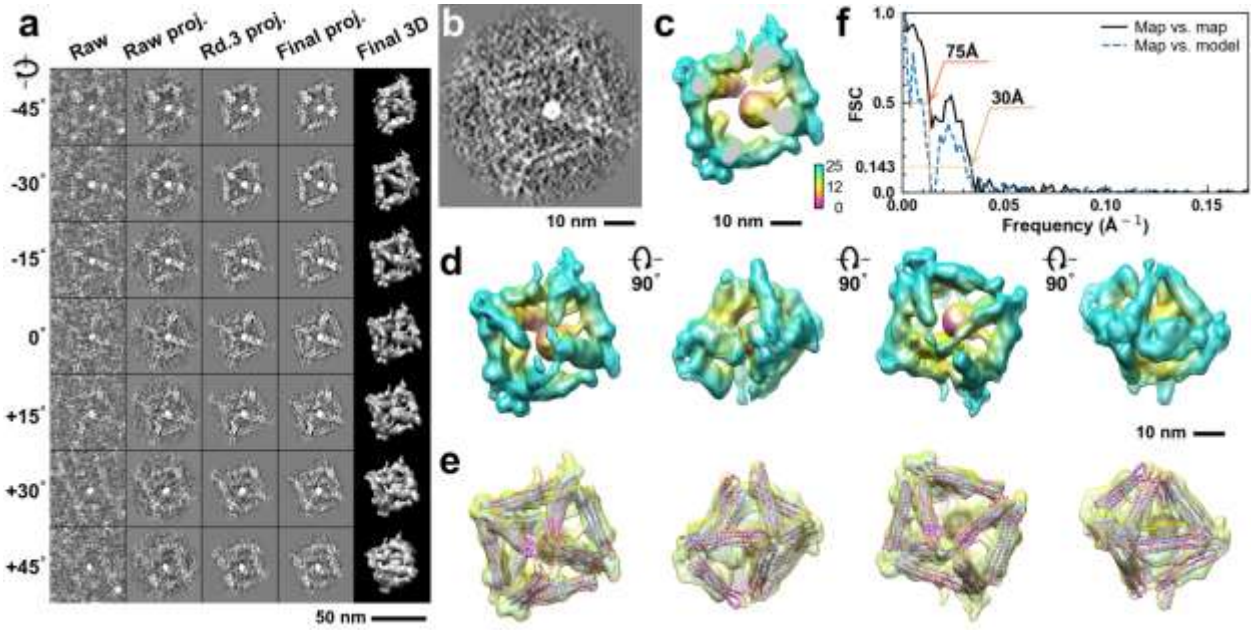

Supplementary Fig. 67: IPET 3D reconstruction and model fitting of an individual unit-cell particle (Index: 059) within a 2D lattice with 100% ferritin loading. a, Seven representative tilt images of a single unit-cell particle are shown in the first column (from left). The tilt images are aligned to a common center using IPET through iterative refinement. The projections of the raw, intermediate, and final 3D reconstruction at the corresponding angles are displayed in the subsequent four columns. **b**, A central cross-section (~23 nm thick) of the final reconstruction before masking is applied. **c**, 3D views of the central cross-section. **d**, Final 3D density map of this particle, viewed from four perpendicular directions. **e**, Final 3D reconstruction superimposed with the fitted model, viewed from four perpendicular directions. **f**, FSC analyses of the final map resolution using two methods: map-map FSC, where each map is reconstructed from one half of the images (even vs. odd tilt angle indices), and map-model FSC, where the model map is generated from the fitted model. Resolution assessments are provided based on tilt-based map-map and map-model FSC analyses at thresholds of FSC=0.5 and 0.143, respectively.

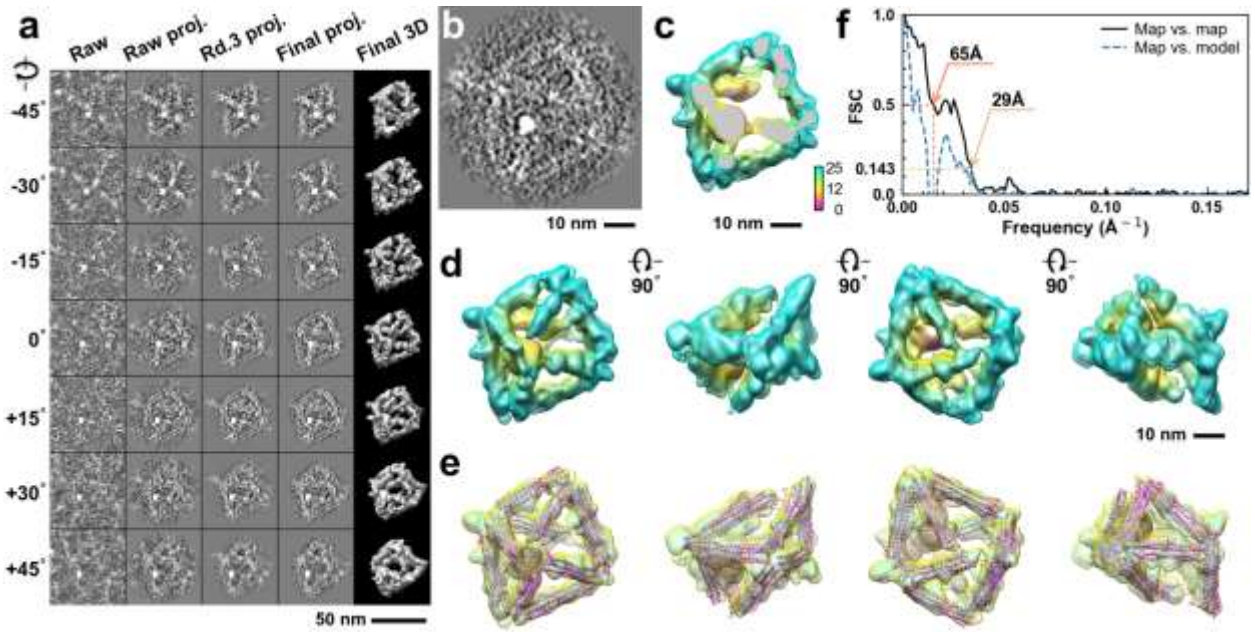

Supplementary Fig. 68: IPET 3D reconstruction and model fitting of an individual unit-cell particle (Index: 060) within a 2D lattice with 100% ferritin loading. a, Seven representative tilt images of a single unit-cell particle are shown in the first column (from left). The tilt images are aligned to a common center using IPET through iterative refinement. The projections of the raw, intermediate, and final 3D reconstruction at the corresponding angles are displayed in the subsequent four columns. **b**, A central cross-section (~23 nm thick) of the final reconstruction before masking is applied. **c**, 3D views of the central cross-section. **d**, Final 3D density map of this particle, viewed from four perpendicular directions. **e**, Final 3D reconstruction superimposed with the fitted model, viewed from four perpendicular directions. **f**, FSC analyses of the final map resolution using two methods: map-map FSC, where each map is reconstructed from one half of the images (even vs. odd tilt angle indices), and map-model FSC, where the model map is generated from the fitted model. Resolution assessments are provided based on tilt-based map-map and map-model FSC analyses at thresholds of FSC=0.5 and 0.143, respectively.

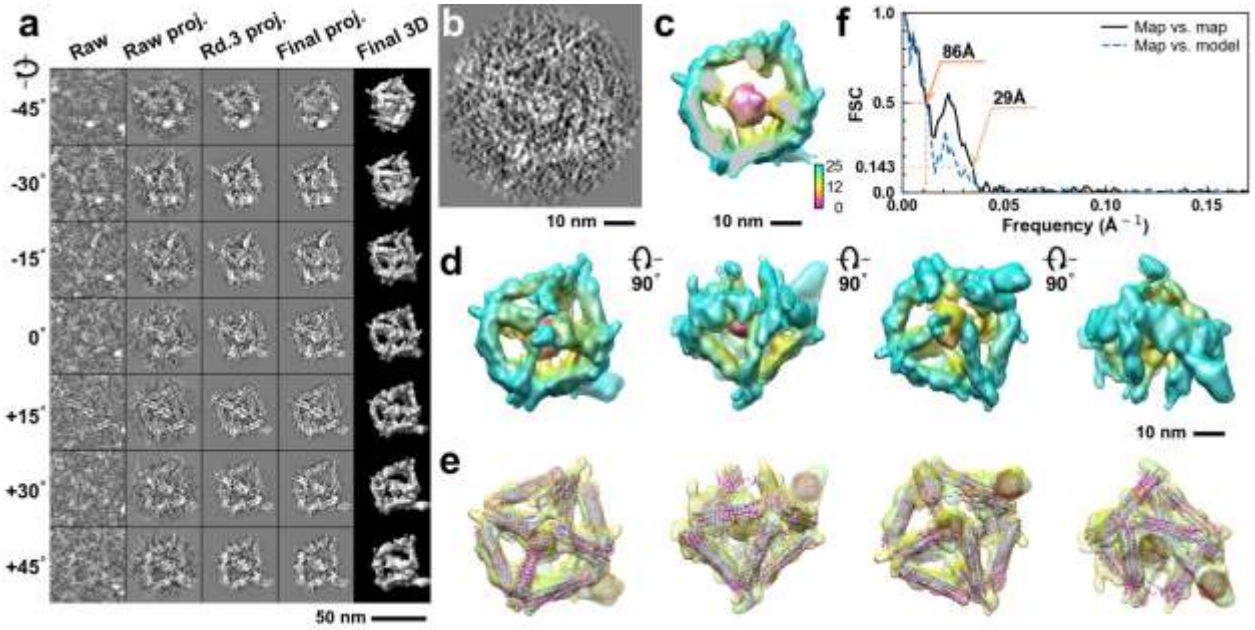

Supplementary Fig. 69: IPET 3D reconstruction and model fitting of an individual unit-cell particle (Index: 061) within a 2D lattice with 100% ferritin loading. a, Seven representative tilt images of a single unit-cell particle are shown in the first column (from left). The tilt images are aligned to a common center using IPET through iterative refinement. The projections of the raw, intermediate, and final 3D reconstruction at the corresponding angles are displayed in the subsequent four columns. **b**, A central cross-section (~23 nm thick) of the final reconstruction before masking is applied. **c**, 3D views of the central cross-section. **d**, Final 3D density map of this particle, viewed from four perpendicular directions. **e**, Final 3D reconstruction superimposed with the fitted model, viewed from four perpendicular directions. **f**, FSC analyses of the final map resolution using two methods: map-map FSC, where each map is reconstructed from one half of the images (even vs. odd tilt angle indices), and map-model FSC, where the model map is generated from the fitted model. Resolution assessments are provided based on tilt-based map-map and map-model FSC analyses at thresholds of FSC=0.5 and 0.143, respectively.

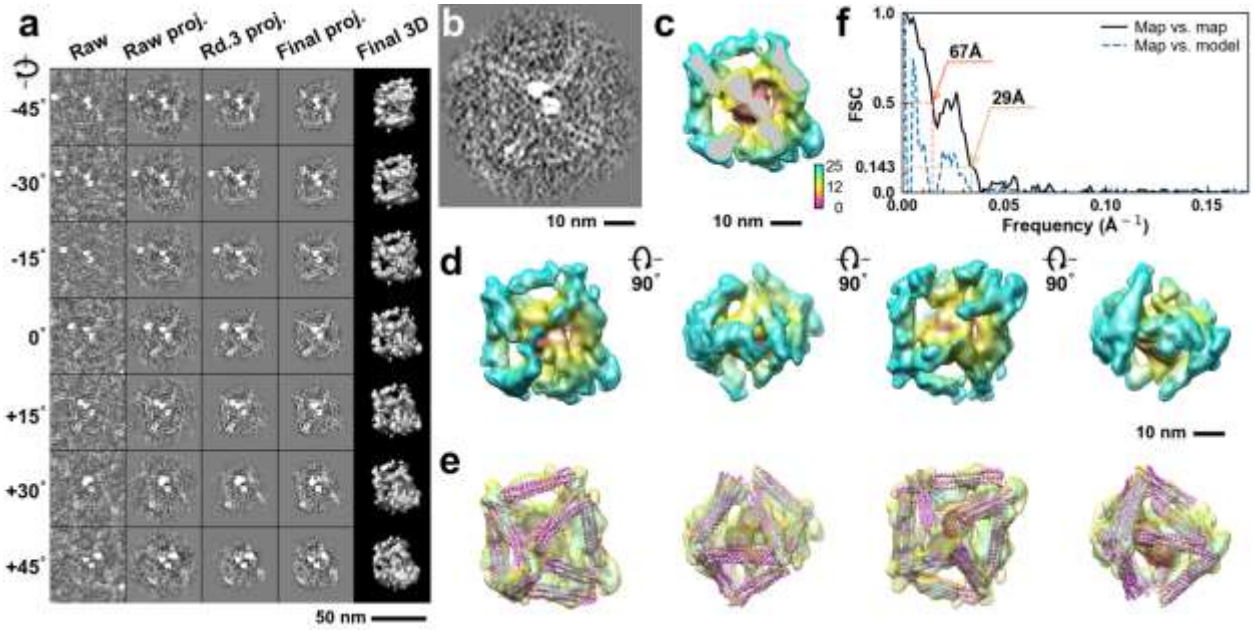

Supplementary Fig. 70: IPET 3D reconstruction and model fitting of an individual unit-cell particle (Index: 062) within a 2D lattice with 100% ferritin loading. a, Seven representative tilt images of a single unit-cell particle are shown in the first column (from left). The tilt images are aligned to a common center using IPET through iterative refinement. The projections of the raw, intermediate, and final 3D reconstruction at the corresponding angles are displayed in the subsequent four columns. **b**, A central cross-section (~23 nm thick) of the final reconstruction before masking is applied. **c**, 3D views of the central cross-section. **d**, Final 3D density map of this particle, viewed from four perpendicular directions. **e**, Final 3D reconstruction superimposed with the fitted model, viewed from four perpendicular directions. **f**, FSC analyses of the final map resolution using two methods: map-map FSC, where each map is reconstructed from one half of the images (even vs. odd tilt angle indices), and map-model FSC, where the model map is generated from the fitted model. Resolution assessments are provided based on tilt-based map-map and map-model FSC analyses at thresholds of FSC=0.5 and 0.143, respectively.

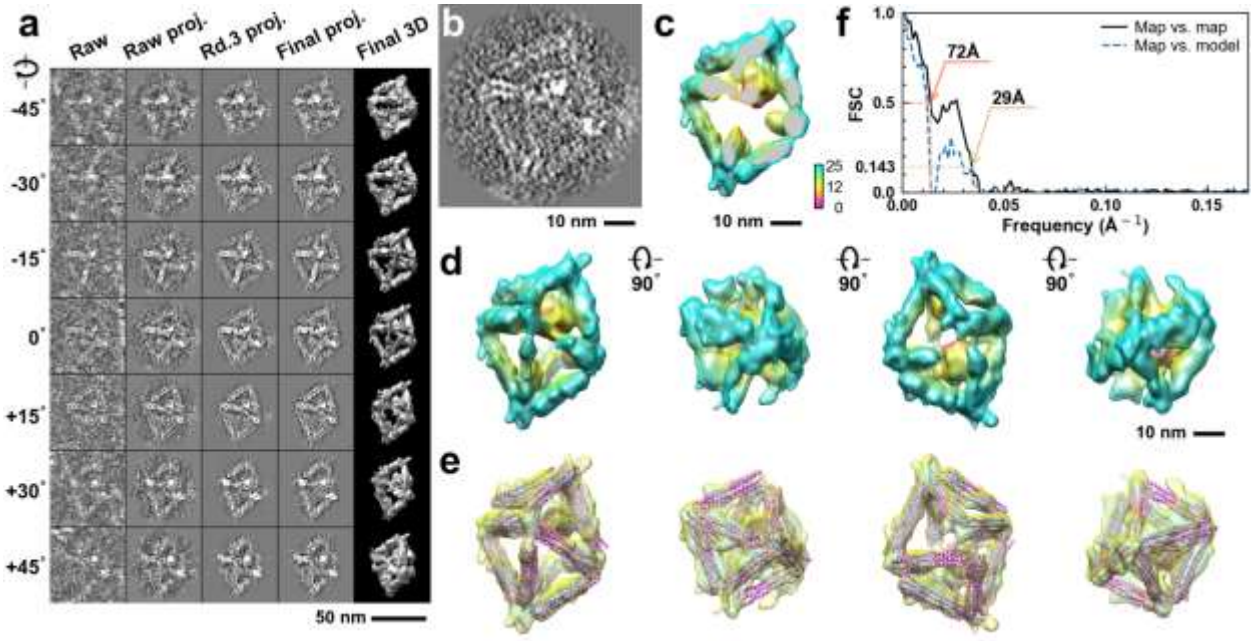

Supplementary Fig. 71: IPET 3D reconstruction and model fitting of an individual unit-cell particle (Index: 063) within a 2D lattice with 100% ferritin loading. a, Seven representative tilt images of a single unit-cell particle are shown in the first column (from left). The tilt images are aligned to a common center using IPET through iterative refinement. The projections of the raw, intermediate, and final 3D reconstruction at the corresponding angles are displayed in the subsequent four columns. **b**, A central cross-section (~23 nm thick) of the final reconstruction before masking is applied. **c**, 3D views of the central cross-section. **d**, Final 3D density map of this particle, viewed from four perpendicular directions. **e**, Final 3D reconstruction superimposed with the fitted model, viewed from four perpendicular directions. **f**, FSC analyses of the final map resolution using two methods: map-map FSC, where each map is reconstructed from one half of the images (even vs. odd tilt angle indices), and map-model FSC, where the model map is generated from the fitted model. Resolution assessments are provided based on tilt-based map-map and map-model FSC analyses at thresholds of FSC=0.5 and 0.143, respectively.

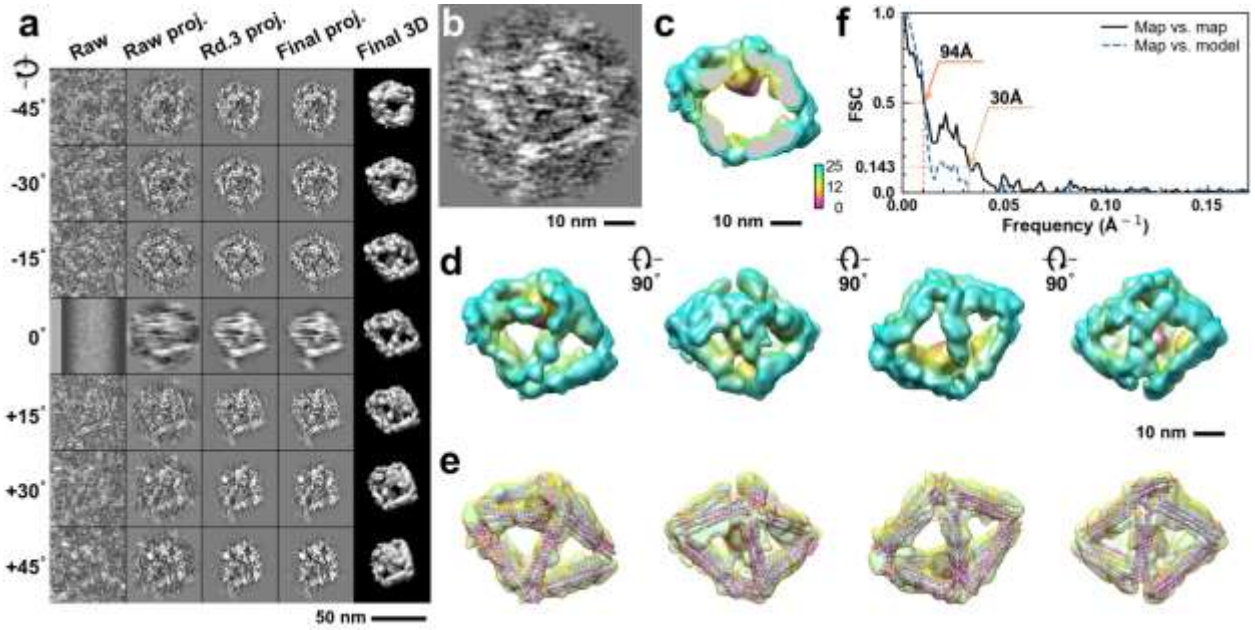

Supplementary Fig. 72: IPET 3D reconstruction and model fitting of an individual unit-cell particle (Index: 064) within a 2D lattice with 100% ferritin loading. a, Seven representative tilt images of a single unit-cell particle are shown in the first column (from left). The tilt images are aligned to a common center using IPET through iterative refinement. The projections of the raw, intermediate, and final 3D reconstruction at the corresponding angles are displayed in the subsequent four columns. **b**, A central cross-section (~23 nm thick) of the final reconstruction before masking is applied. **c**, 3D views of the central cross-section. **d**, Final 3D density map of this particle, viewed from four perpendicular directions. **e**, Final 3D reconstruction superimposed with the fitted model, viewed from four perpendicular directions. **f**, FSC analyses of the final map resolution using two methods: map-map FSC, where each map is reconstructed from one half of the images (even vs. odd tilt angle indices), and map-model FSC, where the model map is generated from the fitted model. Resolution assessments are provided based on tilt-based map-map and map-model FSC analyses at thresholds of FSC=0.5 and 0.143, respectively.

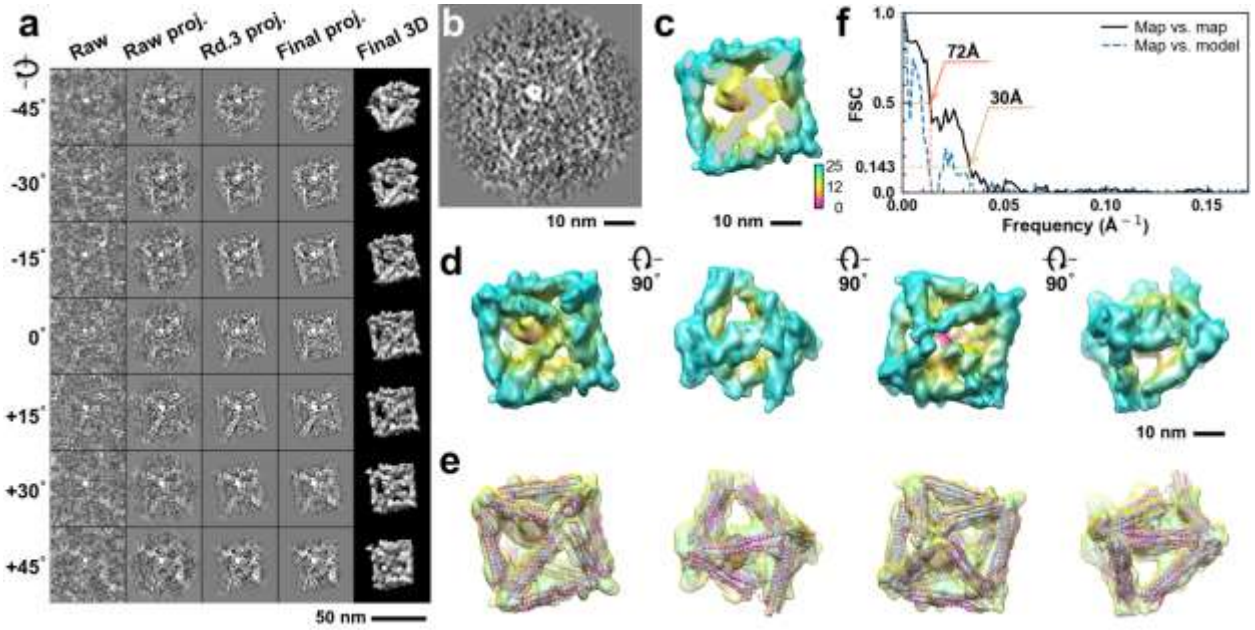

Supplementary Fig. 73: IPET 3D reconstruction and model fitting of an individual unit-cell particle (Index: 065) within a 2D lattice with 100% ferritin loading. a, Seven representative tilt images of a single unit-cell particle are shown in the first column (from left). The tilt images are aligned to a common center using IPET through iterative refinement. The projections of the raw, intermediate, and final 3D reconstruction at the corresponding angles are displayed in the subsequent four columns. **b**, A central cross-section (~23 nm thick) of the final reconstruction before masking is applied. **c**, 3D views of the central cross-section. **d**, Final 3D density map of this particle, viewed from four perpendicular directions. **e**, Final 3D reconstruction superimposed with the fitted model, viewed from four perpendicular directions. **f**, FSC analyses of the final map resolution using two methods: map-map FSC, where each map is reconstructed from one half of the images (even vs. odd tilt angle indices), and map-model FSC, where the model map is generated from the fitted model. Resolution assessments are provided based on tilt-based map-map and map-model FSC analyses at thresholds of FSC=0.5 and 0.143, respectively.

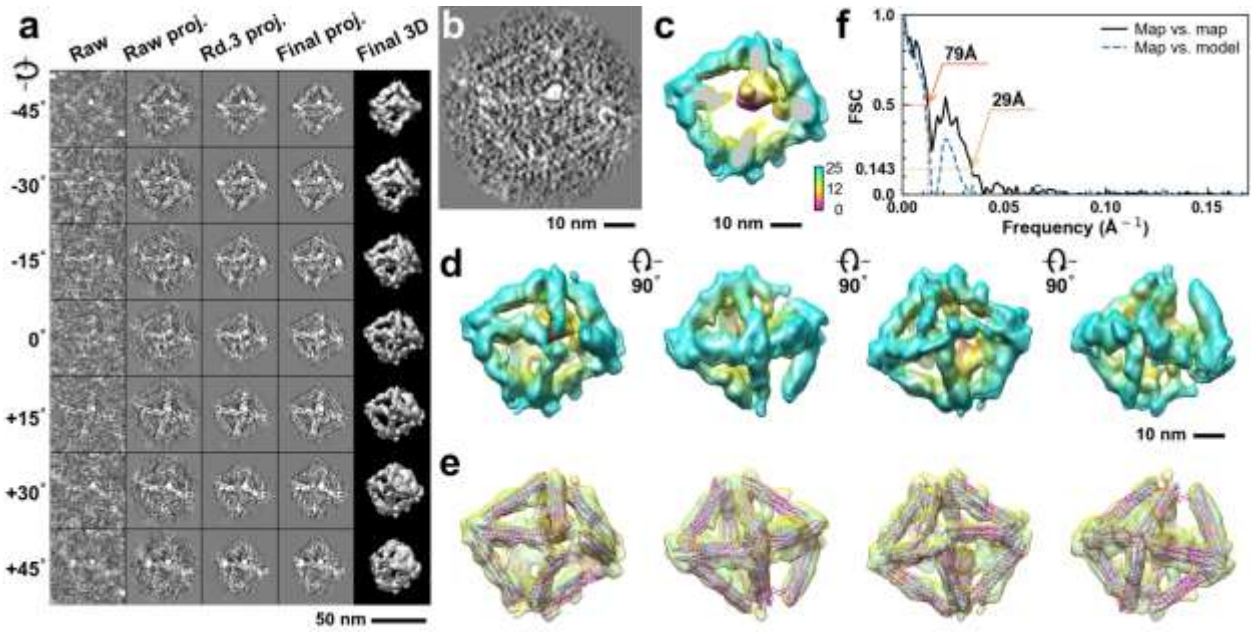

Supplementary Fig. 74: IPET 3D reconstruction and model fitting of an individual unit-cell particle (Index: 066) within a 2D lattice with 100% ferritin loading. a, Seven representative tilt images of a single unit-cell particle are shown in the first column (from left). The tilt images are aligned to a common center using IPET through iterative refinement. The projections of the raw, intermediate, and final 3D reconstruction at the corresponding angles are displayed in the subsequent four columns. **b**, A central cross-section (~23 nm thick) of the final reconstruction before masking is applied. **c**, 3D views of the central cross-section. **d**, Final 3D density map of this particle, viewed from four perpendicular directions. **e**, Final 3D reconstruction superimposed with the fitted model, viewed from four perpendicular directions. **f**, FSC analyses of the final map resolution using two methods: map-map FSC, where each map is reconstructed from one half of the images (even vs. odd tilt angle indices), and map-model FSC, where the model map is generated from the fitted model. Resolution assessments are provided based on tilt-based map-map and map-model FSC analyses at thresholds of FSC=0.5 and 0.143, respectively.

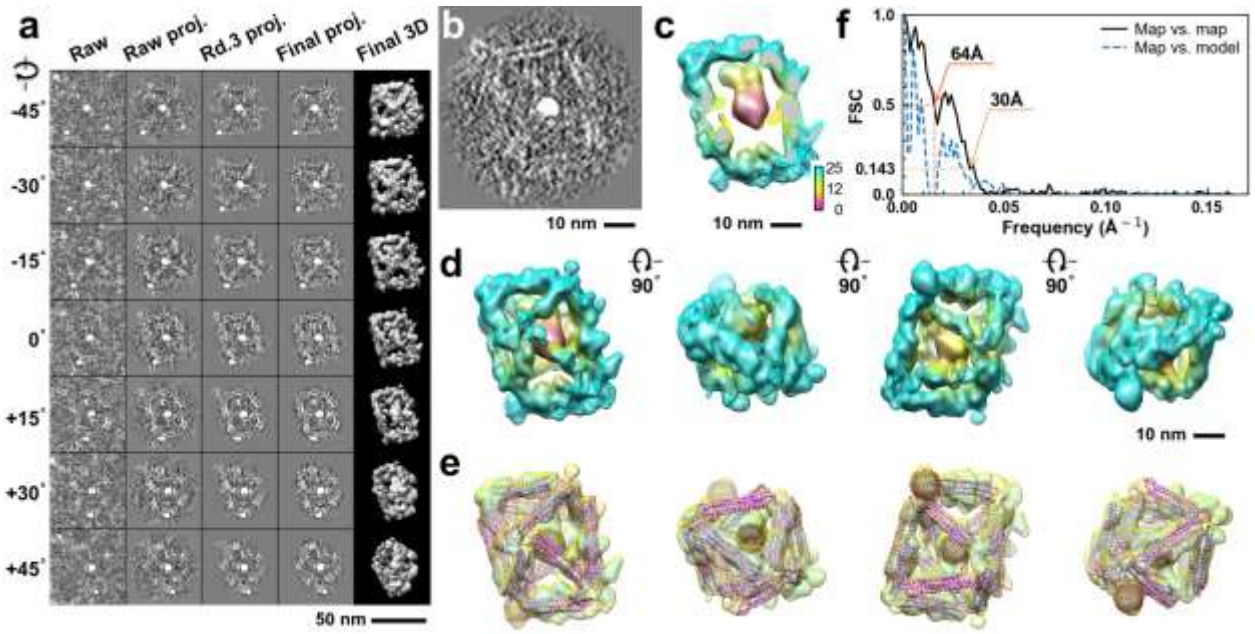

Supplementary Fig. 75: IPET 3D reconstruction and model fitting of an individual unit-cell particle (Index: 067) within a 2D lattice with 100% ferritin loading. a, Seven representative tilt images of a single unit-cell particle are shown in the first column (from left). The tilt images are aligned to a common center using IPET through iterative refinement. The projections of the raw, intermediate, and final 3D reconstruction at the corresponding angles are displayed in the subsequent four columns. **b**, A central cross-section (~23 nm thick) of the final reconstruction before masking is applied. **c**, 3D views of the central cross-section. **d**, Final 3D density map of this particle, viewed from four perpendicular directions. **e**, Final 3D reconstruction superimposed with the fitted model, viewed from four perpendicular directions. **f**, FSC analyses of the final map resolution using two methods: map-map FSC, where each map is reconstructed from one half of the images (even vs. odd tilt angle indices), and map-model FSC, where the model map is generated from the fitted model. Resolution assessments are provided based on tilt-based map-map and map-model FSC analyses at thresholds of FSC=0.5 and 0.143, respectively.

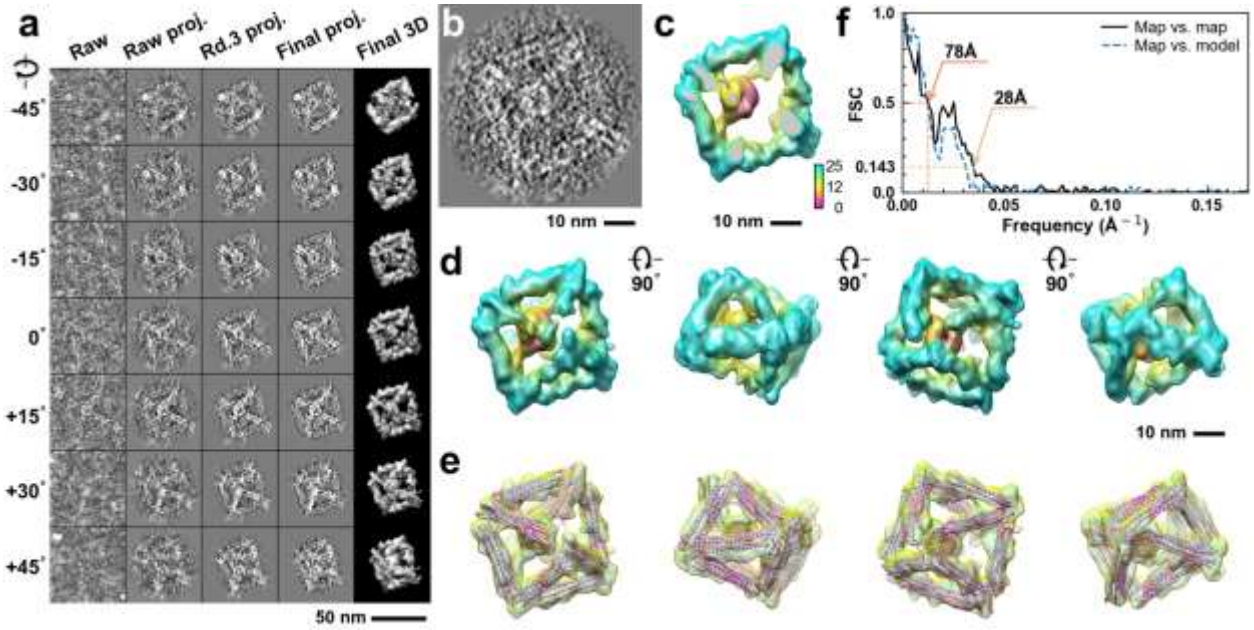

Supplementary Fig. 76: IPET 3D reconstruction and model fitting of an individual unit-cell particle (Index: 068) within a 2D lattice with 100% ferritin loading. a, Seven representative tilt images of a single unit-cell particle are shown in the first column (from left). The tilt images are aligned to a common center using IPET through iterative refinement. The projections of the raw, intermediate, and final 3D reconstruction at the corresponding angles are displayed in the subsequent four columns. **b**, A central cross-section (~23 nm thick) of the final reconstruction before masking is applied. **c**, 3D views of the central cross-section. **d**, Final 3D density map of this particle, viewed from four perpendicular directions. **e**, Final 3D reconstruction superimposed with the fitted model, viewed from four perpendicular directions. **f**, FSC analyses of the final map resolution using two methods: map-map FSC, where each map is reconstructed from one half of the images (even vs. odd tilt angle indices), and map-model FSC, where the model map is generated from the fitted model. Resolution assessments are provided based on tilt-based map-map and map-model FSC analyses at thresholds of FSC=0.5 and 0.143, respectively.

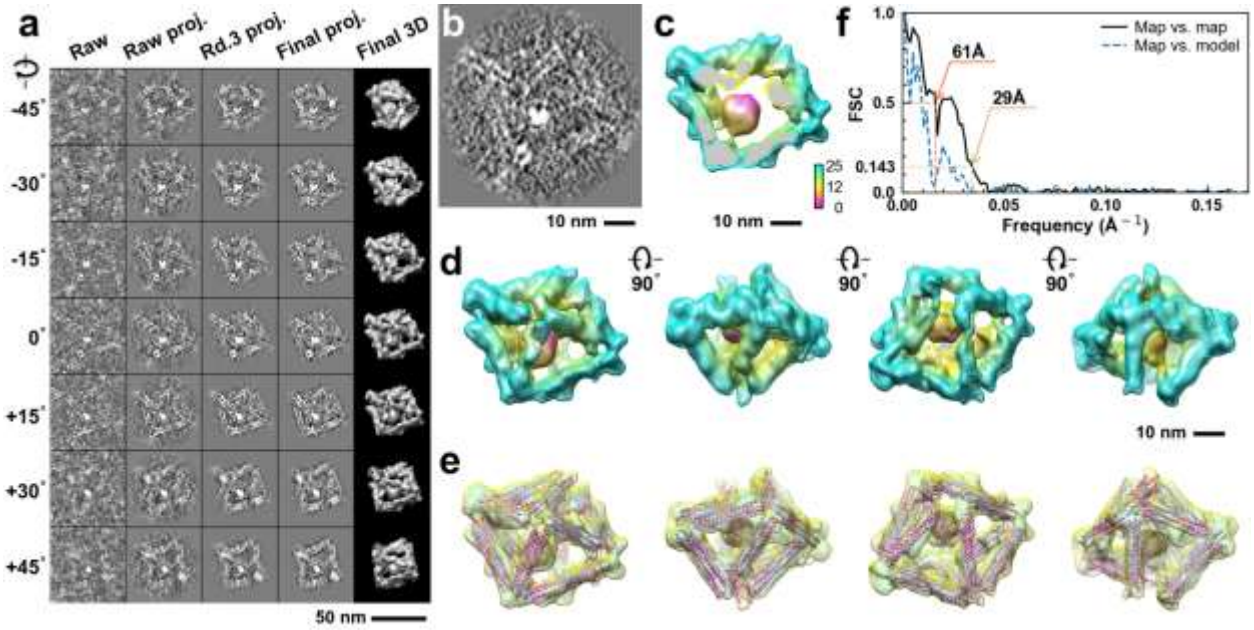

Supplementary Fig. 77: IPET 3D reconstruction and model fitting of an individual unit-cell particle (Index: 069) within a 2D lattice with 100% ferritin loading. a, Seven representative tilt images of a single unit-cell particle are shown in the first column (from left). The tilt images are aligned to a common center using IPET through iterative refinement. The projections of the raw, intermediate, and final 3D reconstruction at the corresponding angles are displayed in the subsequent four columns. **b**, A central cross-section (~23 nm thick) of the final reconstruction before masking is applied. **c**, 3D views of the central cross-section. **d**, Final 3D density map of this particle, viewed from four perpendicular directions. **e**, Final 3D reconstruction superimposed with the fitted model, viewed from four perpendicular directions. **f**, FSC analyses of the final map resolution using two methods: map-map FSC, where each map is reconstructed from one half of the images (even vs. odd tilt angle indices), and map-model FSC, where the model map is generated from the fitted model. Resolution assessments are provided based on tilt-based map-map and map-model FSC analyses at thresholds of FSC=0.5 and 0.143, respectively.

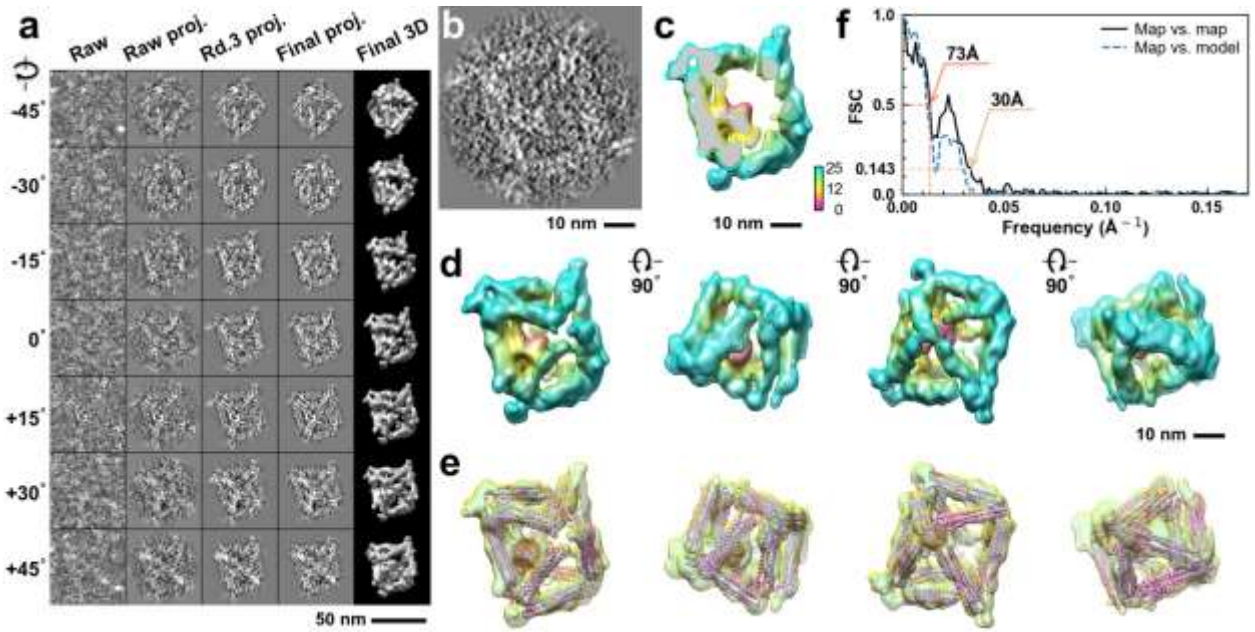

Supplementary Fig. 78: IPET 3D reconstruction and model fitting of an individual unit-cell particle (Index: 070) within a 2D lattice with 100% ferritin loading. a, Seven representative tilt images of a single unit-cell particle are shown in the first column (from left). The tilt images are aligned to a common center using IPET through iterative refinement. The projections of the raw, intermediate, and final 3D reconstruction at the corresponding angles are displayed in the subsequent four columns. **b**, A central cross-section (~23 nm thick) of the final reconstruction before masking is applied. **c**, 3D views of the central cross-section. **d**, Final 3D density map of this particle, viewed from four perpendicular directions. **e**, Final 3D reconstruction superimposed with the fitted model, viewed from four perpendicular directions. **f**, FSC analyses of the final map resolution using two methods: map-map FSC, where each map is reconstructed from one half of the images (even vs. odd tilt angle indices), and map-model FSC, where the model map is generated from the fitted model. Resolution assessments are provided based on tilt-based map-map and map-model FSC analyses at thresholds of FSC=0.5 and 0.143, respectively.

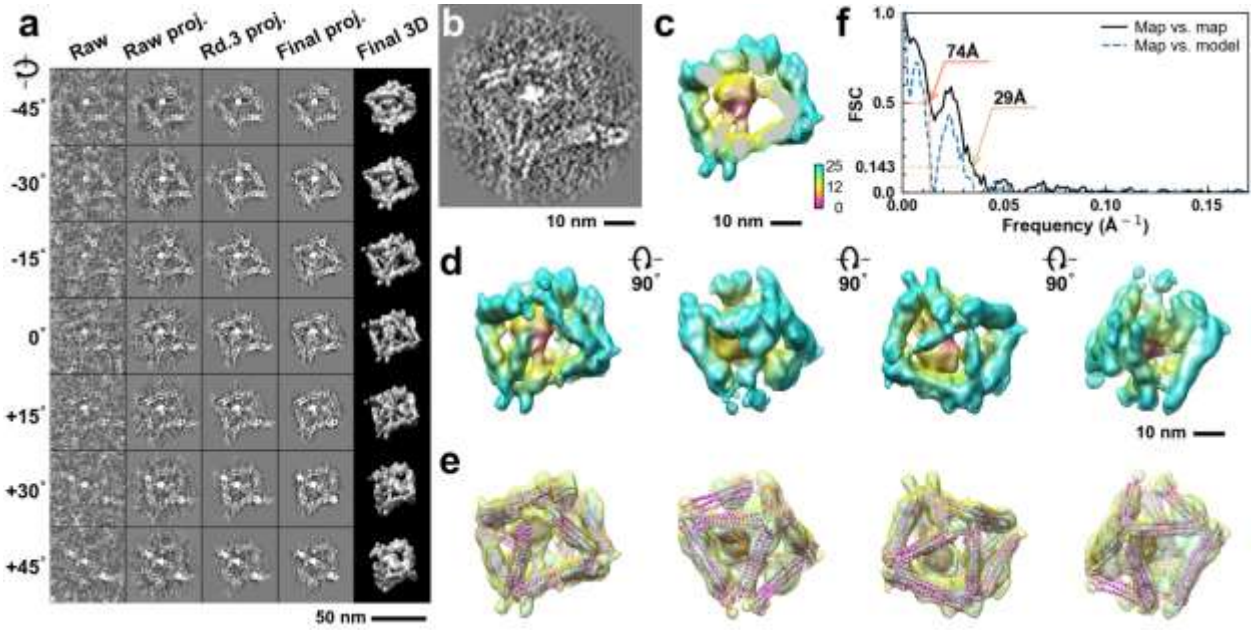

Supplementary Fig. 79: IPET 3D reconstruction and model fitting of an individual unit-cell particle (Index: 071) within a 2D lattice with 100% ferritin loading. a, Seven representative tilt images of a single unit-cell particle are shown in the first column (from left). The tilt images are aligned to a common center using IPET through iterative refinement. The projections of the raw, intermediate, and final 3D reconstruction at the corresponding angles are displayed in the subsequent four columns. **b**, A central cross-section (~23 nm thick) of the final reconstruction before masking is applied. **c**, 3D views of the central cross-section. **d**, Final 3D density map of this particle, viewed from four perpendicular directions. **e**, Final 3D reconstruction superimposed with the fitted model, viewed from four perpendicular directions. **f**, FSC analyses of the final map resolution using two methods: map-map FSC, where each map is reconstructed from one half of the images (even vs. odd tilt angle indices), and map-model FSC, where the model map is generated from the fitted model. Resolution assessments are provided based on tilt-based map-map and map-model FSC analyses at thresholds of FSC=0.5 and 0.143, respectively.

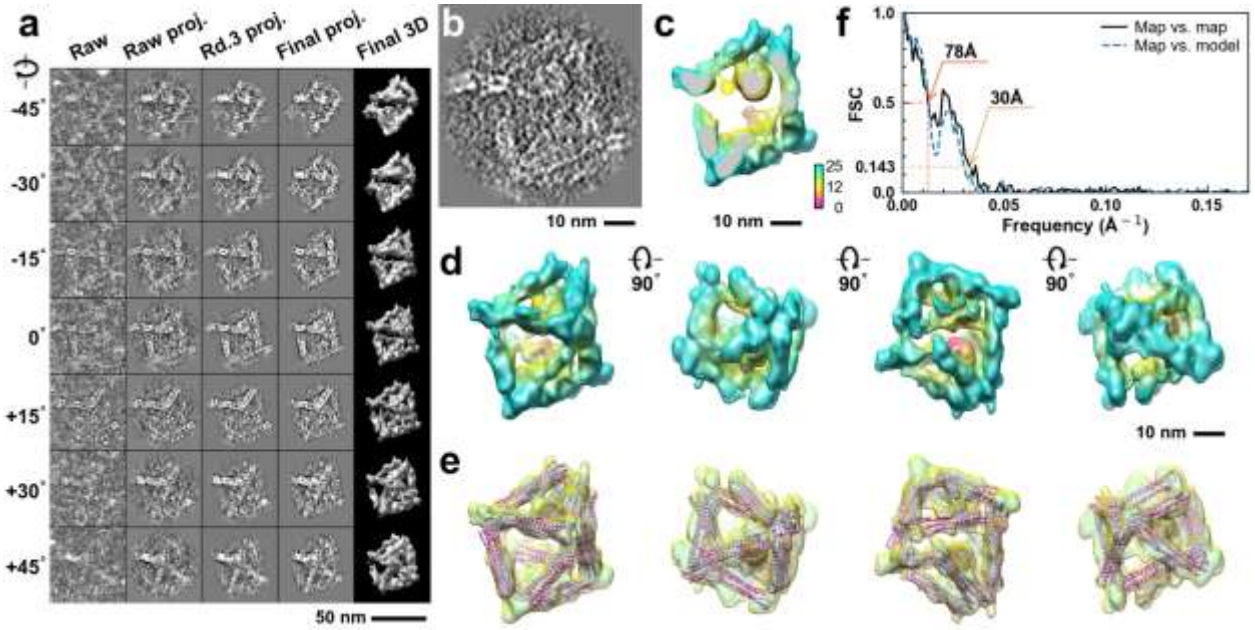

Supplementary Fig. 80: IPET 3D reconstruction and model fitting of an individual unit-cell particle (Index: 072) within a 2D lattice with 100% ferritin loading. a, Seven representative tilt images of a single unit-cell particle are shown in the first column (from left). The tilt images are aligned to a common center using IPET through iterative refinement. The projections of the raw, intermediate, and final 3D reconstruction at the corresponding angles are displayed in the subsequent four columns. **b**, A central cross-section (~23 nm thick) of the final reconstruction before masking is applied. **c**, 3D views of the central cross-section. **d**, Final 3D density map of this particle, viewed from four perpendicular directions. **e**, Final 3D reconstruction superimposed with the fitted model, viewed from four perpendicular directions. **f**, FSC analyses of the final map resolution using two methods: map-map FSC, where each map is reconstructed from one half of the images (even vs. odd tilt angle indices), and map-model FSC, where the model map is generated from the fitted model. Resolution assessments are provided based on tilt-based map-map and map-model FSC analyses at thresholds of FSC=0.5 and 0.143, respectively.

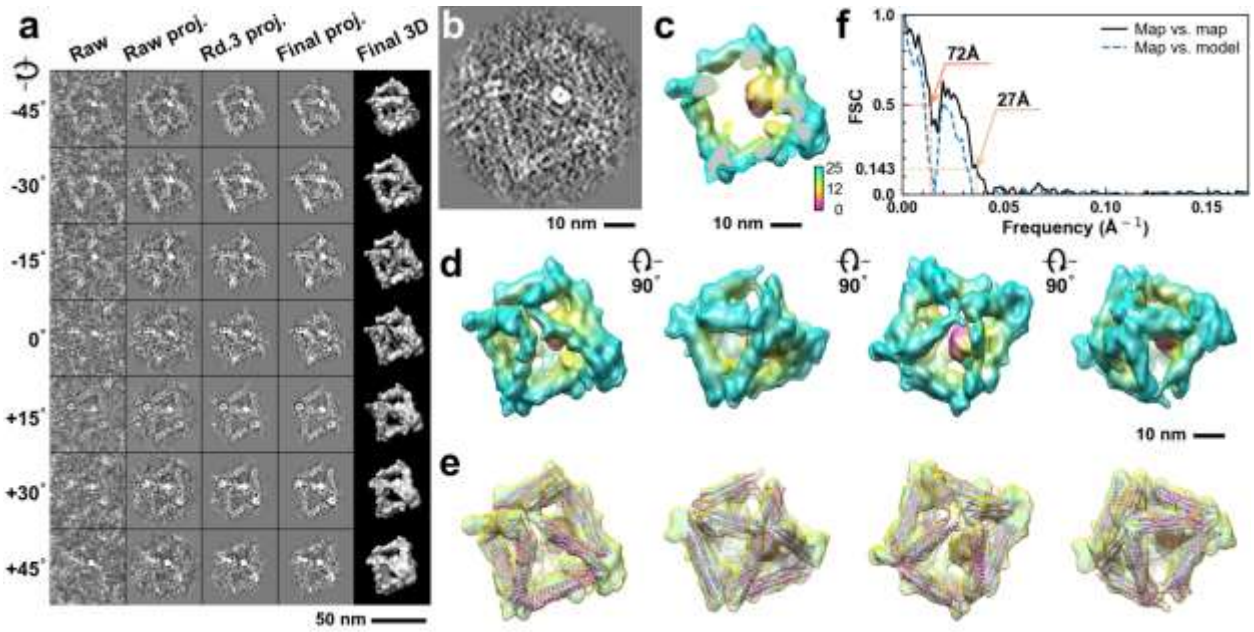

Supplementary Fig. 81: IPET 3D reconstruction and model fitting of an individual unit-cell particle (Index: 073) within a 2D lattice with 100% ferritin loading. a, Seven representative tilt images of a single unit-cell particle are shown in the first column (from left). The tilt images are aligned to a common center using IPET through iterative refinement. The projections of the raw, intermediate, and final 3D reconstruction at the corresponding angles are displayed in the subsequent four columns. **b**, A central cross-section (~23 nm thick) of the final reconstruction before masking is applied. **c**, 3D views of the central cross-section. **d**, Final 3D density map of this particle, viewed from four perpendicular directions. **e**, Final 3D reconstruction superimposed with the fitted model, viewed from four perpendicular directions. **f**, FSC analyses of the final map resolution using two methods: map-map FSC, where each map is reconstructed from one half of the images (even vs. odd tilt angle indices), and map-model FSC, where the model map is generated from the fitted model. Resolution assessments are provided based on tilt-based map-map and map-model FSC analyses at thresholds of FSC=0.5 and 0.143, respectively.

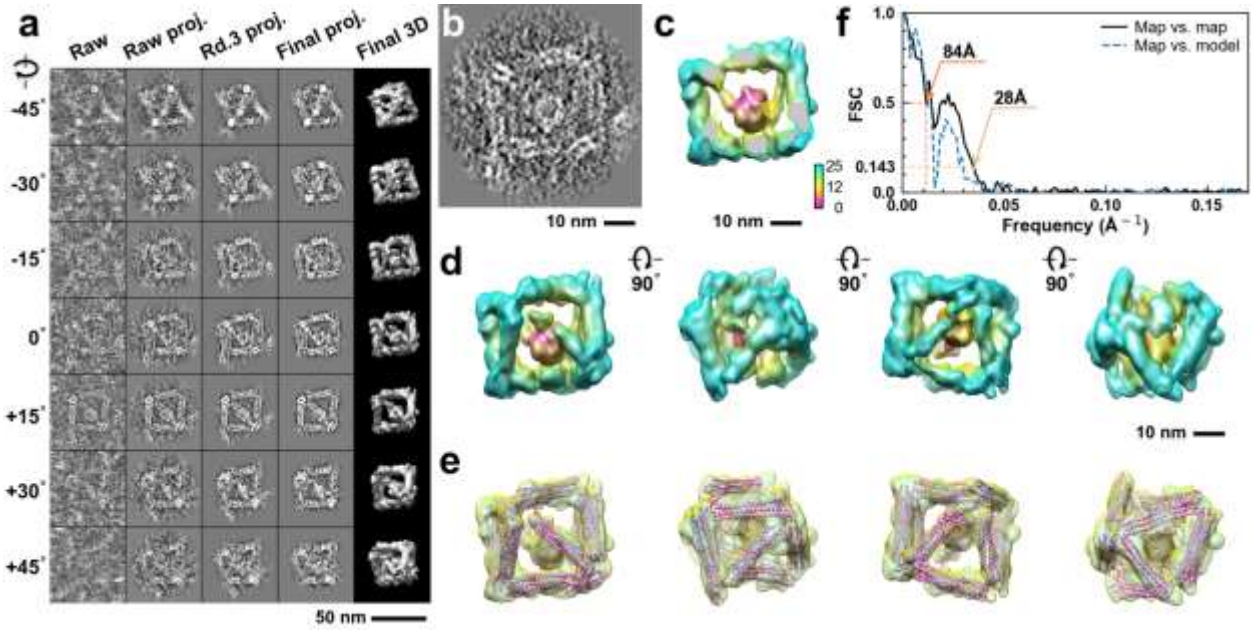

Supplementary Fig. 82: IPET 3D reconstruction and model fitting of an individual unit-cell particle (Index: 074) within a 2D lattice with 100% ferritin loading. a, Seven representative tilt images of a single unit-cell particle are shown in the first column (from left). The tilt images are aligned to a common center using IPET through iterative refinement. The projections of the raw, intermediate, and final 3D reconstruction at the corresponding angles are displayed in the subsequent four columns. **b**, A central cross-section (~23 nm thick) of the final reconstruction before masking is applied. **c**, 3D views of the central cross-section. **d**, Final 3D density map of this particle, viewed from four perpendicular directions. **e**, Final 3D reconstruction superimposed with the fitted model, viewed from four perpendicular directions. **f**, FSC analyses of the final map resolution using two methods: map-map FSC, where each map is reconstructed from one half of the images (even vs. odd tilt angle indices), and map-model FSC, where the model map is generated from the fitted model. Resolution assessments are provided based on tilt-based map-map and map-model FSC analyses at thresholds of FSC=0.5 and 0.143, respectively.

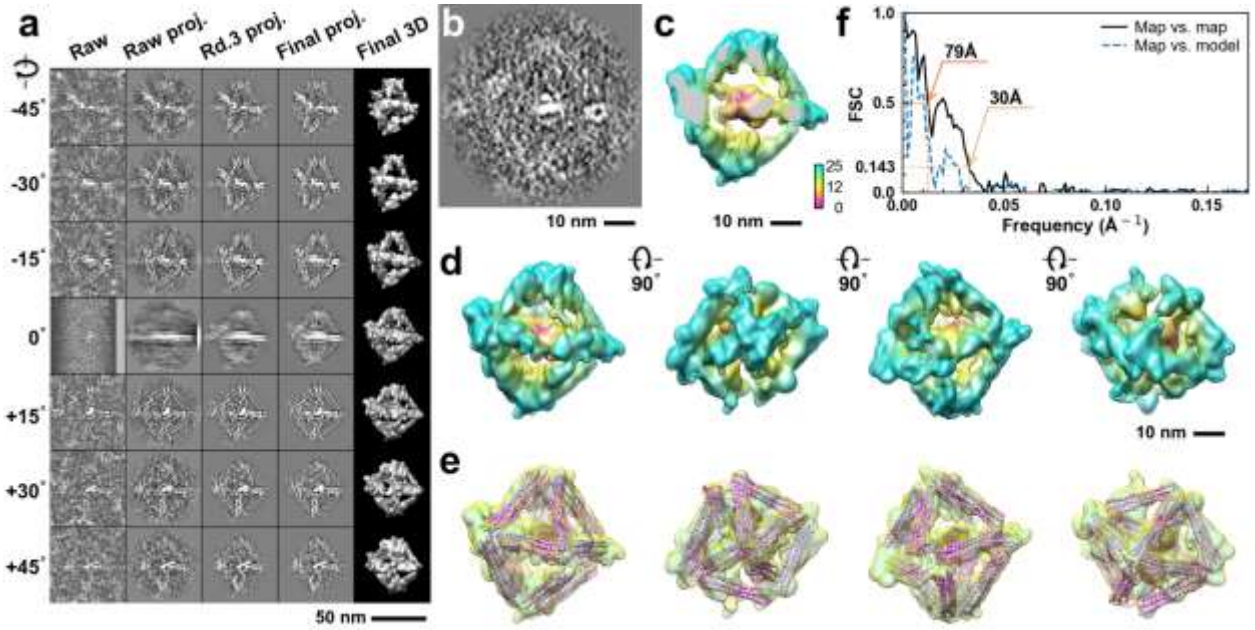

Supplementary Fig. 83: IPET 3D reconstruction and model fitting of an individual unit-cell particle (Index: 075) within a 2D lattice with 100% ferritin loading. a, Seven representative tilt images of a single unit-cell particle are shown in the first column (from left). The tilt images are aligned to a common center using IPET through iterative refinement. The projections of the raw, intermediate, and final 3D reconstruction at the corresponding angles are displayed in the subsequent four columns. **b**, A central cross-section (~23 nm thick) of the final reconstruction before masking is applied. **c**, 3D views of the central cross-section. **d**, Final 3D density map of this particle, viewed from four perpendicular directions. **e**, Final 3D reconstruction superimposed with the fitted model, viewed from four perpendicular directions. **f**, FSC analyses of the final map resolution using two methods: map-map FSC, where each map is reconstructed from one half of the images (even vs. odd tilt angle indices), and map-model FSC, where the model map is generated from the fitted model. Resolution assessments are provided based on tilt-based map-map and map-model FSC analyses at thresholds of FSC=0.5 and 0.143, respectively.

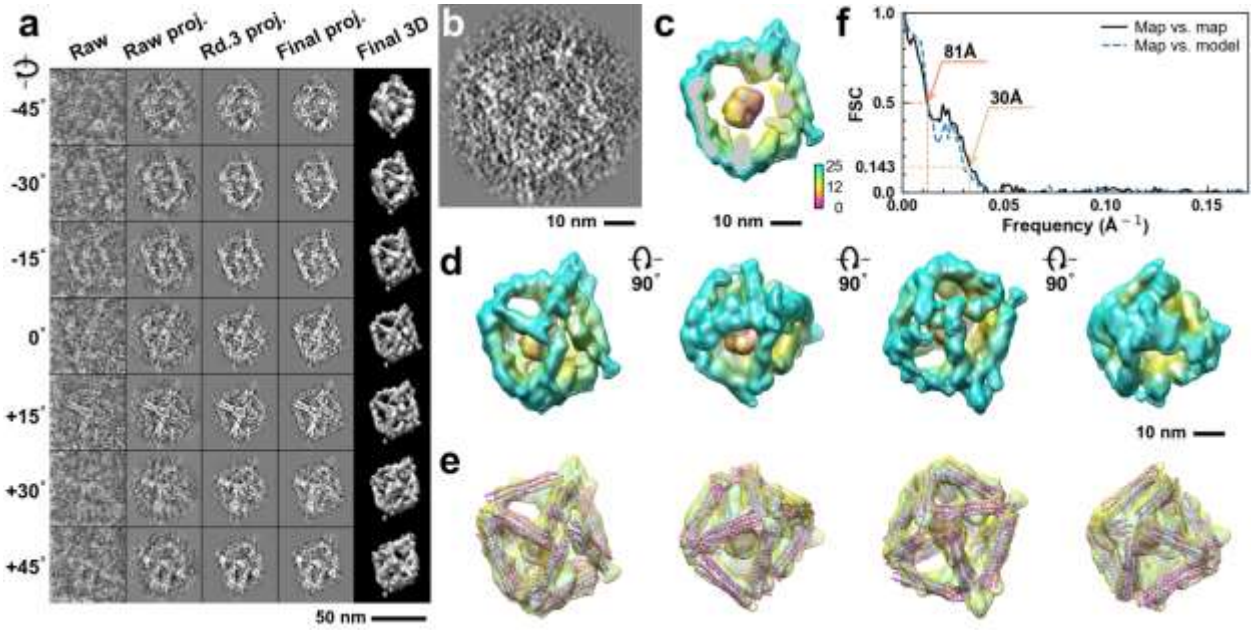

Supplementary Fig. 84: IPET 3D reconstruction and model fitting of an individual unit-cell particle (Index: 076) within a 2D lattice with 100% ferritin loading. a, Seven representative tilt images of a single unit-cell particle are shown in the first column (from left). The tilt images are aligned to a common center using IPET through iterative refinement. The projections of the raw, intermediate, and final 3D reconstruction at the corresponding angles are displayed in the subsequent four columns. **b**, A central cross-section (~23 nm thick) of the final reconstruction before masking is applied. **c**, 3D views of the central cross-section. **d**, Final 3D density map of this particle, viewed from four perpendicular directions. **e**, Final 3D reconstruction superimposed with the fitted model, viewed from four perpendicular directions. **f**, FSC analyses of the final map resolution using two methods: map-map FSC, where each map is reconstructed from one half of the images (even vs. odd tilt angle indices), and map-model FSC, where the model map is generated from the fitted model. Resolution assessments are provided based on tilt-based map-map and map-model FSC analyses at thresholds of FSC=0.5 and 0.143, respectively.

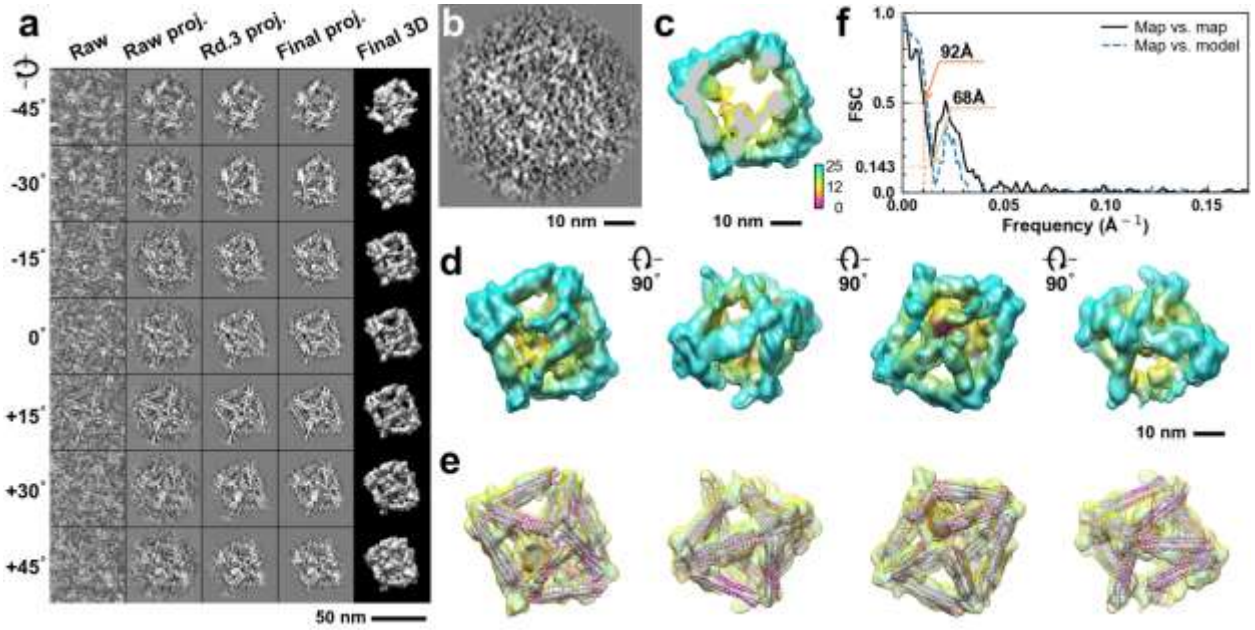

Supplementary Fig. 85: IPET 3D reconstruction and model fitting of an individual unit-cell particle (Index: 077) within a 2D lattice with 100% ferritin loading. a, Seven representative tilt images of a single unit-cell particle are shown in the first column (from left). The tilt images are aligned to a common center using IPET through iterative refinement. The projections of the raw, intermediate, and final 3D reconstruction at the corresponding angles are displayed in the subsequent four columns. **b**, A central cross-section (~23 nm thick) of the final reconstruction before masking is applied. **c**, 3D views of the central cross-section. **d**, Final 3D density map of this particle, viewed from four perpendicular directions. **e**, Final 3D reconstruction superimposed with the fitted model, viewed from four perpendicular directions. **f**, FSC analyses of the final map resolution using two methods: map-map FSC, where each map is reconstructed from one half of the images (even vs. odd tilt angle indices), and map-model FSC, where the model map is generated from the fitted model. Resolution assessments are provided based on tilt-based map-map and map-model FSC analyses at thresholds of FSC=0.5 and 0.143, respectively.

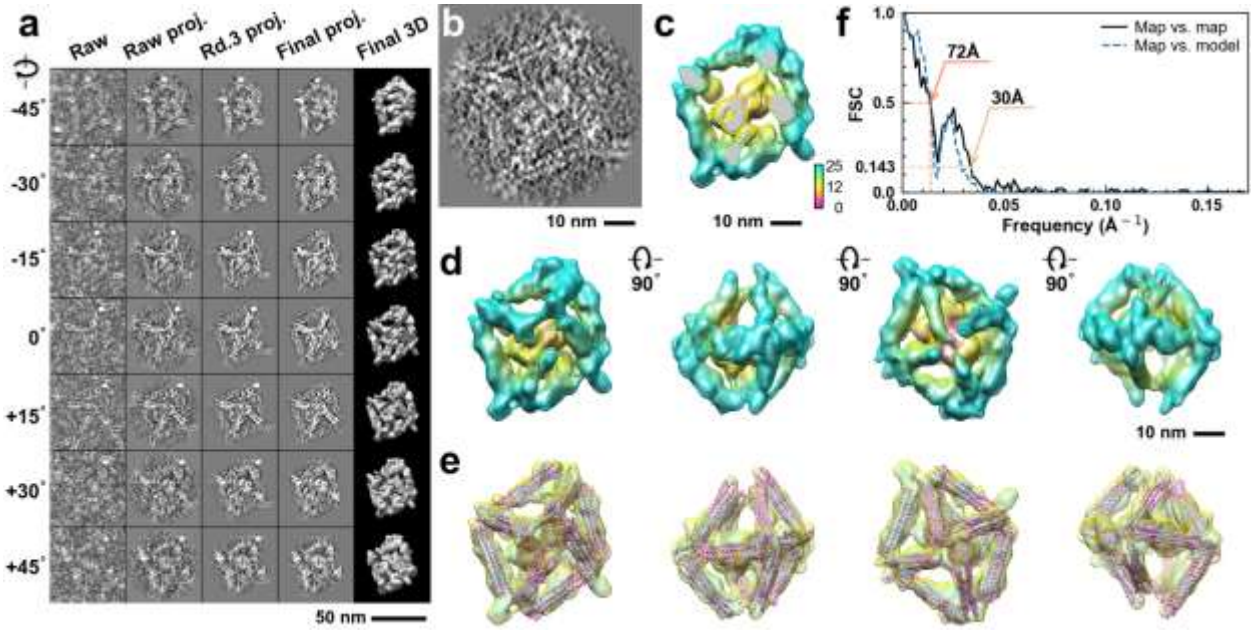

Supplementary Fig. 86: IPET 3D reconstruction and model fitting of an individual unit-cell particle (Index: 078) within a 2D lattice with 100% ferritin loading. a, Seven representative tilt images of a single unit-cell particle are shown in the first column (from left). The tilt images are aligned to a common center using IPET through iterative refinement. The projections of the raw, intermediate, and final 3D reconstruction at the corresponding angles are displayed in the subsequent four columns. **b**, A central cross-section (~23 nm thick) of the final reconstruction before masking is applied. **c**, 3D views of the central cross-section. **d**, Final 3D density map of this particle, viewed from four perpendicular directions. **e**, Final 3D reconstruction superimposed with the fitted model, viewed from four perpendicular directions. **f**, FSC analyses of the final map resolution using two methods: map-map FSC, where each map is reconstructed from one half of the images (even vs. odd tilt angle indices), and map-model FSC, where the model map is generated from the fitted model. Resolution assessments are provided based on tilt-based map-map and map-model FSC analyses at thresholds of FSC=0.5 and 0.143, respectively.

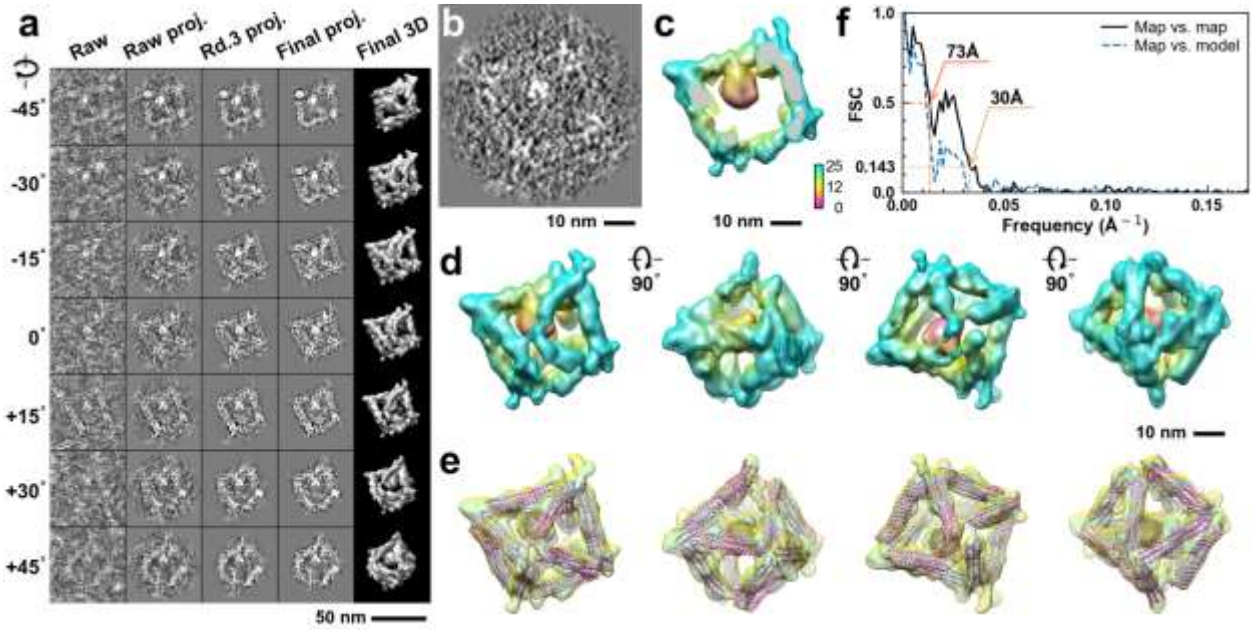

Supplementary Fig. 87: IPET 3D reconstruction and model fitting of an individual unit-cell particle (Index: 079) within a 2D lattice with 100% ferritin loading. a, Seven representative tilt images of a single unit-cell particle are shown in the first column (from left). The tilt images are aligned to a common center using IPET through iterative refinement. The projections of the raw, intermediate, and final 3D reconstruction at the corresponding angles are displayed in the subsequent four columns. **b**, A central cross-section (~23 nm thick) of the final reconstruction before masking is applied. **c**, 3D views of the central cross-section. **d**, Final 3D density map of this particle, viewed from four perpendicular directions. **e**, Final 3D reconstruction superimposed with the fitted model, viewed from four perpendicular directions. **f**, FSC analyses of the final map resolution using two methods: map-map FSC, where each map is reconstructed from one half of the images (even vs. odd tilt angle indices), and map-model FSC, where the model map is generated from the fitted model. Resolution assessments are provided based on tilt-based map-map and map-model FSC analyses at thresholds of FSC=0.5 and 0.143, respectively.

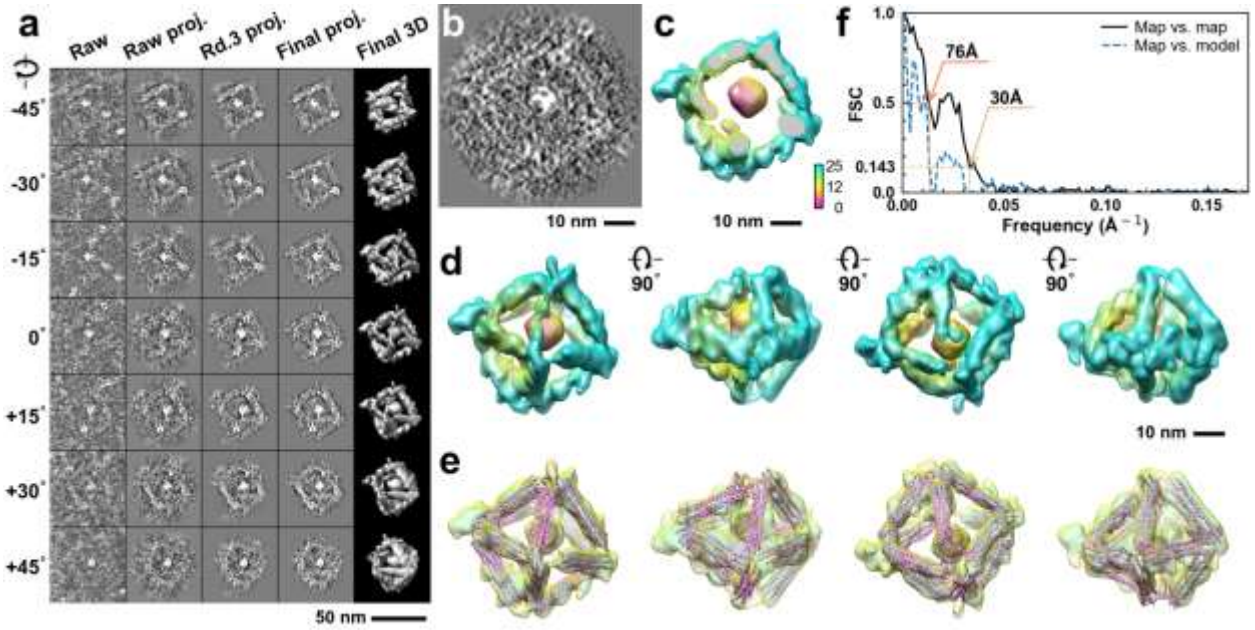

Supplementary Fig. 88: IPET 3D reconstruction and model fitting of an individual unit-cell particle (Index: 080) within a 2D lattice with 100% ferritin loading. a, Seven representative tilt images of a single unit-cell particle are shown in the first column (from left). The tilt images are aligned to a common center using IPET through iterative refinement. The projections of the raw, intermediate, and final 3D reconstruction at the corresponding angles are displayed in the subsequent four columns. **b**, A central cross-section (~23 nm thick) of the final reconstruction before masking is applied. **c**, 3D views of the central cross-section. **d**, Final 3D density map of this particle, viewed from four perpendicular directions. **e**, Final 3D reconstruction superimposed with the fitted model, viewed from four perpendicular directions. **f**, FSC analyses of the final map resolution using two methods: map-map FSC, where each map is reconstructed from one half of the images (even vs. odd tilt angle indices), and map-model FSC, where the model map is generated from the fitted model. Resolution assessments are provided based on tilt-based map-map and map-model FSC analyses at thresholds of FSC=0.5 and 0.143, respectively.

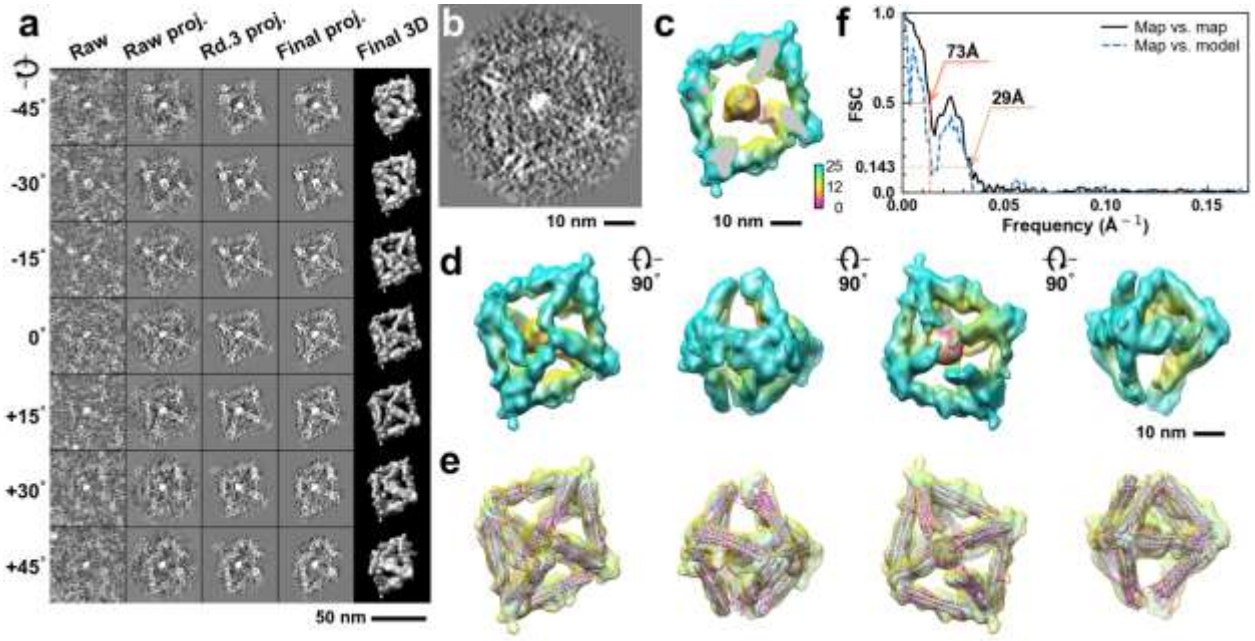

Supplementary Fig. 89: IPET 3D reconstruction and model fitting of an individual unit-cell particle (Index: 081) within a 2D lattice with 100% ferritin loading. a, Seven representative tilt images of a single unit-cell particle are shown in the first column (from left). The tilt images are aligned to a common center using IPET through iterative refinement. The projections of the raw, intermediate, and final 3D reconstruction at the corresponding angles are displayed in the subsequent four columns. **b**, A central cross-section (~23 nm thick) of the final reconstruction before masking is applied. **c**, 3D views of the central cross-section. **d**, Final 3D density map of this particle, viewed from four perpendicular directions. **e**, Final 3D reconstruction superimposed with the fitted model, viewed from four perpendicular directions. **f**, FSC analyses of the final map resolution using two methods: map-map FSC, where each map is reconstructed from one half of the images (even vs. odd tilt angle indices), and map-model FSC, where the model map is generated from the fitted model. Resolution assessments are provided based on tilt-based map-map and map-model FSC analyses at thresholds of FSC=0.5 and 0.143, respectively.

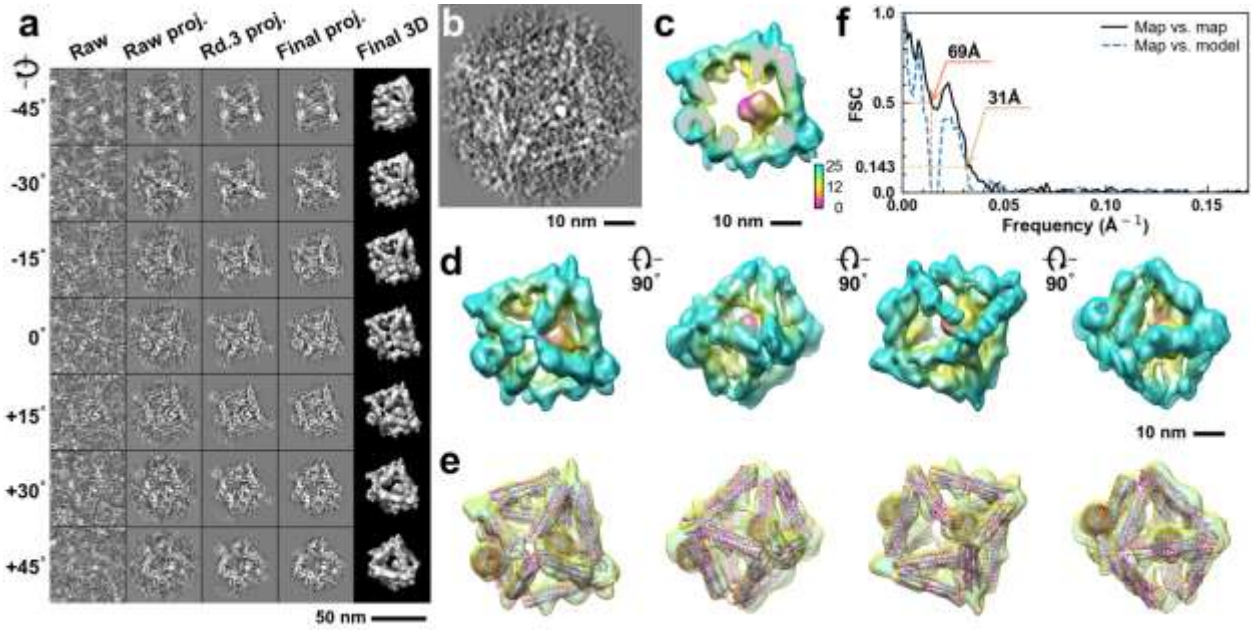

Supplementary Fig. 90: IPET 3D reconstruction and model fitting of an individual unit-cell particle (Index: 082) within a 2D lattice with 100% ferritin loading. a, Seven representative tilt images of a single unit-cell particle are shown in the first column (from left). The tilt images are aligned to a common center using IPET through iterative refinement. The projections of the raw, intermediate, and final 3D reconstruction at the corresponding angles are displayed in the subsequent four columns. **b**, A central cross-section (~23 nm thick) of the final reconstruction before masking is applied. **c**, 3D views of the central cross-section. **d**, Final 3D density map of this particle, viewed from four perpendicular directions. **e**, Final 3D reconstruction superimposed with the fitted model, viewed from four perpendicular directions. **f**, FSC analyses of the final map resolution using two methods: map-map FSC, where each map is reconstructed from one half of the images (even vs. odd tilt angle indices), and map-model FSC, where the model map is generated from the fitted model. Resolution assessments are provided based on tilt-based map-map and map-model FSC analyses at thresholds of FSC=0.5 and 0.143, respectively.

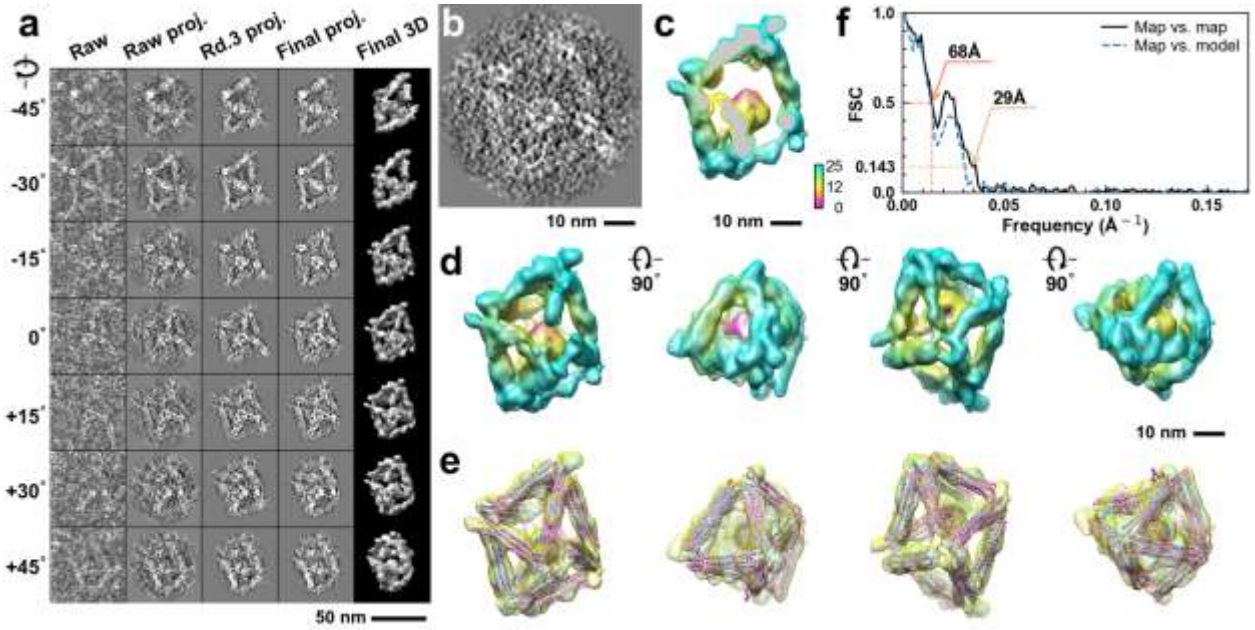

Supplementary Fig. 91: IPET 3D reconstruction and model fitting of an individual unit-cell particle (Index: 083) within a 2D lattice with 100% ferritin loading. a, Seven representative tilt images of a single unit-cell particle are shown in the first column (from left). The tilt images are aligned to a common center using IPET through iterative refinement. The projections of the raw, intermediate, and final 3D reconstruction at the corresponding angles are displayed in the subsequent four columns. **b**, A central cross-section (~23 nm thick) of the final reconstruction before masking is applied. **c**, 3D views of the central cross-section. **d**, Final 3D density map of this particle, viewed from four perpendicular directions. **e**, Final 3D reconstruction superimposed with the fitted model, viewed from four perpendicular directions. **f**, FSC analyses of the final map resolution using two methods: map-map FSC, where each map is reconstructed from one half of the images (even vs. odd tilt angle indices), and map-model FSC, where the model map is generated from the fitted model. Resolution assessments are provided based on tilt-based map-map and map-model FSC analyses at thresholds of FSC=0.5 and 0.143, respectively.

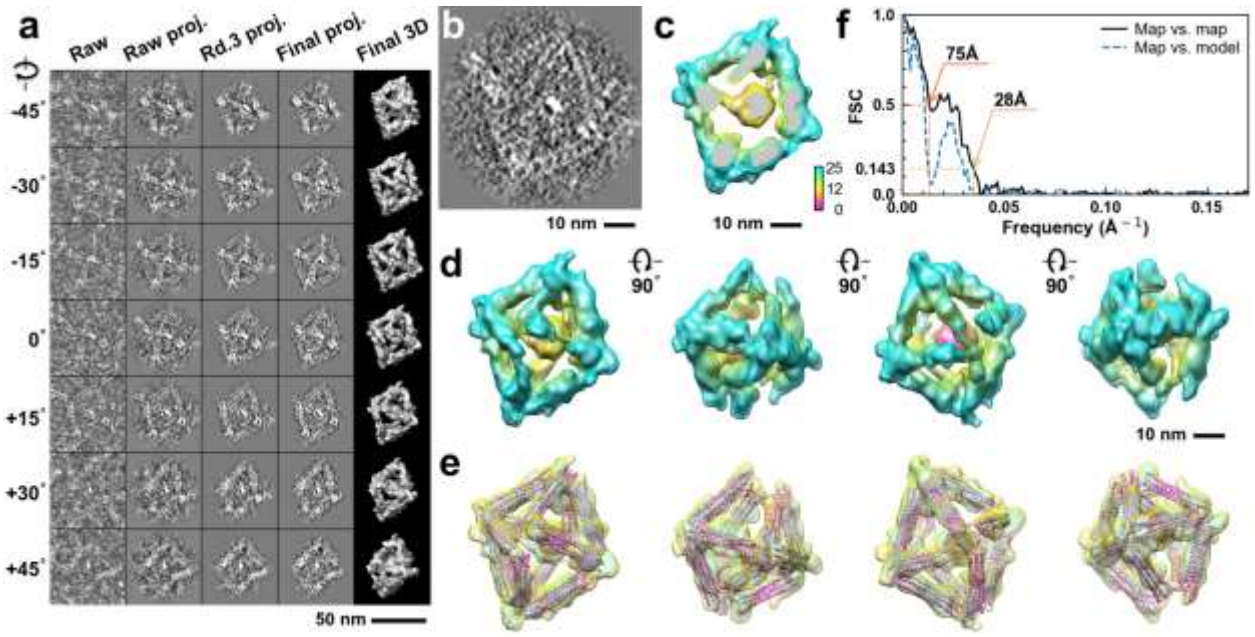

Supplementary Fig. 92: IPET 3D reconstruction and model fitting of an individual unit-cell particle (Index: 084) within a 2D lattice with 100% ferritin loading. a, Seven representative tilt images of a single unit-cell particle are shown in the first column (from left). The tilt images are aligned to a common center using IPET through iterative refinement. The projections of the raw, intermediate, and final 3D reconstruction at the corresponding angles are displayed in the subsequent four columns. **b**, A central cross-section (~23 nm thick) of the final reconstruction before masking is applied. **c**, 3D views of the central cross-section. **d**, Final 3D density map of this particle, viewed from four perpendicular directions. **e**, Final 3D reconstruction superimposed with the fitted model, viewed from four perpendicular directions. **f**, FSC analyses of the final map resolution using two methods: map-map FSC, where each map is reconstructed from one half of the images (even vs. odd tilt angle indices), and map-model FSC, where the model map is generated from the fitted model. Resolution assessments are provided based on tilt-based map-map and map-model FSC analyses at thresholds of FSC=0.5 and 0.143, respectively.

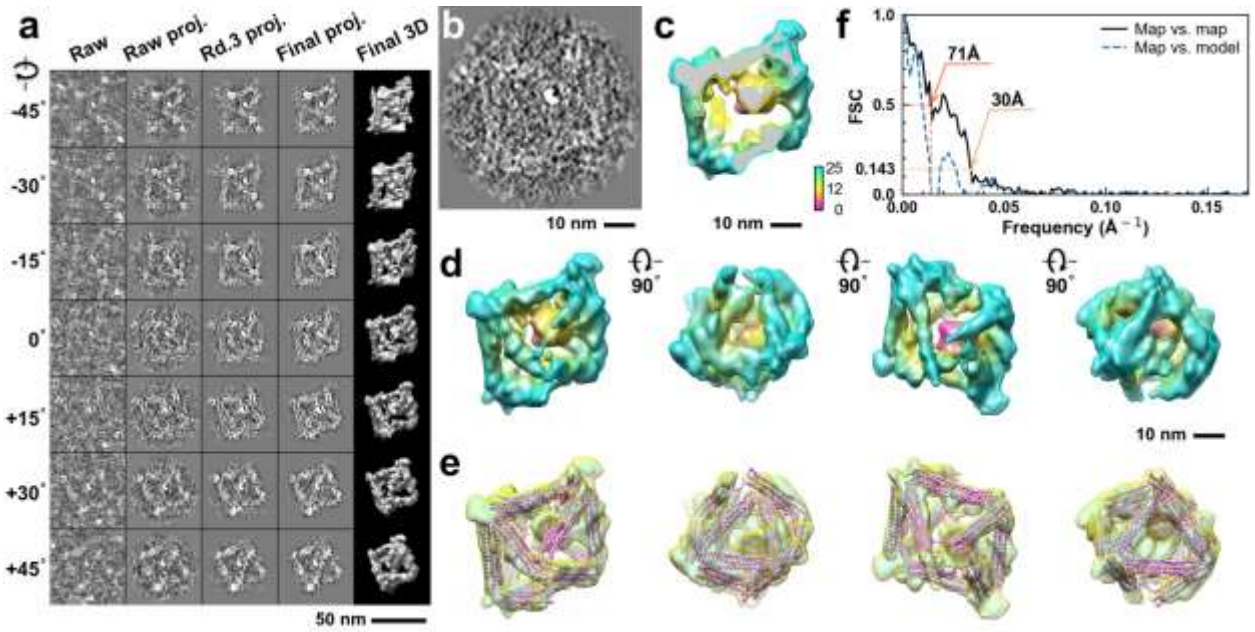

Supplementary Fig. 93: IPET 3D reconstruction and model fitting of an individual unit-cell particle (Index: 085) within a 2D lattice with 100% ferritin loading. a, Seven representative tilt images of a single unit-cell particle are shown in the first column (from left). The tilt images are aligned to a common center using IPET through iterative refinement. The projections of the raw, intermediate, and final 3D reconstruction at the corresponding angles are displayed in the subsequent four columns. **b**, A central cross-section (~23 nm thick) of the final reconstruction before masking is applied. **c**, 3D views of the central cross-section. **d**, Final 3D density map of this particle, viewed from four perpendicular directions. **e**, Final 3D reconstruction superimposed with the fitted model, viewed from four perpendicular directions. **f**, FSC analyses of the final map resolution using two methods: map-map FSC, where each map is reconstructed from one half of the images (even vs. odd tilt angle indices), and map-model FSC, where the model map is generated from the fitted model. Resolution assessments are provided based on tilt-based map-map and map-model FSC analyses at thresholds of FSC=0.5 and 0.143, respectively.

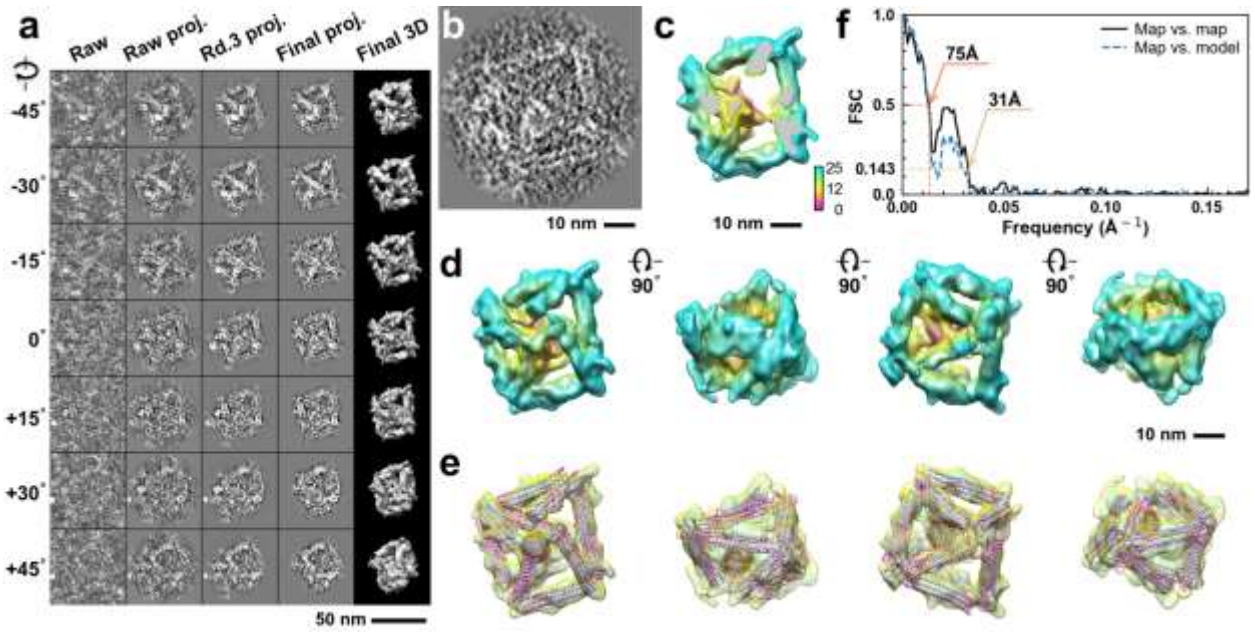

Supplementary Fig. 94: IPET 3D reconstruction and model fitting of an individual unit-cell particle (Index: 086) within a 2D lattice with 100% ferritin loading. a, Seven representative tilt images of a single unit-cell particle are shown in the first column (from left). The tilt images are aligned to a common center using IPET through iterative refinement. The projections of the raw, intermediate, and final 3D reconstruction at the corresponding angles are displayed in the subsequent four columns. **b**, A central cross-section (~23 nm thick) of the final reconstruction before masking is applied. **c**, 3D views of the central cross-section. **d**, Final 3D density map of this particle, viewed from four perpendicular directions. **e**, Final 3D reconstruction superimposed with the fitted model, viewed from four perpendicular directions. **f**, FSC analyses of the final map resolution using two methods: map-map FSC, where each map is reconstructed from one half of the images (even vs. odd tilt angle indices), and map-model FSC, where the model map is generated from the fitted model. Resolution assessments are provided based on tilt-based map-map and map-model FSC analyses at thresholds of FSC=0.5 and 0.143, respectively.

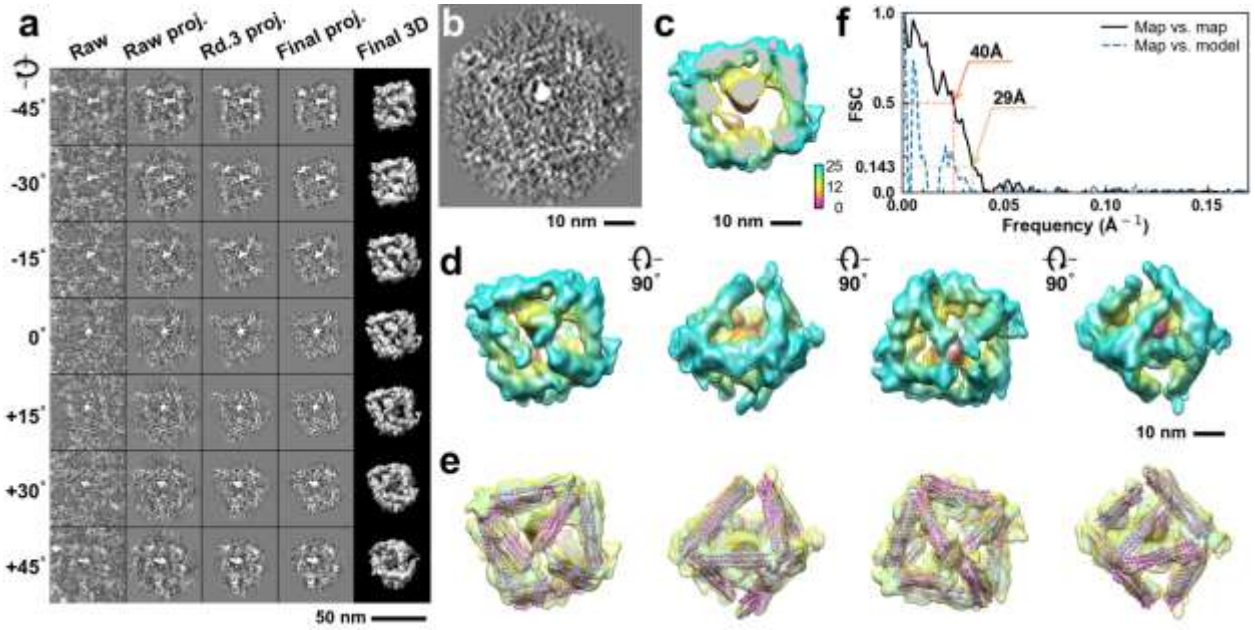

Supplementary Fig. 95: IPET 3D reconstruction and model fitting of an individual unit-cell particle (Index: 087) within a 2D lattice with 100% ferritin loading. a, Seven representative tilt images of a single unit-cell particle are shown in the first column (from left). The tilt images are aligned to a common center using IPET through iterative refinement. The projections of the raw, intermediate, and final 3D reconstruction at the corresponding angles are displayed in the subsequent four columns. **b**, A central cross-section (~23 nm thick) of the final reconstruction before masking is applied. **c**, 3D views of the central cross-section. **d**, Final 3D density map of this particle, viewed from four perpendicular directions. **e**, Final 3D reconstruction superimposed with the fitted model, viewed from four perpendicular directions. **f**, FSC analyses of the final map resolution using two methods: map-map FSC, where each map is reconstructed from one half of the images (even vs. odd tilt angle indices), and map-model FSC, where the model map is generated from the fitted model. Resolution assessments are provided based on tilt-based map-map and map-model FSC analyses at thresholds of FSC=0.5 and 0.143, respectively.

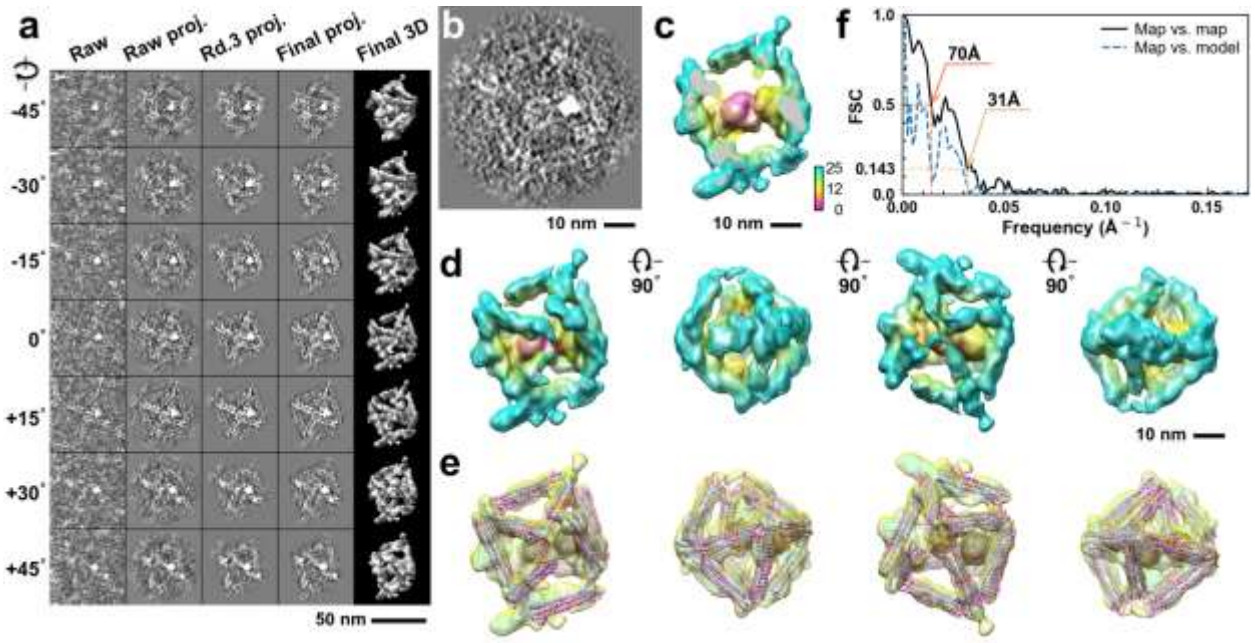

Supplementary Fig. 96: IPET 3D reconstruction and model fitting of an individual unit-cell particle (Index: 088) within a 2D lattice with 100% ferritin loading. a, Seven representative tilt images of a single unit-cell particle are shown in the first column (from left). The tilt images are aligned to a common center using IPET through iterative refinement. The projections of the raw, intermediate, and final 3D reconstruction at the corresponding angles are displayed in the subsequent four columns. **b**, A central cross-section (~23 nm thick) of the final reconstruction before masking is applied. **c**, 3D views of the central cross-section. **d**, Final 3D density map of this particle, viewed from four perpendicular directions. **e**, Final 3D reconstruction superimposed with the fitted model, viewed from four perpendicular directions. **f**, FSC analyses of the final map resolution using two methods: map-map FSC, where each map is reconstructed from one half of the images (even vs. odd tilt angle indices), and map-model FSC, where the model map is generated from the fitted model. Resolution assessments are provided based on tilt-based map-map and map-model FSC analyses at thresholds of FSC=0.5 and 0.143, respectively.

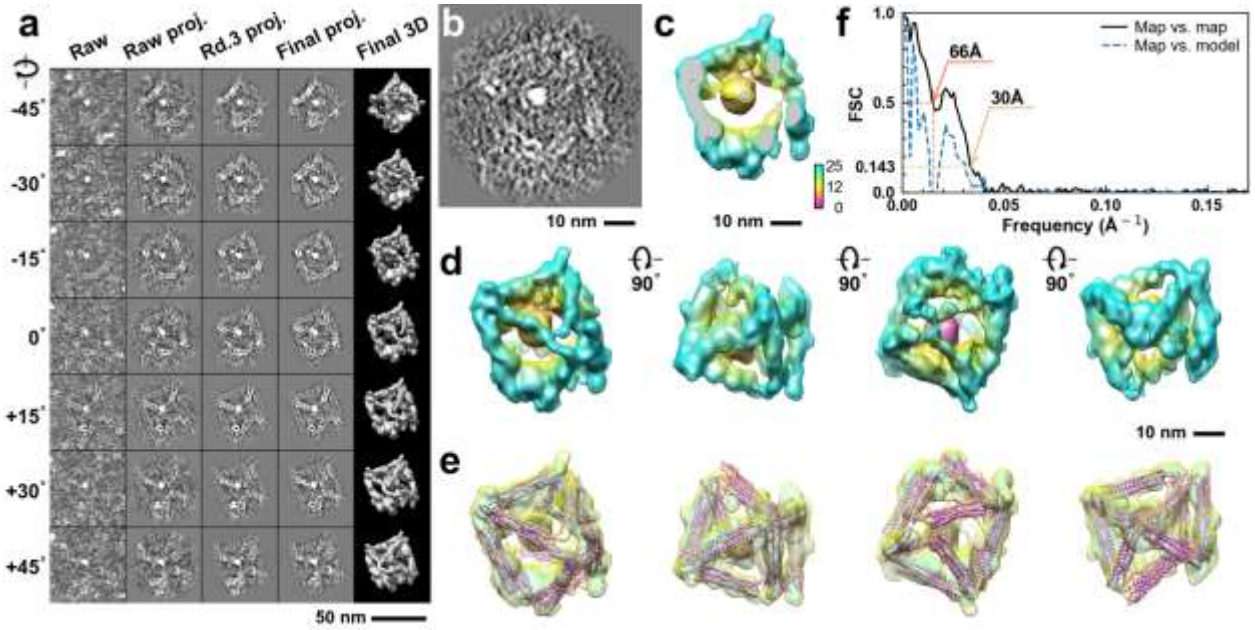

Supplementary Fig. 97: IPET 3D reconstruction and model fitting of an individual unit-cell particle (Index: 089) within a 2D lattice with 100% ferritin loading. a, Seven representative tilt images of a single unit-cell particle are shown in the first column (from left). The tilt images are aligned to a common center using IPET through iterative refinement. The projections of the raw, intermediate, and final 3D reconstruction at the corresponding angles are displayed in the subsequent four columns. **b**, A central cross-section (~23 nm thick) of the final reconstruction before masking is applied. **c**, 3D views of the central cross-section. **d**, Final 3D density map of this particle, viewed from four perpendicular directions. **e**, Final 3D reconstruction superimposed with the fitted model, viewed from four perpendicular directions. **f**, FSC analyses of the final map resolution using two methods: map-map FSC, where each map is reconstructed from one half of the images (even vs. odd tilt angle indices), and map-model FSC, where the model map is generated from the fitted model. Resolution assessments are provided based on tilt-based map-map and map-model FSC analyses at thresholds of FSC=0.5 and 0.143, respectively.

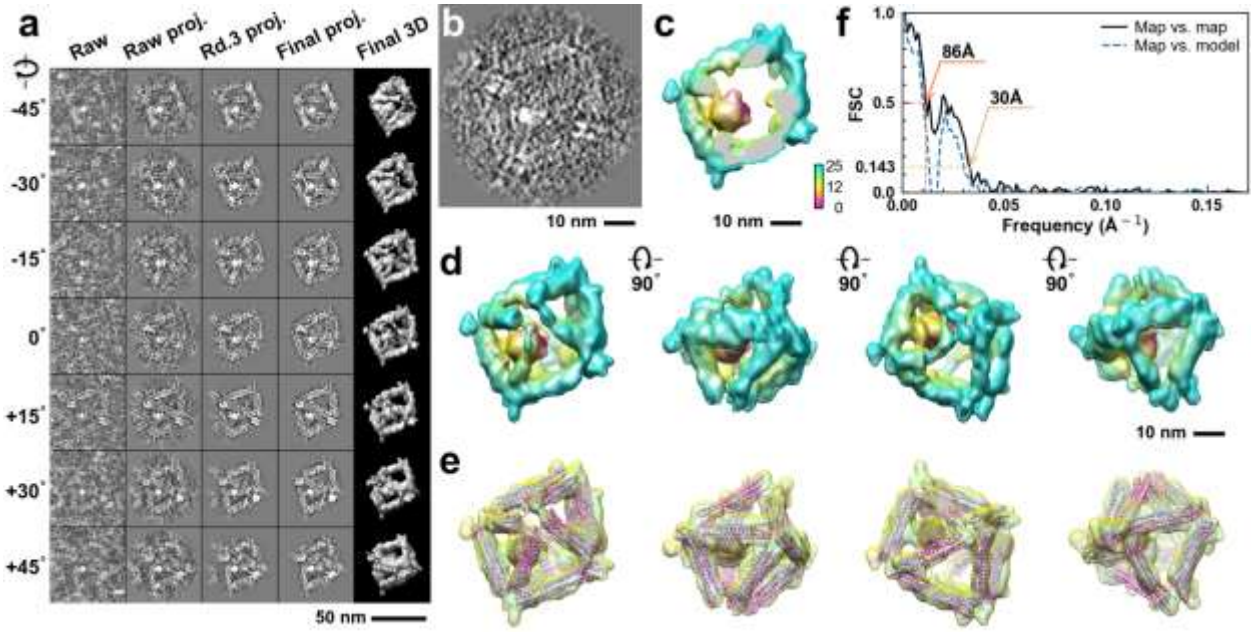

Supplementary Fig. 98: IPET 3D reconstruction and model fitting of an individual unit-cell particle (Index: 090) within a 2D lattice with 100% ferritin loading. a, Seven representative tilt images of a single unit-cell particle are shown in the first column (from left). The tilt images are aligned to a common center using IPET through iterative refinement. The projections of the raw, intermediate, and final 3D reconstruction at the corresponding angles are displayed in the subsequent four columns. **b**, A central cross-section (~23 nm thick) of the final reconstruction before masking is applied. **c**, 3D views of the central cross-section. **d**, Final 3D density map of this particle, viewed from four perpendicular directions. **e**, Final 3D reconstruction superimposed with the fitted model, viewed from four perpendicular directions. **f**, FSC analyses of the final map resolution using two methods: map-map FSC, where each map is reconstructed from one half of the images (even vs. odd tilt angle indices), and map-model FSC, where the model map is generated from the fitted model. Resolution assessments are provided based on tilt-based map-map and map-model FSC analyses at thresholds of FSC=0.5 and 0.143, respectively.

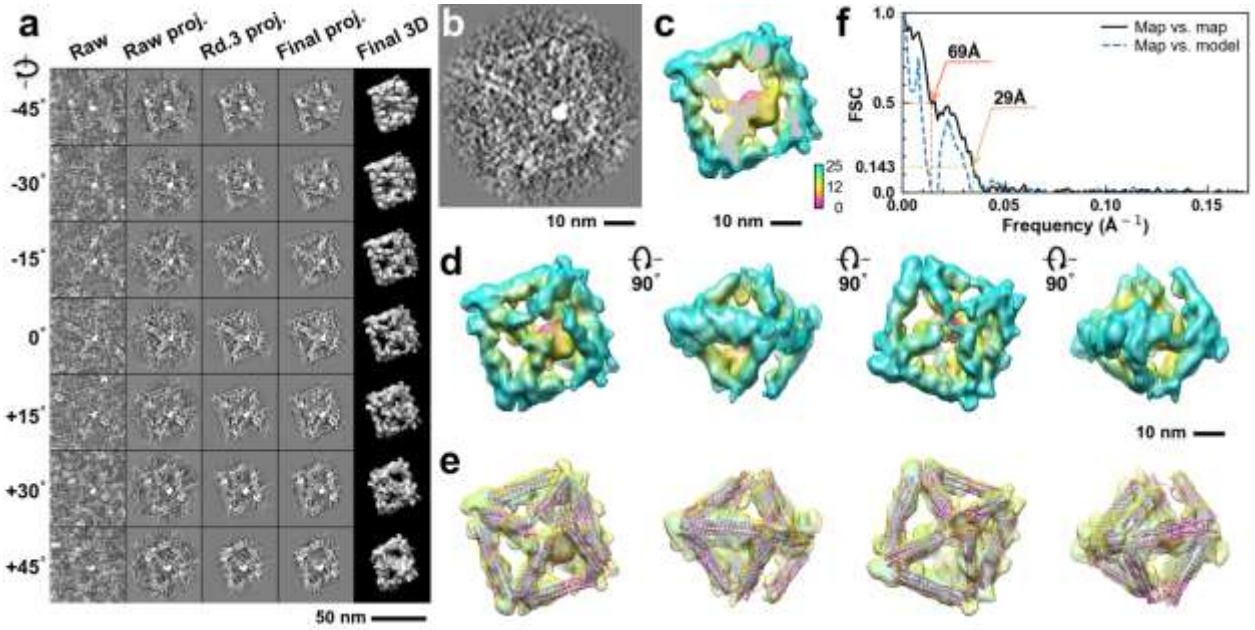

Supplementary Fig. 99: IPET 3D reconstruction and model fitting of an individual unit-cell particle (Index: 091) within a 2D lattice with 100% ferritin loading. a, Seven representative tilt images of a single unit-cell particle are shown in the first column (from left). The tilt images are aligned to a common center using IPET through iterative refinement. The projections of the raw, intermediate, and final 3D reconstruction at the corresponding angles are displayed in the subsequent four columns. **b**, A central cross-section (~23 nm thick) of the final reconstruction before masking is applied. **c**, 3D views of the central cross-section. **d**, Final 3D density map of this particle, viewed from four perpendicular directions. **e**, Final 3D reconstruction superimposed with the fitted model, viewed from four perpendicular directions. **f**, FSC analyses of the final map resolution using two methods: map-map FSC, where each map is reconstructed from one half of the images (even vs. odd tilt angle indices), and map-model FSC, where the model map is generated from the fitted model. Resolution assessments are provided based on tilt-based map-map and map-model FSC analyses at thresholds of FSC=0.5 and 0.143, respectively.

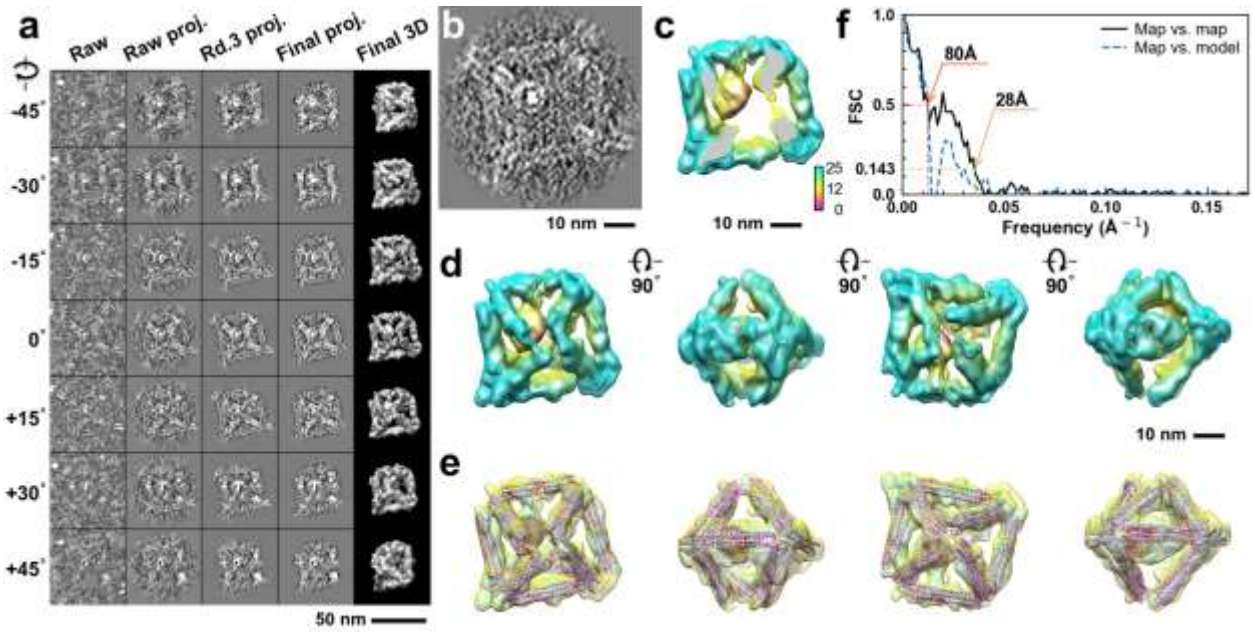

Supplementary Fig. 100: IPET 3D reconstruction and model fitting of an individual unit-cell particle (Index: 092) within a 2D lattice with 100% ferritin loading. a, Seven representative tilt images of a single unit-cell particle are shown in the first column (from left). The tilt images are aligned to a common center using IPET through iterative refinement. The projections of the raw, intermediate, and final 3D reconstruction at the corresponding angles are displayed in the subsequent four columns. **b**, A central cross-section (~23 nm thick) of the final reconstruction before masking is applied. **c**, 3D views of the central cross-section. **d**, Final 3D density map of this particle, viewed from four perpendicular directions. **e**, Final 3D reconstruction superimposed with the fitted model, viewed from four perpendicular directions. **f**, FSC analyses of the final map resolution using two methods: map-map FSC, where each map is reconstructed from one half of the images (even vs. odd tilt angle indices), and map-model FSC, where the model map is generated from the fitted model. Resolution assessments are provided based on tilt-based map-map and map-model FSC analyses at thresholds of FSC=0.5 and 0.143, respectively.

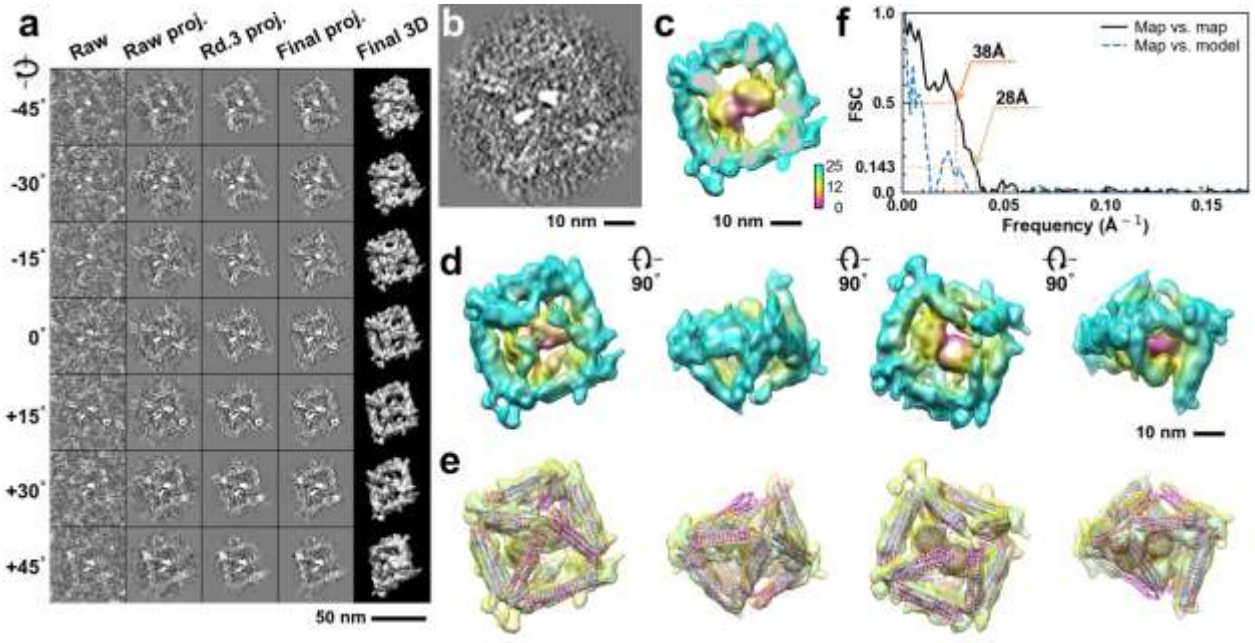

Supplementary Fig. 101: IPET 3D reconstruction and model fitting of an individual unit-cell particle (Index: 093) within a 2D lattice with 100% ferritin loading. a, Seven representative tilt images of a single unit-cell particle are shown in the first column (from left). The tilt images are aligned to a common center using IPET through iterative refinement. The projections of the raw, intermediate, and final 3D reconstruction at the corresponding angles are displayed in the subsequent four columns. **b**, A central cross-section (~23 nm thick) of the final reconstruction before masking is applied. **c**, 3D views of the central cross-section. **d**, Final 3D density map of this particle, viewed from four perpendicular directions. **e**, Final 3D reconstruction superimposed with the fitted model, viewed from four perpendicular directions. **f**, FSC analyses of the final map resolution using two methods: map-map FSC, where each map is reconstructed from one half of the images (even vs. odd tilt angle indices), and map-model FSC, where the model map is generated from the fitted model. Resolution assessments are provided based on tilt-based map-map and map-model FSC analyses at thresholds of FSC=0.5 and 0.143, respectively.

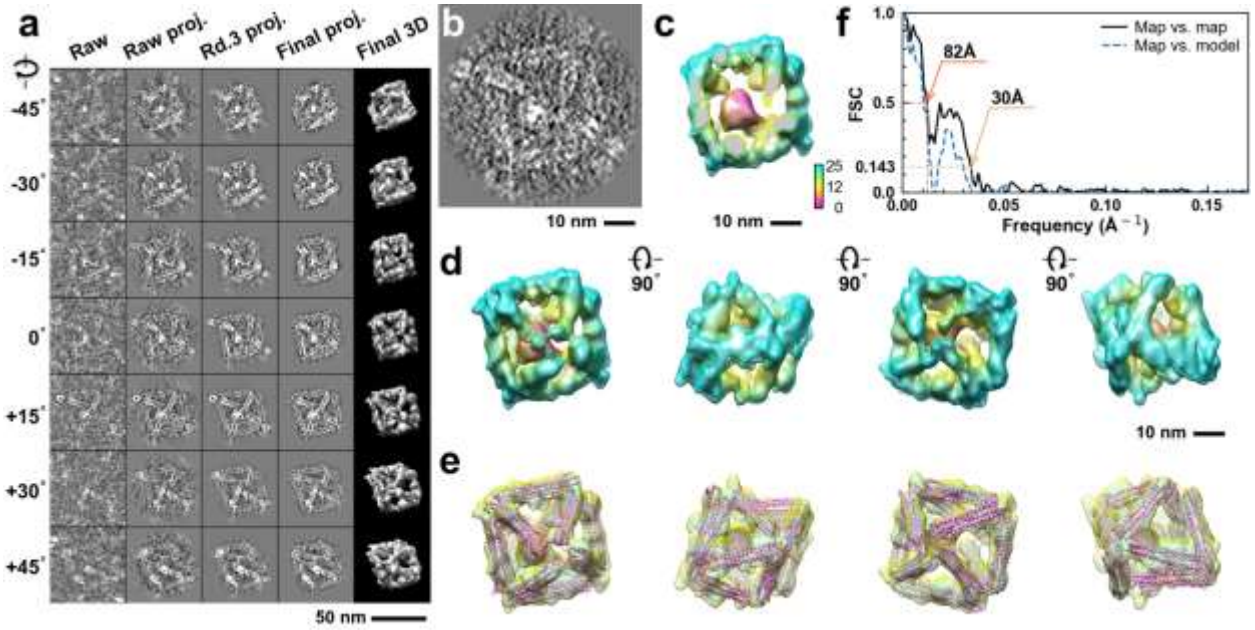

Supplementary Fig. 102: IPET 3D reconstruction and model fitting of an individual unit-cell particle (Index: 094) within a 2D lattice with 100% ferritin loading. a, Seven representative tilt images of a single unit-cell particle are shown in the first column (from left). The tilt images are aligned to a common center using IPET through iterative refinement. The projections of the raw, intermediate, and final 3D reconstruction at the corresponding angles are displayed in the subsequent four columns. **b**, A central cross-section (~23 nm thick) of the final reconstruction before masking is applied. **c**, 3D views of the central cross-section. **d**, Final 3D density map of this particle, viewed from four perpendicular directions. **e**, Final 3D reconstruction superimposed with the fitted model, viewed from four perpendicular directions. **f**, FSC analyses of the final map resolution using two methods: map-map FSC, where each map is reconstructed from one half of the images (even vs. odd tilt angle indices), and map-model FSC, where the model map is generated from the fitted model. Resolution assessments are provided based on tilt-based map-map and map-model FSC analyses at thresholds of FSC=0.5 and 0.143, respectively.

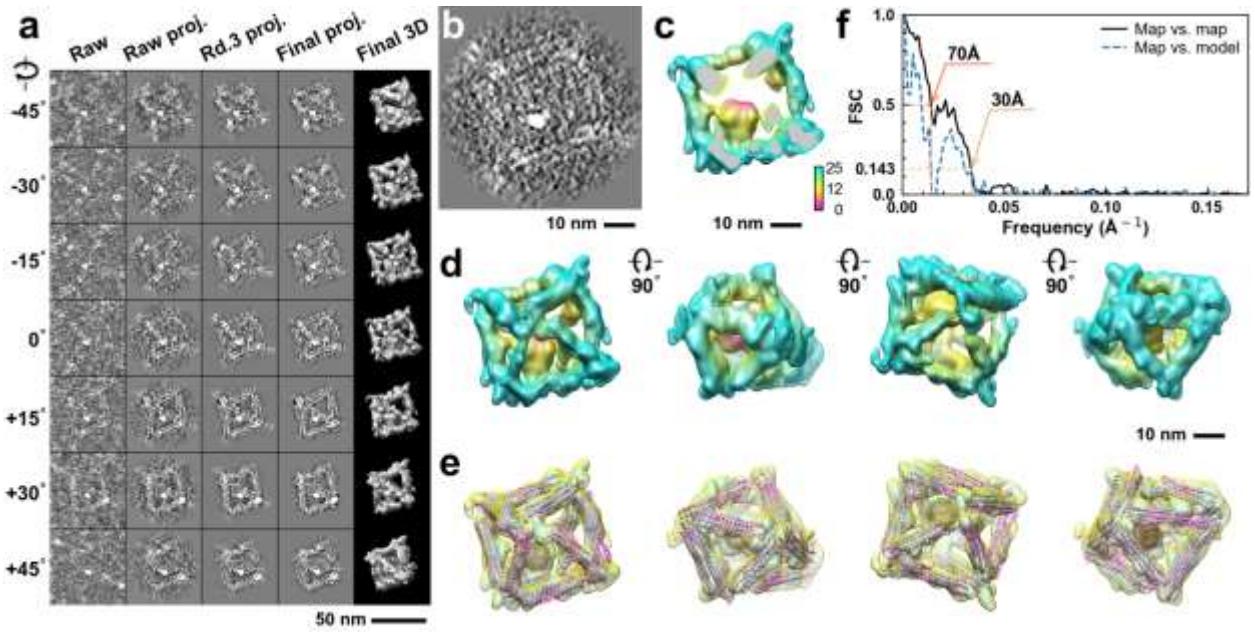

Supplementary Fig. 103: IPET 3D reconstruction and model fitting of an individual unit-cell particle (Index: 095) within a 2D lattice with 100% ferritin loading. a, Seven representative tilt images of a single unit-cell particle are shown in the first column (from left). The tilt images are aligned to a common center using IPET through iterative refinement. The projections of the raw, intermediate, and final 3D reconstruction at the corresponding angles are displayed in the subsequent four columns. **b**, A central cross-section (~23 nm thick) of the final reconstruction before masking is applied. **c**, 3D views of the central cross-section. **d**, Final 3D density map of this particle, viewed from four perpendicular directions. **e**, Final 3D reconstruction superimposed with the fitted model, viewed from four perpendicular directions. **f**, FSC analyses of the final map resolution using two methods: map-map FSC, where each map is reconstructed from one half of the images (even vs. odd tilt angle indices), and map-model FSC, where the model map is generated from the fitted model. Resolution assessments are provided based on tilt-based map-map and map-model FSC analyses at thresholds of FSC=0.5 and 0.143, respectively.

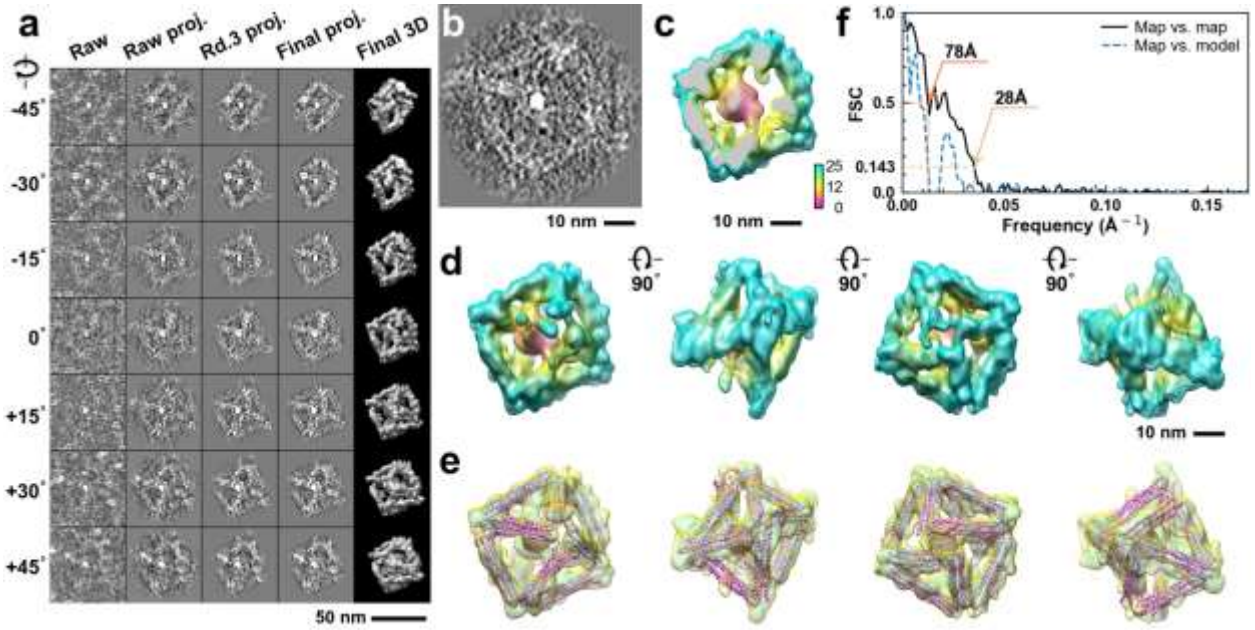

Supplementary Fig. 104: IPET 3D reconstruction and model fitting of an individual unit-cell particle (Index: 096) within a 2D lattice with 100% ferritin loading. a, Seven representative tilt images of a single unit-cell particle are shown in the first column (from left). The tilt images are aligned to a common center using IPET through iterative refinement. The projections of the raw, intermediate, and final 3D reconstruction at the corresponding angles are displayed in the subsequent four columns. **b**, A central cross-section (~23 nm thick) of the final reconstruction before masking is applied. **c**, 3D views of the central cross-section. **d**, Final 3D density map of this particle, viewed from four perpendicular directions. **e**, Final 3D reconstruction superimposed with the fitted model, viewed from four perpendicular directions. **f**, FSC analyses of the final map resolution using two methods: map-map FSC, where each map is reconstructed from one half of the images (even vs. odd tilt angle indices), and map-model FSC, where the model map is generated from the fitted model. Resolution assessments are provided based on tilt-based map-map and map-model FSC analyses at thresholds of FSC=0.5 and 0.143, respectively.

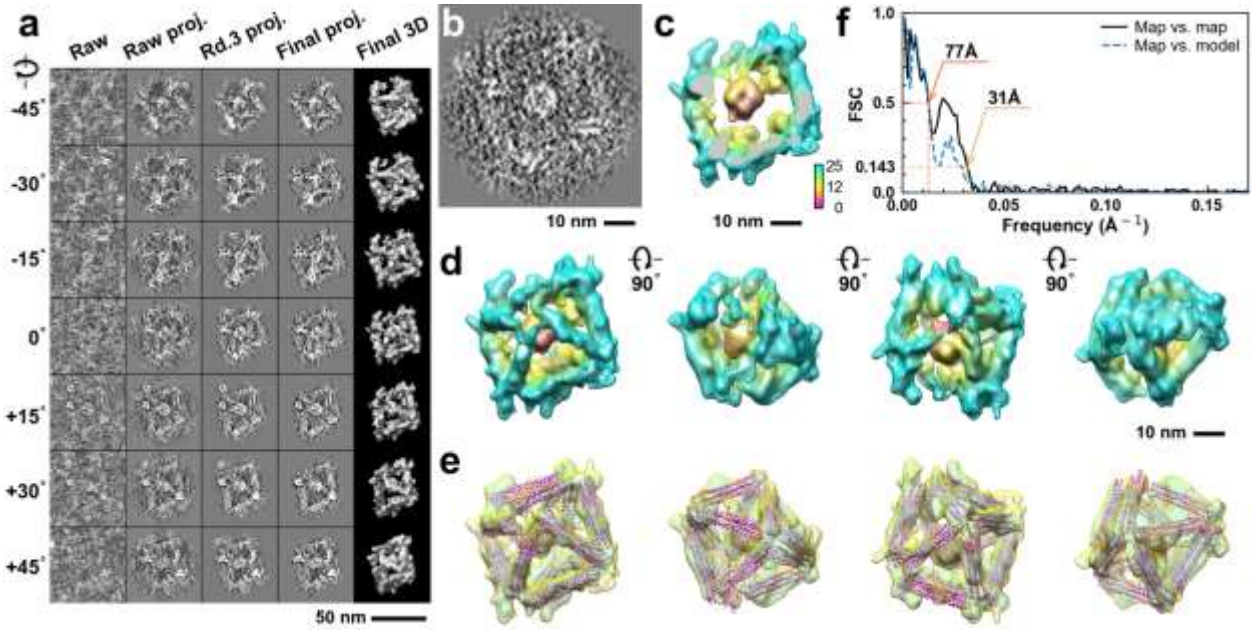

Supplementary Fig. 105: IPET 3D reconstruction and model fitting of an individual unit-cell particle (Index: 097) within a 2D lattice with 100% ferritin loading. a, Seven representative tilt images of a single unit-cell particle are shown in the first column (from left). The tilt images are aligned to a common center using IPET through iterative refinement. The projections of the raw, intermediate, and final 3D reconstruction at the corresponding angles are displayed in the subsequent four columns. **b**, A central cross-section (~23 nm thick) of the final reconstruction before masking is applied. **c**, 3D views of the central cross-section. **d**, Final 3D density map of this particle, viewed from four perpendicular directions. **e**, Final 3D reconstruction superimposed with the fitted model, viewed from four perpendicular directions. **f**, FSC analyses of the final map resolution using two methods: map-map FSC, where each map is reconstructed from one half of the images (even vs. odd tilt angle indices), and map-model FSC, where the model map is generated from the fitted model. Resolution assessments are provided based on tilt-based map-map and map-model FSC analyses at thresholds of FSC=0.5 and 0.143, respectively.

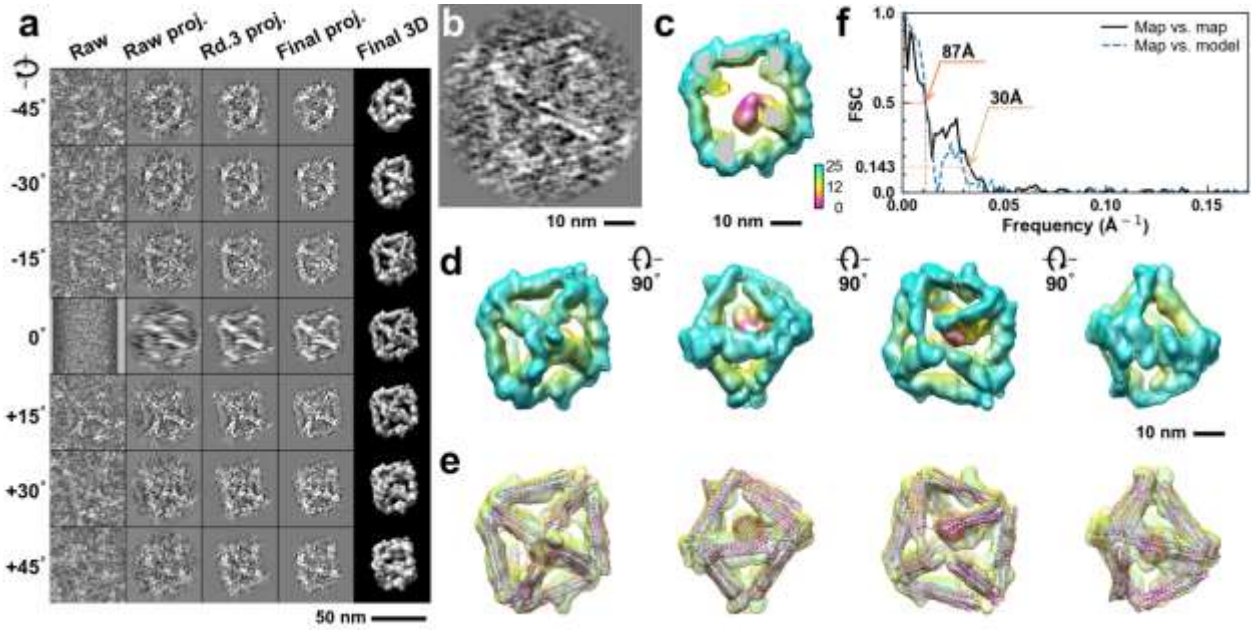

Supplementary Fig. 106: IPET 3D reconstruction and model fitting of an individual unit-cell particle (Index: 098) within a 2D lattice with 100% ferritin loading. a, Seven representative tilt images of a single unit-cell particle are shown in the first column (from left). The tilt images are aligned to a common center using IPET through iterative refinement. The projections of the raw, intermediate, and final 3D reconstruction at the corresponding angles are displayed in the subsequent four columns. **b**, A central cross-section (~23 nm thick) of the final reconstruction before masking is applied. **c**, 3D views of the central cross-section. **d**, Final 3D density map of this particle, viewed from four perpendicular directions. **e**, Final 3D reconstruction superimposed with the fitted model, viewed from four perpendicular directions. **f**, FSC analyses of the final map resolution using two methods: map-map FSC, where each map is reconstructed from one half of the images (even vs. odd tilt angle indices), and map-model FSC, where the model map is generated from the fitted model. Resolution assessments are provided based on tilt-based map-map and map-model FSC analyses at thresholds of FSC=0.5 and 0.143, respectively.

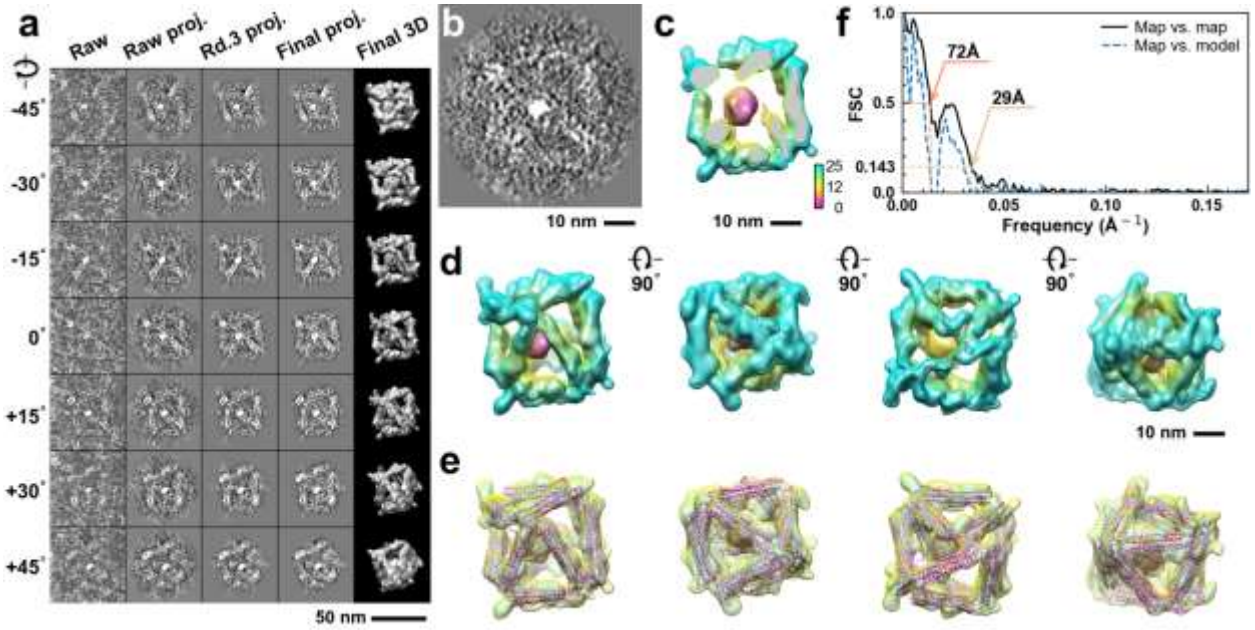

Supplementary Fig. 107: IPET 3D reconstruction and model fitting of an individual unit-cell particle (Index: 099) within a 2D lattice with 100% ferritin loading. a, Seven representative tilt images of a single unit-cell particle are shown in the first column (from left). The tilt images are aligned to a common center using IPET through iterative refinement. The projections of the raw, intermediate, and final 3D reconstruction at the corresponding angles are displayed in the subsequent four columns. **b**, A central cross-section (~23 nm thick) of the final reconstruction before masking is applied. **c**, 3D views of the central cross-section. **d**, Final 3D density map of this particle, viewed from four perpendicular directions. **e**, Final 3D reconstruction superimposed with the fitted model, viewed from four perpendicular directions. **f**, FSC analyses of the final map resolution using two methods: map-map FSC, where each map is reconstructed from one half of the images (even vs. odd tilt angle indices), and map-model FSC, where the model map is generated from the fitted model. Resolution assessments are provided based on tilt-based map-map and map-model FSC analyses at thresholds of FSC=0.5 and 0.143, respectively.

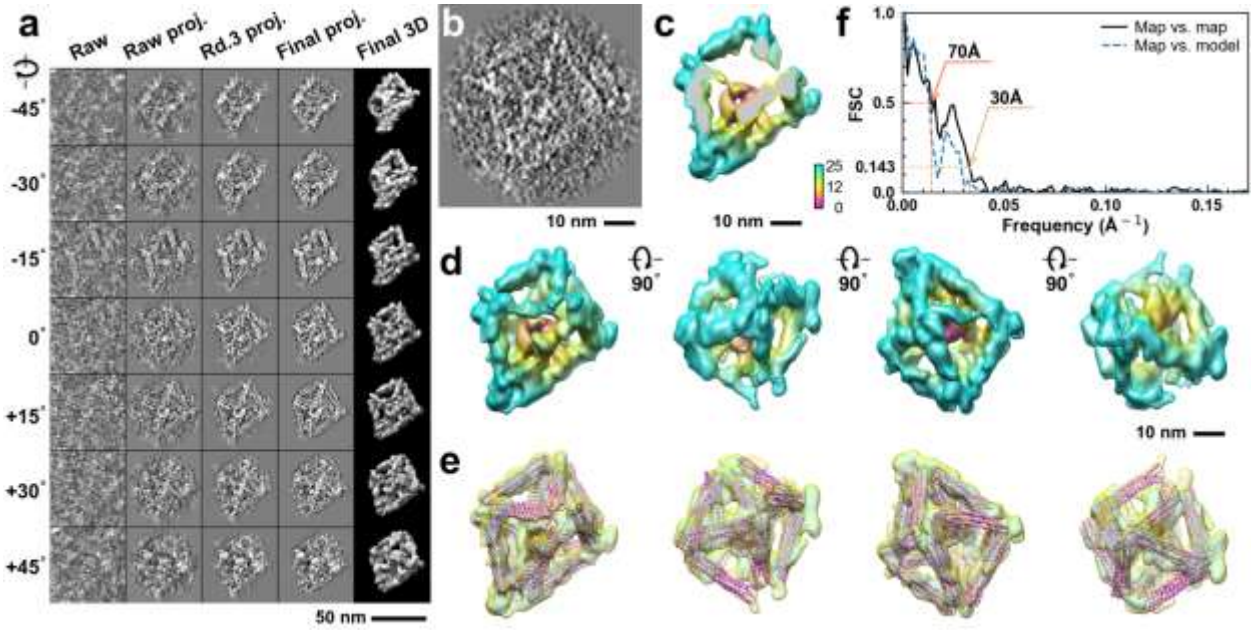

Supplementary Fig. 108: IPET 3D reconstruction and model fitting of an individual unit-cell particle (Index: 100) within a 2D lattice with 100% ferritin loading. a, Seven representative tilt images of a single unit-cell particle are shown in the first column (from left). The tilt images are aligned to a common center using IPET through iterative refinement. The projections of the raw, intermediate, and final 3D reconstruction at the corresponding angles are displayed in the subsequent four columns. **b**, A central cross-section (~23 nm thick) of the final reconstruction before masking is applied. **c**, 3D views of the central cross-section. **d**, Final 3D density map of this particle, viewed from four perpendicular directions. **e**, Final 3D reconstruction superimposed with the fitted model, viewed from four perpendicular directions. **f**, FSC analyses of the final map resolution using two methods: map-map FSC, where each map is reconstructed from one half of the images (even vs. odd tilt angle indices), and map-model FSC, where the model map is generated from the fitted model. Resolution assessments are provided based on tilt-based map-map and map-model FSC analyses at thresholds of FSC=0.5 and 0.143, respectively.

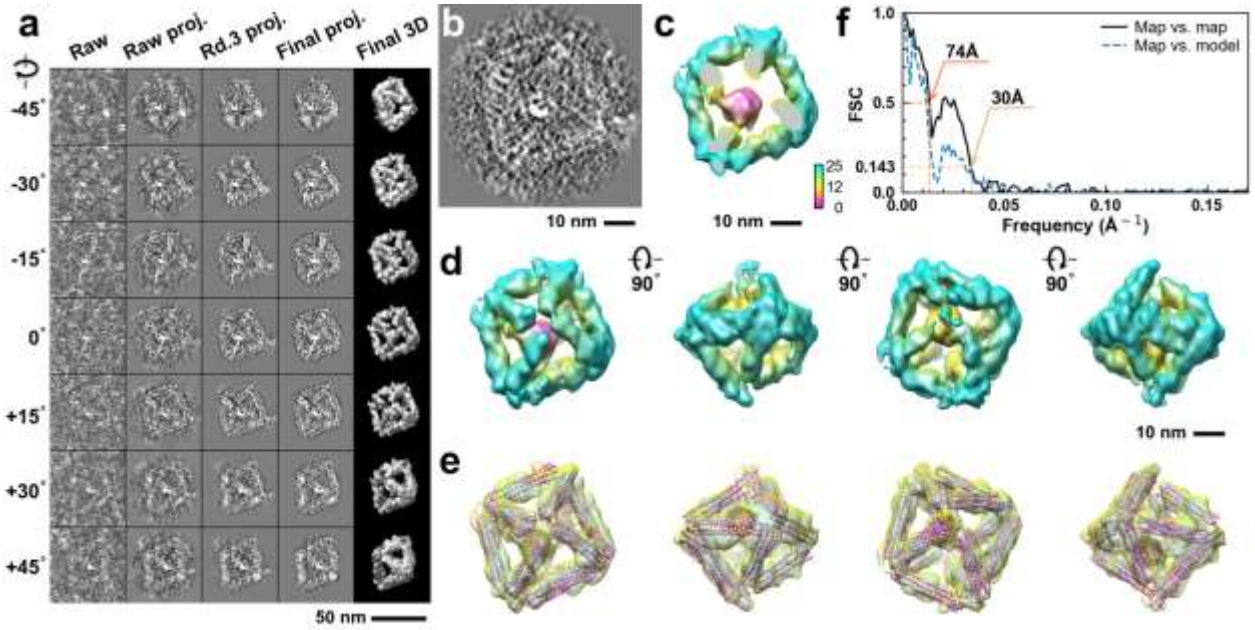

Supplementary Fig. 109: IPET 3D reconstruction and model fitting of an individual unit-cell particle (Index: 101) within a 2D lattice with 100% ferritin loading. a, Seven representative tilt images of a single unit-cell particle are shown in the first column (from left). The tilt images are aligned to a common center using IPET through iterative refinement. The projections of the raw, intermediate, and final 3D reconstruction at the corresponding angles are displayed in the subsequent four columns. **b**, A central cross-section (~23 nm thick) of the final reconstruction before masking is applied. **c**, 3D views of the central cross-section. **d**, Final 3D density map of this particle, viewed from four perpendicular directions. **e**, Final 3D reconstruction superimposed with the fitted model, viewed from four perpendicular directions. **f**, FSC analyses of the final map resolution using two methods: map-map FSC, where each map is reconstructed from one half of the images (even vs. odd tilt angle indices), and map-model FSC, where the model map is generated from the fitted model. Resolution assessments are provided based on tilt-based map-map and map-model FSC analyses at thresholds of FSC=0.5 and 0.143, respectively.

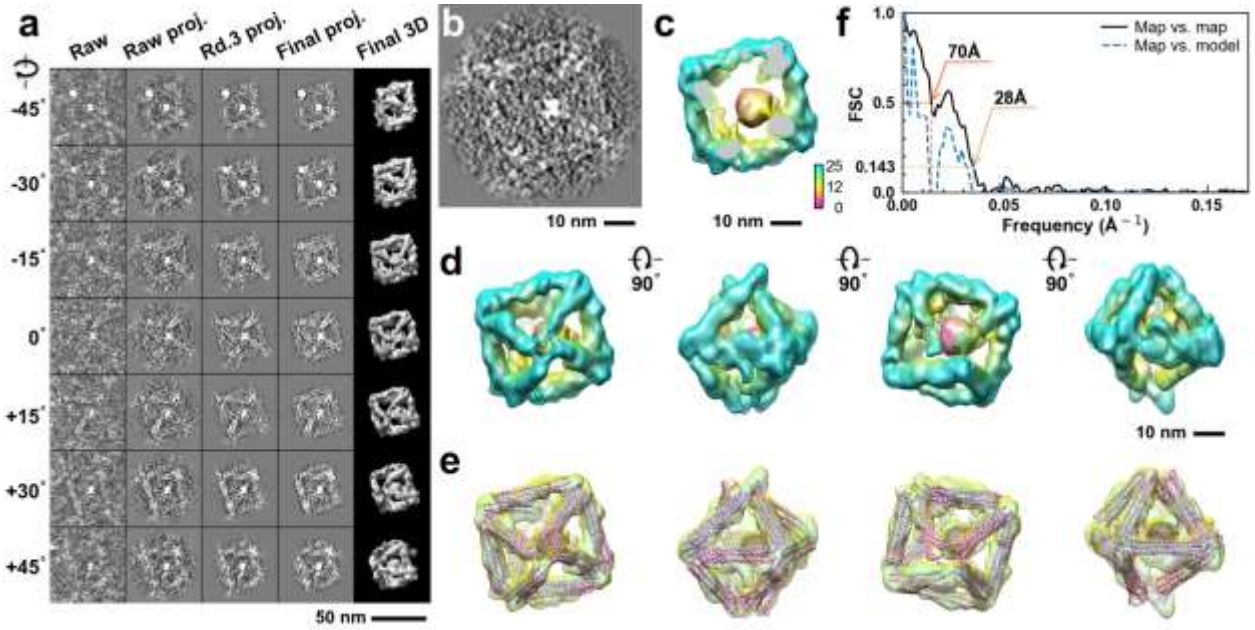

Supplementary Fig. 110: IPET 3D reconstruction and model fitting of an individual unit-cell particle (Index: 102) within a 2D lattice with 100% ferritin loading. a, Seven representative tilt images of a single unit-cell particle are shown in the first column (from left). The tilt images are aligned to a common center using IPET through iterative refinement. The projections of the raw, intermediate, and final 3D reconstruction at the corresponding angles are displayed in the subsequent four columns. **b**, A central cross-section (~23 nm thick) of the final reconstruction before masking is applied. **c**, 3D views of the central cross-section. **d**, Final 3D density map of this particle, viewed from four perpendicular directions. **e**, Final 3D reconstruction superimposed with the fitted model, viewed from four perpendicular directions. **f**, FSC analyses of the final map resolution using two methods: map-map FSC, where each map is reconstructed from one half of the images (even vs. odd tilt angle indices), and map-model FSC, where the model map is generated from the fitted model. Resolution assessments are provided based on tilt-based map-map and map-model FSC analyses at thresholds of FSC=0.5 and 0.143, respectively.

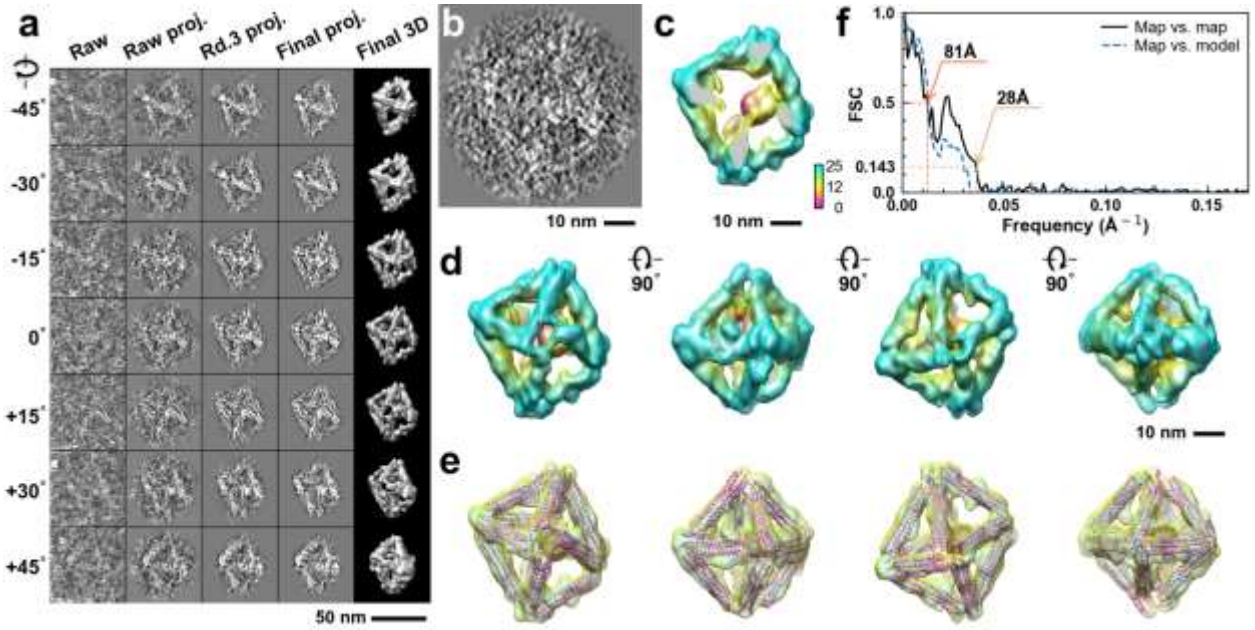

Supplementary Fig. 111: IPET 3D reconstruction and model fitting of an individual unit-cell particle (Index: 103) within a 2D lattice with 100% ferritin loading. a, Seven representative tilt images of a single unit-cell particle are shown in the first column (from left). The tilt images are aligned to a common center using IPET through iterative refinement. The projections of the raw, intermediate, and final 3D reconstruction at the corresponding angles are displayed in the subsequent four columns. **b**, A central cross-section (~23 nm thick) of the final reconstruction before masking is applied. **c**, 3D views of the central cross-section. **d**, Final 3D density map of this particle, viewed from four perpendicular directions. **e**, Final 3D reconstruction superimposed with the fitted model, viewed from four perpendicular directions. **f**, FSC analyses of the final map resolution using two methods: map-map FSC, where each map is reconstructed from one half of the images (even vs. odd tilt angle indices), and map-model FSC, where the model map is generated from the fitted model. Resolution assessments are provided based on tilt-based map-map and map-model FSC analyses at thresholds of FSC=0.5 and 0.143, respectively.

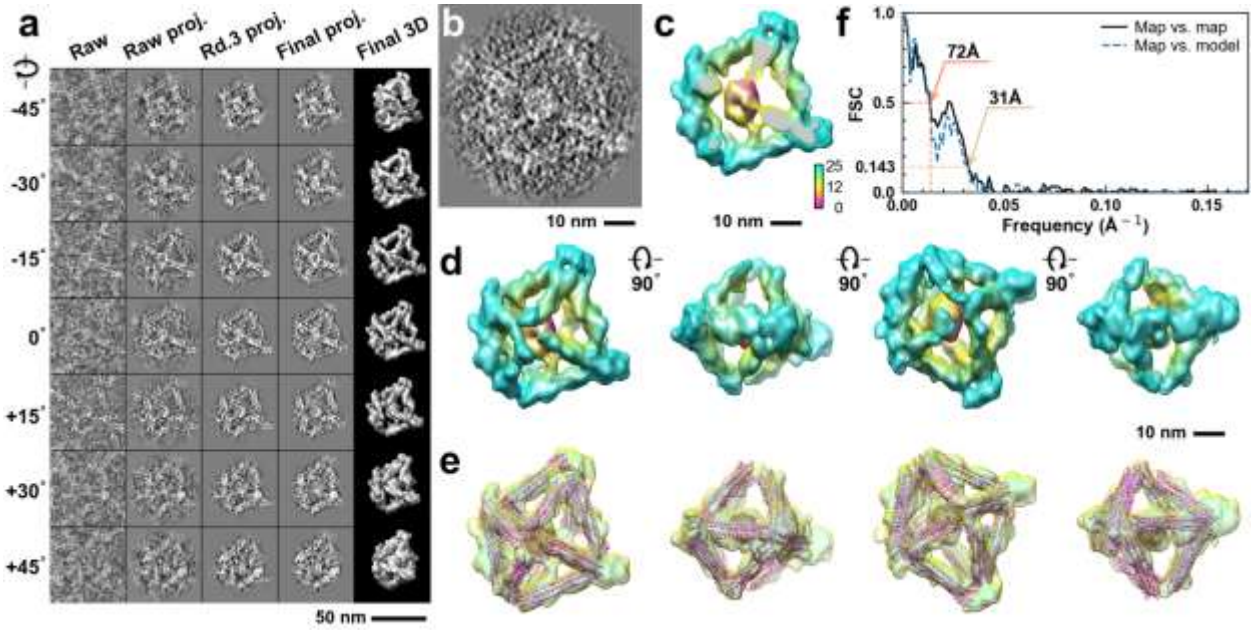

Supplementary Fig. 112: IPET 3D reconstruction and model fitting of an individual unit-cell particle (Index: 104) within a 2D lattice with 100% ferritin loading. a, Seven representative tilt images of a single unit-cell particle are shown in the first column (from left). The tilt images are aligned to a common center using IPET through iterative refinement. The projections of the raw, intermediate, and final 3D reconstruction at the corresponding angles are displayed in the subsequent four columns. **b**, A central cross-section (~23 nm thick) of the final reconstruction before masking is applied. **c**, 3D views of the central cross-section. **d**, Final 3D density map of this particle, viewed from four perpendicular directions. **e**, Final 3D reconstruction superimposed with the fitted model, viewed from four perpendicular directions. **f**, FSC analyses of the final map resolution using two methods: map-map FSC, where each map is reconstructed from one half of the images (even vs. odd tilt angle indices), and map-model FSC, where the model map is generated from the fitted model. Resolution assessments are provided based on tilt-based map-map and map-model FSC analyses at thresholds of FSC=0.5 and 0.143, respectively.

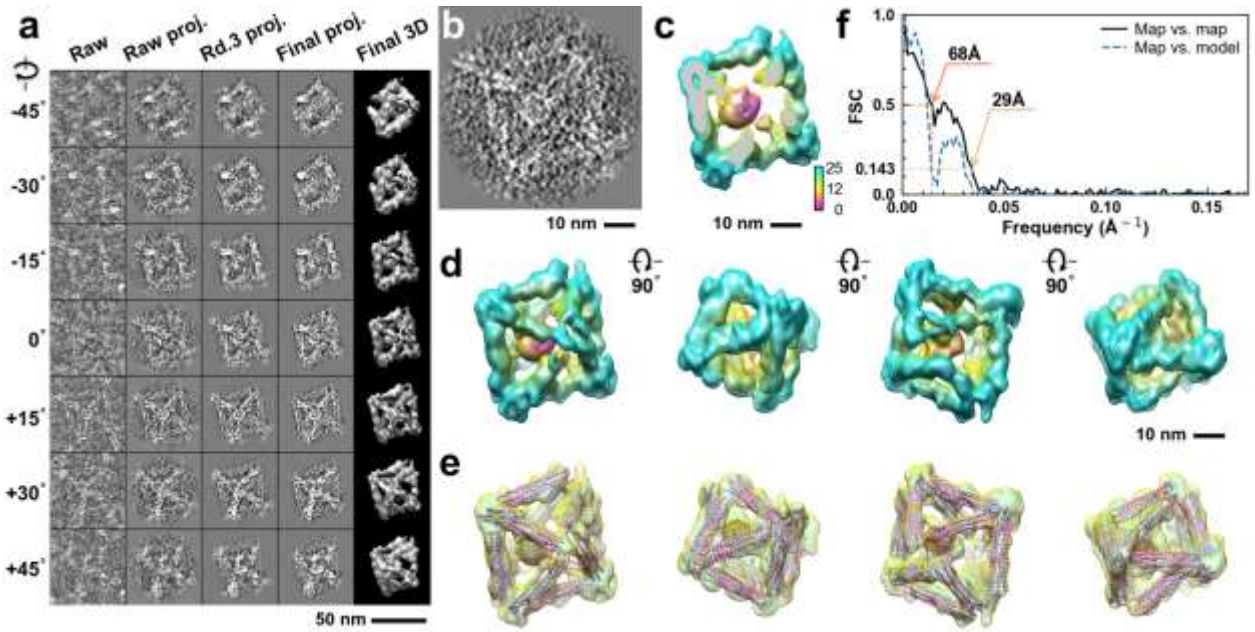

Supplementary Fig. 113: IPET 3D reconstruction and model fitting of an individual unit-cell particle (Index: 105) within a 2D lattice with 100% ferritin loading. a, Seven representative tilt images of a single unit-cell particle are shown in the first column (from left). The tilt images are aligned to a common center using IPET through iterative refinement. The projections of the raw, intermediate, and final 3D reconstruction at the corresponding angles are displayed in the subsequent four columns. **b**, A central cross-section (~23 nm thick) of the final reconstruction before masking is applied. **c**, 3D views of the central cross-section. **d**, Final 3D density map of this particle, viewed from four perpendicular directions. **e**, Final 3D reconstruction superimposed with the fitted model, viewed from four perpendicular directions. **f**, FSC analyses of the final map resolution using two methods: map-map FSC, where each map is reconstructed from one half of the images (even vs. odd tilt angle indices), and map-model FSC, where the model map is generated from the fitted model. Resolution assessments are provided based on tilt-based map-map and map-model FSC analyses at thresholds of FSC=0.5 and 0.143, respectively.

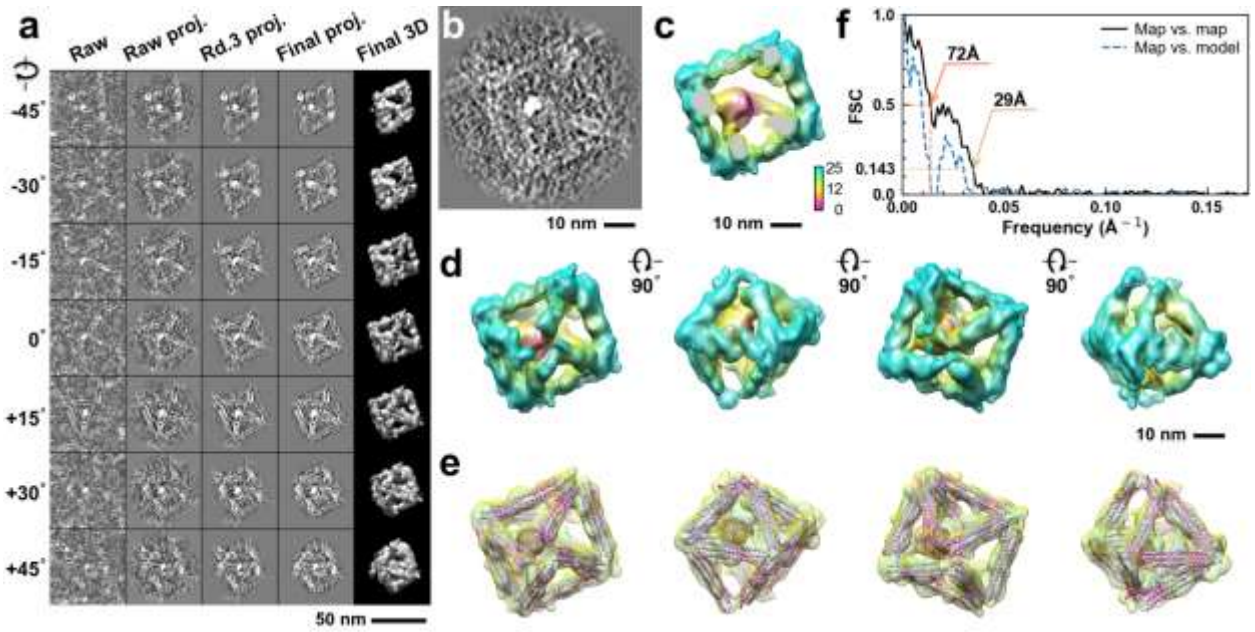

Supplementary Fig. 114: IPET 3D reconstruction and model fitting of an individual unit-cell particle (Index: 106) within a 2D lattice with 100% ferritin loading. a, Seven representative tilt images of a single unit-cell particle are shown in the first column (from left). The tilt images are aligned to a common center using IPET through iterative refinement. The projections of the raw, intermediate, and final 3D reconstruction at the corresponding angles are displayed in the subsequent four columns. **b**, A central cross-section (~23 nm thick) of the final reconstruction before masking is applied. **c**, 3D views of the central cross-section. **d**, Final 3D density map of this particle, viewed from four perpendicular directions. **e**, Final 3D reconstruction superimposed with the fitted model, viewed from four perpendicular directions. **f**, FSC analyses of the final map resolution using two methods: map-map FSC, where each map is reconstructed from one half of the images (even vs. odd tilt angle indices), and map-model FSC, where the model map is generated from the fitted model. Resolution assessments are provided based on tilt-based map-map and map-model FSC analyses at thresholds of FSC=0.5 and 0.143, respectively.

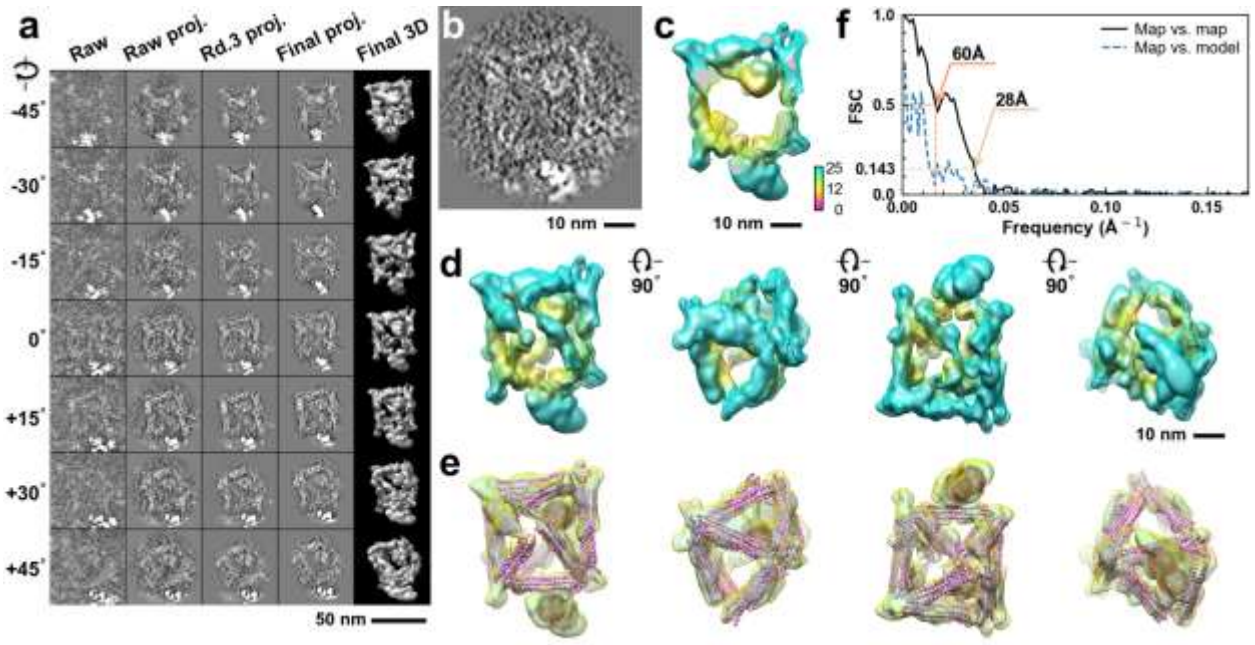

Supplementary Fig. 115: IPET 3D reconstruction and model fitting of an individual unit-cell particle (Index: 107) within a 2D lattice with 100% ferritin loading. a, Seven representative tilt images of a single unit-cell particle are shown in the first column (from left). The tilt images are aligned to a common center using IPET through iterative refinement. The projections of the raw, intermediate, and final 3D reconstruction at the corresponding angles are displayed in the subsequent four columns. **b**, A central cross-section (~23 nm thick) of the final reconstruction before masking is applied. **c**, 3D views of the central cross-section. **d**, Final 3D density map of this particle, viewed from four perpendicular directions. **e**, Final 3D reconstruction superimposed with the fitted model, viewed from four perpendicular directions. **f**, FSC analyses of the final map resolution using two methods: map-map FSC, where each map is reconstructed from one half of the images (even vs. odd tilt angle indices), and map-model FSC, where the model map is generated from the fitted model. Resolution assessments are provided based on tilt-based map-map and map-model FSC analyses at thresholds of FSC=0.5 and 0.143, respectively.

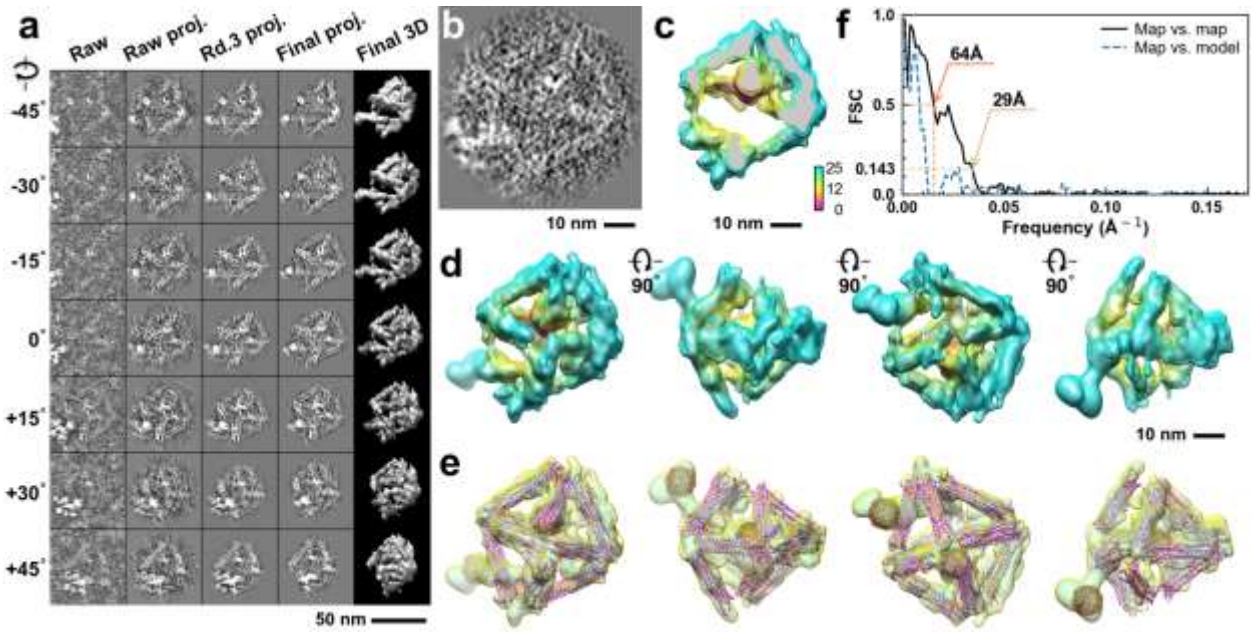

Supplementary Fig. 116: IPET 3D reconstruction and model fitting of an individual unit-cell particle (Index: 108) within a 2D lattice with 100% ferritin loading. a, Seven representative tilt images of a single unit-cell particle are shown in the first column (from left). The tilt images are aligned to a common center using IPET through iterative refinement. The projections of the raw, intermediate, and final 3D reconstruction at the corresponding angles are displayed in the subsequent four columns. **b**, A central cross-section (~23 nm thick) of the final reconstruction before masking is applied. **c**, 3D views of the central cross-section. **d**, Final 3D density map of this particle, viewed from four perpendicular directions. **e**, Final 3D reconstruction superimposed with the fitted model, viewed from four perpendicular directions. **f**, FSC analyses of the final map resolution using two methods: map-map FSC, where each map is reconstructed from one half of the images (even vs. odd tilt angle indices), and map-model FSC, where the model map is generated from the fitted model. Resolution assessments are provided based on tilt-based map-map and map-model FSC analyses at thresholds of FSC=0.5 and 0.143, respectively.

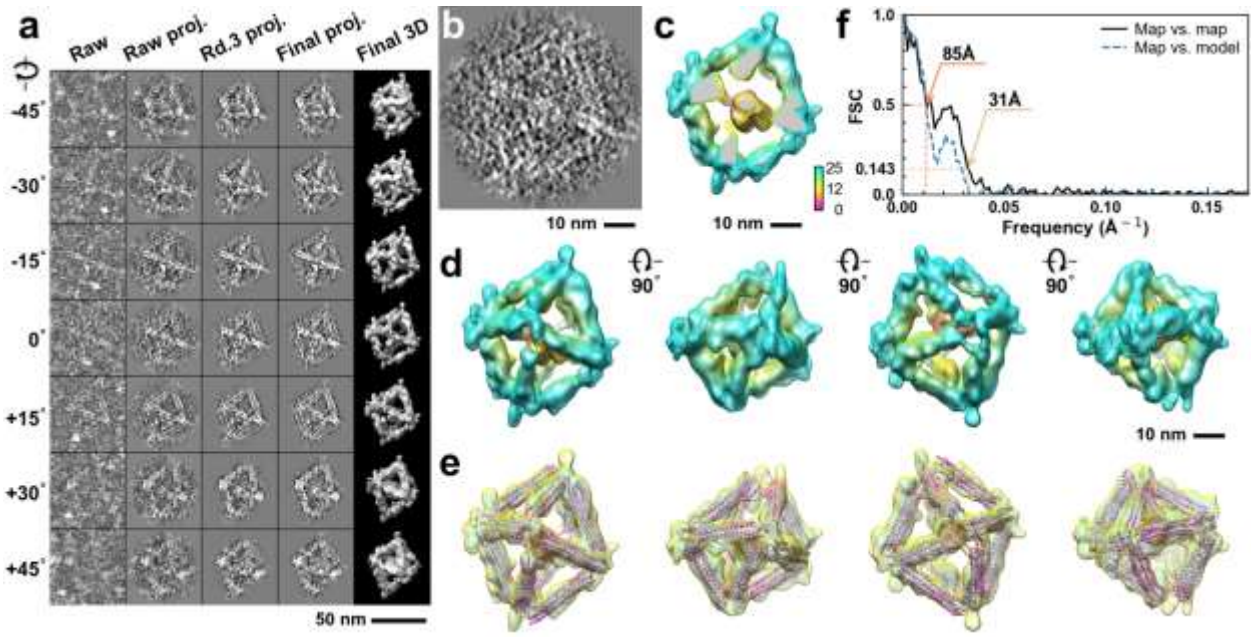

Supplementary Fig. 117: IPET 3D reconstruction and model fitting of an individual unit-cell particle (Index: 109) within a 2D lattice with 100% ferritin loading. a, Seven representative tilt images of a single unit-cell particle are shown in the first column (from left). The tilt images are aligned to a common center using IPET through iterative refinement. The projections of the raw, intermediate, and final 3D reconstruction at the corresponding angles are displayed in the subsequent four columns. **b**, A central cross-section (~23 nm thick) of the final reconstruction before masking is applied. **c**, 3D views of the central cross-section. **d**, Final 3D density map of this particle, viewed from four perpendicular directions. **e**, Final 3D reconstruction superimposed with the fitted model, viewed from four perpendicular directions. **f**, FSC analyses of the final map resolution using two methods: map-map FSC, where each map is reconstructed from one half of the images (even vs. odd tilt angle indices), and map-model FSC, where the model map is generated from the fitted model. Resolution assessments are provided based on tilt-based map-map and map-model FSC analyses at thresholds of FSC=0.5 and 0.143, respectively.

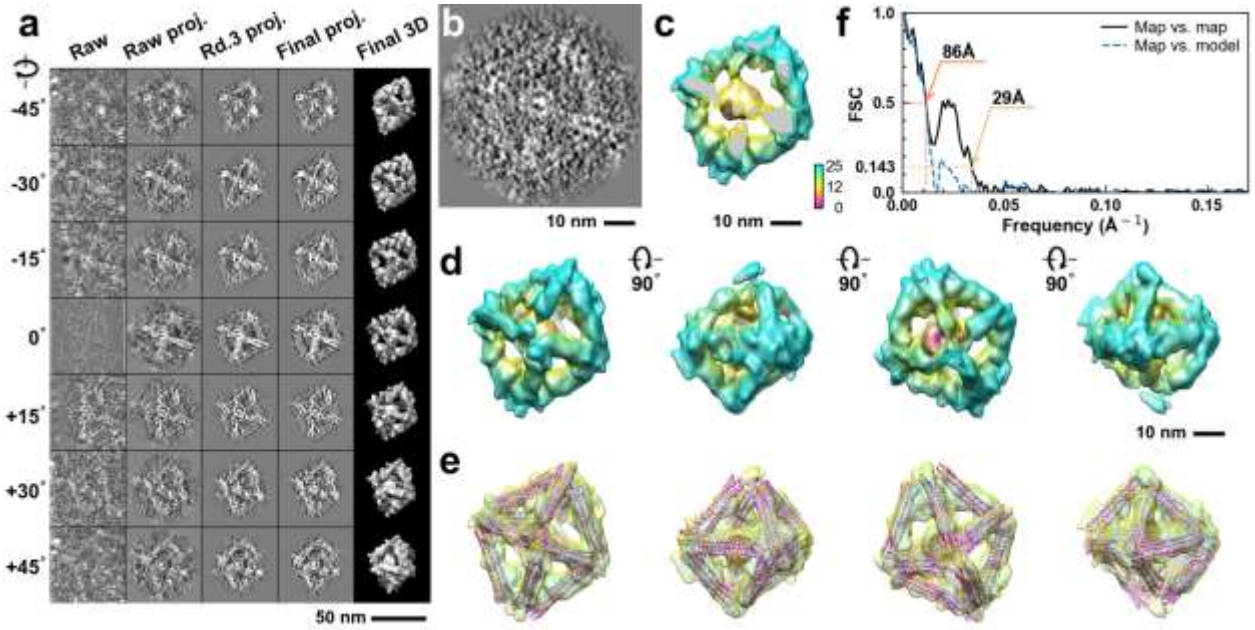

Supplementary Fig. 118: IPET 3D reconstruction and model fitting of an individual unit-cell particle (Index: 110) within a 2D lattice with 100% ferritin loading. a, Seven representative tilt images of a single unit-cell particle are shown in the first column (from left). The tilt images are aligned to a common center using IPET through iterative refinement. The projections of the raw, intermediate, and final 3D reconstruction at the corresponding angles are displayed in the subsequent four columns. **b**, A central cross-section (~23 nm thick) of the final reconstruction before masking is applied. **c**, 3D views of the central cross-section. **d**, Final 3D density map of this particle, viewed from four perpendicular directions. **e**, Final 3D reconstruction superimposed with the fitted model, viewed from four perpendicular directions. **f**, FSC analyses of the final map resolution using two methods: map-map FSC, where each map is reconstructed from one half of the images (even vs. odd tilt angle indices), and map-model FSC, where the model map is generated from the fitted model. Resolution assessments are provided based on tilt-based map-map and map-model FSC analyses at thresholds of FSC=0.5 and 0.143, respectively.

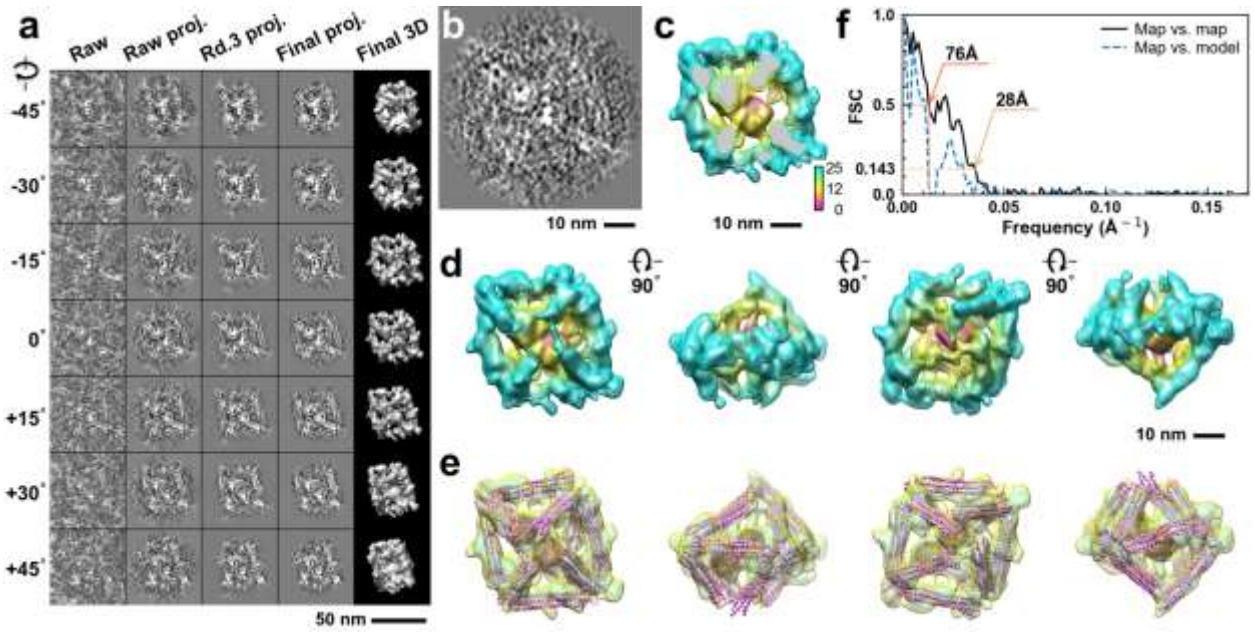

Supplementary Fig. 119: IPET 3D reconstruction and model fitting of an individual unit-cell particle (Index: 111) within a 2D lattice with 100% ferritin loading. a, Seven representative tilt images of a single unit-cell particle are shown in the first column (from left). The tilt images are aligned to a common center using IPET through iterative refinement. The projections of the raw, intermediate, and final 3D reconstruction at the corresponding angles are displayed in the subsequent four columns. **b**, A central cross-section (~23 nm thick) of the final reconstruction before masking is applied. **c**, 3D views of the central cross-section. **d**, Final 3D density map of this particle, viewed from four perpendicular directions. **e**, Final 3D reconstruction superimposed with the fitted model, viewed from four perpendicular directions. **f**, FSC analyses of the final map resolution using two methods: map-map FSC, where each map is reconstructed from one half of the images (even vs. odd tilt angle indices), and map-model FSC, where the model map is generated from the fitted model. Resolution assessments are provided based on tilt-based map-map and map-model FSC analyses at thresholds of FSC=0.5 and 0.143, respectively.

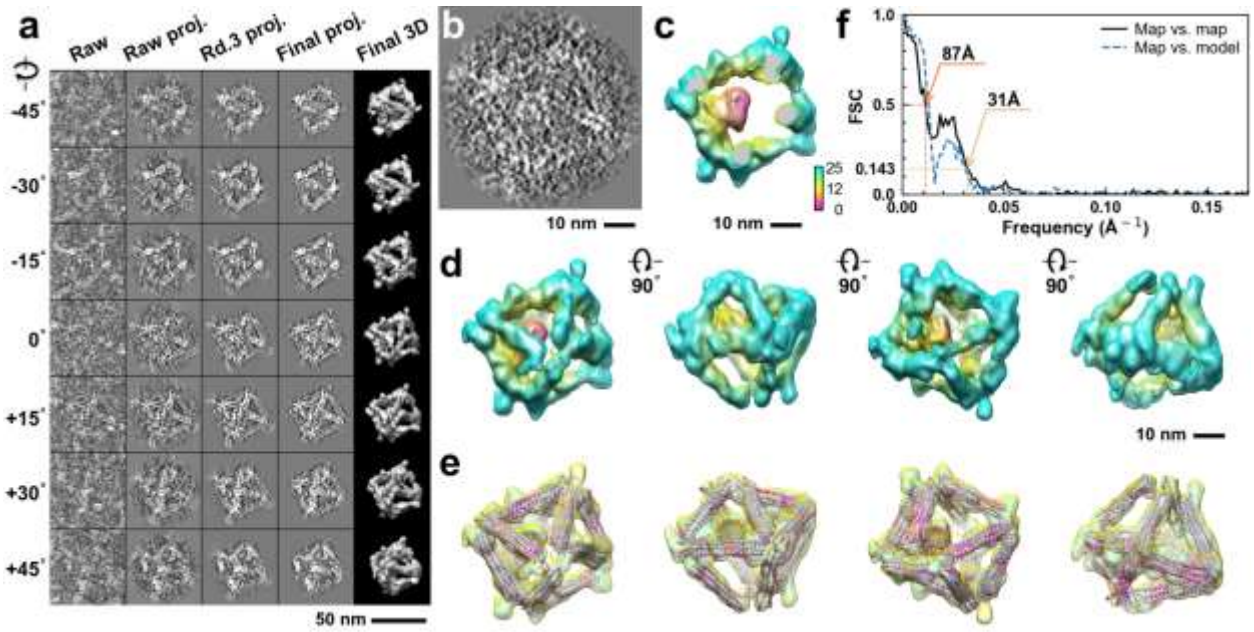

Supplementary Fig. 120: IPET 3D reconstruction and model fitting of an individual unit-cell particle (Index: 112) within a 2D lattice with 100% ferritin loading. a, Seven representative tilt images of a single unit-cell particle are shown in the first column (from left). The tilt images are aligned to a common center using IPET through iterative refinement. The projections of the raw, intermediate, and final 3D reconstruction at the corresponding angles are displayed in the subsequent four columns. **b**, A central cross-section (~23 nm thick) of the final reconstruction before masking is applied. **c**, 3D views of the central cross-section. **d**, Final 3D density map of this particle, viewed from four perpendicular directions. **e**, Final 3D reconstruction superimposed with the fitted model, viewed from four perpendicular directions. **f**, FSC analyses of the final map resolution using two methods: map-map FSC, where each map is reconstructed from one half of the images (even vs. odd tilt angle indices), and map-model FSC, where the model map is generated from the fitted model. Resolution assessments are provided based on tilt-based map-map and map-model FSC analyses at thresholds of FSC=0.5 and 0.143, respectively.

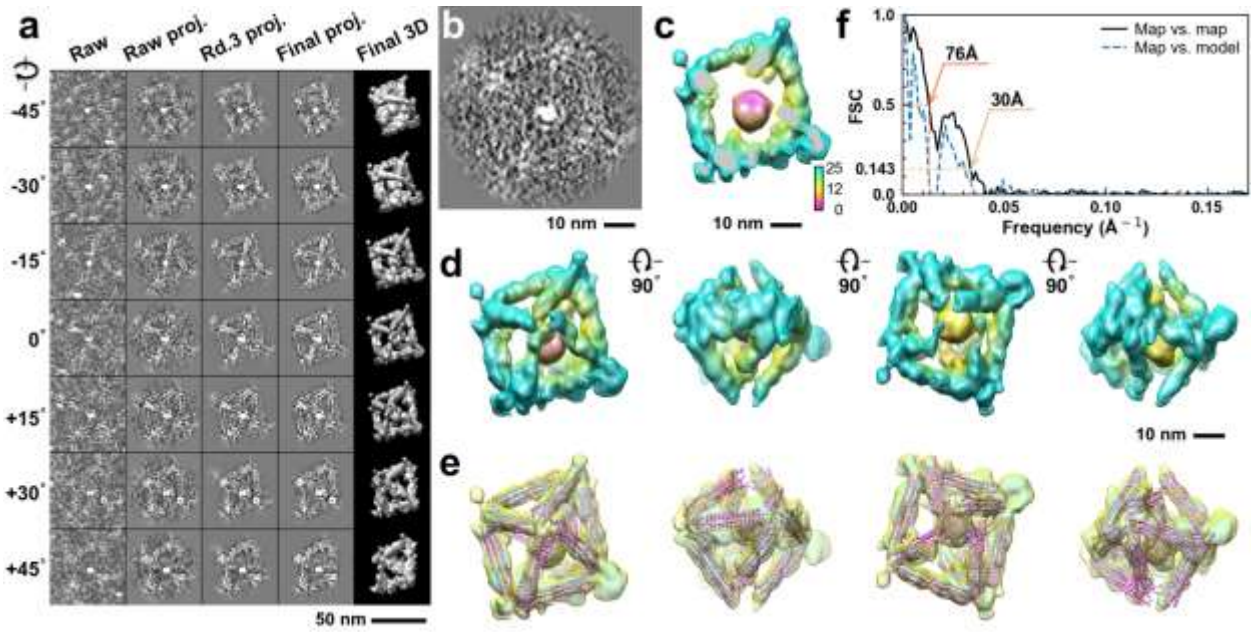

Supplementary Fig. 121: IPET 3D reconstruction and model fitting of an individual unit-cell particle (Index: 113) within a 2D lattice with 100% ferritin loading. a, Seven representative tilt images of a single unit-cell particle are shown in the first column (from left). The tilt images are aligned to a common center using IPET through iterative refinement. The projections of the raw, intermediate, and final 3D reconstruction at the corresponding angles are displayed in the subsequent four columns. **b**, A central cross-section (~23 nm thick) of the final reconstruction before masking is applied. **c**, 3D views of the central cross-section. **d**, Final 3D density map of this particle, viewed from four perpendicular directions. **e**, Final 3D reconstruction superimposed with the fitted model, viewed from four perpendicular directions. **f**, FSC analyses of the final map resolution using two methods: map-map FSC, where each map is reconstructed from one half of the images (even vs. odd tilt angle indices), and map-model FSC, where the model map is generated from the fitted model. Resolution assessments are provided based on tilt-based map-map and map-model FSC analyses at thresholds of FSC=0.5 and 0.143, respectively.

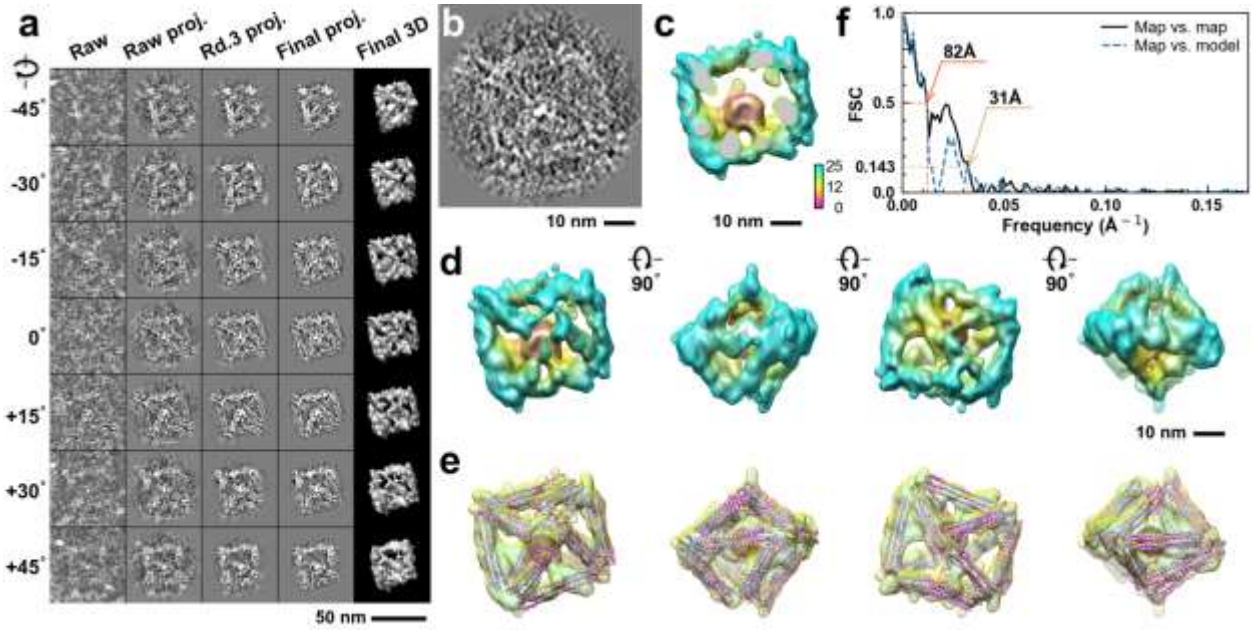

Supplementary Fig. 122: IPET 3D reconstruction and model fitting of an individual unit-cell particle (Index: 114) within a 2D lattice with 100% ferritin loading. a, Seven representative tilt images of a single unit-cell particle are shown in the first column (from left). The tilt images are aligned to a common center using IPET through iterative refinement. The projections of the raw, intermediate, and final 3D reconstruction at the corresponding angles are displayed in the subsequent four columns. **b**, A central cross-section (~23 nm thick) of the final reconstruction before masking is applied. **c**, 3D views of the central cross-section. **d**, Final 3D density map of this particle, viewed from four perpendicular directions. **e**, Final 3D reconstruction superimposed with the fitted model, viewed from four perpendicular directions. **f**, FSC analyses of the final map resolution using two methods: map-map FSC, where each map is reconstructed from one half of the images (even vs. odd tilt angle indices), and map-model FSC, where the model map is generated from the fitted model. Resolution assessments are provided based on tilt-based map-map and map-model FSC analyses at thresholds of FSC=0.5 and 0.143, respectively.

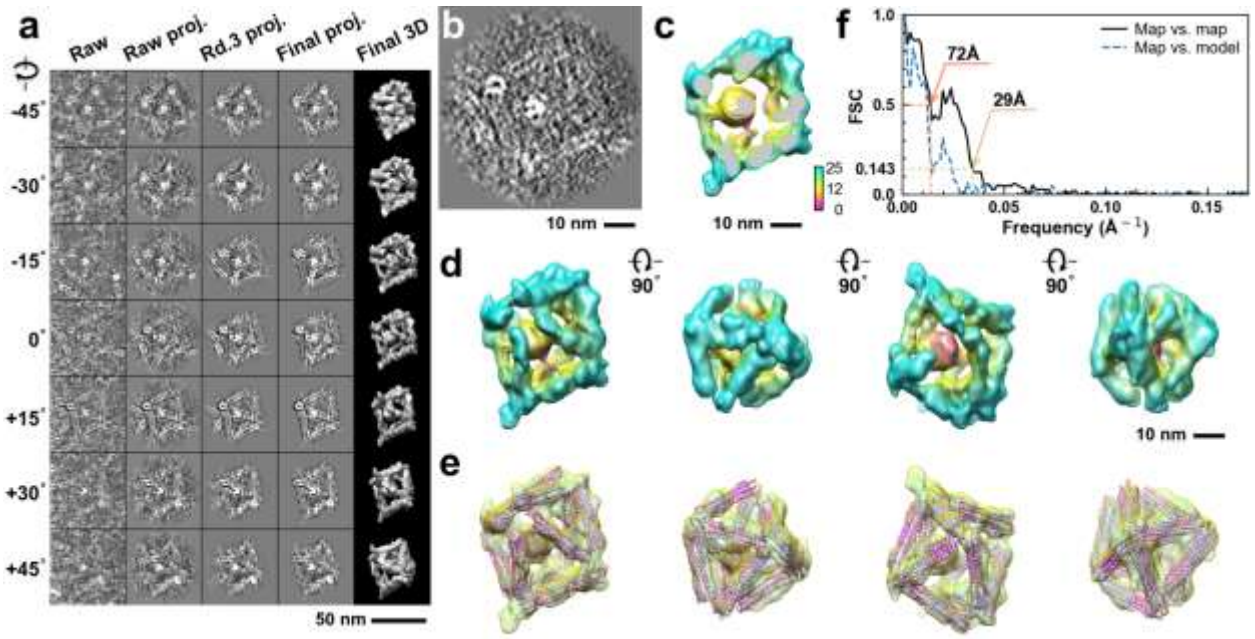

Supplementary Fig. 123: IPET 3D reconstruction and model fitting of an individual unit-cell particle (Index: 115) within a 2D lattice with 100% ferritin loading. a, Seven representative tilt images of a single unit-cell particle are shown in the first column (from left). The tilt images are aligned to a common center using IPET through iterative refinement. The projections of the raw, intermediate, and final 3D reconstruction at the corresponding angles are displayed in the subsequent four columns. **b**, A central cross-section (~23 nm thick) of the final reconstruction before masking is applied. **c**, 3D views of the central cross-section. **d**, Final 3D density map of this particle, viewed from four perpendicular directions. **e**, Final 3D reconstruction superimposed with the fitted model, viewed from four perpendicular directions. **f**, FSC analyses of the final map resolution using two methods: map-map FSC, where each map is reconstructed from one half of the images (even vs. odd tilt angle indices), and map-model FSC, where the model map is generated from the fitted model. Resolution assessments are provided based on tilt-based map-map and map-model FSC analyses at thresholds of FSC=0.5 and 0.143, respectively.

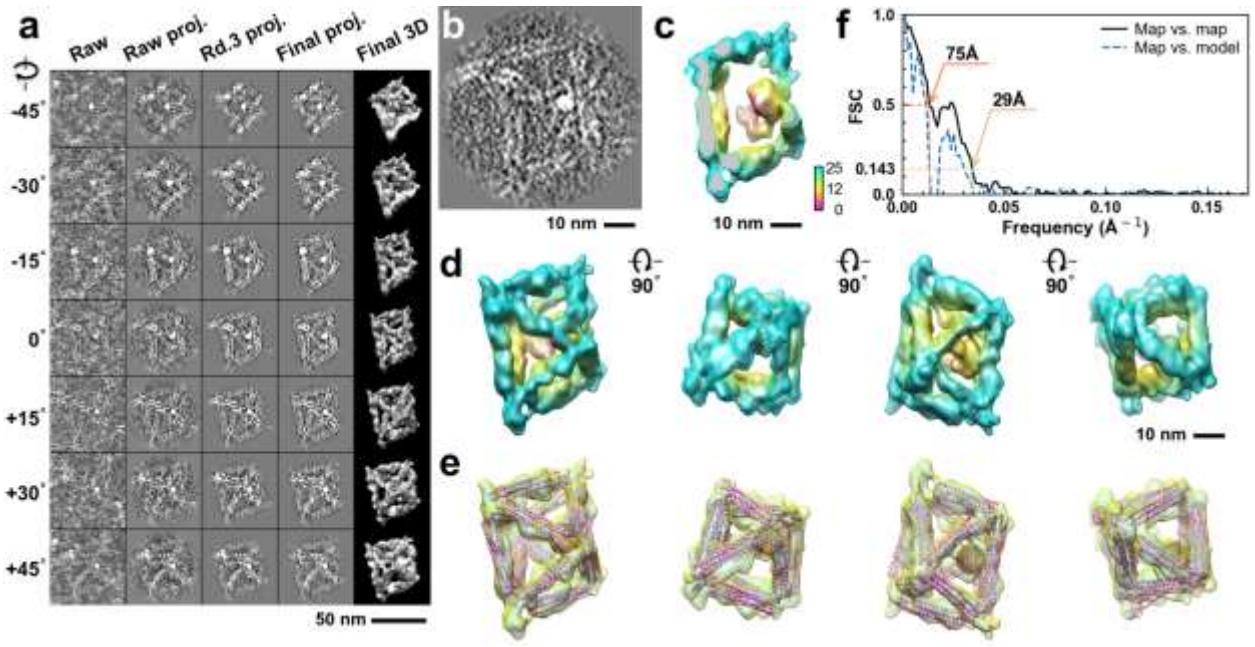

Supplementary Fig. 124: IPET 3D reconstruction and model fitting of an individual unit-cell particle (Index: 116) within a 2D lattice with 100% ferritin loading. a, Seven representative tilt images of a single unit-cell particle are shown in the first column (from left). The tilt images are aligned to a common center using IPET through iterative refinement. The projections of the raw, intermediate, and final 3D reconstruction at the corresponding angles are displayed in the subsequent four columns. **b**, A central cross-section (~23 nm thick) of the final reconstruction before masking is applied. **c**, 3D views of the central cross-section. **d**, Final 3D density map of this particle, viewed from four perpendicular directions. **e**, Final 3D reconstruction superimposed with the fitted model, viewed from four perpendicular directions. **f**, FSC analyses of the final map resolution using two methods: map-map FSC, where each map is reconstructed from one half of the images (even vs. odd tilt angle indices), and map-model FSC, where the model map is generated from the fitted model. Resolution assessments are provided based on tilt-based map-map and map-model FSC analyses at thresholds of FSC=0.5 and 0.143, respectively.

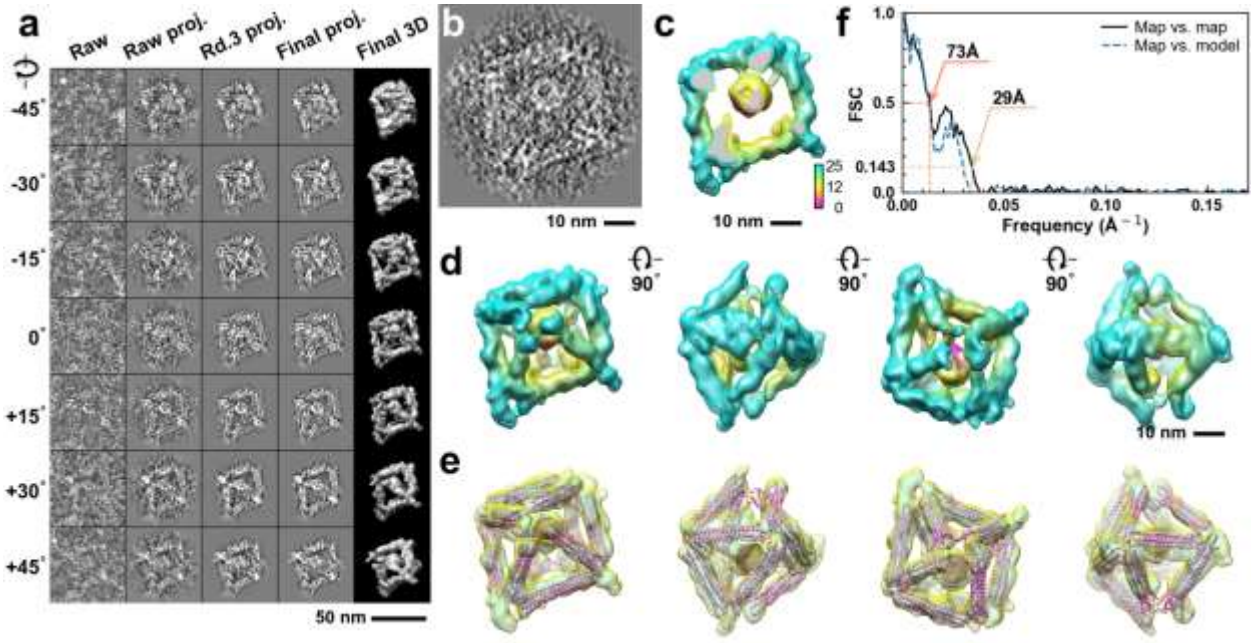

Supplementary Fig. 125: IPET 3D reconstruction and model fitting of an individual unit-cell particle (Index: 117) within a 2D lattice with 100% ferritin loading. a, Seven representative tilt images of a single unit-cell particle are shown in the first column (from left). The tilt images are aligned to a common center using IPET through iterative refinement. The projections of the raw, intermediate, and final 3D reconstruction at the corresponding angles are displayed in the subsequent four columns. **b**, A central cross-section (~23 nm thick) of the final reconstruction before masking is applied. **c**, 3D views of the central cross-section. **d**, Final 3D density map of this particle, viewed from four perpendicular directions. **e**, Final 3D reconstruction superimposed with the fitted model, viewed from four perpendicular directions. **f**, FSC analyses of the final map resolution using two methods: map-map FSC, where each map is reconstructed from one half of the images (even vs. odd tilt angle indices), and map-model FSC, where the model map is generated from the fitted model. Resolution assessments are provided based on tilt-based map-map and map-model FSC analyses at thresholds of FSC=0.5 and 0.143, respectively.

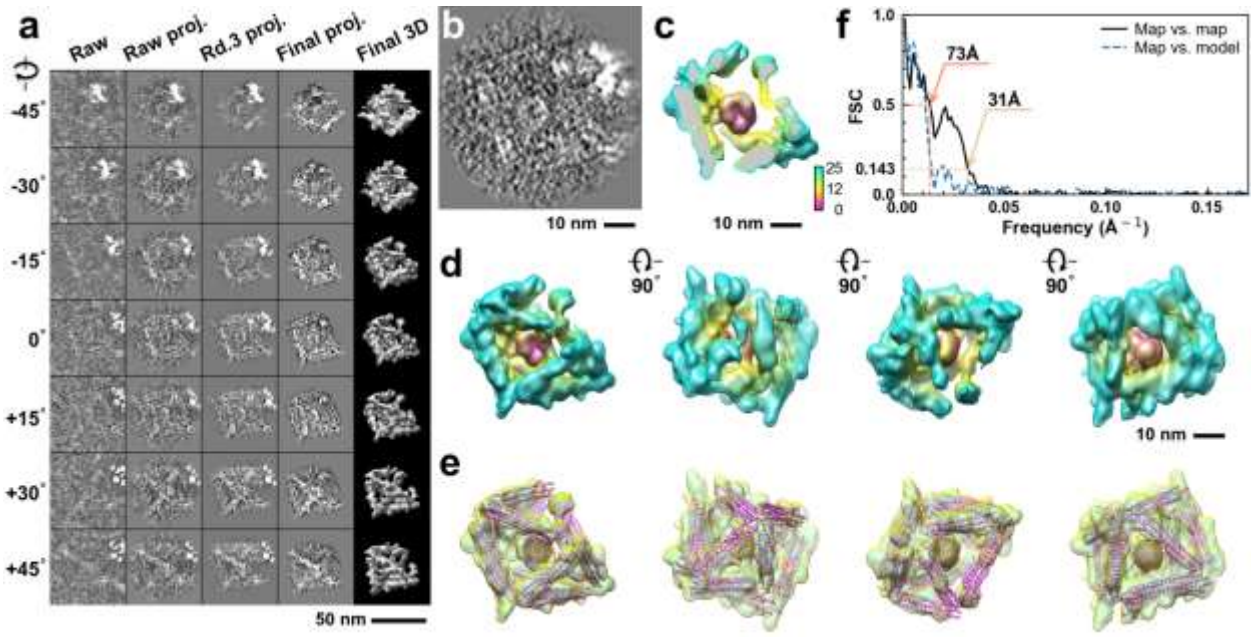

Supplementary Fig. 126: IPET 3D reconstruction and model fitting of an individual unit-cell particle (Index: 118) within a 2D lattice with 100% ferritin loading. a, Seven representative tilt images of a single unit-cell particle are shown in the first column (from left). The tilt images are aligned to a common center using IPET through iterative refinement. The projections of the raw, intermediate, and final 3D reconstruction at the corresponding angles are displayed in the subsequent four columns. **b**, A central cross-section (~23 nm thick) of the final reconstruction before masking is applied. **c**, 3D views of the central cross-section. **d**, Final 3D density map of this particle, viewed from four perpendicular directions. **e**, Final 3D reconstruction superimposed with the fitted model, viewed from four perpendicular directions. **f**, FSC analyses of the final map resolution using two methods: map-map FSC, where each map is reconstructed from one half of the images (even vs. odd tilt angle indices), and map-model FSC, where the model map is generated from the fitted model. Resolution assessments are provided based on tilt-based map-map and map-model FSC analyses at thresholds of FSC=0.5 and 0.143, respectively.

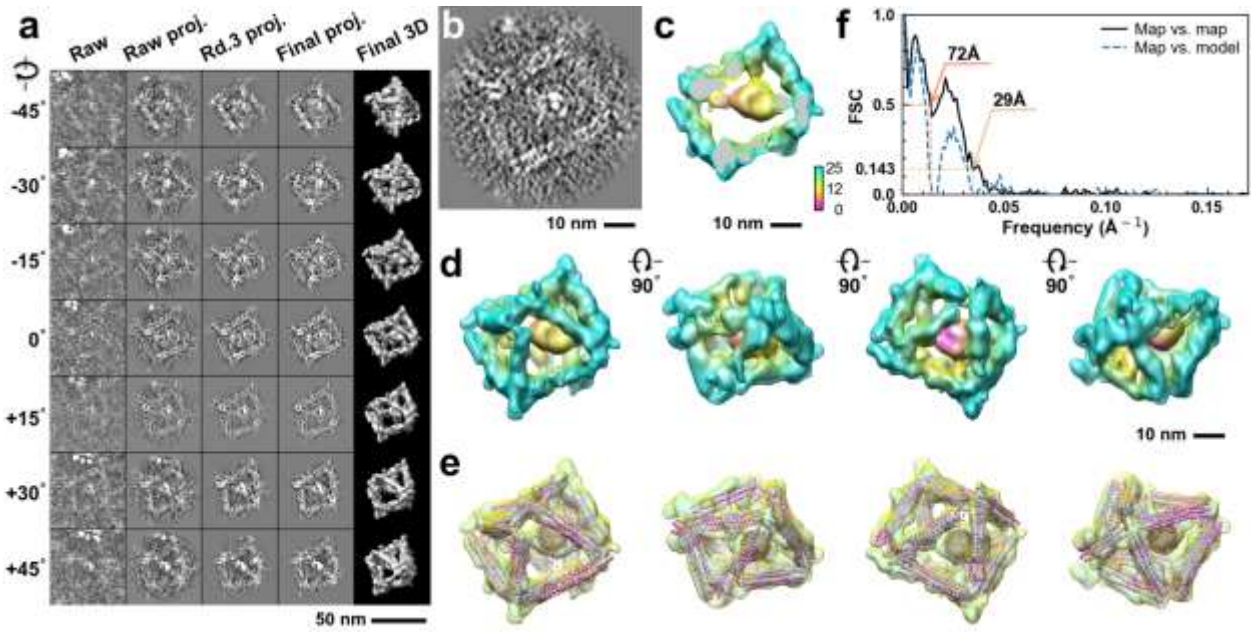

Supplementary Fig. 127: IPET 3D reconstruction and model fitting of an individual unit-cell particle (Index: 119) within a 2D lattice with 100% ferritin loading. a, Seven representative tilt images of a single unit-cell particle are shown in the first column (from left). The tilt images are aligned to a common center using IPET through iterative refinement. The projections of the raw, intermediate, and final 3D reconstruction at the corresponding angles are displayed in the subsequent four columns. **b**, A central cross-section (~23 nm thick) of the final reconstruction before masking is applied. **c**, 3D views of the central cross-section. **d**, Final 3D density map of this particle, viewed from four perpendicular directions. **e**, Final 3D reconstruction superimposed with the fitted model, viewed from four perpendicular directions. **f**, FSC analyses of the final map resolution using two methods: map-map FSC, where each map is reconstructed from one half of the images (even vs. odd tilt angle indices), and map-model FSC, where the model map is generated from the fitted model. Resolution assessments are provided based on tilt-based map-map and map-model FSC analyses at thresholds of FSC=0.5 and 0.143, respectively.

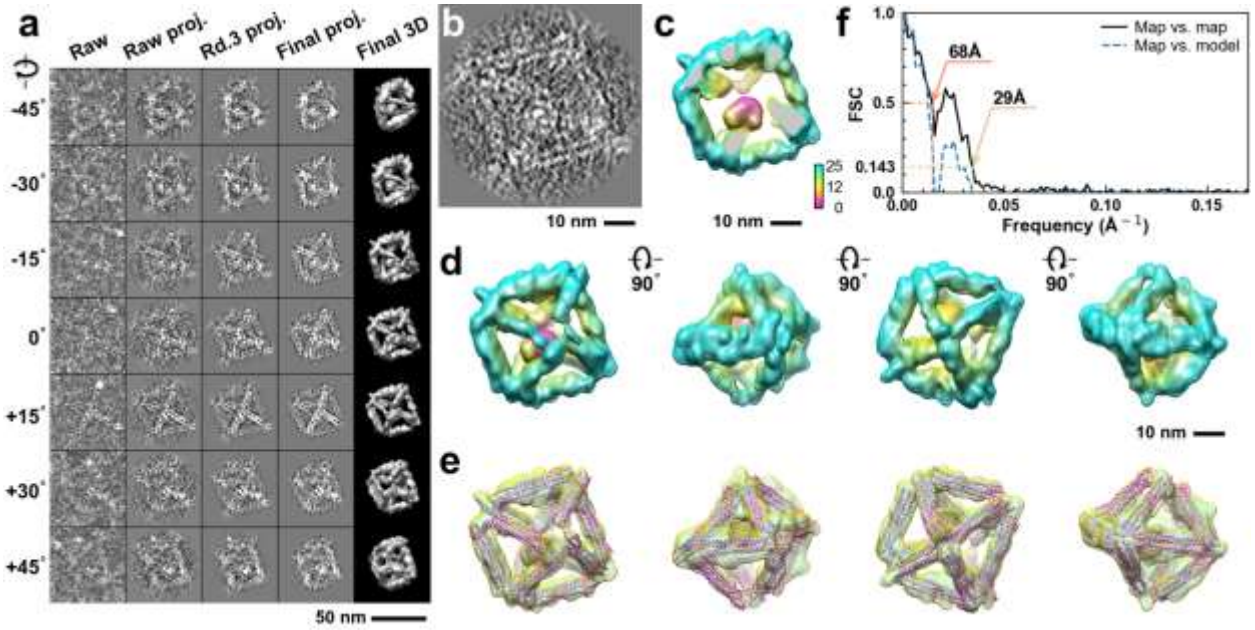

Supplementary Fig. 128: IPET 3D reconstruction and model fitting of an individual unit-cell particle (Index: 120) within a 2D lattice with 100% ferritin loading. a, Seven representative tilt images of a single unit-cell particle are shown in the first column (from left). The tilt images are aligned to a common center using IPET through iterative refinement. The projections of the raw, intermediate, and final 3D reconstruction at the corresponding angles are displayed in the subsequent four columns. **b**, A central cross-section (~23 nm thick) of the final reconstruction before masking is applied. **c**, 3D views of the central cross-section. **d**, Final 3D density map of this particle, viewed from four perpendicular directions. **e**, Final 3D reconstruction superimposed with the fitted model, viewed from four perpendicular directions. **f**, FSC analyses of the final map resolution using two methods: map-map FSC, where each map is reconstructed from one half of the images (even vs. odd tilt angle indices), and map-model FSC, where the model map is generated from the fitted model. Resolution assessments are provided based on tilt-based map-map and map-model FSC analyses at thresholds of FSC=0.5 and 0.143, respectively.

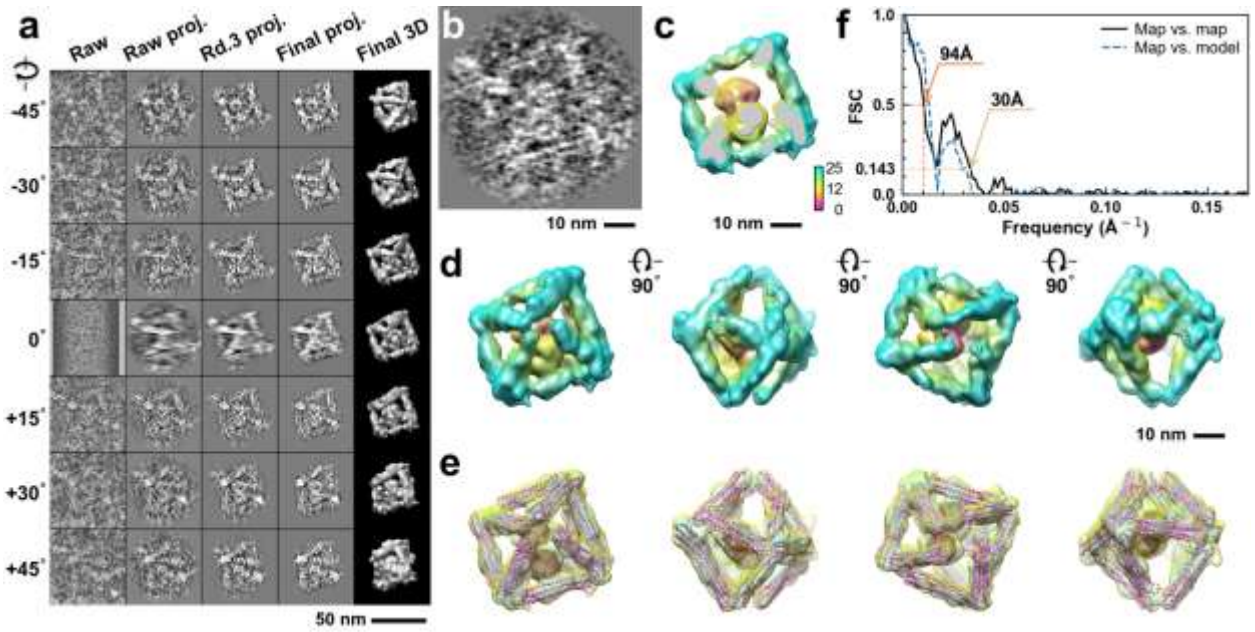

Supplementary Fig. 129: IPET 3D reconstruction and model fitting of an individual unit-cell particle (Index: 121) within a 2D lattice with 100% ferritin loading. a, Seven representative tilt images of a single unit-cell particle are shown in the first column (from left). The tilt images are aligned to a common center using IPET through iterative refinement. The projections of the raw, intermediate, and final 3D reconstruction at the corresponding angles are displayed in the subsequent four columns. **b**, A central cross-section (~23 nm thick) of the final reconstruction before masking is applied. **c**, 3D views of the central cross-section. **d**, Final 3D density map of this particle, viewed from four perpendicular directions. **e**, Final 3D reconstruction superimposed with the fitted model, viewed from four perpendicular directions. **f**, FSC analyses of the final map resolution using two methods: map-map FSC, where each map is reconstructed from one half of the images (even vs. odd tilt angle indices), and map-model FSC, where the model map is generated from the fitted model. Resolution assessments are provided based on tilt-based map-map and map-model FSC analyses at thresholds of FSC=0.5 and 0.143, respectively.

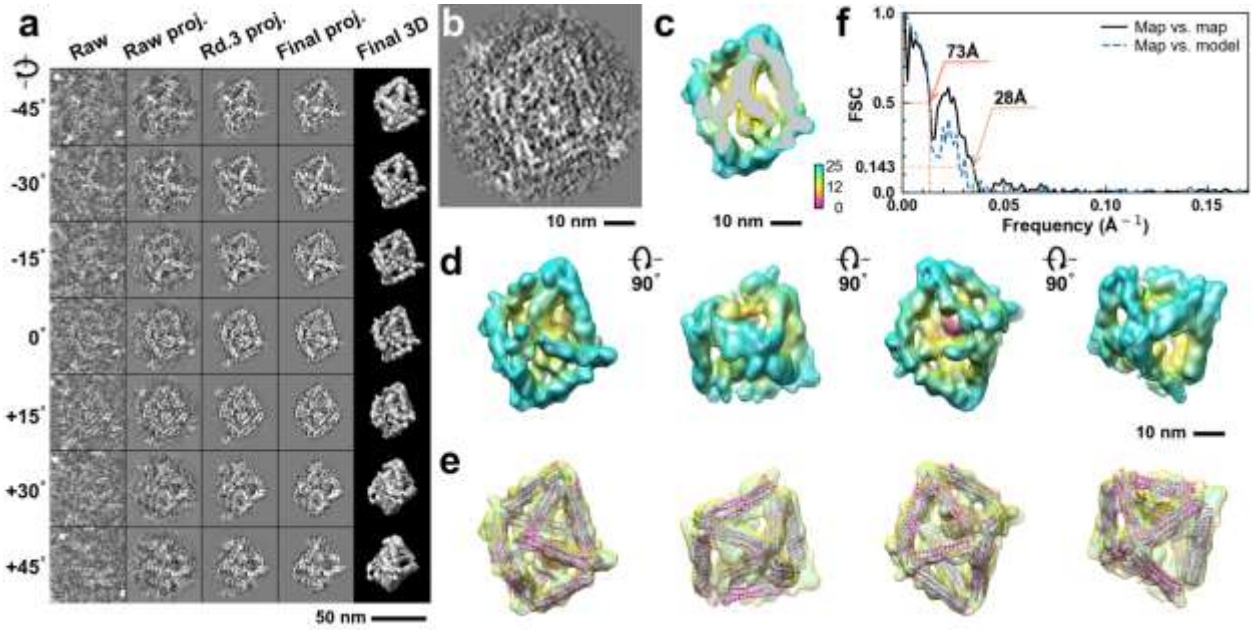

Supplementary Fig. 130: IPET 3D reconstruction and model fitting of an individual unit-cell particle (Index: 122) within a 2D lattice with 100% ferritin loading. a, Seven representative tilt images of a single unit-cell particle are shown in the first column (from left). The tilt images are aligned to a common center using IPET through iterative refinement. The projections of the raw, intermediate, and final 3D reconstruction at the corresponding angles are displayed in the subsequent four columns. **b**, A central cross-section (~23 nm thick) of the final reconstruction before masking is applied. **c**, 3D views of the central cross-section. **d**, Final 3D density map of this particle, viewed from four perpendicular directions. **e**, Final 3D reconstruction superimposed with the fitted model, viewed from four perpendicular directions. **f**, FSC analyses of the final map resolution using two methods: map-map FSC, where each map is reconstructed from one half of the images (even vs. odd tilt angle indices), and map-model FSC, where the model map is generated from the fitted model. Resolution assessments are provided based on tilt-based map-map and map-model FSC analyses at thresholds of FSC=0.5 and 0.143, respectively.

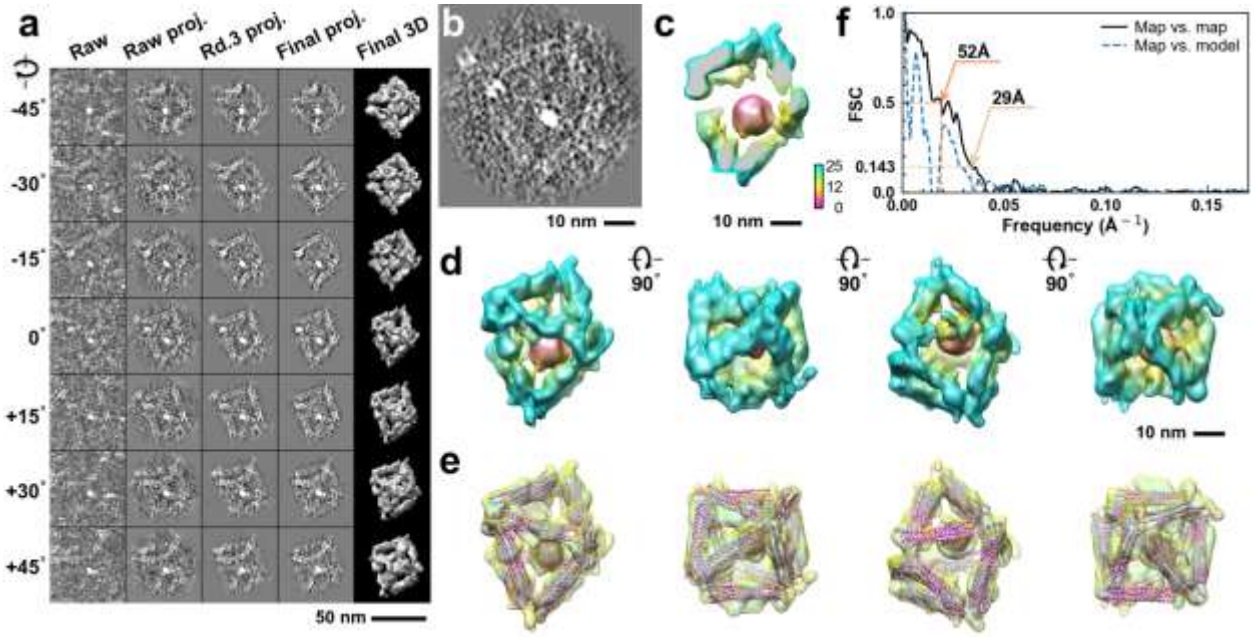

Supplementary Fig. 131: IPET 3D reconstruction and model fitting of an individual unit-cell particle (Index: 123) within a 2D lattice with 100% ferritin loading. a, Seven representative tilt images of a single unit-cell particle are shown in the first column (from left). The tilt images are aligned to a common center using IPET through iterative refinement. The projections of the raw, intermediate, and final 3D reconstruction at the corresponding angles are displayed in the subsequent four columns. **b**, A central cross-section (~23 nm thick) of the final reconstruction before masking is applied. **c**, 3D views of the central cross-section. **d**, Final 3D density map of this particle, viewed from four perpendicular directions. **e**, Final 3D reconstruction superimposed with the fitted model, viewed from four perpendicular directions. **f**, FSC analyses of the final map resolution using two methods: map-map FSC, where each map is reconstructed from one half of the images (even vs. odd tilt angle indices), and map-model FSC, where the model map is generated from the fitted model. Resolution assessments are provided based on tilt-based map-map and map-model FSC analyses at thresholds of FSC=0.5 and 0.143, respectively.

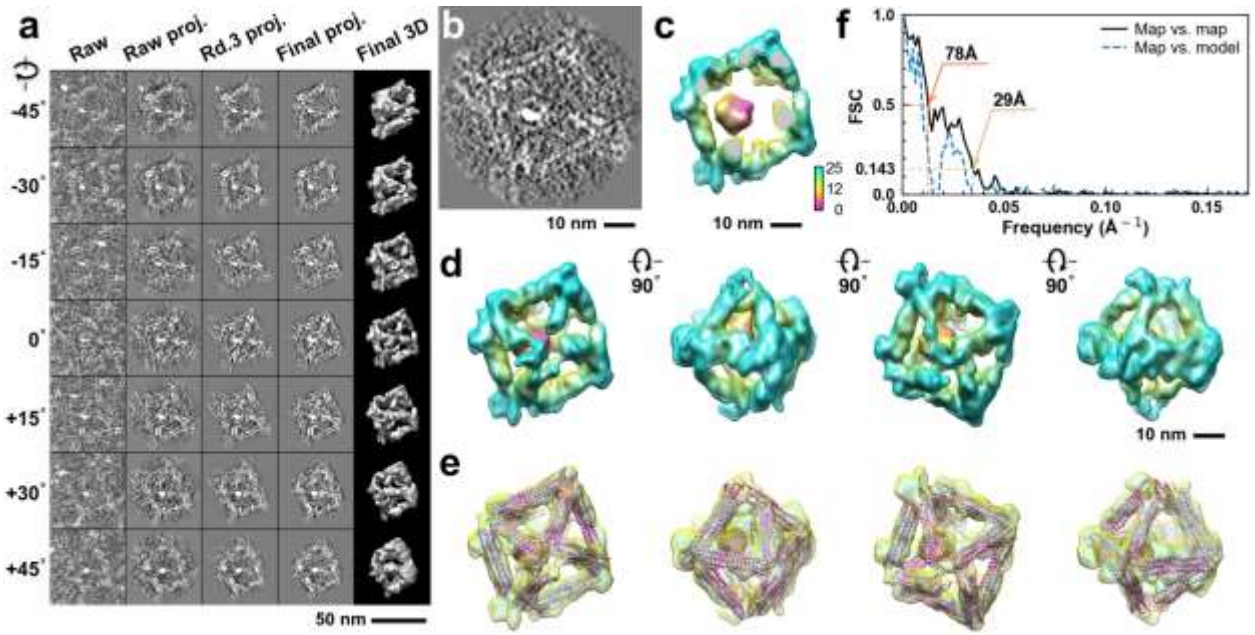

Supplementary Fig. 132: IPET 3D reconstruction and model fitting of an individual unit-cell particle (Index: 124) within a 2D lattice with 100% ferritin loading. a, Seven representative tilt images of a single unit-cell particle are shown in the first column (from left). The tilt images are aligned to a common center using IPET through iterative refinement. The projections of the raw, intermediate, and final 3D reconstruction at the corresponding angles are displayed in the subsequent four columns. **b**, A central cross-section (~23 nm thick) of the final reconstruction before masking is applied. **c**, 3D views of the central cross-section. **d**, Final 3D density map of this particle, viewed from four perpendicular directions. **e**, Final 3D reconstruction superimposed with the fitted model, viewed from four perpendicular directions. **f**, FSC analyses of the final map resolution using two methods: map-map FSC, where each map is reconstructed from one half of the images (even vs. odd tilt angle indices), and map-model FSC, where the model map is generated from the fitted model. Resolution assessments are provided based on tilt-based map-map and map-model FSC analyses at thresholds of FSC=0.5 and 0.143, respectively.

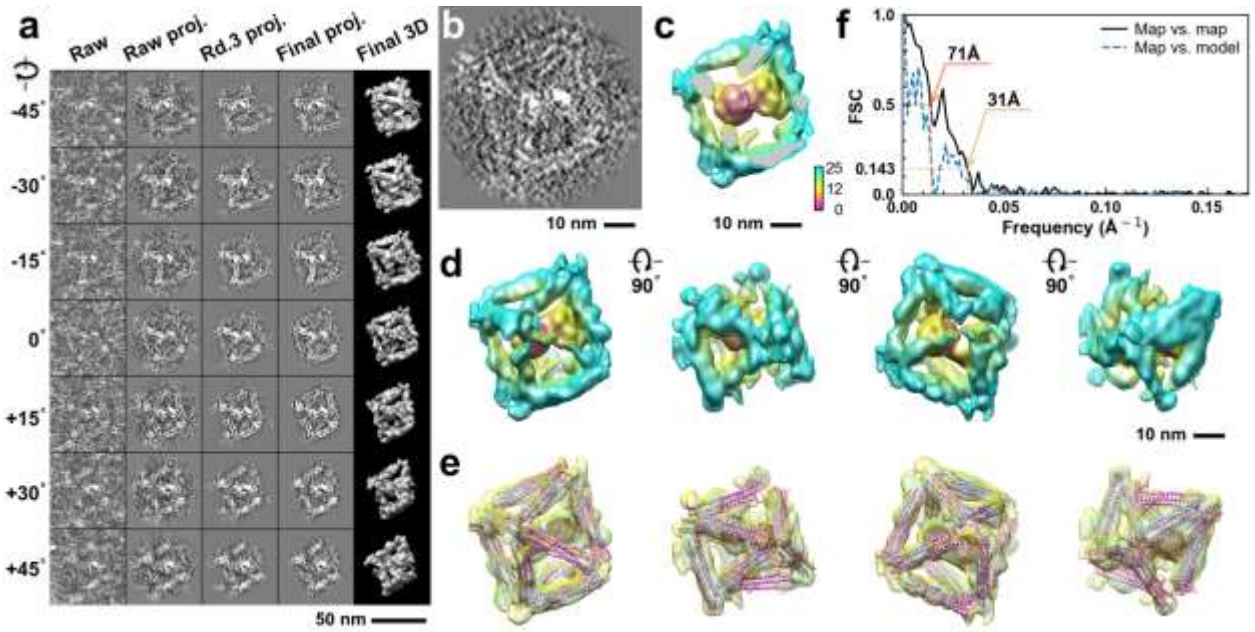

Supplementary Fig. 133: IPET 3D reconstruction and model fitting of an individual unit-cell particle (Index: 125) within a 2D lattice with 100% ferritin loading. a, Seven representative tilt images of a single unit-cell particle are shown in the first column (from left). The tilt images are aligned to a common center using IPET through iterative refinement. The projections of the raw, intermediate, and final 3D reconstruction at the corresponding angles are displayed in the subsequent four columns. **b**, A central cross-section (~23 nm thick) of the final reconstruction before masking is applied. **c**, 3D views of the central cross-section. **d**, Final 3D density map of this particle, viewed from four perpendicular directions. **e**, Final 3D reconstruction superimposed with the fitted model, viewed from four perpendicular directions. **f**, FSC analyses of the final map resolution using two methods: map-map FSC, where each map is reconstructed from one half of the images (even vs. odd tilt angle indices), and map-model FSC, where the model map is generated from the fitted model. Resolution assessments are provided based on tilt-based map-map and map-model FSC analyses at thresholds of FSC=0.5 and 0.143, respectively.

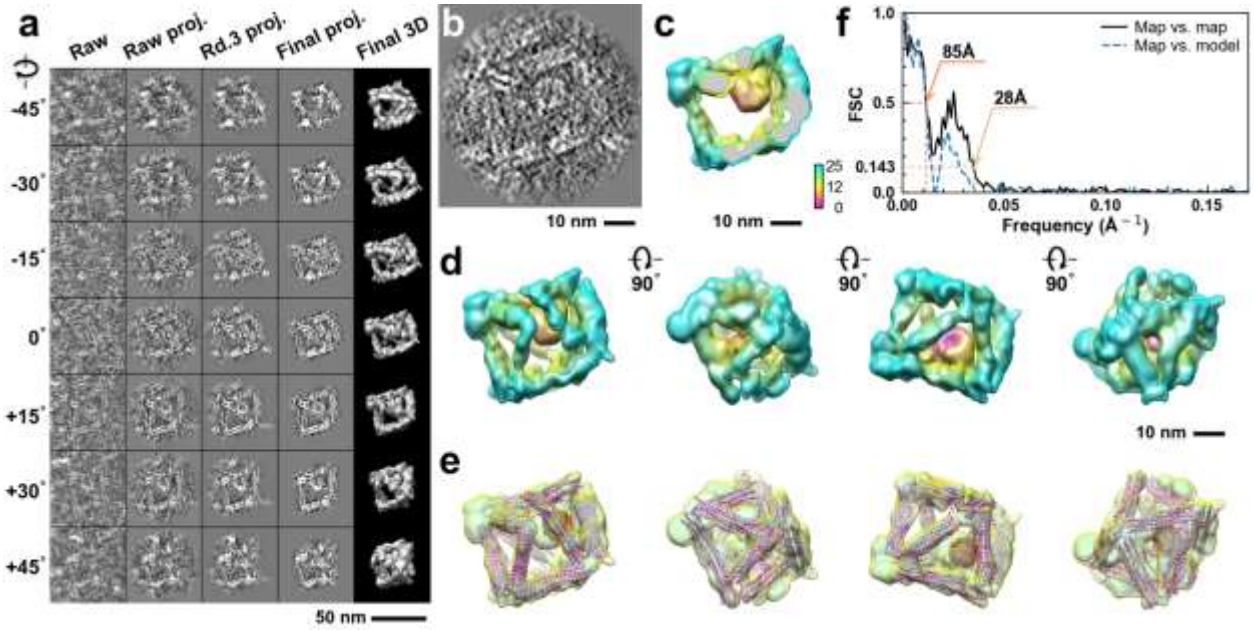

Supplementary Fig. 134: IPET 3D reconstruction and model fitting of an individual unit-cell particle (Index: 126) within a 2D lattice with 100% ferritin loading. a, Seven representative tilt images of a single unit-cell particle are shown in the first column (from left). The tilt images are aligned to a common center using IPET through iterative refinement. The projections of the raw, intermediate, and final 3D reconstruction at the corresponding angles are displayed in the subsequent four columns. **b**, A central cross-section (~23 nm thick) of the final reconstruction before masking is applied. **c**, 3D views of the central cross-section. **d**, Final 3D density map of this particle, viewed from four perpendicular directions. **e**, Final 3D reconstruction superimposed with the fitted model, viewed from four perpendicular directions. **f**, FSC analyses of the final map resolution using two methods: map-map FSC, where each map is reconstructed from one half of the images (even vs. odd tilt angle indices), and map-model FSC, where the model map is generated from the fitted model. Resolution assessments are provided based on tilt-based map-map and map-model FSC analyses at thresholds of FSC=0.5 and 0.143, respectively.

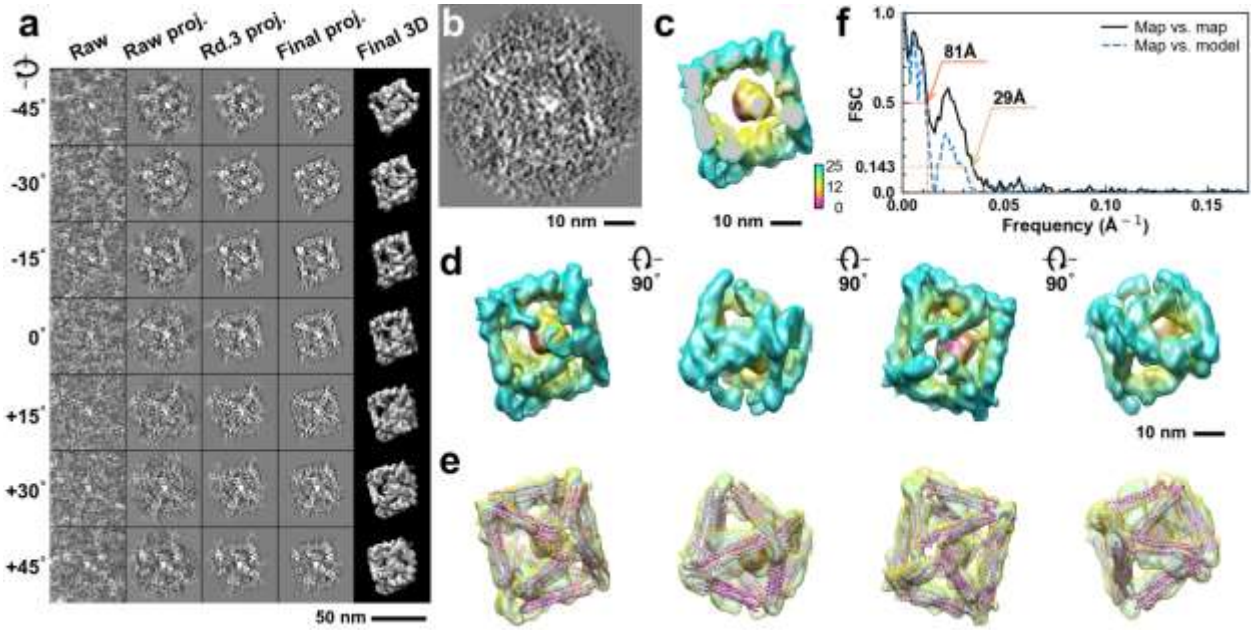

Supplementary Fig. 135: IPET 3D reconstruction and model fitting of an individual unit-cell particle (Index: 127) within a 2D lattice with 100% ferritin loading. a, Seven representative tilt images of a single unit-cell particle are shown in the first column (from left). The tilt images are aligned to a common center using IPET through iterative refinement. The projections of the raw, intermediate, and final 3D reconstruction at the corresponding angles are displayed in the subsequent four columns. **b**, A central cross-section (~23 nm thick) of the final reconstruction before masking is applied. **c**, 3D views of the central cross-section. **d**, Final 3D density map of this particle, viewed from four perpendicular directions. **e**, Final 3D reconstruction superimposed with the fitted model, viewed from four perpendicular directions. **f**, FSC analyses of the final map resolution using two methods: map-map FSC, where each map is reconstructed from one half of the images (even vs. odd tilt angle indices), and map-model FSC, where the model map is generated from the fitted model. Resolution assessments are provided based on tilt-based map-map and map-model FSC analyses at thresholds of FSC=0.5 and 0.143, respectively.

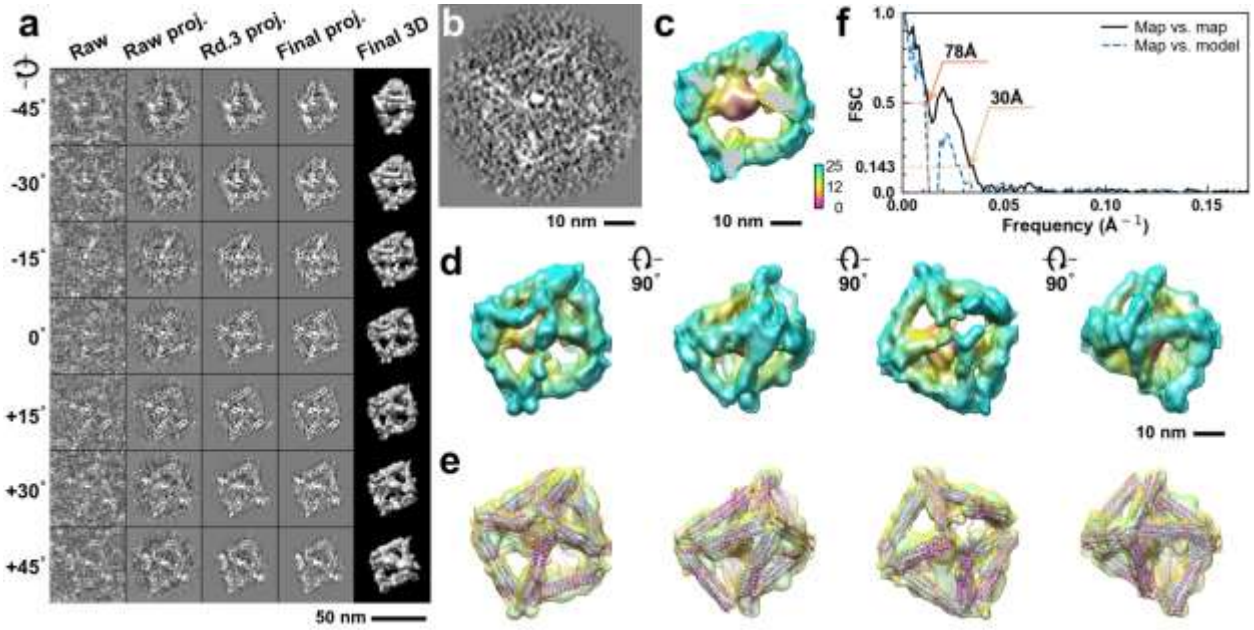

Supplementary Fig. 136: IPET 3D reconstruction and model fitting of an individual unit-cell particle (Index: 128) within a 2D lattice with 100% ferritin loading. a, Seven representative tilt images of a single unit-cell particle are shown in the first column (from left). The tilt images are aligned to a common center using IPET through iterative refinement. The projections of the raw, intermediate, and final 3D reconstruction at the corresponding angles are displayed in the subsequent four columns. **b**, A central cross-section (~23 nm thick) of the final reconstruction before masking is applied. **c**, 3D views of the central cross-section. **d**, Final 3D density map of this particle, viewed from four perpendicular directions. **e**, Final 3D reconstruction superimposed with the fitted model, viewed from four perpendicular directions. **f**, FSC analyses of the final map resolution using two methods: map-map FSC, where each map is reconstructed from one half of the images (even vs. odd tilt angle indices), and map-model FSC, where the model map is generated from the fitted model. Resolution assessments are provided based on tilt-based map-map and map-model FSC analyses at thresholds of FSC=0.5 and 0.143, respectively.

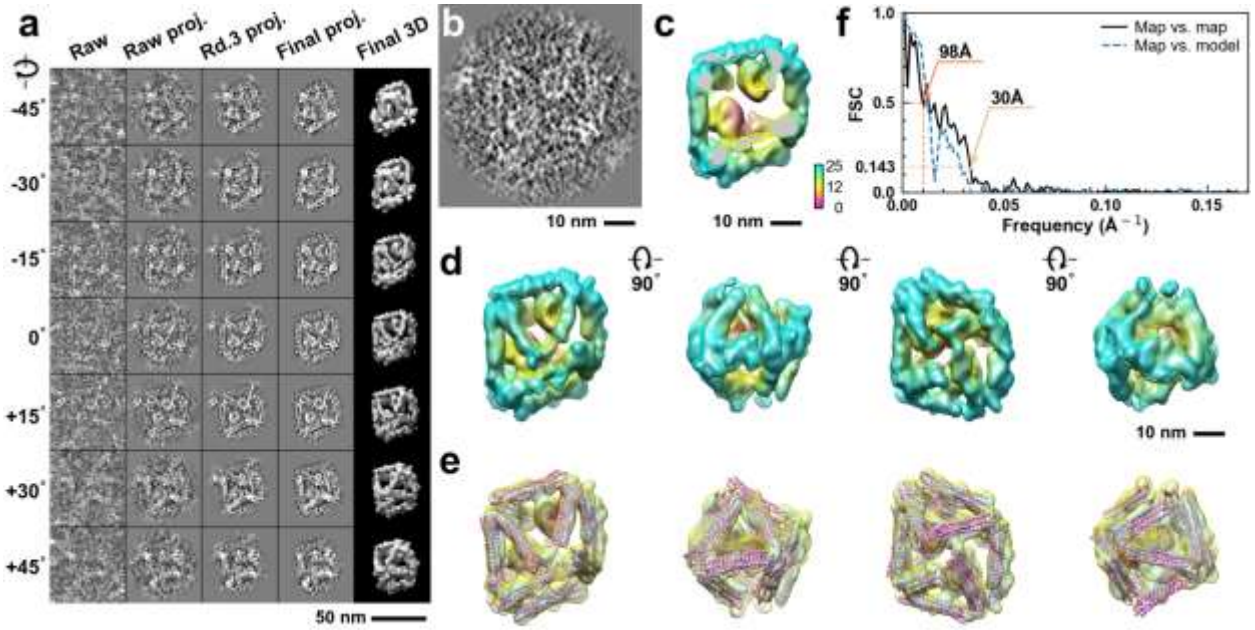

Supplementary Fig. 137: IPET 3D reconstruction and model fitting of an individual unit-cell particle (Index: 129) within a 2D lattice with 100% ferritin loading. a, Seven representative tilt images of a single unit-cell particle are shown in the first column (from left). The tilt images are aligned to a common center using IPET through iterative refinement. The projections of the raw, intermediate, and final 3D reconstruction at the corresponding angles are displayed in the subsequent four columns. **b**, A central cross-section (~23 nm thick) of the final reconstruction before masking is applied. **c**, 3D views of the central cross-section. **d**, Final 3D density map of this particle, viewed from four perpendicular directions. **e**, Final 3D reconstruction superimposed with the fitted model, viewed from four perpendicular directions. **f**, FSC analyses of the final map resolution using two methods: map-map FSC, where each map is reconstructed from one half of the images (even vs. odd tilt angle indices), and map-model FSC, where the model map is generated from the fitted model. Resolution assessments are provided based on tilt-based map-map and map-model FSC analyses at thresholds of FSC=0.5 and 0.143, respectively.

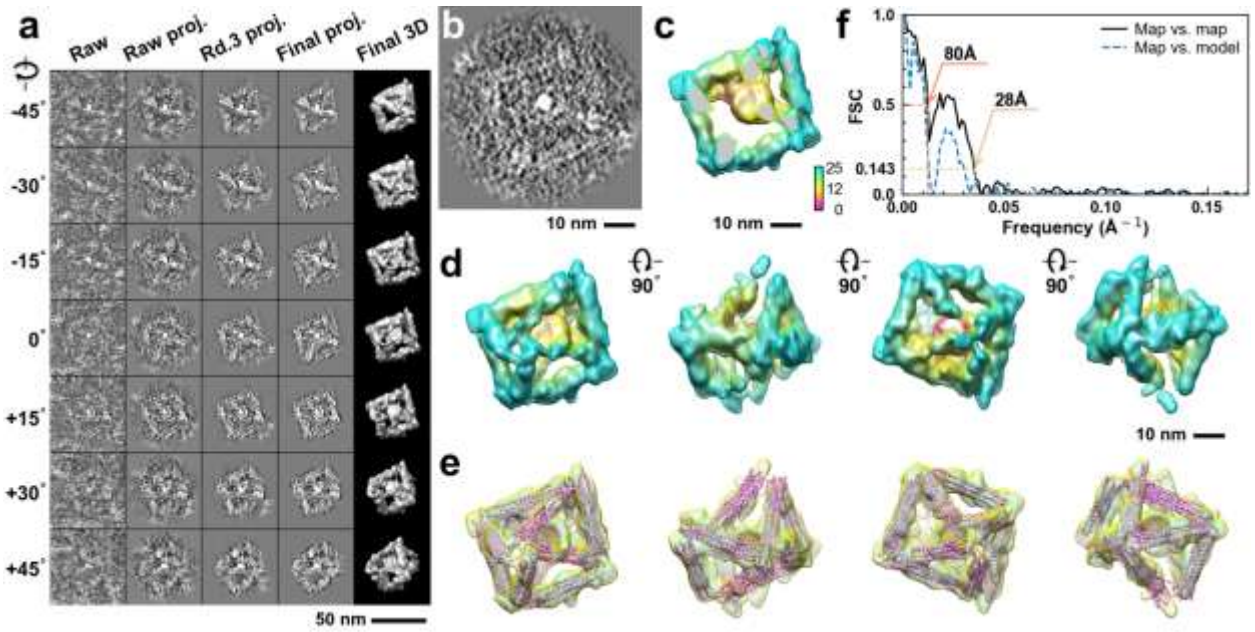

Supplementary Fig. 138: IPET 3D reconstruction and model fitting of an individual unit-cell particle (Index: 130) within a 2D lattice with 100% ferritin loading. a, Seven representative tilt images of a single unit-cell particle are shown in the first column (from left). The tilt images are aligned to a common center using IPET through iterative refinement. The projections of the raw, intermediate, and final 3D reconstruction at the corresponding angles are displayed in the subsequent four columns. **b**, A central cross-section (~23 nm thick) of the final reconstruction before masking is applied. **c**, 3D views of the central cross-section. **d**, Final 3D density map of this particle, viewed from four perpendicular directions. **e**, Final 3D reconstruction superimposed with the fitted model, viewed from four perpendicular directions. **f**, FSC analyses of the final map resolution using two methods: map-map FSC, where each map is reconstructed from one half of the images (even vs. odd tilt angle indices), and map-model FSC, where the model map is generated from the fitted model. Resolution assessments are provided based on tilt-based map-map and map-model FSC analyses at thresholds of FSC=0.5 and 0.143, respectively.

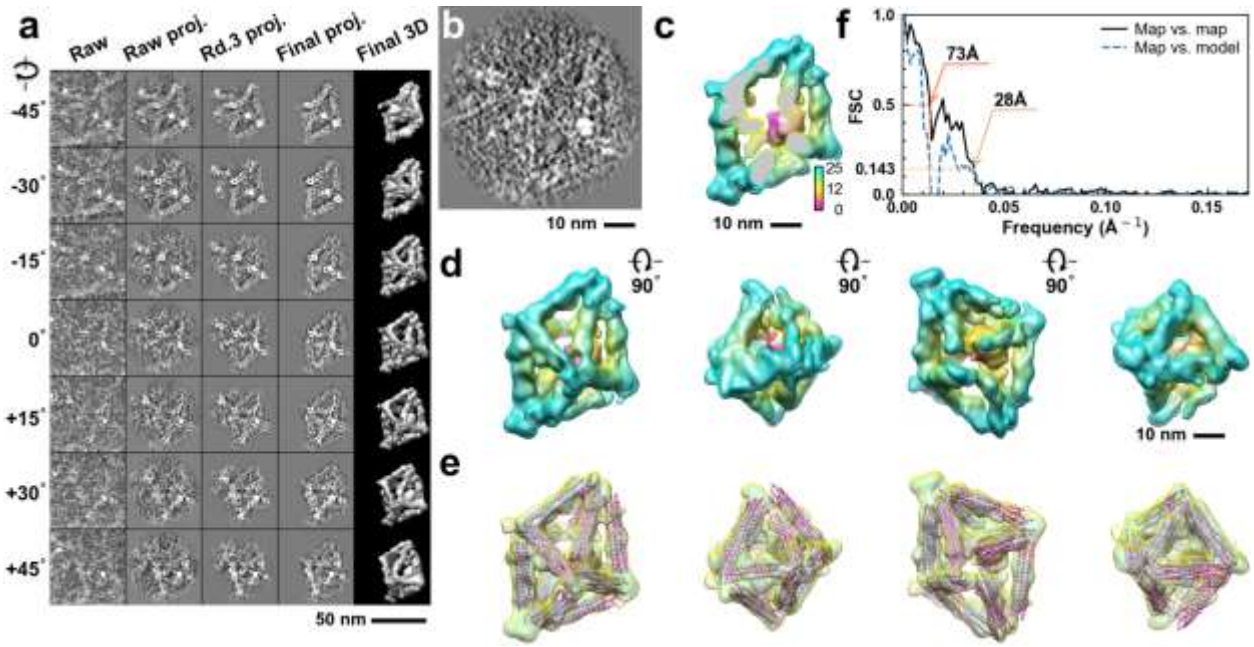

Supplementary Fig. 139: IPET 3D reconstruction and model fitting of an individual unit-cell particle (Index: 131) within a 2D lattice with 100% ferritin loading. a, Seven representative tilt images of a single unit-cell particle are shown in the first column (from left). The tilt images are aligned to a common center using IPET through iterative refinement. The projections of the raw, intermediate, and final 3D reconstruction at the corresponding angles are displayed in the subsequent four columns. **b**, A central cross-section (~23 nm thick) of the final reconstruction before masking is applied. **c**, 3D views of the central cross-section. **d**, Final 3D density map of this particle, viewed from four perpendicular directions. **e**, Final 3D reconstruction superimposed with the fitted model, viewed from four perpendicular directions. **f**, FSC analyses of the final map resolution using two methods: map-map FSC, where each map is reconstructed from one half of the images (even vs. odd tilt angle indices), and map-model FSC, where the model map is generated from the fitted model. Resolution assessments are provided based on tilt-based map-map and map-model FSC analyses at thresholds of FSC=0.5 and 0.143, respectively.

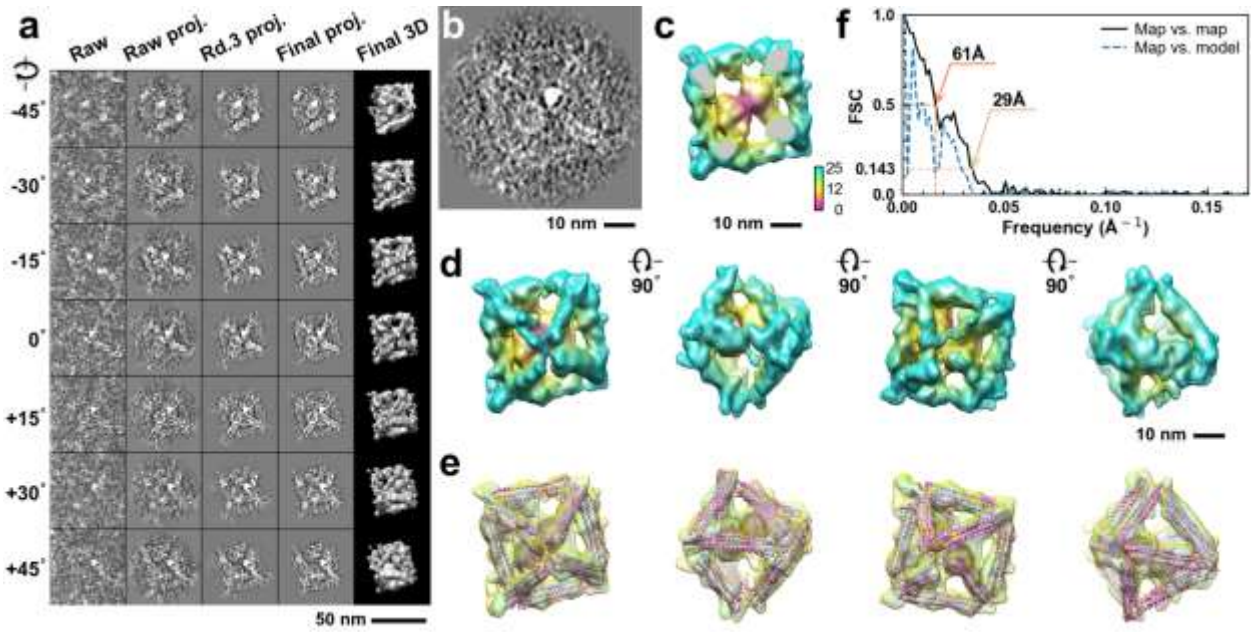

Supplementary Fig. 140: IPET 3D reconstruction and model fitting of an individual unit-cell particle (Index: 132) within a 2D lattice with 100% ferritin loading. a, Seven representative tilt images of a single unit-cell particle are shown in the first column (from left). The tilt images are aligned to a common center using IPET through iterative refinement. The projections of the raw, intermediate, and final 3D reconstruction at the corresponding angles are displayed in the subsequent four columns. **b**, A central cross-section (~23 nm thick) of the final reconstruction before masking is applied. **c**, 3D views of the central cross-section. **d**, Final 3D density map of this particle, viewed from four perpendicular directions. **e**, Final 3D reconstruction superimposed with the fitted model, viewed from four perpendicular directions. **f**, FSC analyses of the final map resolution using two methods: map-map FSC, where each map is reconstructed from one half of the images (even vs. odd tilt angle indices), and map-model FSC, where the model map is generated from the fitted model. Resolution assessments are provided based on tilt-based map-map and map-model FSC analyses at thresholds of FSC=0.5 and 0.143, respectively.

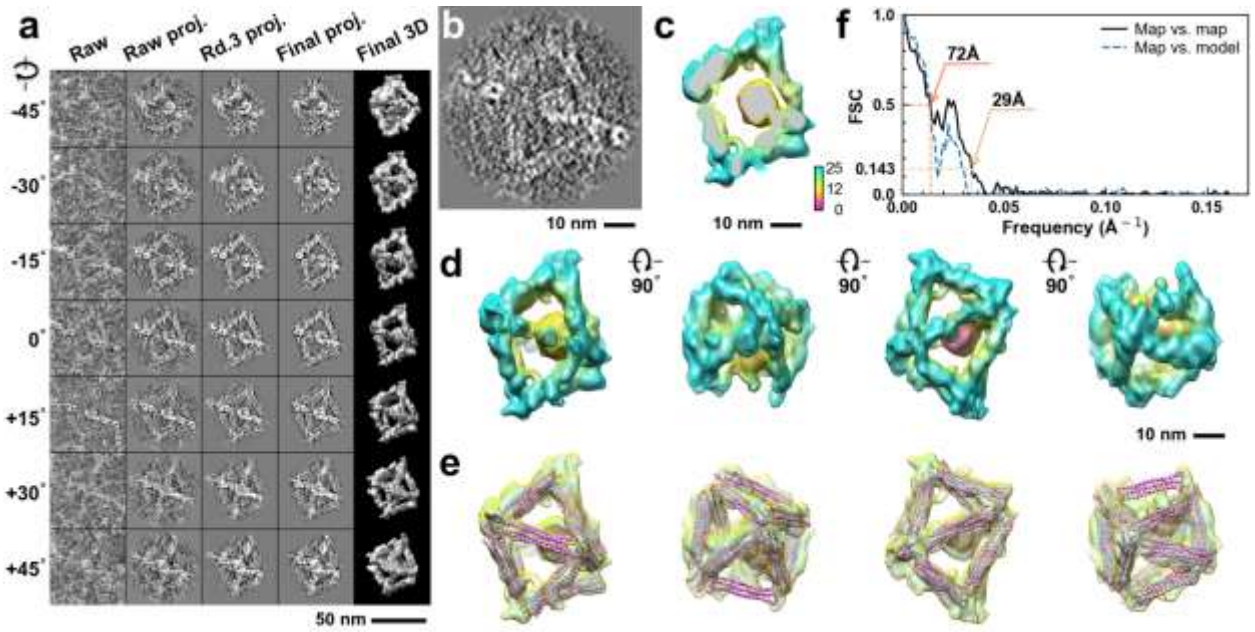

Supplementary Fig. 141: IPET 3D reconstruction and model fitting of an individual unit-cell particle (Index: 133) within a 2D lattice with 100% ferritin loading. a, Seven representative tilt images of a single unit-cell particle are shown in the first column (from left). The tilt images are aligned to a common center using IPET through iterative refinement. The projections of the raw, intermediate, and final 3D reconstruction at the corresponding angles are displayed in the subsequent four columns. **b**, A central cross-section (~23 nm thick) of the final reconstruction before masking is applied. **c**, 3D views of the central cross-section. **d**, Final 3D density map of this particle, viewed from four perpendicular directions. **e**, Final 3D reconstruction superimposed with the fitted model, viewed from four perpendicular directions. **f**, FSC analyses of the final map resolution using two methods: map-map FSC, where each map is reconstructed from one half of the images (even vs. odd tilt angle indices), and map-model FSC, where the model map is generated from the fitted model. Resolution assessments are provided based on tilt-based map-map and map-model FSC analyses at thresholds of FSC=0.5 and 0.143, respectively.

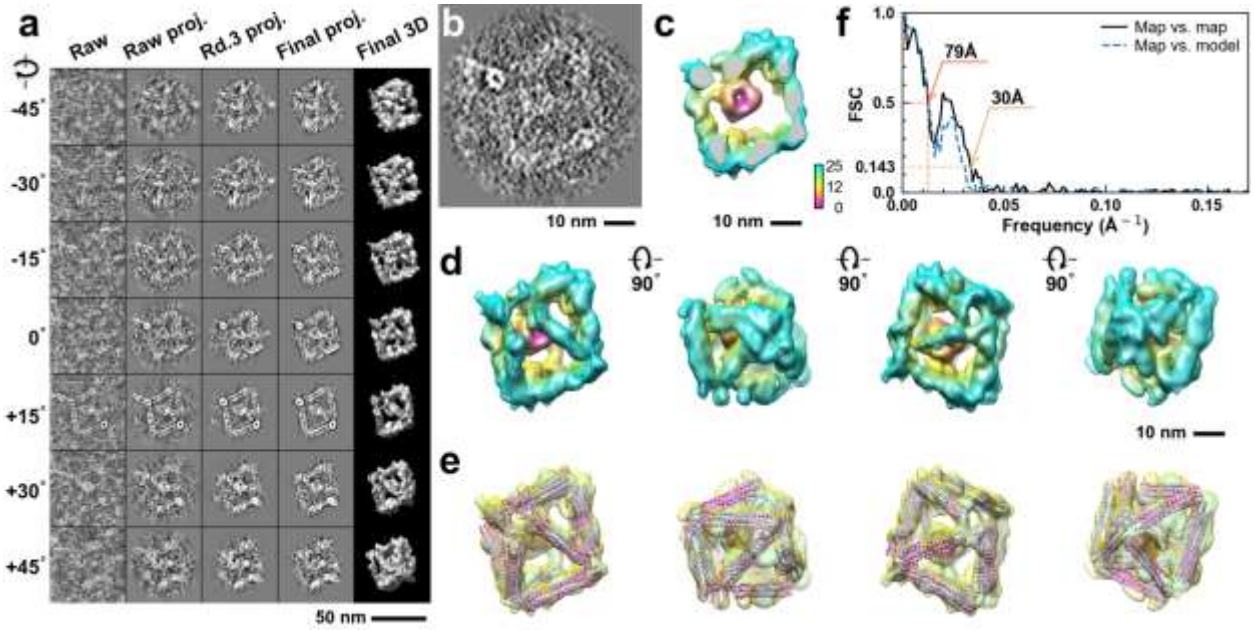

Supplementary Fig. 142: IPET 3D reconstruction and model fitting of an individual unit-cell particle (Index: 134) within a 2D lattice with 100% ferritin loading. a, Seven representative tilt images of a single unit-cell particle are shown in the first column (from left). The tilt images are aligned to a common center using IPET through iterative refinement. The projections of the raw, intermediate, and final 3D reconstruction at the corresponding angles are displayed in the subsequent four columns. **b**, A central cross-section (~23 nm thick) of the final reconstruction before masking is applied. **c**, 3D views of the central cross-section. **d**, Final 3D density map of this particle, viewed from four perpendicular directions. **e**, Final 3D reconstruction superimposed with the fitted model, viewed from four perpendicular directions. **f**, FSC analyses of the final map resolution using two methods: map-map FSC, where each map is reconstructed from one half of the images (even vs. odd tilt angle indices), and map-model FSC, where the model map is generated from the fitted model. Resolution assessments are provided based on tilt-based map-map and map-model FSC analyses at thresholds of FSC=0.5 and 0.143, respectively.

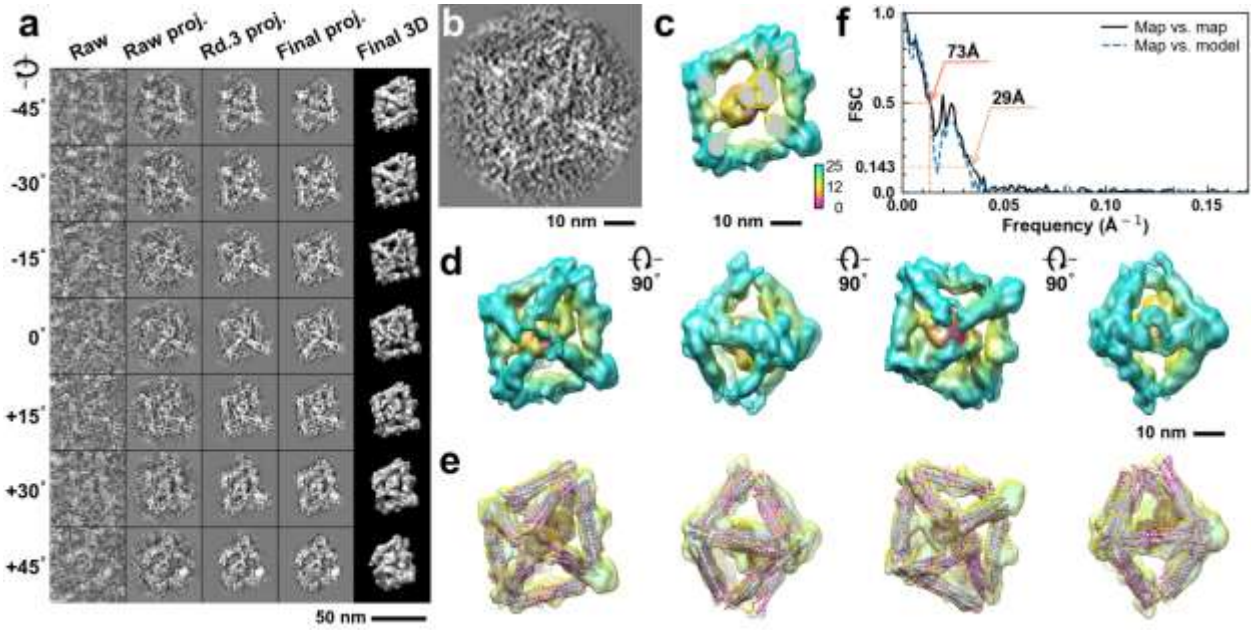

Supplementary Fig. 143: IPET 3D reconstruction and model fitting of an individual unit-cell particle (Index: 135) within a 2D lattice with 100% ferritin loading. a, Seven representative tilt images of a single unit-cell particle are shown in the first column (from left). The tilt images are aligned to a common center using IPET through iterative refinement. The projections of the raw, intermediate, and final 3D reconstruction at the corresponding angles are displayed in the subsequent four columns. **b**, A central cross-section (~23 nm thick) of the final reconstruction before masking is applied. **c**, 3D views of the central cross-section. **d**, Final 3D density map of this particle, viewed from four perpendicular directions. **e**, Final 3D reconstruction superimposed with the fitted model, viewed from four perpendicular directions. **f**, FSC analyses of the final map resolution using two methods: map-map FSC, where each map is reconstructed from one half of the images (even vs. odd tilt angle indices), and map-model FSC, where the model map is generated from the fitted model. Resolution assessments are provided based on tilt-based map-map and map-model FSC analyses at thresholds of FSC=0.5 and 0.143, respectively.

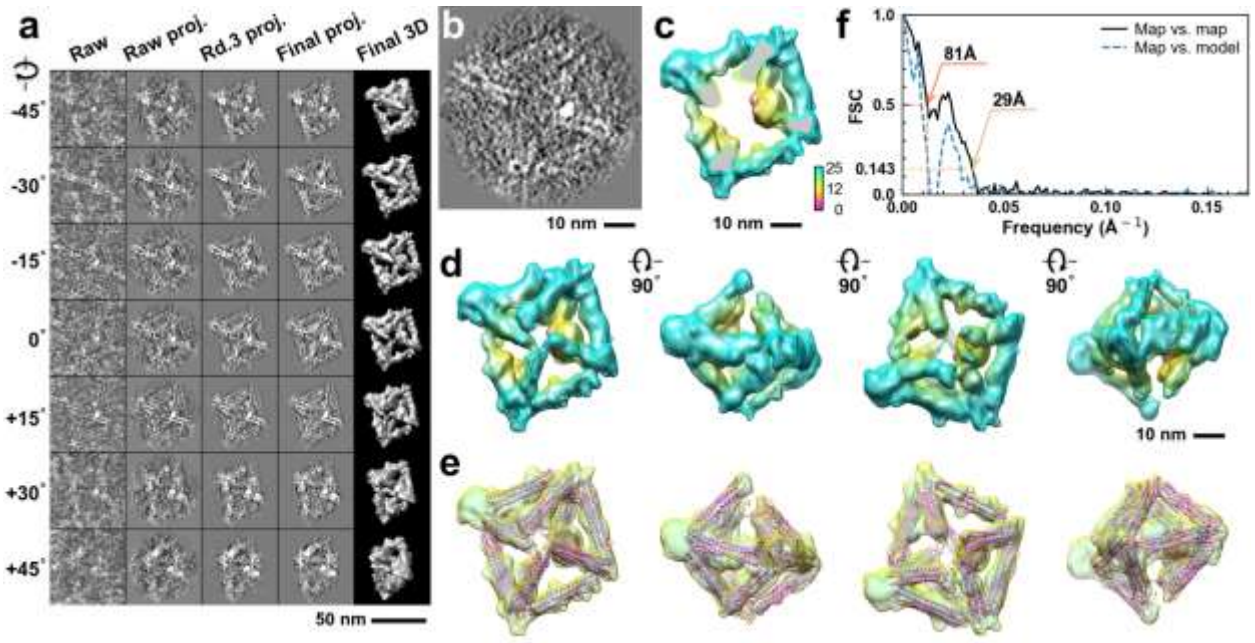

Supplementary Fig. 144: IPET 3D reconstruction and model fitting of an individual unit-cell particle (Index: 136) within a 2D lattice with 100% ferritin loading. a, Seven representative tilt images of a single unit-cell particle are shown in the first column (from left). The tilt images are aligned to a common center using IPET through iterative refinement. The projections of the raw, intermediate, and final 3D reconstruction at the corresponding angles are displayed in the subsequent four columns. **b**, A central cross-section (~23 nm thick) of the final reconstruction before masking is applied. **c**, 3D views of the central cross-section. **d**, Final 3D density map of this particle, viewed from four perpendicular directions. **e**, Final 3D reconstruction superimposed with the fitted model, viewed from four perpendicular directions. **f**, FSC analyses of the final map resolution using two methods: map-map FSC, where each map is reconstructed from one half of the images (even vs. odd tilt angle indices), and map-model FSC, where the model map is generated from the fitted model. Resolution assessments are provided based on tilt-based map-map and map-model FSC analyses at thresholds of FSC=0.5 and 0.143, respectively.

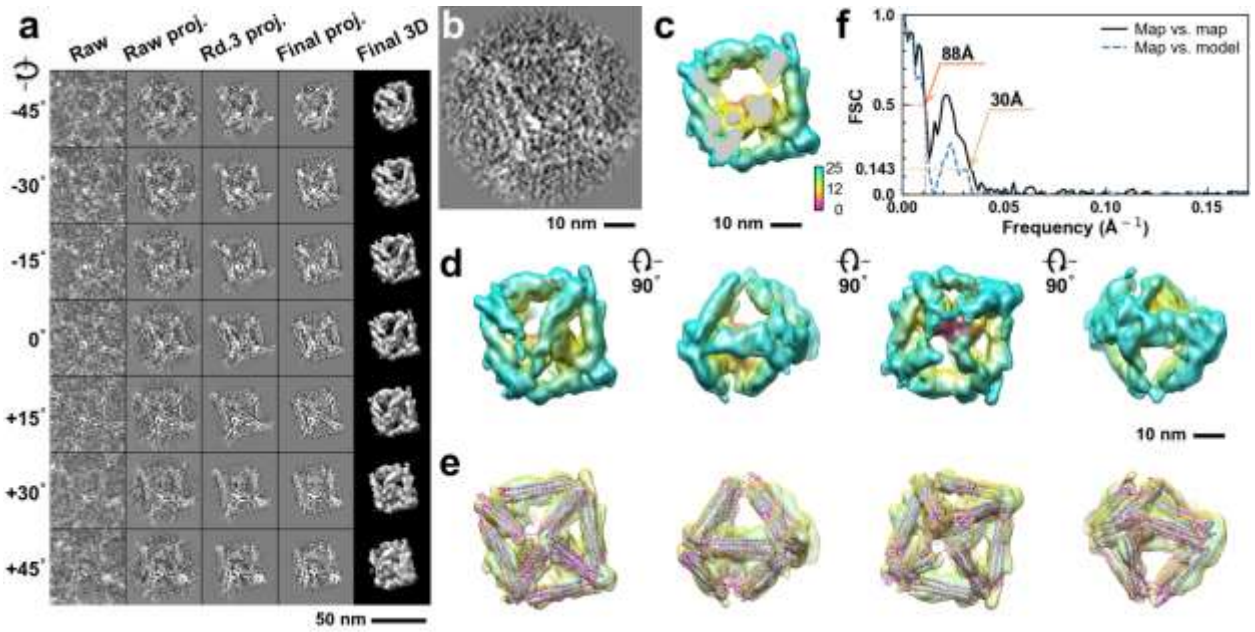

Supplementary Fig. 145: IPET 3D reconstruction and model fitting of an individual unit-cell particle (Index: 137) within a 2D lattice with 100% ferritin loading. a, Seven representative tilt images of a single unit-cell particle are shown in the first column (from left). The tilt images are aligned to a common center using IPET through iterative refinement. The projections of the raw, intermediate, and final 3D reconstruction at the corresponding angles are displayed in the subsequent four columns. **b**, A central cross-section (~23 nm thick) of the final reconstruction before masking is applied. **c**, 3D views of the central cross-section. **d**, Final 3D density map of this particle, viewed from four perpendicular directions. **e**, Final 3D reconstruction superimposed with the fitted model, viewed from four perpendicular directions. **f**, FSC analyses of the final map resolution using two methods: map-map FSC, where each map is reconstructed from one half of the images (even vs. odd tilt angle indices), and map-model FSC, where the model map is generated from the fitted model. Resolution assessments are provided based on tilt-based map-map and map-model FSC analyses at thresholds of FSC=0.5 and 0.143, respectively.

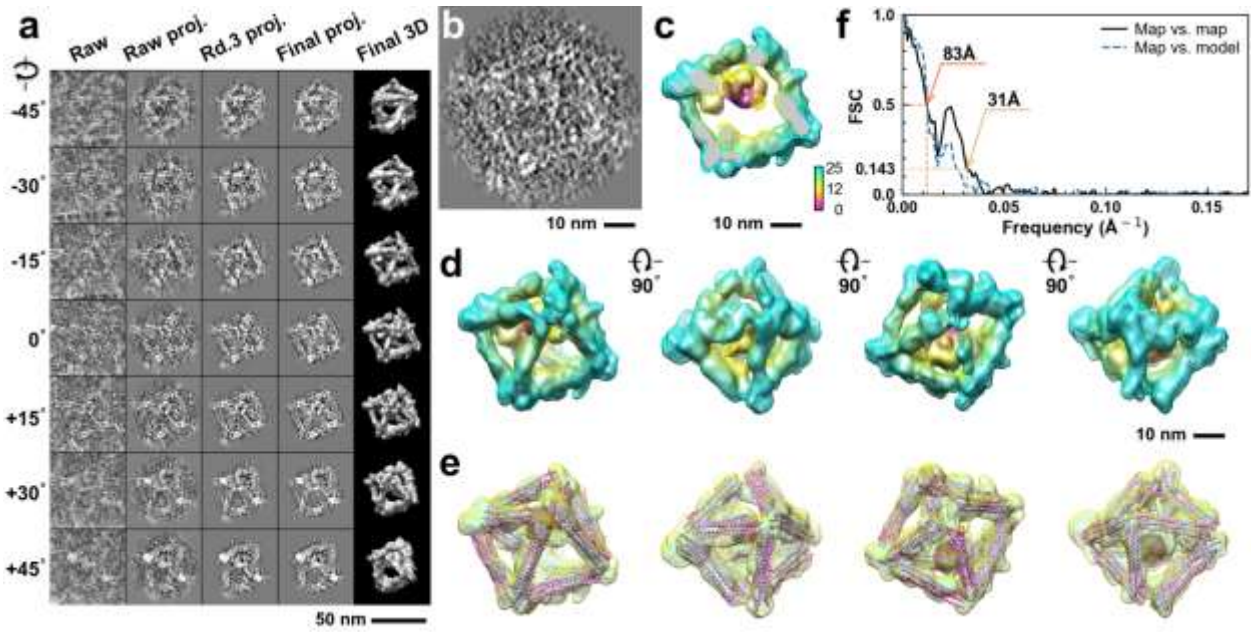

Supplementary Fig. 146: IPET 3D reconstruction and model fitting of an individual unit-cell particle (Index: 138) within a 2D lattice with 100% ferritin loading. a, Seven representative tilt images of a single unit-cell particle are shown in the first column (from left). The tilt images are aligned to a common center using IPET through iterative refinement. The projections of the raw, intermediate, and final 3D reconstruction at the corresponding angles are displayed in the subsequent four columns. **b**, A central cross-section (~23 nm thick) of the final reconstruction before masking is applied. **c**, 3D views of the central cross-section. **d**, Final 3D density map of this particle, viewed from four perpendicular directions. **e**, Final 3D reconstruction superimposed with the fitted model, viewed from four perpendicular directions. **f**, FSC analyses of the final map resolution using two methods: map-map FSC, where each map is reconstructed from one half of the images (even vs. odd tilt angle indices), and map-model FSC, where the model map is generated from the fitted model. Resolution assessments are provided based on tilt-based map-map and map-model FSC analyses at thresholds of FSC=0.5 and 0.143, respectively.

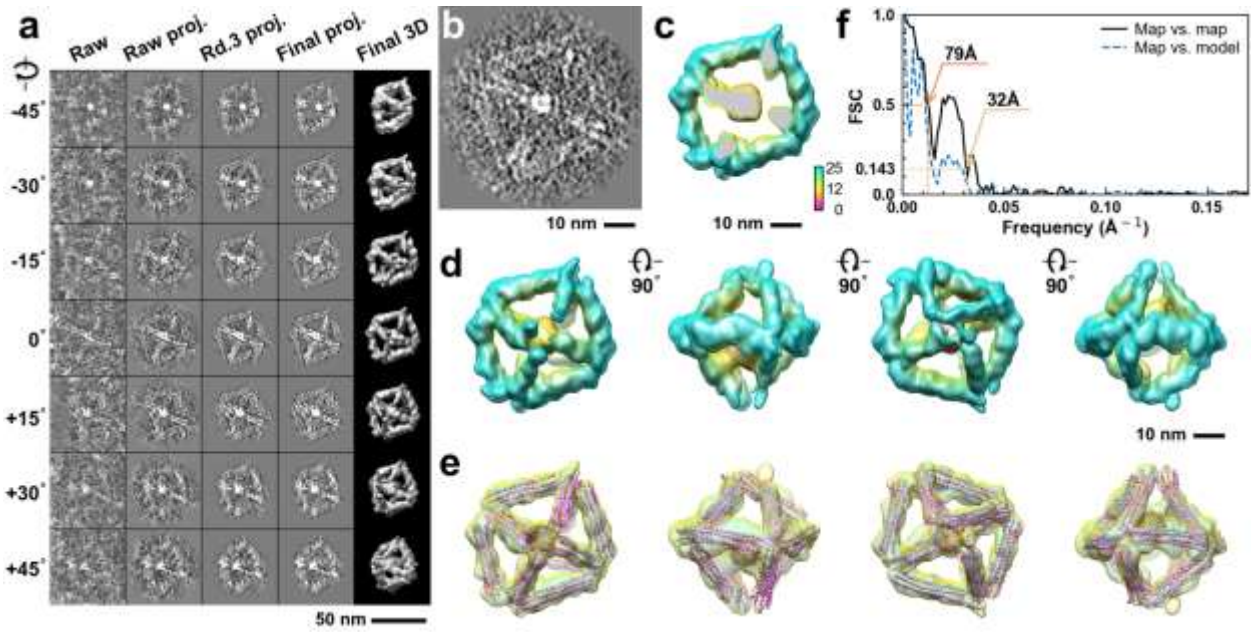

Supplementary Fig. 147: IPET 3D reconstruction and model fitting of an individual unit-cell particle (Index: 139) within a 2D lattice with 100% ferritin loading. a, Seven representative tilt images of a single unit-cell particle are shown in the first column (from left). The tilt images are aligned to a common center using IPET through iterative refinement. The projections of the raw, intermediate, and final 3D reconstruction at the corresponding angles are displayed in the subsequent four columns. **b**, A central cross-section (~23 nm thick) of the final reconstruction before masking is applied. **c**, 3D views of the central cross-section. **d**, Final 3D density map of this particle, viewed from four perpendicular directions. **e**, Final 3D reconstruction superimposed with the fitted model, viewed from four perpendicular directions. **f**, FSC analyses of the final map resolution using two methods: map-map FSC, where each map is reconstructed from one half of the images (even vs. odd tilt angle indices), and map-model FSC, where the model map is generated from the fitted model. Resolution assessments are provided based on tilt-based map-map and map-model FSC analyses at thresholds of FSC=0.5 and 0.143, respectively.

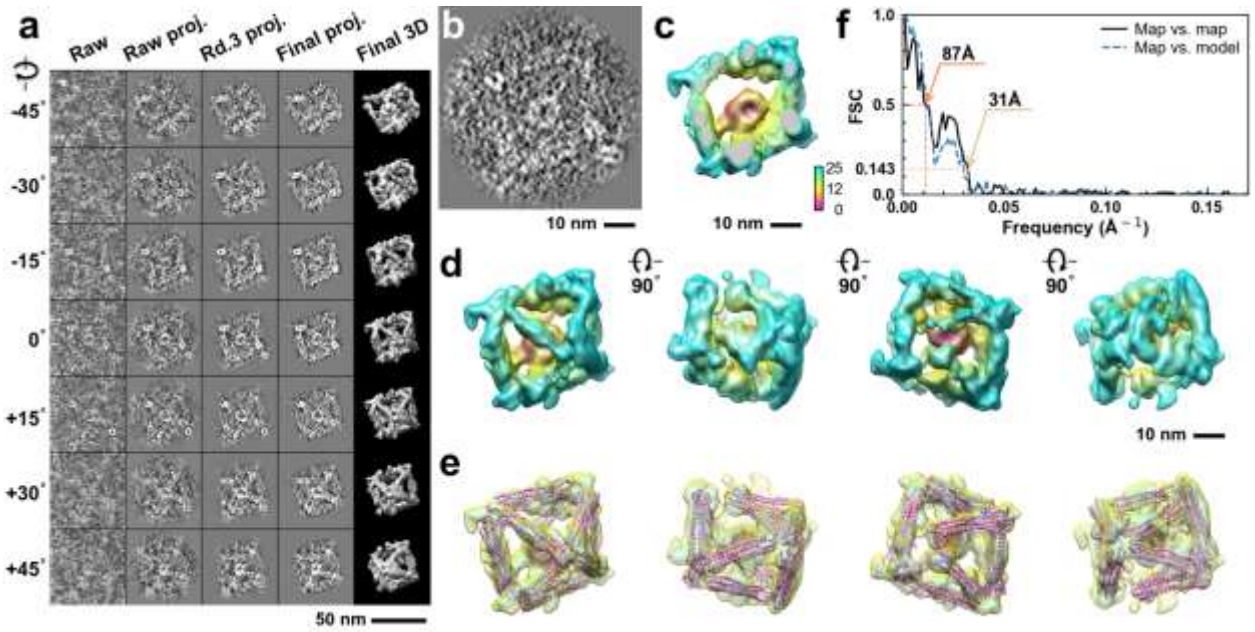

Supplementary Fig. 148: IPET 3D reconstruction and model fitting of an individual unit-cell particle (Index: 140) within a 2D lattice with 100% ferritin loading. a, Seven representative tilt images of a single unit-cell particle are shown in the first column (from left). The tilt images are aligned to a common center using IPET through iterative refinement. The projections of the raw, intermediate, and final 3D reconstruction at the corresponding angles are displayed in the subsequent four columns. **b**, A central cross-section (~23 nm thick) of the final reconstruction before masking is applied. **c**, 3D views of the central cross-section. **d**, Final 3D density map of this particle, viewed from four perpendicular directions. **e**, Final 3D reconstruction superimposed with the fitted model, viewed from four perpendicular directions. **f**, FSC analyses of the final map resolution using two methods: map-map FSC, where each map is reconstructed from one half of the images (even vs. odd tilt angle indices), and map-model FSC, where the model map is generated from the fitted model. Resolution assessments are provided based on tilt-based map-map and map-model FSC analyses at thresholds of FSC=0.5 and 0.143, respectively.

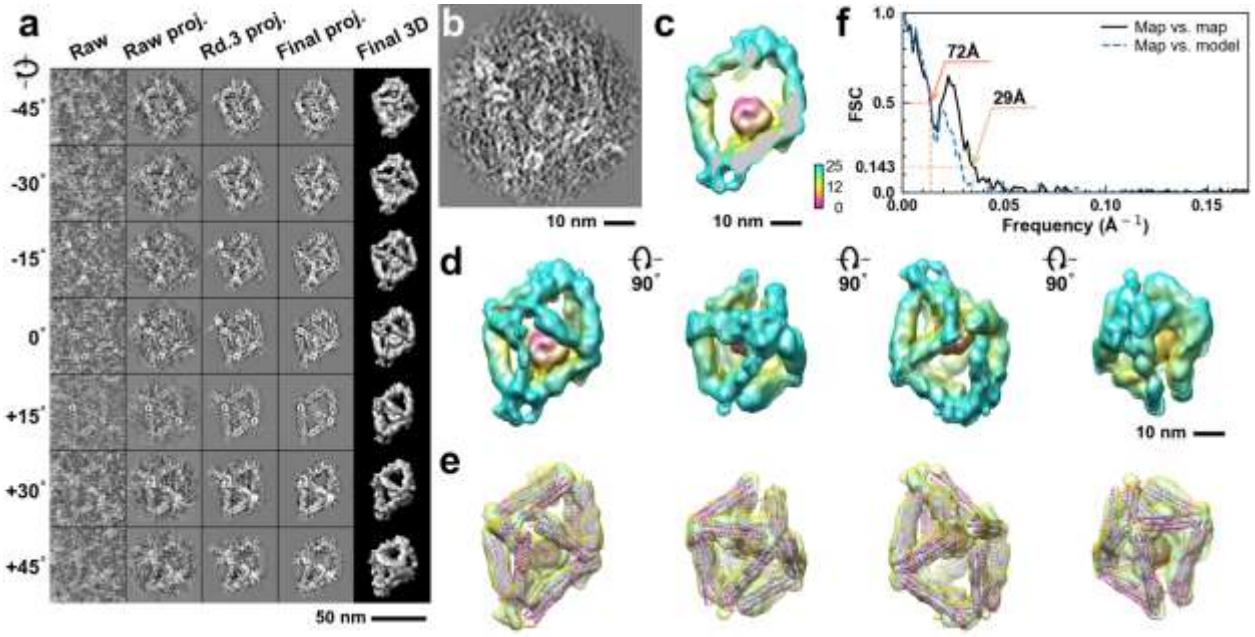

Supplementary Fig. 149: IPET 3D reconstruction and model fitting of an individual unit-cell particle (Index: 141) within a 2D lattice with 100% ferritin loading. a, Seven representative tilt images of a single unit-cell particle are shown in the first column (from left). The tilt images are aligned to a common center using IPET through iterative refinement. The projections of the raw, intermediate, and final 3D reconstruction at the corresponding angles are displayed in the subsequent four columns. **b**, A central cross-section (~23 nm thick) of the final reconstruction before masking is applied. **c**, 3D views of the central cross-section. **d**, Final 3D density map of this particle, viewed from four perpendicular directions. **e**, Final 3D reconstruction superimposed with the fitted model, viewed from four perpendicular directions. **f**, FSC analyses of the final map resolution using two methods: map-map FSC, where each map is reconstructed from one half of the images (even vs. odd tilt angle indices), and map-model FSC, where the model map is generated from the fitted model. Resolution assessments are provided based on tilt-based map-map and map-model FSC analyses at thresholds of FSC=0.5 and 0.143, respectively.

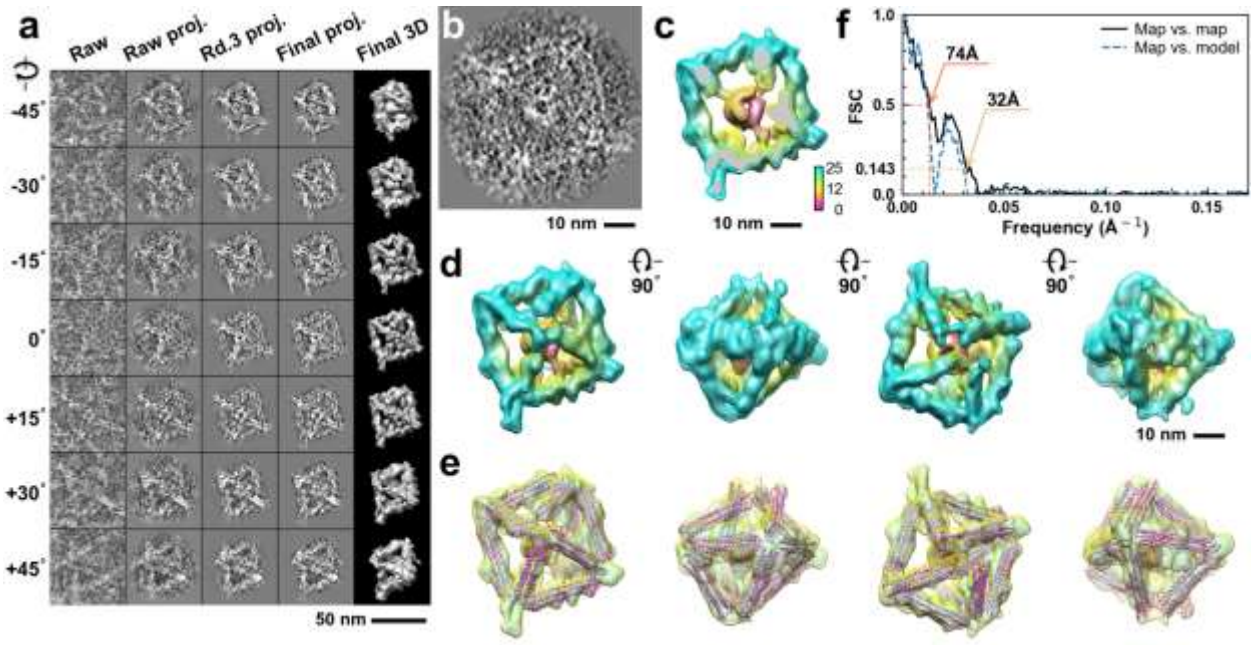

Supplementary Fig. 150: IPET 3D reconstruction and model fitting of an individual unit-cell particle (Index: 142) within a 2D lattice with 100% ferritin loading. a, Seven representative tilt images of a single unit-cell particle are shown in the first column (from left). The tilt images are aligned to a common center using IPET through iterative refinement. The projections of the raw, intermediate, and final 3D reconstruction at the corresponding angles are displayed in the subsequent four columns. **b**, A central cross-section (~23 nm thick) of the final reconstruction before masking is applied. **c**, 3D views of the central cross-section. **d**, Final 3D density map of this particle, viewed from four perpendicular directions. **e**, Final 3D reconstruction superimposed with the fitted model, viewed from four perpendicular directions. **f**, FSC analyses of the final map resolution using two methods: map-map FSC, where each map is reconstructed from one half of the images (even vs. odd tilt angle indices), and map-model FSC, where the model map is generated from the fitted model. Resolution assessments are provided based on tilt-based map-map and map-model FSC analyses at thresholds of FSC=0.5 and 0.143, respectively.

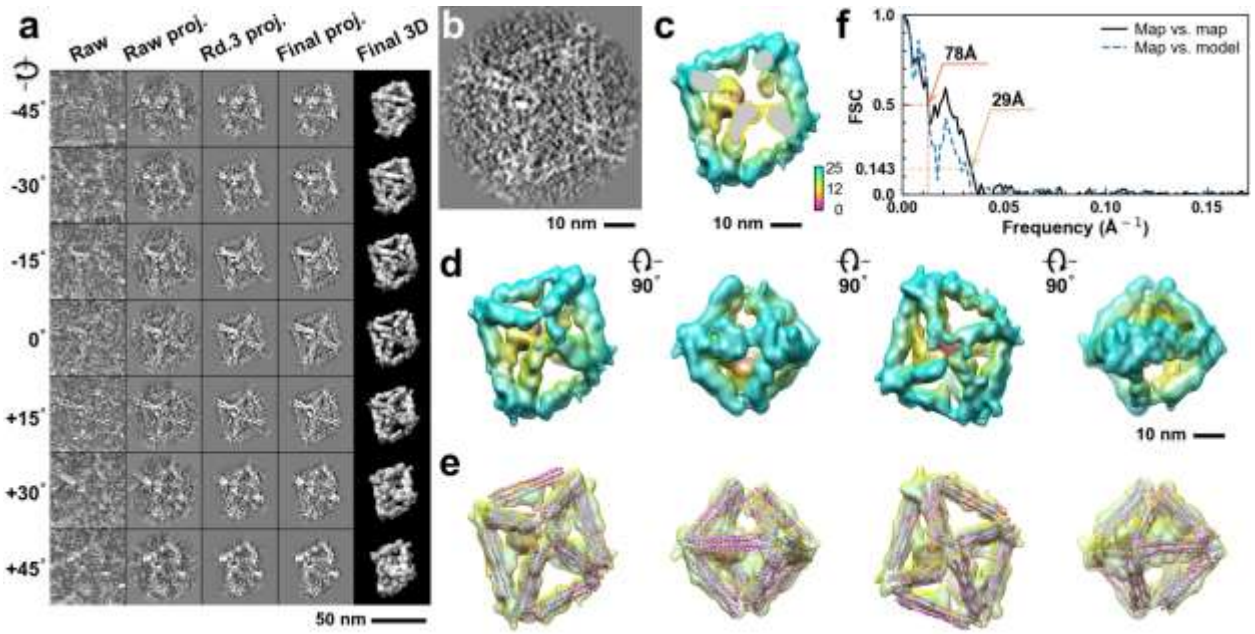

Supplementary Fig. 151: IPET 3D reconstruction and model fitting of an individual unit-cell particle (Index: 143) within a 2D lattice with 100% ferritin loading. a, Seven representative tilt images of a single unit-cell particle are shown in the first column (from left). The tilt images are aligned to a common center using IPET through iterative refinement. The projections of the raw, intermediate, and final 3D reconstruction at the corresponding angles are displayed in the subsequent four columns. **b**, A central cross-section (~23 nm thick) of the final reconstruction before masking is applied. **c**, 3D views of the central cross-section. **d**, Final 3D density map of this particle, viewed from four perpendicular directions. **e**, Final 3D reconstruction superimposed with the fitted model, viewed from four perpendicular directions. **f**, FSC analyses of the final map resolution using two methods: map-map FSC, where each map is reconstructed from one half of the images (even vs. odd tilt angle indices), and map-model FSC, where the model map is generated from the fitted model. Resolution assessments are provided based on tilt-based map-map and map-model FSC analyses at thresholds of FSC=0.5 and 0.143, respectively.

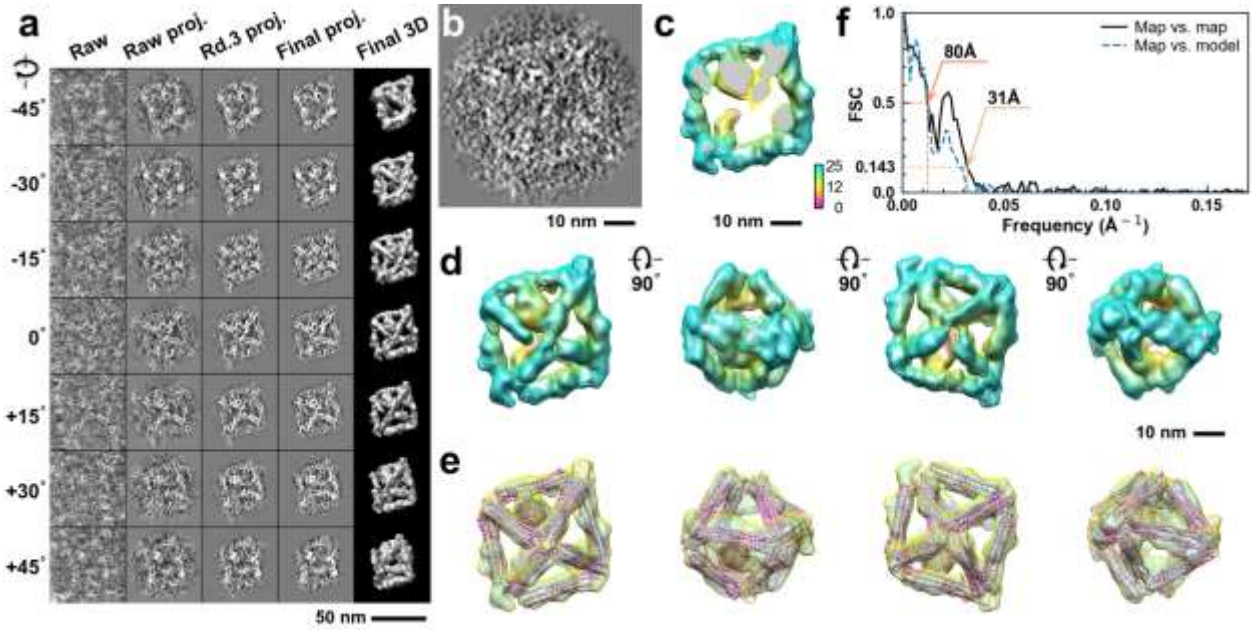

Supplementary Fig. 152: IPET 3D reconstruction and model fitting of an individual unit-cell particle (Index: 144) within a 2D lattice with 100% ferritin loading. a, Seven representative tilt images of a single unit-cell particle are shown in the first column (from left). The tilt images are aligned to a common center using IPET through iterative refinement. The projections of the raw, intermediate, and final 3D reconstruction at the corresponding angles are displayed in the subsequent four columns. **b**, A central cross-section (~23 nm thick) of the final reconstruction before masking is applied. **c**, 3D views of the central cross-section. **d**, Final 3D density map of this particle, viewed from four perpendicular directions. **e**, Final 3D reconstruction superimposed with the fitted model, viewed from four perpendicular directions. **f**, FSC analyses of the final map resolution using two methods: map-map FSC, where each map is reconstructed from one half of the images (even vs. odd tilt angle indices), and map-model FSC, where the model map is generated from the fitted model. Resolution assessments are provided based on tilt-based map-map and map-model FSC analyses at thresholds of FSC=0.5 and 0.143, respectively.

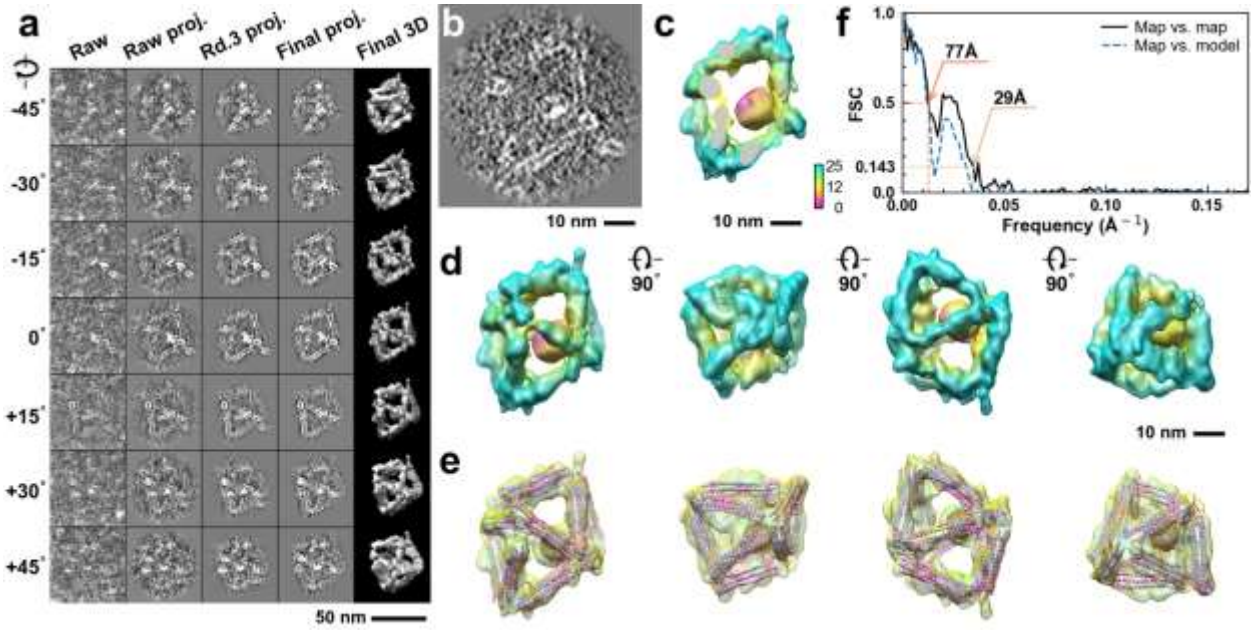

Supplementary Fig. 153: IPET 3D reconstruction and model fitting of an individual unit-cell particle (Index: 145) within a 2D lattice with 100% ferritin loading. a, Seven representative tilt images of a single unit-cell particle are shown in the first column (from left). The tilt images are aligned to a common center using IPET through iterative refinement. The projections of the raw, intermediate, and final 3D reconstruction at the corresponding angles are displayed in the subsequent four columns. **b**, A central cross-section (~23 nm thick) of the final reconstruction before masking is applied. **c**, 3D views of the central cross-section. **d**, Final 3D density map of this particle, viewed from four perpendicular directions. **e**, Final 3D reconstruction superimposed with the fitted model, viewed from four perpendicular directions. **f**, FSC analyses of the final map resolution using two methods: map-map FSC, where each map is reconstructed from one half of the images (even vs. odd tilt angle indices), and map-model FSC, where the model map is generated from the fitted model. Resolution assessments are provided based on tilt-based map-map and map-model FSC analyses at thresholds of FSC=0.5 and 0.143, respectively.

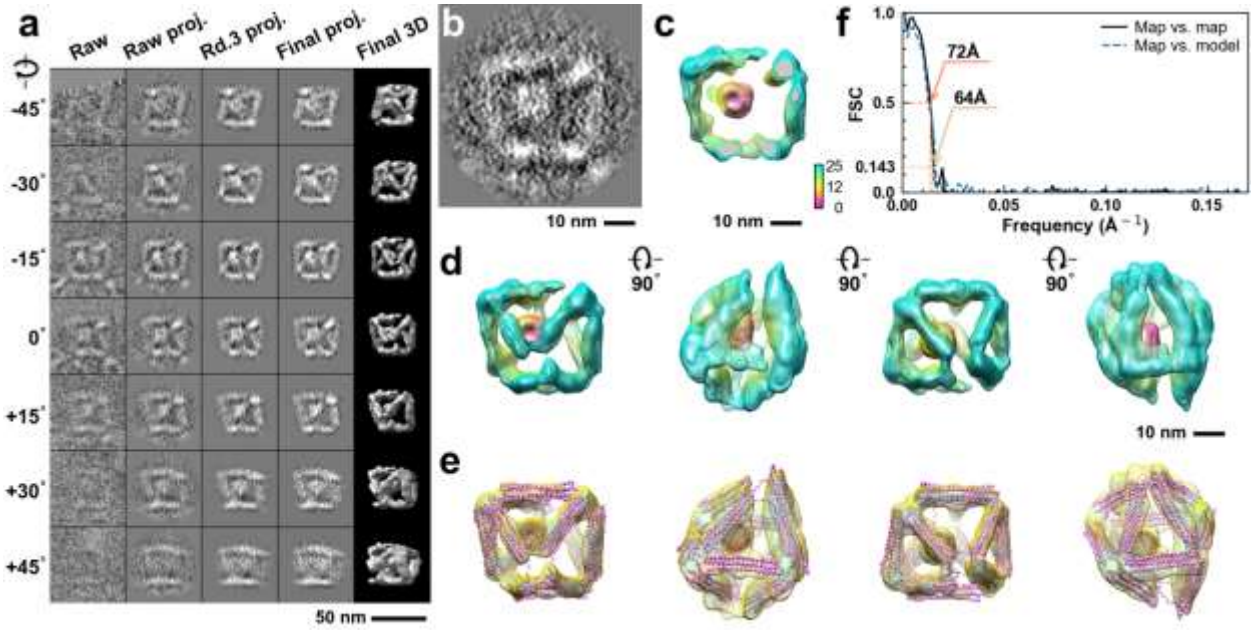

Supplementary Fig. 154: IPET 3D reconstruction and model fitting of an individual unit-cell particle (Index: 146) within a 2D lattice with 70% ferritin loading. a, Seven representative tilt images of a single unit-cell particle are shown in the first column (from left). The tilt images are aligned to a common center using IPET through iterative refinement. The projections of the raw, intermediate, and final 3D reconstruction at the corresponding angles are displayed in the subsequent four columns. **b**, A central cross-section (~23 nm thick) of the final reconstruction before masking is applied. **c**, 3D views of the central cross-section. **d**, Final 3D density map of this particle, viewed from four perpendicular directions. **e**, Final 3D reconstruction superimposed with the fitted model, viewed from four perpendicular directions. **f**, FSC analyses of the final map resolution using two methods: map-map FSC, where each map is reconstructed from one half of the images (even vs. odd tilt angle indices), and map-model FSC, where the model map is generated from the fitted model. Resolution assessments are provided based on tilt-based map-map and map-model FSC analyses at thresholds of FSC=0.5 and 0.143, respectively.

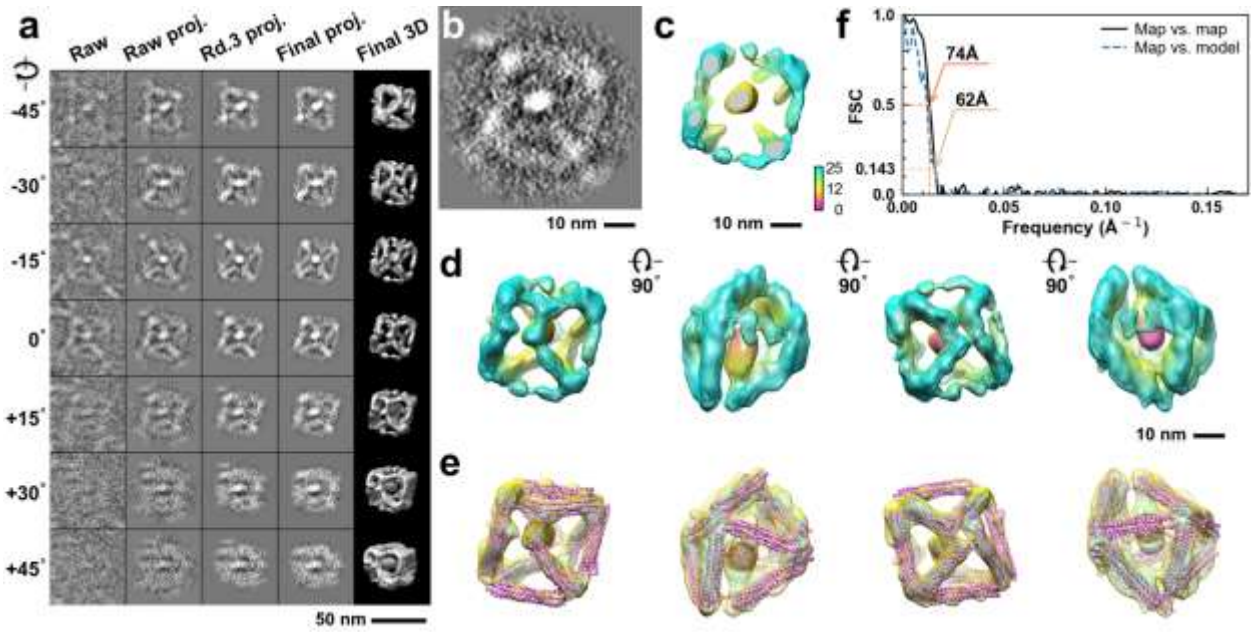

Supplementary Fig. 155: IPET 3D reconstruction and model fitting of an individual unit-cell particle (Index: 147) within a 2D lattice with 70% ferritin loading. a, Seven representative tilt images of a single unit-cell particle are shown in the first column (from left). The tilt images are aligned to a common center using IPET through iterative refinement. The projections of the raw, intermediate, and final 3D reconstruction at the corresponding angles are displayed in the subsequent four columns. **b**, A central cross-section (~23 nm thick) of the final reconstruction before masking is applied. **c**, 3D views of the central cross-section. **d**, Final 3D density map of this particle, viewed from four perpendicular directions. **e**, Final 3D reconstruction superimposed with the fitted model, viewed from four perpendicular directions. **f**, FSC analyses of the final map resolution using two methods: map-map FSC, where each map is reconstructed from one half of the images (even vs. odd tilt angle indices), and map-model FSC, where the model map is generated from the fitted model. Resolution assessments are provided based on tilt-based map-map and map-model FSC analyses at thresholds of FSC=0.5 and 0.143, respectively.

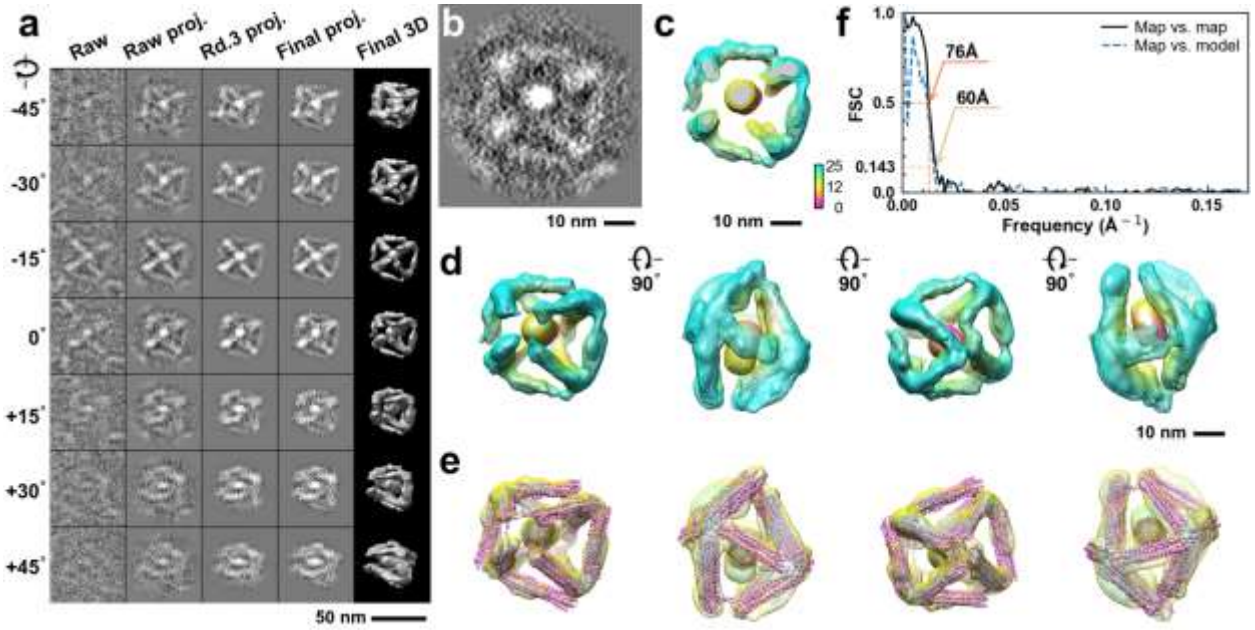

Supplementary Fig. 156: IPET 3D reconstruction and model fitting of an individual unit-cell particle (Index: 148) within a 2D lattice with 70% ferritin loading. a, Seven representative tilt images of a single unit-cell particle are shown in the first column (from left). The tilt images are aligned to a common center using IPET through iterative refinement. The projections of the raw, intermediate, and final 3D reconstruction at the corresponding angles are displayed in the subsequent four columns. **b**, A central cross-section (~23 nm thick) of the final reconstruction before masking is applied. **c**, 3D views of the central cross-section. **d**, Final 3D density map of this particle, viewed from four perpendicular directions. **e**, Final 3D reconstruction superimposed with the fitted model, viewed from four perpendicular directions. **f**, FSC analyses of the final map resolution using two methods: map-map FSC, where each map is reconstructed from one half of the images (even vs. odd tilt angle indices), and map-model FSC, where the model map is generated from the fitted model. Resolution assessments are provided based on tilt-based map-map and map-model FSC analyses at thresholds of FSC=0.5 and 0.143, respectively.

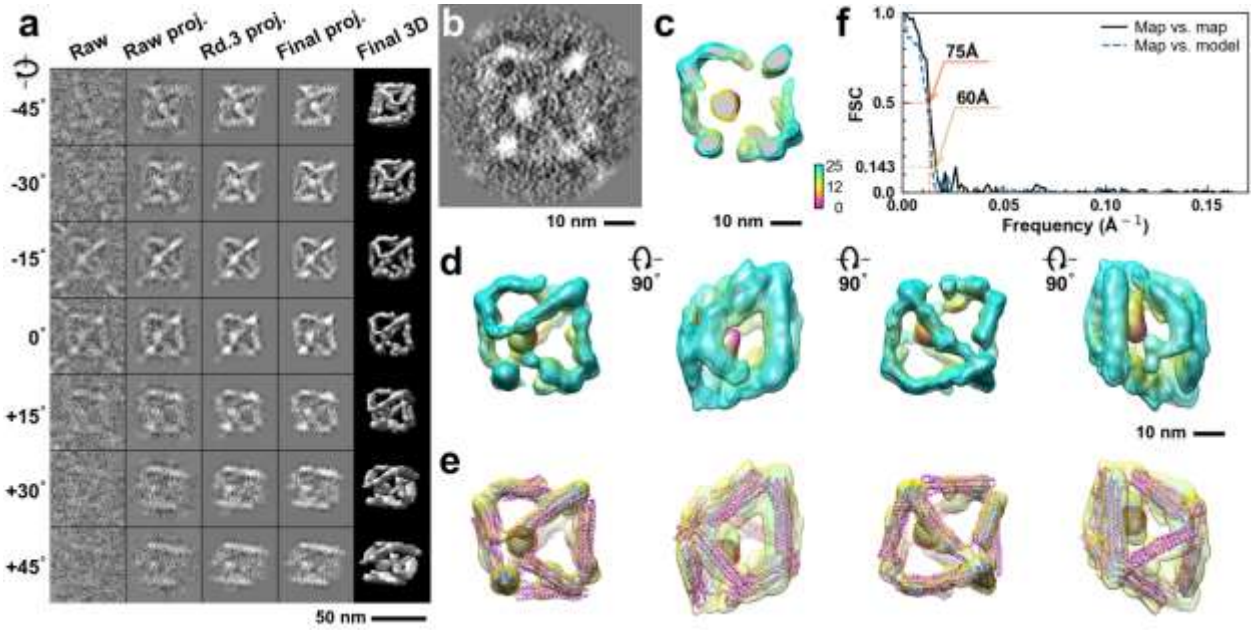

Supplementary Fig. 157: IPET 3D reconstruction and model fitting of an individual unit-cell particle (Index: 149) within a 2D lattice with 70% ferritin loading. a, Seven representative tilt images of a single unit-cell particle are shown in the first column (from left). The tilt images are aligned to a common center using IPET through iterative refinement. The projections of the raw, intermediate, and final 3D reconstruction at the corresponding angles are displayed in the subsequent four columns. **b**, A central cross-section (~23 nm thick) of the final reconstruction before masking is applied. **c**, 3D views of the central cross-section. **d**, Final 3D density map of this particle, viewed from four perpendicular directions. **e**, Final 3D reconstruction superimposed with the fitted model, viewed from four perpendicular directions. **f**, FSC analyses of the final map resolution using two methods: map-map FSC, where each map is reconstructed from one half of the images (even vs. odd tilt angle indices), and map-model FSC, where the model map is generated from the fitted model. Resolution assessments are provided based on tilt-based map-map and map-model FSC analyses at thresholds of FSC=0.5 and 0.143, respectively.

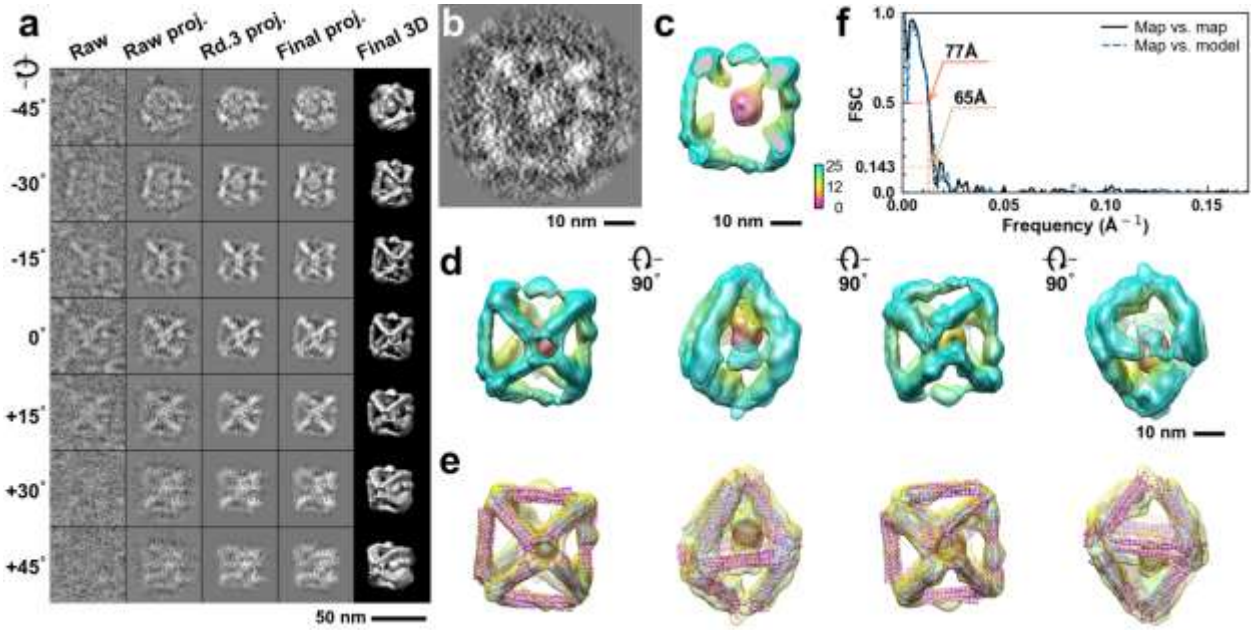

Supplementary Fig. 158: IPET 3D reconstruction and model fitting of an individual unit-cell particle (Index: 150) within a 2D lattice with 70% ferritin loading. a, Seven representative tilt images of a single unit-cell particle are shown in the first column (from left). The tilt images are aligned to a common center using IPET through iterative refinement. The projections of the raw, intermediate, and final 3D reconstruction at the corresponding angles are displayed in the subsequent four columns. **b**, A central cross-section (~23 nm thick) of the final reconstruction before masking is applied. **c**, 3D views of the central cross-section. **d**, Final 3D density map of this particle, viewed from four perpendicular directions. **e**, Final 3D reconstruction superimposed with the fitted model, viewed from four perpendicular directions. **f**, FSC analyses of the final map resolution using two methods: map-map FSC, where each map is reconstructed from one half of the images (even vs. odd tilt angle indices), and map-model FSC, where the model map is generated from the fitted model. Resolution assessments are provided based on tilt-based map-map and map-model FSC analyses at thresholds of FSC=0.5 and 0.143, respectively.

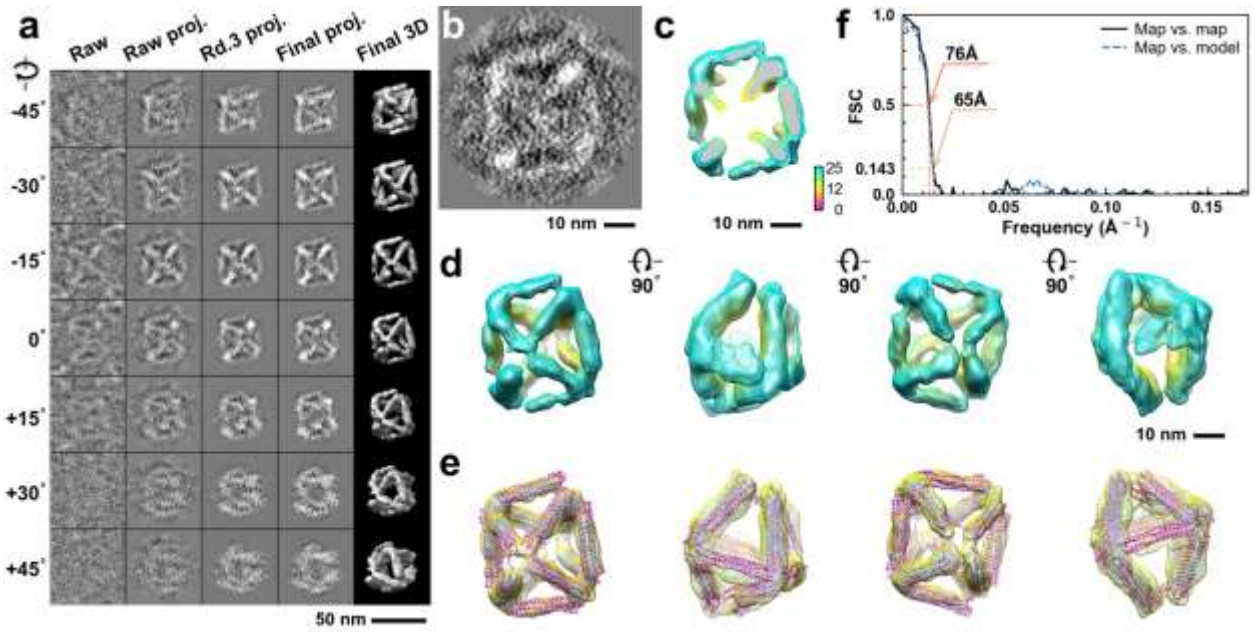

Supplementary Fig. 159: IPET 3D reconstruction and model fitting of an individual unit-cell particle (Index: 151) within a 2D lattice with 70% ferritin loading. a, Seven representative tilt images of a single unit-cell particle are shown in the first column (from left). The tilt images are aligned to a common center using IPET through iterative refinement. The projections of the raw, intermediate, and final 3D reconstruction at the corresponding angles are displayed in the subsequent four columns. **b**, A central cross-section (~23 nm thick) of the final reconstruction before masking is applied. **c**, 3D views of the central cross-section. **d**, Final 3D density map of this particle, viewed from four perpendicular directions. **e**, Final 3D reconstruction superimposed with the fitted model, viewed from four perpendicular directions. **f**, FSC analyses of the final map resolution using two methods: map-map FSC, where each map is reconstructed from one half of the images (even vs. odd tilt angle indices), and map-model FSC, where the model map is generated from the fitted model. Resolution assessments are provided based on tilt-based map-map and map-model FSC analyses at thresholds of FSC=0.5 and 0.143, respectively.

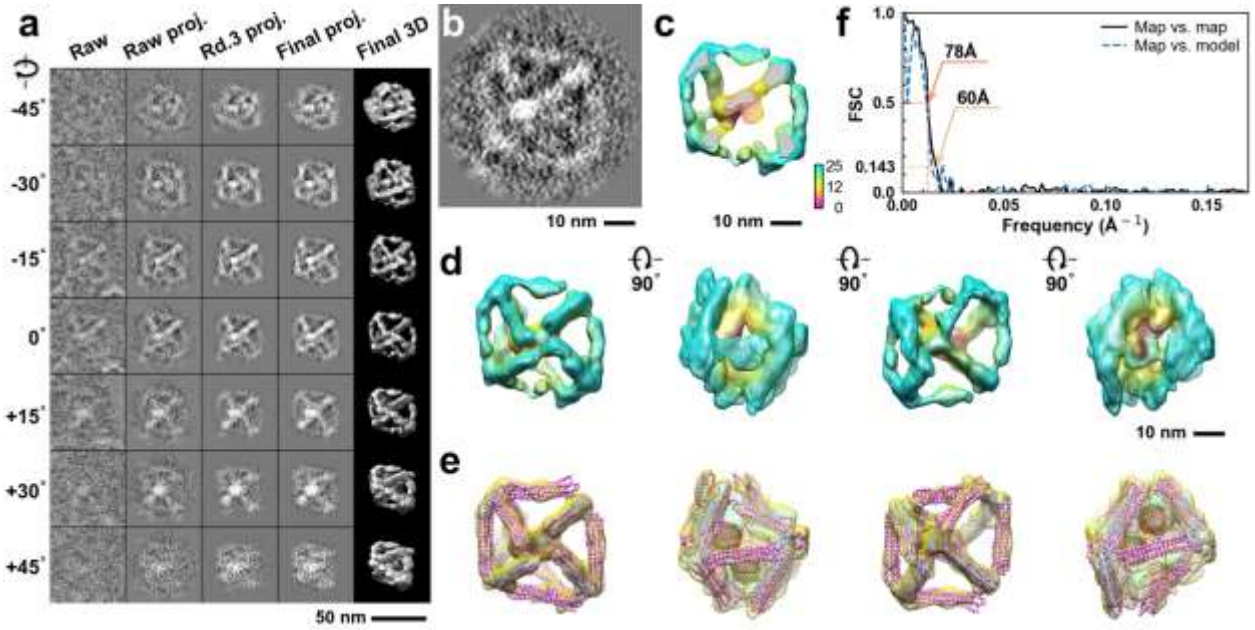

Supplementary Fig. 160: IPET 3D reconstruction and model fitting of an individual unit-cell particle (Index: 152) within a 2D lattice with 70% ferritin loading. a, Seven representative tilt images of a single unit-cell particle are shown in the first column (from left). The tilt images are aligned to a common center using IPET through iterative refinement. The projections of the raw, intermediate, and final 3D reconstruction at the corresponding angles are displayed in the subsequent four columns. **b**, A central cross-section (~23 nm thick) of the final reconstruction before masking is applied. **c**, 3D views of the central cross-section. **d**, Final 3D density map of this particle, viewed from four perpendicular directions. **e**, Final 3D reconstruction superimposed with the fitted model, viewed from four perpendicular directions. **f**, FSC analyses of the final map resolution using two methods: map-map FSC, where each map is reconstructed from one half of the images (even vs. odd tilt angle indices), and map-model FSC, where the model map is generated from the fitted model. Resolution assessments are provided based on tilt-based map-map and map-model FSC analyses at thresholds of FSC=0.5 and 0.143, respectively.

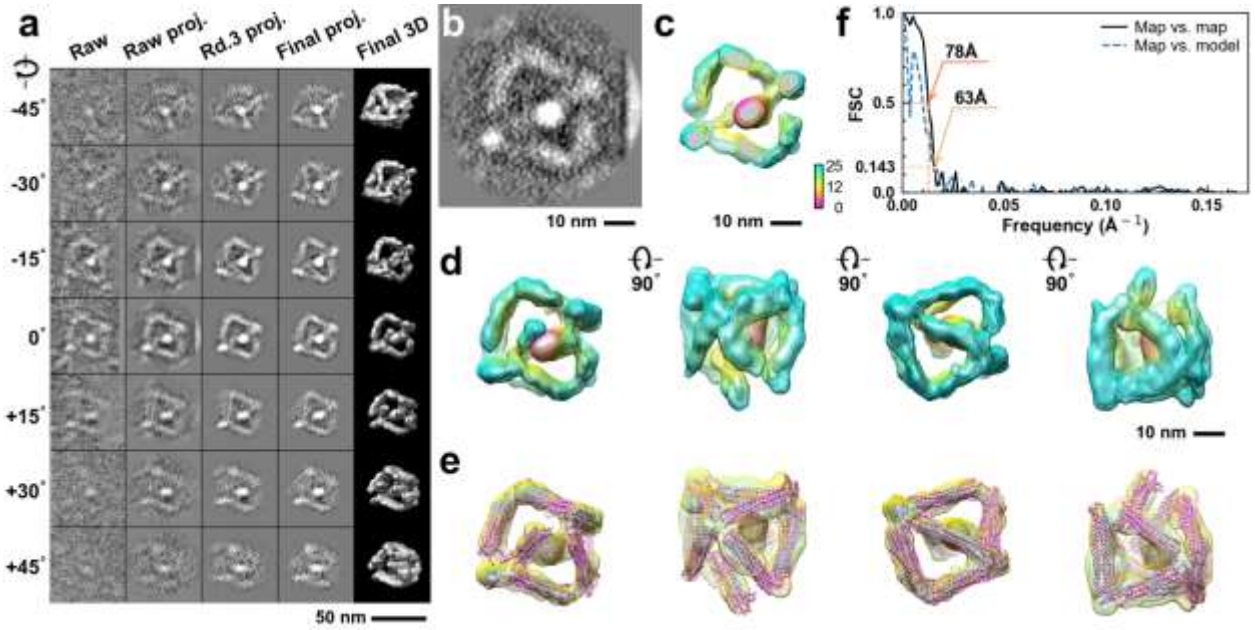

Supplementary Fig. 161: IPET 3D reconstruction and model fitting of an individual unit-cell particle (Index: 153) within a 2D lattice with 70% ferritin loading. a, Seven representative tilt images of a single unit-cell particle are shown in the first column (from left). The tilt images are aligned to a common center using IPET through iterative refinement. The projections of the raw, intermediate, and final 3D reconstruction at the corresponding angles are displayed in the subsequent four columns. **b**, A central cross-section (~23 nm thick) of the final reconstruction before masking is applied. **c**, 3D views of the central cross-section. **d**, Final 3D density map of this particle, viewed from four perpendicular directions. **e**, Final 3D reconstruction superimposed with the fitted model, viewed from four perpendicular directions. **f**, FSC analyses of the final map resolution using two methods: map-map FSC, where each map is reconstructed from one half of the images (even vs. odd tilt angle indices), and map-model FSC, where the model map is generated from the fitted model. Resolution assessments are provided based on tilt-based map-map and map-model FSC analyses at thresholds of FSC=0.5 and 0.143, respectively.

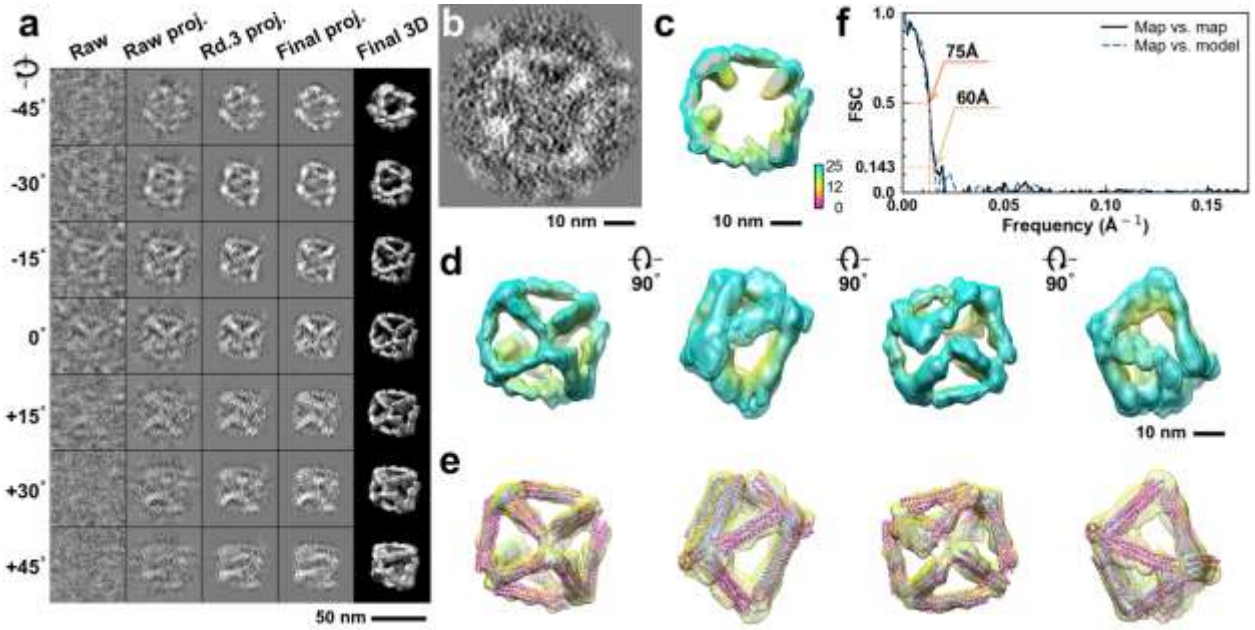

Supplementary Fig. 162: IPET 3D reconstruction and model fitting of an individual unit-cell particle (Index: 154) within a 2D lattice with 70% ferritin loading. a, Seven representative tilt images of a single unit-cell particle are shown in the first column (from left). The tilt images are aligned to a common center using IPET through iterative refinement. The projections of the raw, intermediate, and final 3D reconstruction at the corresponding angles are displayed in the subsequent four columns. **b**, A central cross-section (~23 nm thick) of the final reconstruction before masking is applied. **c**, 3D views of the central cross-section. **d**, Final 3D density map of this particle, viewed from four perpendicular directions. **e**, Final 3D reconstruction superimposed with the fitted model, viewed from four perpendicular directions. **f**, FSC analyses of the final map resolution using two methods: map-map FSC, where each map is reconstructed from one half of the images (even vs. odd tilt angle indices), and map-model FSC, where the model map is generated from the fitted model. Resolution assessments are provided based on tilt-based map-map and map-model FSC analyses at thresholds of FSC=0.5 and 0.143, respectively.

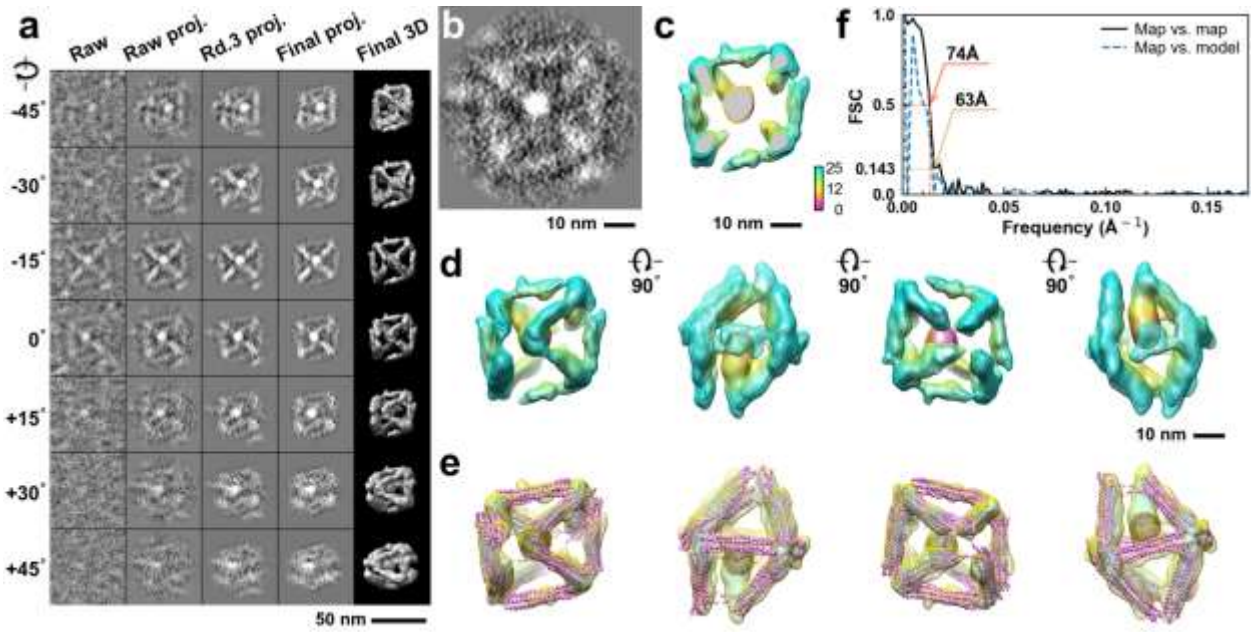

Supplementary Fig. 163: IPET 3D reconstruction and model fitting of an individual unit-cell particle (Index: 155) within a 2D lattice with 70% ferritin loading. a, Seven representative tilt images of a single unit-cell particle are shown in the first column (from left). The tilt images are aligned to a common center using IPET through iterative refinement. The projections of the raw, intermediate, and final 3D reconstruction at the corresponding angles are displayed in the subsequent four columns. **b**, A central cross-section (~23 nm thick) of the final reconstruction before masking is applied. **c**, 3D views of the central cross-section. **d**, Final 3D density map of this particle, viewed from four perpendicular directions. **e**, Final 3D reconstruction superimposed with the fitted model, viewed from four perpendicular directions. **f**, FSC analyses of the final map resolution using two methods: map-map FSC, where each map is reconstructed from one half of the images (even vs. odd tilt angle indices), and map-model FSC, where the model map is generated from the fitted model. Resolution assessments are provided based on tilt-based map-map and map-model FSC analyses at thresholds of FSC=0.5 and 0.143, respectively.

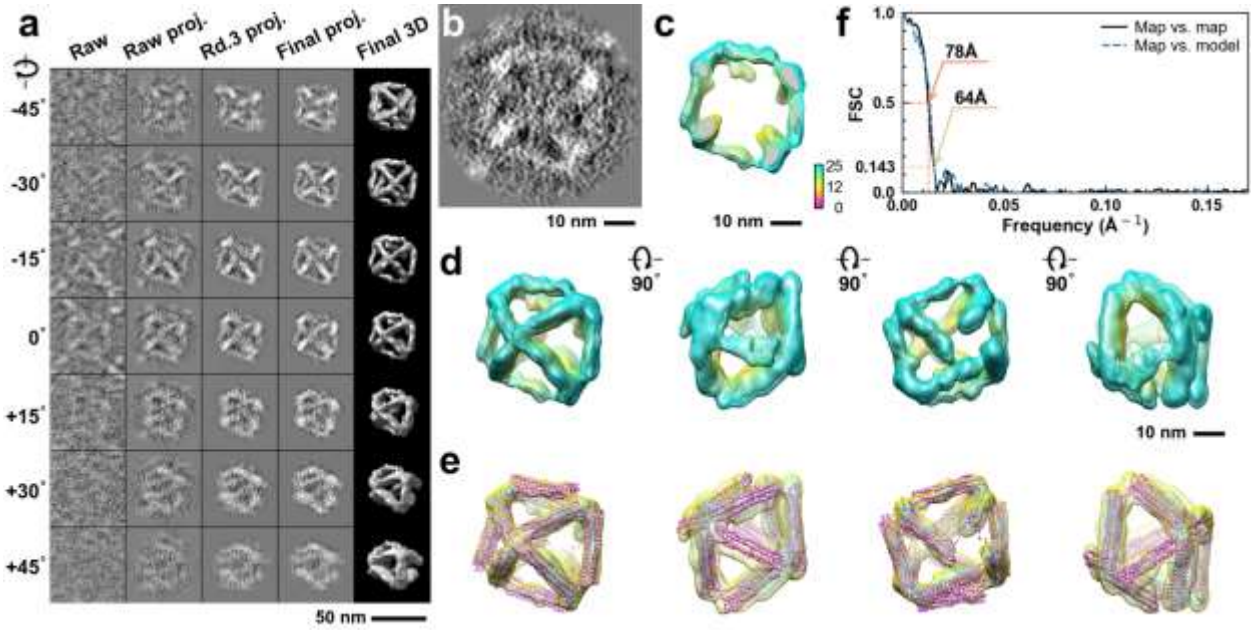

Supplementary Fig. 164: IPET 3D reconstruction and model fitting of an individual unit-cell particle (Index: 156) within a 2D lattice with 70% ferritin loading. a, Seven representative tilt images of a single unit-cell particle are shown in the first column (from left). The tilt images are aligned to a common center using IPET through iterative refinement. The projections of the raw, intermediate, and final 3D reconstruction at the corresponding angles are displayed in the subsequent four columns. **b**, A central cross-section (~23 nm thick) of the final reconstruction before masking is applied. **c**, 3D views of the central cross-section. **d**, Final 3D density map of this particle, viewed from four perpendicular directions. **e**, Final 3D reconstruction superimposed with the fitted model, viewed from four perpendicular directions. **f**, FSC analyses of the final map resolution using two methods: map-map FSC, where each map is reconstructed from one half of the images (even vs. odd tilt angle indices), and map-model FSC, where the model map is generated from the fitted model. Resolution assessments are provided based on tilt-based map-map and map-model FSC analyses at thresholds of FSC=0.5 and 0.143, respectively.

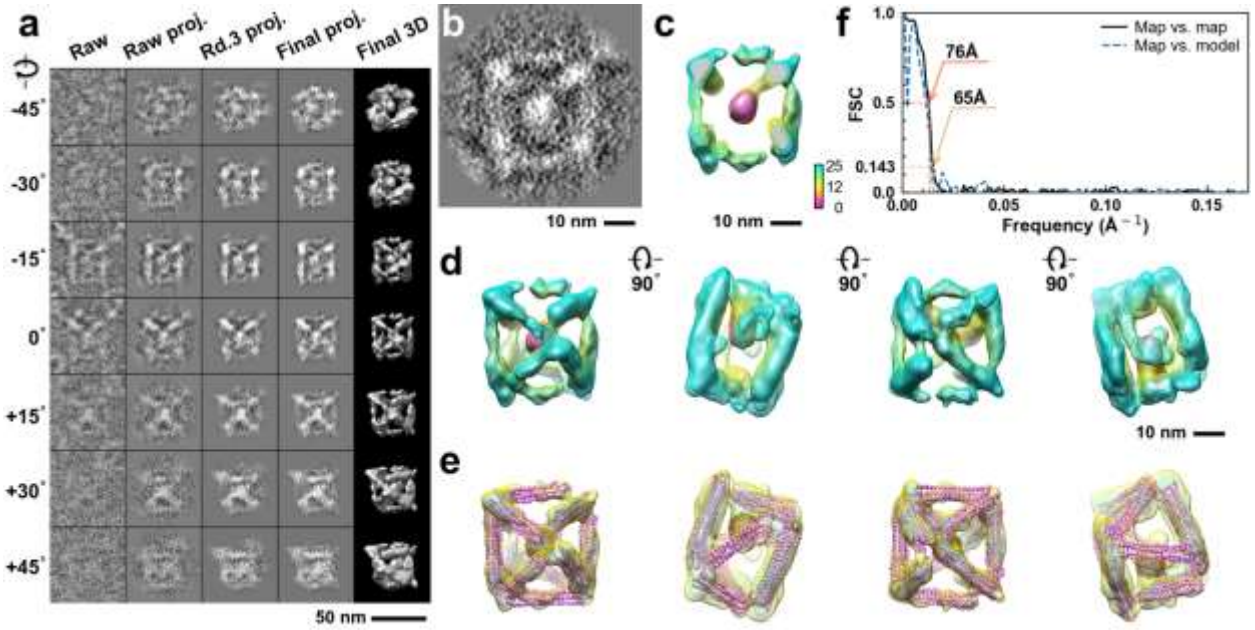

Supplementary Fig. 165: IPET 3D reconstruction and model fitting of an individual unit-cell particle (Index: 157) within a 2D lattice with 70% ferritin loading. a, Seven representative tilt images of a single unit-cell particle are shown in the first column (from left). The tilt images are aligned to a common center using IPET through iterative refinement. The projections of the raw, intermediate, and final 3D reconstruction at the corresponding angles are displayed in the subsequent four columns. **b**, A central cross-section (~23 nm thick) of the final reconstruction before masking is applied. **c**, 3D views of the central cross-section. **d**, Final 3D density map of this particle, viewed from four perpendicular directions. **e**, Final 3D reconstruction superimposed with the fitted model, viewed from four perpendicular directions. **f**, FSC analyses of the final map resolution using two methods: map-map FSC, where each map is reconstructed from one half of the images (even vs. odd tilt angle indices), and map-model FSC, where the model map is generated from the fitted model. Resolution assessments are provided based on tilt-based map-map and map-model FSC analyses at thresholds of FSC=0.5 and 0.143, respectively.

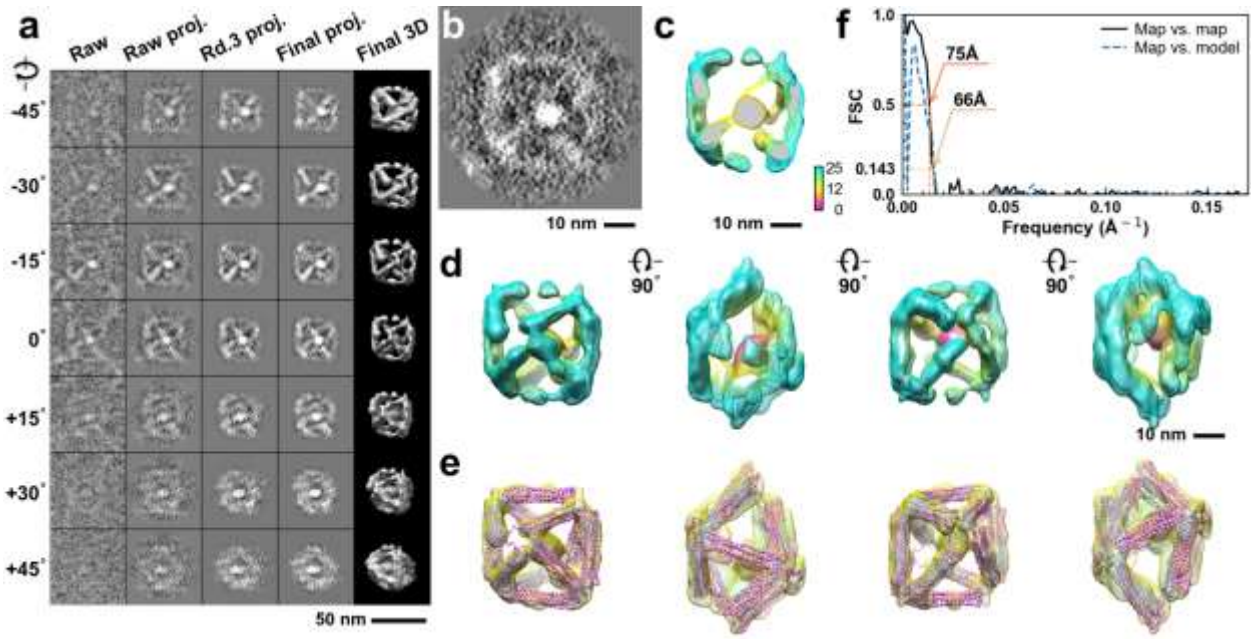

Supplementary Fig. 166: IPET 3D reconstruction and model fitting of an individual unit-cell particle (Index: 158) within a 2D lattice with 70% ferritin loading. a, Seven representative tilt images of a single unit-cell particle are shown in the first column (from left). The tilt images are aligned to a common center using IPET through iterative refinement. The projections of the raw, intermediate, and final 3D reconstruction at the corresponding angles are displayed in the subsequent four columns. **b**, A central cross-section (~23 nm thick) of the final reconstruction before masking is applied. **c**, 3D views of the central cross-section. **d**, Final 3D density map of this particle, viewed from four perpendicular directions. **e**, Final 3D reconstruction superimposed with the fitted model, viewed from four perpendicular directions. **f**, FSC analyses of the final map resolution using two methods: map-map FSC, where each map is reconstructed from one half of the images (even vs. odd tilt angle indices), and map-model FSC, where the model map is generated from the fitted model. Resolution assessments are provided based on tilt-based map-map and map-model FSC analyses at thresholds of FSC=0.5 and 0.143, respectively.

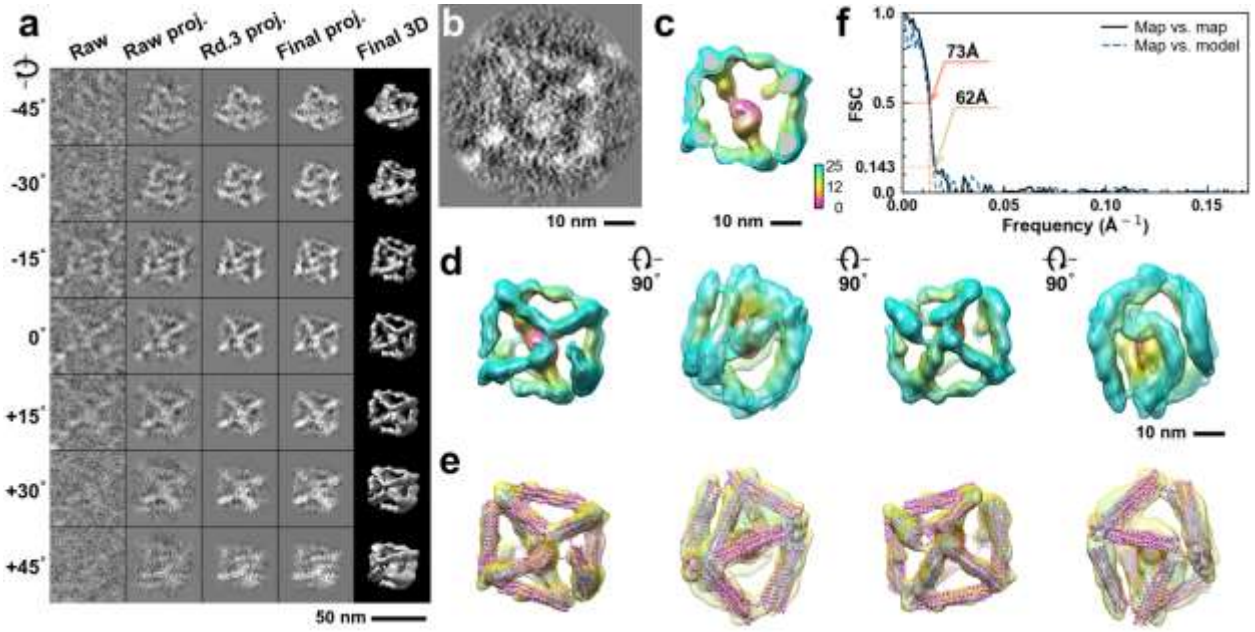

Supplementary Fig. 167: IPET 3D reconstruction and model fitting of an individual unit-cell particle (Index: 159) within a 2D lattice with 70% ferritin loading. a, Seven representative tilt images of a single unit-cell particle are shown in the first column (from left). The tilt images are aligned to a common center using IPET through iterative refinement. The projections of the raw, intermediate, and final 3D reconstruction at the corresponding angles are displayed in the subsequent four columns. **b**, A central cross-section (~23 nm thick) of the final reconstruction before masking is applied. **c**, 3D views of the central cross-section. **d**, Final 3D density map of this particle, viewed from four perpendicular directions. **e**, Final 3D reconstruction superimposed with the fitted model, viewed from four perpendicular directions. **f**, FSC analyses of the final map resolution using two methods: map-map FSC, where each map is reconstructed from one half of the images (even vs. odd tilt angle indices), and map-model FSC, where the model map is generated from the fitted model. Resolution assessments are provided based on tilt-based map-map and map-model FSC analyses at thresholds of FSC=0.5 and 0.143, respectively.

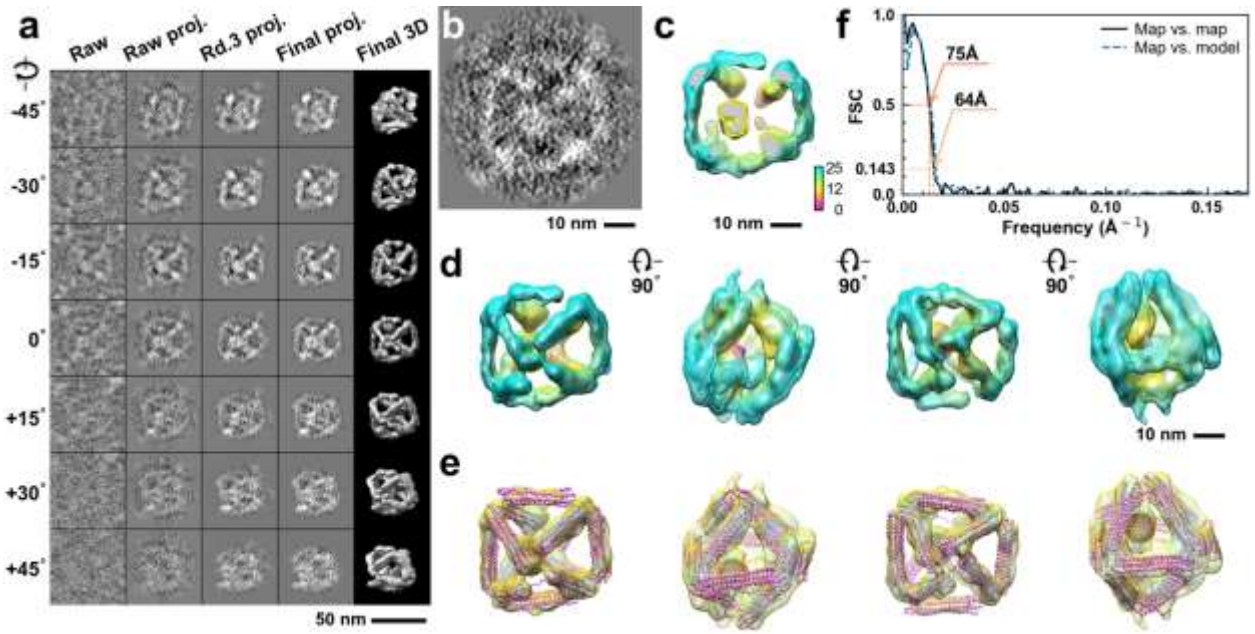

Supplementary Fig. 168: IPET 3D reconstruction and model fitting of an individual unit-cell particle (Index: 160) within a 2D lattice with 70% ferritin loading. a, Seven representative tilt images of a single unit-cell particle are shown in the first column (from left). The tilt images are aligned to a common center using IPET through iterative refinement. The projections of the raw, intermediate, and final 3D reconstruction at the corresponding angles are displayed in the subsequent four columns. **b**, A central cross-section (~23 nm thick) of the final reconstruction before masking is applied. **c**, 3D views of the central cross-section. **d**, Final 3D density map of this particle, viewed from four perpendicular directions. **e**, Final 3D reconstruction superimposed with the fitted model, viewed from four perpendicular directions. **f**, FSC analyses of the final map resolution using two methods: map-map FSC, where each map is reconstructed from one half of the images (even vs. odd tilt angle indices), and map-model FSC, where the model map is generated from the fitted model. Resolution assessments are provided based on tilt-based map-map and map-model FSC analyses at thresholds of FSC=0.5 and 0.143, respectively.

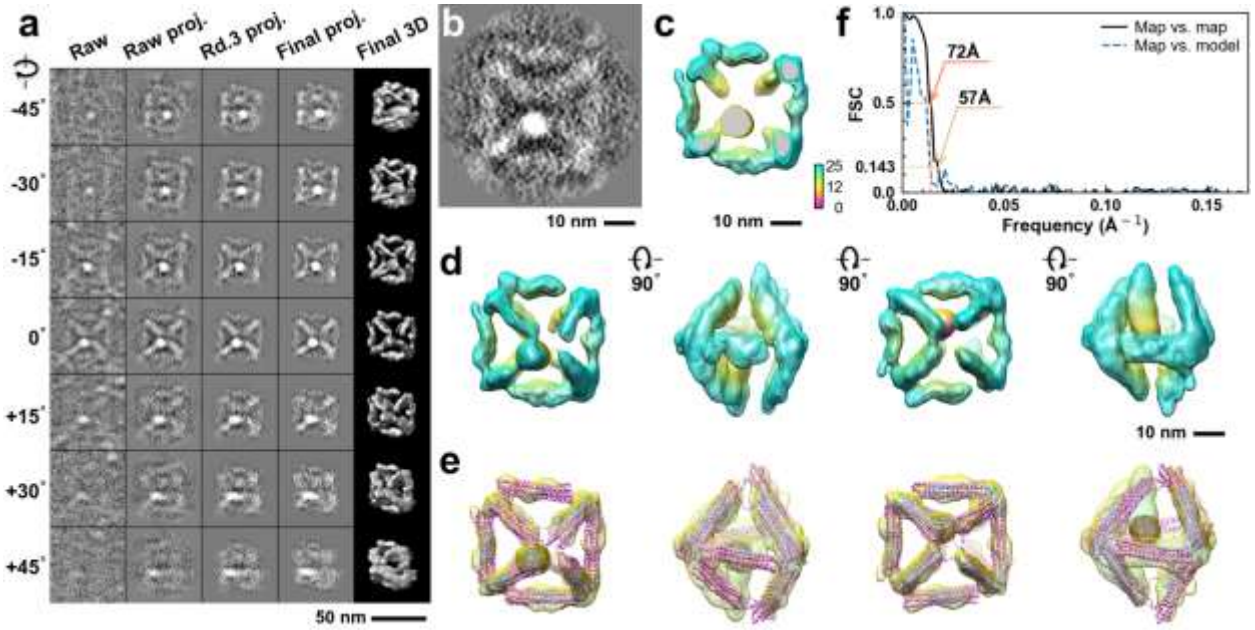

Supplementary Fig. 169: IPET 3D reconstruction and model fitting of an individual unit-cell particle (Index: 161) within a 2D lattice with 70% ferritin loading. a, Seven representative tilt images of a single unit-cell particle are shown in the first column (from left). The tilt images are aligned to a common center using IPET through iterative refinement. The projections of the raw, intermediate, and final 3D reconstruction at the corresponding angles are displayed in the subsequent four columns. **b**, A central cross-section (~23 nm thick) of the final reconstruction before masking is applied. **c**, 3D views of the central cross-section. **d**, Final 3D density map of this particle, viewed from four perpendicular directions. **e**, Final 3D reconstruction superimposed with the fitted model, viewed from four perpendicular directions. **f**, FSC analyses of the final map resolution using two methods: map-map FSC, where each map is reconstructed from one half of the images (even vs. odd tilt angle indices), and map-model FSC, where the model map is generated from the fitted model. Resolution assessments are provided based on tilt-based map-map and map-model FSC analyses at thresholds of FSC=0.5 and 0.143, respectively.

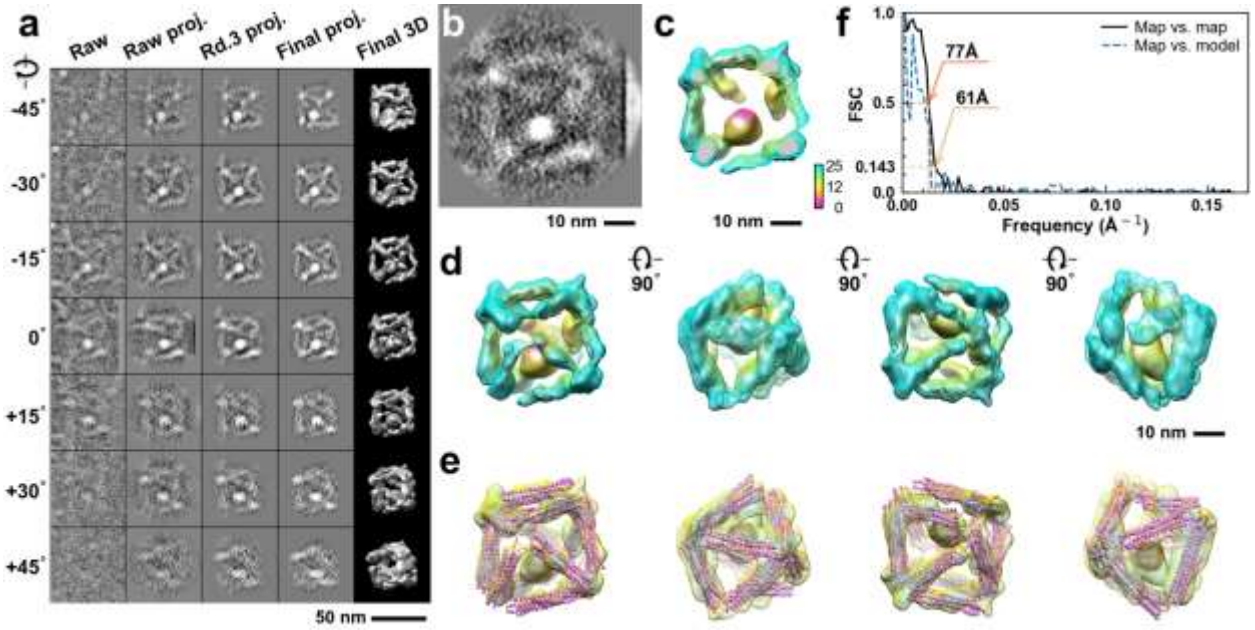

Supplementary Fig. 170: IPET 3D reconstruction and model fitting of an individual unit-cell particle (Index: 162) within a 2D lattice with 70% ferritin loading. a, Seven representative tilt images of a single unit-cell particle are shown in the first column (from left). The tilt images are aligned to a common center using IPET through iterative refinement. The projections of the raw, intermediate, and final 3D reconstruction at the corresponding angles are displayed in the subsequent four columns. **b**, A central cross-section (~23 nm thick) of the final reconstruction before masking is applied. **c**, 3D views of the central cross-section. **d**, Final 3D density map of this particle, viewed from four perpendicular directions. **e**, Final 3D reconstruction superimposed with the fitted model, viewed from four perpendicular directions. **f**, FSC analyses of the final map resolution using two methods: map-map FSC, where each map is reconstructed from one half of the images (even vs. odd tilt angle indices), and map-model FSC, where the model map is generated from the fitted model. Resolution assessments are provided based on tilt-based map-map and map-model FSC analyses at thresholds of FSC=0.5 and 0.143, respectively.

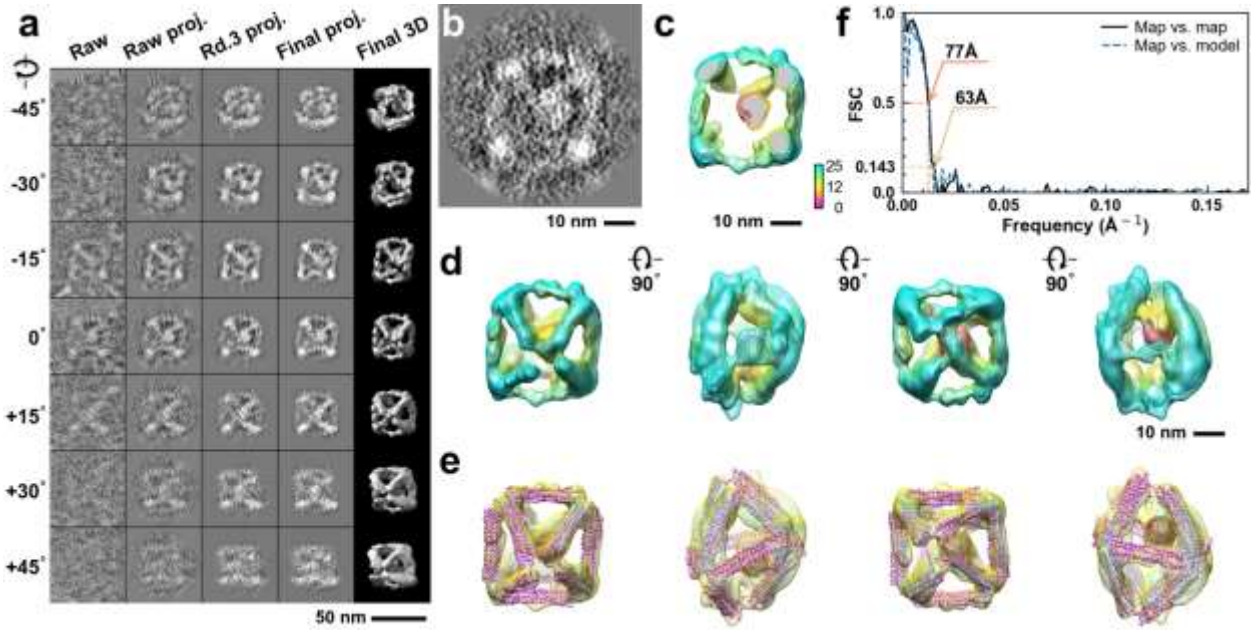

Supplementary Fig. 171: IPET 3D reconstruction and model fitting of an individual unit-cell particle (Index: 163) within a 2D lattice with 70% ferritin loading. a, Seven representative tilt images of a single unit-cell particle are shown in the first column (from left). The tilt images are aligned to a common center using IPET through iterative refinement. The projections of the raw, intermediate, and final 3D reconstruction at the corresponding angles are displayed in the subsequent four columns. **b**, A central cross-section (~23 nm thick) of the final reconstruction before masking is applied. **c**, 3D views of the central cross-section. **d**, Final 3D density map of this particle, viewed from four perpendicular directions. **e**, Final 3D reconstruction superimposed with the fitted model, viewed from four perpendicular directions. **f**, FSC analyses of the final map resolution using two methods: map-map FSC, where each map is reconstructed from one half of the images (even vs. odd tilt angle indices), and map-model FSC, where the model map is generated from the fitted model. Resolution assessments are provided based on tilt-based map-map and map-model FSC analyses at thresholds of FSC=0.5 and 0.143, respectively.

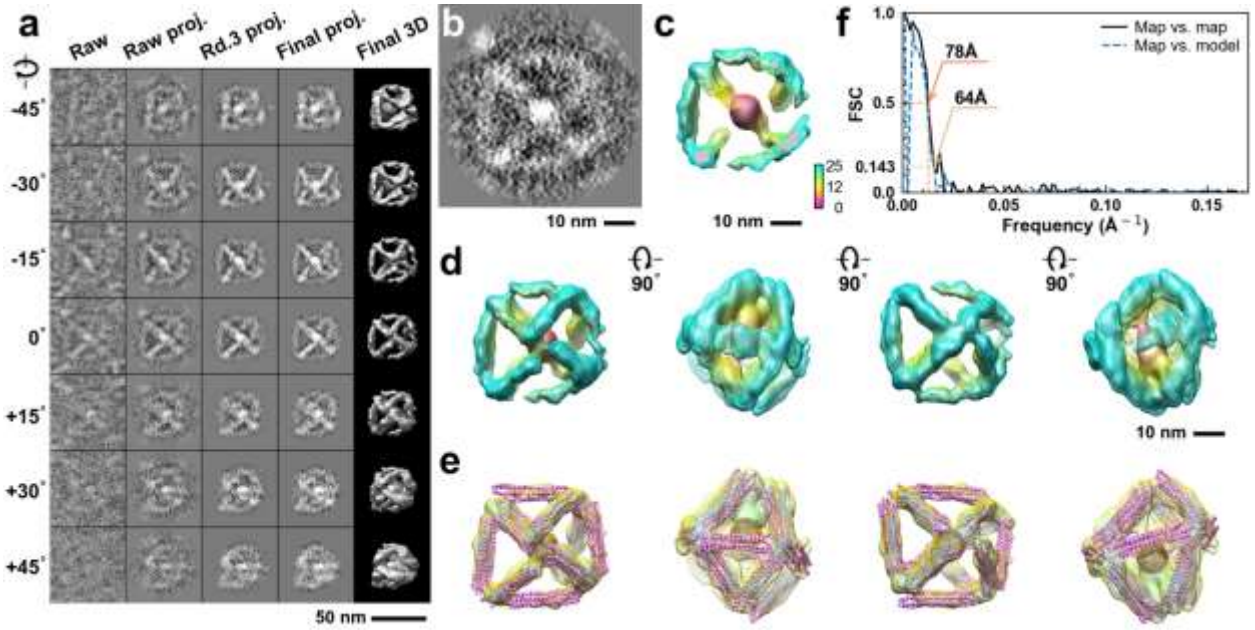

Supplementary Fig. 172: IPET 3D reconstruction and model fitting of an individual unit-cell particle (Index: 164) within a 2D lattice with 70% ferritin loading. a, Seven representative tilt images of a single unit-cell particle are shown in the first column (from left). The tilt images are aligned to a common center using IPET through iterative refinement. The projections of the raw, intermediate, and final 3D reconstruction at the corresponding angles are displayed in the subsequent four columns. **b**, A central cross-section (~23 nm thick) of the final reconstruction before masking is applied. **c**, 3D views of the central cross-section. **d**, Final 3D density map of this particle, viewed from four perpendicular directions. **e**, Final 3D reconstruction superimposed with the fitted model, viewed from four perpendicular directions. **f**, FSC analyses of the final map resolution using two methods: map-map FSC, where each map is reconstructed from one half of the images (even vs. odd tilt angle indices), and map-model FSC, where the model map is generated from the fitted model. Resolution assessments are provided based on tilt-based map-map and map-model FSC analyses at thresholds of FSC=0.5 and 0.143, respectively.

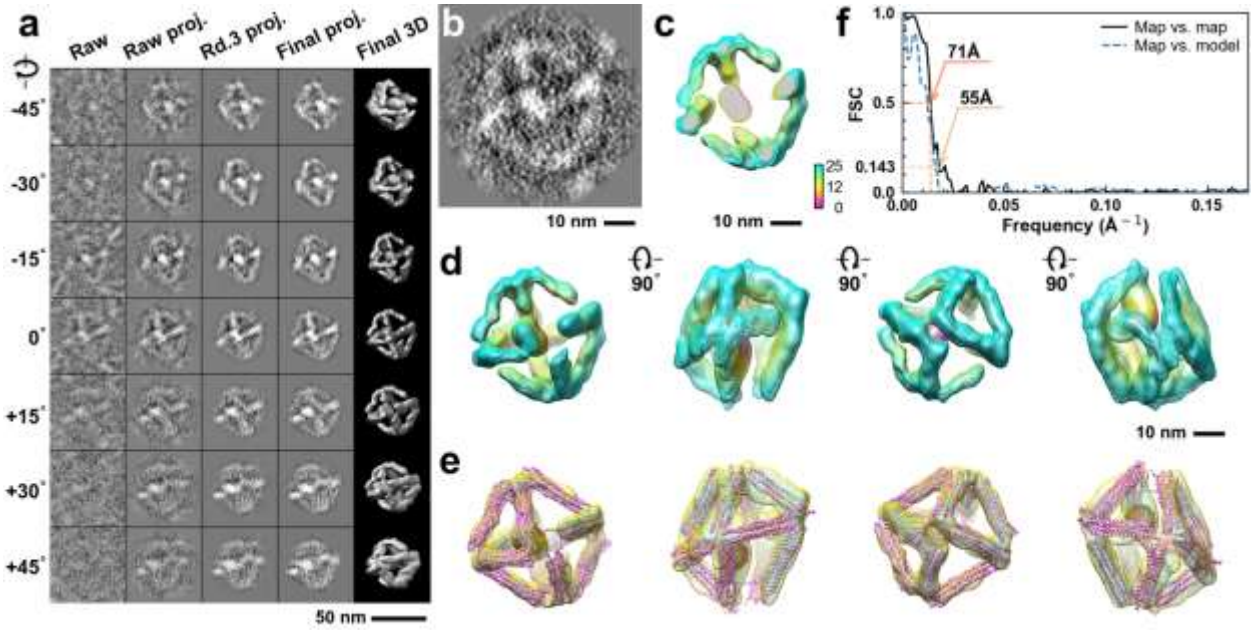

Supplementary Fig. 173: IPET 3D reconstruction and model fitting of an individual unit-cell particle (Index: 165) within a 2D lattice with 70% ferritin loading. a, Seven representative tilt images of a single unit-cell particle are shown in the first column (from left). The tilt images are aligned to a common center using IPET through iterative refinement. The projections of the raw, intermediate, and final 3D reconstruction at the corresponding angles are displayed in the subsequent four columns. **b**, A central cross-section (~23 nm thick) of the final reconstruction before masking is applied. **c**, 3D views of the central cross-section. **d**, Final 3D density map of this particle, viewed from four perpendicular directions. **e**, Final 3D reconstruction superimposed with the fitted model, viewed from four perpendicular directions. **f**, FSC analyses of the final map resolution using two methods: map-map FSC, where each map is reconstructed from one half of the images (even vs. odd tilt angle indices), and map-model FSC, where the model map is generated from the fitted model. Resolution assessments are provided based on tilt-based map-map and map-model FSC analyses at thresholds of FSC=0.5 and 0.143, respectively.

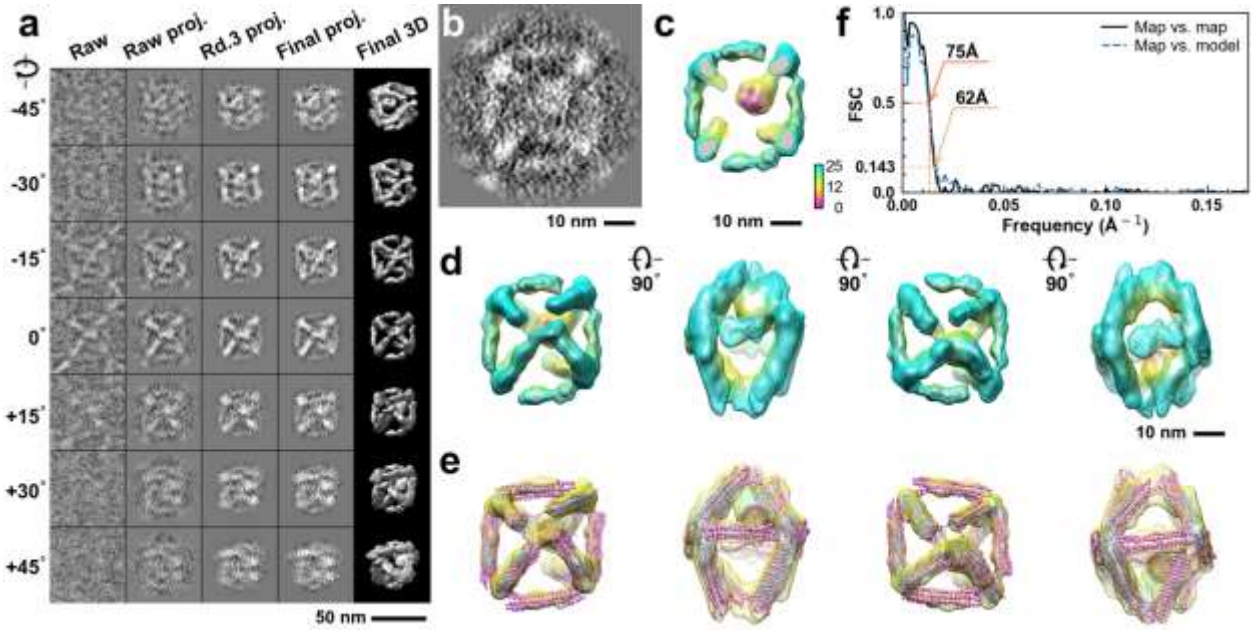

Supplementary Fig. 174: IPET 3D reconstruction and model fitting of an individual unit-cell particle (Index: 166) within a 2D lattice with 70% ferritin loading. a, Seven representative tilt images of a single unit-cell particle are shown in the first column (from left). The tilt images are aligned to a common center using IPET through iterative refinement. The projections of the raw, intermediate, and final 3D reconstruction at the corresponding angles are displayed in the subsequent four columns. **b**, A central cross-section (~23 nm thick) of the final reconstruction before masking is applied. **c**, 3D views of the central cross-section. **d**, Final 3D density map of this particle, viewed from four perpendicular directions. **e**, Final 3D reconstruction superimposed with the fitted model, viewed from four perpendicular directions. **f**, FSC analyses of the final map resolution using two methods: map-map FSC, where each map is reconstructed from one half of the images (even vs. odd tilt angle indices), and map-model FSC, where the model map is generated from the fitted model. Resolution assessments are provided based on tilt-based map-map and map-model FSC analyses at thresholds of FSC=0.5 and 0.143, respectively.

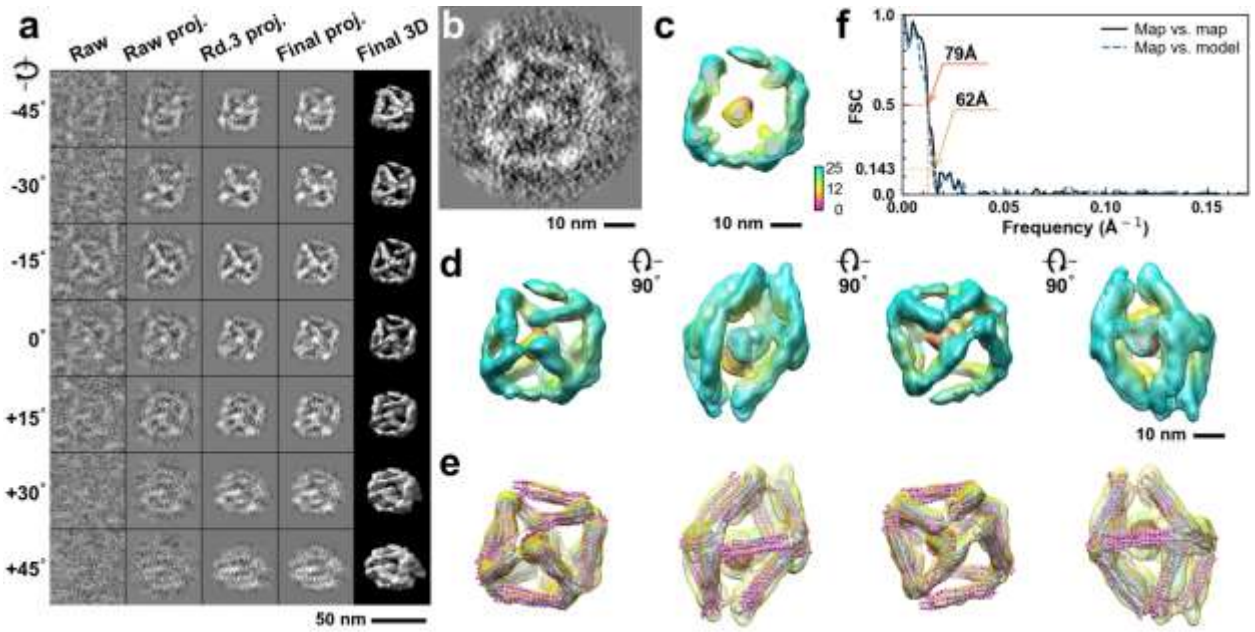

Supplementary Fig. 175: IPET 3D reconstruction and model fitting of an individual unit-cell particle (Index: 167) within a 2D lattice with 70% ferritin loading. a, Seven representative tilt images of a single unit-cell particle are shown in the first column (from left). The tilt images are aligned to a common center using IPET through iterative refinement. The projections of the raw, intermediate, and final 3D reconstruction at the corresponding angles are displayed in the subsequent four columns. **b**, A central cross-section (~23 nm thick) of the final reconstruction before masking is applied. **c**, 3D views of the central cross-section. **d**, Final 3D density map of this particle, viewed from four perpendicular directions. **e**, Final 3D reconstruction superimposed with the fitted model, viewed from four perpendicular directions. **f**, FSC analyses of the final map resolution using two methods: map-map FSC, where each map is reconstructed from one half of the images (even vs. odd tilt angle indices), and map-model FSC, where the model map is generated from the fitted model. Resolution assessments are provided based on tilt-based map-map and map-model FSC analyses at thresholds of FSC=0.5 and 0.143, respectively.

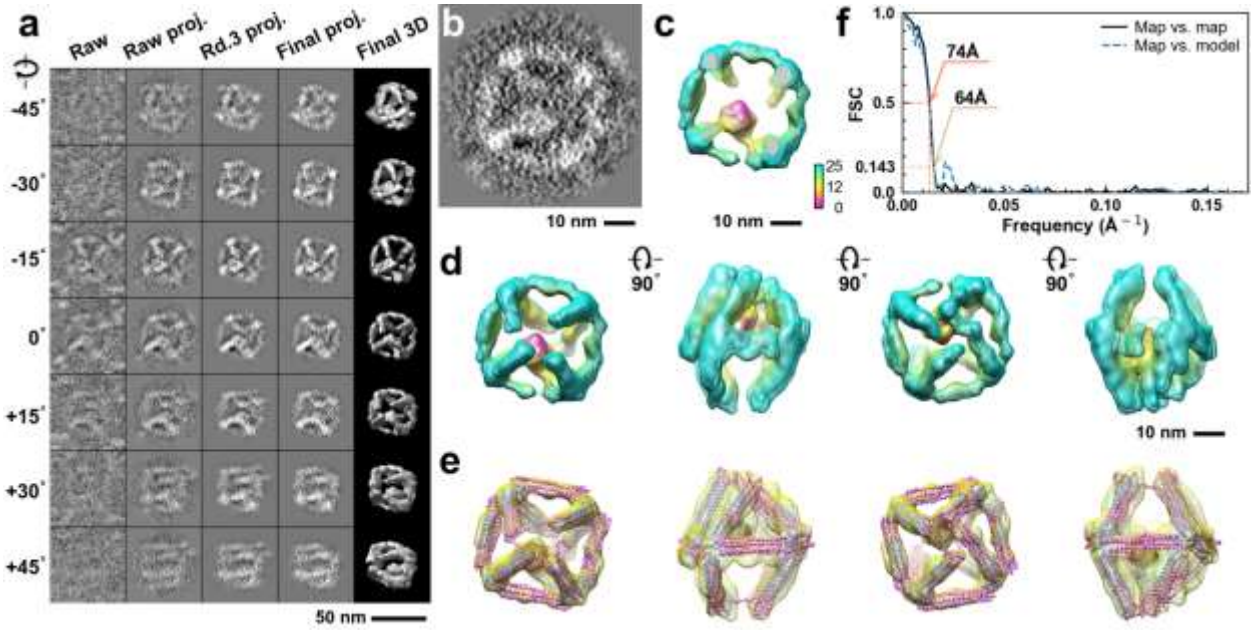

Supplementary Fig. 176: IPET 3D reconstruction and model fitting of an individual unit-cell particle (Index: 168) within a 2D lattice with 70% ferritin loading. a, Seven representative tilt images of a single unit-cell particle are shown in the first column (from left). The tilt images are aligned to a common center using IPET through iterative refinement. The projections of the raw, intermediate, and final 3D reconstruction at the corresponding angles are displayed in the subsequent four columns. **b**, A central cross-section (~23 nm thick) of the final reconstruction before masking is applied. **c**, 3D views of the central cross-section. **d**, Final 3D density map of this particle, viewed from four perpendicular directions. **e**, Final 3D reconstruction superimposed with the fitted model, viewed from four perpendicular directions. **f**, FSC analyses of the final map resolution using two methods: map-map FSC, where each map is reconstructed from one half of the images (even vs. odd tilt angle indices), and map-model FSC, where the model map is generated from the fitted model. Resolution assessments are provided based on tilt-based map-map and map-model FSC analyses at thresholds of FSC=0.5 and 0.143, respectively.

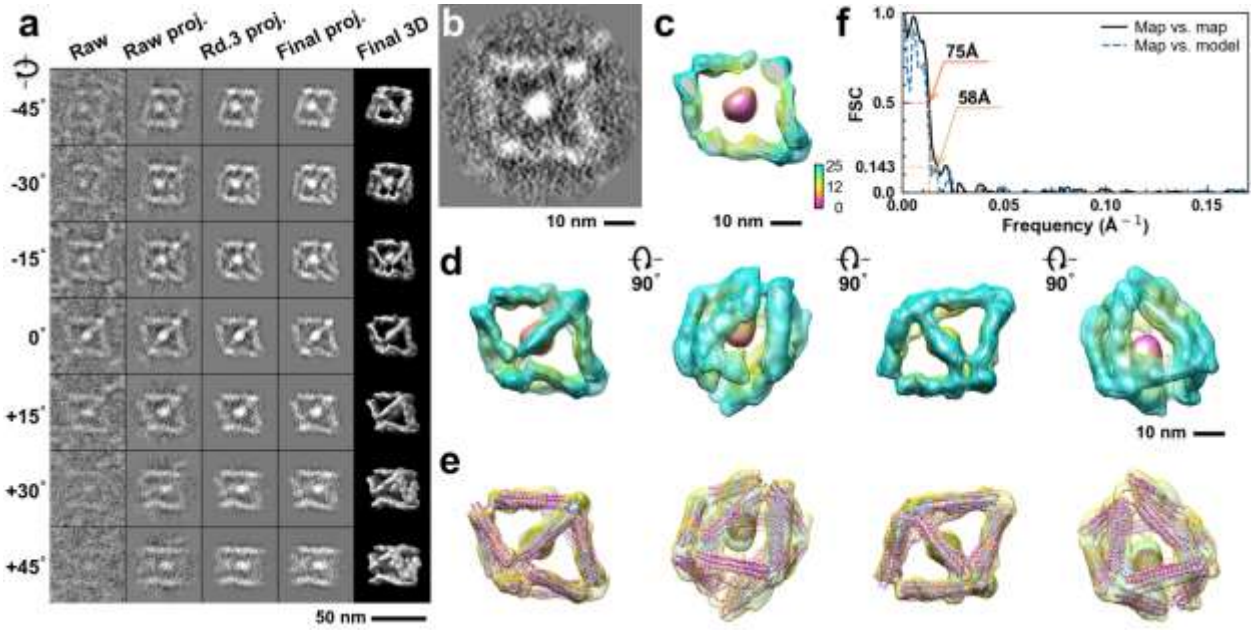

Supplementary Fig. 177: IPET 3D reconstruction and model fitting of an individual unit-cell particle (Index: 169) within a 2D lattice with 70% ferritin loading. a, Seven representative tilt images of a single unit-cell particle are shown in the first column (from left). The tilt images are aligned to a common center using IPET through iterative refinement. The projections of the raw, intermediate, and final 3D reconstruction at the corresponding angles are displayed in the subsequent four columns. **b**, A central cross-section (~23 nm thick) of the final reconstruction before masking is applied. **c**, 3D views of the central cross-section. **d**, Final 3D density map of this particle, viewed from four perpendicular directions. **e**, Final 3D reconstruction superimposed with the fitted model, viewed from four perpendicular directions. **f**, FSC analyses of the final map resolution using two methods: map-map FSC, where each map is reconstructed from one half of the images (even vs. odd tilt angle indices), and map-model FSC, where the model map is generated from the fitted model. Resolution assessments are provided based on tilt-based map-map and map-model FSC analyses at thresholds of FSC=0.5 and 0.143, respectively.

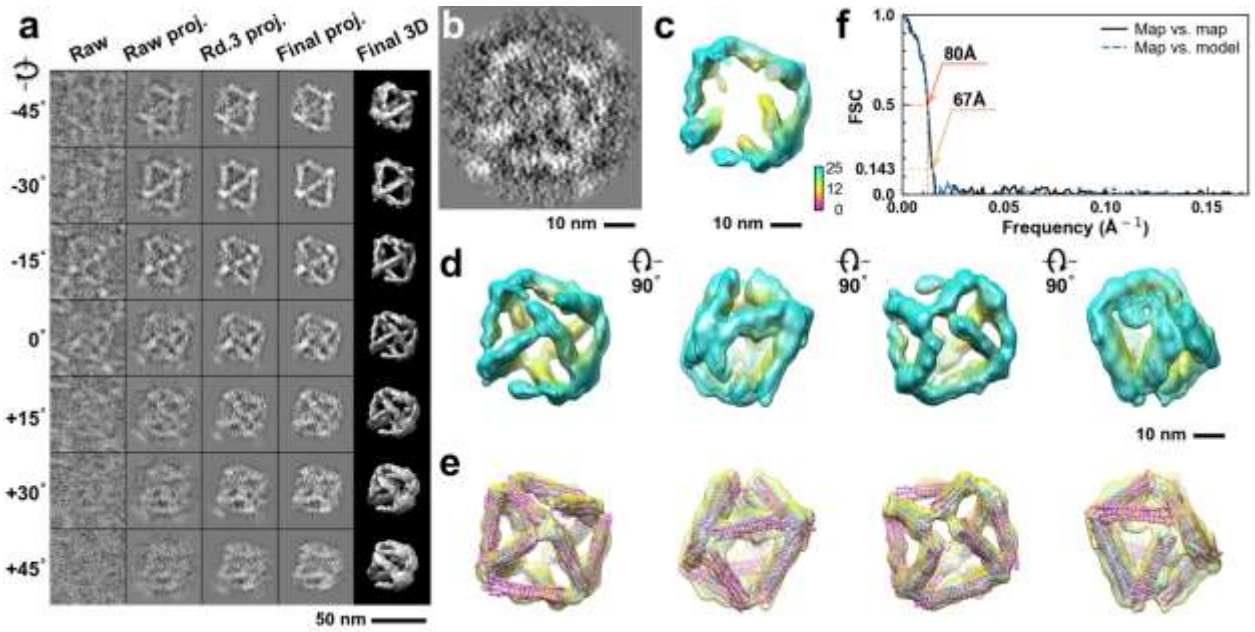

Supplementary Fig. 178: IPET 3D reconstruction and model fitting of an individual unit-cell particle (Index: 170) within a 2D lattice with 70% ferritin loading. a, Seven representative tilt images of a single unit-cell particle are shown in the first column (from left). The tilt images are aligned to a common center using IPET through iterative refinement. The projections of the raw, intermediate, and final 3D reconstruction at the corresponding angles are displayed in the subsequent four columns. **b**, A central cross-section (~23 nm thick) of the final reconstruction before masking is applied. **c**, 3D views of the central cross-section. **d**, Final 3D density map of this particle, viewed from four perpendicular directions. **e**, Final 3D reconstruction superimposed with the fitted model, viewed from four perpendicular directions. **f**, FSC analyses of the final map resolution using two methods: map-map FSC, where each map is reconstructed from one half of the images (even vs. odd tilt angle indices), and map-model FSC, where the model map is generated from the fitted model. Resolution assessments are provided based on tilt-based map-map and map-model FSC analyses at thresholds of FSC=0.5 and 0.143, respectively.

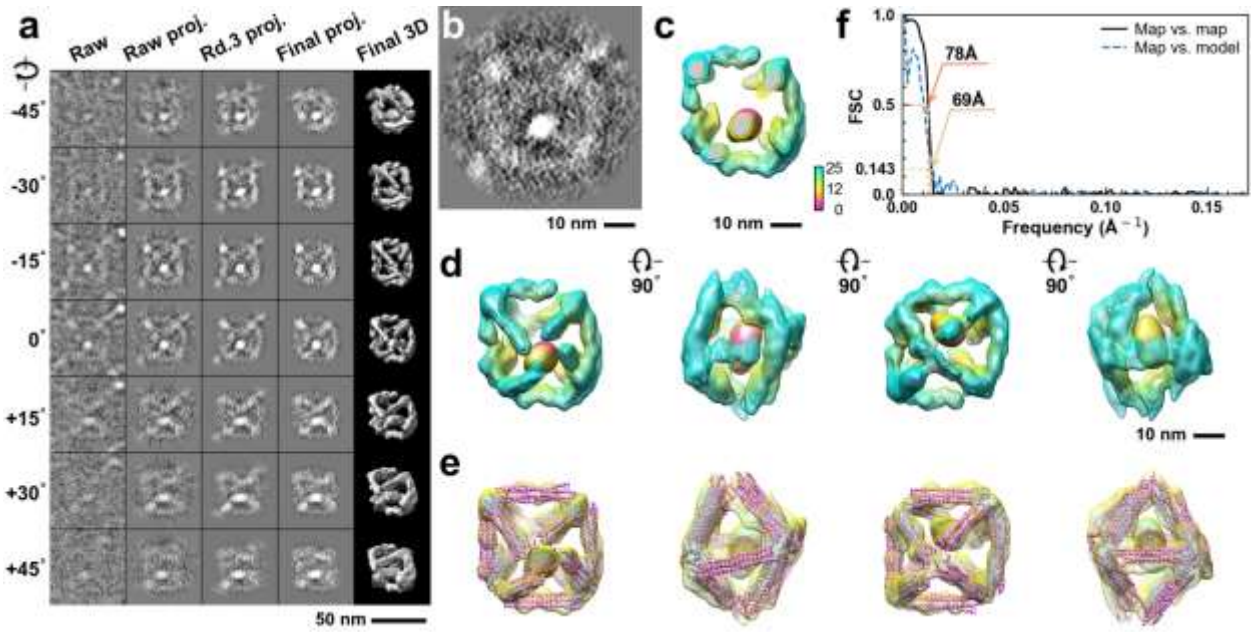

Supplementary Fig. 179: IPET 3D reconstruction and model fitting of an individual unit-cell particle (Index: 171) within a 2D lattice with 70% ferritin loading. a, Seven representative tilt images of a single unit-cell particle are shown in the first column (from left). The tilt images are aligned to a common center using IPET through iterative refinement. The projections of the raw, intermediate, and final 3D reconstruction at the corresponding angles are displayed in the subsequent four columns. **b**, A central cross-section (~23 nm thick) of the final reconstruction before masking is applied. **c**, 3D views of the central cross-section. **d**, Final 3D density map of this particle, viewed from four perpendicular directions. **e**, Final 3D reconstruction superimposed with the fitted model, viewed from four perpendicular directions. **f**, FSC analyses of the final map resolution using two methods: map-map FSC, where each map is reconstructed from one half of the images (even vs. odd tilt angle indices), and map-model FSC, where the model map is generated from the fitted model. Resolution assessments are provided based on tilt-based map-map and map-model FSC analyses at thresholds of FSC=0.5 and 0.143, respectively.

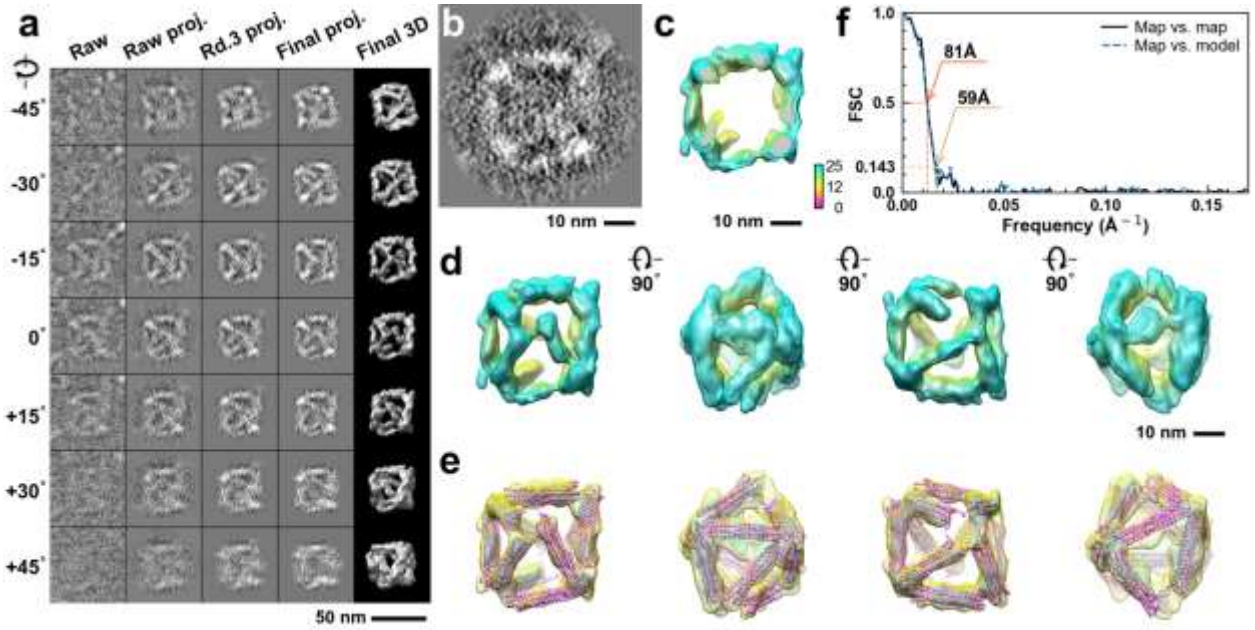

Supplementary Fig. 180: IPET 3D reconstruction and model fitting of an individual unit-cell particle (Index: 172) within a 2D lattice with 70% ferritin loading. a, Seven representative tilt images of a single unit-cell particle are shown in the first column (from left). The tilt images are aligned to a common center using IPET through iterative refinement. The projections of the raw, intermediate, and final 3D reconstruction at the corresponding angles are displayed in the subsequent four columns. **b**, A central cross-section (~23 nm thick) of the final reconstruction before masking is applied. **c**, 3D views of the central cross-section. **d**, Final 3D density map of this particle, viewed from four perpendicular directions. **e**, Final 3D reconstruction superimposed with the fitted model, viewed from four perpendicular directions. **f**, FSC analyses of the final map resolution using two methods: map-map FSC, where each map is reconstructed from one half of the images (even vs. odd tilt angle indices), and map-model FSC, where the model map is generated from the fitted model. Resolution assessments are provided based on tilt-based map-map and map-model FSC analyses at thresholds of FSC=0.5 and 0.143, respectively.

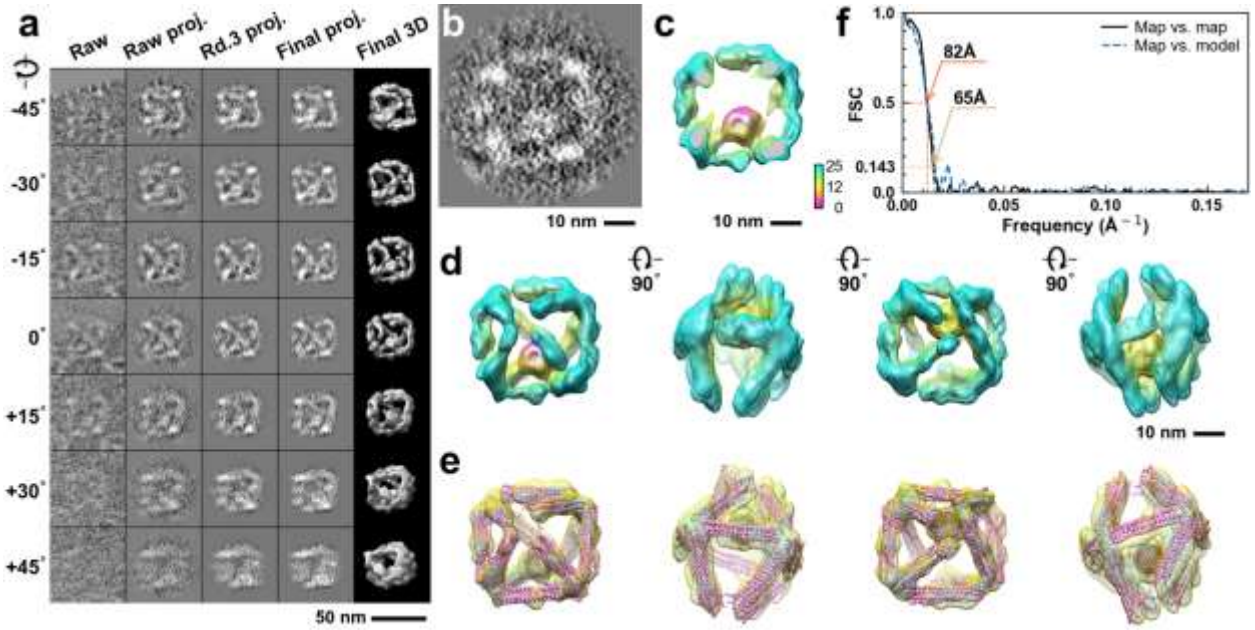

Supplementary Fig. 181: IPET 3D reconstruction and model fitting of an individual unit-cell particle (Index: 173) within a 2D lattice with 70% ferritin loading. a, Seven representative tilt images of a single unit-cell particle are shown in the first column (from left). The tilt images are aligned to a common center using IPET through iterative refinement. The projections of the raw, intermediate, and final 3D reconstruction at the corresponding angles are displayed in the subsequent four columns. **b**, A central cross-section (~23 nm thick) of the final reconstruction before masking is applied. **c**, 3D views of the central cross-section. **d**, Final 3D density map of this particle, viewed from four perpendicular directions. **e**, Final 3D reconstruction superimposed with the fitted model, viewed from four perpendicular directions. **f**, FSC analyses of the final map resolution using two methods: map-map FSC, where each map is reconstructed from one half of the images (even vs. odd tilt angle indices), and map-model FSC, where the model map is generated from the fitted model. Resolution assessments are provided based on tilt-based map-map and map-model FSC analyses at thresholds of FSC=0.5 and 0.143, respectively.

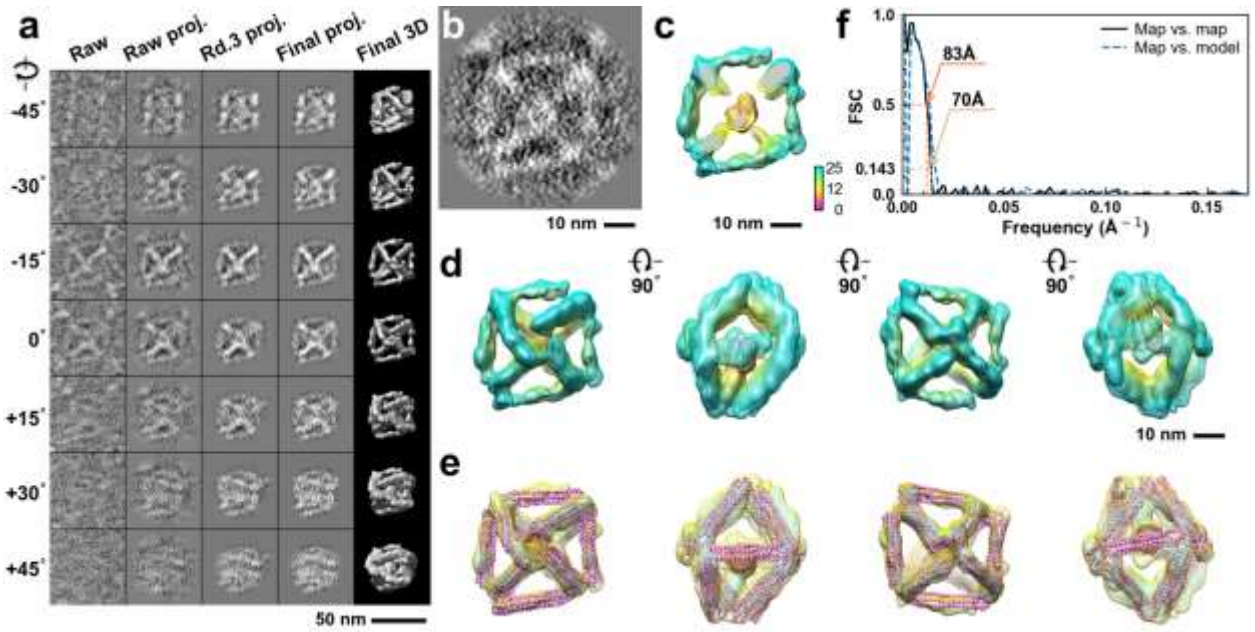

Supplementary Fig. 182: IPET 3D reconstruction and model fitting of an individual unit-cell particle (Index: 174) within a 2D lattice with 70% ferritin loading. a, Seven representative tilt images of a single unit-cell particle are shown in the first column (from left). The tilt images are aligned to a common center using IPET through iterative refinement. The projections of the raw, intermediate, and final 3D reconstruction at the corresponding angles are displayed in the subsequent four columns. **b**, A central cross-section (~23 nm thick) of the final reconstruction before masking is applied. **c**, 3D views of the central cross-section. **d**, Final 3D density map of this particle, viewed from four perpendicular directions. **e**, Final 3D reconstruction superimposed with the fitted model, viewed from four perpendicular directions. **f**, FSC analyses of the final map resolution using two methods: map-map FSC, where each map is reconstructed from one half of the images (even vs. odd tilt angle indices), and map-model FSC, where the model map is generated from the fitted model. Resolution assessments are provided based on tilt-based map-map and map-model FSC analyses at thresholds of FSC=0.5 and 0.143, respectively.

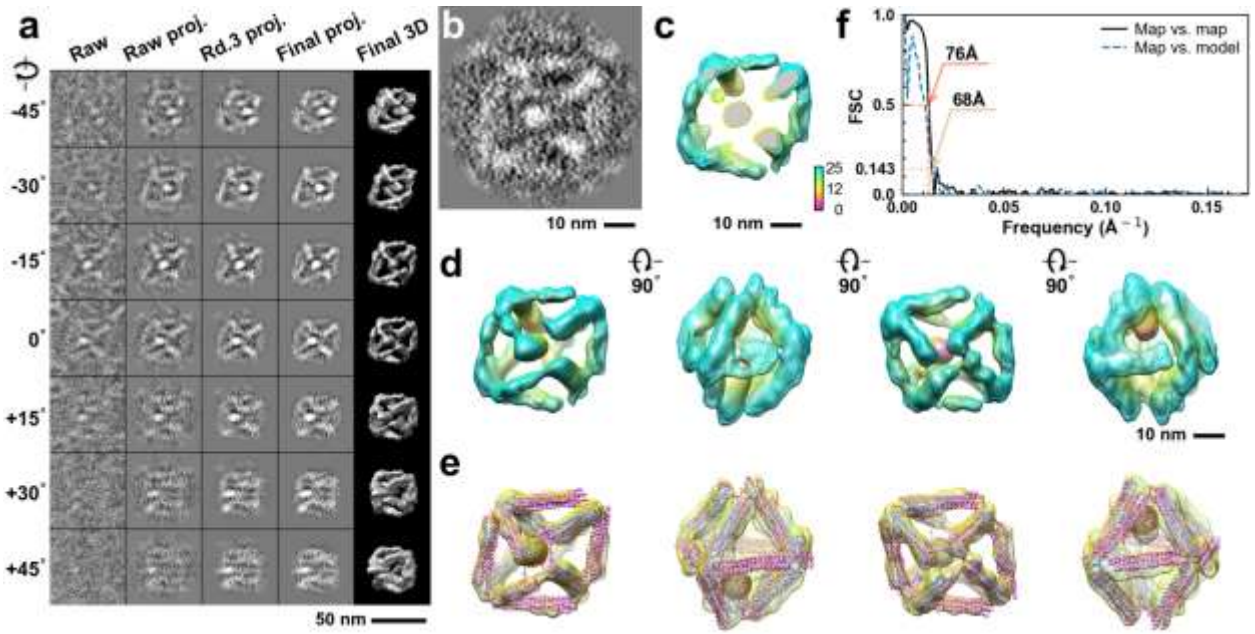

Supplementary Fig. 183: IPET 3D reconstruction and model fitting of an individual unit-cell particle (Index: 175) within a 2D lattice with 70% ferritin loading. a, Seven representative tilt images of a single unit-cell particle are shown in the first column (from left). The tilt images are aligned to a common center using IPET through iterative refinement. The projections of the raw, intermediate, and final 3D reconstruction at the corresponding angles are displayed in the subsequent four columns. **b**, A central cross-section (~23 nm thick) of the final reconstruction before masking is applied. **c**, 3D views of the central cross-section. **d**, Final 3D density map of this particle, viewed from four perpendicular directions. **e**, Final 3D reconstruction superimposed with the fitted model, viewed from four perpendicular directions. **f**, FSC analyses of the final map resolution using two methods: map-map FSC, where each map is reconstructed from one half of the images (even vs. odd tilt angle indices), and map-model FSC, where the model map is generated from the fitted model. Resolution assessments are provided based on tilt-based map-map and map-model FSC analyses at thresholds of FSC=0.5 and 0.143, respectively.

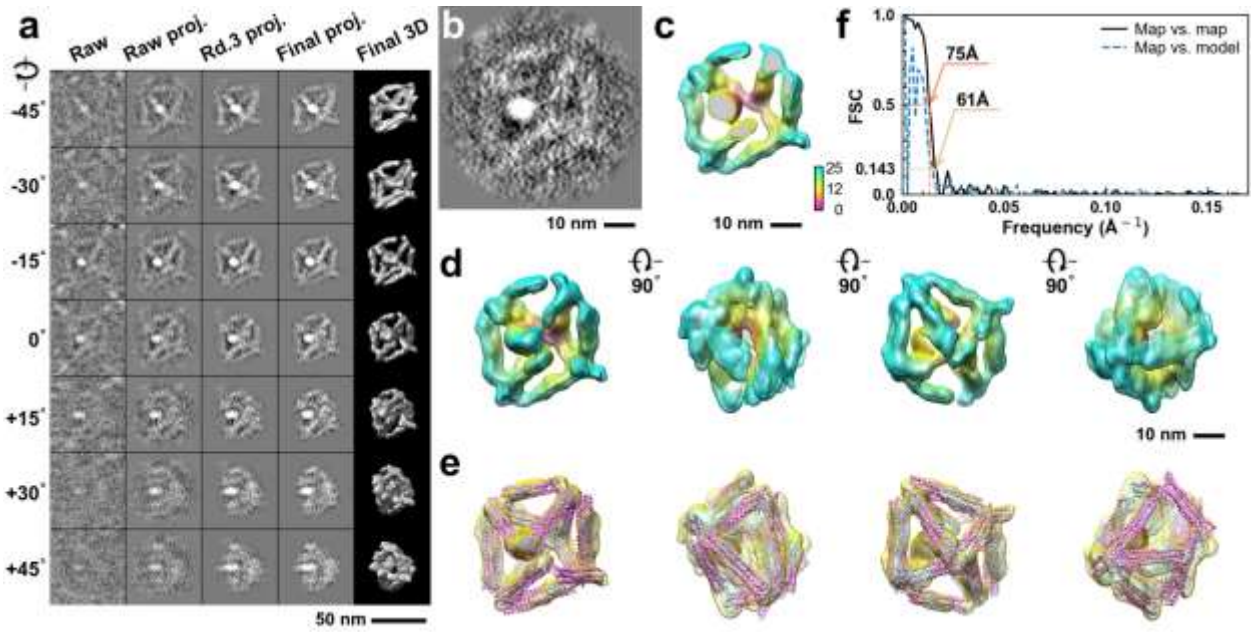

Supplementary Fig. 184: IPET 3D reconstruction and model fitting of an individual unit-cell particle (Index: 176) within a 2D lattice with 70% ferritin loading. a, Seven representative tilt images of a single unit-cell particle are shown in the first column (from left). The tilt images are aligned to a common center using IPET through iterative refinement. The projections of the raw, intermediate, and final 3D reconstruction at the corresponding angles are displayed in the subsequent four columns. **b**, A central cross-section (~23 nm thick) of the final reconstruction before masking is applied. **c**, 3D views of the central cross-section. **d**, Final 3D density map of this particle, viewed from four perpendicular directions. **e**, Final 3D reconstruction superimposed with the fitted model, viewed from four perpendicular directions. **f**, FSC analyses of the final map resolution using two methods: map-map FSC, where each map is reconstructed from one half of the images (even vs. odd tilt angle indices), and map-model FSC, where the model map is generated from the fitted model. Resolution assessments are provided based on tilt-based map-map and map-model FSC analyses at thresholds of FSC=0.5 and 0.143, respectively.

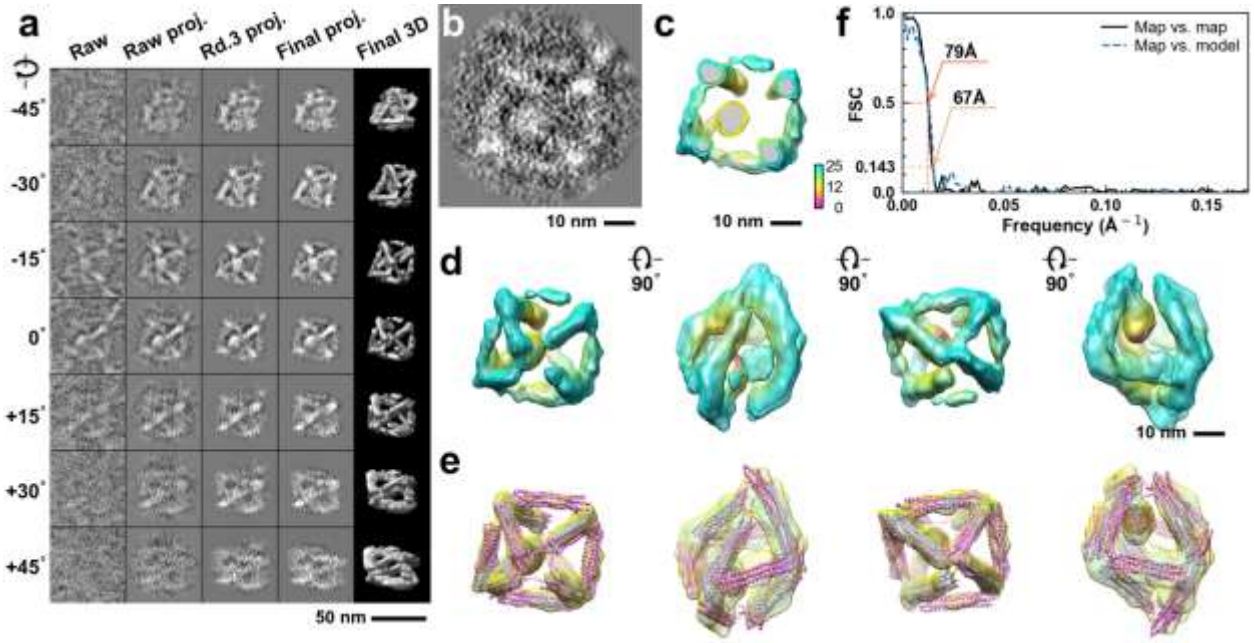

Supplementary Fig. 185: IPET 3D reconstruction and model fitting of an individual unit-cell particle (Index: 177) within a 2D lattice with 70% ferritin loading. a, Seven representative tilt images of a single unit-cell particle are shown in the first column (from left). The tilt images are aligned to a common center using IPET through iterative refinement. The projections of the raw, intermediate, and final 3D reconstruction at the corresponding angles are displayed in the subsequent four columns. **b**, A central cross-section (~23 nm thick) of the final reconstruction before masking is applied. **c**, 3D views of the central cross-section. **d**, Final 3D density map of this particle, viewed from four perpendicular directions. **e**, Final 3D reconstruction superimposed with the fitted model, viewed from four perpendicular directions. **f**, FSC analyses of the final map resolution using two methods: map-map FSC, where each map is reconstructed from one half of the images (even vs. odd tilt angle indices), and map-model FSC, where the model map is generated from the fitted model. Resolution assessments are provided based on tilt-based map-map and map-model FSC analyses at thresholds of FSC=0.5 and 0.143, respectively.

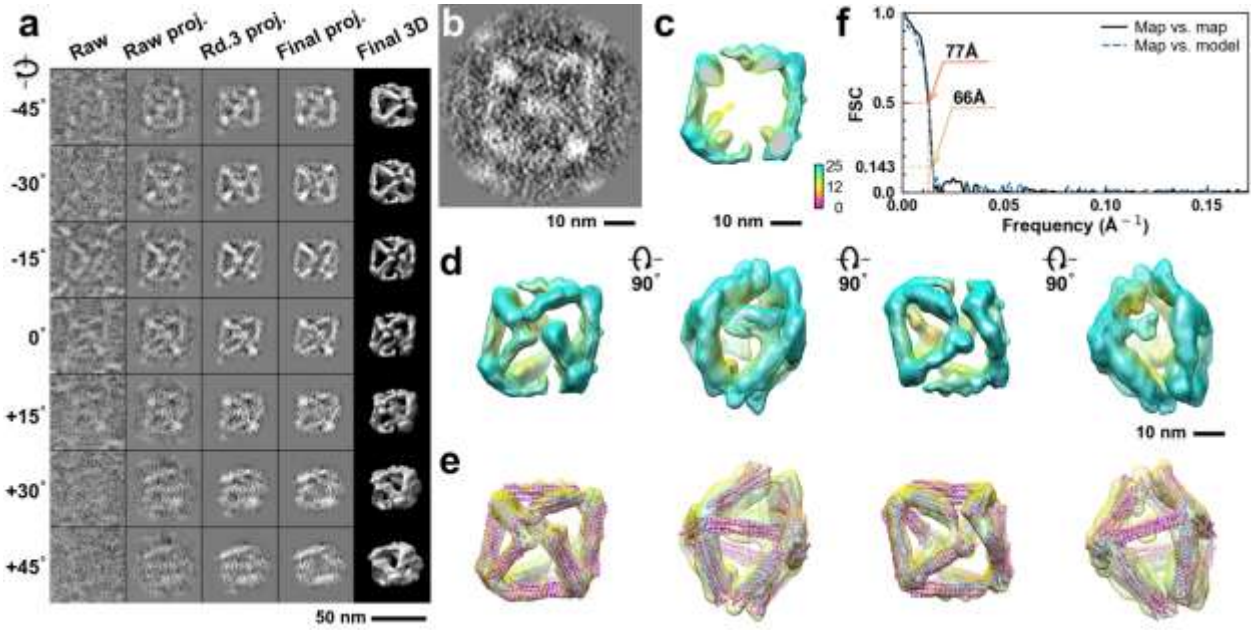

Supplementary Fig. 186: IPET 3D reconstruction and model fitting of an individual unit-cell particle (Index: 178) within a 2D lattice with 70% ferritin loading. a, Seven representative tilt images of a single unit-cell particle are shown in the first column (from left). The tilt images are aligned to a common center using IPET through iterative refinement. The projections of the raw, intermediate, and final 3D reconstruction at the corresponding angles are displayed in the subsequent four columns. **b**, A central cross-section (~23 nm thick) of the final reconstruction before masking is applied. **c**, 3D views of the central cross-section. **d**, Final 3D density map of this particle, viewed from four perpendicular directions. **e**, Final 3D reconstruction superimposed with the fitted model, viewed from four perpendicular directions. **f**, FSC analyses of the final map resolution using two methods: map-map FSC, where each map is reconstructed from one half of the images (even vs. odd tilt angle indices), and map-model FSC, where the model map is generated from the fitted model. Resolution assessments are provided based on tilt-based map-map and map-model FSC analyses at thresholds of FSC=0.5 and 0.143, respectively.

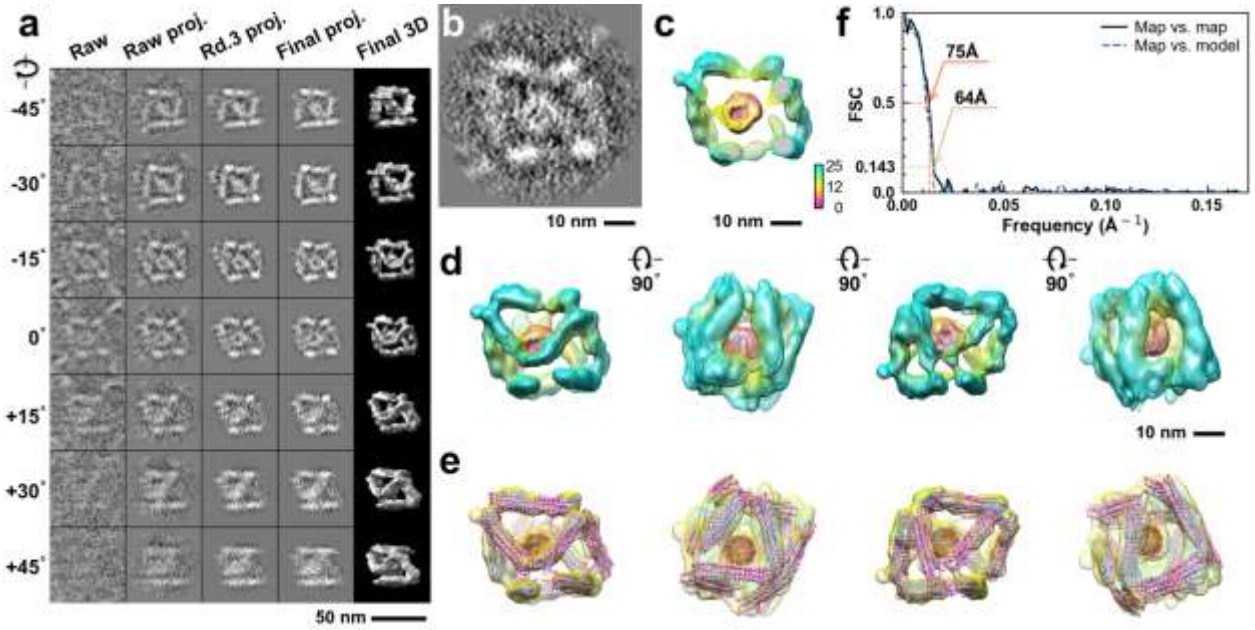

Supplementary Fig. 187: IPET 3D reconstruction and model fitting of an individual unit-cell particle (Index: 179) within a 2D lattice with 70% ferritin loading. a, Seven representative tilt images of a single unit-cell particle are shown in the first column (from left). The tilt images are aligned to a common center using IPET through iterative refinement. The projections of the raw, intermediate, and final 3D reconstruction at the corresponding angles are displayed in the subsequent four columns. **b**, A central cross-section (~23 nm thick) of the final reconstruction before masking is applied. **c**, 3D views of the central cross-section. **d**, Final 3D density map of this particle, viewed from four perpendicular directions. **e**, Final 3D reconstruction superimposed with the fitted model, viewed from four perpendicular directions. **f**, FSC analyses of the final map resolution using two methods: map-map FSC, where each map is reconstructed from one half of the images (even vs. odd tilt angle indices), and map-model FSC, where the model map is generated from the fitted model. Resolution assessments are provided based on tilt-based map-map and map-model FSC analyses at thresholds of FSC=0.5 and 0.143, respectively.

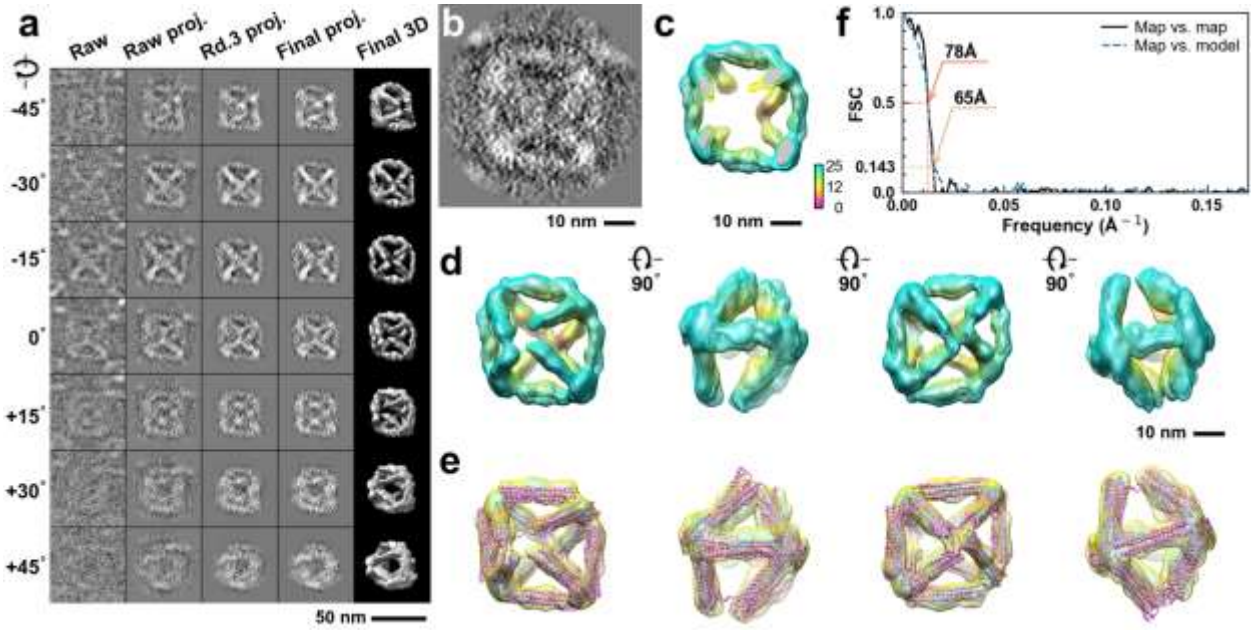

Supplementary Fig. 188: IPET 3D reconstruction and model fitting of an individual unit-cell particle (Index: 180) within a 2D lattice with 70% ferritin loading. a, Seven representative tilt images of a single unit-cell particle are shown in the first column (from left). The tilt images are aligned to a common center using IPET through iterative refinement. The projections of the raw, intermediate, and final 3D reconstruction at the corresponding angles are displayed in the subsequent four columns. **b**, A central cross-section (~23 nm thick) of the final reconstruction before masking is applied. **c**, 3D views of the central cross-section. **d**, Final 3D density map of this particle, viewed from four perpendicular directions. **e**, Final 3D reconstruction superimposed with the fitted model, viewed from four perpendicular directions. **f**, FSC analyses of the final map resolution using two methods: map-map FSC, where each map is reconstructed from one half of the images (even vs. odd tilt angle indices), and map-model FSC, where the model map is generated from the fitted model. Resolution assessments are provided based on tilt-based map-map and map-model FSC analyses at thresholds of FSC=0.5 and 0.143, respectively.

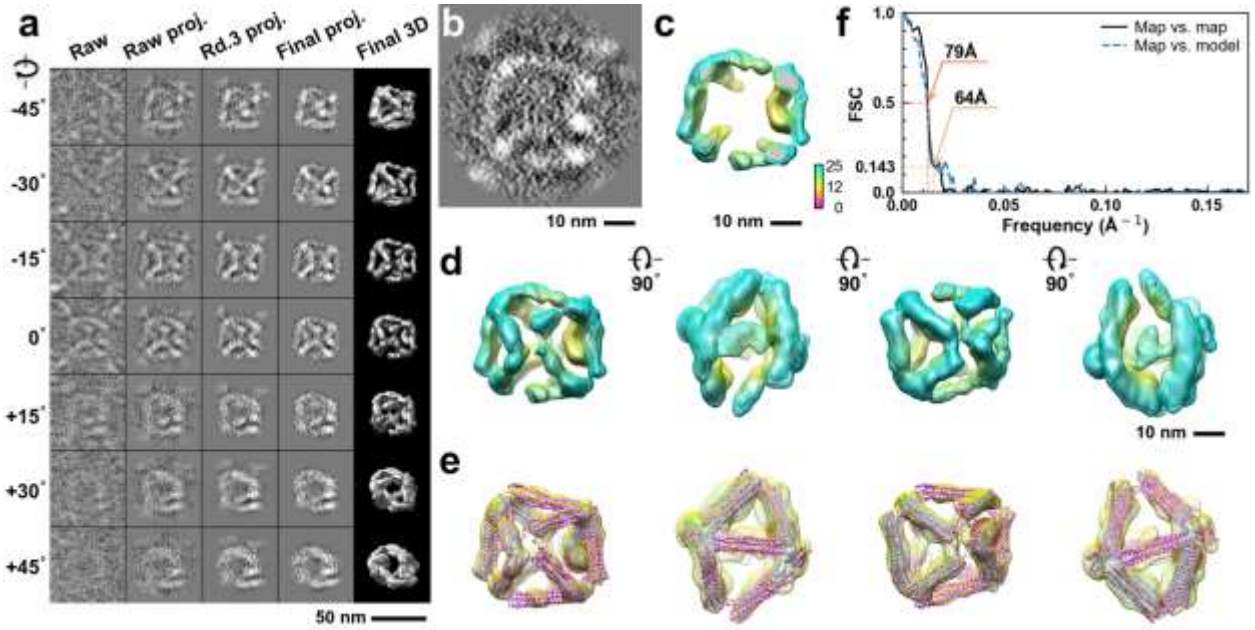

Supplementary Fig. 189: IPET 3D reconstruction and model fitting of an individual unit-cell particle (Index: 181) within a 2D lattice with 70% ferritin loading. a, Seven representative tilt images of a single unit-cell particle are shown in the first column (from left). The tilt images are aligned to a common center using IPET through iterative refinement. The projections of the raw, intermediate, and final 3D reconstruction at the corresponding angles are displayed in the subsequent four columns. **b**, A central cross-section (~23 nm thick) of the final reconstruction before masking is applied. **c**, 3D views of the central cross-section. **d**, Final 3D density map of this particle, viewed from four perpendicular directions. **e**, Final 3D reconstruction superimposed with the fitted model, viewed from four perpendicular directions. **f**, FSC analyses of the final map resolution using two methods: map-map FSC, where each map is reconstructed from one half of the images (even vs. odd tilt angle indices), and map-model FSC, where the model map is generated from the fitted model. Resolution assessments are provided based on tilt-based map-map and map-model FSC analyses at thresholds of FSC=0.5 and 0.143, respectively.

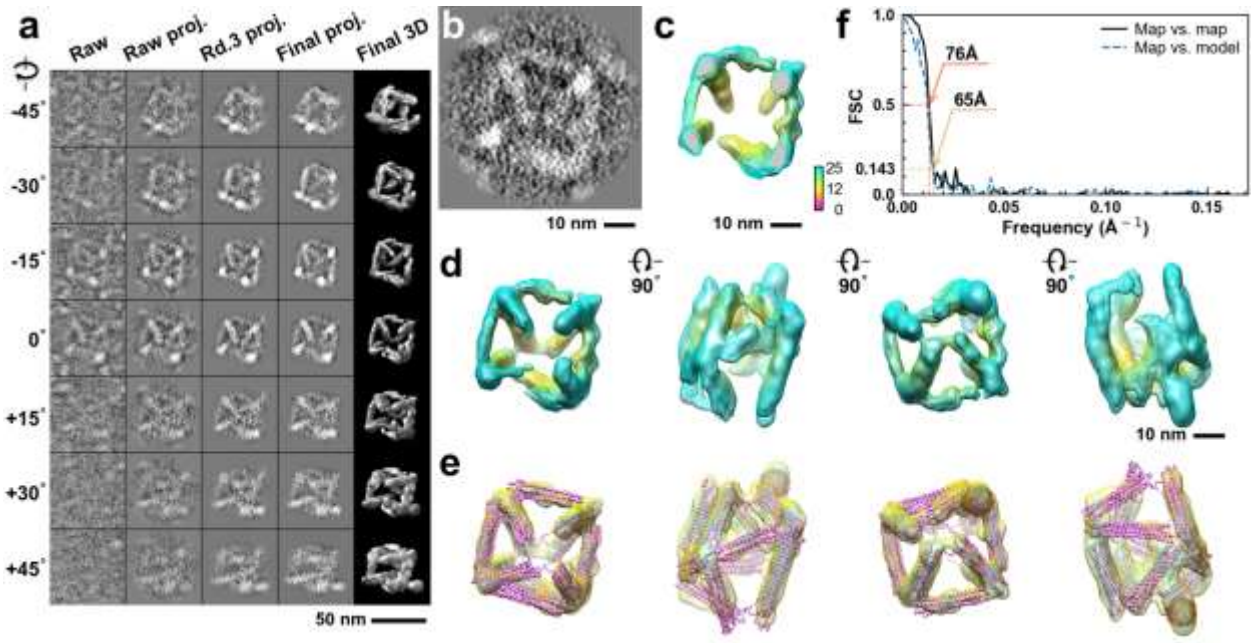

Supplementary Fig. 190: IPET 3D reconstruction and model fitting of an individual unit-cell particle (Index: 182) within a 2D lattice with 70% ferritin loading. a, Seven representative tilt images of a single unit-cell particle are shown in the first column (from left). The tilt images are aligned to a common center using IPET through iterative refinement. The projections of the raw, intermediate, and final 3D reconstruction at the corresponding angles are displayed in the subsequent four columns. **b**, A central cross-section (~23 nm thick) of the final reconstruction before masking is applied. **c**, 3D views of the central cross-section. **d**, Final 3D density map of this particle, viewed from four perpendicular directions. **e**, Final 3D reconstruction superimposed with the fitted model, viewed from four perpendicular directions. **f**, FSC analyses of the final map resolution using two methods: map-map FSC, where each map is reconstructed from one half of the images (even vs. odd tilt angle indices), and map-model FSC, where the model map is generated from the fitted model. Resolution assessments are provided based on tilt-based map-map and map-model FSC analyses at thresholds of FSC=0.5 and 0.143, respectively.

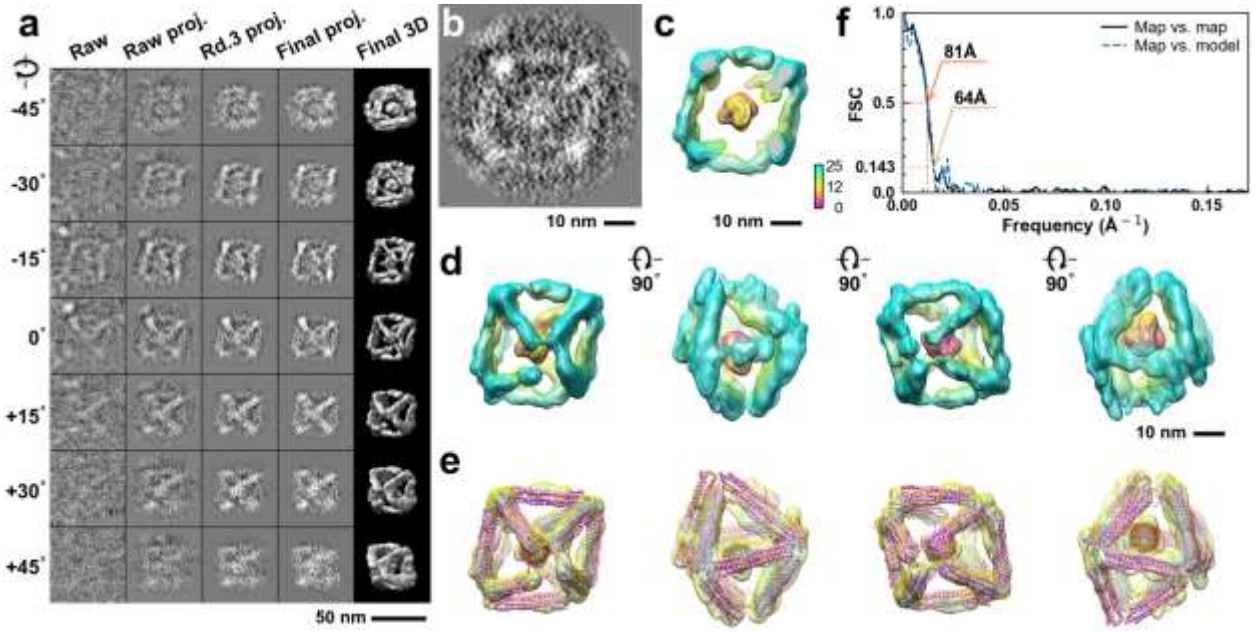

Supplementary Fig. 191: IPET 3D reconstruction and model fitting of an individual unit-cell particle (Index: 183) within a 2D lattice with 70% ferritin loading. a, Seven representative tilt images of a single unit-cell particle are shown in the first column (from left). The tilt images are aligned to a common center using IPET through iterative refinement. The projections of the raw, intermediate, and final 3D reconstruction at the corresponding angles are displayed in the subsequent four columns. **b**, A central cross-section (~23 nm thick) of the final reconstruction before masking is applied. **c**, 3D views of the central cross-section. **d**, Final 3D density map of this particle, viewed from four perpendicular directions. **e**, Final 3D reconstruction superimposed with the fitted model, viewed from four perpendicular directions. **f**, FSC analyses of the final map resolution using two methods: map-map FSC, where each map is reconstructed from one half of the images (even vs. odd tilt angle indices), and map-model FSC, where the model map is generated from the fitted model. Resolution assessments are provided based on tilt-based map-map and map-model FSC analyses at thresholds of FSC=0.5 and 0.143, respectively.

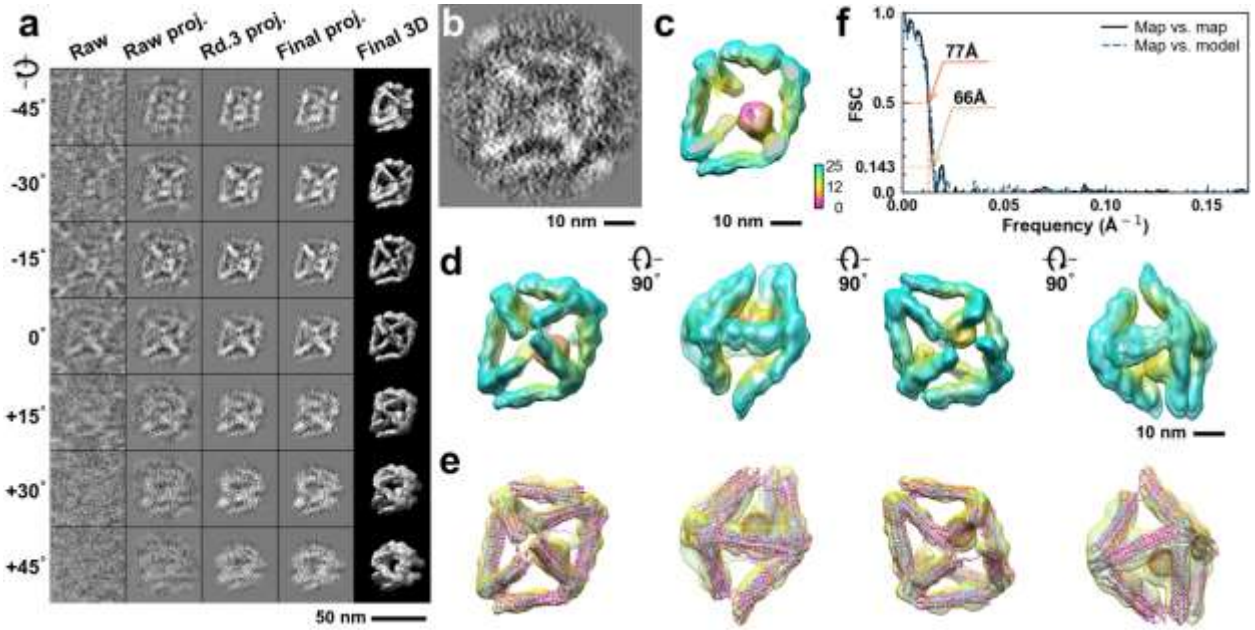

Supplementary Fig. 192: IPET 3D reconstruction and model fitting of an individual unit-cell particle (Index: 184) within a 2D lattice with 70% ferritin loading. a, Seven representative tilt images of a single unit-cell particle are shown in the first column (from left). The tilt images are aligned to a common center using IPET through iterative refinement. The projections of the raw, intermediate, and final 3D reconstruction at the corresponding angles are displayed in the subsequent four columns. **b**, A central cross-section (~23 nm thick) of the final reconstruction before masking is applied. **c**, 3D views of the central cross-section. **d**, Final 3D density map of this particle, viewed from four perpendicular directions. **e**, Final 3D reconstruction superimposed with the fitted model, viewed from four perpendicular directions. **f**, FSC analyses of the final map resolution using two methods: map-map FSC, where each map is reconstructed from one half of the images (even vs. odd tilt angle indices), and map-model FSC, where the model map is generated from the fitted model. Resolution assessments are provided based on tilt-based map-map and map-model FSC analyses at thresholds of FSC=0.5 and 0.143, respectively.

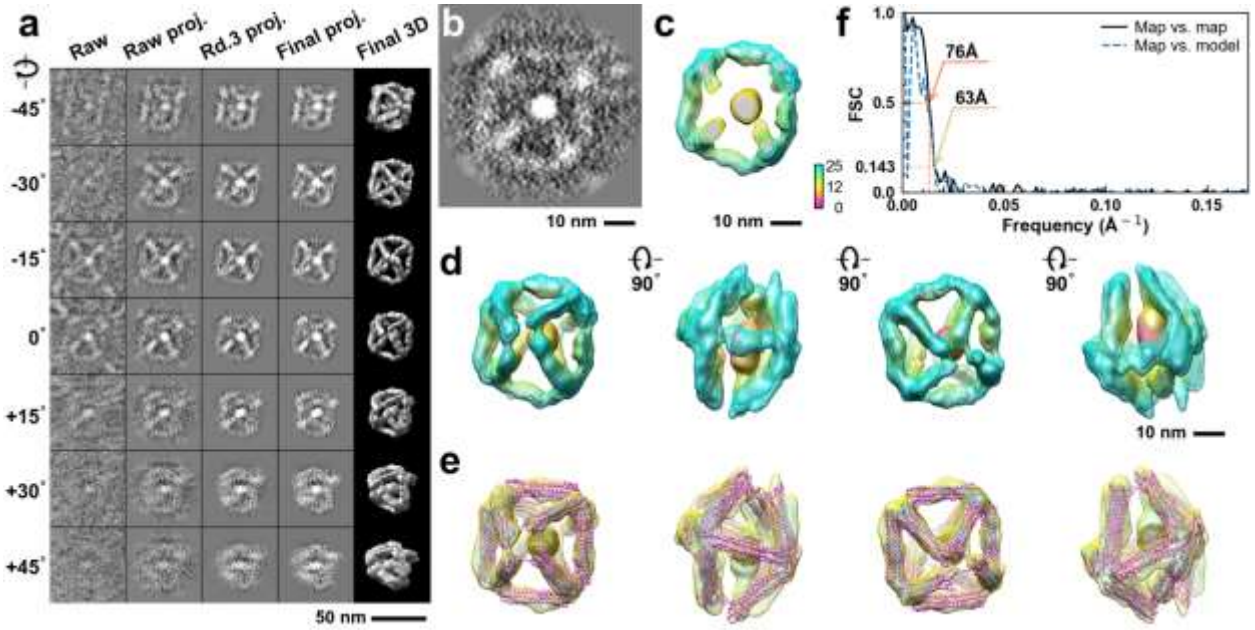

Supplementary Fig. 193: IPET 3D reconstruction and model fitting of an individual unit-cell particle (Index: 185) within a 2D lattice with 70% ferritin loading. a, Seven representative tilt images of a single unit-cell particle are shown in the first column (from left). The tilt images are aligned to a common center using IPET through iterative refinement. The projections of the raw, intermediate, and final 3D reconstruction at the corresponding angles are displayed in the subsequent four columns. **b**, A central cross-section (~23 nm thick) of the final reconstruction before masking is applied. **c**, 3D views of the central cross-section. **d**, Final 3D density map of this particle, viewed from four perpendicular directions. **e**, Final 3D reconstruction superimposed with the fitted model, viewed from four perpendicular directions. **f**, FSC analyses of the final map resolution using two methods: map-map FSC, where each map is reconstructed from one half of the images (even vs. odd tilt angle indices), and map-model FSC, where the model map is generated from the fitted model. Resolution assessments are provided based on tilt-based map-map and map-model FSC analyses at thresholds of FSC=0.5 and 0.143, respectively.

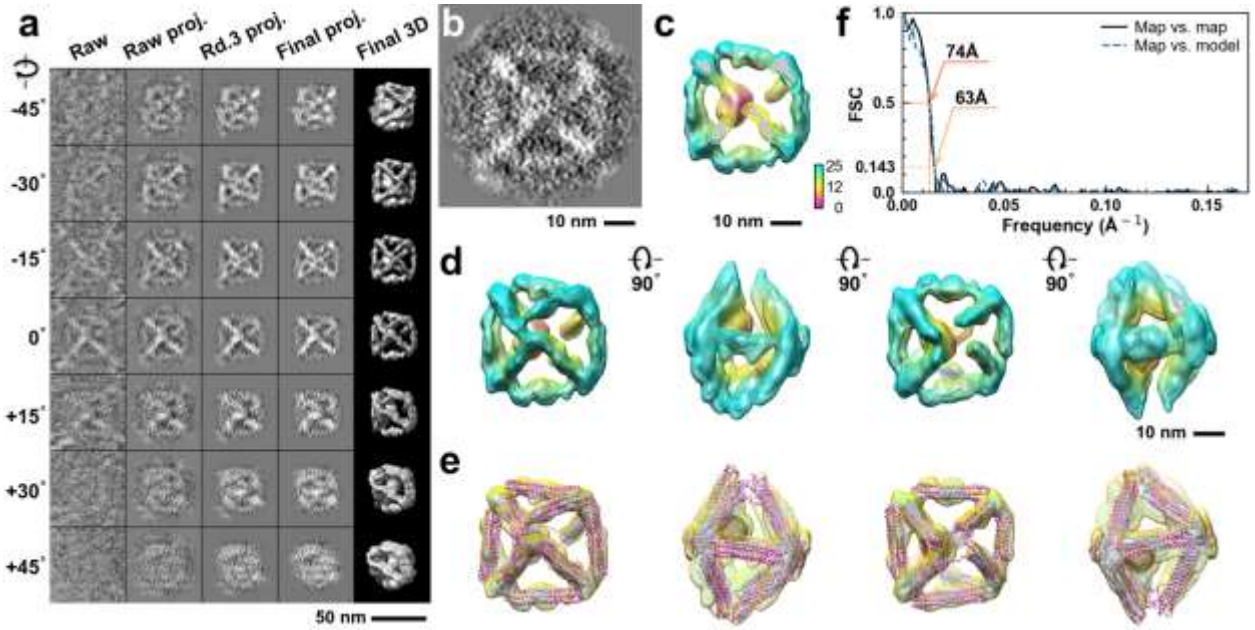

Supplementary Fig. 194: IPET 3D reconstruction and model fitting of an individual unit-cell particle (Index: 186) within a 2D lattice with 70% ferritin loading. a, Seven representative tilt images of a single unit-cell particle are shown in the first column (from left). The tilt images are aligned to a common center using IPET through iterative refinement. The projections of the raw, intermediate, and final 3D reconstruction at the corresponding angles are displayed in the subsequent four columns. **b**, A central cross-section (~23 nm thick) of the final reconstruction before masking is applied. **c**, 3D views of the central cross-section. **d**, Final 3D density map of this particle, viewed from four perpendicular directions. **e**, Final 3D reconstruction superimposed with the fitted model, viewed from four perpendicular directions. **f**, FSC analyses of the final map resolution using two methods: map-map FSC, where each map is reconstructed from one half of the images (even vs. odd tilt angle indices), and map-model FSC, where the model map is generated from the fitted model. Resolution assessments are provided based on tilt-based map-map and map-model FSC analyses at thresholds of FSC=0.5 and 0.143, respectively.

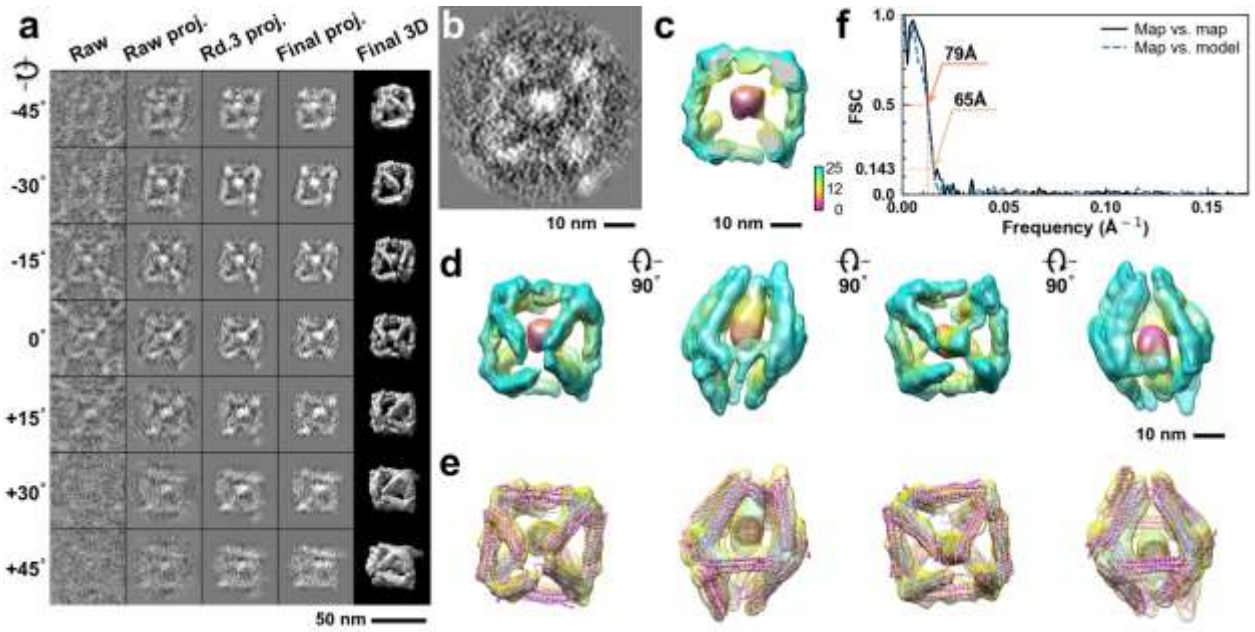

Supplementary Fig. 195: IPET 3D reconstruction and model fitting of an individual unit-cell particle (Index: 187) within a 2D lattice with 70% ferritin loading. a, Seven representative tilt images of a single unit-cell particle are shown in the first column (from left). The tilt images are aligned to a common center using IPET through iterative refinement. The projections of the raw, intermediate, and final 3D reconstruction at the corresponding angles are displayed in the subsequent four columns. **b**, A central cross-section (~23 nm thick) of the final reconstruction before masking is applied. **c**, 3D views of the central cross-section. **d**, Final 3D density map of this particle, viewed from four perpendicular directions. **e**, Final 3D reconstruction superimposed with the fitted model, viewed from four perpendicular directions. **f**, FSC analyses of the final map resolution using two methods: map-map FSC, where each map is reconstructed from one half of the images (even vs. odd tilt angle indices), and map-model FSC, where the model map is generated from the fitted model. Resolution assessments are provided based on tilt-based map-map and map-model FSC analyses at thresholds of FSC=0.5 and 0.143, respectively.

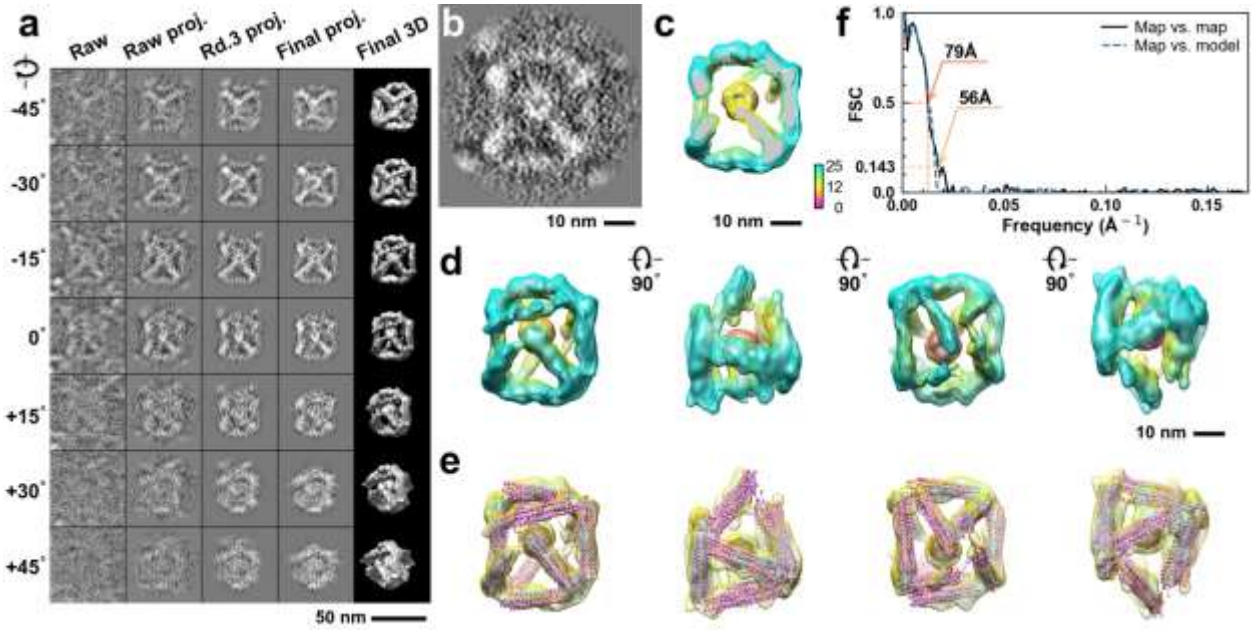

Supplementary Fig. 196: IPET 3D reconstruction and model fitting of an individual unit-cell particle (Index: 188) within a 2D lattice with 70% ferritin loading. a, Seven representative tilt images of a single unit-cell particle are shown in the first column (from left). The tilt images are aligned to a common center using IPET through iterative refinement. The projections of the raw, intermediate, and final 3D reconstruction at the corresponding angles are displayed in the subsequent four columns. **b**, A central cross-section (~23 nm thick) of the final reconstruction before masking is applied. **c**, 3D views of the central cross-section. **d**, Final 3D density map of this particle, viewed from four perpendicular directions. **e**, Final 3D reconstruction superimposed with the fitted model, viewed from four perpendicular directions. **f**, FSC analyses of the final map resolution using two methods: map-map FSC, where each map is reconstructed from one half of the images (even vs. odd tilt angle indices), and map-model FSC, where the model map is generated from the fitted model. Resolution assessments are provided based on tilt-based map-map and map-model FSC analyses at thresholds of FSC=0.5 and 0.143, respectively.

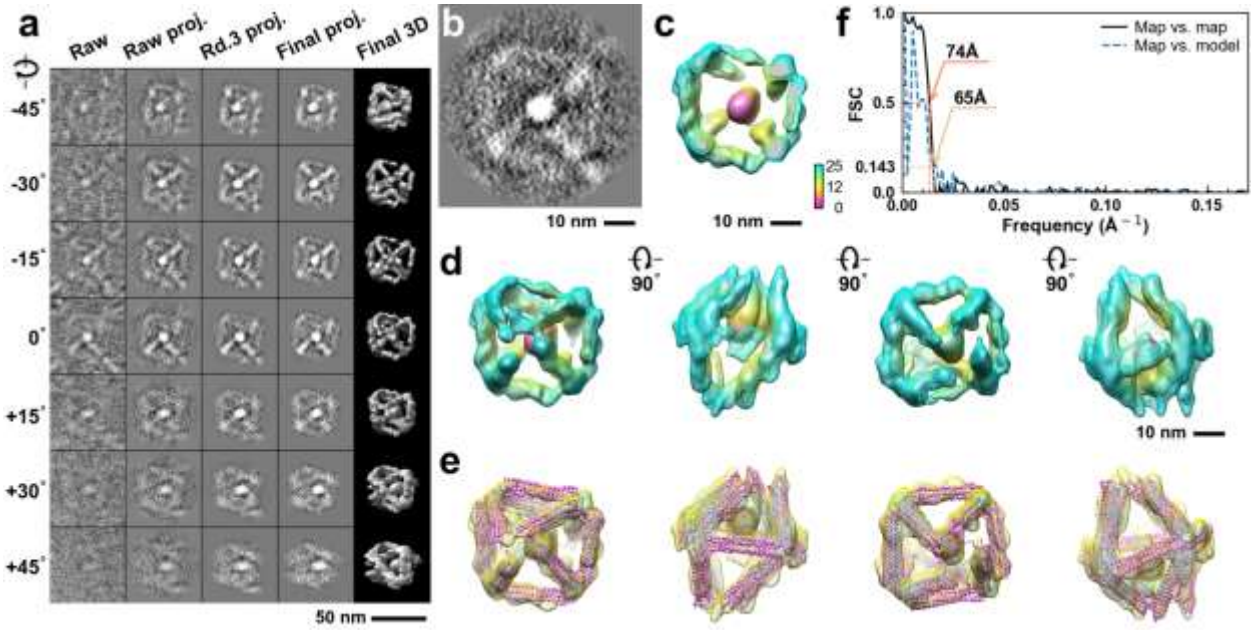

Supplementary Fig. 197: IPET 3D reconstruction and model fitting of an individual unit-cell particle (Index: 189) within a 2D lattice with 70% ferritin loading. a, Seven representative tilt images of a single unit-cell particle are shown in the first column (from left). The tilt images are aligned to a common center using IPET through iterative refinement. The projections of the raw, intermediate, and final 3D reconstruction at the corresponding angles are displayed in the subsequent four columns. **b**, A central cross-section (~23 nm thick) of the final reconstruction before masking is applied. **c**, 3D views of the central cross-section. **d**, Final 3D density map of this particle, viewed from four perpendicular directions. **e**, Final 3D reconstruction superimposed with the fitted model, viewed from four perpendicular directions. **f**, FSC analyses of the final map resolution using two methods: map-map FSC, where each map is reconstructed from one half of the images (even vs. odd tilt angle indices), and map-model FSC, where the model map is generated from the fitted model. Resolution assessments are provided based on tilt-based map-map and map-model FSC analyses at thresholds of FSC=0.5 and 0.143, respectively.

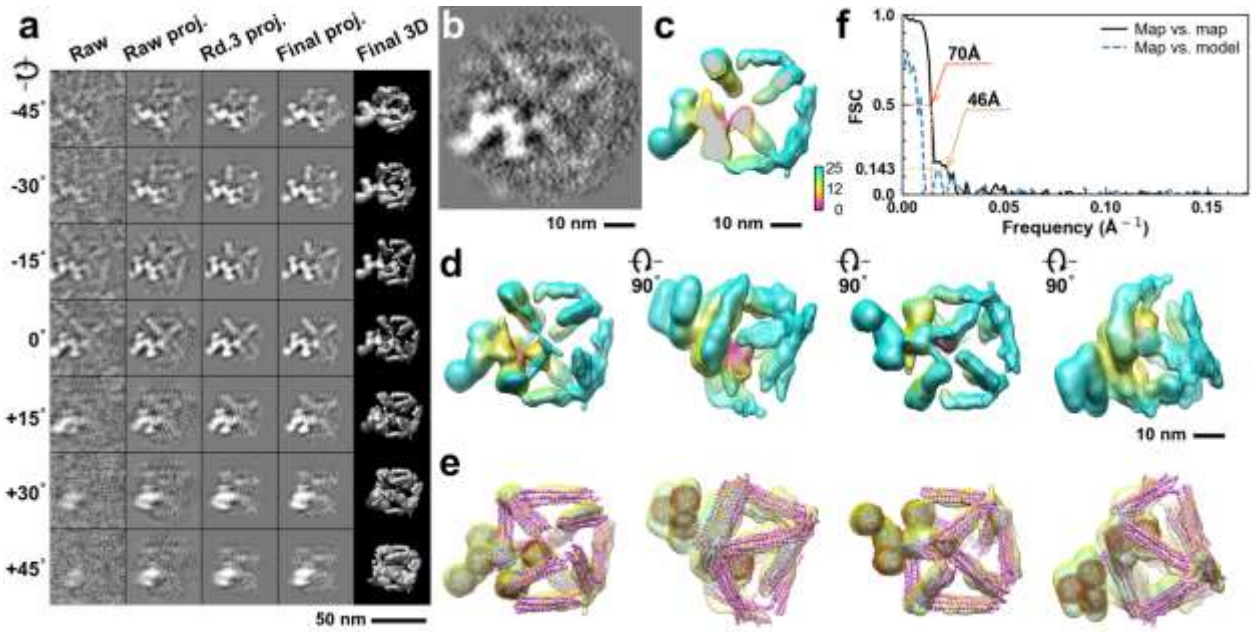

Supplementary Fig. 198: IPET 3D reconstruction and model fitting of an individual unit-cell particle (Index: 190) within a 2D lattice with 70% ferritin loading. a, Seven representative tilt images of a single unit-cell particle are shown in the first column (from left). The tilt images are aligned to a common center using IPET through iterative refinement. The projections of the raw, intermediate, and final 3D reconstruction at the corresponding angles are displayed in the subsequent four columns. **b**, A central cross-section (~23 nm thick) of the final reconstruction before masking is applied. **c**, 3D views of the central cross-section. **d**, Final 3D density map of this particle, viewed from four perpendicular directions. **e**, Final 3D reconstruction superimposed with the fitted model, viewed from four perpendicular directions. **f**, FSC analyses of the final map resolution using two methods: map-map FSC, where each map is reconstructed from one half of the images (even vs. odd tilt angle indices), and map-model FSC, where the model map is generated from the fitted model. Resolution assessments are provided based on tilt-based map-map and map-model FSC analyses at thresholds of FSC=0.5 and 0.143, respectively.

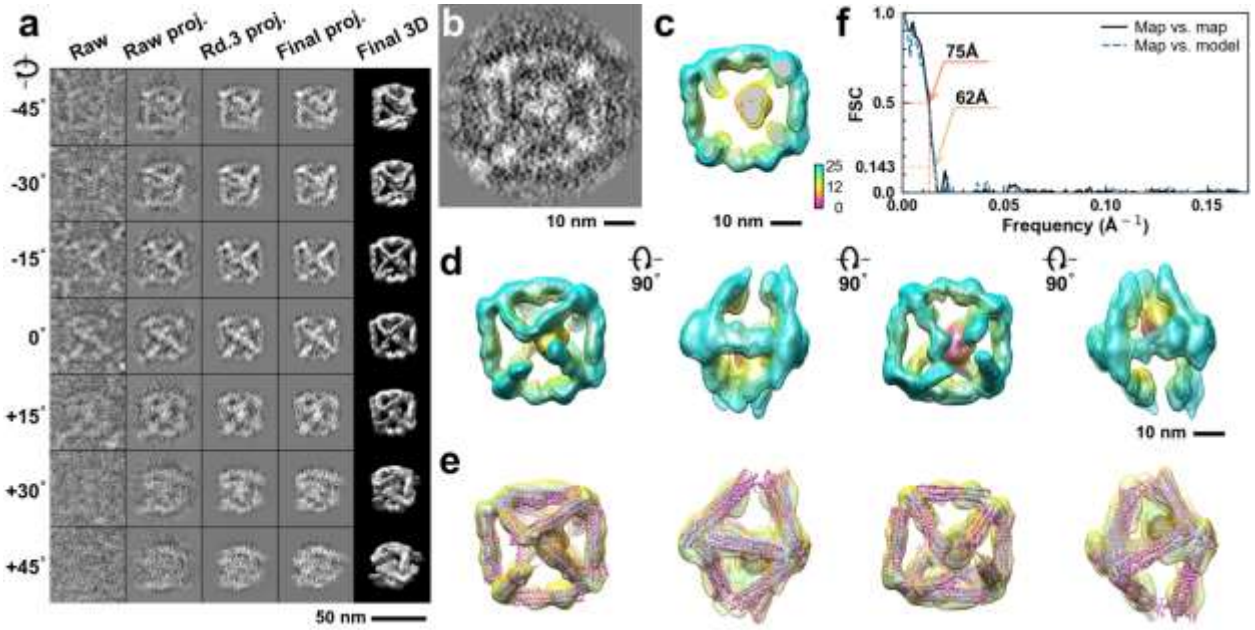

Supplementary Fig. 199: IPET 3D reconstruction and model fitting of an individual unit-cell particle (Index: 191) within a 2D lattice with 70% ferritin loading. a, Seven representative tilt images of a single unit-cell particle are shown in the first column (from left). The tilt images are aligned to a common center using IPET through iterative refinement. The projections of the raw, intermediate, and final 3D reconstruction at the corresponding angles are displayed in the subsequent four columns. **b**, A central cross-section (~23 nm thick) of the final reconstruction before masking is applied. **c**, 3D views of the central cross-section. **d**, Final 3D density map of this particle, viewed from four perpendicular directions. **e**, Final 3D reconstruction superimposed with the fitted model, viewed from four perpendicular directions. **f**, FSC analyses of the final map resolution using two methods: map-map FSC, where each map is reconstructed from one half of the images (even vs. odd tilt angle indices), and map-model FSC, where the model map is generated from the fitted model. Resolution assessments are provided based on tilt-based map-map and map-model FSC analyses at thresholds of FSC=0.5 and 0.143, respectively.

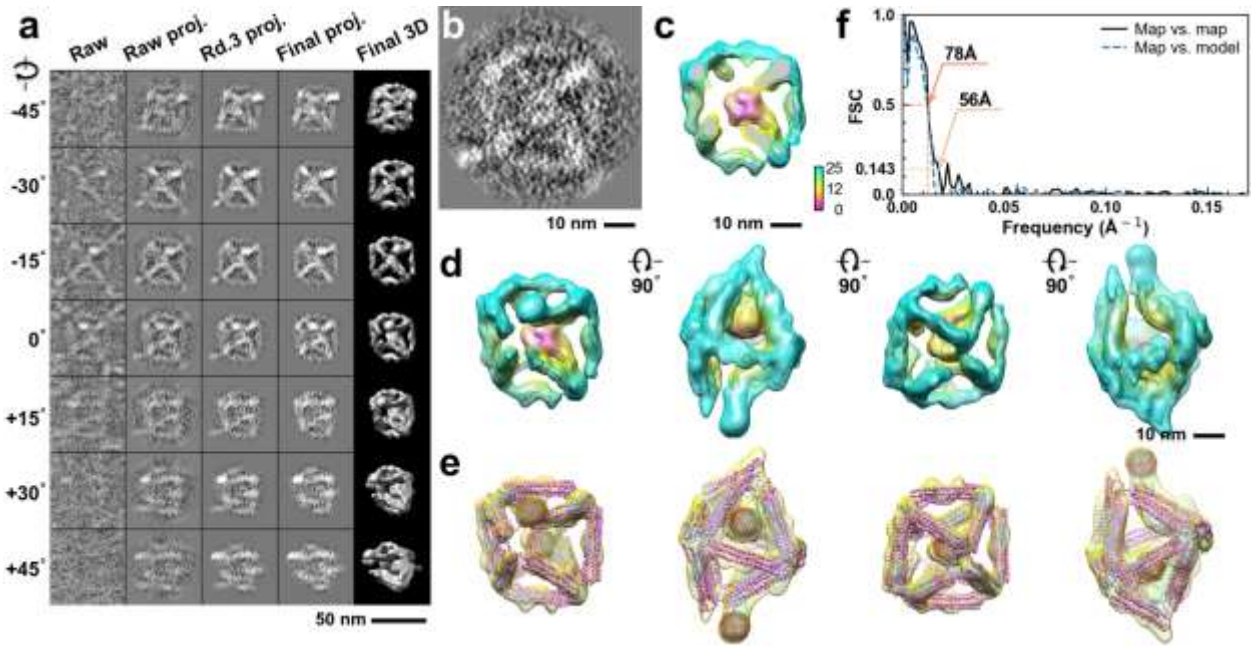

Supplementary Fig. 200: IPET 3D reconstruction and model fitting of an individual unit-cell particle (Index: 192) within a 2D lattice with 70% ferritin loading. a, Seven representative tilt images of a single unit-cell particle are shown in the first column (from left). The tilt images are aligned to a common center using IPET through iterative refinement. The projections of the raw, intermediate, and final 3D reconstruction at the corresponding angles are displayed in the subsequent four columns. **b**, A central cross-section (~23 nm thick) of the final reconstruction before masking is applied. **c**, 3D views of the central cross-section. **d**, Final 3D density map of this particle, viewed from four perpendicular directions. **e**, Final 3D reconstruction superimposed with the fitted model, viewed from four perpendicular directions. **f**, FSC analyses of the final map resolution using two methods: map-map FSC, where each map is reconstructed from one half of the images (even vs. odd tilt angle indices), and map-model FSC, where the model map is generated from the fitted model. Resolution assessments are provided based on tilt-based map-map and map-model FSC analyses at thresholds of FSC=0.5 and 0.143, respectively.

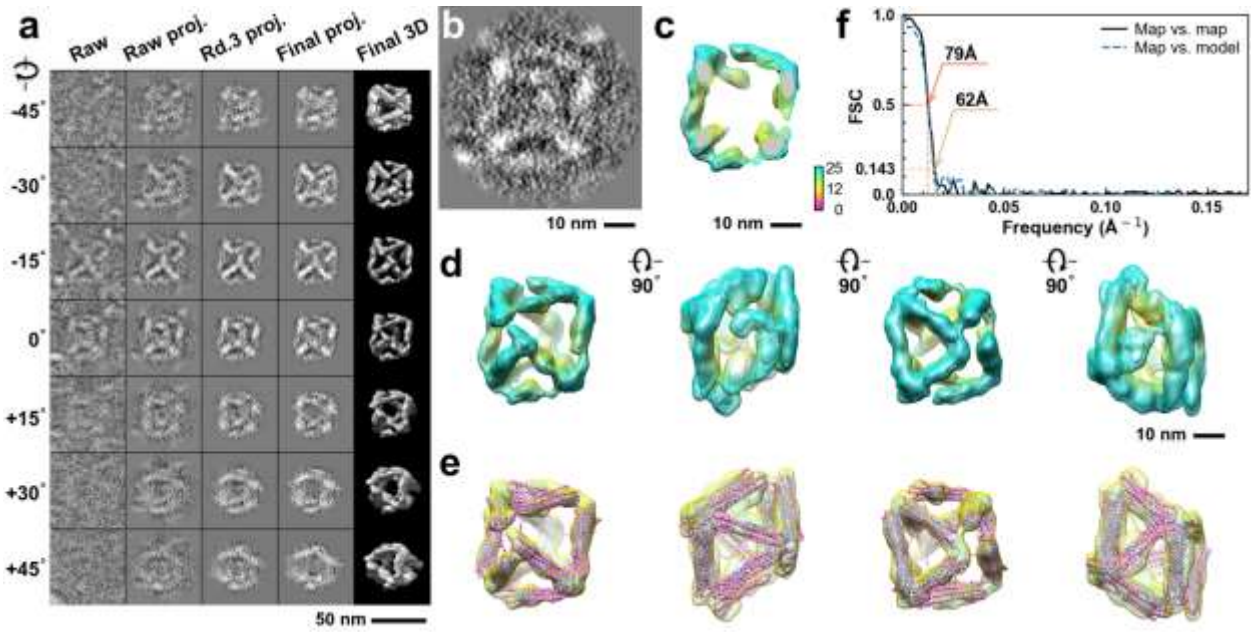

Supplementary Fig. 201: IPET 3D reconstruction and model fitting of an individual unit-cell particle (Index: 193) within a 2D lattice with 70% ferritin loading. a, Seven representative tilt images of a single unit-cell particle are shown in the first column (from left). The tilt images are aligned to a common center using IPET through iterative refinement. The projections of the raw, intermediate, and final 3D reconstruction at the corresponding angles are displayed in the subsequent four columns. **b**, A central cross-section (~23 nm thick) of the final reconstruction before masking is applied. **c**, 3D views of the central cross-section. **d**, Final 3D density map of this particle, viewed from four perpendicular directions. **e**, Final 3D reconstruction superimposed with the fitted model, viewed from four perpendicular directions. **f**, FSC analyses of the final map resolution using two methods: map-map FSC, where each map is reconstructed from one half of the images (even vs. odd tilt angle indices), and map-model FSC, where the model map is generated from the fitted model. Resolution assessments are provided based on tilt-based map-map and map-model FSC analyses at thresholds of FSC=0.5 and 0.143, respectively.

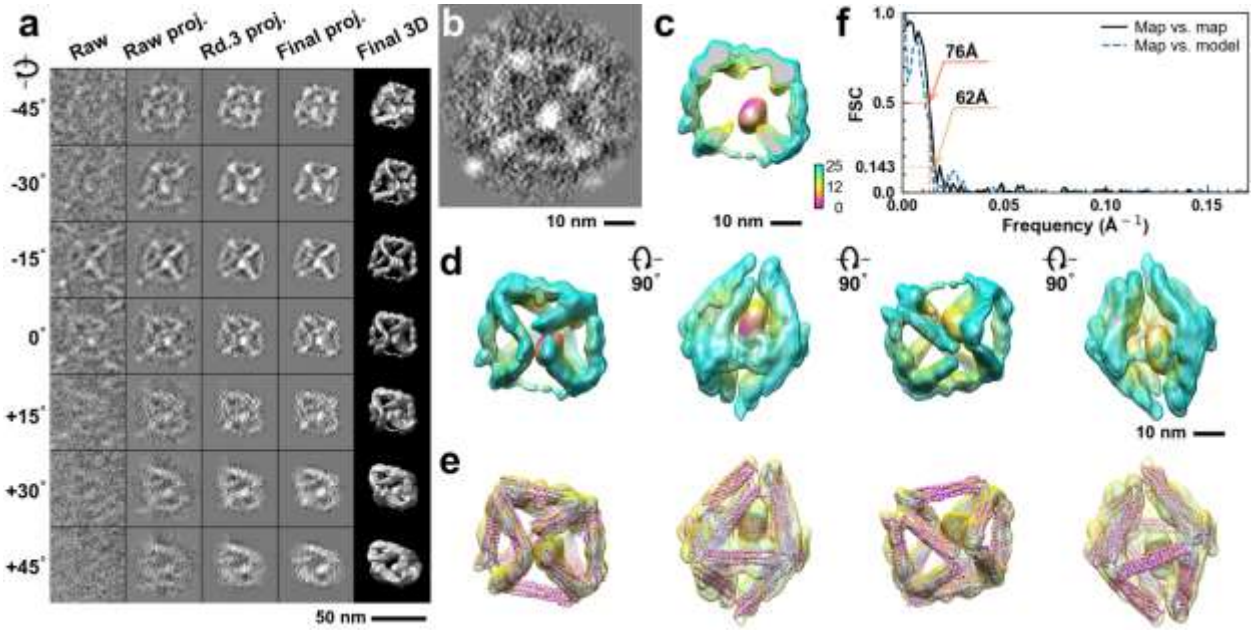

Supplementary Fig. 202: IPET 3D reconstruction and model fitting of an individual unit-cell particle (Index: 194) within a 2D lattice with 70% ferritin loading. a, Seven representative tilt images of a single unit-cell particle are shown in the first column (from left). The tilt images are aligned to a common center using IPET through iterative refinement. The projections of the raw, intermediate, and final 3D reconstruction at the corresponding angles are displayed in the subsequent four columns. **b**, A central cross-section (~23 nm thick) of the final reconstruction before masking is applied. **c**, 3D views of the central cross-section. **d**, Final 3D density map of this particle, viewed from four perpendicular directions. **e**, Final 3D reconstruction superimposed with the fitted model, viewed from four perpendicular directions. **f**, FSC analyses of the final map resolution using two methods: map-map FSC, where each map is reconstructed from one half of the images (even vs. odd tilt angle indices), and map-model FSC, where the model map is generated from the fitted model. Resolution assessments are provided based on tilt-based map-map and map-model FSC analyses at thresholds of FSC=0.5 and 0.143, respectively.

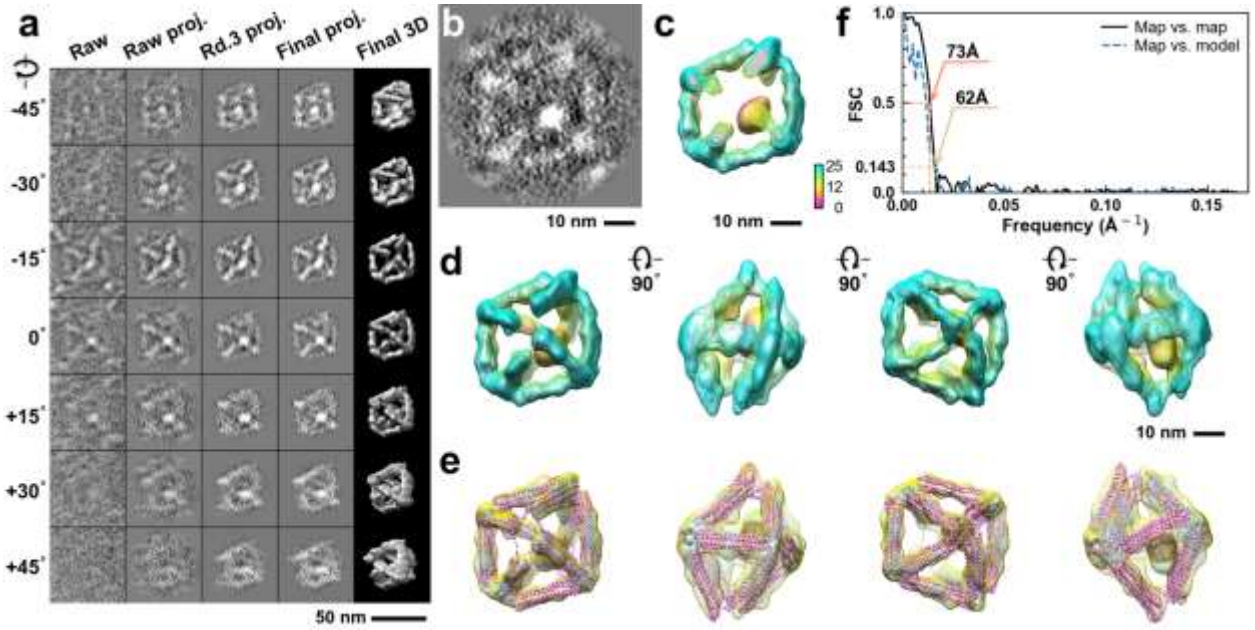

Supplementary Fig. 203: IPET 3D reconstruction and model fitting of an individual unit-cell particle (Index: 195) within a 2D lattice with 70% ferritin loading. a, Seven representative tilt images of a single unit-cell particle are shown in the first column (from left). The tilt images are aligned to a common center using IPET through iterative refinement. The projections of the raw, intermediate, and final 3D reconstruction at the corresponding angles are displayed in the subsequent four columns. **b**, A central cross-section (~23 nm thick) of the final reconstruction before masking is applied. **c**, 3D views of the central cross-section. **d**, Final 3D density map of this particle, viewed from four perpendicular directions. **e**, Final 3D reconstruction superimposed with the fitted model, viewed from four perpendicular directions. **f**, FSC analyses of the final map resolution using two methods: map-map FSC, where each map is reconstructed from one half of the images (even vs. odd tilt angle indices), and map-model FSC, where the model map is generated from the fitted model. Resolution assessments are provided based on tilt-based map-map and map-model FSC analyses at thresholds of FSC=0.5 and 0.143, respectively.

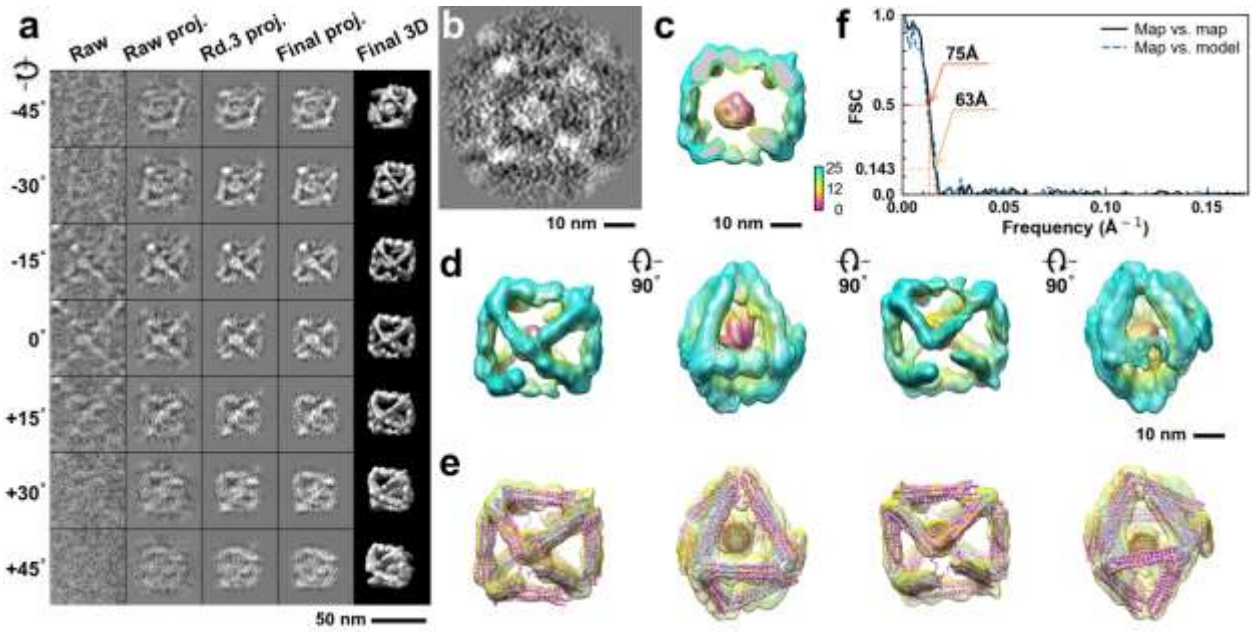

Supplementary Fig. 204: IPET 3D reconstruction and model fitting of an individual unit-cell particle (Index: 196) within a 2D lattice with 70% ferritin loading. a, Seven representative tilt images of a single unit-cell particle are shown in the first column (from left). The tilt images are aligned to a common center using IPET through iterative refinement. The projections of the raw, intermediate, and final 3D reconstruction at the corresponding angles are displayed in the subsequent four columns. **b**, A central cross-section (~23 nm thick) of the final reconstruction before masking is applied. **c**, 3D views of the central cross-section. **d**, Final 3D density map of this particle, viewed from four perpendicular directions. **e**, Final 3D reconstruction superimposed with the fitted model, viewed from four perpendicular directions. **f**, FSC analyses of the final map resolution using two methods: map-map FSC, where each map is reconstructed from one half of the images (even vs. odd tilt angle indices), and map-model FSC, where the model map is generated from the fitted model. Resolution assessments are provided based on tilt-based map-map and map-model FSC analyses at thresholds of FSC=0.5 and 0.143, respectively.

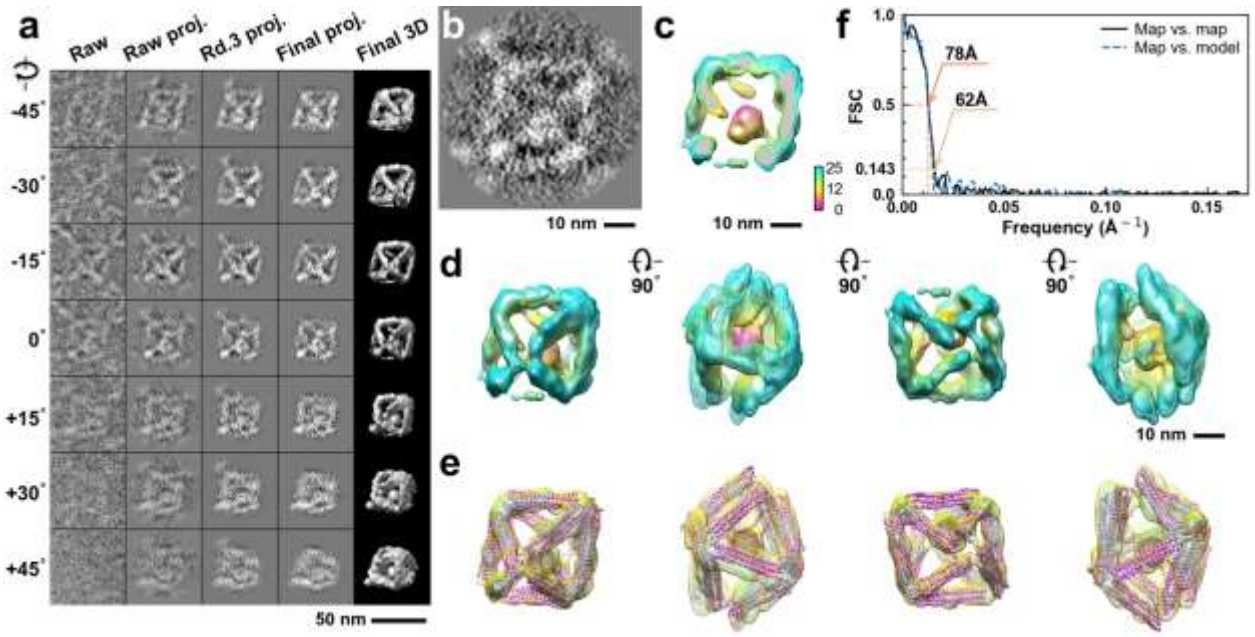

Supplementary Fig. 205: IPET 3D reconstruction and model fitting of an individual unit-cell particle (Index: 197) within a 2D lattice with 70% ferritin loading. a, Seven representative tilt images of a single unit-cell particle are shown in the first column (from left). The tilt images are aligned to a common center using IPET through iterative refinement. The projections of the raw, intermediate, and final 3D reconstruction at the corresponding angles are displayed in the subsequent four columns. **b**, A central cross-section (~23 nm thick) of the final reconstruction before masking is applied. **c**, 3D views of the central cross-section. **d**, Final 3D density map of this particle, viewed from four perpendicular directions. **e**, Final 3D reconstruction superimposed with the fitted model, viewed from four perpendicular directions. **f**, FSC analyses of the final map resolution using two methods: map-map FSC, where each map is reconstructed from one half of the images (even vs. odd tilt angle indices), and map-model FSC, where the model map is generated from the fitted model. Resolution assessments are provided based on tilt-based map-map and map-model FSC analyses at thresholds of FSC=0.5 and 0.143, respectively.

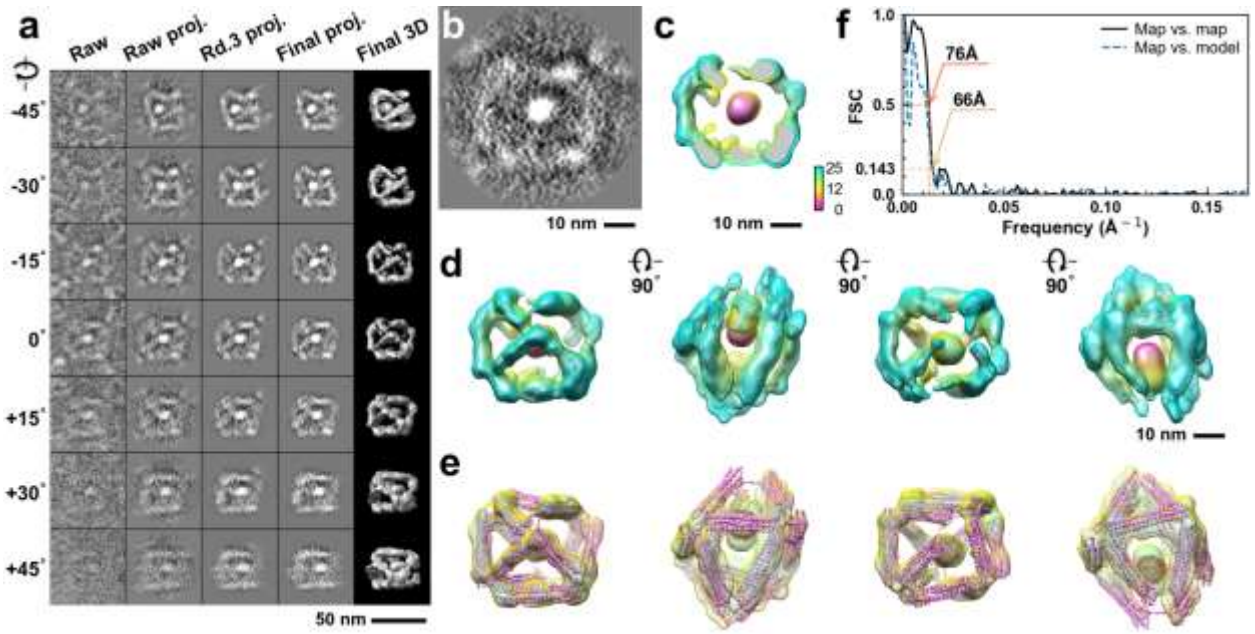

Supplementary Fig. 206: IPET 3D reconstruction and model fitting of an individual unit-cell particle (Index: 198) within a 2D lattice with 70% ferritin loading. a, Seven representative tilt images of a single unit-cell particle are shown in the first column (from left). The tilt images are aligned to a common center using IPET through iterative refinement. The projections of the raw, intermediate, and final 3D reconstruction at the corresponding angles are displayed in the subsequent four columns. **b**, A central cross-section (~23 nm thick) of the final reconstruction before masking is applied. **c**, 3D views of the central cross-section. **d**, Final 3D density map of this particle, viewed from four perpendicular directions. **e**, Final 3D reconstruction superimposed with the fitted model, viewed from four perpendicular directions. **f**, FSC analyses of the final map resolution using two methods: map-map FSC, where each map is reconstructed from one half of the images (even vs. odd tilt angle indices), and map-model FSC, where the model map is generated from the fitted model. Resolution assessments are provided based on tilt-based map-map and map-model FSC analyses at thresholds of FSC=0.5 and 0.143, respectively.

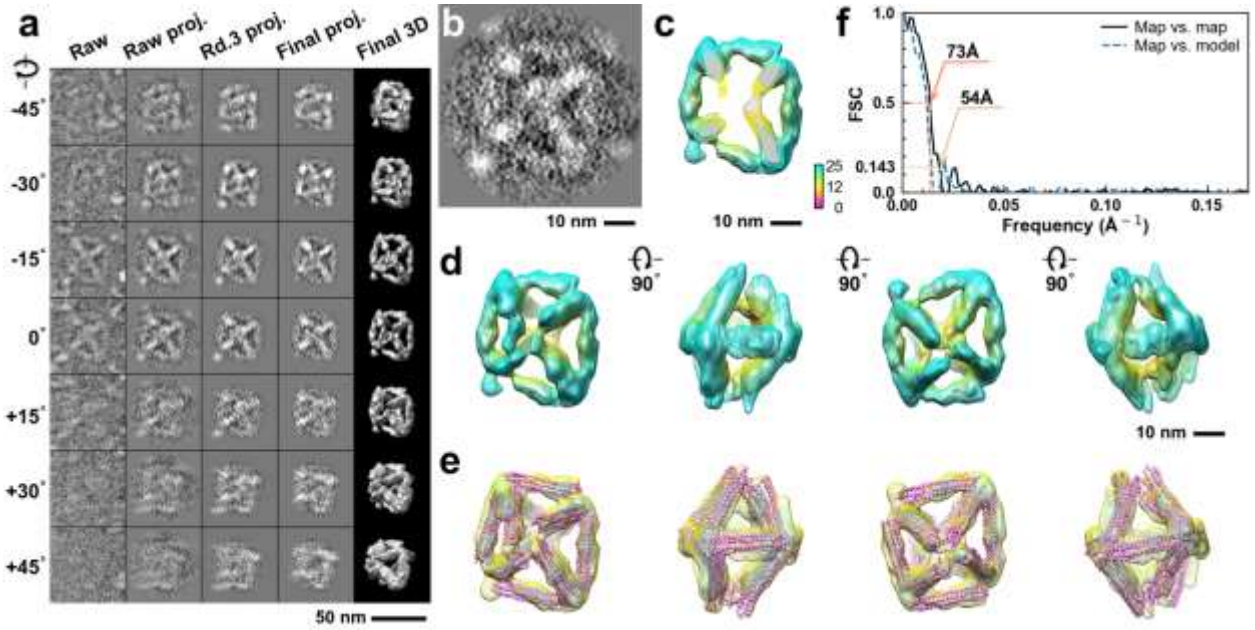

Supplementary Fig. 207: IPET 3D reconstruction and model fitting of an individual unit-cell particle (Index: 199) within a 2D lattice with 70% ferritin loading. a, Seven representative tilt images of a single unit-cell particle are shown in the first column (from left). The tilt images are aligned to a common center using IPET through iterative refinement. The projections of the raw, intermediate, and final 3D reconstruction at the corresponding angles are displayed in the subsequent four columns. **b**, A central cross-section (~23 nm thick) of the final reconstruction before masking is applied. **c**, 3D views of the central cross-section. **d**, Final 3D density map of this particle, viewed from four perpendicular directions. **e**, Final 3D reconstruction superimposed with the fitted model, viewed from four perpendicular directions. **f**, FSC analyses of the final map resolution using two methods: map-map FSC, where each map is reconstructed from one half of the images (even vs. odd tilt angle indices), and map-model FSC, where the model map is generated from the fitted model. Resolution assessments are provided based on tilt-based map-map and map-model FSC analyses at thresholds of FSC=0.5 and 0.143, respectively.

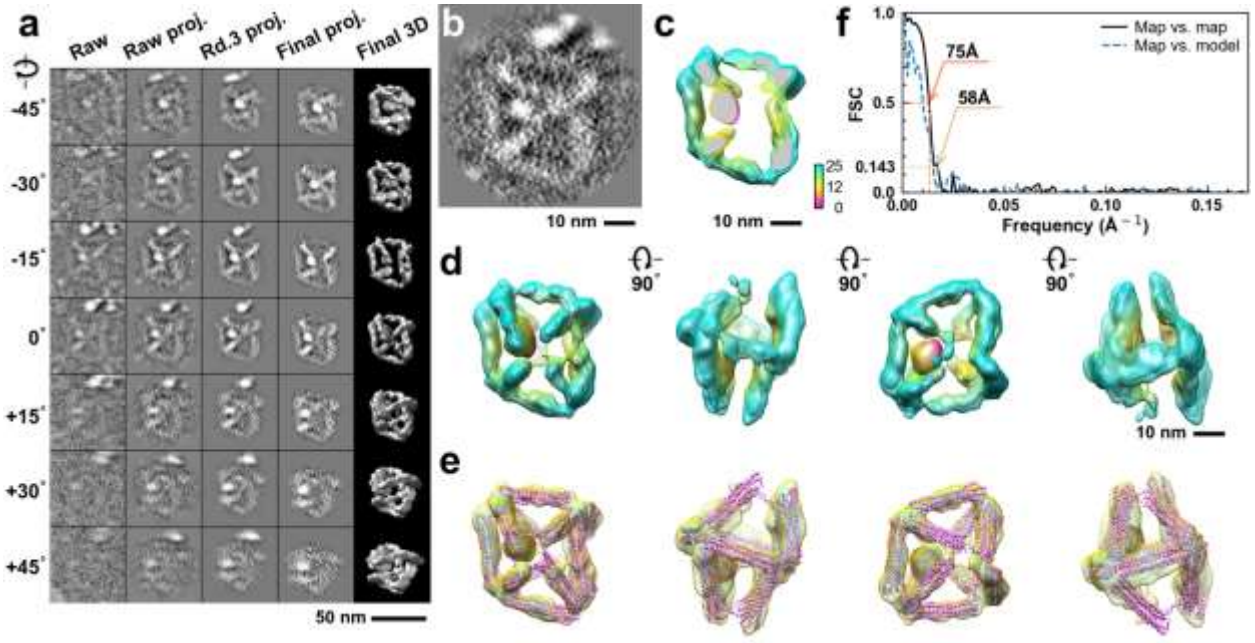

Supplementary Fig. 208: IPET 3D reconstruction and model fitting of an individual unit-cell particle (Index: 200) within a 2D lattice with 70% ferritin loading. a, Seven representative tilt images of a single unit-cell particle are shown in the first column (from left). The tilt images are aligned to a common center using IPET through iterative refinement. The projections of the raw, intermediate, and final 3D reconstruction at the corresponding angles are displayed in the subsequent four columns. **b**, A central cross-section (~23 nm thick) of the final reconstruction before masking is applied. **c**, 3D views of the central cross-section. **d**, Final 3D density map of this particle, viewed from four perpendicular directions. **e**, Final 3D reconstruction superimposed with the fitted model, viewed from four perpendicular directions. **f**, FSC analyses of the final map resolution using two methods: map-map FSC, where each map is reconstructed from one half of the images (even vs. odd tilt angle indices), and map-model FSC, where the model map is generated from the fitted model. Resolution assessments are provided based on tilt-based map-map and map-model FSC analyses at thresholds of FSC=0.5 and 0.143, respectively.

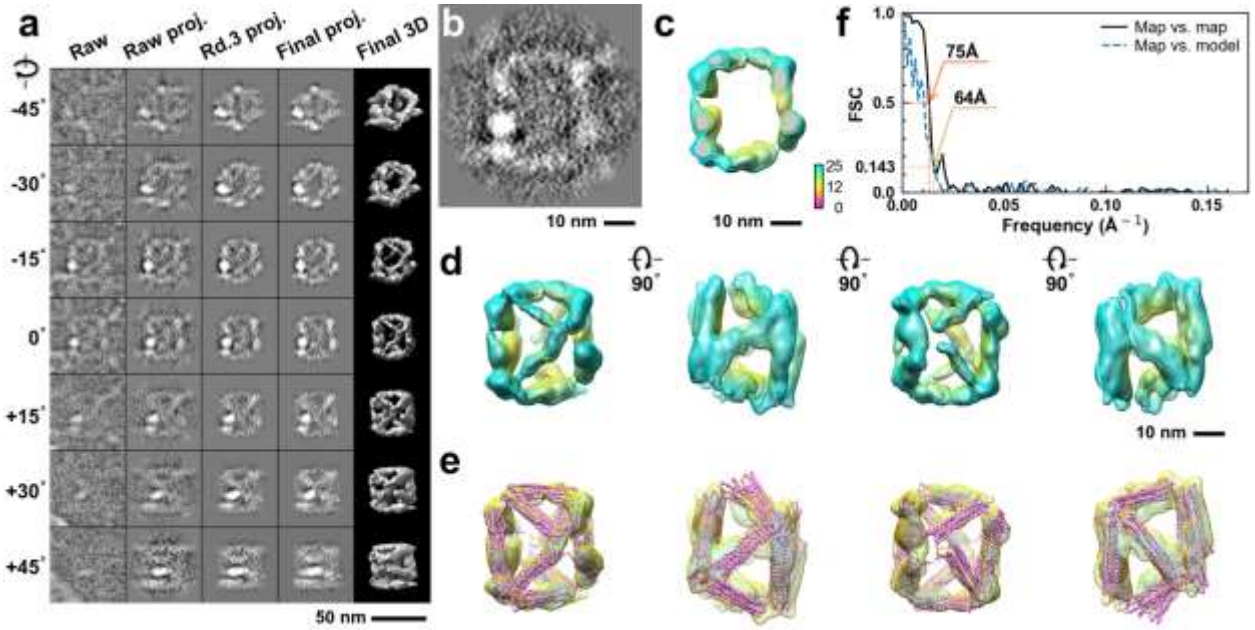

Supplementary Fig. 209: IPET 3D reconstruction and model fitting of an individual unit-cell particle (Index: 201) within a 2D lattice with 70% ferritin loading. a, Seven representative tilt images of a single unit-cell particle are shown in the first column (from left). The tilt images are aligned to a common center using IPET through iterative refinement. The projections of the raw, intermediate, and final 3D reconstruction at the corresponding angles are displayed in the subsequent four columns. **b**, A central cross-section (~23 nm thick) of the final reconstruction before masking is applied. **c**, 3D views of the central cross-section. **d**, Final 3D density map of this particle, viewed from four perpendicular directions. **e**, Final 3D reconstruction superimposed with the fitted model, viewed from four perpendicular directions. **f**, FSC analyses of the final map resolution using two methods: map-map FSC, where each map is reconstructed from one half of the images (even vs. odd tilt angle indices), and map-model FSC, where the model map is generated from the fitted model. Resolution assessments are provided based on tilt-based map-map and map-model FSC analyses at thresholds of FSC=0.5 and 0.143, respectively.

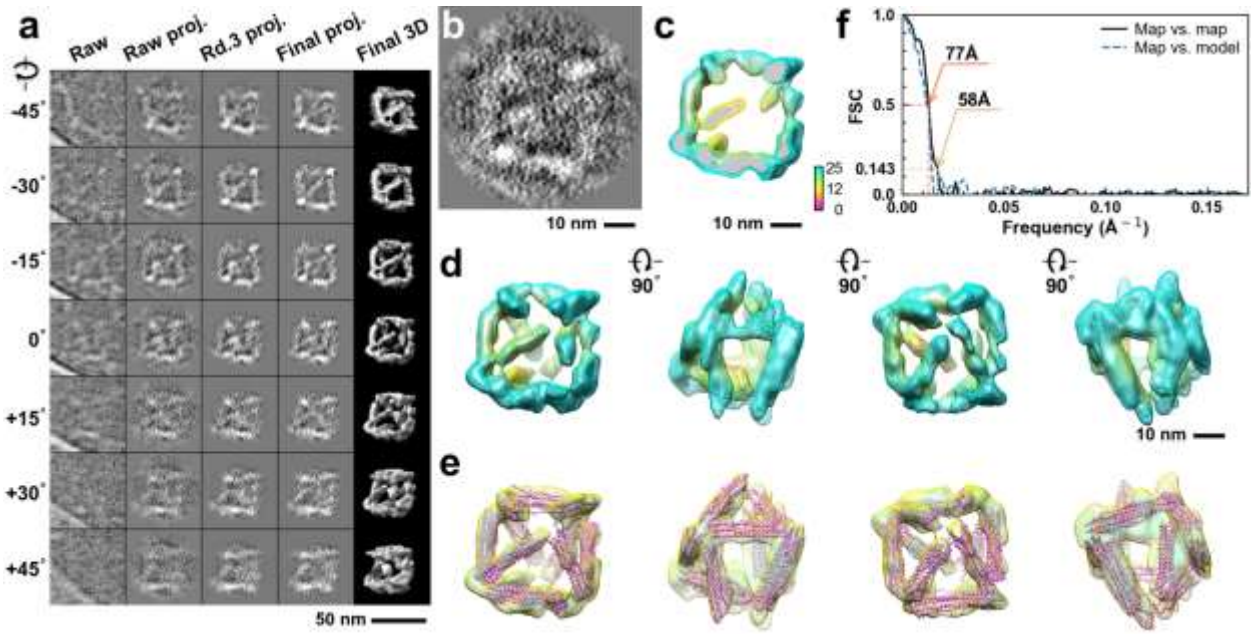

Supplementary Fig. 210: IPET 3D reconstruction and model fitting of an individual unit-cell particle (Index: 202) within a 2D lattice with 70% ferritin loading. a, Seven representative tilt images of a single unit-cell particle are shown in the first column (from left). The tilt images are aligned to a common center using IPET through iterative refinement. The projections of the raw, intermediate, and final 3D reconstruction at the corresponding angles are displayed in the subsequent four columns. **b**, A central cross-section (~23 nm thick) of the final reconstruction before masking is applied. **c**, 3D views of the central cross-section. **d**, Final 3D density map of this particle, viewed from four perpendicular directions. **e**, Final 3D reconstruction superimposed with the fitted model, viewed from four perpendicular directions. **f**, FSC analyses of the final map resolution using two methods: map-map FSC, where each map is reconstructed from one half of the images (even vs. odd tilt angle indices), and map-model FSC, where the model map is generated from the fitted model. Resolution assessments are provided based on tilt-based map-map and map-model FSC analyses at thresholds of FSC=0.5 and 0.143, respectively.

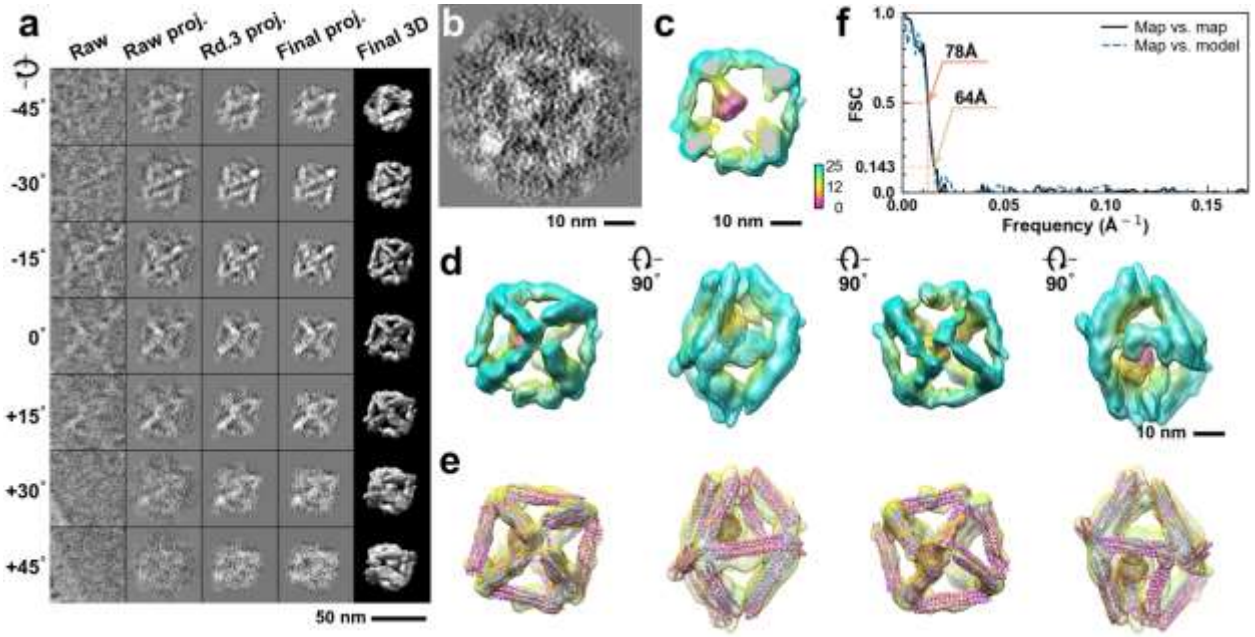

Supplementary Fig. 211: IPET 3D reconstruction and model fitting of an individual unit-cell particle (Index: 203) within a 2D lattice with 70% ferritin loading. a, Seven representative tilt images of a single unit-cell particle are shown in the first column (from left). The tilt images are aligned to a common center using IPET through iterative refinement. The projections of the raw, intermediate, and final 3D reconstruction at the corresponding angles are displayed in the subsequent four columns. **b**, A central cross-section (~23 nm thick) of the final reconstruction before masking is applied. **c**, 3D views of the central cross-section. **d**, Final 3D density map of this particle, viewed from four perpendicular directions. **e**, Final 3D reconstruction superimposed with the fitted model, viewed from four perpendicular directions. **f**, FSC analyses of the final map resolution using two methods: map-map FSC, where each map is reconstructed from one half of the images (even vs. odd tilt angle indices), and map-model FSC, where the model map is generated from the fitted model. Resolution assessments are provided based on tilt-based map-map and map-model FSC analyses at thresholds of FSC=0.5 and 0.143, respectively.

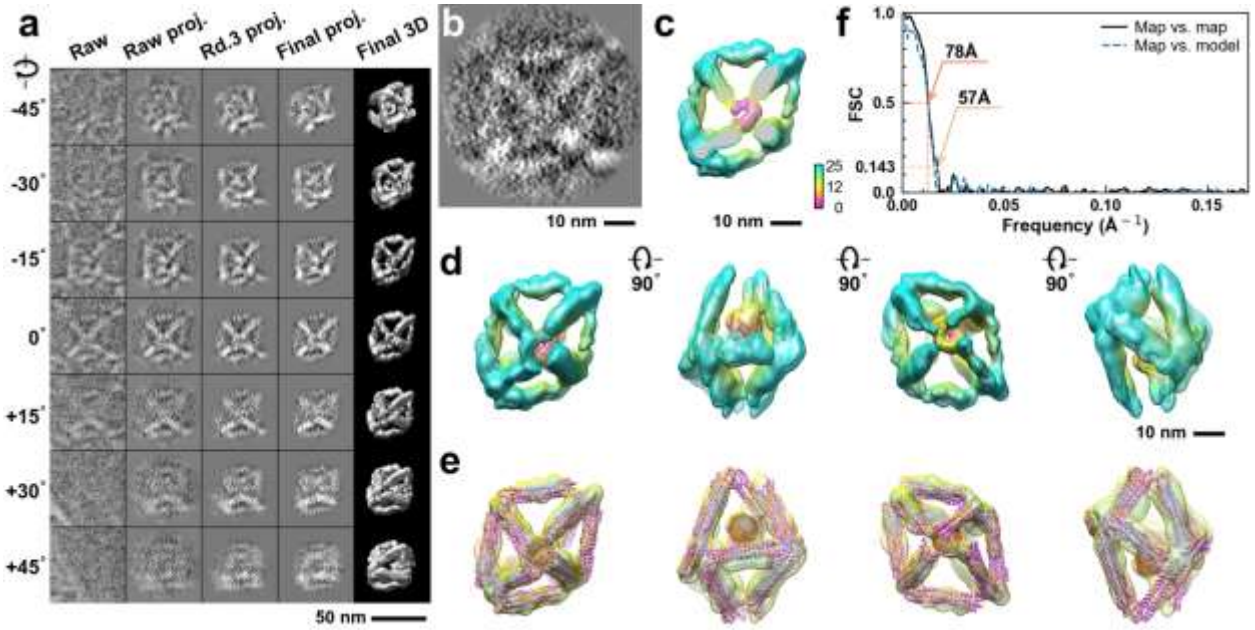

Supplementary Fig. 212: IPET 3D reconstruction and model fitting of an individual unit-cell particle (Index: 204) within a 2D lattice with 70% ferritin loading. a, Seven representative tilt images of a single unit-cell particle are shown in the first column (from left). The tilt images are aligned to a common center using IPET through iterative refinement. The projections of the raw, intermediate, and final 3D reconstruction at the corresponding angles are displayed in the subsequent four columns. **b**, A central cross-section (~23 nm thick) of the final reconstruction before masking is applied. **c**, 3D views of the central cross-section. **d**, Final 3D density map of this particle, viewed from four perpendicular directions. **e**, Final 3D reconstruction superimposed with the fitted model, viewed from four perpendicular directions. **f**, FSC analyses of the final map resolution using two methods: map-map FSC, where each map is reconstructed from one half of the images (even vs. odd tilt angle indices), and map-model FSC, where the model map is generated from the fitted model. Resolution assessments are provided based on tilt-based map-map and map-model FSC analyses at thresholds of FSC=0.5 and 0.143, respectively.

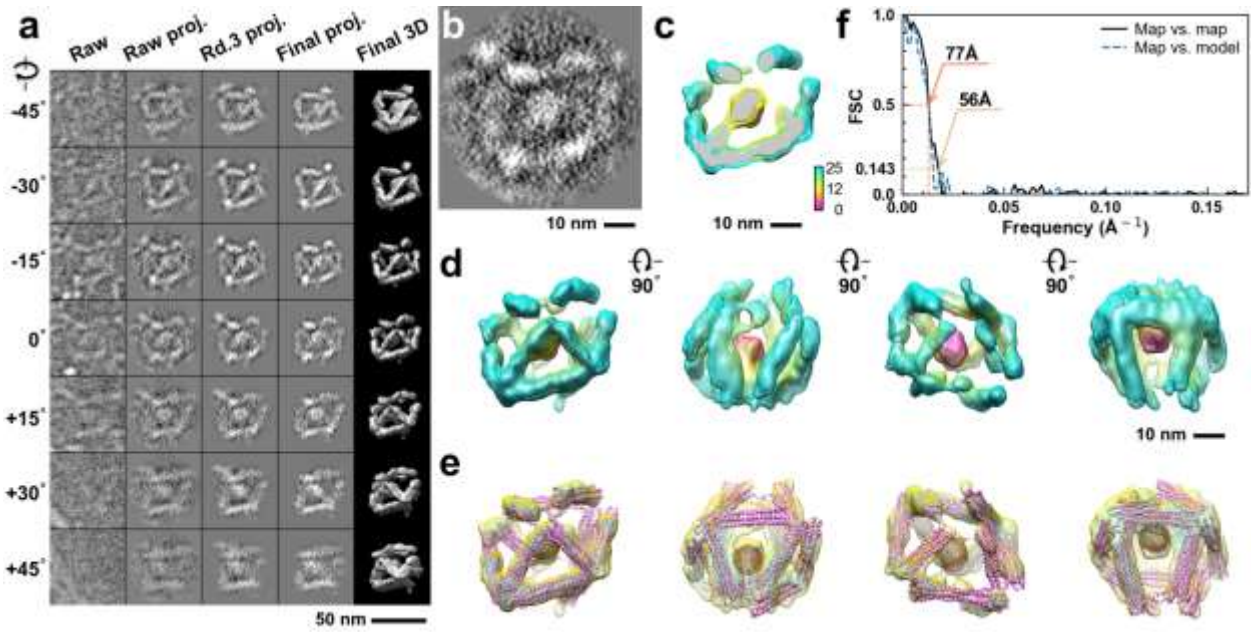

Supplementary Fig. 213: IPET 3D reconstruction and model fitting of an individual unit-cell particle (Index: 205) within a 2D lattice with 70% ferritin loading. a, Seven representative tilt images of a single unit-cell particle are shown in the first column (from left). The tilt images are aligned to a common center using IPET through iterative refinement. The projections of the raw, intermediate, and final 3D reconstruction at the corresponding angles are displayed in the subsequent four columns. **b**, A central cross-section (~23 nm thick) of the final reconstruction before masking is applied. **c**, 3D views of the central cross-section. **d**, Final 3D density map of this particle, viewed from four perpendicular directions. **e**, Final 3D reconstruction superimposed with the fitted model, viewed from four perpendicular directions. **f**, FSC analyses of the final map resolution using two methods: map-map FSC, where each map is reconstructed from one half of the images (even vs. odd tilt angle indices), and map-model FSC, where the model map is generated from the fitted model. Resolution assessments are provided based on tilt-based map-map and map-model FSC analyses at thresholds of FSC=0.5 and 0.143, respectively.

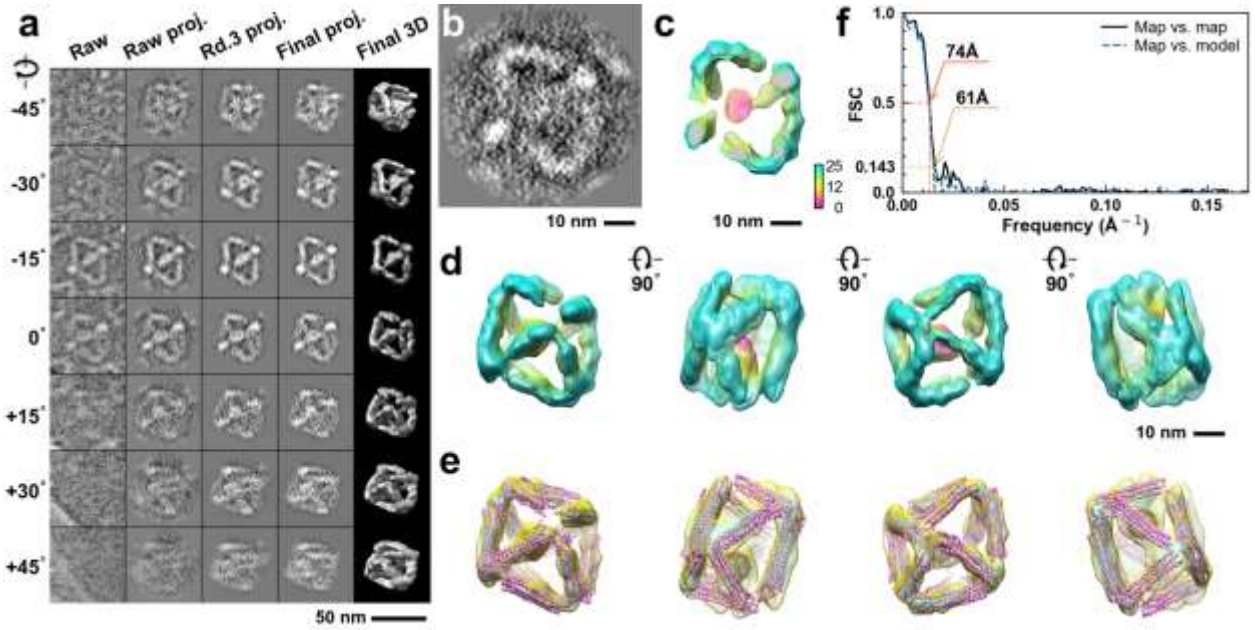

Supplementary Fig. 214: IPET 3D reconstruction and model fitting of an individual unit-cell particle (Index: 206) within a 2D lattice with 70% ferritin loading. a, Seven representative tilt images of a single unit-cell particle are shown in the first column (from left). The tilt images are aligned to a common center using IPET through iterative refinement. The projections of the raw, intermediate, and final 3D reconstruction at the corresponding angles are displayed in the subsequent four columns. **b**, A central cross-section (~23 nm thick) of the final reconstruction before masking is applied. **c**, 3D views of the central cross-section. **d**, Final 3D density map of this particle, viewed from four perpendicular directions. **e**, Final 3D reconstruction superimposed with the fitted model, viewed from four perpendicular directions. **f**, FSC analyses of the final map resolution using two methods: map-map FSC, where each map is reconstructed from one half of the images (even vs. odd tilt angle indices), and map-model FSC, where the model map is generated from the fitted model. Resolution assessments are provided based on tilt-based map-map and map-model FSC analyses at thresholds of FSC=0.5 and 0.143, respectively.

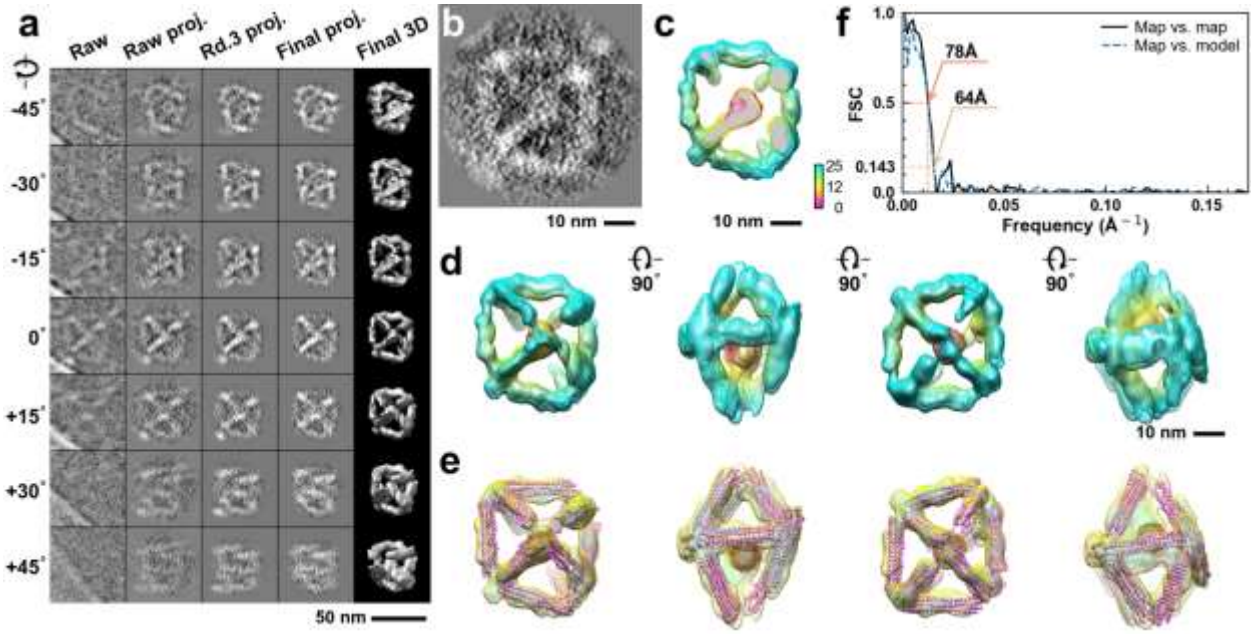

Supplementary Fig. 215: IPET 3D reconstruction and model fitting of an individual unit-cell particle (Index: 207) within a 2D lattice with 70% ferritin loading. a, Seven representative tilt images of a single unit-cell particle are shown in the first column (from left). The tilt images are aligned to a common center using IPET through iterative refinement. The projections of the raw, intermediate, and final 3D reconstruction at the corresponding angles are displayed in the subsequent four columns. **b**, A central cross-section (~23 nm thick) of the final reconstruction before masking is applied. **c**, 3D views of the central cross-section. **d**, Final 3D density map of this particle, viewed from four perpendicular directions. **e**, Final 3D reconstruction superimposed with the fitted model, viewed from four perpendicular directions. **f**, FSC analyses of the final map resolution using two methods: map-map FSC, where each map is reconstructed from one half of the images (even vs. odd tilt angle indices), and map-model FSC, where the model map is generated from the fitted model. Resolution assessments are provided based on tilt-based map-map and map-model FSC analyses at thresholds of FSC=0.5 and 0.143, respectively.

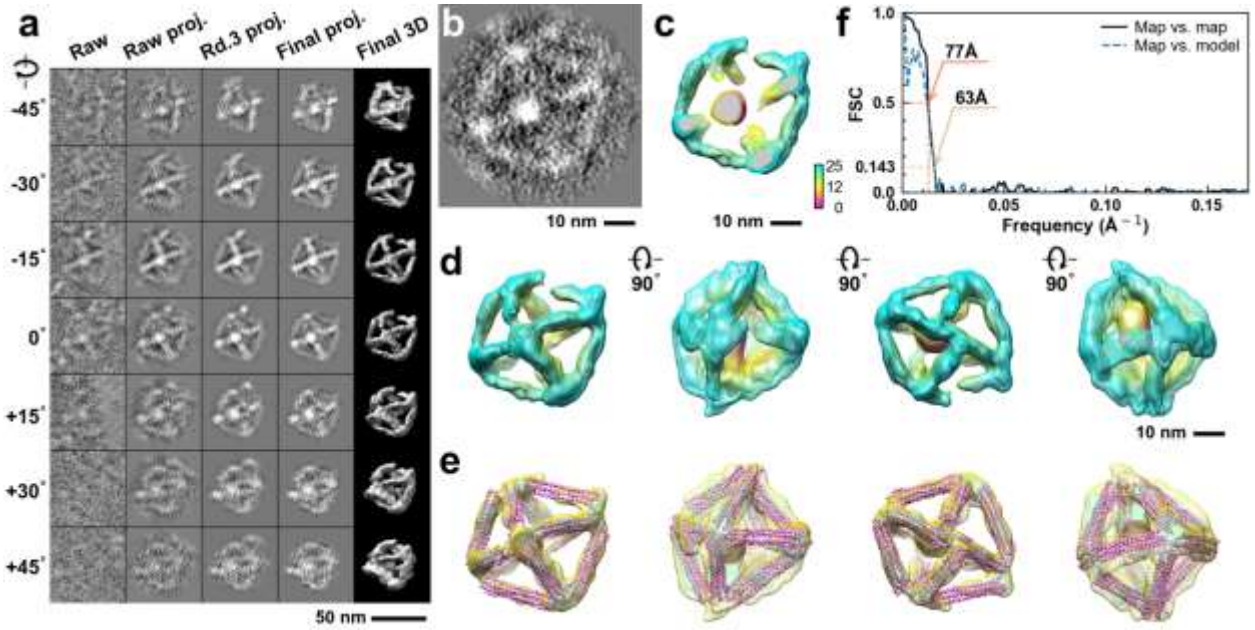

Supplementary Fig. 216: IPET 3D reconstruction and model fitting of an individual unit-cell particle (Index: 208) within a 2D lattice with 70% ferritin loading. a, Seven representative tilt images of a single unit-cell particle are shown in the first column (from left). The tilt images are aligned to a common center using IPET through iterative refinement. The projections of the raw, intermediate, and final 3D reconstruction at the corresponding angles are displayed in the subsequent four columns. **b**, A central cross-section (~23 nm thick) of the final reconstruction before masking is applied. **c**, 3D views of the central cross-section. **d**, Final 3D density map of this particle, viewed from four perpendicular directions. **e**, Final 3D reconstruction superimposed with the fitted model, viewed from four perpendicular directions. **f**, FSC analyses of the final map resolution using two methods: map-map FSC, where each map is reconstructed from one half of the images (even vs. odd tilt angle indices), and map-model FSC, where the model map is generated from the fitted model. Resolution assessments are provided based on tilt-based map-map and map-model FSC analyses at thresholds of FSC=0.5 and 0.143, respectively.

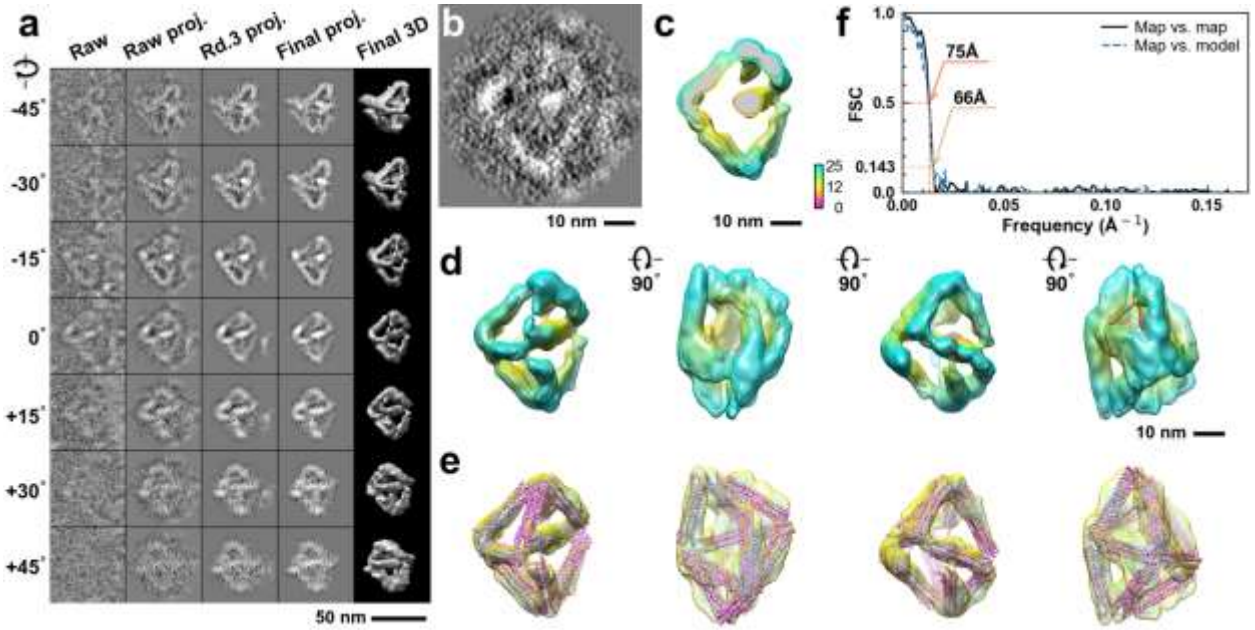

Supplementary Fig. 217: IPET 3D reconstruction and model fitting of an individual unit-cell particle (Index: 209) within a 2D lattice with 70% ferritin loading. a, Seven representative tilt images of a single unit-cell particle are shown in the first column (from left). The tilt images are aligned to a common center using IPET through iterative refinement. The projections of the raw, intermediate, and final 3D reconstruction at the corresponding angles are displayed in the subsequent four columns. **b**, A central cross-section (~23 nm thick) of the final reconstruction before masking is applied. **c**, 3D views of the central cross-section. **d**, Final 3D density map of this particle, viewed from four perpendicular directions. **e**, Final 3D reconstruction superimposed with the fitted model, viewed from four perpendicular directions. **f**, FSC analyses of the final map resolution using two methods: map-map FSC, where each map is reconstructed from one half of the images (even vs. odd tilt angle indices), and map-model FSC, where the model map is generated from the fitted model. Resolution assessments are provided based on tilt-based map-map and map-model FSC analyses at thresholds of FSC=0.5 and 0.143, respectively.

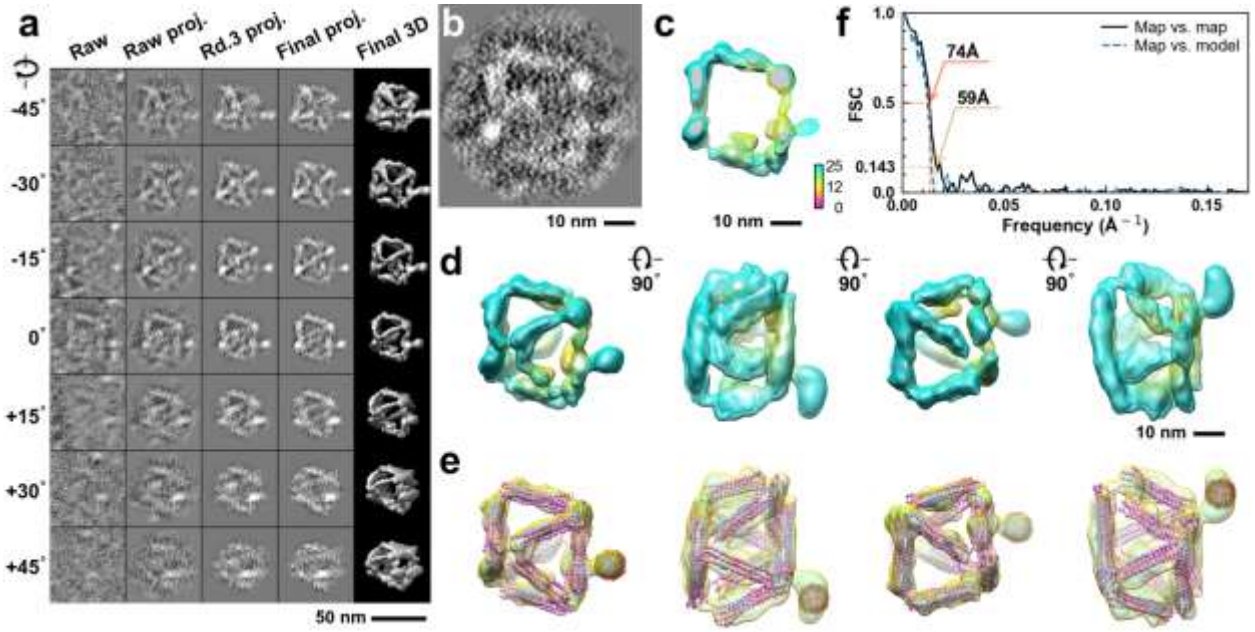

Supplementary Fig. 218: IPET 3D reconstruction and model fitting of an individual unit-cell particle (Index: 210) within a 2D lattice with 70% ferritin loading. a, Seven representative tilt images of a single unit-cell particle are shown in the first column (from left). The tilt images are aligned to a common center using IPET through iterative refinement. The projections of the raw, intermediate, and final 3D reconstruction at the corresponding angles are displayed in the subsequent four columns. **b**, A central cross-section (~23 nm thick) of the final reconstruction before masking is applied. **c**, 3D views of the central cross-section. **d**, Final 3D density map of this particle, viewed from four perpendicular directions. **e**, Final 3D reconstruction superimposed with the fitted model, viewed from four perpendicular directions. **f**, FSC analyses of the final map resolution using two methods: map-map FSC, where each map is reconstructed from one half of the images (even vs. odd tilt angle indices), and map-model FSC, where the model map is generated from the fitted model. Resolution assessments are provided based on tilt-based map-map and map-model FSC analyses at thresholds of FSC=0.5 and 0.143, respectively.

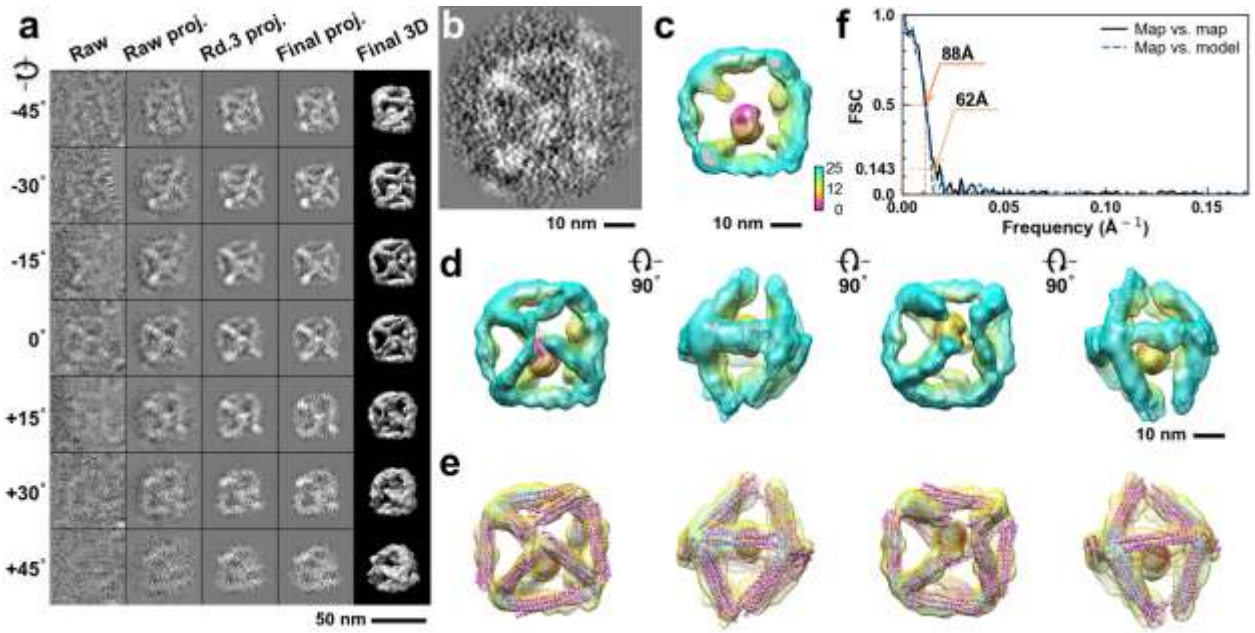

Supplementary Fig. 219: IPET 3D reconstruction and model fitting of an individual unit-cell particle (Index: 211) within a 2D lattice with 70% ferritin loading. a, Seven representative tilt images of a single unit-cell particle are shown in the first column (from left). The tilt images are aligned to a common center using IPET through iterative refinement. The projections of the raw, intermediate, and final 3D reconstruction at the corresponding angles are displayed in the subsequent four columns. **b**, A central cross-section (~23 nm thick) of the final reconstruction before masking is applied. **c**, 3D views of the central cross-section. **d**, Final 3D density map of this particle, viewed from four perpendicular directions. **e**, Final 3D reconstruction superimposed with the fitted model, viewed from four perpendicular directions. **f**, FSC analyses of the final map resolution using two methods: map-map FSC, where each map is reconstructed from one half of the images (even vs. odd tilt angle indices), and map-model FSC, where the model map is generated from the fitted model. Resolution assessments are provided based on tilt-based map-map and map-model FSC analyses at thresholds of FSC=0.5 and 0.143, respectively.

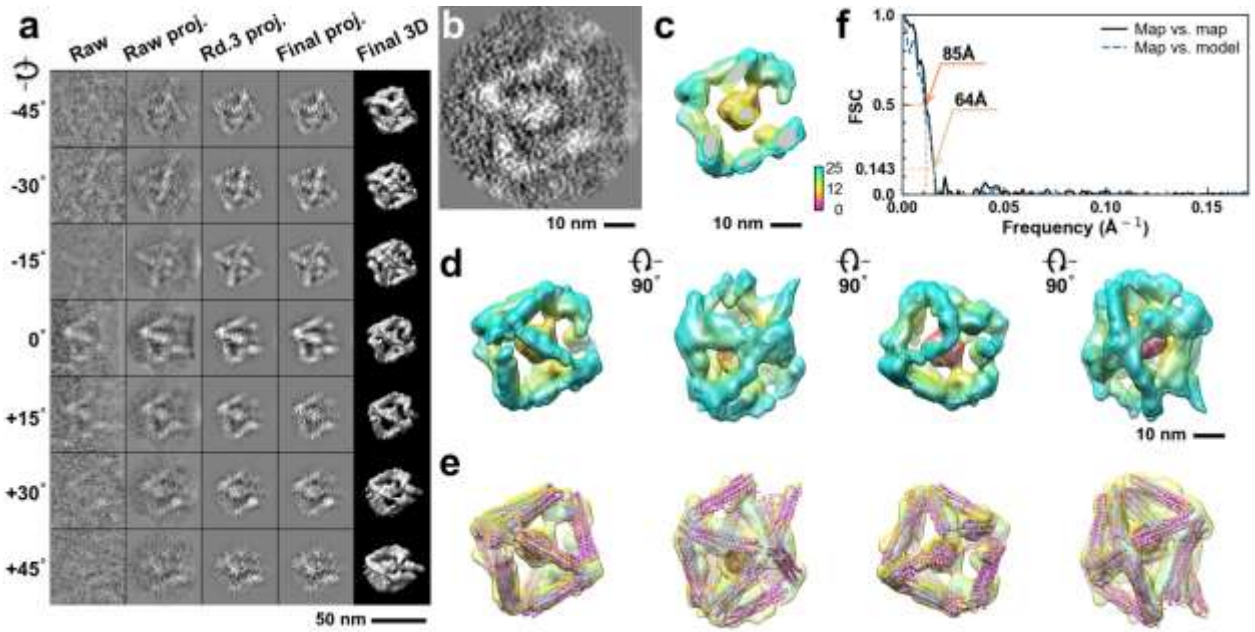

Supplementary Fig. 220: IPET 3D reconstruction and model fitting of an individual unit-cell particle (Index: 212) within a 2D lattice with 70% ferritin loading. a, Seven representative tilt images of a single unit-cell particle are shown in the first column (from left). The tilt images are aligned to a common center using IPET through iterative refinement. The projections of the raw, intermediate, and final 3D reconstruction at the corresponding angles are displayed in the subsequent four columns. **b**, A central cross-section (~23 nm thick) of the final reconstruction before masking is applied. **c**, 3D views of the central cross-section. **d**, Final 3D density map of this particle, viewed from four perpendicular directions. **e**, Final 3D reconstruction superimposed with the fitted model, viewed from four perpendicular directions. **f**, FSC analyses of the final map resolution using two methods: map-map FSC, where each map is reconstructed from one half of the images (even vs. odd tilt angle indices), and map-model FSC, where the model map is generated from the fitted model. Resolution assessments are provided based on tilt-based map-map and map-model FSC analyses at thresholds of FSC=0.5 and 0.143, respectively.

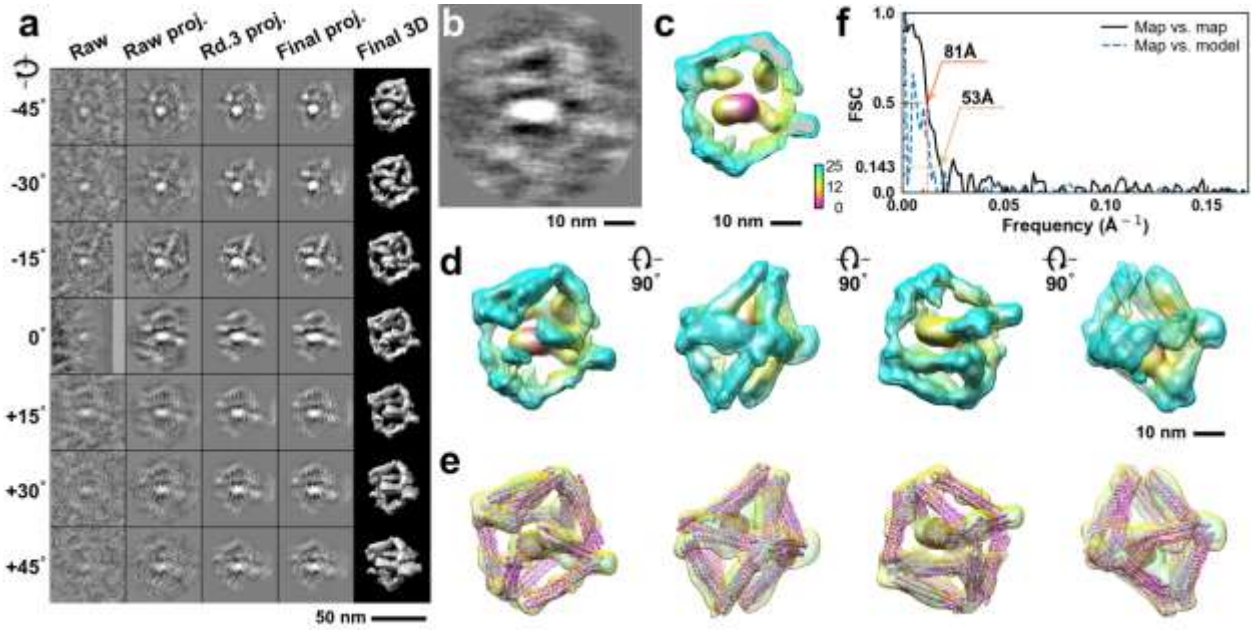

Supplementary Fig. 221: IPET 3D reconstruction and model fitting of an individual unit-cell particle (Index: 213) within a 2D lattice with 70% ferritin loading. a, Seven representative tilt images of a single unit-cell particle are shown in the first column (from left). The tilt images are aligned to a common center using IPET through iterative refinement. The projections of the raw, intermediate, and final 3D reconstruction at the corresponding angles are displayed in the subsequent four columns. **b**, A central cross-section (~23 nm thick) of the final reconstruction before masking is applied. **c**, 3D views of the central cross-section. **d**, Final 3D density map of this particle, viewed from four perpendicular directions. **e**, Final 3D reconstruction superimposed with the fitted model, viewed from four perpendicular directions. **f**, FSC analyses of the final map resolution using two methods: map-map FSC, where each map is reconstructed from one half of the images (even vs. odd tilt angle indices), and map-model FSC, where the model map is generated from the fitted model. Resolution assessments are provided based on tilt-based map-map and map-model FSC analyses at thresholds of FSC=0.5 and 0.143, respectively.

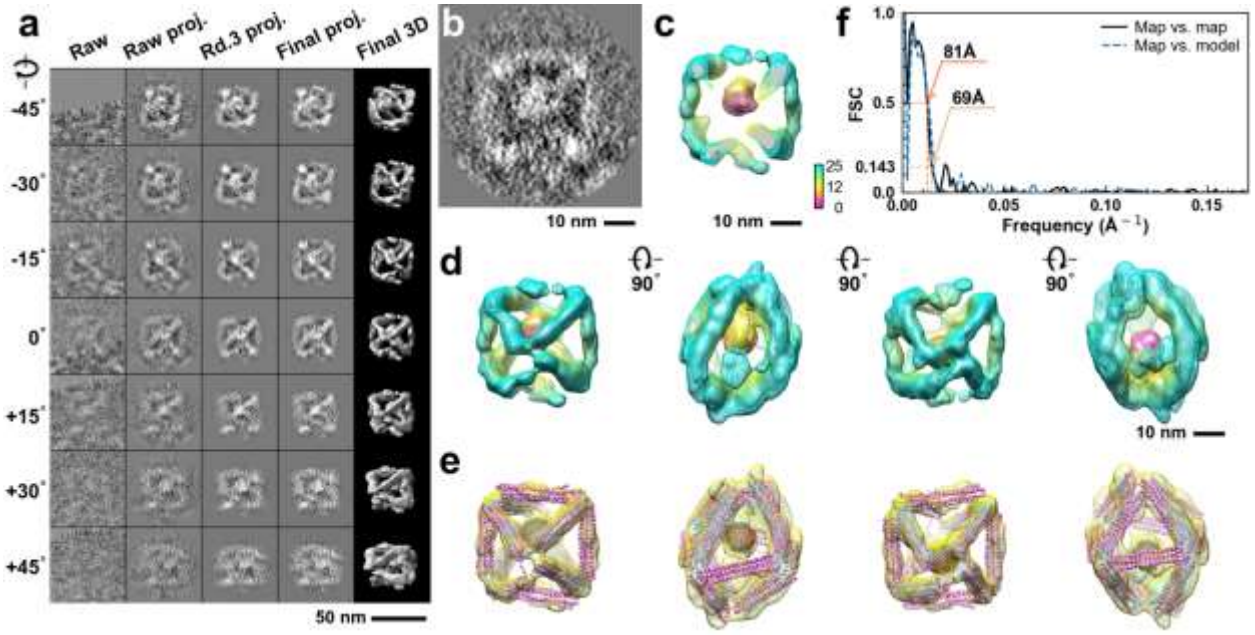

Supplementary Fig. 222: IPET 3D reconstruction and model fitting of an individual unit-cell particle (Index: 214) within a 2D lattice with 70% ferritin loading. a, Seven representative tilt images of a single unit-cell particle are shown in the first column (from left). The tilt images are aligned to a common center using IPET through iterative refinement. The projections of the raw, intermediate, and final 3D reconstruction at the corresponding angles are displayed in the subsequent four columns. **b**, A central cross-section (~23 nm thick) of the final reconstruction before masking is applied. **c**, 3D views of the central cross-section. **d**, Final 3D density map of this particle, viewed from four perpendicular directions. **e**, Final 3D reconstruction superimposed with the fitted model, viewed from four perpendicular directions. **f**, FSC analyses of the final map resolution using two methods: map-map FSC, where each map is reconstructed from one half of the images (even vs. odd tilt angle indices), and map-model FSC, where the model map is generated from the fitted model. Resolution assessments are provided based on tilt-based map-map and map-model FSC analyses at thresholds of FSC=0.5 and 0.143, respectively.

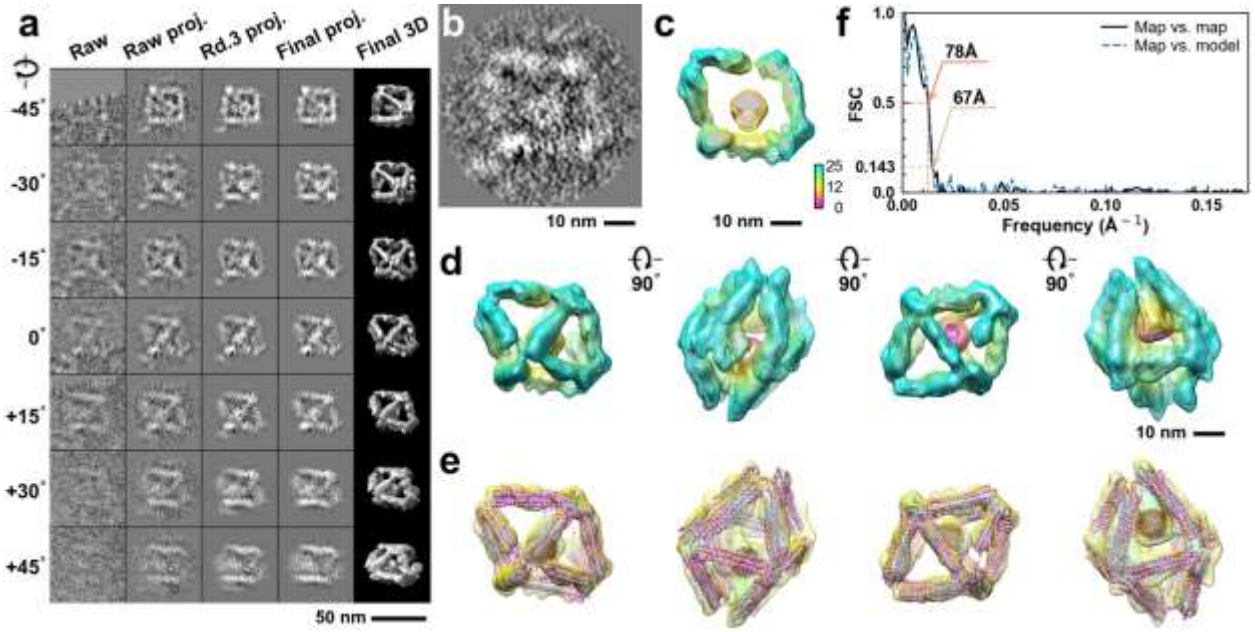

Supplementary Fig. 223: IPET 3D reconstruction and model fitting of an individual unit-cell particle (Index: 215) within a 2D lattice with 70% ferritin loading. a, Seven representative tilt images of a single unit-cell particle are shown in the first column (from left). The tilt images are aligned to a common center using IPET through iterative refinement. The projections of the raw, intermediate, and final 3D reconstruction at the corresponding angles are displayed in the subsequent four columns. **b**, A central cross-section (~23 nm thick) of the final reconstruction before masking is applied. **c**, 3D views of the central cross-section. **d**, Final 3D density map of this particle, viewed from four perpendicular directions. **e**, Final 3D reconstruction superimposed with the fitted model, viewed from four perpendicular directions. **f**, FSC analyses of the final map resolution using two methods: map-map FSC, where each map is reconstructed from one half of the images (even vs. odd tilt angle indices), and map-model FSC, where the model map is generated from the fitted model. Resolution assessments are provided based on tilt-based map-map and map-model FSC analyses at thresholds of FSC=0.5 and 0.143, respectively.

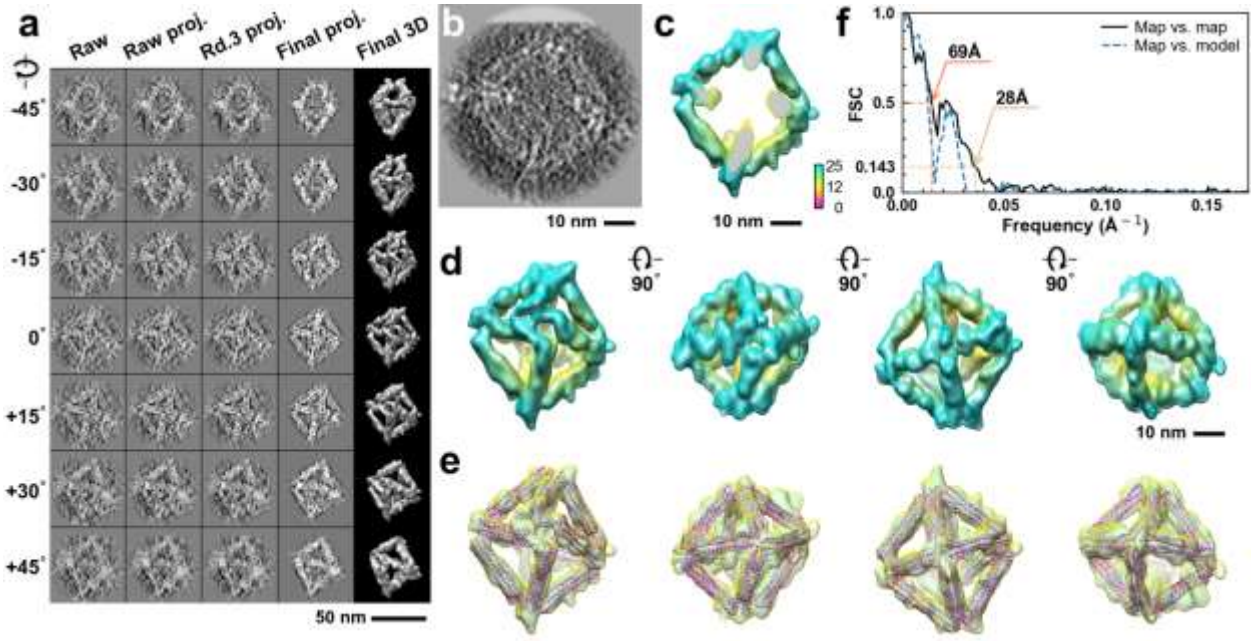

Supplementary Fig. 224: IPET 3D reconstruction and model fitting of an individual unit-cell particle (Index: 216) within a 2D lattice with 0% ferritin loading. a, Seven representative tilt images of a single unit-cell particle are shown in the first column (from left). The tilt images are aligned to a common center using IPET through iterative refinement. The projections of the raw, intermediate, and final 3D reconstruction at the corresponding angles are displayed in the subsequent four columns. **b**, A central cross-section (~23 nm thick) of the final reconstruction before masking is applied. **c**, 3D views of the central cross-section. **d**, Final 3D density map of this particle, viewed from four perpendicular directions. **e**, Final 3D reconstruction superimposed with the fitted model, viewed from four perpendicular directions. **f**, FSC analyses of the final map resolution using two methods: map-map FSC, where each map is reconstructed from one half of the images (even vs. odd tilt angle indices), and map-model FSC, where the model map is generated from the fitted model. Resolution assessments are provided based on tilt-based map-map and map-model FSC analyses at thresholds of FSC=0.5 and 0.143, respectively.

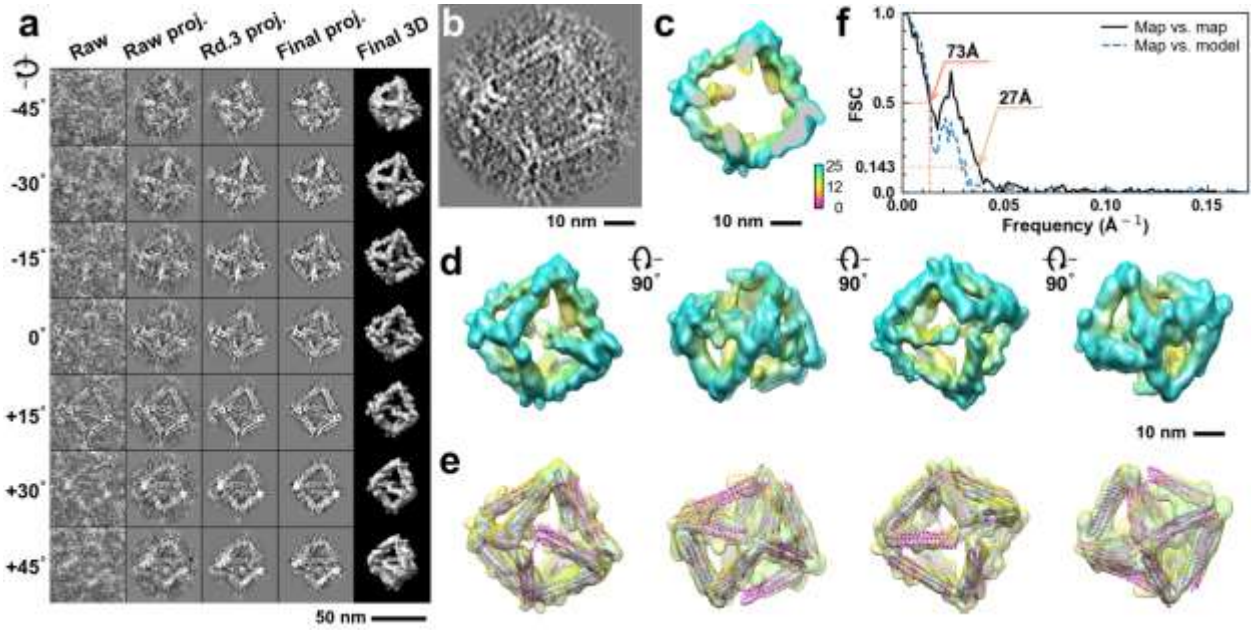

Supplementary Fig. 225: IPET 3D reconstruction and model fitting of an individual unit-cell particle (Index: 217) within a 2D lattice with 0% ferritin loading. a, Seven representative tilt images of a single unit-cell particle are shown in the first column (from left). The tilt images are aligned to a common center using IPET through iterative refinement. The projections of the raw, intermediate, and final 3D reconstruction at the corresponding angles are displayed in the subsequent four columns. **b**, A central cross-section (~23 nm thick) of the final reconstruction before masking is applied. **c**, 3D views of the central cross-section. **d**, Final 3D density map of this particle, viewed from four perpendicular directions. **e**, Final 3D reconstruction superimposed with the fitted model, viewed from four perpendicular directions. **f**, FSC analyses of the final map resolution using two methods: map-map FSC, where each map is reconstructed from one half of the images (even vs. odd tilt angle indices), and map-model FSC, where the model map is generated from the fitted model. Resolution assessments are provided based on tilt-based map-map and map-model FSC analyses at thresholds of FSC=0.5 and 0.143, respectively.

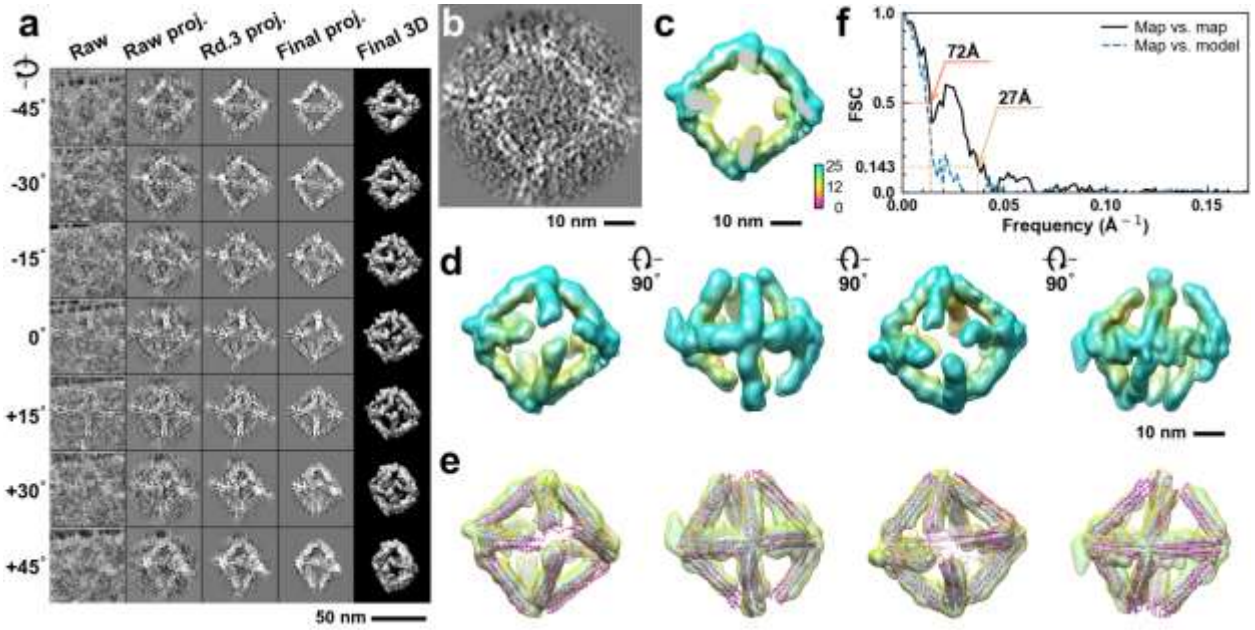

Supplementary Fig. 226: IPET 3D reconstruction and model fitting of an individual unit-cell particle (Index: 218) within a 2D lattice with 0% ferritin loading. a, Seven representative tilt images of a single unit-cell particle are shown in the first column (from left). The tilt images are aligned to a common center using IPET through iterative refinement. The projections of the raw, intermediate, and final 3D reconstruction at the corresponding angles are displayed in the subsequent four columns. **b**, A central cross-section (~23 nm thick) of the final reconstruction before masking is applied. **c**, 3D views of the central cross-section. **d**, Final 3D density map of this particle, viewed from four perpendicular directions. **e**, Final 3D reconstruction superimposed with the fitted model, viewed from four perpendicular directions. **f**, FSC analyses of the final map resolution using two methods: map-map FSC, where each map is reconstructed from one half of the images (even vs. odd tilt angle indices), and map-model FSC, where the model map is generated from the fitted model. Resolution assessments are provided based on tilt-based map-map and map-model FSC analyses at thresholds of FSC=0.5 and 0.143, respectively.

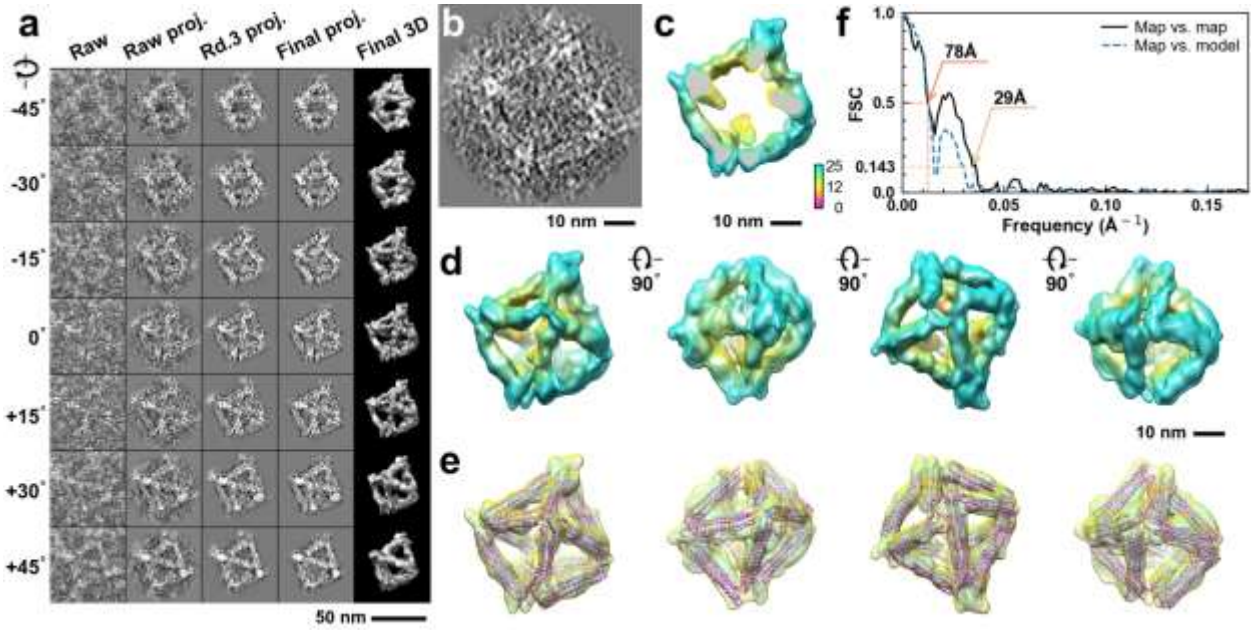

Supplementary Fig. 227: IPET 3D reconstruction and model fitting of an individual unit-cell particle (Index: 219) within a 2D lattice with 0% ferritin loading. a, Seven representative tilt images of a single unit-cell particle are shown in the first column (from left). The tilt images are aligned to a common center using IPET through iterative refinement. The projections of the raw, intermediate, and final 3D reconstruction at the corresponding angles are displayed in the subsequent four columns. **b**, A central cross-section (~23 nm thick) of the final reconstruction before masking is applied. **c**, 3D views of the central cross-section. **d**, Final 3D density map of this particle, viewed from four perpendicular directions. **e**, Final 3D reconstruction superimposed with the fitted model, viewed from four perpendicular directions. **f**, FSC analyses of the final map resolution using two methods: map-map FSC, where each map is reconstructed from one half of the images (even vs. odd tilt angle indices), and map-model FSC, where the model map is generated from the fitted model. Resolution assessments are provided based on tilt-based map-map and map-model FSC analyses at thresholds of FSC=0.5 and 0.143, respectively.

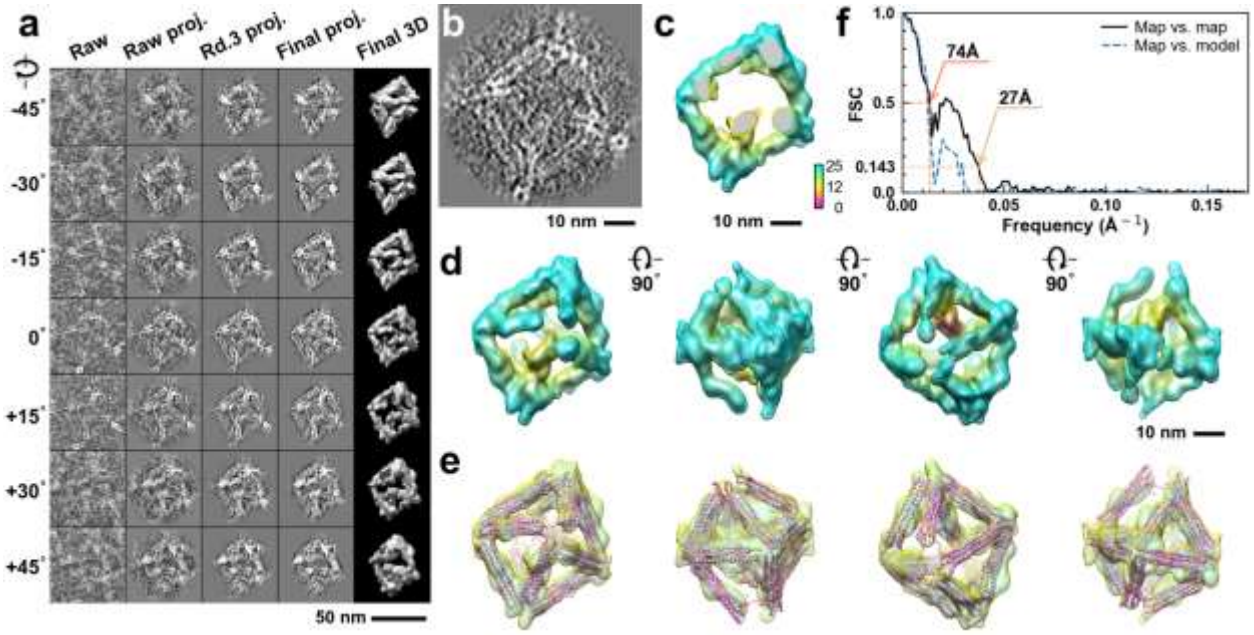

Supplementary Fig. 228: IPET 3D reconstruction and model fitting of an individual unit-cell particle (Index: 220) within a 2D lattice with 0% ferritin loading. a, Seven representative tilt images of a single unit-cell particle are shown in the first column (from left). The tilt images are aligned to a common center using IPET through iterative refinement. The projections of the raw, intermediate, and final 3D reconstruction at the corresponding angles are displayed in the subsequent four columns. **b**, A central cross-section (~23 nm thick) of the final reconstruction before masking is applied. **c**, 3D views of the central cross-section. **d**, Final 3D density map of this particle, viewed from four perpendicular directions. **e**, Final 3D reconstruction superimposed with the fitted model, viewed from four perpendicular directions. **f**, FSC analyses of the final map resolution using two methods: map-map FSC, where each map is reconstructed from one half of the images (even vs. odd tilt angle indices), and map-model FSC, where the model map is generated from the fitted model. Resolution assessments are provided based on tilt-based map-map and map-model FSC analyses at thresholds of FSC=0.5 and 0.143, respectively.

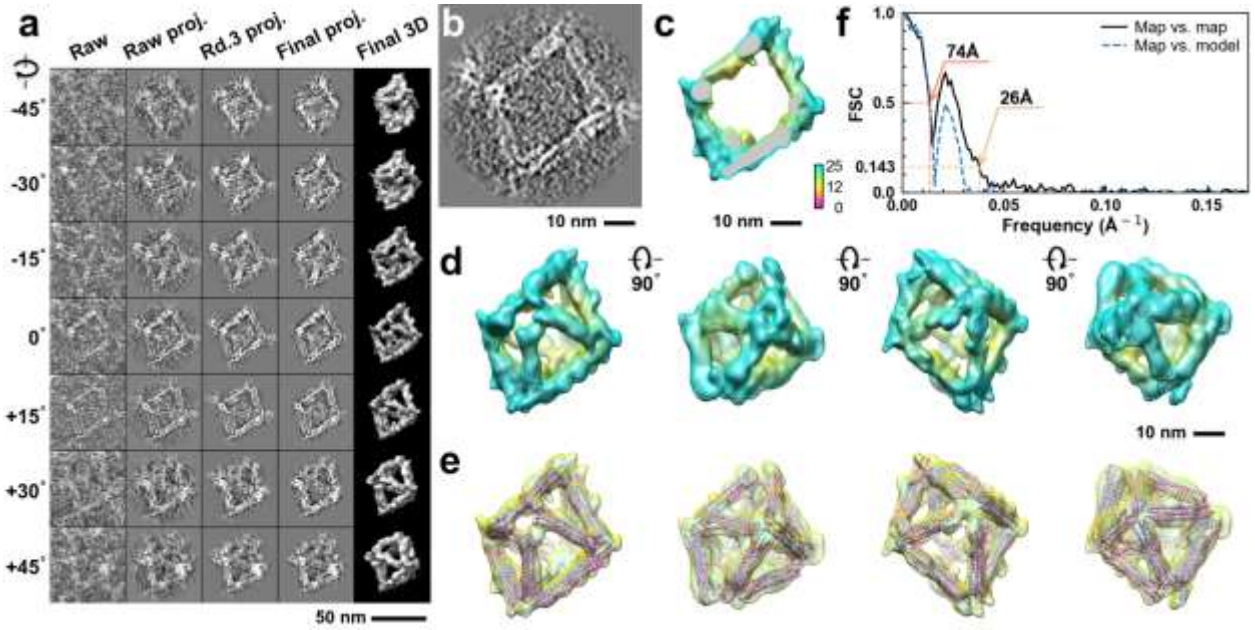

Supplementary Fig. 229: IPET 3D reconstruction and model fitting of an individual unit-cell particle (Index: 221) within a 2D lattice with 0% ferritin loading. a, Seven representative tilt images of a single unit-cell particle are shown in the first column (from left). The tilt images are aligned to a common center using IPET through iterative refinement. The projections of the raw, intermediate, and final 3D reconstruction at the corresponding angles are displayed in the subsequent four columns. **b**, A central cross-section (~23 nm thick) of the final reconstruction before masking is applied. **c**, 3D views of the central cross-section. **d**, Final 3D density map of this particle, viewed from four perpendicular directions. **e**, Final 3D reconstruction superimposed with the fitted model, viewed from four perpendicular directions. **f**, FSC analyses of the final map resolution using two methods: map-map FSC, where each map is reconstructed from one half of the images (even vs. odd tilt angle indices), and map-model FSC, where the model map is generated from the fitted model. Resolution assessments are provided based on tilt-based map-map and map-model FSC analyses at thresholds of FSC=0.5 and 0.143, respectively.

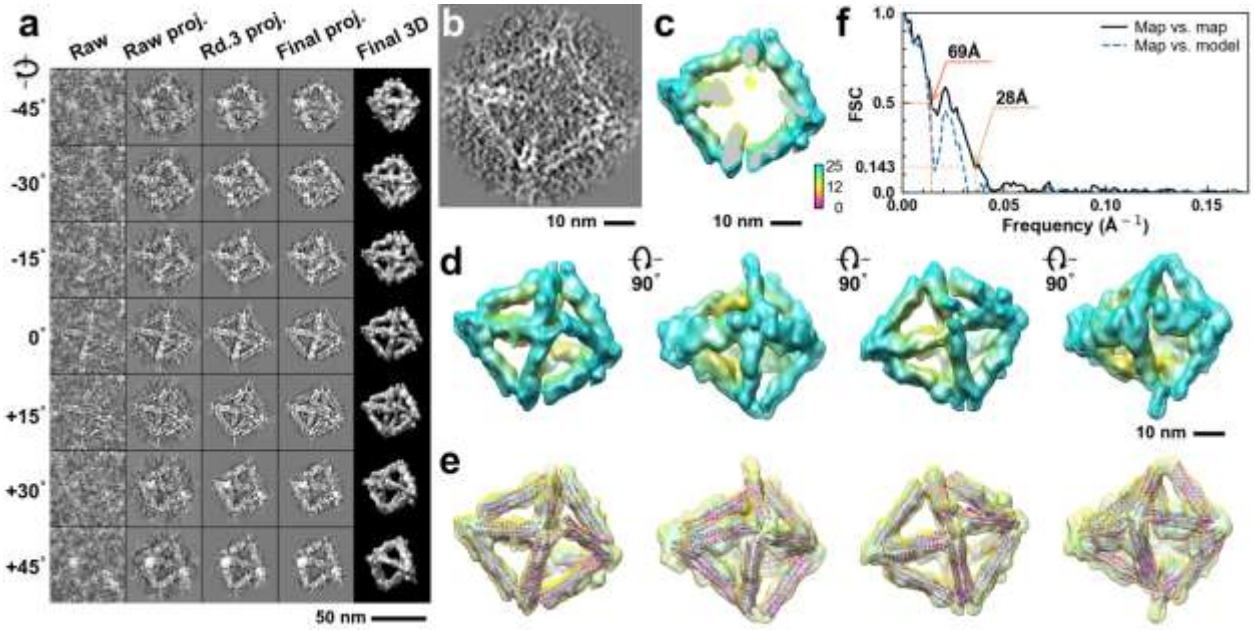

Supplementary Fig. 230: IPET 3D reconstruction and model fitting of an individual unit-cell particle (Index: 222) within a 2D lattice with 0% ferritin loading. a, Seven representative tilt images of a single unit-cell particle are shown in the first column (from left). The tilt images are aligned to a common center using IPET through iterative refinement. The projections of the raw, intermediate, and final 3D reconstruction at the corresponding angles are displayed in the subsequent four columns. **b**, A central cross-section (~23 nm thick) of the final reconstruction before masking is applied. **c**, 3D views of the central cross-section. **d**, Final 3D density map of this particle, viewed from four perpendicular directions. **e**, Final 3D reconstruction superimposed with the fitted model, viewed from four perpendicular directions. **f**, FSC analyses of the final map resolution using two methods: map-map FSC, where each map is reconstructed from one half of the images (even vs. odd tilt angle indices), and map-model FSC, where the model map is generated from the fitted model. Resolution assessments are provided based on tilt-based map-map and map-model FSC analyses at thresholds of FSC=0.5 and 0.143, respectively.

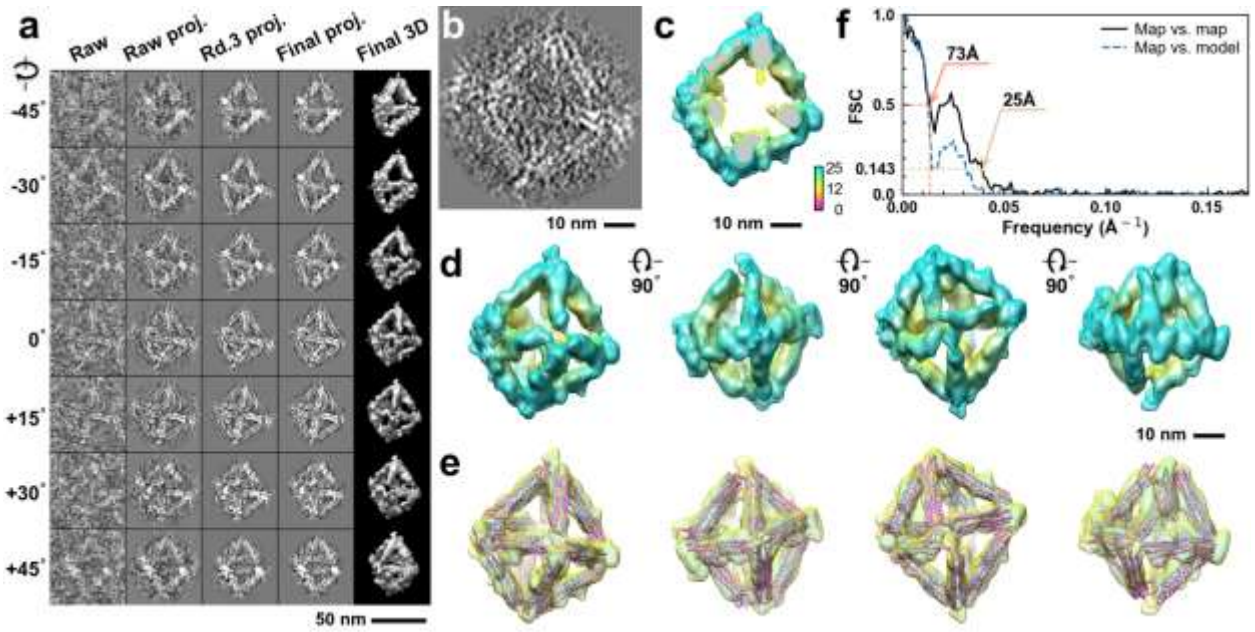

Supplementary Fig. 231: IPET 3D reconstruction and model fitting of an individual unit-cell particle (Index: 223) within a 2D lattice with 0% ferritin loading. a, Seven representative tilt images of a single unit-cell particle are shown in the first column (from left). The tilt images are aligned to a common center using IPET through iterative refinement. The projections of the raw, intermediate, and final 3D reconstruction at the corresponding angles are displayed in the subsequent four columns. **b**, A central cross-section (~23 nm thick) of the final reconstruction before masking is applied. **c**, 3D views of the central cross-section. **d**, Final 3D density map of this particle, viewed from four perpendicular directions. **e**, Final 3D reconstruction superimposed with the fitted model, viewed from four perpendicular directions. **f**, FSC analyses of the final map resolution using two methods: map-map FSC, where each map is reconstructed from one half of the images (even vs. odd tilt angle indices), and map-model FSC, where the model map is generated from the fitted model. Resolution assessments are provided based on tilt-based map-map and map-model FSC analyses at thresholds of FSC=0.5 and 0.143, respectively.

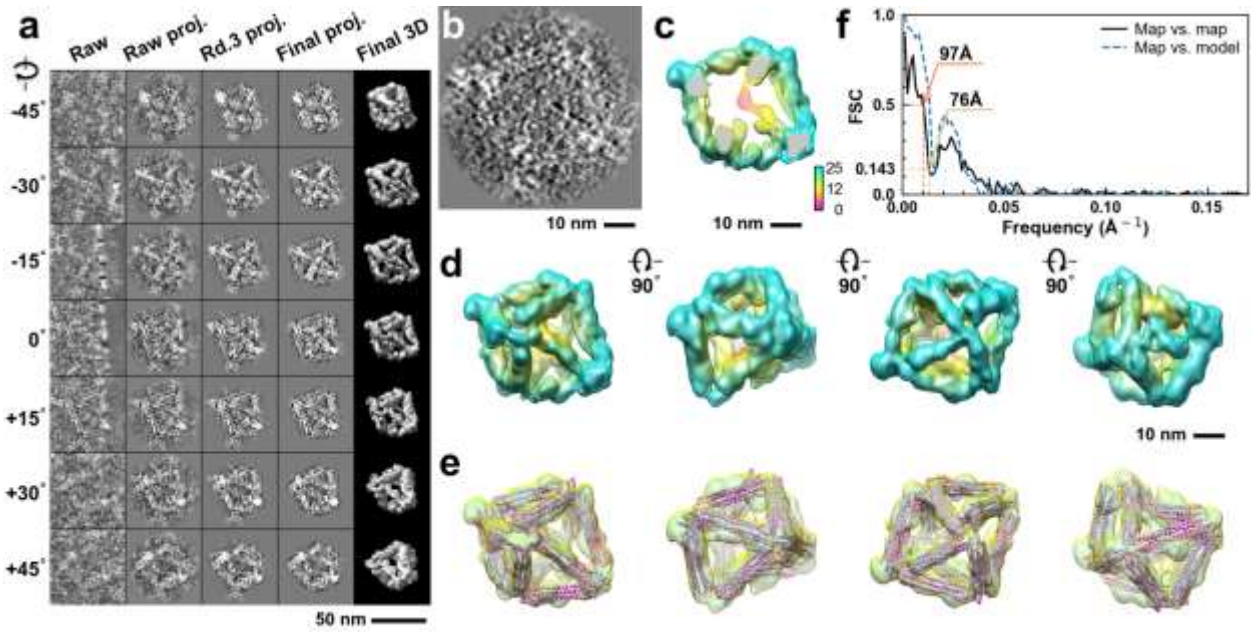

Supplementary Fig. 232: IPET 3D reconstruction and model fitting of an individual unit-cell particle (Index: 224) within a 2D lattice with 0% ferritin loading. a, Seven representative tilt images of a single unit-cell particle are shown in the first column (from left). The tilt images are aligned to a common center using IPET through iterative refinement. The projections of the raw, intermediate, and final 3D reconstruction at the corresponding angles are displayed in the subsequent four columns. **b**, A central cross-section (~23 nm thick) of the final reconstruction before masking is applied. **c**, 3D views of the central cross-section. **d**, Final 3D density map of this particle, viewed from four perpendicular directions. **e**, Final 3D reconstruction superimposed with the fitted model, viewed from four perpendicular directions. **f**, FSC analyses of the final map resolution using two methods: map-map FSC, where each map is reconstructed from one half of the images (even vs. odd tilt angle indices), and map-model FSC, where the model map is generated from the fitted model. Resolution assessments are provided based on tilt-based map-map and map-model FSC analyses at thresholds of FSC=0.5 and 0.143, respectively.

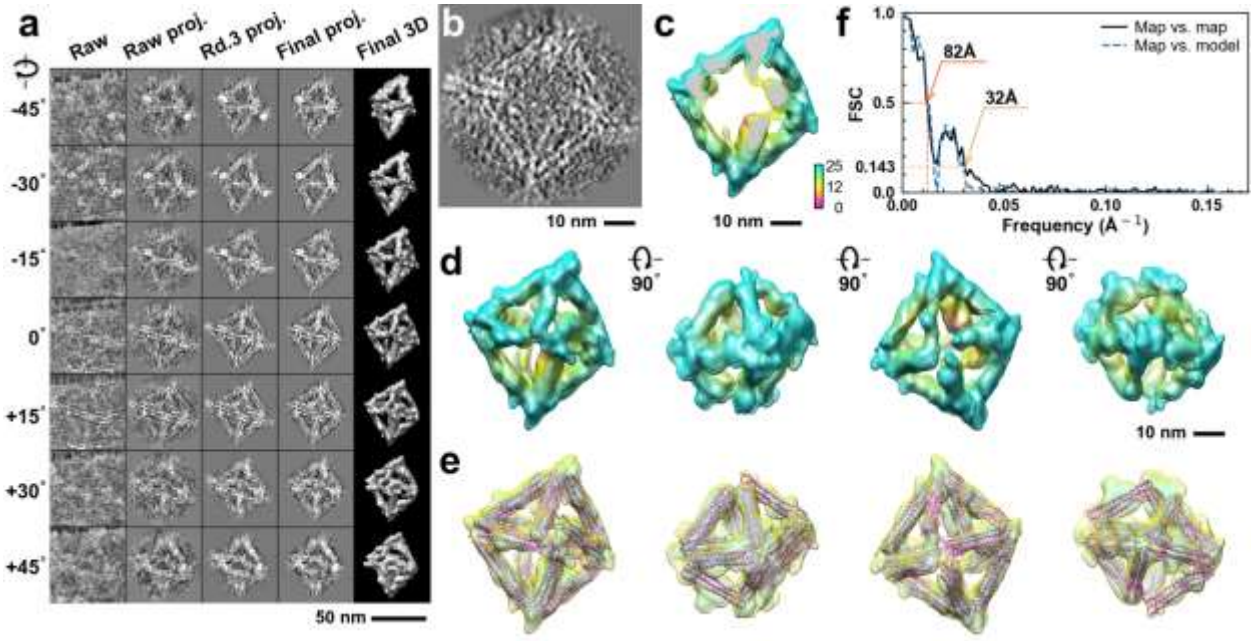

Supplementary Fig. 233: IPET 3D reconstruction and model fitting of an individual unit-cell particle (Index: 225) within a 2D lattice with 0% ferritin loading. a, Seven representative tilt images of a single unit-cell particle are shown in the first column (from left). The tilt images are aligned to a common center using IPET through iterative refinement. The projections of the raw, intermediate, and final 3D reconstruction at the corresponding angles are displayed in the subsequent four columns. **b**, A central cross-section (~23 nm thick) of the final reconstruction before masking is applied. **c**, 3D views of the central cross-section. **d**, Final 3D density map of this particle, viewed from four perpendicular directions. **e**, Final 3D reconstruction superimposed with the fitted model, viewed from four perpendicular directions. **f**, FSC analyses of the final map resolution using two methods: map-map FSC, where each map is reconstructed from one half of the images (even vs. odd tilt angle indices), and map-model FSC, where the model map is generated from the fitted model. Resolution assessments are provided based on tilt-based map-map and map-model FSC analyses at thresholds of FSC=0.5 and 0.143, respectively.

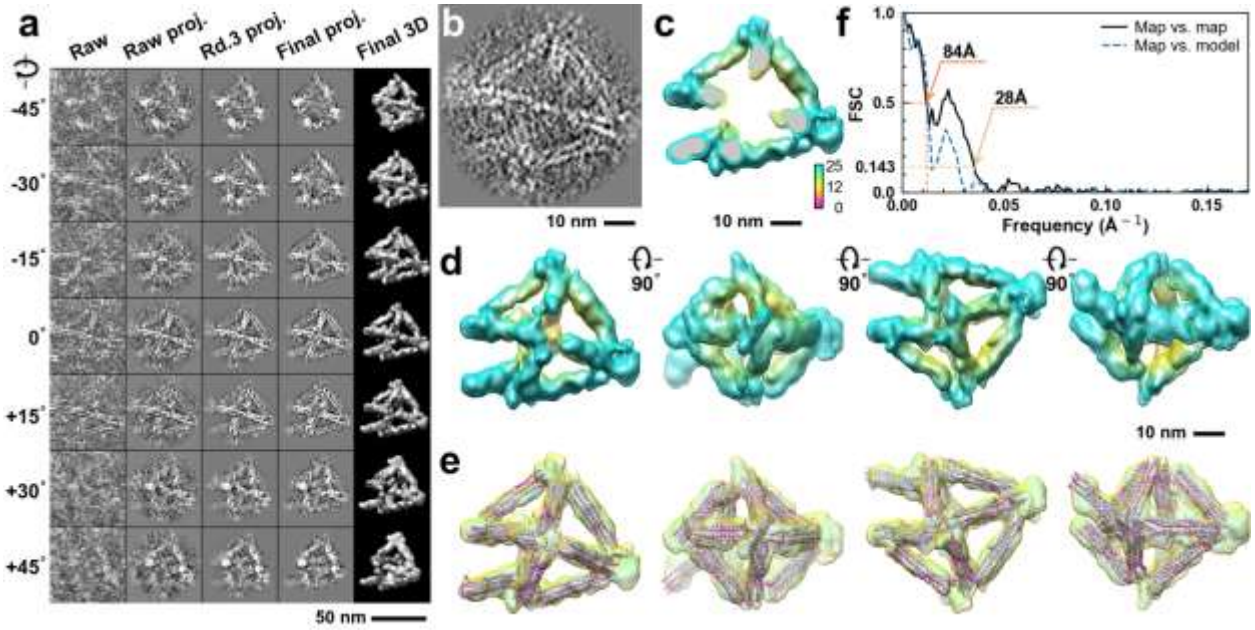

Supplementary Fig. 234: IPET 3D reconstruction and model fitting of an individual unit-cell particle (Index: 226) within a 2D lattice with 0% ferritin loading. a, Seven representative tilt images of a single unit-cell particle are shown in the first column (from left). The tilt images are aligned to a common center using IPET through iterative refinement. The projections of the raw, intermediate, and final 3D reconstruction at the corresponding angles are displayed in the subsequent four columns. **b**, A central cross-section (~23 nm thick) of the final reconstruction before masking is applied. **c**, 3D views of the central cross-section. **d**, Final 3D density map of this particle, viewed from four perpendicular directions. **e**, Final 3D reconstruction superimposed with the fitted model, viewed from four perpendicular directions. **f**, FSC analyses of the final map resolution using two methods: map-map FSC, where each map is reconstructed from one half of the images (even vs. odd tilt angle indices), and map-model FSC, where the model map is generated from the fitted model. Resolution assessments are provided based on tilt-based map-map and map-model FSC analyses at thresholds of FSC=0.5 and 0.143, respectively.

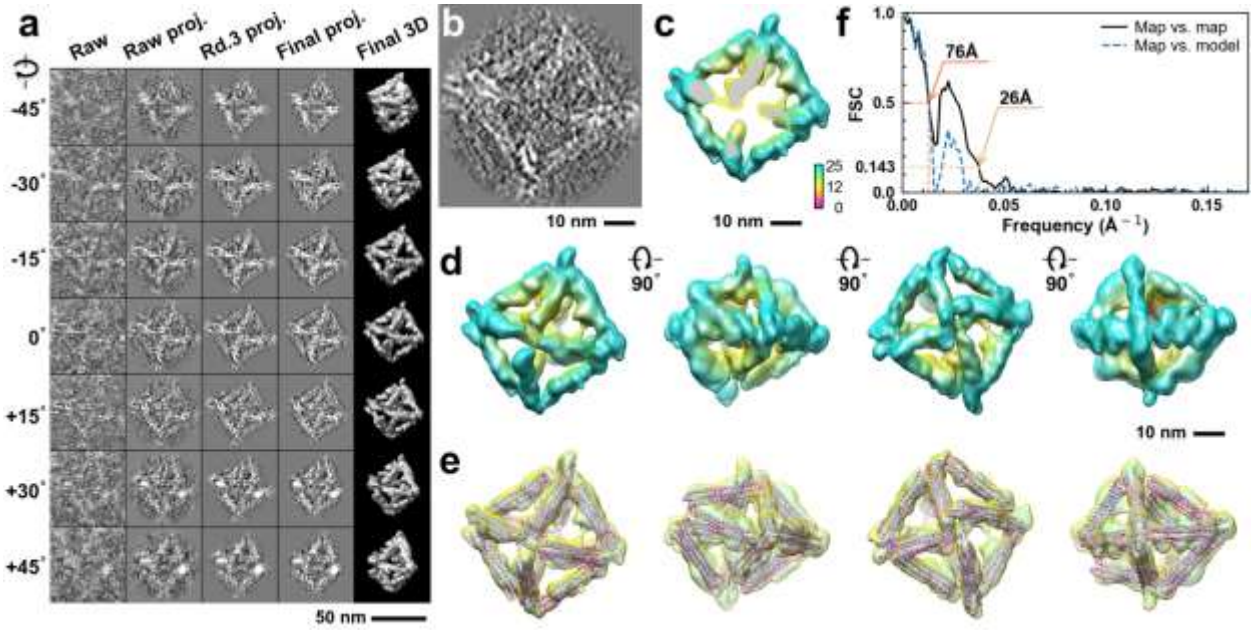

Supplementary Fig. 235: IPET 3D reconstruction and model fitting of an individual unit-cell particle (Index: 227) within a 2D lattice with 0% ferritin loading. a, Seven representative tilt images of a single unit-cell particle are shown in the first column (from left). The tilt images are aligned to a common center using IPET through iterative refinement. The projections of the raw, intermediate, and final 3D reconstruction at the corresponding angles are displayed in the subsequent four columns. **b**, A central cross-section (~23 nm thick) of the final reconstruction before masking is applied. **c**, 3D views of the central cross-section. **d**, Final 3D density map of this particle, viewed from four perpendicular directions. **e**, Final 3D reconstruction superimposed with the fitted model, viewed from four perpendicular directions. **f**, FSC analyses of the final map resolution using two methods: map-map FSC, where each map is reconstructed from one half of the images (even vs. odd tilt angle indices), and map-model FSC, where the model map is generated from the fitted model. Resolution assessments are provided based on tilt-based map-map and map-model FSC analyses at thresholds of FSC=0.5 and 0.143, respectively.

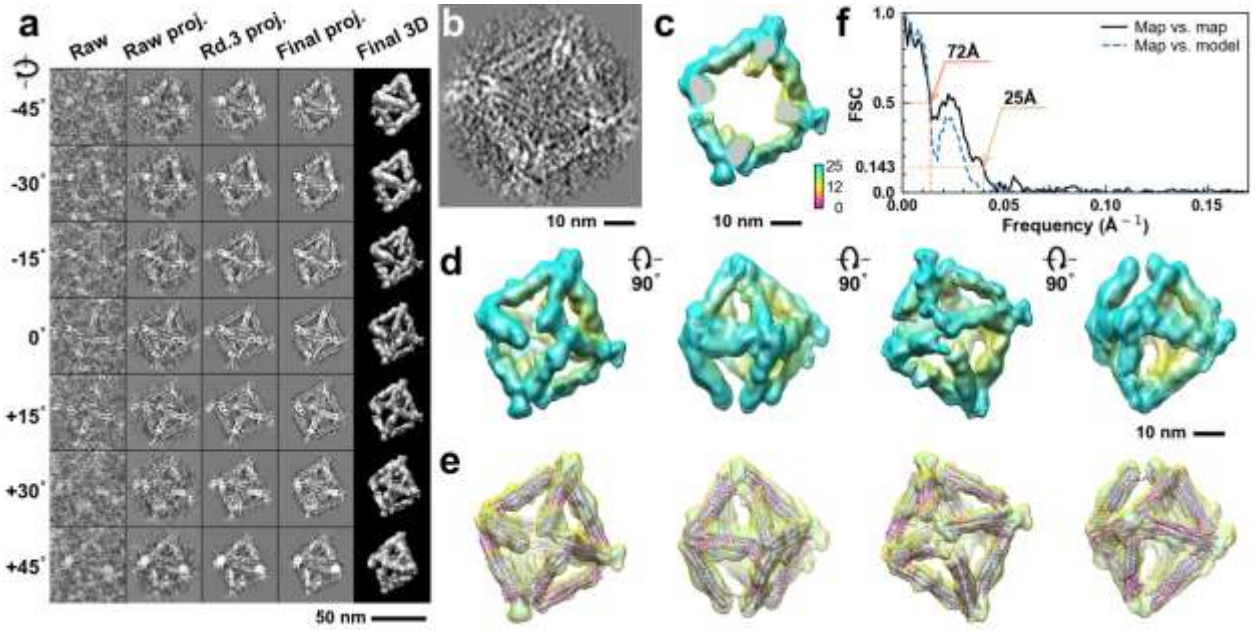

Supplementary Fig. 236: IPET 3D reconstruction and model fitting of an individual unit-cell particle (Index: 228) within a 2D lattice with 0% ferritin loading. a, Seven representative tilt images of a single unit-cell particle are shown in the first column (from left). The tilt images are aligned to a common center using IPET through iterative refinement. The projections of the raw, intermediate, and final 3D reconstruction at the corresponding angles are displayed in the subsequent four columns. **b**, A central cross-section (~23 nm thick) of the final reconstruction before masking is applied. **c**, 3D views of the central cross-section. **d**, Final 3D density map of this particle, viewed from four perpendicular directions. **e**, Final 3D reconstruction superimposed with the fitted model, viewed from four perpendicular directions. **f**, FSC analyses of the final map resolution using two methods: map-map FSC, where each map is reconstructed from one half of the images (even vs. odd tilt angle indices), and map-model FSC, where the model map is generated from the fitted model. Resolution assessments are provided based on tilt-based map-map and map-model FSC analyses at thresholds of FSC=0.5 and 0.143, respectively.

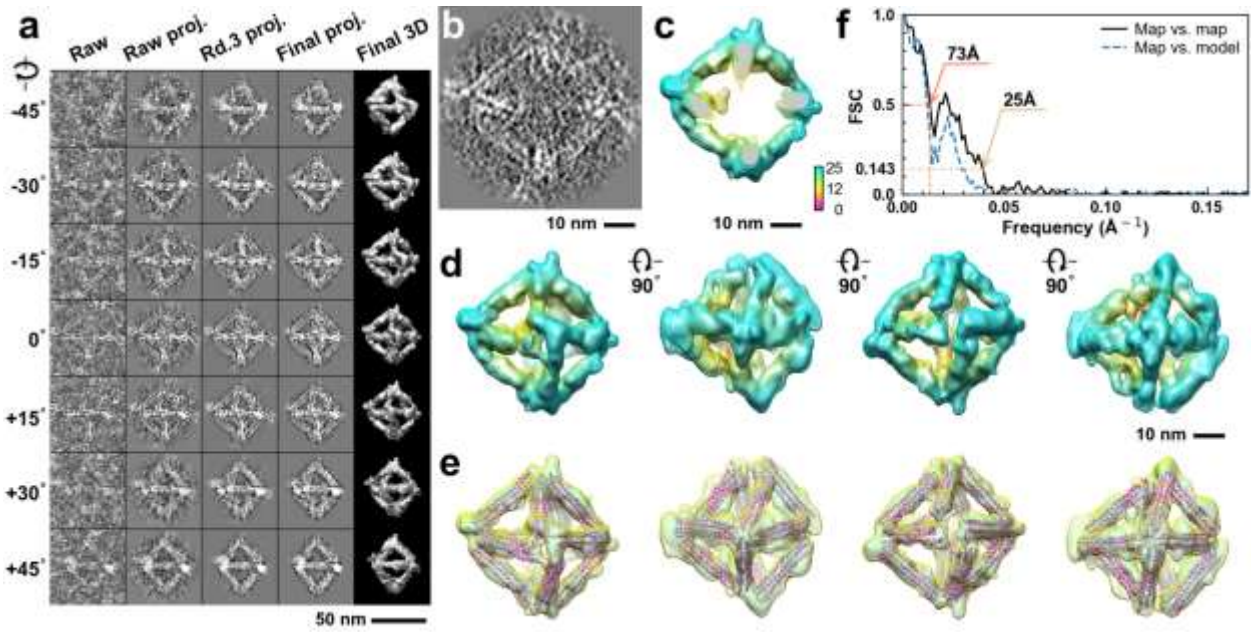

Supplementary Fig. 237: IPET 3D reconstruction and model fitting of an individual unit-cell particle (Index: 229) within a 2D lattice with 0% ferritin loading. a, Seven representative tilt images of a single unit-cell particle are shown in the first column (from left). The tilt images are aligned to a common center using IPET through iterative refinement. The projections of the raw, intermediate, and final 3D reconstruction at the corresponding angles are displayed in the subsequent four columns. **b**, A central cross-section (~23 nm thick) of the final reconstruction before masking is applied. **c**, 3D views of the central cross-section. **d**, Final 3D density map of this particle, viewed from four perpendicular directions. **e**, Final 3D reconstruction superimposed with the fitted model, viewed from four perpendicular directions. **f**, FSC analyses of the final map resolution using two methods: map-map FSC, where each map is reconstructed from one half of the images (even vs. odd tilt angle indices), and map-model FSC, where the model map is generated from the fitted model. Resolution assessments are provided based on tilt-based map-map and map-model FSC analyses at thresholds of FSC=0.5 and 0.143, respectively.

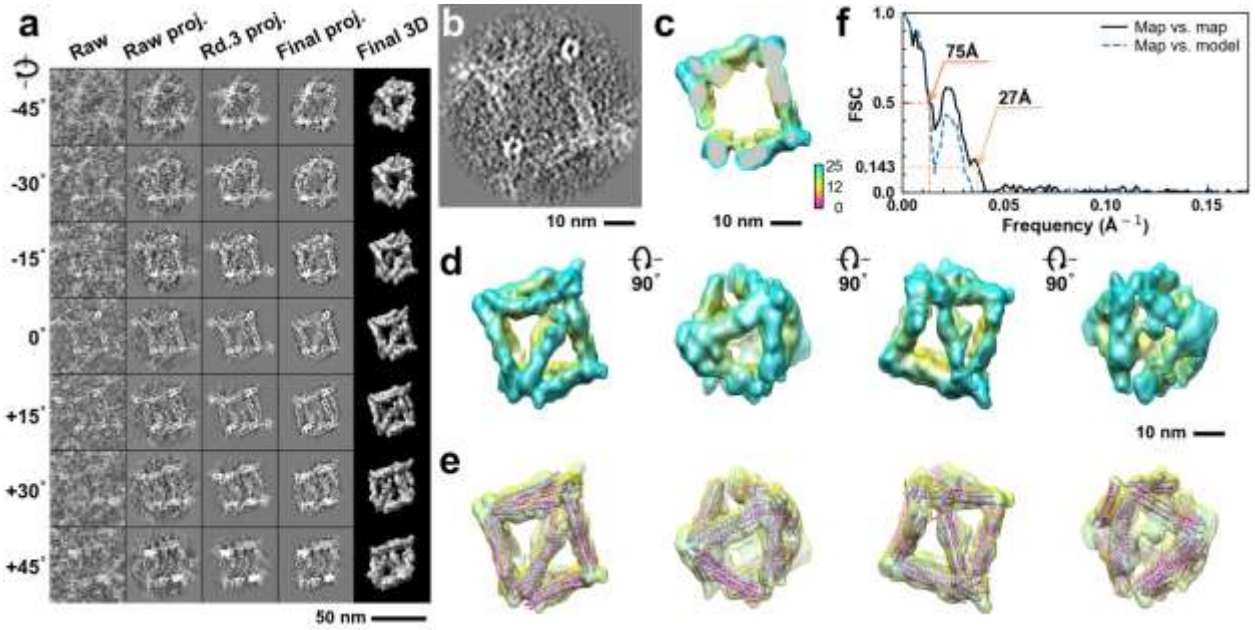

Supplementary Fig. 238: IPET 3D reconstruction and model fitting of an individual unit-cell particle (Index: 230) within a 2D lattice with 0% ferritin loading. a, Seven representative tilt images of a single unit-cell particle are shown in the first column (from left). The tilt images are aligned to a common center using IPET through iterative refinement. The projections of the raw, intermediate, and final 3D reconstruction at the corresponding angles are displayed in the subsequent four columns. **b**, A central cross-section (~23 nm thick) of the final reconstruction before masking is applied. **c**, 3D views of the central cross-section. **d**, Final 3D density map of this particle, viewed from four perpendicular directions. **e**, Final 3D reconstruction superimposed with the fitted model, viewed from four perpendicular directions. **f**, FSC analyses of the final map resolution using two methods: map-map FSC, where each map is reconstructed from one half of the images (even vs. odd tilt angle indices), and map-model FSC, where the model map is generated from the fitted model. Resolution assessments are provided based on tilt-based map-map and map-model FSC analyses at thresholds of FSC=0.5 and 0.143, respectively.

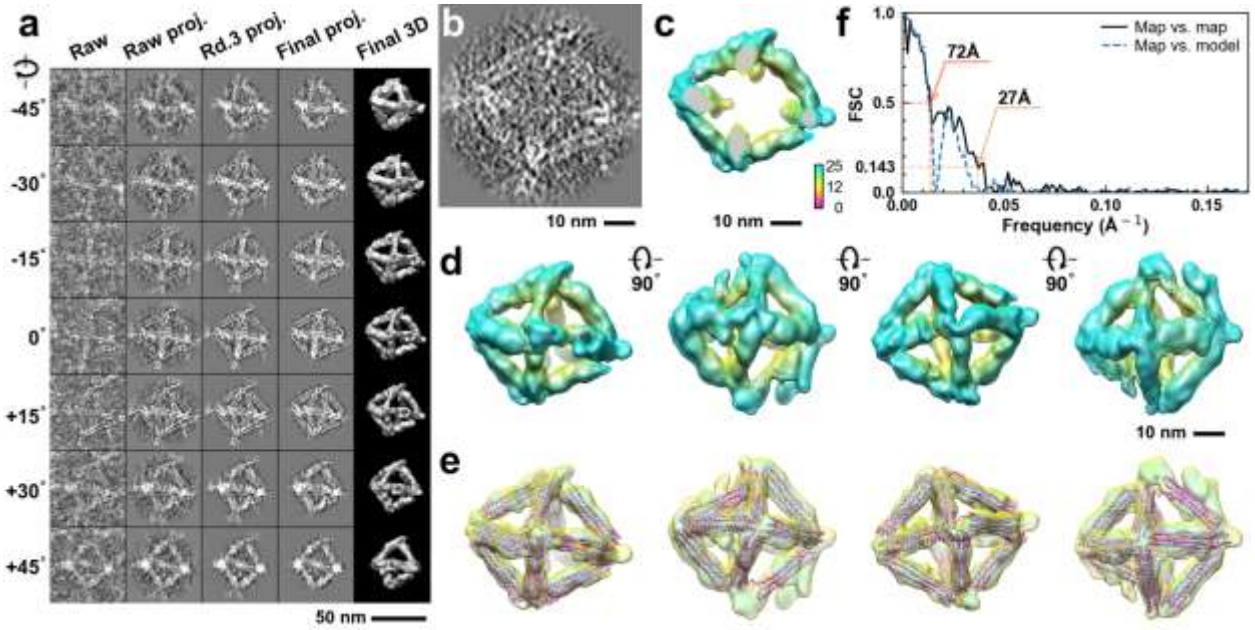

Supplementary Fig. 239: IPET 3D reconstruction and model fitting of an individual unit-cell particle (Index: 231) within a 2D lattice with 0% ferritin loading. a, Seven representative tilt images of a single unit-cell particle are shown in the first column (from left). The tilt images are aligned to a common center using IPET through iterative refinement. The projections of the raw, intermediate, and final 3D reconstruction at the corresponding angles are displayed in the subsequent four columns. **b**, A central cross-section (~23 nm thick) of the final reconstruction before masking is applied. **c**, 3D views of the central cross-section. **d**, Final 3D density map of this particle, viewed from four perpendicular directions. **e**, Final 3D reconstruction superimposed with the fitted model, viewed from four perpendicular directions. **f**, FSC analyses of the final map resolution using two methods: map-map FSC, where each map is reconstructed from one half of the images (even vs. odd tilt angle indices), and map-model FSC, where the model map is generated from the fitted model. Resolution assessments are provided based on tilt-based map-map and map-model FSC analyses at thresholds of FSC=0.5 and 0.143, respectively.

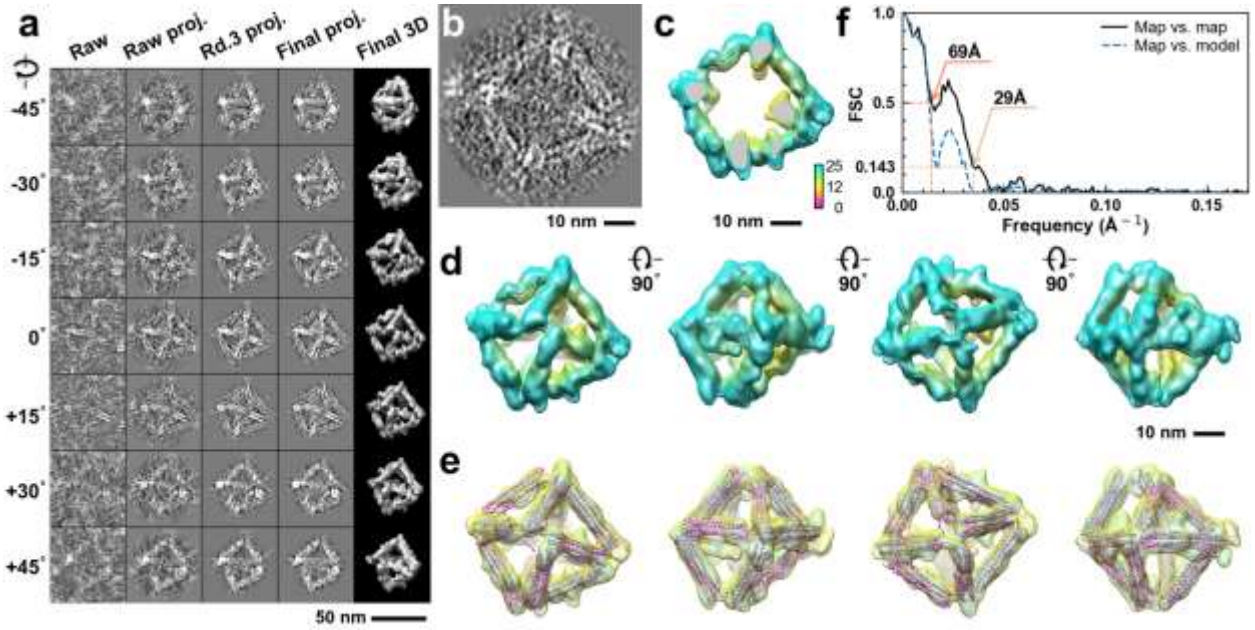

Supplementary Fig. 240: IPET 3D reconstruction and model fitting of an individual unit-cell particle (Index: 232) within a 2D lattice with 0% ferritin loading. a, Seven representative tilt images of a single unit-cell particle are shown in the first column (from left). The tilt images are aligned to a common center using IPET through iterative refinement. The projections of the raw, intermediate, and final 3D reconstruction at the corresponding angles are displayed in the subsequent four columns. **b**, A central cross-section (~23 nm thick) of the final reconstruction before masking is applied. **c**, 3D views of the central cross-section. **d**, Final 3D density map of this particle, viewed from four perpendicular directions. **e**, Final 3D reconstruction superimposed with the fitted model, viewed from four perpendicular directions. **f**, FSC analyses of the final map resolution using two methods: map-map FSC, where each map is reconstructed from one half of the images (even vs. odd tilt angle indices), and map-model FSC, where the model map is generated from the fitted model. Resolution assessments are provided based on tilt-based map-map and map-model FSC analyses at thresholds of FSC=0.5 and 0.143, respectively.

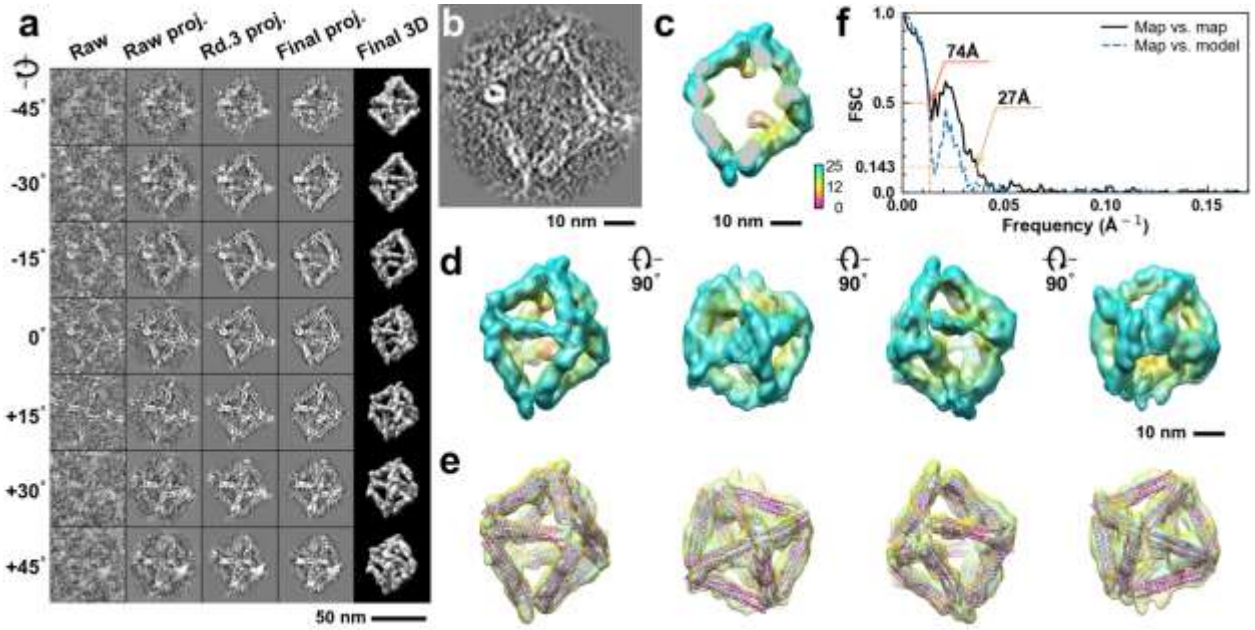

Supplementary Fig. 241: IPET 3D reconstruction and model fitting of an individual unit-cell particle (Index: 233) within a 2D lattice with 0% ferritin loading. a, Seven representative tilt images of a single unit-cell particle are shown in the first column (from left). The tilt images are aligned to a common center using IPET through iterative refinement. The projections of the raw, intermediate, and final 3D reconstruction at the corresponding angles are displayed in the subsequent four columns. **b**, A central cross-section (~23 nm thick) of the final reconstruction before masking is applied. **c**, 3D views of the central cross-section. **d**, Final 3D density map of this particle, viewed from four perpendicular directions. **e**, Final 3D reconstruction superimposed with the fitted model, viewed from four perpendicular directions. **f**, FSC analyses of the final map resolution using two methods: map-map FSC, where each map is reconstructed from one half of the images (even vs. odd tilt angle indices), and map-model FSC, where the model map is generated from the fitted model. Resolution assessments are provided based on tilt-based map-map and map-model FSC analyses at thresholds of FSC=0.5 and 0.143, respectively.

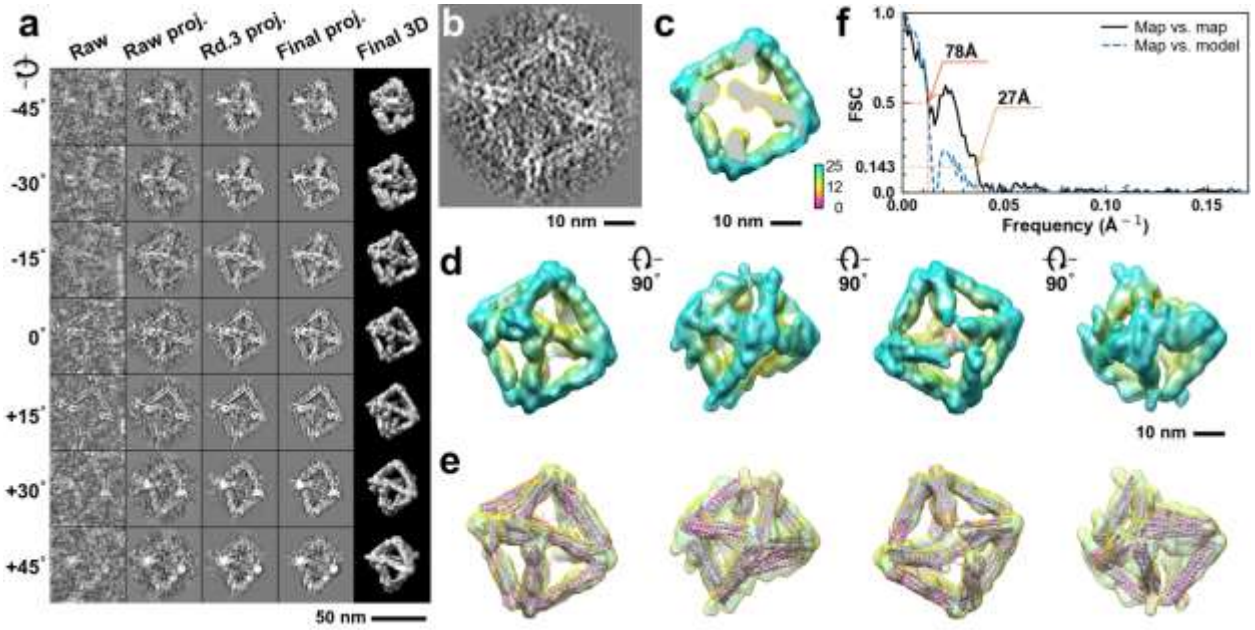

Supplementary Fig. 242: IPET 3D reconstruction and model fitting of an individual unit-cell particle (Index: 234) within a 2D lattice with 0% ferritin loading. a, Seven representative tilt images of a single unit-cell particle are shown in the first column (from left). The tilt images are aligned to a common center using IPET through iterative refinement. The projections of the raw, intermediate, and final 3D reconstruction at the corresponding angles are displayed in the subsequent four columns. **b**, A central cross-section (~23 nm thick) of the final reconstruction before masking is applied. **c**, 3D views of the central cross-section. **d**, Final 3D density map of this particle, viewed from four perpendicular directions. **e**, Final 3D reconstruction superimposed with the fitted model, viewed from four perpendicular directions. **f**, FSC analyses of the final map resolution using two methods: map-map FSC, where each map is reconstructed from one half of the images (even vs. odd tilt angle indices), and map-model FSC, where the model map is generated from the fitted model. Resolution assessments are provided based on tilt-based map-map and map-model FSC analyses at thresholds of FSC=0.5 and 0.143, respectively.

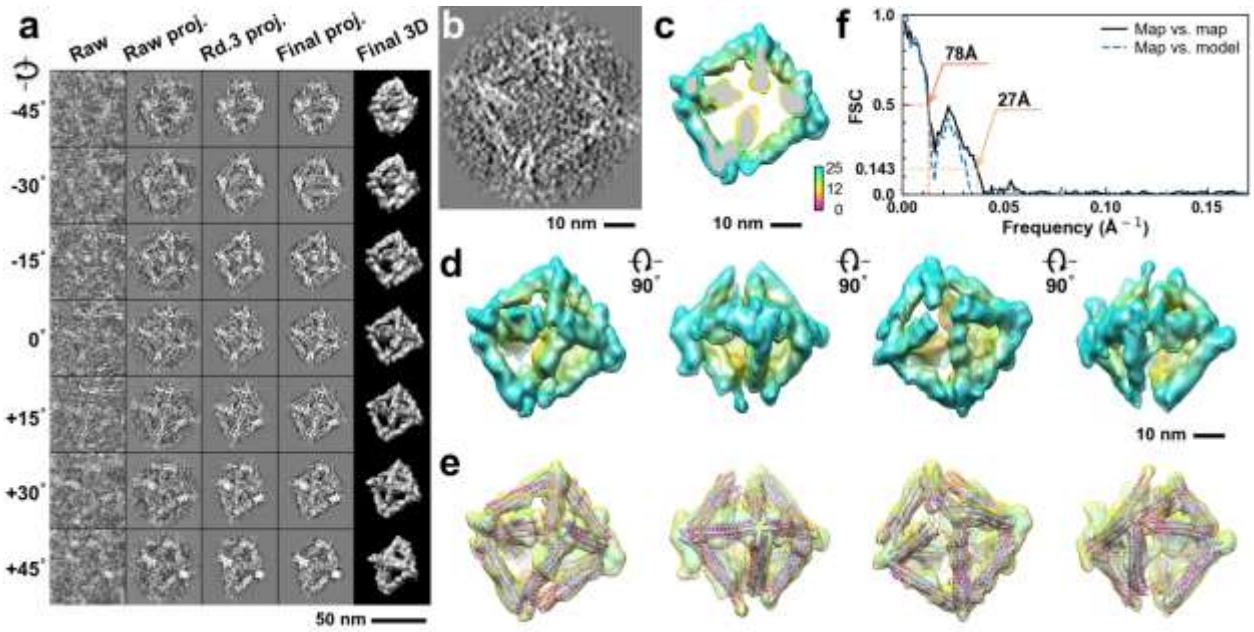

Supplementary Fig. 243: IPET 3D reconstruction and model fitting of an individual unit-cell particle (Index: 235) within a 2D lattice with 0% ferritin loading. a, Seven representative tilt images of a single unit-cell particle are shown in the first column (from left). The tilt images are aligned to a common center using IPET through iterative refinement. The projections of the raw, intermediate, and final 3D reconstruction at the corresponding angles are displayed in the subsequent four columns. **b**, A central cross-section (~23 nm thick) of the final reconstruction before masking is applied. **c**, 3D views of the central cross-section. **d**, Final 3D density map of this particle, viewed from four perpendicular directions. **e**, Final 3D reconstruction superimposed with the fitted model, viewed from four perpendicular directions. **f**, FSC analyses of the final map resolution using two methods: map-map FSC, where each map is reconstructed from one half of the images (even vs. odd tilt angle indices), and map-model FSC, where the model map is generated from the fitted model. Resolution assessments are provided based on tilt-based map-map and map-model FSC analyses at thresholds of FSC=0.5 and 0.143, respectively.

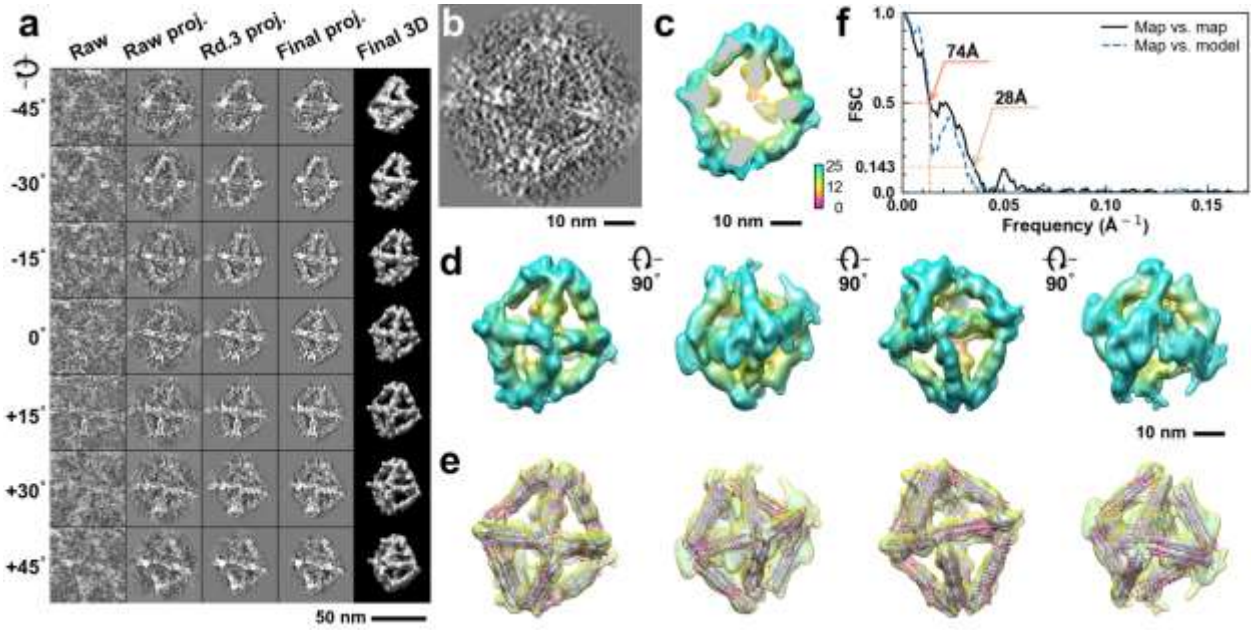

Supplementary Fig. 244: IPET 3D reconstruction and model fitting of an individual unit-cell particle (Index: 236) within a 2D lattice with 0% ferritin loading. a, Seven representative tilt images of a single unit-cell particle are shown in the first column (from left). The tilt images are aligned to a common center using IPET through iterative refinement. The projections of the raw, intermediate, and final 3D reconstruction at the corresponding angles are displayed in the subsequent four columns. **b**, A central cross-section (~23 nm thick) of the final reconstruction before masking is applied. **c**, 3D views of the central cross-section. **d**, Final 3D density map of this particle, viewed from four perpendicular directions. **e**, Final 3D reconstruction superimposed with the fitted model, viewed from four perpendicular directions. **f**, FSC analyses of the final map resolution using two methods: map-map FSC, where each map is reconstructed from one half of the images (even vs. odd tilt angle indices), and map-model FSC, where the model map is generated from the fitted model. Resolution assessments are provided based on tilt-based map-map and map-model FSC analyses at thresholds of FSC=0.5 and 0.143, respectively.

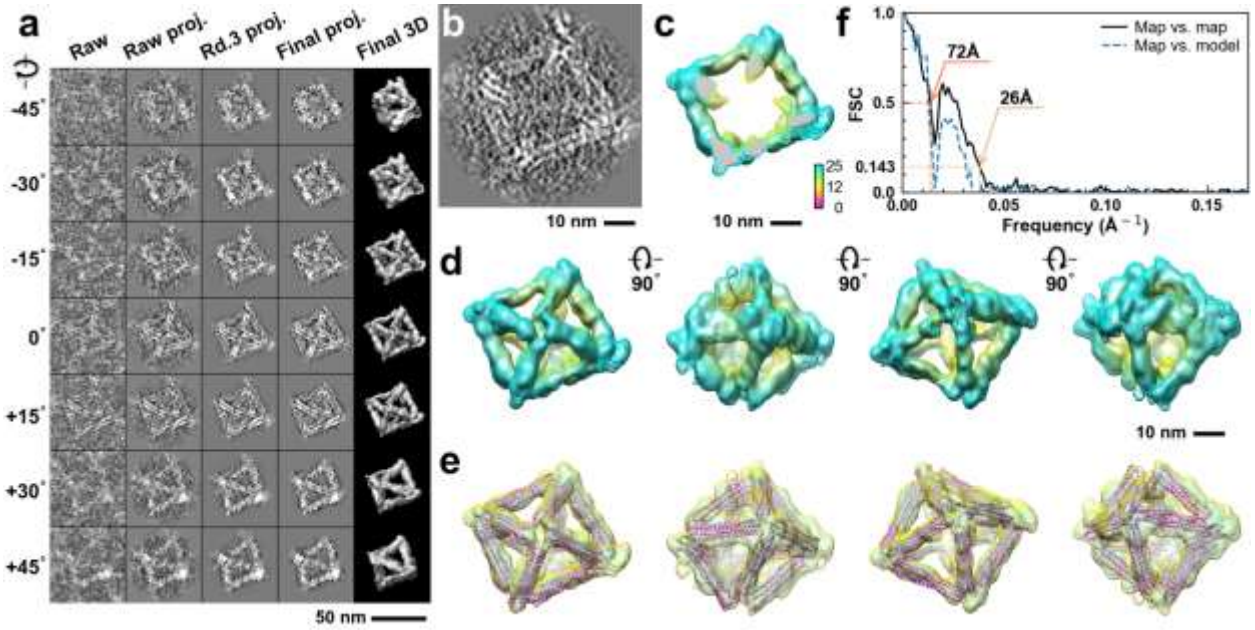

Supplementary Fig. 245: IPET 3D reconstruction and model fitting of an individual unit-cell particle (Index: 237) within a 2D lattice with 0% ferritin loading. a, Seven representative tilt images of a single unit-cell particle are shown in the first column (from left). The tilt images are aligned to a common center using IPET through iterative refinement. The projections of the raw, intermediate, and final 3D reconstruction at the corresponding angles are displayed in the subsequent four columns. **b**, A central cross-section (~23 nm thick) of the final reconstruction before masking is applied. **c**, 3D views of the central cross-section. **d**, Final 3D density map of this particle, viewed from four perpendicular directions. **e**, Final 3D reconstruction superimposed with the fitted model, viewed from four perpendicular directions. **f**, FSC analyses of the final map resolution using two methods: map-map FSC, where each map is reconstructed from one half of the images (even vs. odd tilt angle indices), and map-model FSC, where the model map is generated from the fitted model. Resolution assessments are provided based on tilt-based map-map and map-model FSC analyses at thresholds of FSC=0.5 and 0.143, respectively.

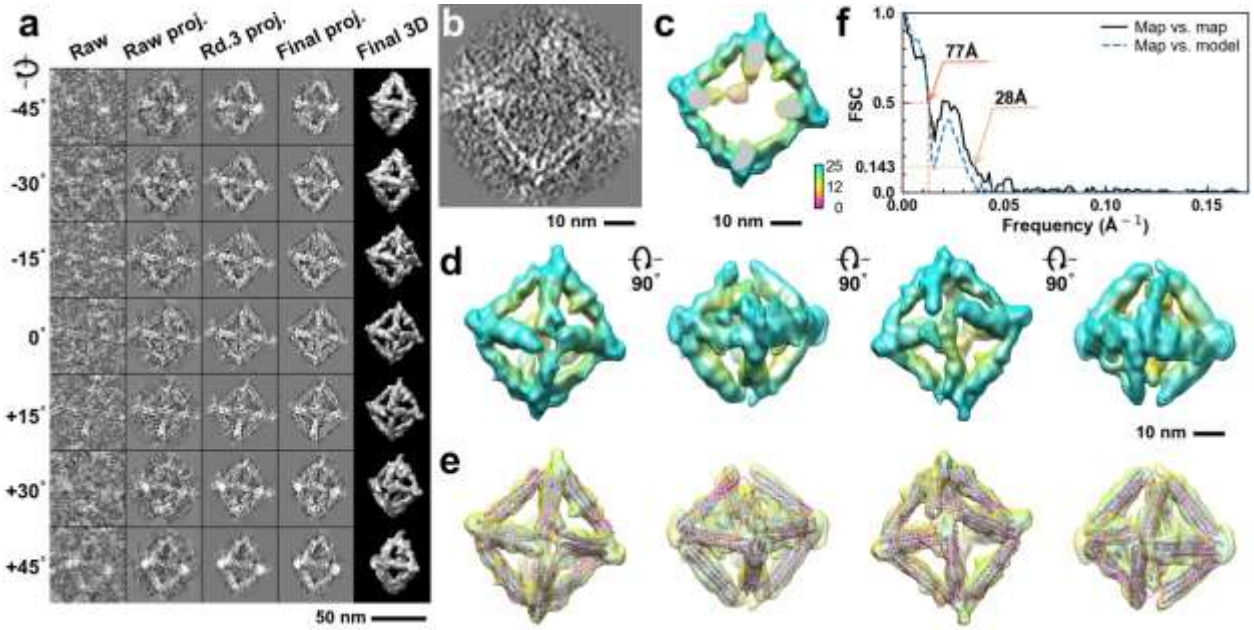

Supplementary Fig. 246: IPET 3D reconstruction and model fitting of an individual unit-cell particle (Index: 238) within a 2D lattice with 0% ferritin loading. a, Seven representative tilt images of a single unit-cell particle are shown in the first column (from left). The tilt images are aligned to a common center using IPET through iterative refinement. The projections of the raw, intermediate, and final 3D reconstruction at the corresponding angles are displayed in the subsequent four columns. **b**, A central cross-section (~23 nm thick) of the final reconstruction before masking is applied. **c**, 3D views of the central cross-section. **d**, Final 3D density map of this particle, viewed from four perpendicular directions. **e**, Final 3D reconstruction superimposed with the fitted model, viewed from four perpendicular directions. **f**, FSC analyses of the final map resolution using two methods: map-map FSC, where each map is reconstructed from one half of the images (even vs. odd tilt angle indices), and map-model FSC, where the model map is generated from the fitted model. Resolution assessments are provided based on tilt-based map-map and map-model FSC analyses at thresholds of FSC=0.5 and 0.143, respectively.

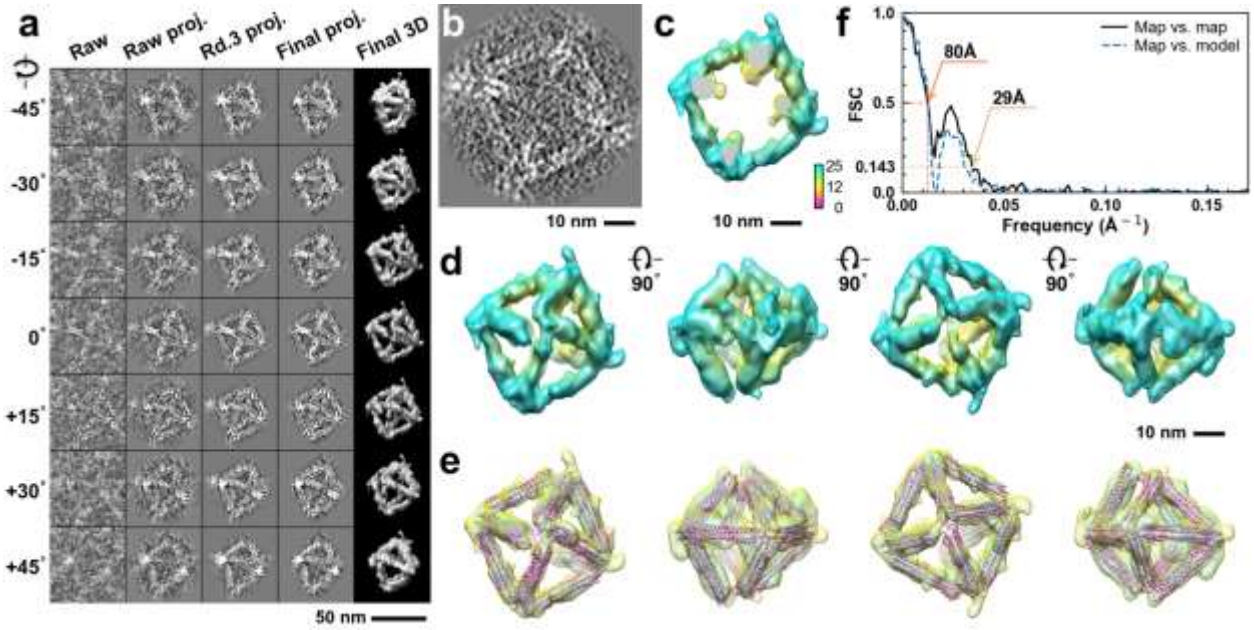

Supplementary Fig. 247: IPET 3D reconstruction and model fitting of an individual unit-cell particle (Index: 239) within a 2D lattice with 0% ferritin loading. a, Seven representative tilt images of a single unit-cell particle are shown in the first column (from left). The tilt images are aligned to a common center using IPET through iterative refinement. The projections of the raw, intermediate, and final 3D reconstruction at the corresponding angles are displayed in the subsequent four columns. **b**, A central cross-section (~23 nm thick) of the final reconstruction before masking is applied. **c**, 3D views of the central cross-section. **d**, Final 3D density map of this particle, viewed from four perpendicular directions. **e**, Final 3D reconstruction superimposed with the fitted model, viewed from four perpendicular directions. **f**, FSC analyses of the final map resolution using two methods: map-map FSC, where each map is reconstructed from one half of the images (even vs. odd tilt angle indices), and map-model FSC, where the model map is generated from the fitted model. Resolution assessments are provided based on tilt-based map-map and map-model FSC analyses at thresholds of FSC=0.5 and 0.143, respectively.

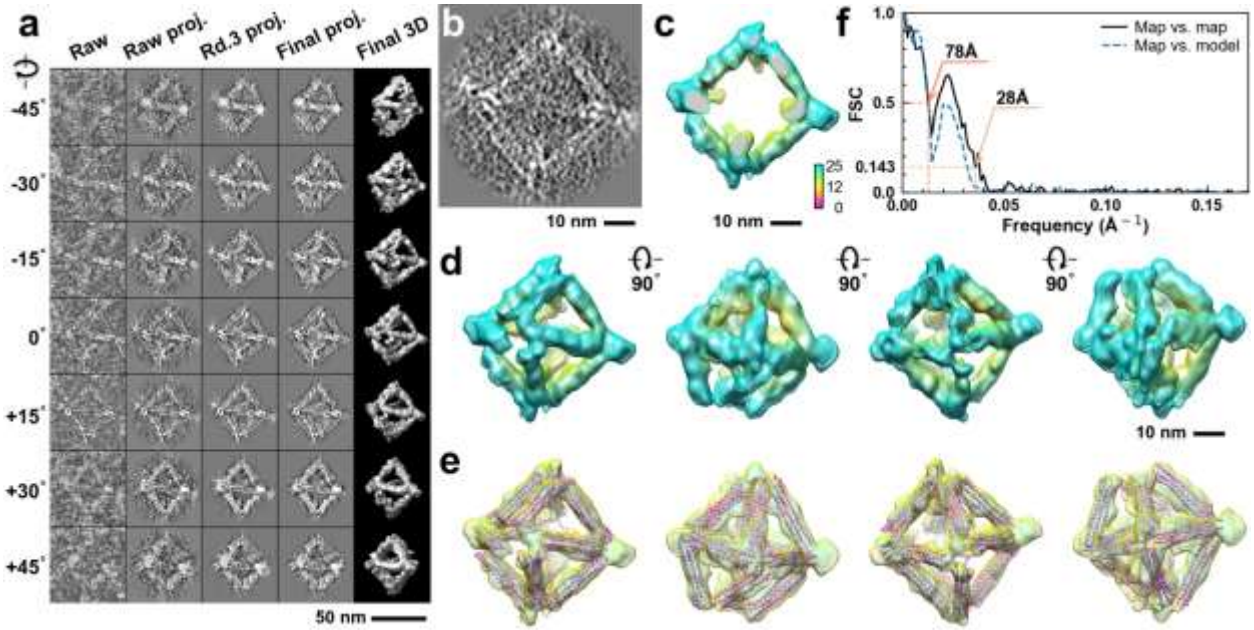

Supplementary Fig. 248: IPET 3D reconstruction and model fitting of an individual unit-cell particle (Index: 240) within a 2D lattice with 0% ferritin loading. a, Seven representative tilt images of a single unit-cell particle are shown in the first column (from left). The tilt images are aligned to a common center using IPET through iterative refinement. The projections of the raw, intermediate, and final 3D reconstruction at the corresponding angles are displayed in the subsequent four columns. **b**, A central cross-section (~23 nm thick) of the final reconstruction before masking is applied. **c**, 3D views of the central cross-section. **d**, Final 3D density map of this particle, viewed from four perpendicular directions. **e**, Final 3D reconstruction superimposed with the fitted model, viewed from four perpendicular directions. **f**, FSC analyses of the final map resolution using two methods: map-map FSC, where each map is reconstructed from one half of the images (even vs. odd tilt angle indices), and map-model FSC, where the model map is generated from the fitted model. Resolution assessments are provided based on tilt-based map-map and map-model FSC analyses at thresholds of FSC=0.5 and 0.143, respectively.

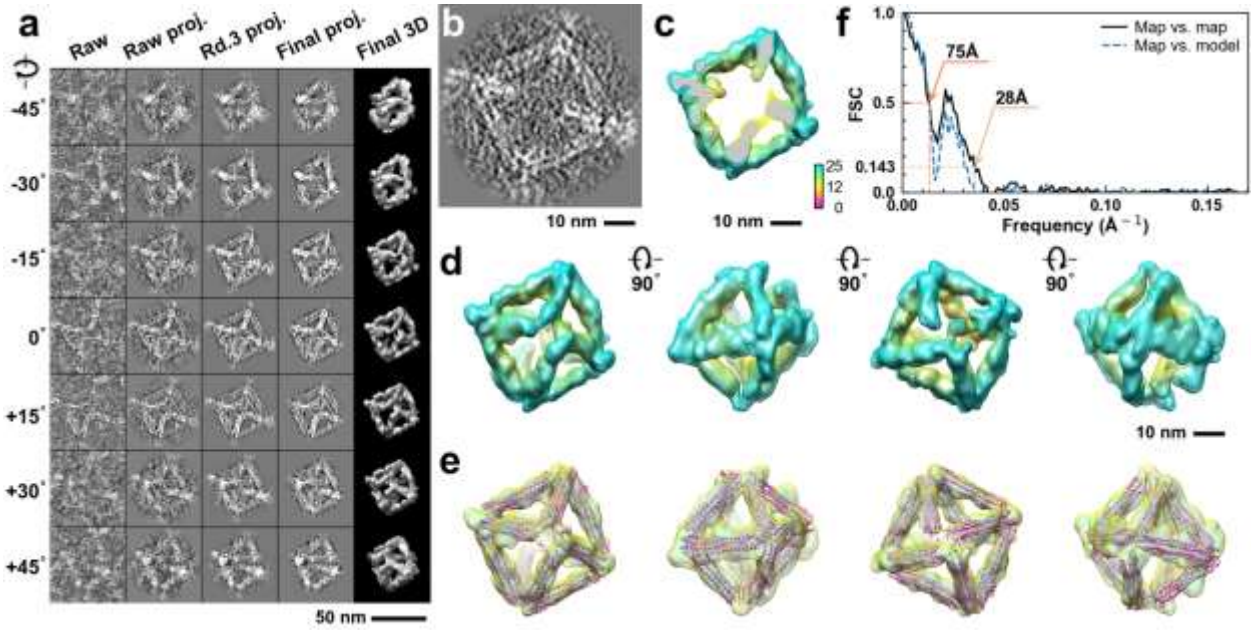

Supplementary Fig. 249: IPET 3D reconstruction and model fitting of an individual unit-cell particle (Index: 241) within a 2D lattice with 0% ferritin loading. a, Seven representative tilt images of a single unit-cell particle are shown in the first column (from left). The tilt images are aligned to a common center using IPET through iterative refinement. The projections of the raw, intermediate, and final 3D reconstruction at the corresponding angles are displayed in the subsequent four columns. **b**, A central cross-section (~23 nm thick) of the final reconstruction before masking is applied. **c**, 3D views of the central cross-section. **d**, Final 3D density map of this particle, viewed from four perpendicular directions. **e**, Final 3D reconstruction superimposed with the fitted model, viewed from four perpendicular directions. **f**, FSC analyses of the final map resolution using two methods: map-map FSC, where each map is reconstructed from one half of the images (even vs. odd tilt angle indices), and map-model FSC, where the model map is generated from the fitted model. Resolution assessments are provided based on tilt-based map-map and map-model FSC analyses at thresholds of FSC=0.5 and 0.143, respectively.

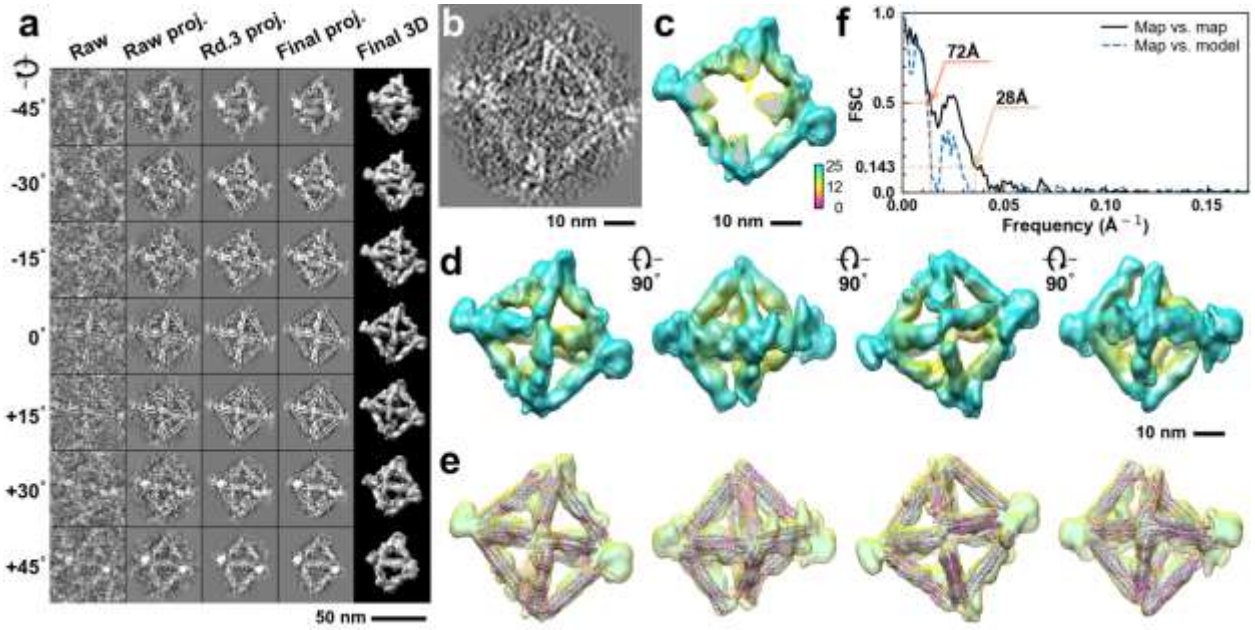

Supplementary Fig. 250: IPET 3D reconstruction and model fitting of an individual unit-cell particle (Index: 242) within a 2D lattice with 0% ferritin loading. a, Seven representative tilt images of a single unit-cell particle are shown in the first column (from left). The tilt images are aligned to a common center using IPET through iterative refinement. The projections of the raw, intermediate, and final 3D reconstruction at the corresponding angles are displayed in the subsequent four columns. **b**, A central cross-section (~23 nm thick) of the final reconstruction before masking is applied. **c**, 3D views of the central cross-section. **d**, Final 3D density map of this particle, viewed from four perpendicular directions. **e**, Final 3D reconstruction superimposed with the fitted model, viewed from four perpendicular directions. **f**, FSC analyses of the final map resolution using two methods: map-map FSC, where each map is reconstructed from one half of the images (even vs. odd tilt angle indices), and map-model FSC, where the model map is generated from the fitted model. Resolution assessments are provided based on tilt-based map-map and map-model FSC analyses at thresholds of FSC=0.5 and 0.143, respectively.

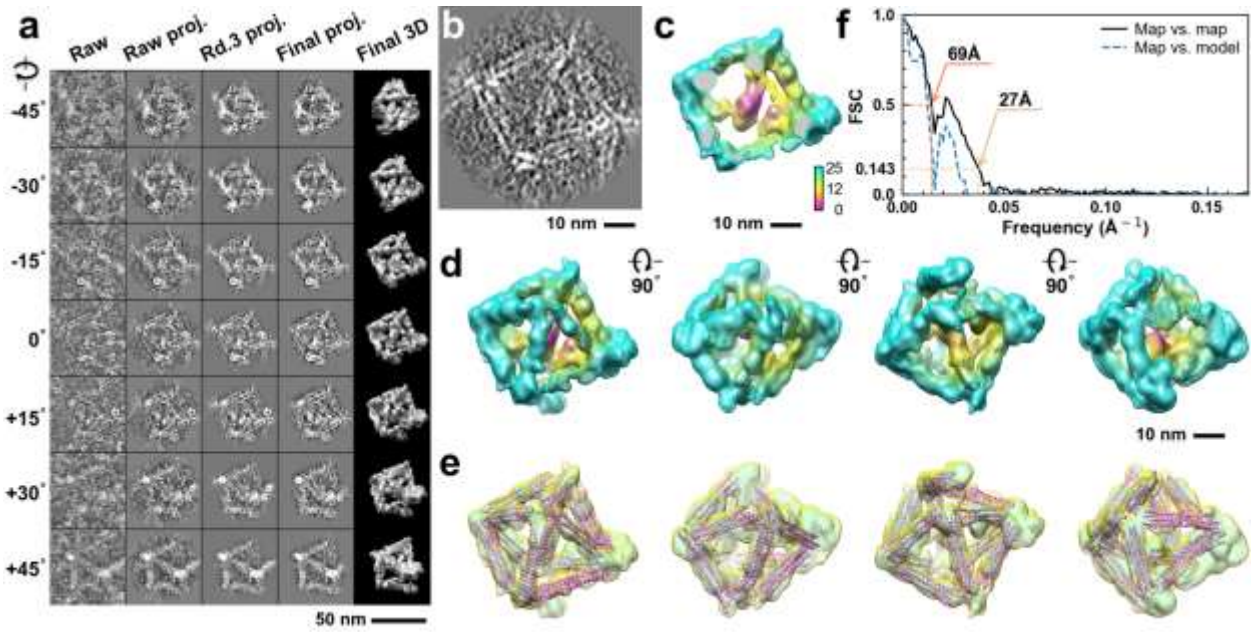

Supplementary Fig. 251: IPET 3D reconstruction and model fitting of an individual unit-cell particle (Index: 243) within a 2D lattice with 0% ferritin loading. a, Seven representative tilt images of a single unit-cell particle are shown in the first column (from left). The tilt images are aligned to a common center using IPET through iterative refinement. The projections of the raw, intermediate, and final 3D reconstruction at the corresponding angles are displayed in the subsequent four columns. **b**, A central cross-section (~23 nm thick) of the final reconstruction before masking is applied. **c**, 3D views of the central cross-section. **d**, Final 3D density map of this particle, viewed from four perpendicular directions. **e**, Final 3D reconstruction superimposed with the fitted model, viewed from four perpendicular directions. **f**, FSC analyses of the final map resolution using two methods: map-map FSC, where each map is reconstructed from one half of the images (even vs. odd tilt angle indices), and map-model FSC, where the model map is generated from the fitted model. Resolution assessments are provided based on tilt-based map-map and map-model FSC analyses at thresholds of FSC=0.5 and 0.143, respectively.

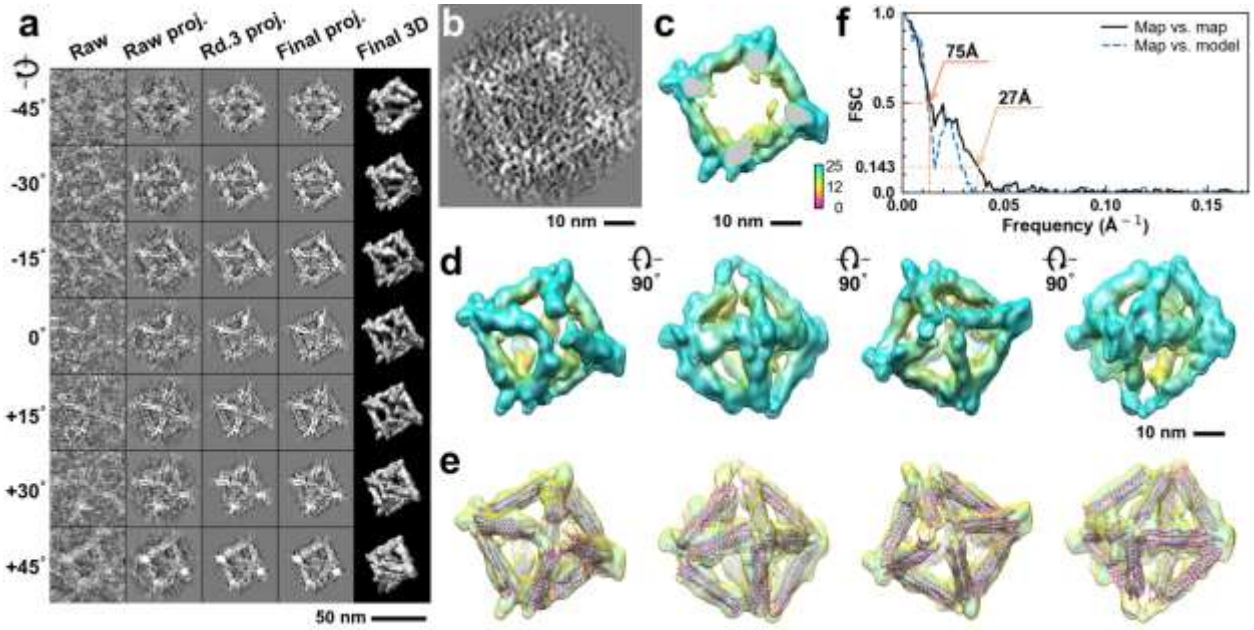

Supplementary Fig. 252: IPET 3D reconstruction and model fitting of an individual unit-cell particle (Index: 244) within a 2D lattice with 0% ferritin loading. a, Seven representative tilt images of a single unit-cell particle are shown in the first column (from left). The tilt images are aligned to a common center using IPET through iterative refinement. The projections of the raw, intermediate, and final 3D reconstruction at the corresponding angles are displayed in the subsequent four columns. **b**, A central cross-section (~23 nm thick) of the final reconstruction before masking is applied. **c**, 3D views of the central cross-section. **d**, Final 3D density map of this particle, viewed from four perpendicular directions. **e**, Final 3D reconstruction superimposed with the fitted model, viewed from four perpendicular directions. **f**, FSC analyses of the final map resolution using two methods: map-map FSC, where each map is reconstructed from one half of the images (even vs. odd tilt angle indices), and map-model FSC, where the model map is generated from the fitted model. Resolution assessments are provided based on tilt-based map-map and map-model FSC analyses at thresholds of FSC=0.5 and 0.143, respectively.

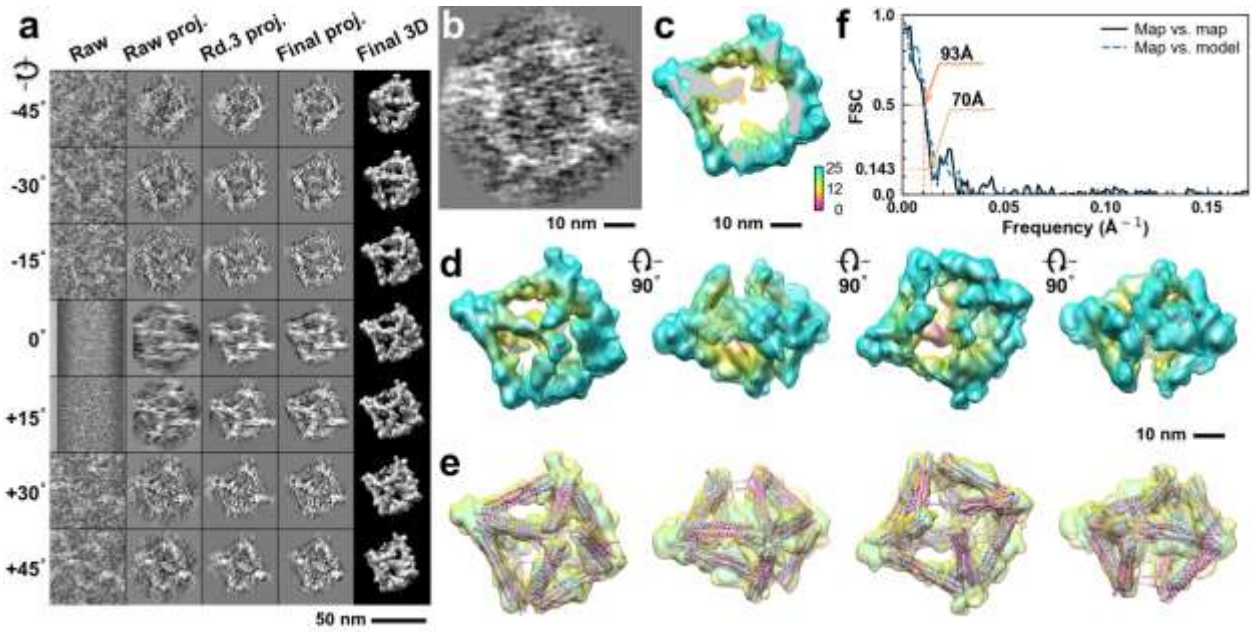

Supplementary Fig. 253: IPET 3D reconstruction and model fitting of an individual unit-cell particle (Index: 245) within a 2D lattice with 0% ferritin loading. a, Seven representative tilt images of a single unit-cell particle are shown in the first column (from left). The tilt images are aligned to a common center using IPET through iterative refinement. The projections of the raw, intermediate, and final 3D reconstruction at the corresponding angles are displayed in the subsequent four columns. **b**, A central cross-section (~23 nm thick) of the final reconstruction before masking is applied. **c**, 3D views of the central cross-section. **d**, Final 3D density map of this particle, viewed from four perpendicular directions. **e**, Final 3D reconstruction superimposed with the fitted model, viewed from four perpendicular directions. **f**, FSC analyses of the final map resolution using two methods: map-map FSC, where each map is reconstructed from one half of the images (even vs. odd tilt angle indices), and map-model FSC, where the model map is generated from the fitted model. Resolution assessments are provided based on tilt-based map-map and map-model FSC analyses at thresholds of FSC=0.5 and 0.143, respectively.

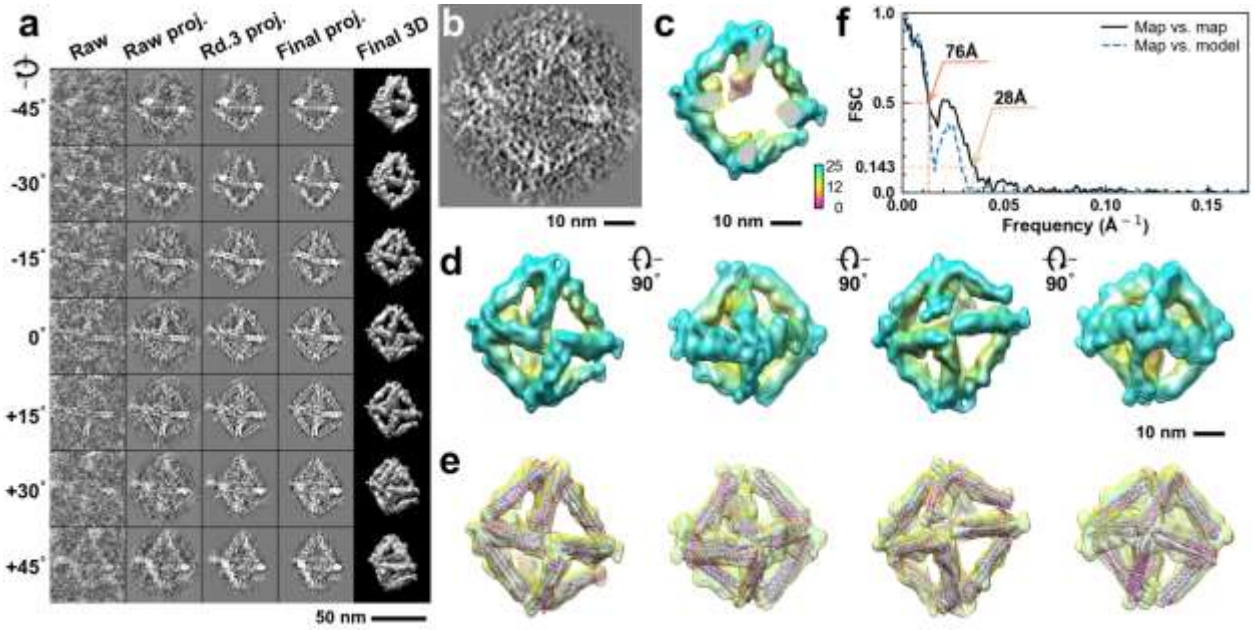

Supplementary Fig. 254: IPET 3D reconstruction and model fitting of an individual unit-cell particle (Index: 246) within a 2D lattice with 0% ferritin loading. a, Seven representative tilt images of a single unit-cell particle are shown in the first column (from left). The tilt images are aligned to a common center using IPET through iterative refinement. The projections of the raw, intermediate, and final 3D reconstruction at the corresponding angles are displayed in the subsequent four columns. **b**, A central cross-section (~23 nm thick) of the final reconstruction before masking is applied. **c**, 3D views of the central cross-section. **d**, Final 3D density map of this particle, viewed from four perpendicular directions. **e**, Final 3D reconstruction superimposed with the fitted model, viewed from four perpendicular directions. **f**, FSC analyses of the final map resolution using two methods: map-map FSC, where each map is reconstructed from one half of the images (even vs. odd tilt angle indices), and map-model FSC, where the model map is generated from the fitted model. Resolution assessments are provided based on tilt-based map-map and map-model FSC analyses at thresholds of FSC=0.5 and 0.143, respectively.

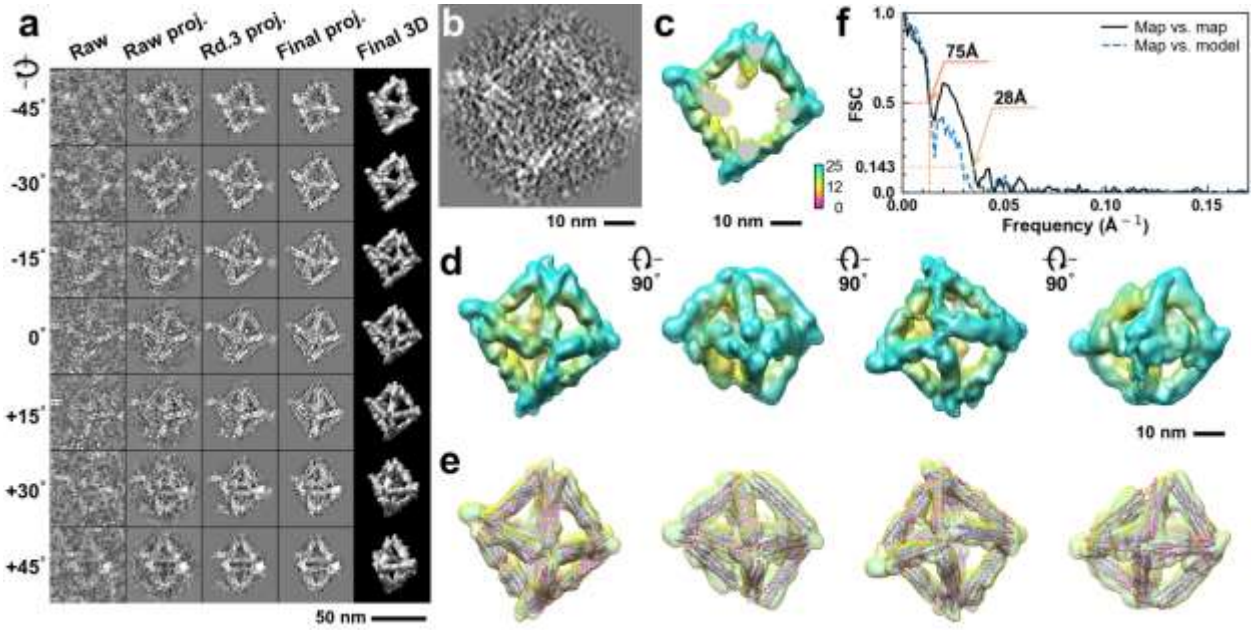

Supplementary Fig. 255: IPET 3D reconstruction and model fitting of an individual unit-cell particle (Index: 247) within a 2D lattice with 0% ferritin loading. a, Seven representative tilt images of a single unit-cell particle are shown in the first column (from left). The tilt images are aligned to a common center using IPET through iterative refinement. The projections of the raw, intermediate, and final 3D reconstruction at the corresponding angles are displayed in the subsequent four columns. **b**, A central cross-section (~23 nm thick) of the final reconstruction before masking is applied. **c**, 3D views of the central cross-section. **d**, Final 3D density map of this particle, viewed from four perpendicular directions. **e**, Final 3D reconstruction superimposed with the fitted model, viewed from four perpendicular directions. **f**, FSC analyses of the final map resolution using two methods: map-map FSC, where each map is reconstructed from one half of the images (even vs. odd tilt angle indices), and map-model FSC, where the model map is generated from the fitted model. Resolution assessments are provided based on tilt-based map-map and map-model FSC analyses at thresholds of FSC=0.5 and 0.143, respectively.

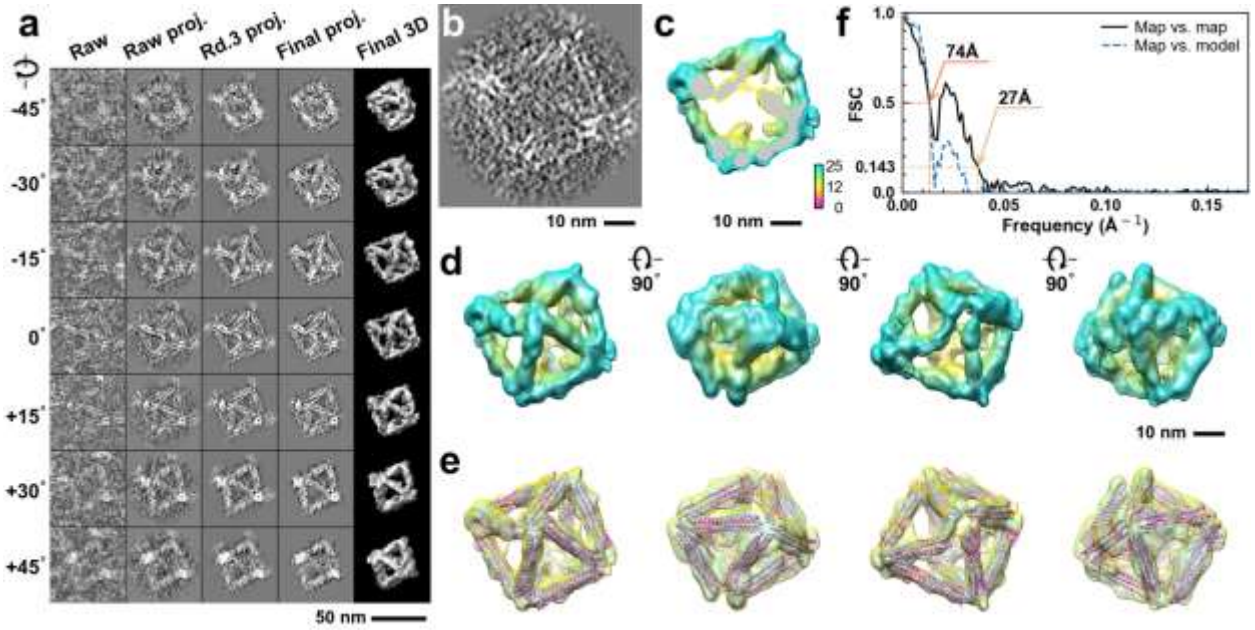

Supplementary Fig. 256: IPET 3D reconstruction and model fitting of an individual unit-cell particle (Index: 248) within a 2D lattice with 0% ferritin loading. a, Seven representative tilt images of a single unit-cell particle are shown in the first column (from left). The tilt images are aligned to a common center using IPET through iterative refinement. The projections of the raw, intermediate, and final 3D reconstruction at the corresponding angles are displayed in the subsequent four columns. **b**, A central cross-section (~23 nm thick) of the final reconstruction before masking is applied. **c**, 3D views of the central cross-section. **d**, Final 3D density map of this particle, viewed from four perpendicular directions. **e**, Final 3D reconstruction superimposed with the fitted model, viewed from four perpendicular directions. **f**, FSC analyses of the final map resolution using two methods: map-map FSC, where each map is reconstructed from one half of the images (even vs. odd tilt angle indices), and map-model FSC, where the model map is generated from the fitted model. Resolution assessments are provided based on tilt-based map-map and map-model FSC analyses at thresholds of FSC=0.5 and 0.143, respectively.

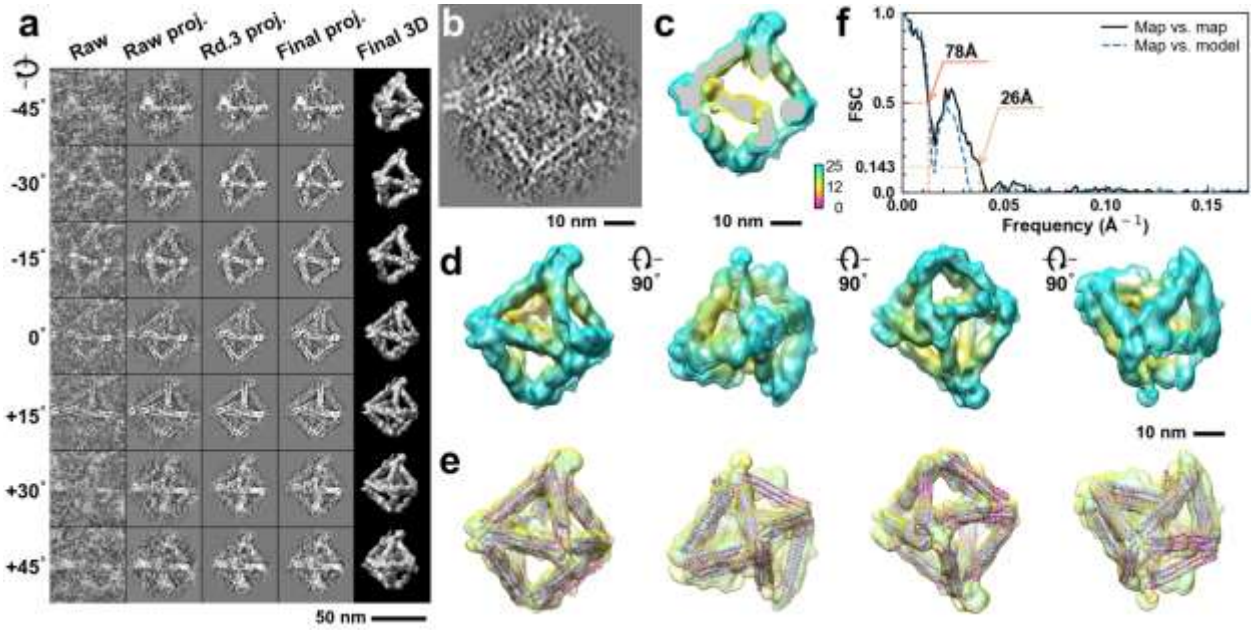

Supplementary Fig. 257: IPET 3D reconstruction and model fitting of an individual unit-cell particle (Index: 249) within a 2D lattice with 0% ferritin loading. a, Seven representative tilt images of a single unit-cell particle are shown in the first column (from left). The tilt images are aligned to a common center using IPET through iterative refinement. The projections of the raw, intermediate, and final 3D reconstruction at the corresponding angles are displayed in the subsequent four columns. **b**, A central cross-section (~23 nm thick) of the final reconstruction before masking is applied. **c**, 3D views of the central cross-section. **d**, Final 3D density map of this particle, viewed from four perpendicular directions. **e**, Final 3D reconstruction superimposed with the fitted model, viewed from four perpendicular directions. **f**, FSC analyses of the final map resolution using two methods: map-map FSC, where each map is reconstructed from one half of the images (even vs. odd tilt angle indices), and map-model FSC, where the model map is generated from the fitted model. Resolution assessments are provided based on tilt-based map-map and map-model FSC analyses at thresholds of FSC=0.5 and 0.143, respectively.

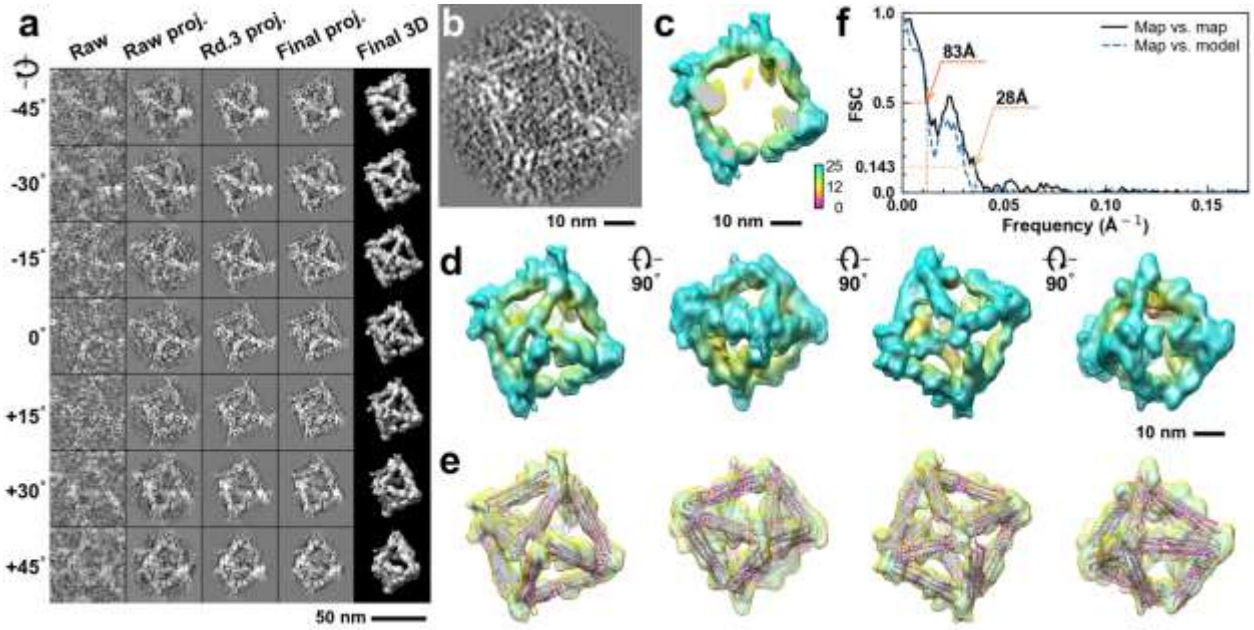

Supplementary Fig. 258: IPET 3D reconstruction and model fitting of an individual unit-cell particle (Index: 250) within a 2D lattice with 0% ferritin loading. a, Seven representative tilt images of a single unit-cell particle are shown in the first column (from left). The tilt images are aligned to a common center using IPET through iterative refinement. The projections of the raw, intermediate, and final 3D reconstruction at the corresponding angles are displayed in the subsequent four columns. **b**, A central cross-section (~23 nm thick) of the final reconstruction before masking is applied. **c**, 3D views of the central cross-section. **d**, Final 3D density map of this particle, viewed from four perpendicular directions. **e**, Final 3D reconstruction superimposed with the fitted model, viewed from four perpendicular directions. **f**, FSC analyses of the final map resolution using two methods: map-map FSC, where each map is reconstructed from one half of the images (even vs. odd tilt angle indices), and map-model FSC, where the model map is generated from the fitted model. Resolution assessments are provided based on tilt-based map-map and map-model FSC analyses at thresholds of FSC=0.5 and 0.143, respectively.

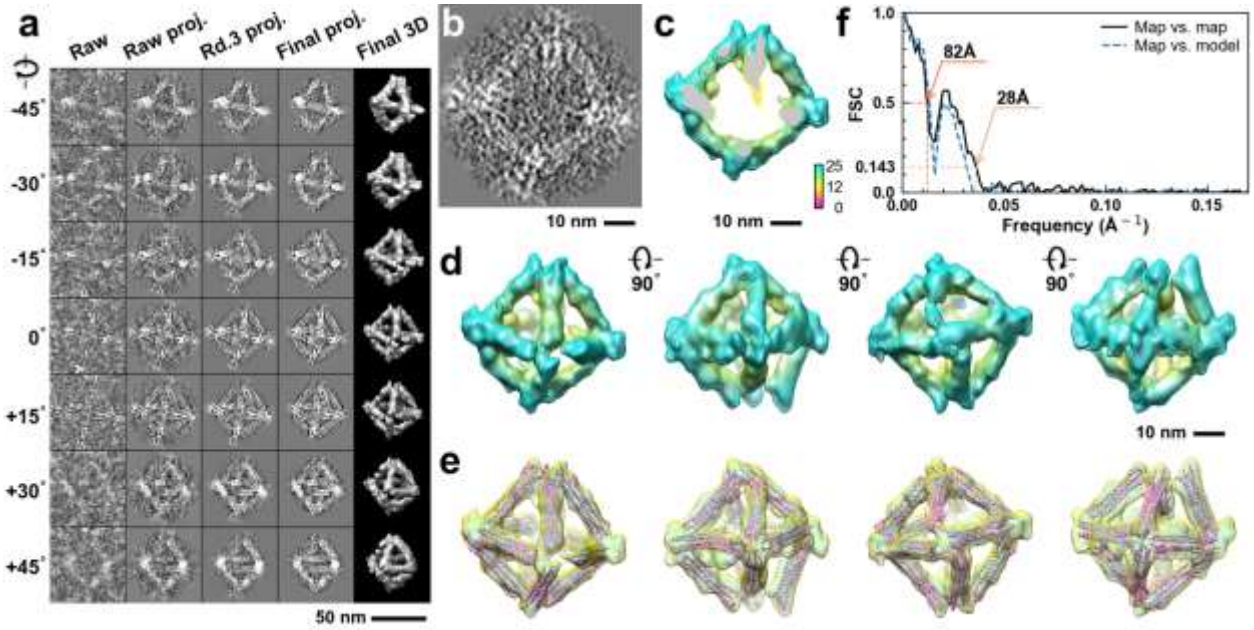

Supplementary Fig. 259: IPET 3D reconstruction and model fitting of an individual unit-cell particle (Index: 251) within a 2D lattice with 0% ferritin loading. a, Seven representative tilt images of a single unit-cell particle are shown in the first column (from left). The tilt images are aligned to a common center using IPET through iterative refinement. The projections of the raw, intermediate, and final 3D reconstruction at the corresponding angles are displayed in the subsequent four columns. **b**, A central cross-section (~23 nm thick) of the final reconstruction before masking is applied. **c**, 3D views of the central cross-section. **d**, Final 3D density map of this particle, viewed from four perpendicular directions. **e**, Final 3D reconstruction superimposed with the fitted model, viewed from four perpendicular directions. **f**, FSC analyses of the final map resolution using two methods: map-map FSC, where each map is reconstructed from one half of the images (even vs. odd tilt angle indices), and map-model FSC, where the model map is generated from the fitted model. Resolution assessments are provided based on tilt-based map-map and map-model FSC analyses at thresholds of FSC=0.5 and 0.143, respectively.

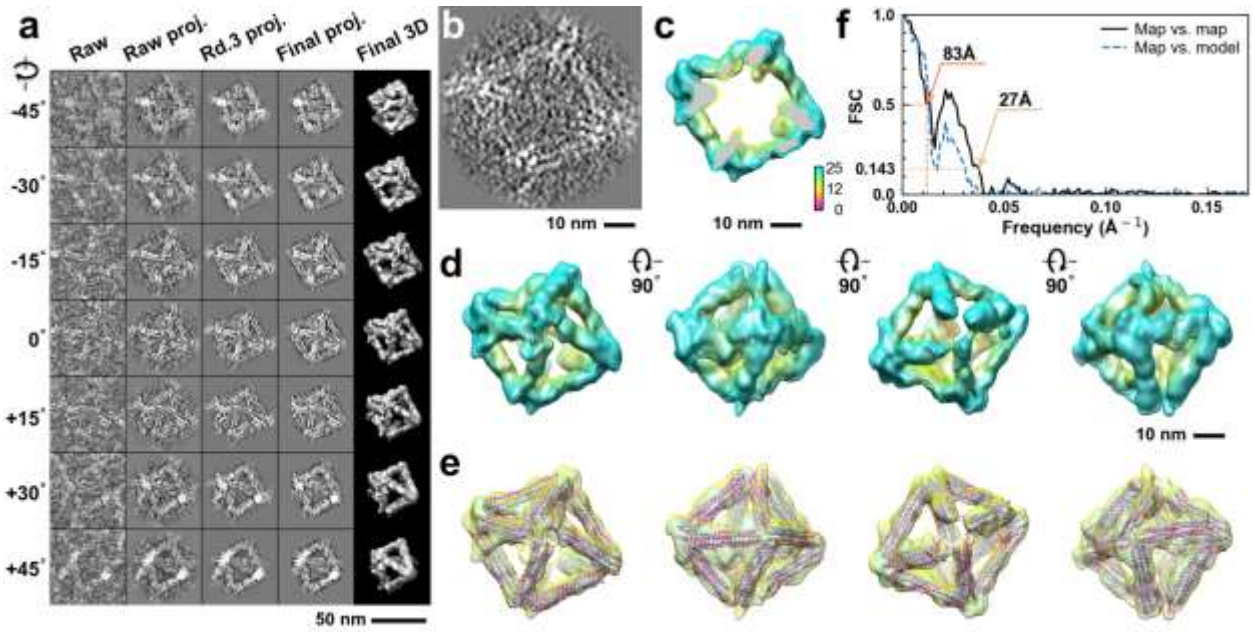

Supplementary Fig. 260: IPET 3D reconstruction and model fitting of an individual unit-cell particle (Index: 252) within a 2D lattice with 0% ferritin loading. a, Seven representative tilt images of a single unit-cell particle are shown in the first column (from left). The tilt images are aligned to a common center using IPET through iterative refinement. The projections of the raw, intermediate, and final 3D reconstruction at the corresponding angles are displayed in the subsequent four columns. **b**, A central cross-section (~23 nm thick) of the final reconstruction before masking is applied. **c**, 3D views of the central cross-section. **d**, Final 3D density map of this particle, viewed from four perpendicular directions. **e**, Final 3D reconstruction superimposed with the fitted model, viewed from four perpendicular directions. **f**, FSC analyses of the final map resolution using two methods: map-map FSC, where each map is reconstructed from one half of the images (even vs. odd tilt angle indices), and map-model FSC, where the model map is generated from the fitted model. Resolution assessments are provided based on tilt-based map-map and map-model FSC analyses at thresholds of FSC=0.5 and 0.143, respectively.

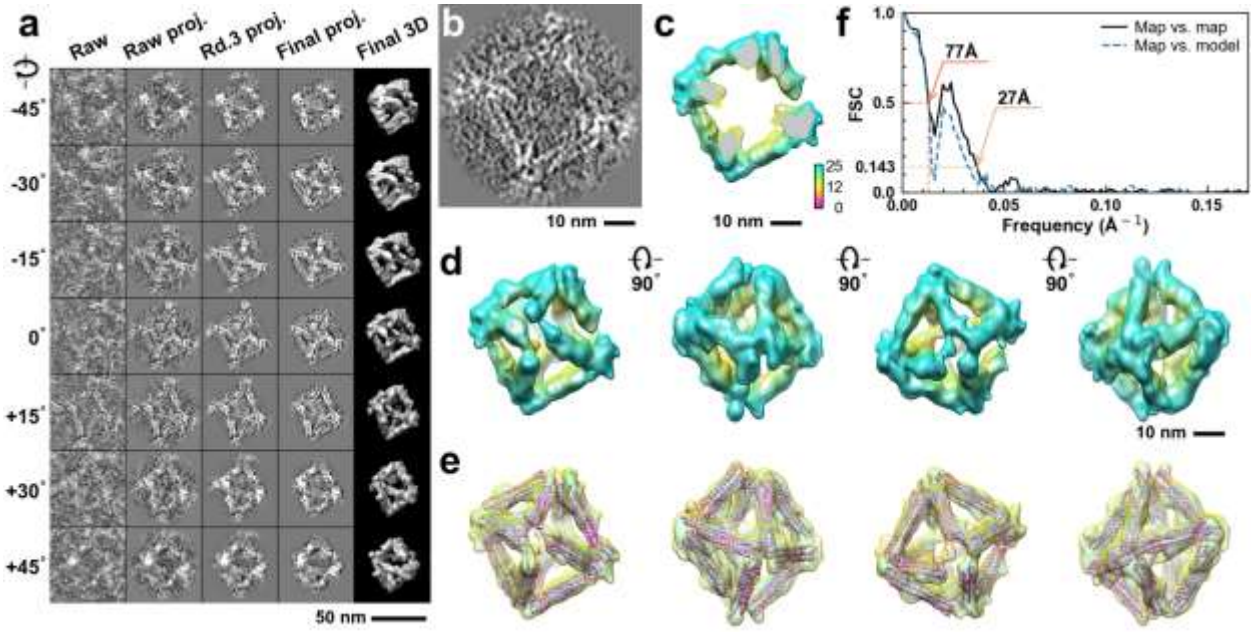

Supplementary Fig. 261: IPET 3D reconstruction and model fitting of an individual unit-cell particle (Index: 253) within a 2D lattice with 0% ferritin loading. a, Seven representative tilt images of a single unit-cell particle are shown in the first column (from left). The tilt images are aligned to a common center using IPET through iterative refinement. The projections of the raw, intermediate, and final 3D reconstruction at the corresponding angles are displayed in the subsequent four columns. **b**, A central cross-section (~23 nm thick) of the final reconstruction before masking is applied. **c**, 3D views of the central cross-section. **d**, Final 3D density map of this particle, viewed from four perpendicular directions. **e**, Final 3D reconstruction superimposed with the fitted model, viewed from four perpendicular directions. **f**, FSC analyses of the final map resolution using two methods: map-map FSC, where each map is reconstructed from one half of the images (even vs. odd tilt angle indices), and map-model FSC, where the model map is generated from the fitted model. Resolution assessments are provided based on tilt-based map-map and map-model FSC analyses at thresholds of FSC=0.5 and 0.143, respectively.

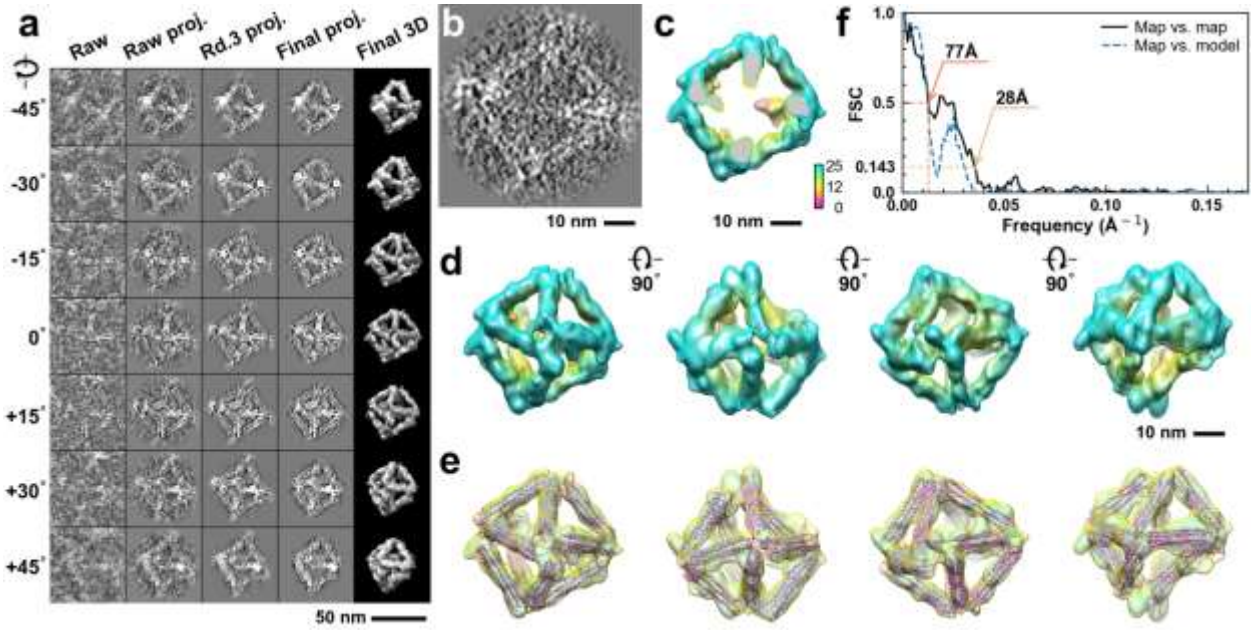

Supplementary Fig. 262: IPET 3D reconstruction and model fitting of an individual unit-cell particle (Index: 254) within a 2D lattice with 0% ferritin loading. a, Seven representative tilt images of a single unit-cell particle are shown in the first column (from left). The tilt images are aligned to a common center using IPET through iterative refinement. The projections of the raw, intermediate, and final 3D reconstruction at the corresponding angles are displayed in the subsequent four columns. **b**, A central cross-section (~23 nm thick) of the final reconstruction before masking is applied. **c**, 3D views of the central cross-section. **d**, Final 3D density map of this particle, viewed from four perpendicular directions. **e**, Final 3D reconstruction superimposed with the fitted model, viewed from four perpendicular directions. **f**, FSC analyses of the final map resolution using two methods: map-map FSC, where each map is reconstructed from one half of the images (even vs. odd tilt angle indices), and map-model FSC, where the model map is generated from the fitted model. Resolution assessments are provided based on tilt-based map-map and map-model FSC analyses at thresholds of FSC=0.5 and 0.143, respectively.

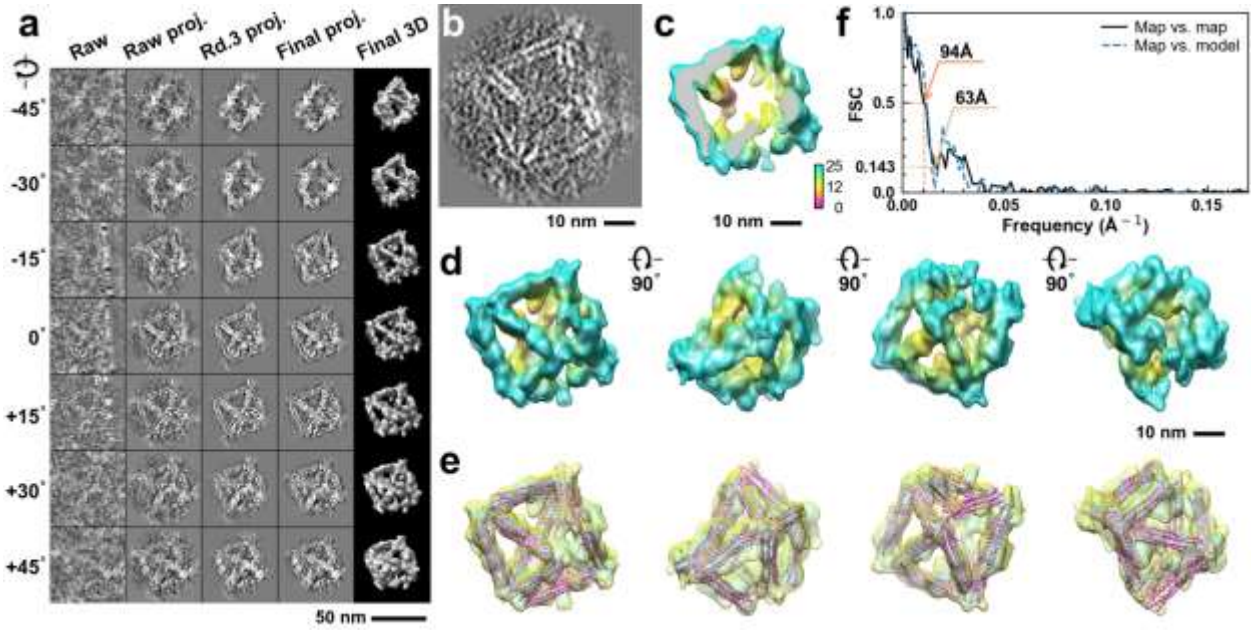

Supplementary Fig. 263: IPET 3D reconstruction and model fitting of an individual unit-cell particle (Index: 255) within a 2D lattice with 0% ferritin loading. a, Seven representative tilt images of a single unit-cell particle are shown in the first column (from left). The tilt images are aligned to a common center using IPET through iterative refinement. The projections of the raw, intermediate, and final 3D reconstruction at the corresponding angles are displayed in the subsequent four columns. **b**, A central cross-section (~23 nm thick) of the final reconstruction before masking is applied. **c**, 3D views of the central cross-section. **d**, Final 3D density map of this particle, viewed from four perpendicular directions. **e**, Final 3D reconstruction superimposed with the fitted model, viewed from four perpendicular directions. **f**, FSC analyses of the final map resolution using two methods: map-map FSC, where each map is reconstructed from one half of the images (even vs. odd tilt angle indices), and map-model FSC, where the model map is generated from the fitted model. Resolution assessments are provided based on tilt-based map-map and map-model FSC analyses at thresholds of FSC=0.5 and 0.143, respectively.

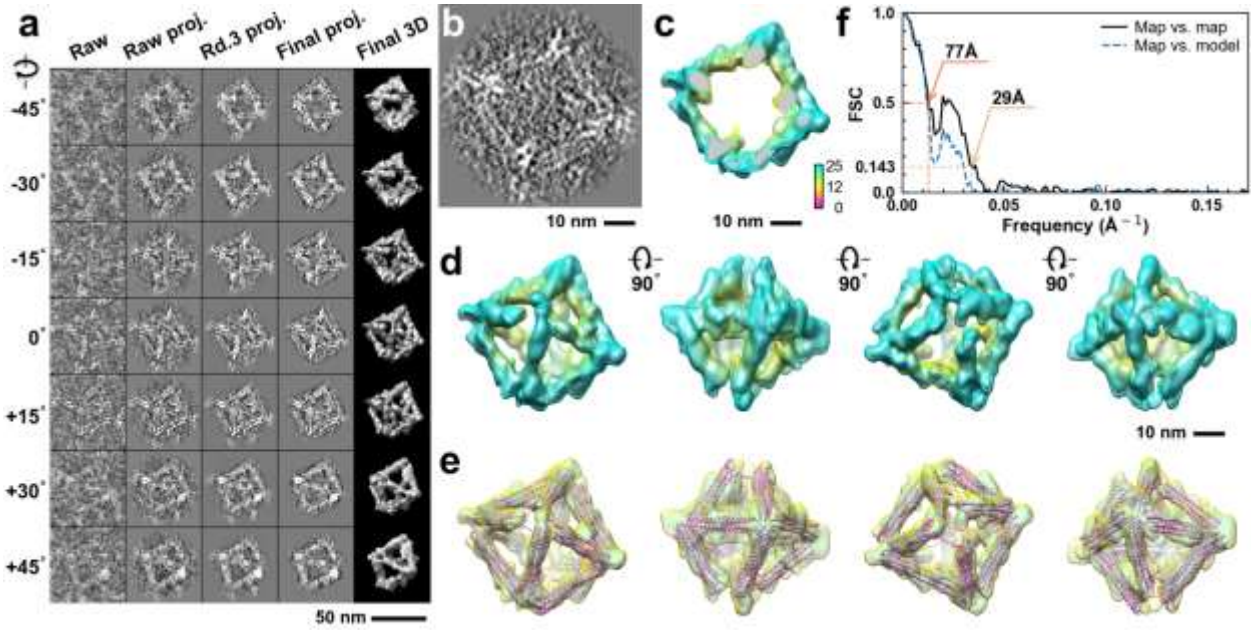

Supplementary Fig. 264: IPET 3D reconstruction and model fitting of an individual unit-cell particle (Index: 256) within a 2D lattice with 0% ferritin loading. a, Seven representative tilt images of a single unit-cell particle are shown in the first column (from left). The tilt images are aligned to a common center using IPET through iterative refinement. The projections of the raw, intermediate, and final 3D reconstruction at the corresponding angles are displayed in the subsequent four columns. **b**, A central cross-section (~23 nm thick) of the final reconstruction before masking is applied. **c**, 3D views of the central cross-section. **d**, Final 3D density map of this particle, viewed from four perpendicular directions. **e**, Final 3D reconstruction superimposed with the fitted model, viewed from four perpendicular directions. **f**, FSC analyses of the final map resolution using two methods: map-map FSC, where each map is reconstructed from one half of the images (even vs. odd tilt angle indices), and map-model FSC, where the model map is generated from the fitted model. Resolution assessments are provided based on tilt-based map-map and map-model FSC analyses at thresholds of FSC=0.5 and 0.143, respectively.

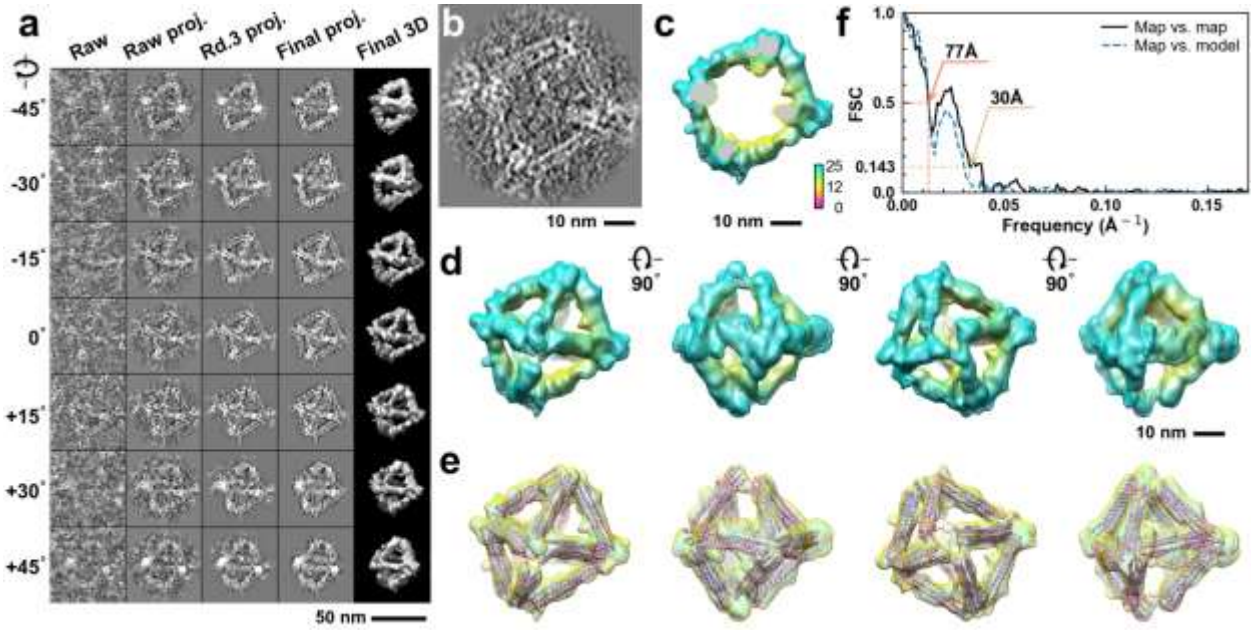

Supplementary Fig. 265: IPET 3D reconstruction and model fitting of an individual unit-cell particle (Index: 257) within a 2D lattice with 0% ferritin loading. a, Seven representative tilt images of a single unit-cell particle are shown in the first column (from left). The tilt images are aligned to a common center using IPET through iterative refinement. The projections of the raw, intermediate, and final 3D reconstruction at the corresponding angles are displayed in the subsequent four columns. **b**, A central cross-section (~23 nm thick) of the final reconstruction before masking is applied. **c**, 3D views of the central cross-section. **d**, Final 3D density map of this particle, viewed from four perpendicular directions. **e**, Final 3D reconstruction superimposed with the fitted model, viewed from four perpendicular directions. **f**, FSC analyses of the final map resolution using two methods: map-map FSC, where each map is reconstructed from one half of the images (even vs. odd tilt angle indices), and map-model FSC, where the model map is generated from the fitted model. Resolution assessments are provided based on tilt-based map-map and map-model FSC analyses at thresholds of FSC=0.5 and 0.143, respectively.

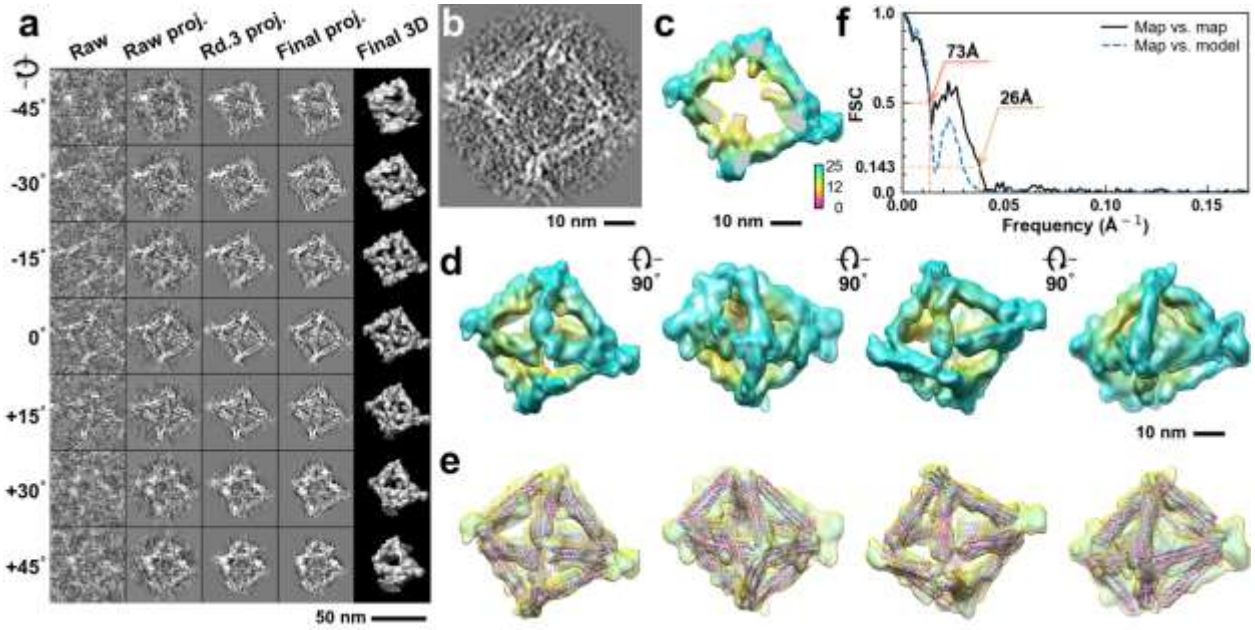

Supplementary Fig. 266: IPET 3D reconstruction and model fitting of an individual unit-cell particle (Index: 258) within a 2D lattice with 0% ferritin loading. a, Seven representative tilt images of a single unit-cell particle are shown in the first column (from left). The tilt images are aligned to a common center using IPET through iterative refinement. The projections of the raw, intermediate, and final 3D reconstruction at the corresponding angles are displayed in the subsequent four columns. **b**, A central cross-section (~23 nm thick) of the final reconstruction before masking is applied. **c**, 3D views of the central cross-section. **d**, Final 3D density map of this particle, viewed from four perpendicular directions. **e**, Final 3D reconstruction superimposed with the fitted model, viewed from four perpendicular directions. **f**, FSC analyses of the final map resolution using two methods: map-map FSC, where each map is reconstructed from one half of the images (even vs. odd tilt angle indices), and map-model FSC, where the model map is generated from the fitted model. Resolution assessments are provided based on tilt-based map-map and map-model FSC analyses at thresholds of FSC=0.5 and 0.143, respectively.

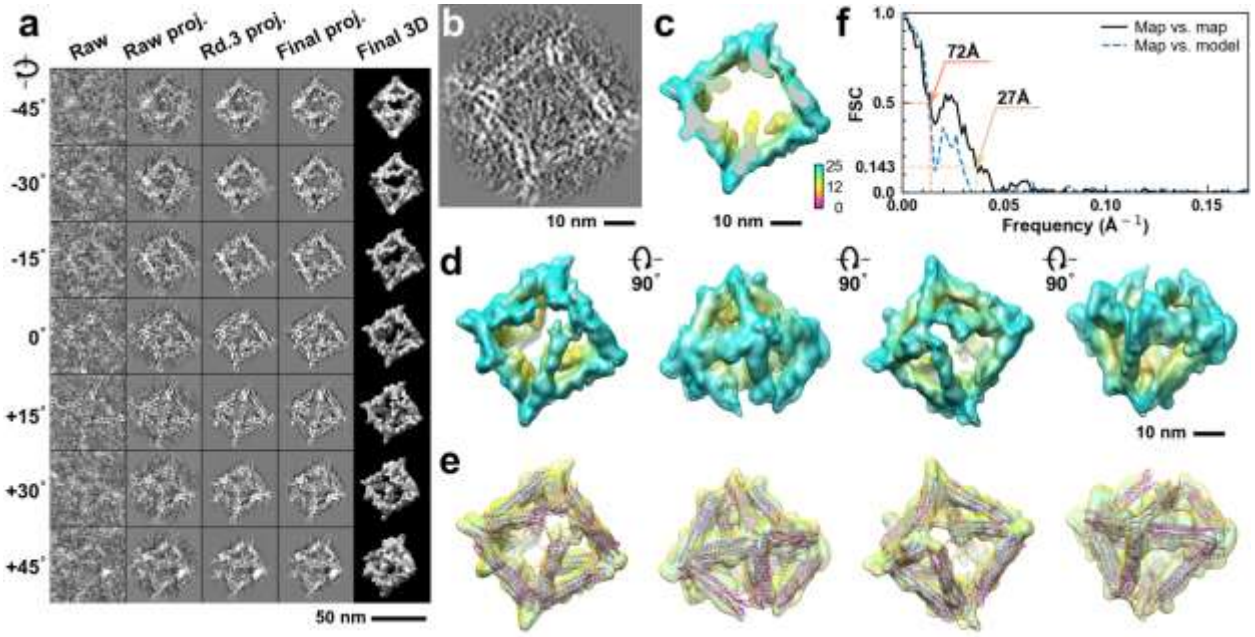

Supplementary Fig. 267: IPET 3D reconstruction and model fitting of an individual unit-cell particle (Index: 259) within a 2D lattice with 0% ferritin loading. a, Seven representative tilt images of a single unit-cell particle are shown in the first column (from left). The tilt images are aligned to a common center using IPET through iterative refinement. The projections of the raw, intermediate, and final 3D reconstruction at the corresponding angles are displayed in the subsequent four columns. **b**, A central cross-section (~23 nm thick) of the final reconstruction before masking is applied. **c**, 3D views of the central cross-section. **d**, Final 3D density map of this particle, viewed from four perpendicular directions. **e**, Final 3D reconstruction superimposed with the fitted model, viewed from four perpendicular directions. **f**, FSC analyses of the final map resolution using two methods: map-map FSC, where each map is reconstructed from one half of the images (even vs. odd tilt angle indices), and map-model FSC, where the model map is generated from the fitted model. Resolution assessments are provided based on tilt-based map-map and map-model FSC analyses at thresholds of FSC=0.5 and 0.143, respectively.

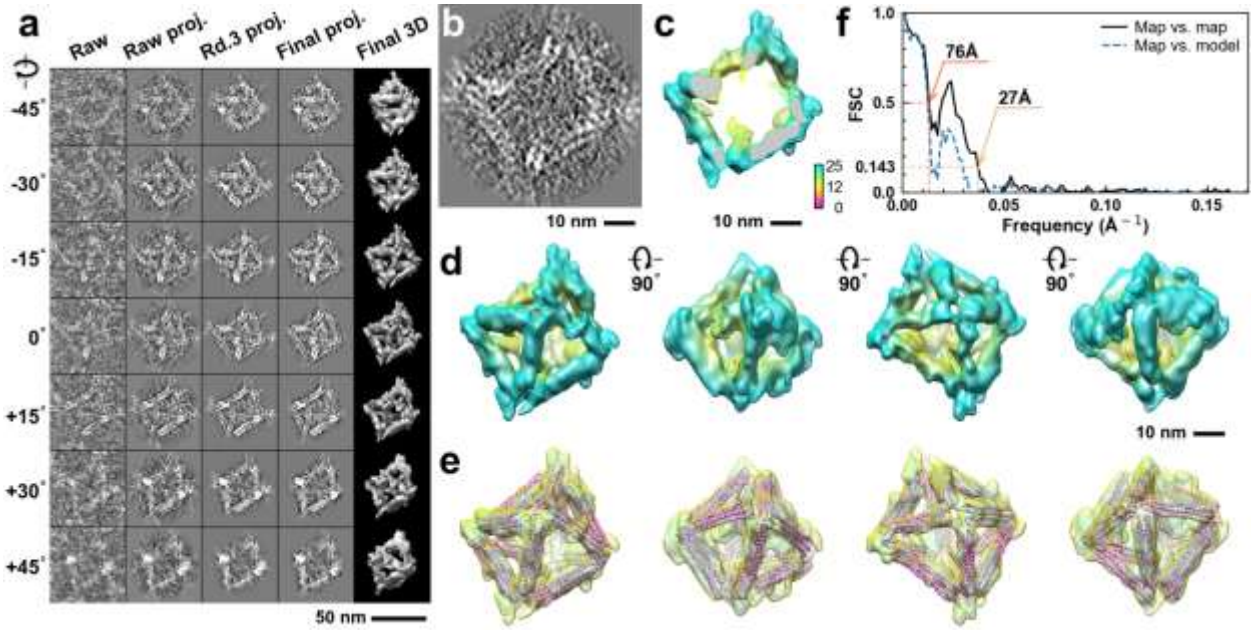

Supplementary Fig. 268: IPET 3D reconstruction and model fitting of an individual unit-cell particle (Index: 260) within a 2D lattice with 0% ferritin loading. a, Seven representative tilt images of a single unit-cell particle are shown in the first column (from left). The tilt images are aligned to a common center using IPET through iterative refinement. The projections of the raw, intermediate, and final 3D reconstruction at the corresponding angles are displayed in the subsequent four columns. **b**, A central cross-section (~23 nm thick) of the final reconstruction before masking is applied. **c**, 3D views of the central cross-section. **d**, Final 3D density map of this particle, viewed from four perpendicular directions. **e**, Final 3D reconstruction superimposed with the fitted model, viewed from four perpendicular directions. **f**, FSC analyses of the final map resolution using two methods: map-map FSC, where each map is reconstructed from one half of the images (even vs. odd tilt angle indices), and map-model FSC, where the model map is generated from the fitted model. Resolution assessments are provided based on tilt-based map-map and map-model FSC analyses at thresholds of FSC=0.5 and 0.143, respectively.

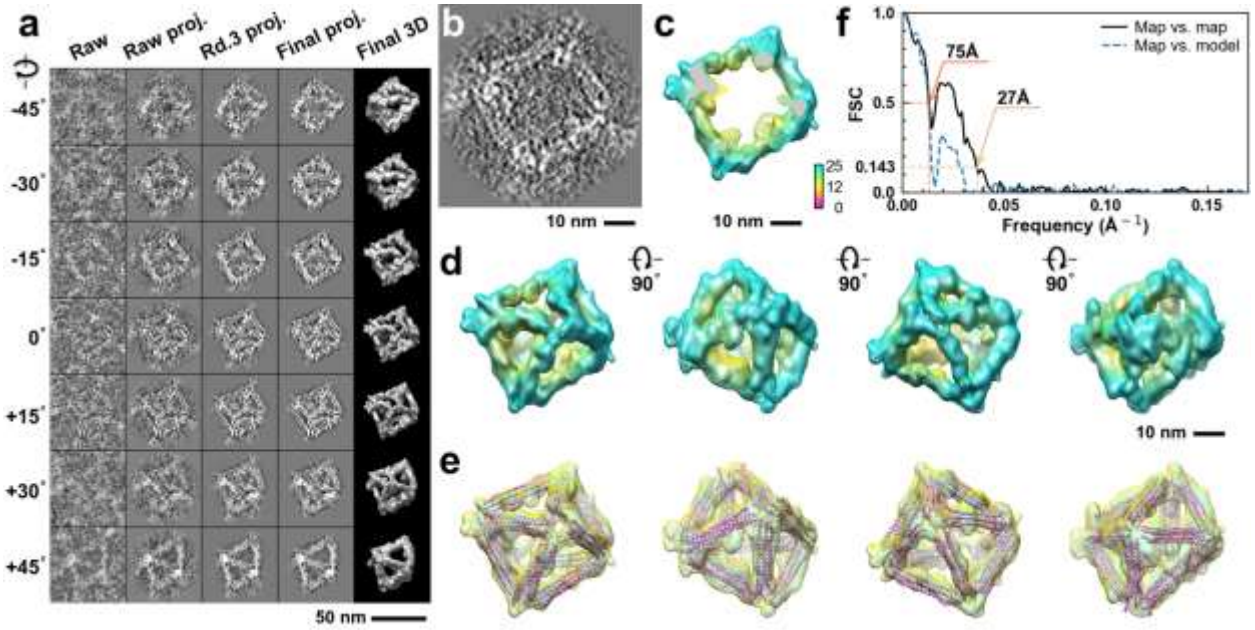

Supplementary Fig. 269: IPET 3D reconstruction and model fitting of an individual unit-cell particle (Index: 261) within a 2D lattice with 0% ferritin loading. a, Seven representative tilt images of a single unit-cell particle are shown in the first column (from left). The tilt images are aligned to a common center using IPET through iterative refinement. The projections of the raw, intermediate, and final 3D reconstruction at the corresponding angles are displayed in the subsequent four columns. **b**, A central cross-section (~23 nm thick) of the final reconstruction before masking is applied. **c**, 3D views of the central cross-section. **d**, Final 3D density map of this particle, viewed from four perpendicular directions. **e**, Final 3D reconstruction superimposed with the fitted model, viewed from four perpendicular directions. **f**, FSC analyses of the final map resolution using two methods: map-map FSC, where each map is reconstructed from one half of the images (even vs. odd tilt angle indices), and map-model FSC, where the model map is generated from the fitted model. Resolution assessments are provided based on tilt-based map-map and map-model FSC analyses at thresholds of FSC=0.5 and 0.143, respectively.

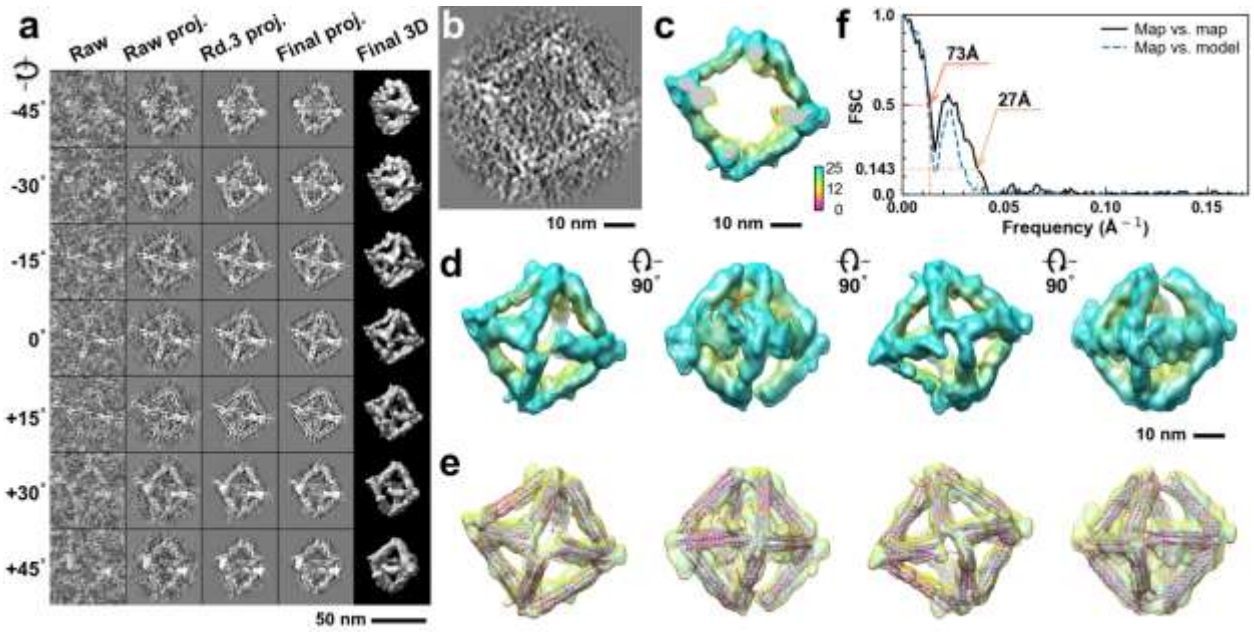

Supplementary Fig. 270: IPET 3D reconstruction and model fitting of an individual unit-cell particle (Index: 262) within a 2D lattice with 0% ferritin loading. a, Seven representative tilt images of a single unit-cell particle are shown in the first column (from left). The tilt images are aligned to a common center using IPET through iterative refinement. The projections of the raw, intermediate, and final 3D reconstruction at the corresponding angles are displayed in the subsequent four columns. **b**, A central cross-section (~23 nm thick) of the final reconstruction before masking is applied. **c**, 3D views of the central cross-section. **d**, Final 3D density map of this particle, viewed from four perpendicular directions. **e**, Final 3D reconstruction superimposed with the fitted model, viewed from four perpendicular directions. **f**, FSC analyses of the final map resolution using two methods: map-map FSC, where each map is reconstructed from one half of the images (even vs. odd tilt angle indices), and map-model FSC, where the model map is generated from the fitted model. Resolution assessments are provided based on tilt-based map-map and map-model FSC analyses at thresholds of FSC=0.5 and 0.143, respectively.

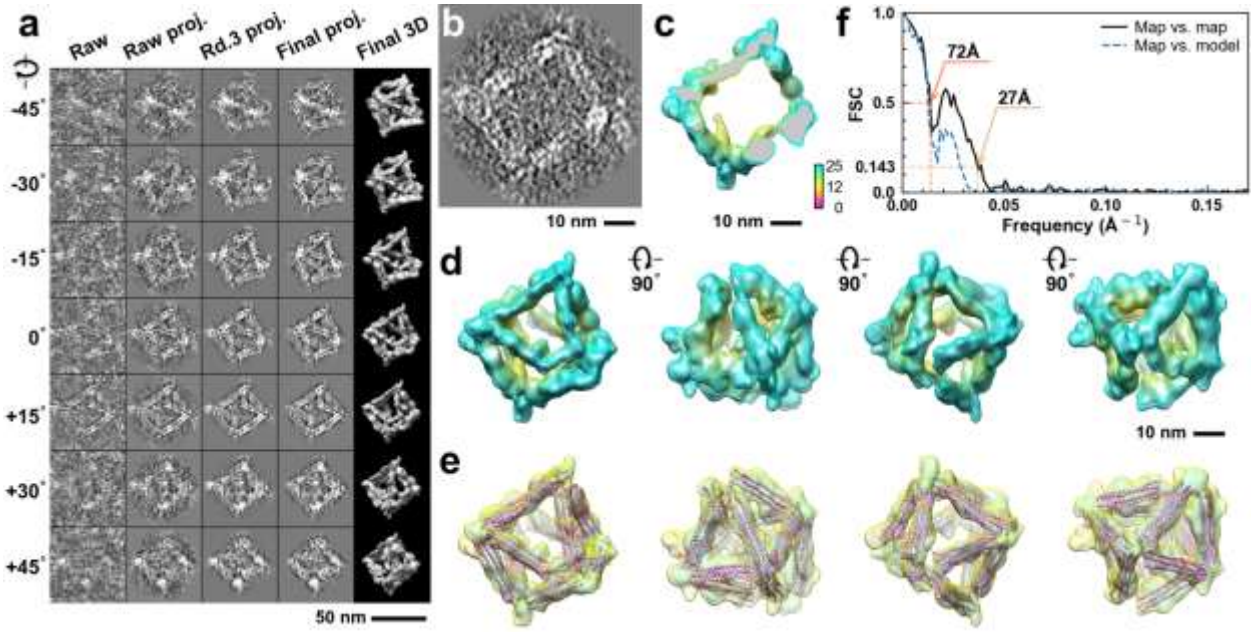

Supplementary Fig. 271: IPET 3D reconstruction and model fitting of an individual unit-cell particle (Index: 263) within a 2D lattice with 0% ferritin loading. a, Seven representative tilt images of a single unit-cell particle are shown in the first column (from left). The tilt images are aligned to a common center using IPET through iterative refinement. The projections of the raw, intermediate, and final 3D reconstruction at the corresponding angles are displayed in the subsequent four columns. **b**, A central cross-section (~23 nm thick) of the final reconstruction before masking is applied. **c**, 3D views of the central cross-section. **d**, Final 3D density map of this particle, viewed from four perpendicular directions. **e**, Final 3D reconstruction superimposed with the fitted model, viewed from four perpendicular directions. **f**, FSC analyses of the final map resolution using two methods: map-map FSC, where each map is reconstructed from one half of the images (even vs. odd tilt angle indices), and map-model FSC, where the model map is generated from the fitted model. Resolution assessments are provided based on tilt-based map-map and map-model FSC analyses at thresholds of FSC=0.5 and 0.143, respectively.

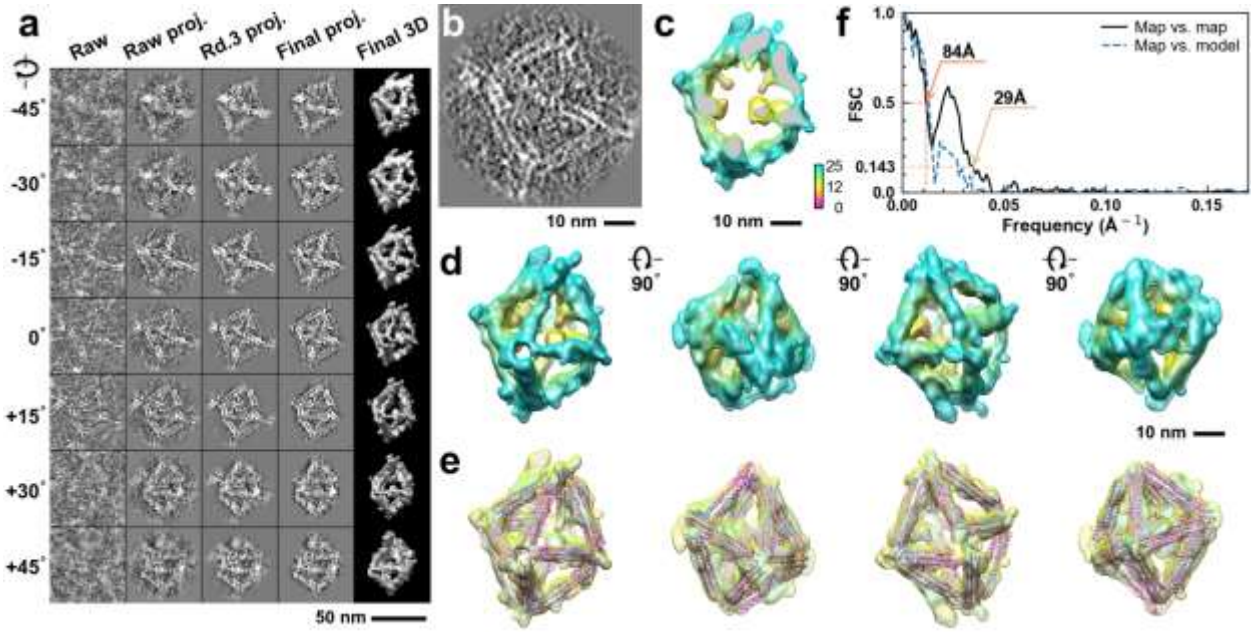

Supplementary Fig. 272: IPET 3D reconstruction and model fitting of an individual unit-cell particle (Index: 264) within a 2D lattice with 0% ferritin loading. a, Seven representative tilt images of a single unit-cell particle are shown in the first column (from left). The tilt images are aligned to a common center using IPET through iterative refinement. The projections of the raw, intermediate, and final 3D reconstruction at the corresponding angles are displayed in the subsequent four columns. **b**, A central cross-section (~23 nm thick) of the final reconstruction before masking is applied. **c**, 3D views of the central cross-section. **d**, Final 3D density map of this particle, viewed from four perpendicular directions. **e**, Final 3D reconstruction superimposed with the fitted model, viewed from four perpendicular directions. **f**, FSC analyses of the final map resolution using two methods: map-map FSC, where each map is reconstructed from one half of the images (even vs. odd tilt angle indices), and map-model FSC, where the model map is generated from the fitted model. Resolution assessments are provided based on tilt-based map-map and map-model FSC analyses at thresholds of FSC=0.5 and 0.143, respectively.

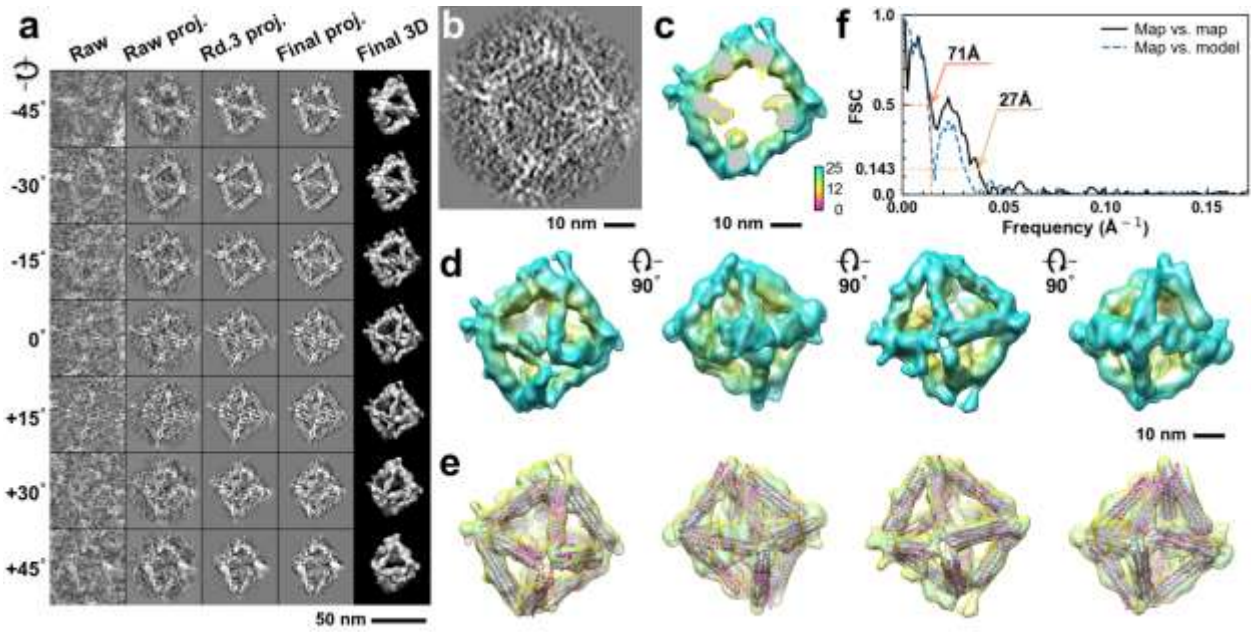

Supplementary Fig. 273: IPET 3D reconstruction and model fitting of an individual unit-cell particle (Index: 265) within a 2D lattice with 0% ferritin loading. a, Seven representative tilt images of a single unit-cell particle are shown in the first column (from left). The tilt images are aligned to a common center using IPET through iterative refinement. The projections of the raw, intermediate, and final 3D reconstruction at the corresponding angles are displayed in the subsequent four columns. **b**, A central cross-section (~23 nm thick) of the final reconstruction before masking is applied. **c**, 3D views of the central cross-section. **d**, Final 3D density map of this particle, viewed from four perpendicular directions. **e**, Final 3D reconstruction superimposed with the fitted model, viewed from four perpendicular directions. **f**, FSC analyses of the final map resolution using two methods: map-map FSC, where each map is reconstructed from one half of the images (even vs. odd tilt angle indices), and map-model FSC, where the model map is generated from the fitted model. Resolution assessments are provided based on tilt-based map-map and map-model FSC analyses at thresholds of FSC=0.5 and 0.143, respectively.

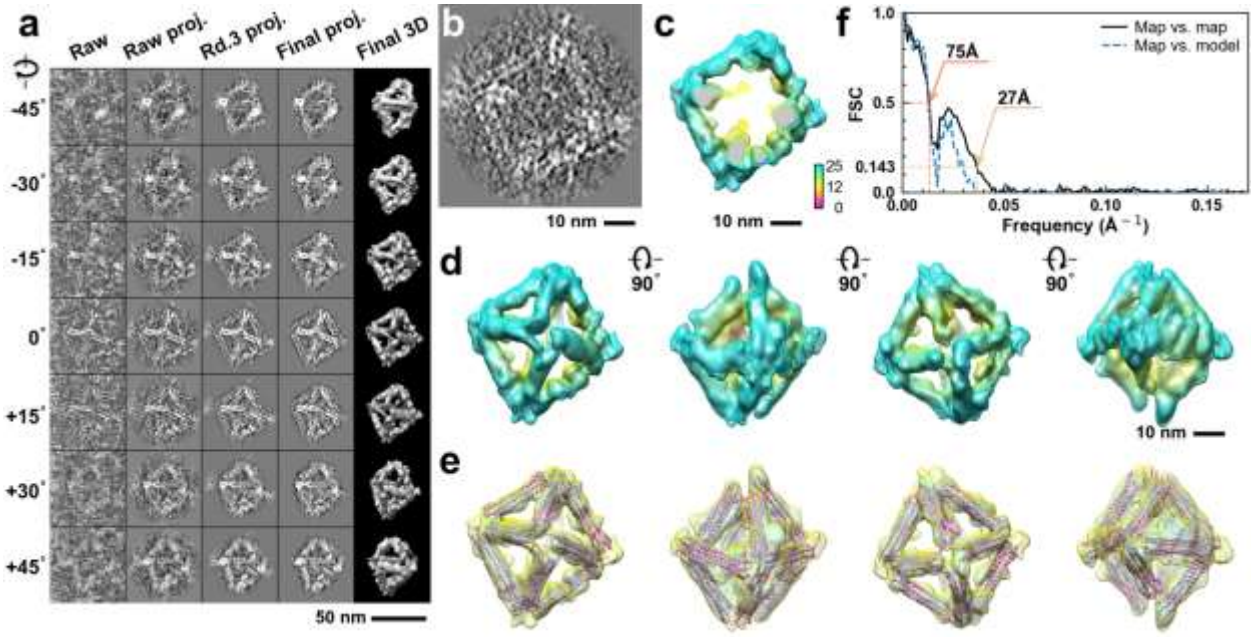

Supplementary Fig. 274: IPET 3D reconstruction and model fitting of an individual unit-cell particle (Index: 266) within a 2D lattice with 0% ferritin loading. a, Seven representative tilt images of a single unit-cell particle are shown in the first column (from left). The tilt images are aligned to a common center using IPET through iterative refinement. The projections of the raw, intermediate, and final 3D reconstruction at the corresponding angles are displayed in the subsequent four columns. **b**, A central cross-section (~23 nm thick) of the final reconstruction before masking is applied. **c**, 3D views of the central cross-section. **d**, Final 3D density map of this particle, viewed from four perpendicular directions. **e**, Final 3D reconstruction superimposed with the fitted model, viewed from four perpendicular directions. **f**, FSC analyses of the final map resolution using two methods: map-map FSC, where each map is reconstructed from one half of the images (even vs. odd tilt angle indices), and map-model FSC, where the model map is generated from the fitted model. Resolution assessments are provided based on tilt-based map-map and map-model FSC analyses at thresholds of FSC=0.5 and 0.143, respectively.

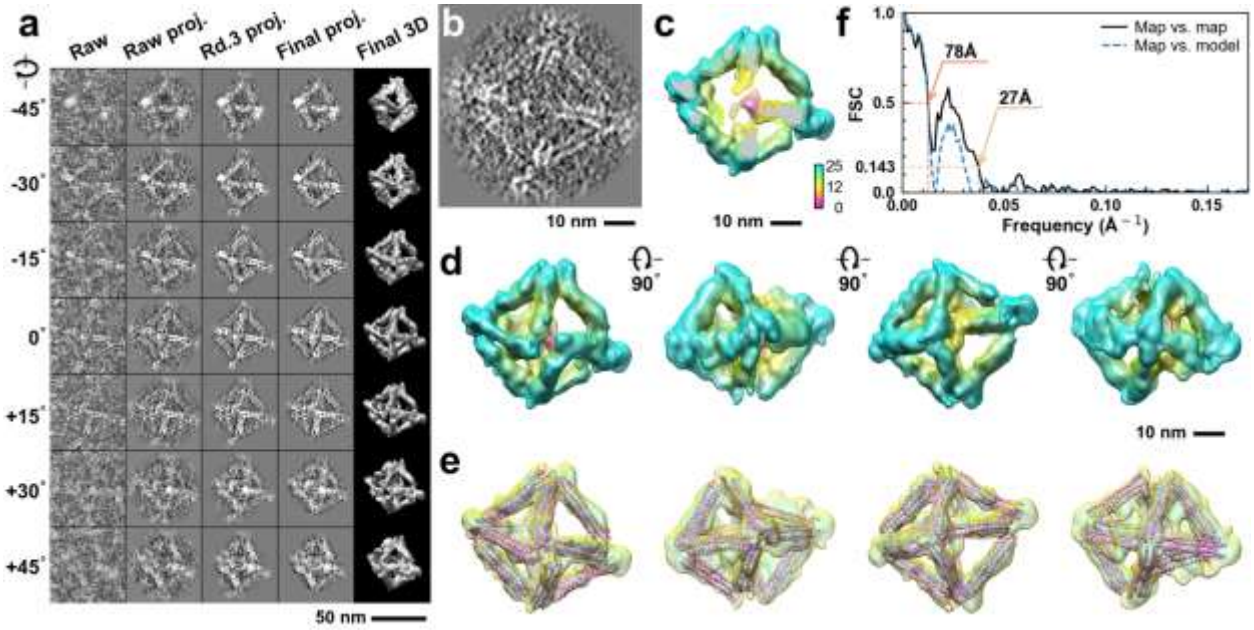

Supplementary Fig. 275: IPET 3D reconstruction and model fitting of an individual unit-cell particle (Index: 267) within a 2D lattice with 0% ferritin loading. a, Seven representative tilt images of a single unit-cell particle are shown in the first column (from left). The tilt images are aligned to a common center using IPET through iterative refinement. The projections of the raw, intermediate, and final 3D reconstruction at the corresponding angles are displayed in the subsequent four columns. **b**, A central cross-section (~23 nm thick) of the final reconstruction before masking is applied. **c**, 3D views of the central cross-section. **d**, Final 3D density map of this particle, viewed from four perpendicular directions. **e**, Final 3D reconstruction superimposed with the fitted model, viewed from four perpendicular directions. **f**, FSC analyses of the final map resolution using two methods: map-map FSC, where each map is reconstructed from one half of the images (even vs. odd tilt angle indices), and map-model FSC, where the model map is generated from the fitted model. Resolution assessments are provided based on tilt-based map-map and map-model FSC analyses at thresholds of FSC=0.5 and 0.143, respectively.

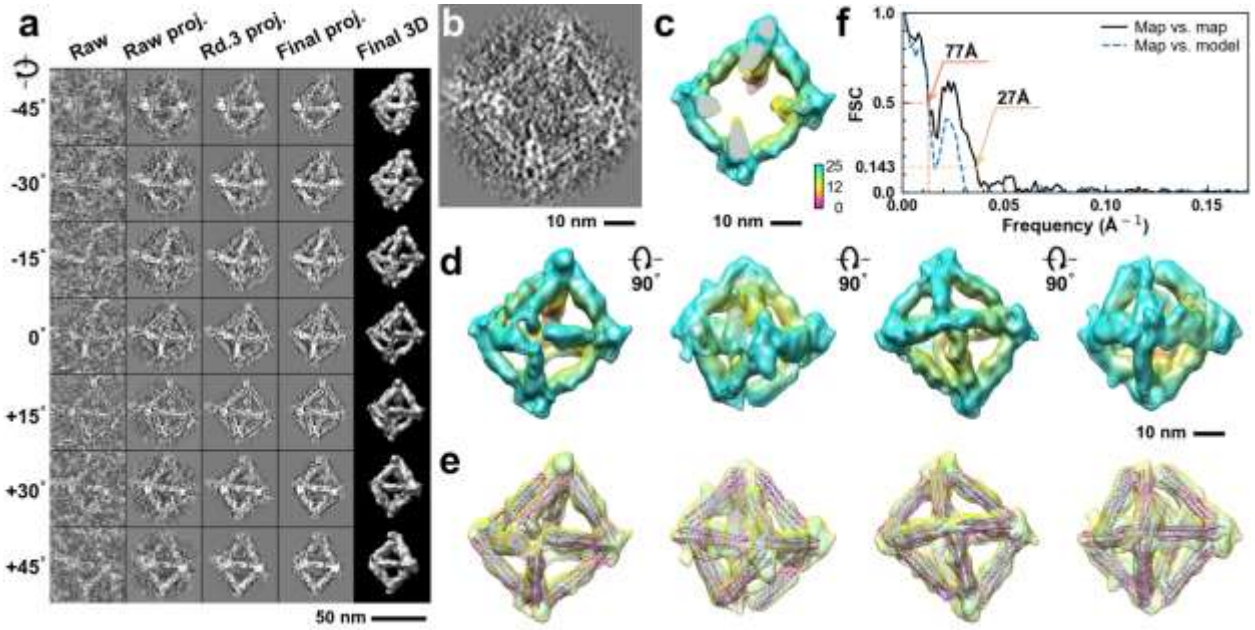

Supplementary Fig. 276: IPET 3D reconstruction and model fitting of an individual unit-cell particle (Index: 268) within a 2D lattice with 0% ferritin loading. a, Seven representative tilt images of a single unit-cell particle are shown in the first column (from left). The tilt images are aligned to a common center using IPET through iterative refinement. The projections of the raw, intermediate, and final 3D reconstruction at the corresponding angles are displayed in the subsequent four columns. **b**, A central cross-section (~23 nm thick) of the final reconstruction before masking is applied. **c**, 3D views of the central cross-section. **d**, Final 3D density map of this particle, viewed from four perpendicular directions. **e**, Final 3D reconstruction superimposed with the fitted model, viewed from four perpendicular directions. **f**, FSC analyses of the final map resolution using two methods: map-map FSC, where each map is reconstructed from one half of the images (even vs. odd tilt angle indices), and map-model FSC, where the model map is generated from the fitted model. Resolution assessments are provided based on tilt-based map-map and map-model FSC analyses at thresholds of FSC=0.5 and 0.143, respectively.

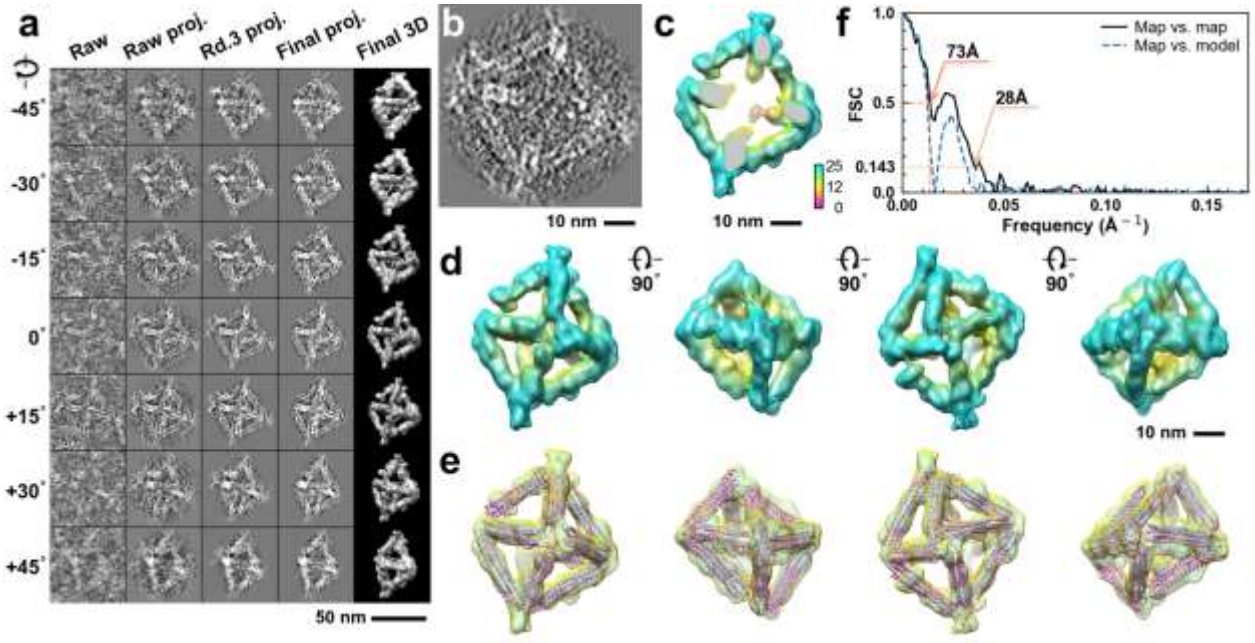

Supplementary Fig. 277: IPET 3D reconstruction and model fitting of an individual unit-cell particle (Index: 269) within a 2D lattice with 0% ferritin loading. a, Seven representative tilt images of a single unit-cell particle are shown in the first column (from left). The tilt images are aligned to a common center using IPET through iterative refinement. The projections of the raw, intermediate, and final 3D reconstruction at the corresponding angles are displayed in the subsequent four columns. **b**, A central cross-section (~23 nm thick) of the final reconstruction before masking is applied. **c**, 3D views of the central cross-section. **d**, Final 3D density map of this particle, viewed from four perpendicular directions. **e**, Final 3D reconstruction superimposed with the fitted model, viewed from four perpendicular directions. **f**, FSC analyses of the final map resolution using two methods: map-map FSC, where each map is reconstructed from one half of the images (even vs. odd tilt angle indices), and map-model FSC, where the model map is generated from the fitted model. Resolution assessments are provided based on tilt-based map-map and map-model FSC analyses at thresholds of FSC=0.5 and 0.143, respectively.

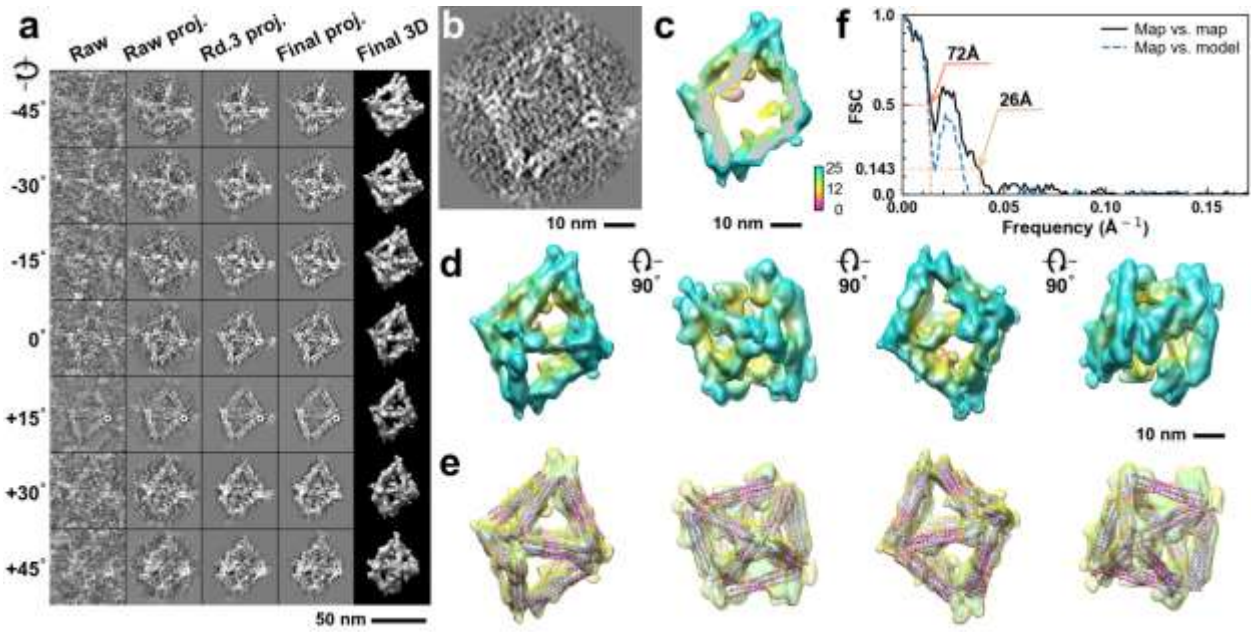

Supplementary Fig. 278: IPET 3D reconstruction and model fitting of an individual unit-cell particle (Index: 270) within a 2D lattice with 0% ferritin loading. a, Seven representative tilt images of a single unit-cell particle are shown in the first column (from left). The tilt images are aligned to a common center using IPET through iterative refinement. The projections of the raw, intermediate, and final 3D reconstruction at the corresponding angles are displayed in the subsequent four columns. **b**, A central cross-section (~23 nm thick) of the final reconstruction before masking is applied. **c**, 3D views of the central cross-section. **d**, Final 3D density map of this particle, viewed from four perpendicular directions. **e**, Final 3D reconstruction superimposed with the fitted model, viewed from four perpendicular directions. **f**, FSC analyses of the final map resolution using two methods: map-map FSC, where each map is reconstructed from one half of the images (even vs. odd tilt angle indices), and map-model FSC, where the model map is generated from the fitted model. Resolution assessments are provided based on tilt-based map-map and map-model FSC analyses at thresholds of FSC=0.5 and 0.143, respectively.

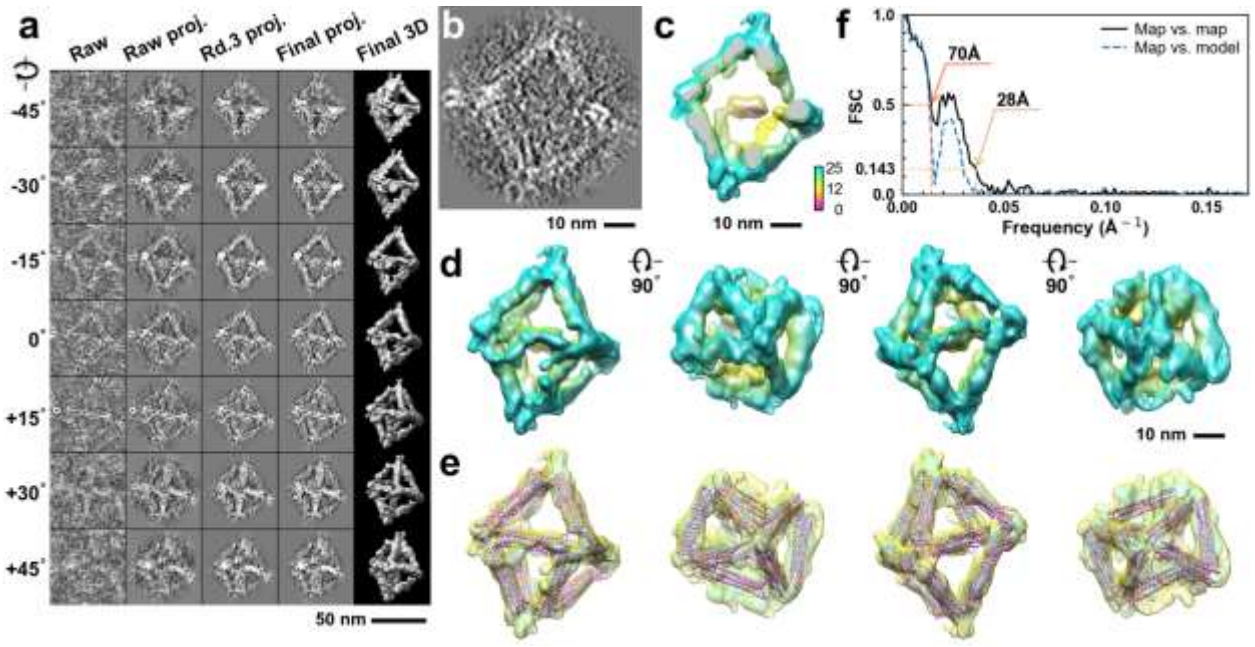

Supplementary Fig. 279: IPET 3D reconstruction and model fitting of an individual unit-cell particle (Index: 271) within a 2D lattice with 0% ferritin loading. a, Seven representative tilt images of a single unit-cell particle are shown in the first column (from left). The tilt images are aligned to a common center using IPET through iterative refinement. The projections of the raw, intermediate, and final 3D reconstruction at the corresponding angles are displayed in the subsequent four columns. **b**, A central cross-section (~23 nm thick) of the final reconstruction before masking is applied. **c**, 3D views of the central cross-section. **d**, Final 3D density map of this particle, viewed from four perpendicular directions. **e**, Final 3D reconstruction superimposed with the fitted model, viewed from four perpendicular directions. **f**, FSC analyses of the final map resolution using two methods: map-map FSC, where each map is reconstructed from one half of the images (even vs. odd tilt angle indices), and map-model FSC, where the model map is generated from the fitted model. Resolution assessments are provided based on tilt-based map-map and map-model FSC analyses at thresholds of FSC=0.5 and 0.143, respectively.

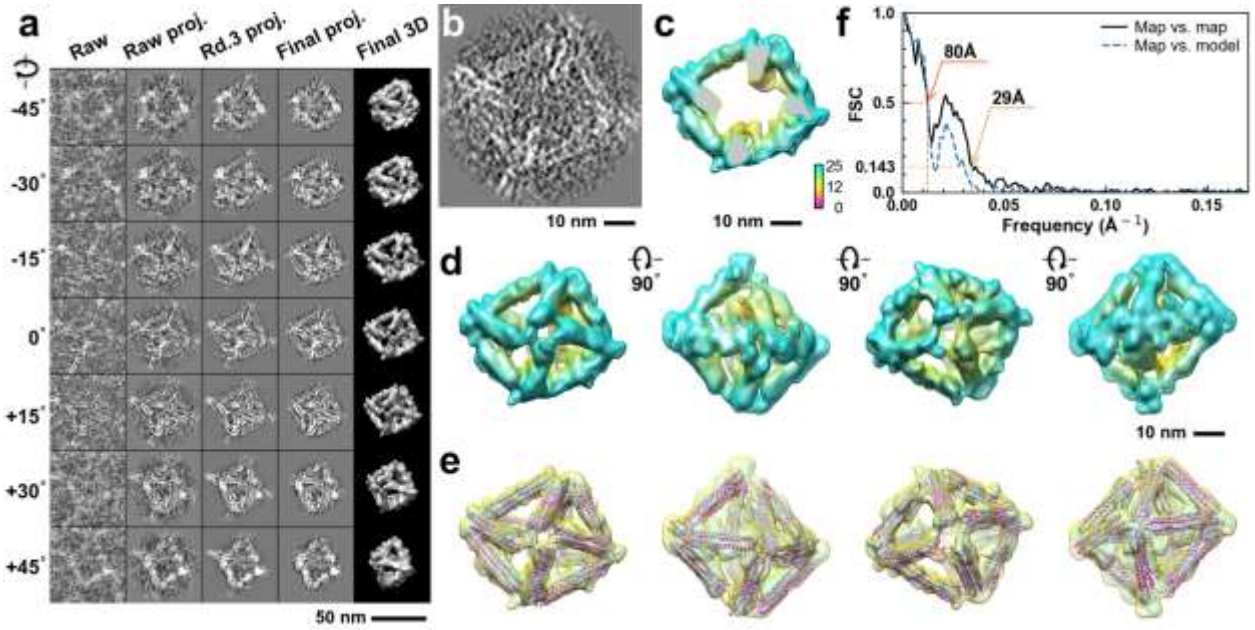

Supplementary Fig. 280: IPET 3D reconstruction and model fitting of an individual unit-cell particle (Index: 272) within a 2D lattice with 0% ferritin loading. a, Seven representative tilt images of a single unit-cell particle are shown in the first column (from left). The tilt images are aligned to a common center using IPET through iterative refinement. The projections of the raw, intermediate, and final 3D reconstruction at the corresponding angles are displayed in the subsequent four columns. **b**, A central cross-section (~23 nm thick) of the final reconstruction before masking is applied. **c**, 3D views of the central cross-section. **d**, Final 3D density map of this particle, viewed from four perpendicular directions. **e**, Final 3D reconstruction superimposed with the fitted model, viewed from four perpendicular directions. **f**, FSC analyses of the final map resolution using two methods: map-map FSC, where each map is reconstructed from one half of the images (even vs. odd tilt angle indices), and map-model FSC, where the model map is generated from the fitted model. Resolution assessments are provided based on tilt-based map-map and map-model FSC analyses at thresholds of FSC=0.5 and 0.143, respectively.

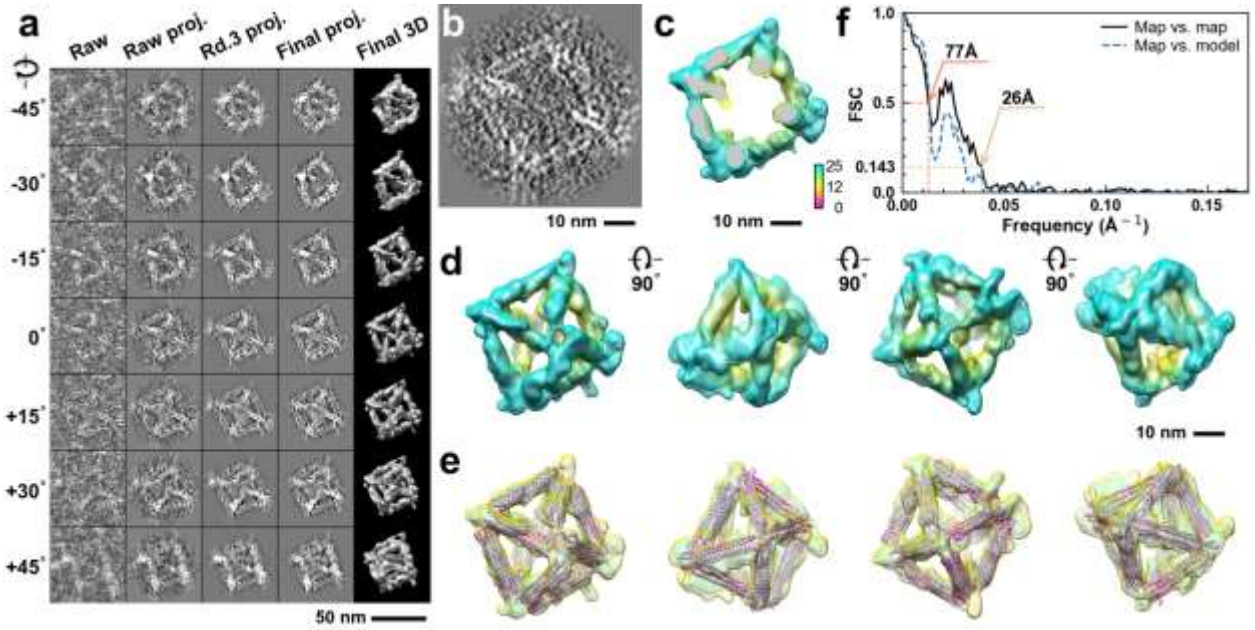

Supplementary Fig. 281: IPET 3D reconstruction and model fitting of an individual unit-cell particle (Index: 273) within a 2D lattice with 0% ferritin loading. a, Seven representative tilt images of a single unit-cell particle are shown in the first column (from left). The tilt images are aligned to a common center using IPET through iterative refinement. The projections of the raw, intermediate, and final 3D reconstruction at the corresponding angles are displayed in the subsequent four columns. **b**, A central cross-section (~23 nm thick) of the final reconstruction before masking is applied. **c**, 3D views of the central cross-section. **d**, Final 3D density map of this particle, viewed from four perpendicular directions. **e**, Final 3D reconstruction superimposed with the fitted model, viewed from four perpendicular directions. **f**, FSC analyses of the final map resolution using two methods: map-map FSC, where each map is reconstructed from one half of the images (even vs. odd tilt angle indices), and map-model FSC, where the model map is generated from the fitted model. Resolution assessments are provided based on tilt-based map-map and map-model FSC analyses at thresholds of FSC=0.5 and 0.143, respectively.

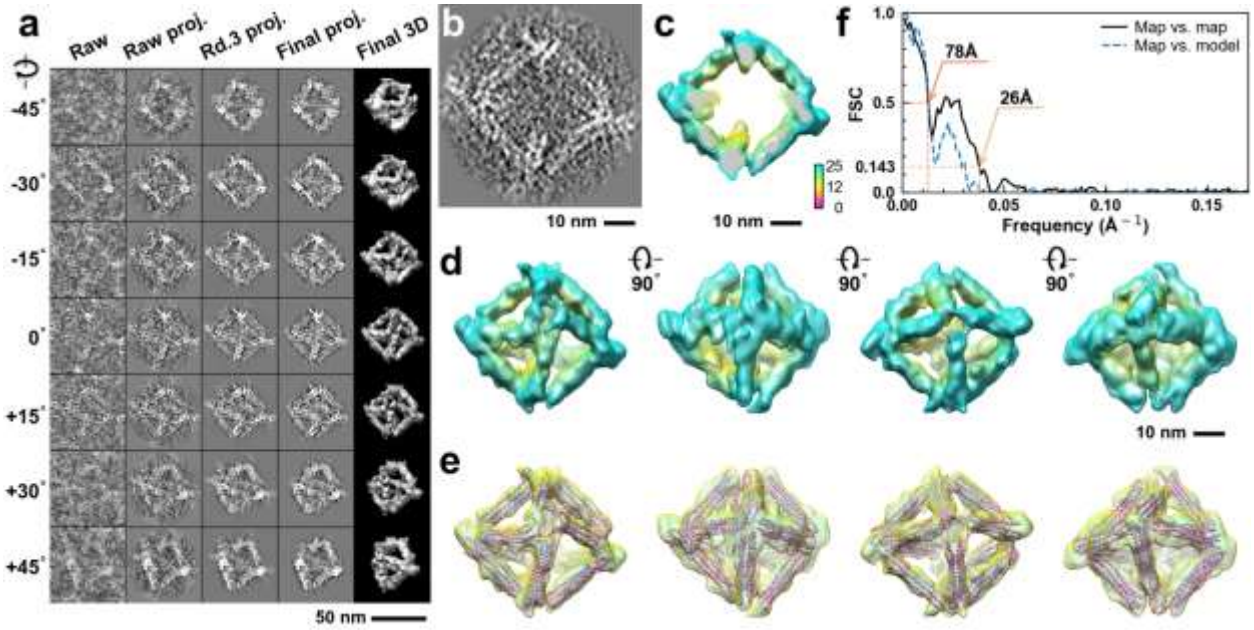

Supplementary Fig. 282: IPET 3D reconstruction and model fitting of an individual unit-cell particle (Index: 274) within a 2D lattice with 0% ferritin loading. a, Seven representative tilt images of a single unit-cell particle are shown in the first column (from left). The tilt images are aligned to a common center using IPET through iterative refinement. The projections of the raw, intermediate, and final 3D reconstruction at the corresponding angles are displayed in the subsequent four columns. **b**, A central cross-section (~23 nm thick) of the final reconstruction before masking is applied. **c**, 3D views of the central cross-section. **d**, Final 3D density map of this particle, viewed from four perpendicular directions. **e**, Final 3D reconstruction superimposed with the fitted model, viewed from four perpendicular directions. **f**, FSC analyses of the final map resolution using two methods: map-map FSC, where each map is reconstructed from one half of the images (even vs. odd tilt angle indices), and map-model FSC, where the model map is generated from the fitted model. Resolution assessments are provided based on tilt-based map-map and map-model FSC analyses at thresholds of FSC=0.5 and 0.143, respectively.

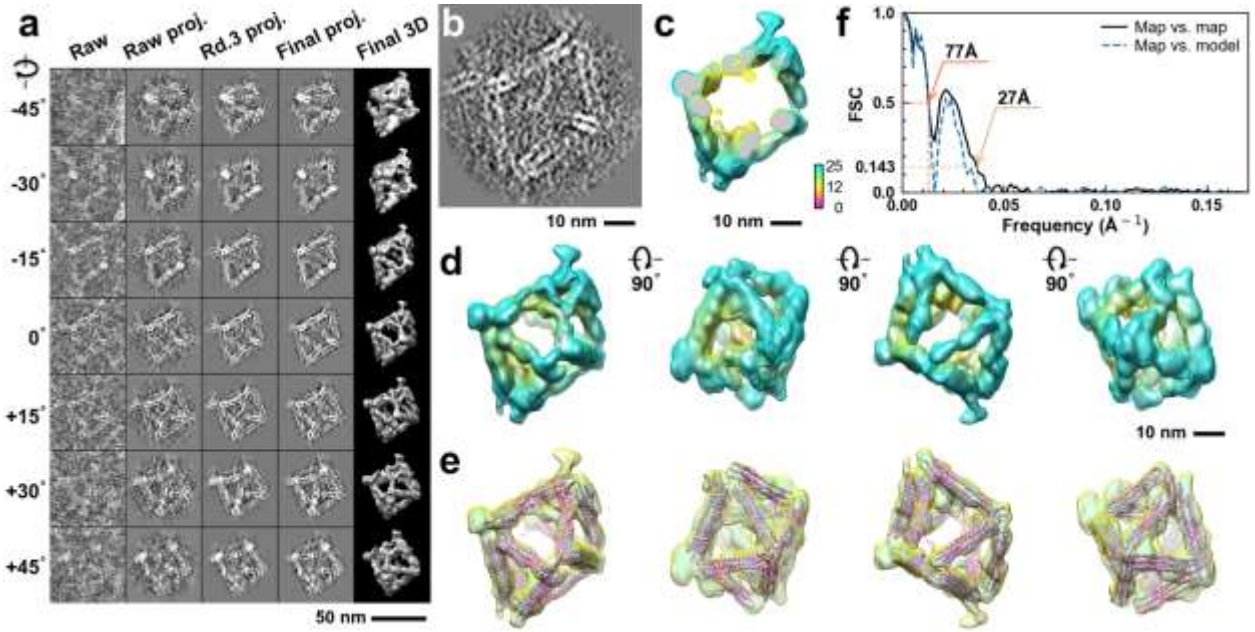

Supplementary Fig. 283: IPET 3D reconstruction and model fitting of an individual unit-cell particle (Index: 275) within a 2D lattice with 0% ferritin loading. a, Seven representative tilt images of a single unit-cell particle are shown in the first column (from left). The tilt images are aligned to a common center using IPET through iterative refinement. The projections of the raw, intermediate, and final 3D reconstruction at the corresponding angles are displayed in the subsequent four columns. **b**, A central cross-section (~23 nm thick) of the final reconstruction before masking is applied. **c**, 3D views of the central cross-section. **d**, Final 3D density map of this particle, viewed from four perpendicular directions. **e**, Final 3D reconstruction superimposed with the fitted model, viewed from four perpendicular directions. **f**, FSC analyses of the final map resolution using two methods: map-map FSC, where each map is reconstructed from one half of the images (even vs. odd tilt angle indices), and map-model FSC, where the model map is generated from the fitted model. Resolution assessments are provided based on tilt-based map-map and map-model FSC analyses at thresholds of FSC=0.5 and 0.143, respectively.

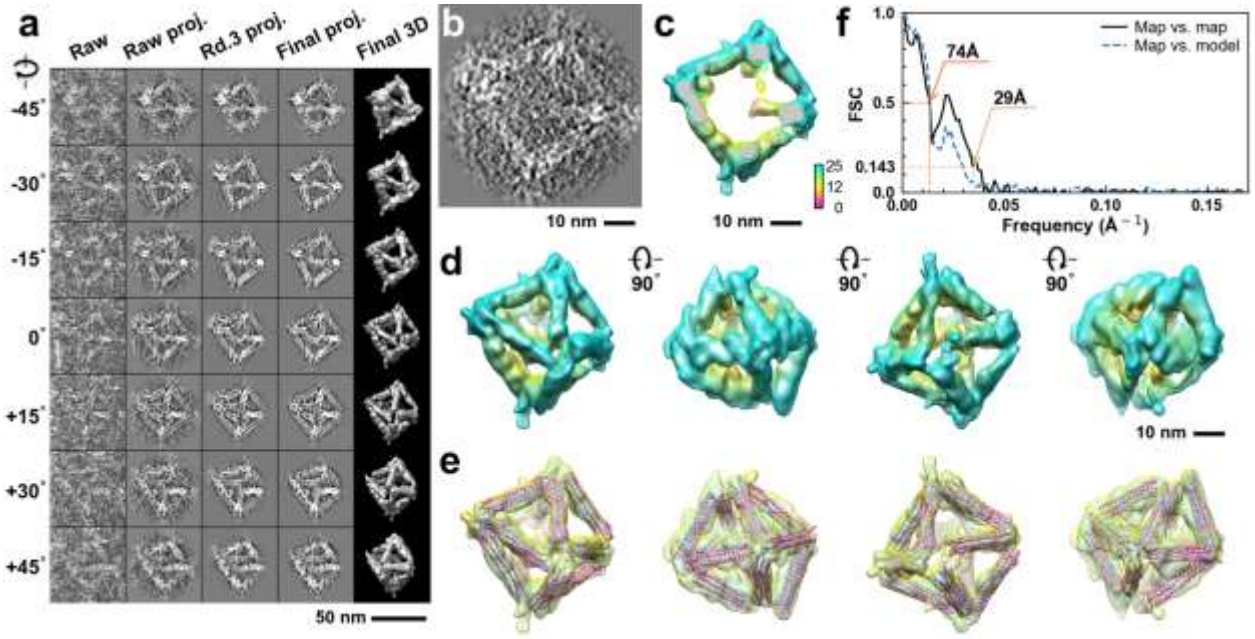

Supplementary Fig. 284: IPET 3D reconstruction and model fitting of an individual unit-cell particle (Index: 276) within a 2D lattice with 0% ferritin loading. a, Seven representative tilt images of a single unit-cell particle are shown in the first column (from left). The tilt images are aligned to a common center using IPET through iterative refinement. The projections of the raw, intermediate, and final 3D reconstruction at the corresponding angles are displayed in the subsequent four columns. **b**, A central cross-section (~23 nm thick) of the final reconstruction before masking is applied. **c**, 3D views of the central cross-section. **d**, Final 3D density map of this particle, viewed from four perpendicular directions. **e**, Final 3D reconstruction superimposed with the fitted model, viewed from four perpendicular directions. **f**, FSC analyses of the final map resolution using two methods: map-map FSC, where each map is reconstructed from one half of the images (even vs. odd tilt angle indices), and map-model FSC, where the model map is generated from the fitted model. Resolution assessments are provided based on tilt-based map-map and map-model FSC analyses at thresholds of FSC=0.5 and 0.143, respectively.

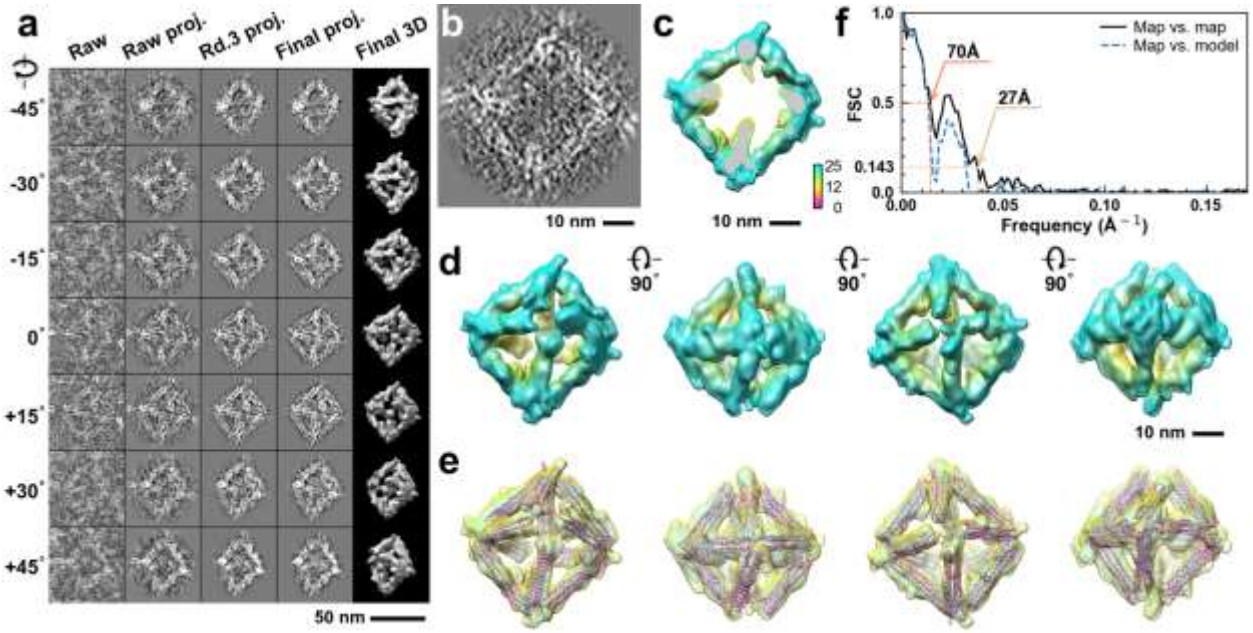

Supplementary Fig. 285: IPET 3D reconstruction and model fitting of an individual unit-cell particle (Index: 277) within a 2D lattice with 0% ferritin loading. a, Seven representative tilt images of a single unit-cell particle are shown in the first column (from left). The tilt images are aligned to a common center using IPET through iterative refinement. The projections of the raw, intermediate, and final 3D reconstruction at the corresponding angles are displayed in the subsequent four columns. **b**, A central cross-section (~23 nm thick) of the final reconstruction before masking is applied. **c**, 3D views of the central cross-section. **d**, Final 3D density map of this particle, viewed from four perpendicular directions. **e**, Final 3D reconstruction superimposed with the fitted model, viewed from four perpendicular directions. **f**, FSC analyses of the final map resolution using two methods: map-map FSC, where each map is reconstructed from one half of the images (even vs. odd tilt angle indices), and map-model FSC, where the model map is generated from the fitted model. Resolution assessments are provided based on tilt-based map-map and map-model FSC analyses at thresholds of FSC=0.5 and 0.143, respectively.

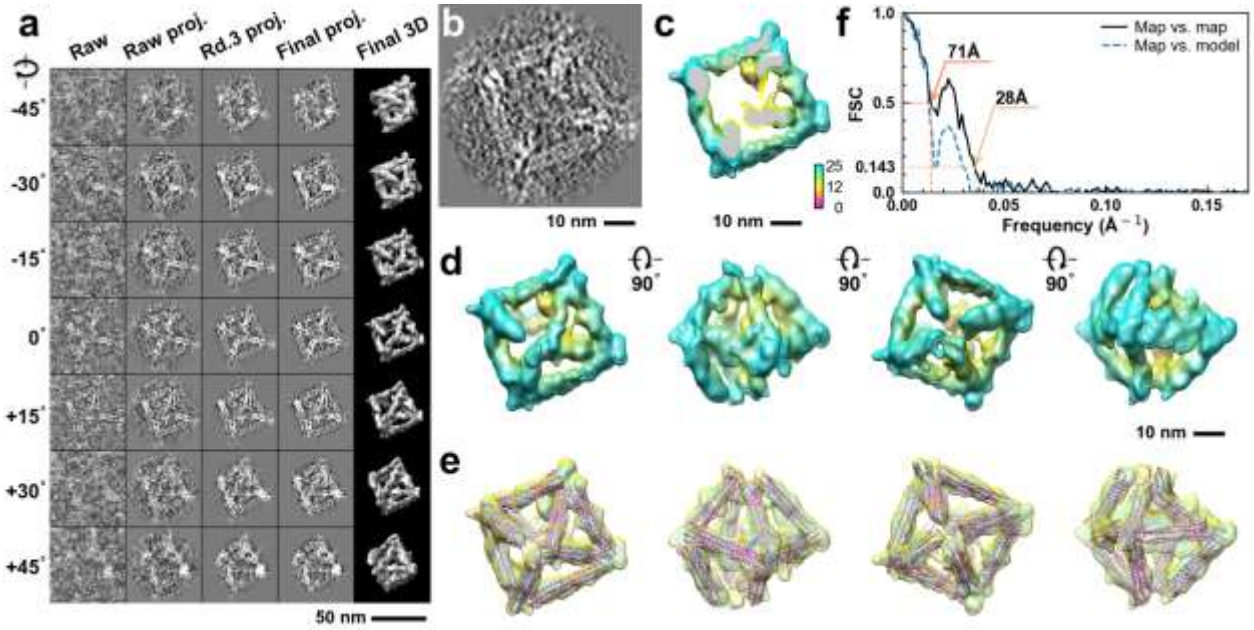

Supplementary Fig. 286: IPET 3D reconstruction and model fitting of an individual unit-cell particle (Index: 278) within a 2D lattice with 0% ferritin loading. a, Seven representative tilt images of a single unit-cell particle are shown in the first column (from left). The tilt images are aligned to a common center using IPET through iterative refinement. The projections of the raw, intermediate, and final 3D reconstruction at the corresponding angles are displayed in the subsequent four columns. **b**, A central cross-section (~23 nm thick) of the final reconstruction before masking is applied. **c**, 3D views of the central cross-section. **d**, Final 3D density map of this particle, viewed from four perpendicular directions. **e**, Final 3D reconstruction superimposed with the fitted model, viewed from four perpendicular directions. **f**, FSC analyses of the final map resolution using two methods: map-map FSC, where each map is reconstructed from one half of the images (even vs. odd tilt angle indices), and map-model FSC, where the model map is generated from the fitted model. Resolution assessments are provided based on tilt-based map-map and map-model FSC analyses at thresholds of FSC=0.5 and 0.143, respectively.

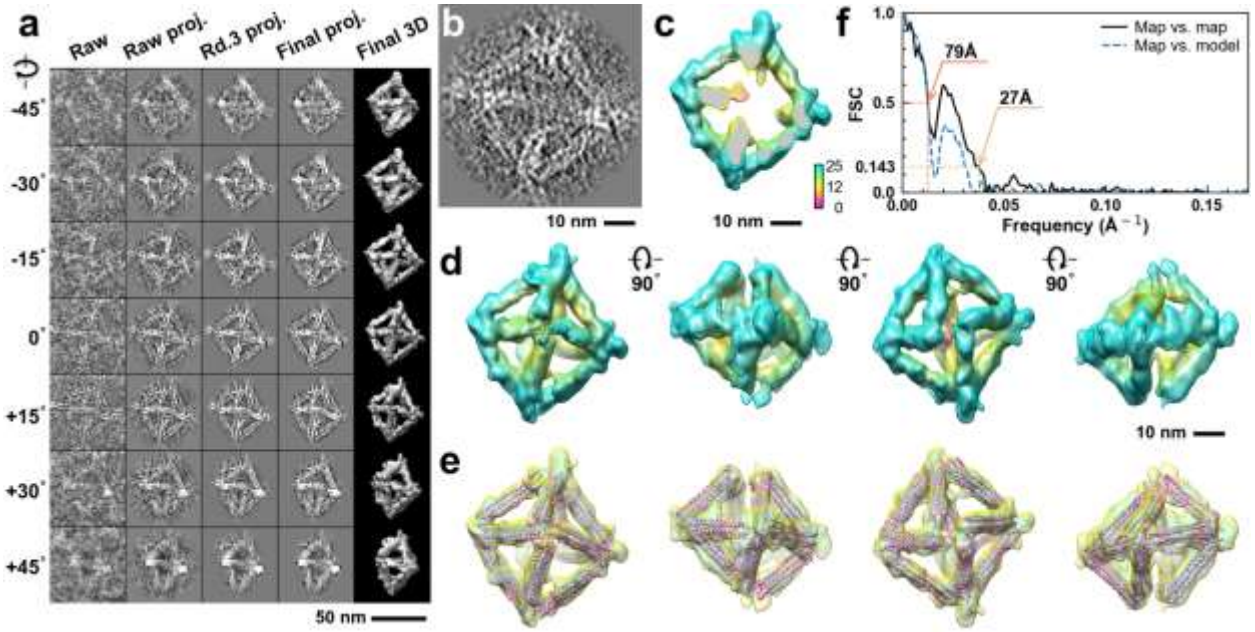

Supplementary Fig. 287: IPET 3D reconstruction and model fitting of an individual unit-cell particle (Index: 279) within a 2D lattice with 0% ferritin loading. a, Seven representative tilt images of a single unit-cell particle are shown in the first column (from left). The tilt images are aligned to a common center using IPET through iterative refinement. The projections of the raw, intermediate, and final 3D reconstruction at the corresponding angles are displayed in the subsequent four columns. **b**, A central cross-section (~23 nm thick) of the final reconstruction before masking is applied. **c**, 3D views of the central cross-section. **d**, Final 3D density map of this particle, viewed from four perpendicular directions. **e**, Final 3D reconstruction superimposed with the fitted model, viewed from four perpendicular directions. **f**, FSC analyses of the final map resolution using two methods: map-map FSC, where each map is reconstructed from one half of the images (even vs. odd tilt angle indices), and map-model FSC, where the model map is generated from the fitted model. Resolution assessments are provided based on tilt-based map-map and map-model FSC analyses at thresholds of FSC=0.5 and 0.143, respectively.

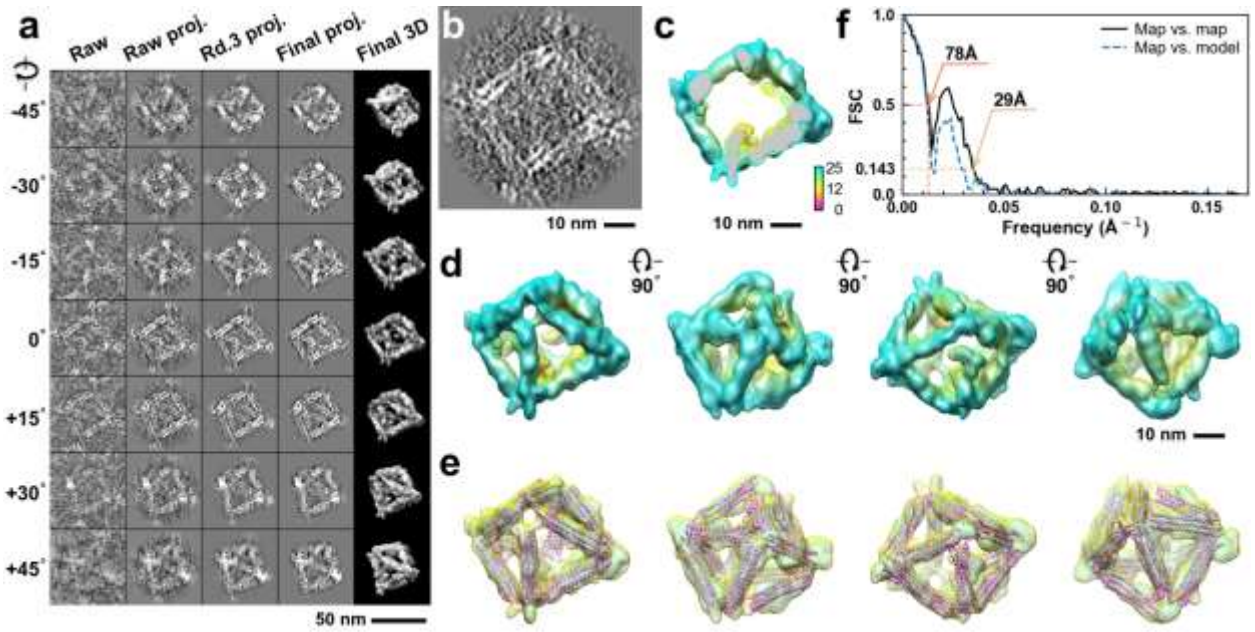

Supplementary Fig. 288: IPET 3D reconstruction and model fitting of an individual unit-cell particle (Index: 280) within a 2D lattice with 0% ferritin loading. a, Seven representative tilt images of a single unit-cell particle are shown in the first column (from left). The tilt images are aligned to a common center using IPET through iterative refinement. The projections of the raw, intermediate, and final 3D reconstruction at the corresponding angles are displayed in the subsequent four columns. **b**, A central cross-section (~23 nm thick) of the final reconstruction before masking is applied. **c**, 3D views of the central cross-section. **d**, Final 3D density map of this particle, viewed from four perpendicular directions. **e**, Final 3D reconstruction superimposed with the fitted model, viewed from four perpendicular directions. **f**, FSC analyses of the final map resolution using two methods: map-map FSC, where each map is reconstructed from one half of the images (even vs. odd tilt angle indices), and map-model FSC, where the model map is generated from the fitted model. Resolution assessments are provided based on tilt-based map-map and map-model FSC analyses at thresholds of FSC=0.5 and 0.143, respectively.

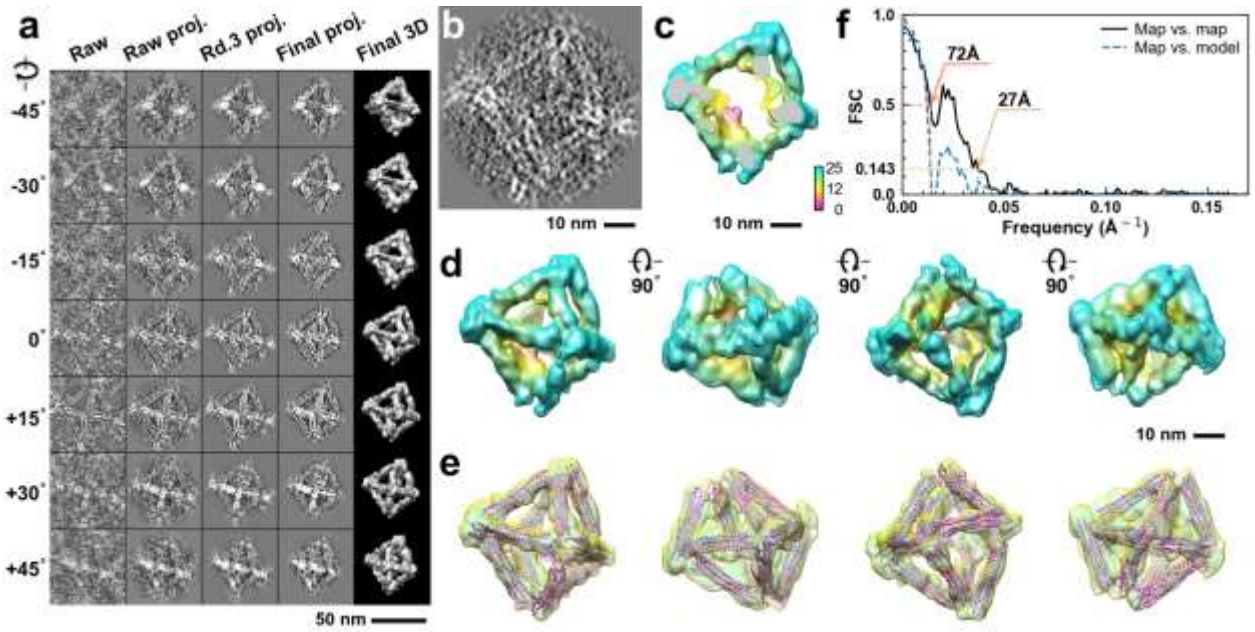

Supplementary Fig. 289: IPET 3D reconstruction and model fitting of an individual unit-cell particle (Index: 281) within a 2D lattice with 0% ferritin loading. a, Seven representative tilt images of a single unit-cell particle are shown in the first column (from left). The tilt images are aligned to a common center using IPET through iterative refinement. The projections of the raw, intermediate, and final 3D reconstruction at the corresponding angles are displayed in the subsequent four columns. **b**, A central cross-section (~23 nm thick) of the final reconstruction before masking is applied. **c**, 3D views of the central cross-section. **d**, Final 3D density map of this particle, viewed from four perpendicular directions. **e**, Final 3D reconstruction superimposed with the fitted model, viewed from four perpendicular directions. **f**, FSC analyses of the final map resolution using two methods: map-map FSC, where each map is reconstructed from one half of the images (even vs. odd tilt angle indices), and map-model FSC, where the model map is generated from the fitted model. Resolution assessments are provided based on tilt-based map-map and map-model FSC analyses at thresholds of FSC=0.5 and 0.143, respectively.

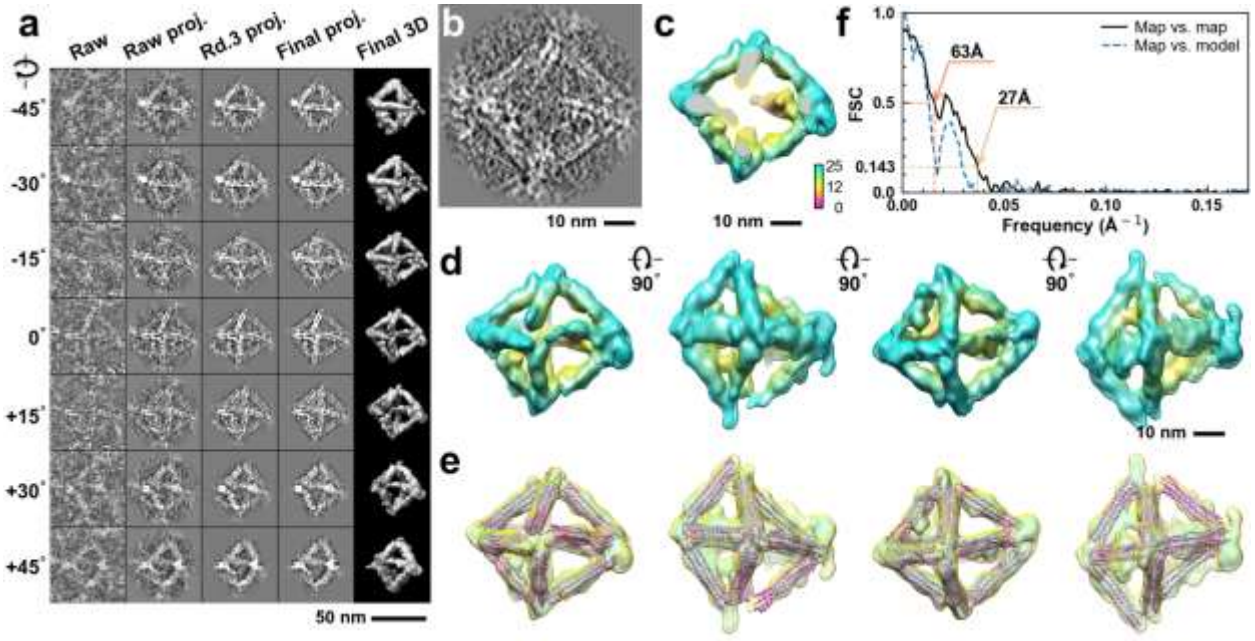

Supplementary Fig. 290: IPET 3D reconstruction and model fitting of an individual unit-cell particle (Index: 282) within a 2D lattice with 0% ferritin loading. a, Seven representative tilt images of a single unit-cell particle are shown in the first column (from left). The tilt images are aligned to a common center using IPET through iterative refinement. The projections of the raw, intermediate, and final 3D reconstruction at the corresponding angles are displayed in the subsequent four columns. **b**, A central cross-section (~23 nm thick) of the final reconstruction before masking is applied. **c**, 3D views of the central cross-section. **d**, Final 3D density map of this particle, viewed from four perpendicular directions. **e**, Final 3D reconstruction superimposed with the fitted model, viewed from four perpendicular directions. **f**, FSC analyses of the final map resolution using two methods: map-map FSC, where each map is reconstructed from one half of the images (even vs. odd tilt angle indices), and map-model FSC, where the model map is generated from the fitted model. Resolution assessments are provided based on tilt-based map-map and map-model FSC analyses at thresholds of FSC=0.5 and 0.143, respectively.

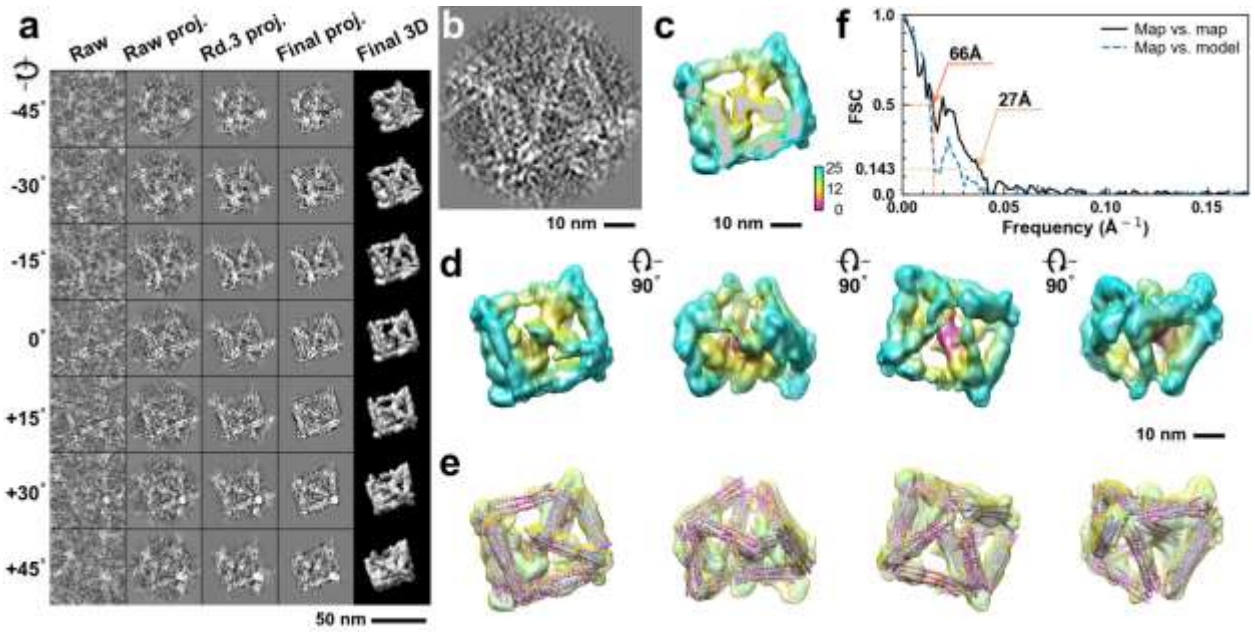

Supplementary Fig. 291: IPET 3D reconstruction and model fitting of an individual unit-cell particle (Index: 283) within a 2D lattice with 0% ferritin loading. a, Seven representative tilt images of a single unit-cell particle are shown in the first column (from left). The tilt images are aligned to a common center using IPET through iterative refinement. The projections of the raw, intermediate, and final 3D reconstruction at the corresponding angles are displayed in the subsequent four columns. **b**, A central cross-section (~23 nm thick) of the final reconstruction before masking is applied. **c**, 3D views of the central cross-section. **d**, Final 3D density map of this particle, viewed from four perpendicular directions. **e**, Final 3D reconstruction superimposed with the fitted model, viewed from four perpendicular directions. **f**, FSC analyses of the final map resolution using two methods: map-map FSC, where each map is reconstructed from one half of the images (even vs. odd tilt angle indices), and map-model FSC, where the model map is generated from the fitted model. Resolution assessments are provided based on tilt-based map-map and map-model FSC analyses at thresholds of FSC=0.5 and 0.143, respectively.

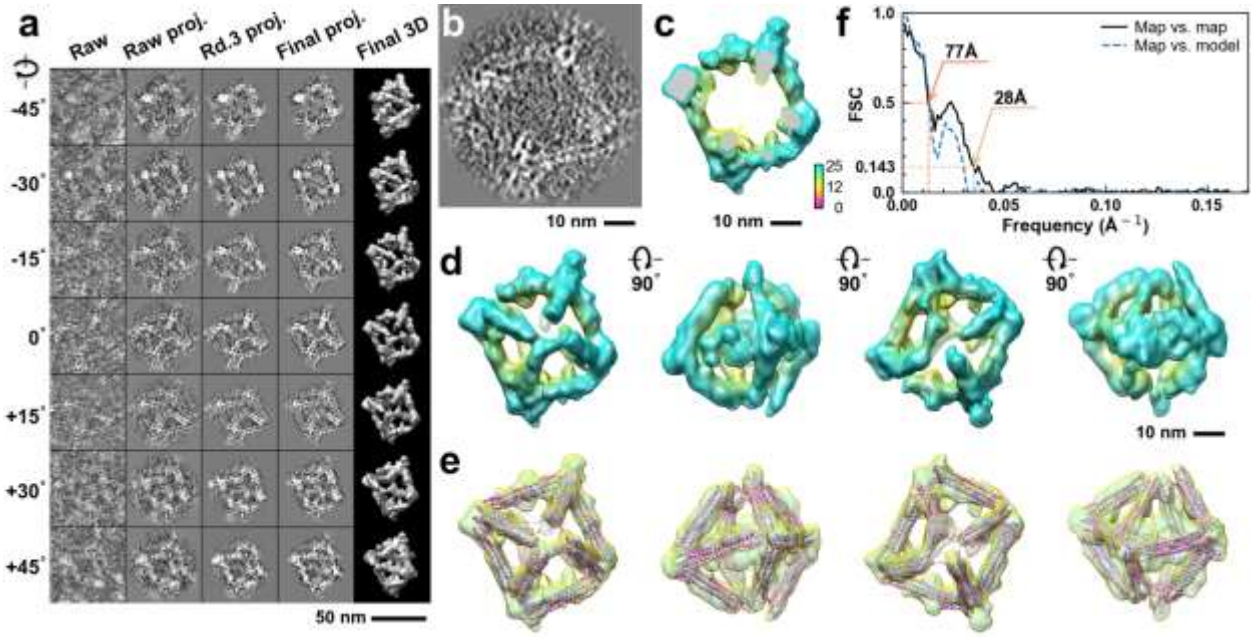

Supplementary Fig. 292: IPET 3D reconstruction and model fitting of an individual unit-cell particle (Index: 284) within a 2D lattice with 0% ferritin loading. a, Seven representative tilt images of a single unit-cell particle are shown in the first column (from left). The tilt images are aligned to a common center using IPET through iterative refinement. The projections of the raw, intermediate, and final 3D reconstruction at the corresponding angles are displayed in the subsequent four columns. **b**, A central cross-section (~23 nm thick) of the final reconstruction before masking is applied. **c**, 3D views of the central cross-section. **d**, Final 3D density map of this particle, viewed from four perpendicular directions. **e**, Final 3D reconstruction superimposed with the fitted model, viewed from four perpendicular directions. **f**, FSC analyses of the final map resolution using two methods: map-map FSC, where each map is reconstructed from one half of the images (even vs. odd tilt angle indices), and map-model FSC, where the model map is generated from the fitted model. Resolution assessments are provided based on tilt-based map-map and map-model FSC analyses at thresholds of FSC=0.5 and 0.143, respectively.

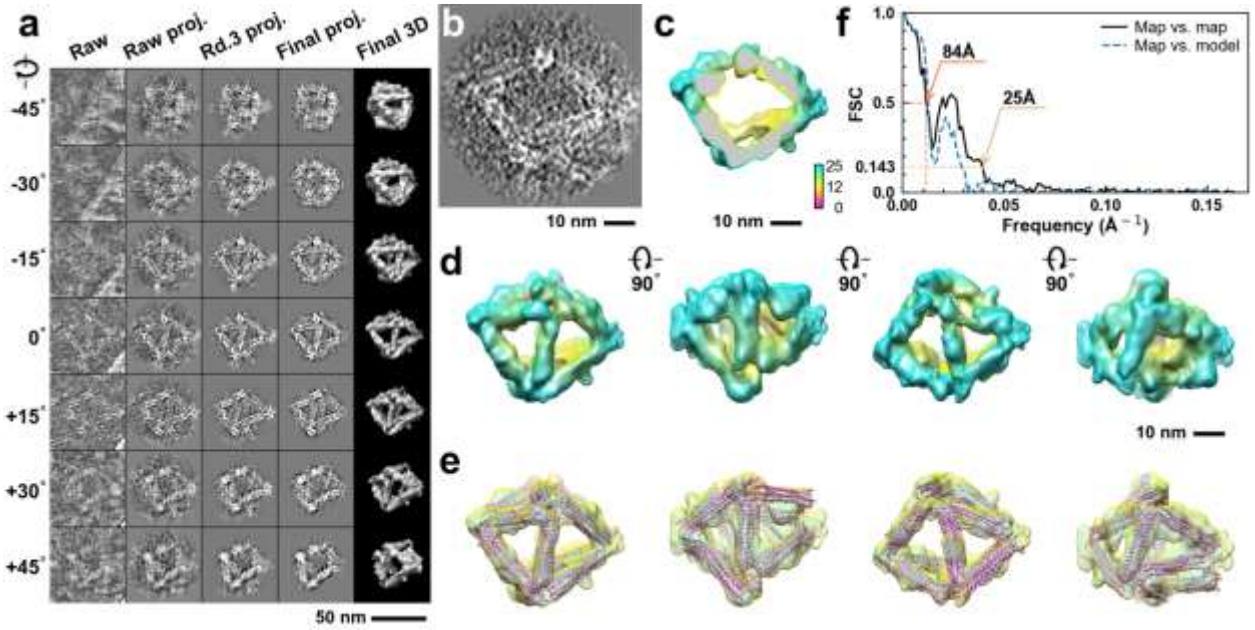

Supplementary Fig. 293: IPET 3D reconstruction and model fitting of an individual unit-cell particle (Index: 285) within a 2D lattice with 0% ferritin loading. a, Seven representative tilt images of a single unit-cell particle are shown in the first column (from left). The tilt images are aligned to a common center using IPET through iterative refinement. The projections of the raw, intermediate, and final 3D reconstruction at the corresponding angles are displayed in the subsequent four columns. **b**, A central cross-section (~23 nm thick) of the final reconstruction before masking is applied. **c**, 3D views of the central cross-section. **d**, Final 3D density map of this particle, viewed from four perpendicular directions. **e**, Final 3D reconstruction superimposed with the fitted model, viewed from four perpendicular directions. **f**, FSC analyses of the final map resolution using two methods: map-map FSC, where each map is reconstructed from one half of the images (even vs. odd tilt angle indices), and map-model FSC, where the model map is generated from the fitted model. Resolution assessments are provided based on tilt-based map-map and map-model FSC analyses at thresholds of FSC=0.5 and 0.143, respectively.

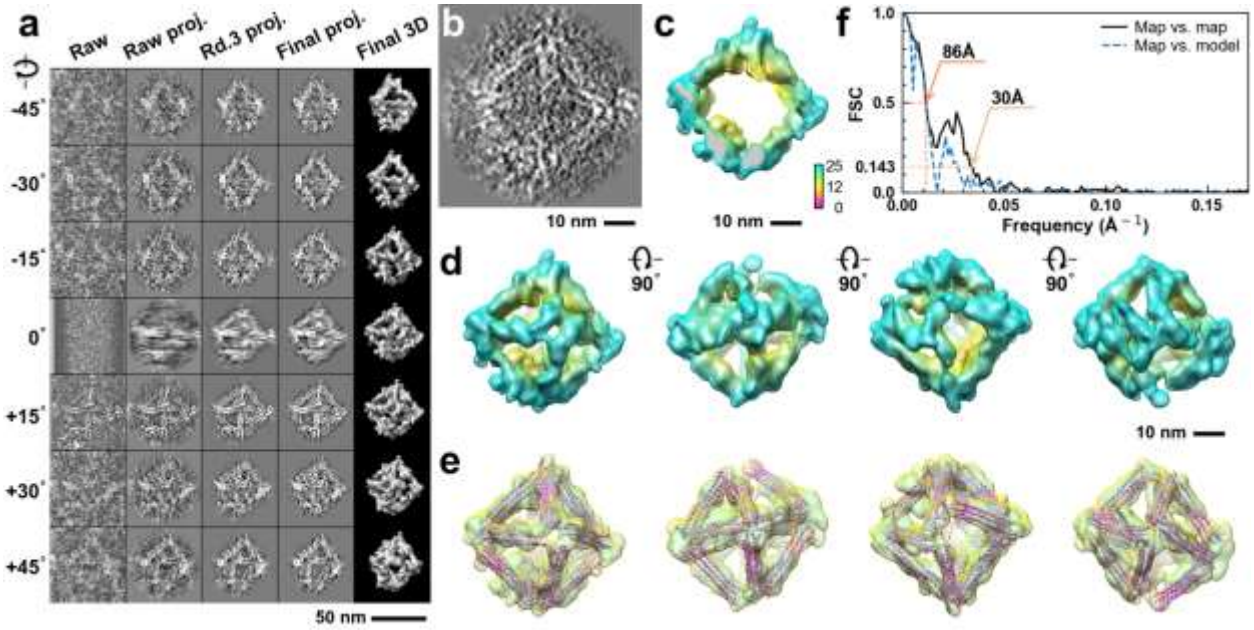

Supplementary Fig. 294: IPET 3D reconstruction and model fitting of an individual unit-cell particle (Index: 286) within a 2D lattice with 0% ferritin loading. a, Seven representative tilt images of a single unit-cell particle are shown in the first column (from left). The tilt images are aligned to a common center using IPET through iterative refinement. The projections of the raw, intermediate, and final 3D reconstruction at the corresponding angles are displayed in the subsequent four columns. **b**, A central cross-section (~23 nm thick) of the final reconstruction before masking is applied. **c**, 3D views of the central cross-section. **d**, Final 3D density map of this particle, viewed from four perpendicular directions. **e**, Final 3D reconstruction superimposed with the fitted model, viewed from four perpendicular directions. **f**, FSC analyses of the final map resolution using two methods: map-map FSC, where each map is reconstructed from one half of the images (even vs. odd tilt angle indices), and map-model FSC, where the model map is generated from the fitted model. Resolution assessments are provided based on tilt-based map-map and map-model FSC analyses at thresholds of FSC=0.5 and 0.143, respectively.

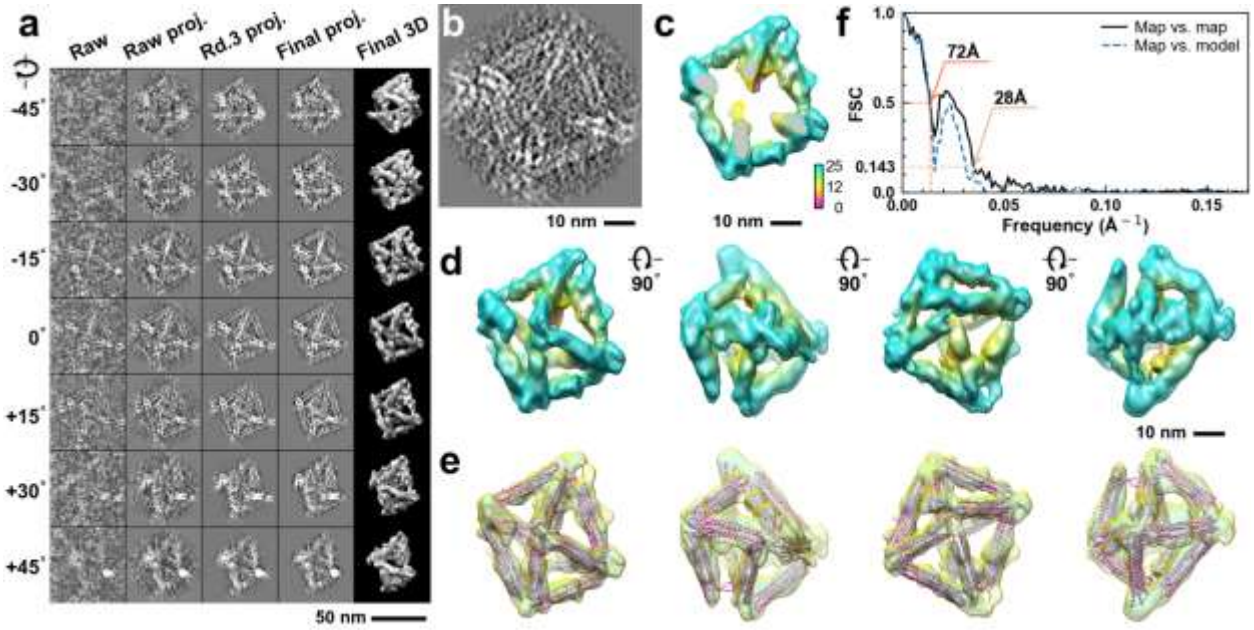

Supplementary Fig. 295: IPET 3D reconstruction and model fitting of an individual unit-cell particle (Index: 287) within a 2D lattice with 0% ferritin loading. a, Seven representative tilt images of a single unit-cell particle are shown in the first column (from left). The tilt images are aligned to a common center using IPET through iterative refinement. The projections of the raw, intermediate, and final 3D reconstruction at the corresponding angles are displayed in the subsequent four columns. **b**, A central cross-section (~23 nm thick) of the final reconstruction before masking is applied. **c**, 3D views of the central cross-section. **d**, Final 3D density map of this particle, viewed from four perpendicular directions. **e**, Final 3D reconstruction superimposed with the fitted model, viewed from four perpendicular directions. **f**, FSC analyses of the final map resolution using two methods: map-map FSC, where each map is reconstructed from one half of the images (even vs. odd tilt angle indices), and map-model FSC, where the model map is generated from the fitted model. Resolution assessments are provided based on tilt-based map-map and map-model FSC analyses at thresholds of FSC=0.5 and 0.143, respectively.

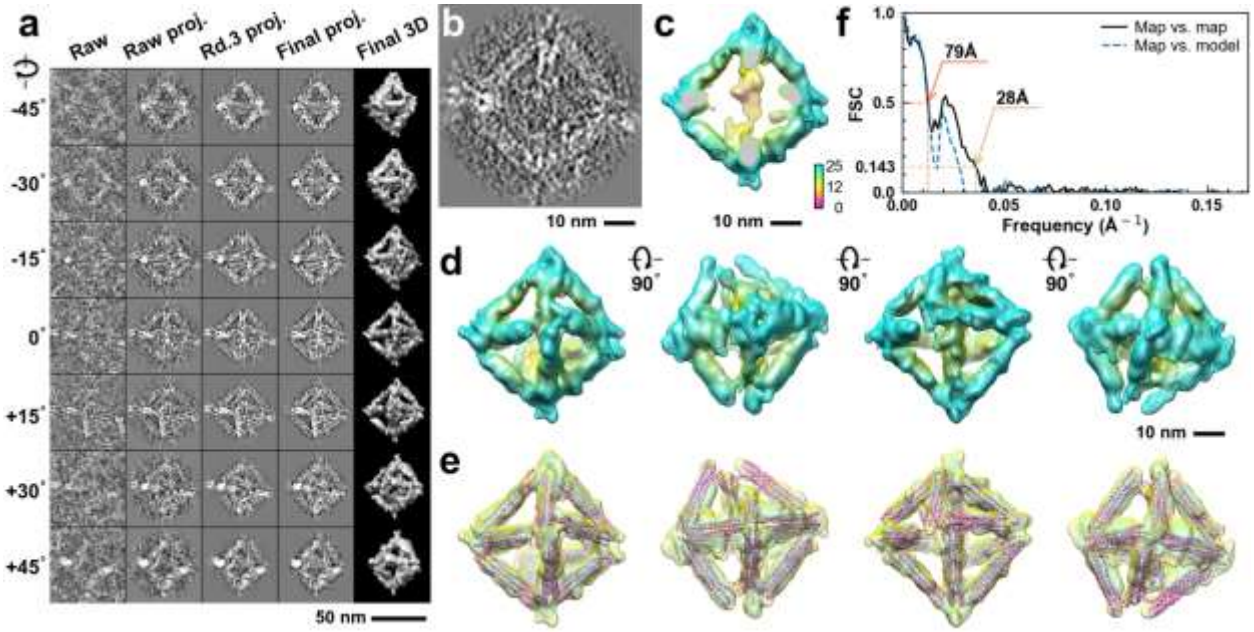

Supplementary Fig. 296: IPET 3D reconstruction and model fitting of an individual unit-cell particle (Index: 288) within a 2D lattice with 0% ferritin loading. a, Seven representative tilt images of a single unit-cell particle are shown in the first column (from left). The tilt images are aligned to a common center using IPET through iterative refinement. The projections of the raw, intermediate, and final 3D reconstruction at the corresponding angles are displayed in the subsequent four columns. **b**, A central cross-section (~23 nm thick) of the final reconstruction before masking is applied. **c**, 3D views of the central cross-section. **d**, Final 3D density map of this particle, viewed from four perpendicular directions. **e**, Final 3D reconstruction superimposed with the fitted model, viewed from four perpendicular directions. **f**, FSC analyses of the final map resolution using two methods: map-map FSC, where each map is reconstructed from one half of the images (even vs. odd tilt angle indices), and map-model FSC, where the model map is generated from the fitted model. Resolution assessments are provided based on tilt-based map-map and map-model FSC analyses at thresholds of FSC=0.5 and 0.143, respectively.

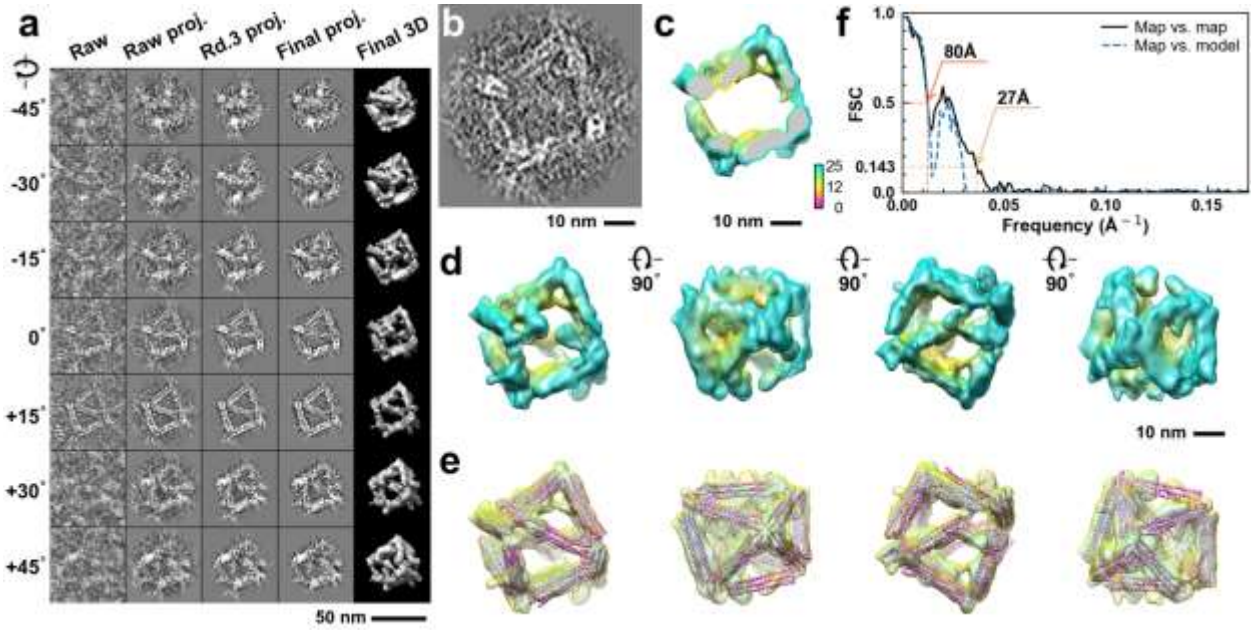

Supplementary Fig. 297: IPET 3D reconstruction and model fitting of an individual unit-cell particle (Index: 289) within a 2D lattice with 0% ferritin loading. a, Seven representative tilt images of a single unit-cell particle are shown in the first column (from left). The tilt images are aligned to a common center using IPET through iterative refinement. The projections of the raw, intermediate, and final 3D reconstruction at the corresponding angles are displayed in the subsequent four columns. **b**, A central cross-section (~23 nm thick) of the final reconstruction before masking is applied. **c**, 3D views of the central cross-section. **d**, Final 3D density map of this particle, viewed from four perpendicular directions. **e**, Final 3D reconstruction superimposed with the fitted model, viewed from four perpendicular directions. **f**, FSC analyses of the final map resolution using two methods: map-map FSC, where each map is reconstructed from one half of the images (even vs. odd tilt angle indices), and map-model FSC, where the model map is generated from the fitted model. Resolution assessments are provided based on tilt-based map-map and map-model FSC analyses at thresholds of FSC=0.5 and 0.143, respectively.

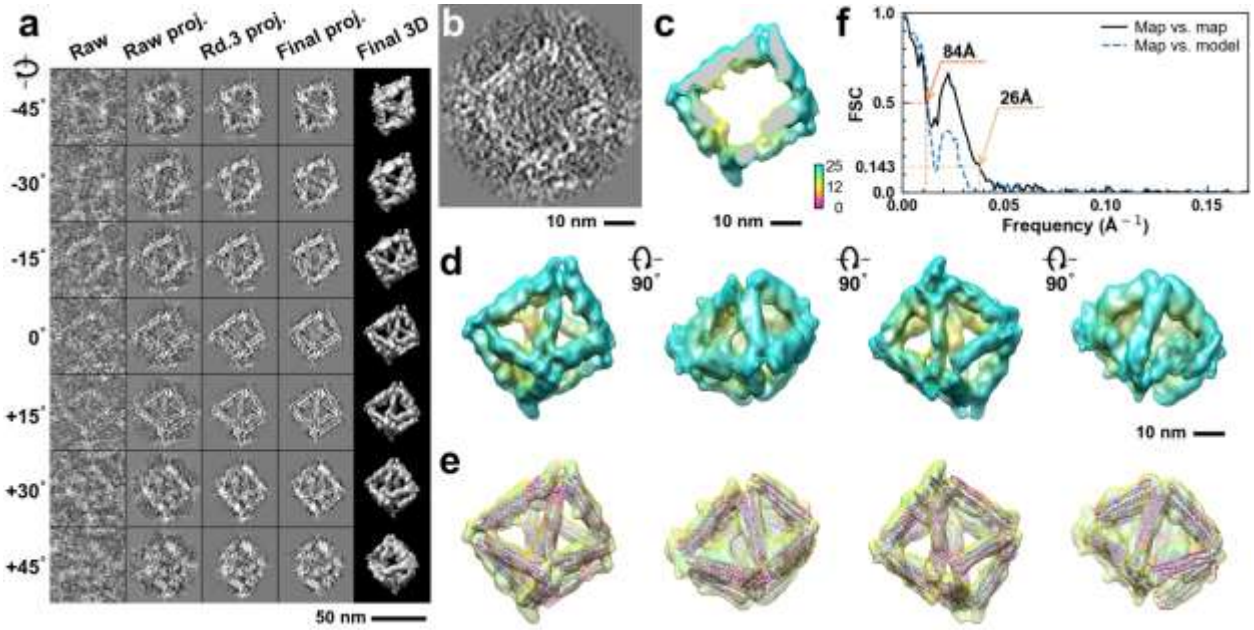

Supplementary Fig. 298: IPET 3D reconstruction and model fitting of an individual unit-cell particle (Index: 290) within a 2D lattice with 0% ferritin loading. a, Seven representative tilt images of a single unit-cell particle are shown in the first column (from left). The tilt images are aligned to a common center using IPET through iterative refinement. The projections of the raw, intermediate, and final 3D reconstruction at the corresponding angles are displayed in the subsequent four columns. **b**, A central cross-section (~23 nm thick) of the final reconstruction before masking is applied. **c**, 3D views of the central cross-section. **d**, Final 3D density map of this particle, viewed from four perpendicular directions. **e**, Final 3D reconstruction superimposed with the fitted model, viewed from four perpendicular directions. **f**, FSC analyses of the final map resolution using two methods: map-map FSC, where each map is reconstructed from one half of the images (even vs. odd tilt angle indices), and map-model FSC, where the model map is generated from the fitted model. Resolution assessments are provided based on tilt-based map-map and map-model FSC analyses at thresholds of FSC=0.5 and 0.143, respectively.

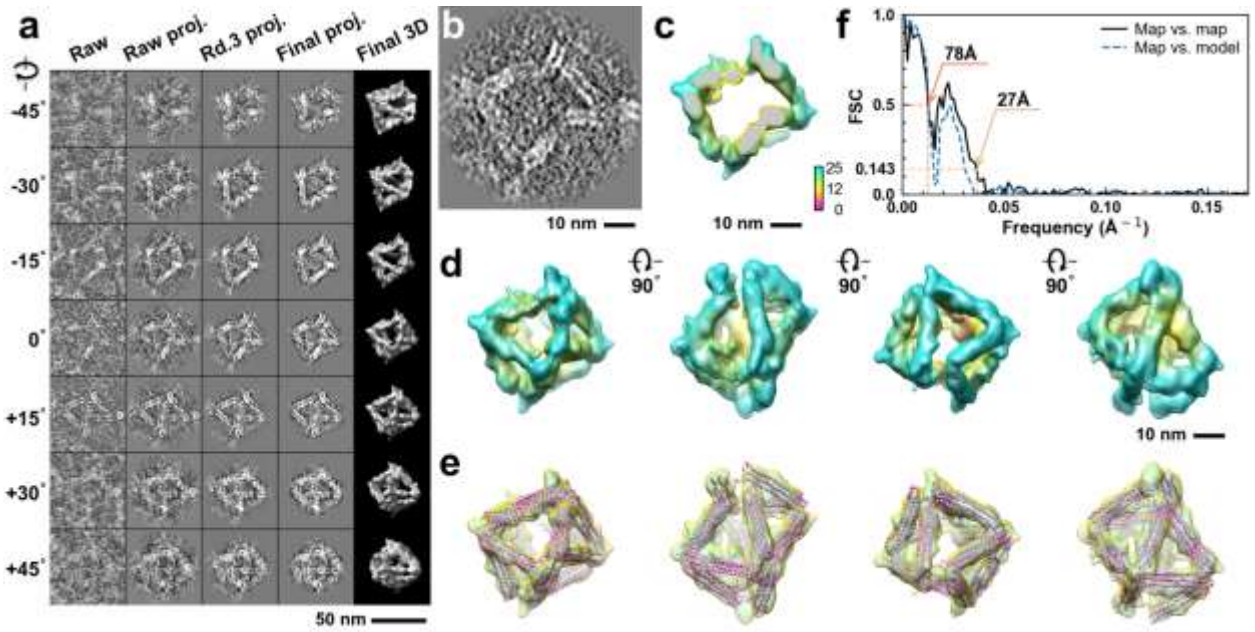

Supplementary Fig. 299: IPET 3D reconstruction and model fitting of an individual unit-cell particle (Index: 291) within a 2D lattice with 0% ferritin loading. a, Seven representative tilt images of a single unit-cell particle are shown in the first column (from left). The tilt images are aligned to a common center using IPET through iterative refinement. The projections of the raw, intermediate, and final 3D reconstruction at the corresponding angles are displayed in the subsequent four columns. **b**, A central cross-section (~23 nm thick) of the final reconstruction before masking is applied. **c**, 3D views of the central cross-section. **d**, Final 3D density map of this particle, viewed from four perpendicular directions. **e**, Final 3D reconstruction superimposed with the fitted model, viewed from four perpendicular directions. **f**, FSC analyses of the final map resolution using two methods: map-map FSC, where each map is reconstructed from one half of the images (even vs. odd tilt angle indices), and map-model FSC, where the model map is generated from the fitted model. Resolution assessments are provided based on tilt-based map-map and map-model FSC analyses at thresholds of FSC=0.5 and 0.143, respectively.

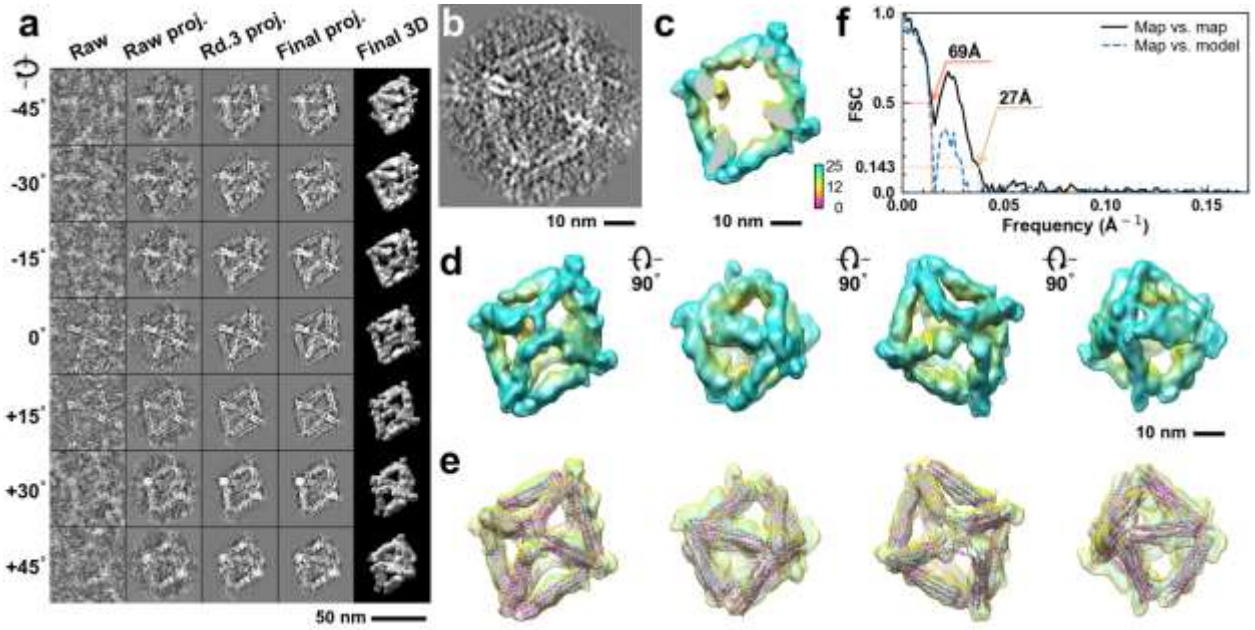

Supplementary Fig. 300: IPET 3D reconstruction and model fitting of an individual unit-cell particle (Index: 292) within a 2D lattice with 0% ferritin loading. a, Seven representative tilt images of a single unit-cell particle are shown in the first column (from left). The tilt images are aligned to a common center using IPET through iterative refinement. The projections of the raw, intermediate, and final 3D reconstruction at the corresponding angles are displayed in the subsequent four columns. **b**, A central cross-section (~23 nm thick) of the final reconstruction before masking is applied. **c**, 3D views of the central cross-section. **d**, Final 3D density map of this particle, viewed from four perpendicular directions. **e**, Final 3D reconstruction superimposed with the fitted model, viewed from four perpendicular directions. **f**, FSC analyses of the final map resolution using two methods: map-map FSC, where each map is reconstructed from one half of the images (even vs. odd tilt angle indices), and map-model FSC, where the model map is generated from the fitted model. Resolution assessments are provided based on tilt-based map-map and map-model FSC analyses at thresholds of FSC=0.5 and 0.143, respectively.

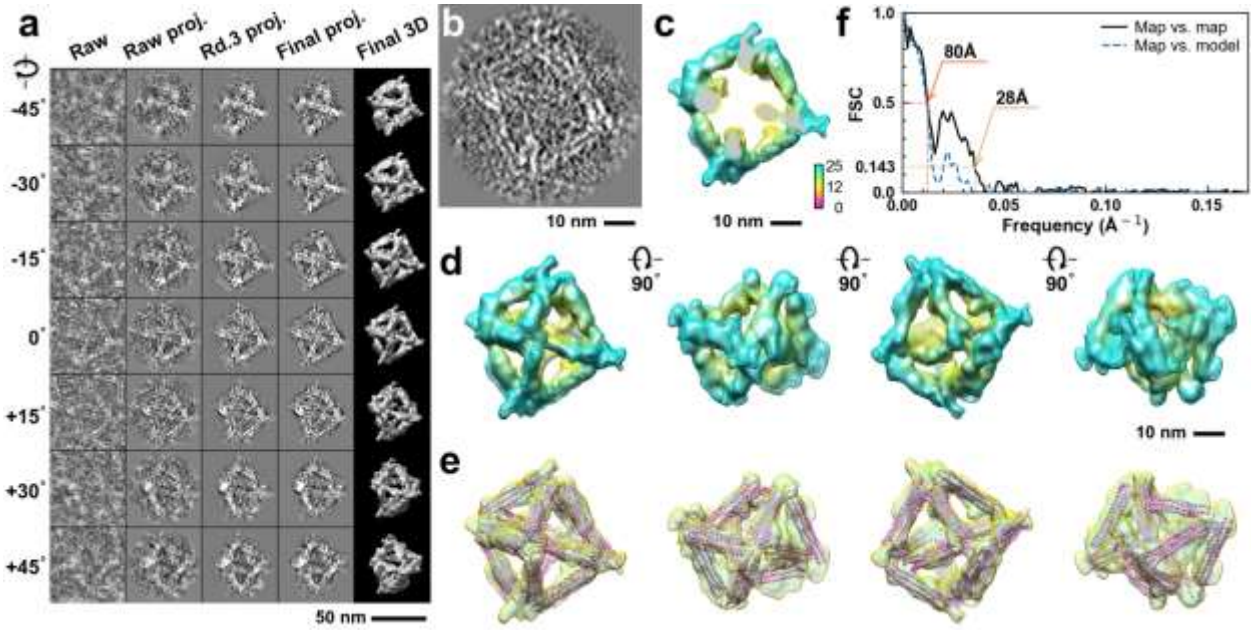

Supplementary Fig. 301: IPET 3D reconstruction and model fitting of an individual unit-cell particle (Index: 293) within a 2D lattice with 0% ferritin loading. a, Seven representative tilt images of a single unit-cell particle are shown in the first column (from left). The tilt images are aligned to a common center using IPET through iterative refinement. The projections of the raw, intermediate, and final 3D reconstruction at the corresponding angles are displayed in the subsequent four columns. **b**, A central cross-section (~23 nm thick) of the final reconstruction before masking is applied. **c**, 3D views of the central cross-section. **d**, Final 3D density map of this particle, viewed from four perpendicular directions. **e**, Final 3D reconstruction superimposed with the fitted model, viewed from four perpendicular directions. **f**, FSC analyses of the final map resolution using two methods: map-map FSC, where each map is reconstructed from one half of the images (even vs. odd tilt angle indices), and map-model FSC, where the model map is generated from the fitted model. Resolution assessments are provided based on tilt-based map-map and map-model FSC analyses at thresholds of FSC=0.5 and 0.143, respectively.

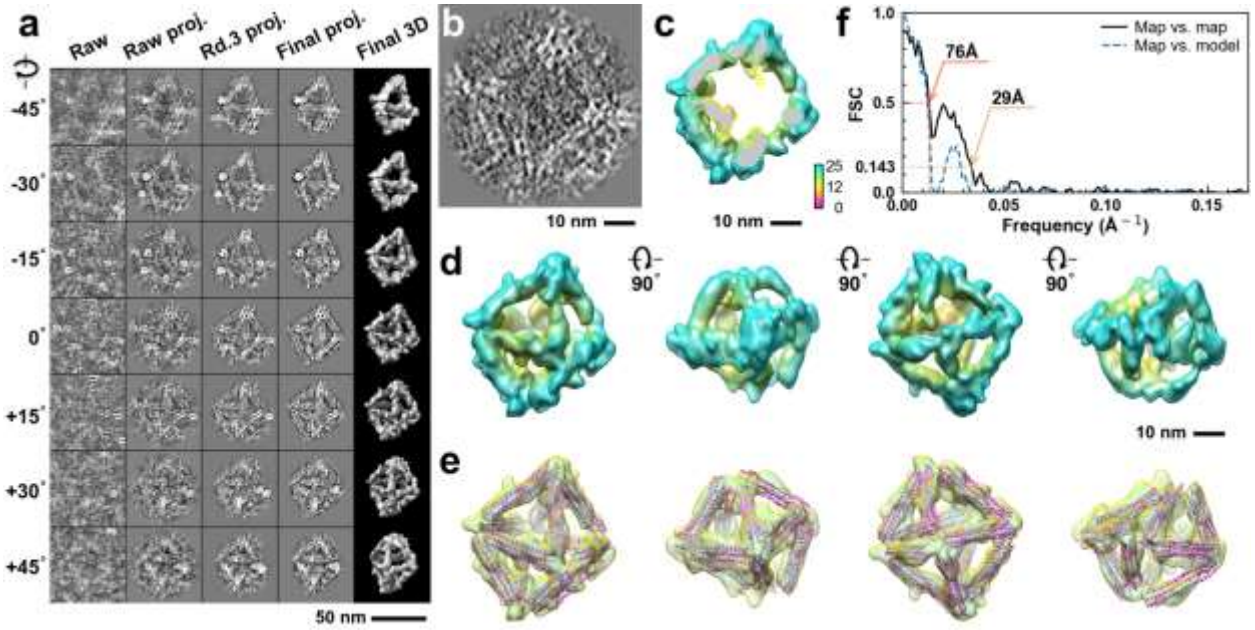

Supplementary Fig. 302: IPET 3D reconstruction and model fitting of an individual unit-cell particle (Index: 294) within a 2D lattice with 0% ferritin loading. a, Seven representative tilt images of a single unit-cell particle are shown in the first column (from left). The tilt images are aligned to a common center using IPET through iterative refinement. The projections of the raw, intermediate, and final 3D reconstruction at the corresponding angles are displayed in the subsequent four columns. **b**, A central cross-section (~23 nm thick) of the final reconstruction before masking is applied. **c**, 3D views of the central cross-section. **d**, Final 3D density map of this particle, viewed from four perpendicular directions. **e**, Final 3D reconstruction superimposed with the fitted model, viewed from four perpendicular directions. **f**, FSC analyses of the final map resolution using two methods: map-map FSC, where each map is reconstructed from one half of the images (even vs. odd tilt angle indices), and map-model FSC, where the model map is generated from the fitted model. Resolution assessments are provided based on tilt-based map-map and map-model FSC analyses at thresholds of FSC=0.5 and 0.143, respectively.

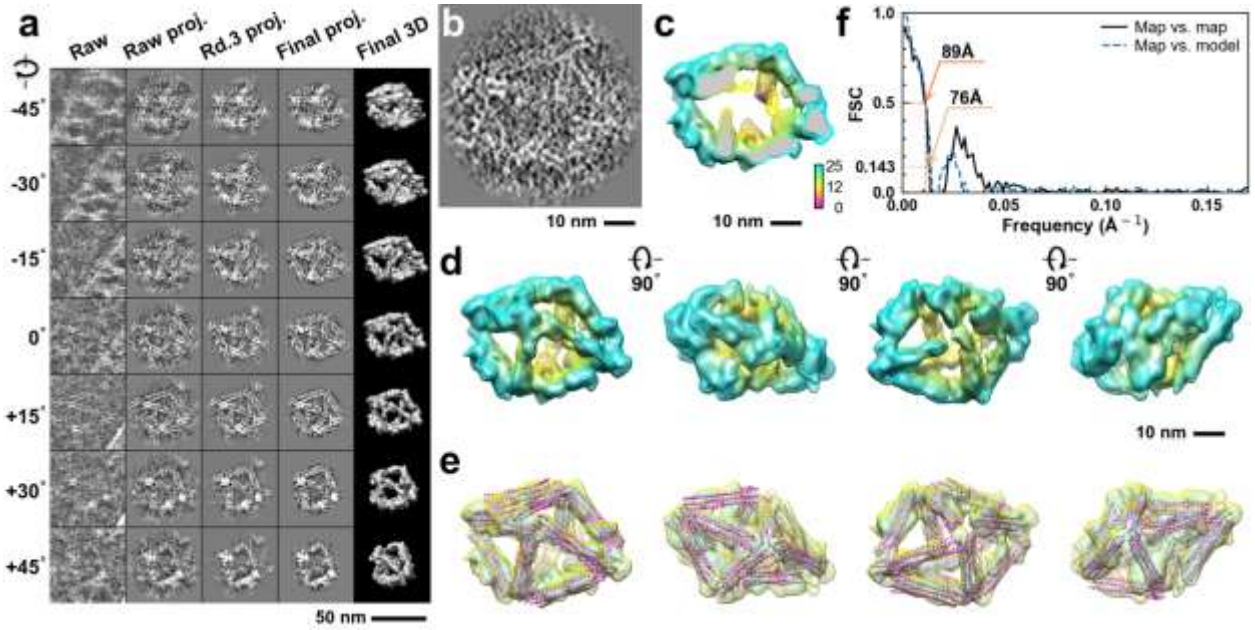

Supplementary Fig. 303: IPET 3D reconstruction and model fitting of an individual unit-cell particle (Index: 295) within a 2D lattice with 0% ferritin loading. a, Seven representative tilt images of a single unit-cell particle are shown in the first column (from left). The tilt images are aligned to a common center using IPET through iterative refinement. The projections of the raw, intermediate, and final 3D reconstruction at the corresponding angles are displayed in the subsequent four columns. **b**, A central cross-section (~23 nm thick) of the final reconstruction before masking is applied. **c**, 3D views of the central cross-section. **d**, Final 3D density map of this particle, viewed from four perpendicular directions. **e**, Final 3D reconstruction superimposed with the fitted model, viewed from four perpendicular directions. **f**, FSC analyses of the final map resolution using two methods: map-map FSC, where each map is reconstructed from one half of the images (even vs. odd tilt angle indices), and map-model FSC, where the model map is generated from the fitted model. Resolution assessments are provided based on tilt-based map-map and map-model FSC analyses at thresholds of FSC=0.5 and 0.143, respectively.

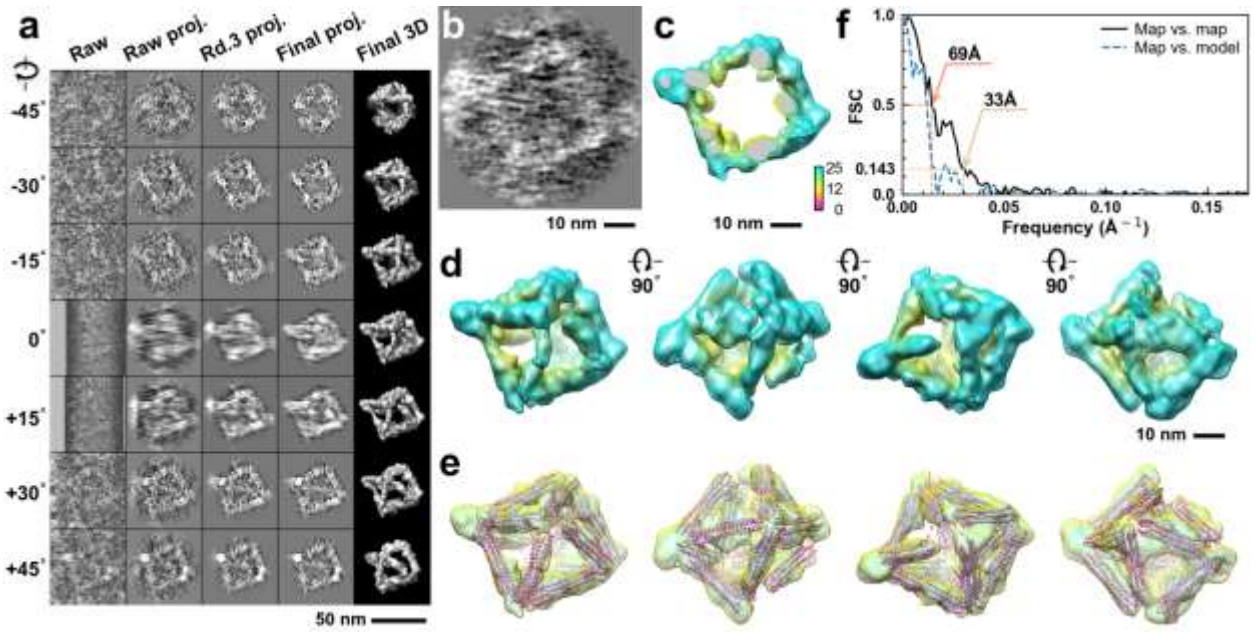

Supplementary Fig. 304: IPET 3D reconstruction and model fitting of an individual unit-cell particle (Index: 296) within a 2D lattice with 0% ferritin loading. a, Seven representative tilt images of a single unit-cell particle are shown in the first column (from left). The tilt images are aligned to a common center using IPET through iterative refinement. The projections of the raw, intermediate, and final 3D reconstruction at the corresponding angles are displayed in the subsequent four columns. **b**, A central cross-section (~23 nm thick) of the final reconstruction before masking is applied. **c**, 3D views of the central cross-section. **d**, Final 3D density map of this particle, viewed from four perpendicular directions. **e**, Final 3D reconstruction superimposed with the fitted model, viewed from four perpendicular directions. **f**, FSC analyses of the final map resolution using two methods: map-map FSC, where each map is reconstructed from one half of the images (even vs. odd tilt angle indices), and map-model FSC, where the model map is generated from the fitted model. Resolution assessments are provided based on tilt-based map-map and map-model FSC analyses at thresholds of FSC=0.5 and 0.143, respectively.

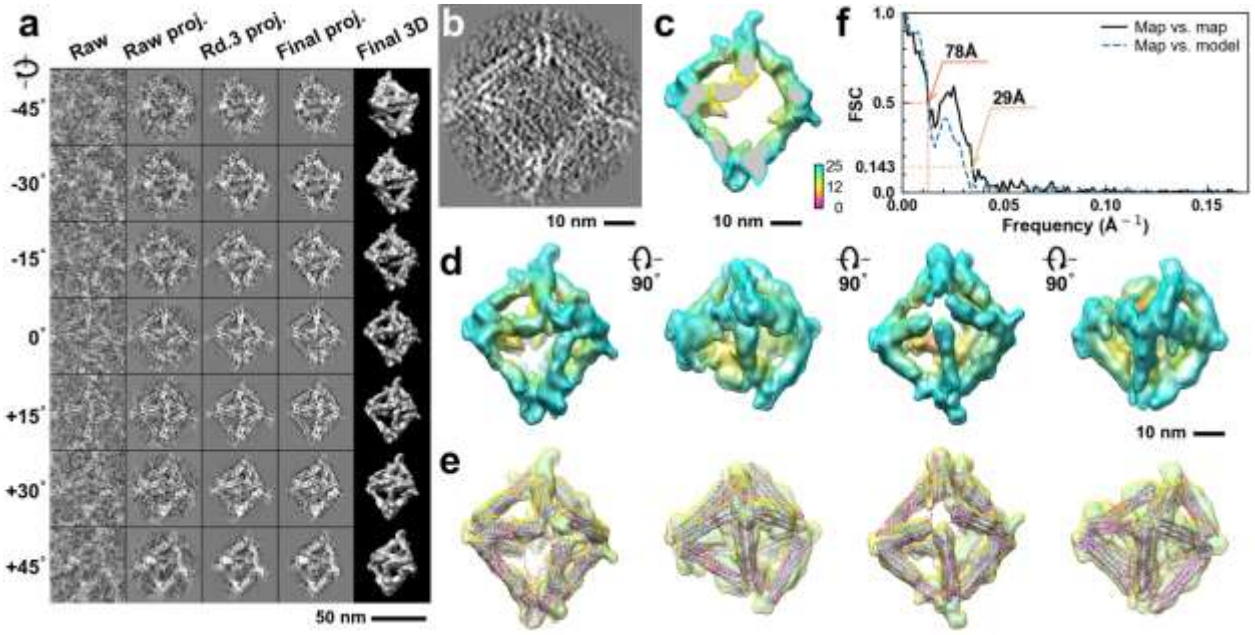

Supplementary Fig. 305: IPET 3D reconstruction and model fitting of an individual unit-cell particle (Index: 297) within a 2D lattice with 0% ferritin loading. a, Seven representative tilt images of a single unit-cell particle are shown in the first column (from left). The tilt images are aligned to a common center using IPET through iterative refinement. The projections of the raw, intermediate, and final 3D reconstruction at the corresponding angles are displayed in the subsequent four columns. **b**, A central cross-section (~23 nm thick) of the final reconstruction before masking is applied. **c**, 3D views of the central cross-section. **d**, Final 3D density map of this particle, viewed from four perpendicular directions. **e**, Final 3D reconstruction superimposed with the fitted model, viewed from four perpendicular directions. **f**, FSC analyses of the final map resolution using two methods: map-map FSC, where each map is reconstructed from one half of the images (even vs. odd tilt angle indices), and map-model FSC, where the model map is generated from the fitted model. Resolution assessments are provided based on tilt-based map-map and map-model FSC analyses at thresholds of FSC=0.5 and 0.143, respectively.

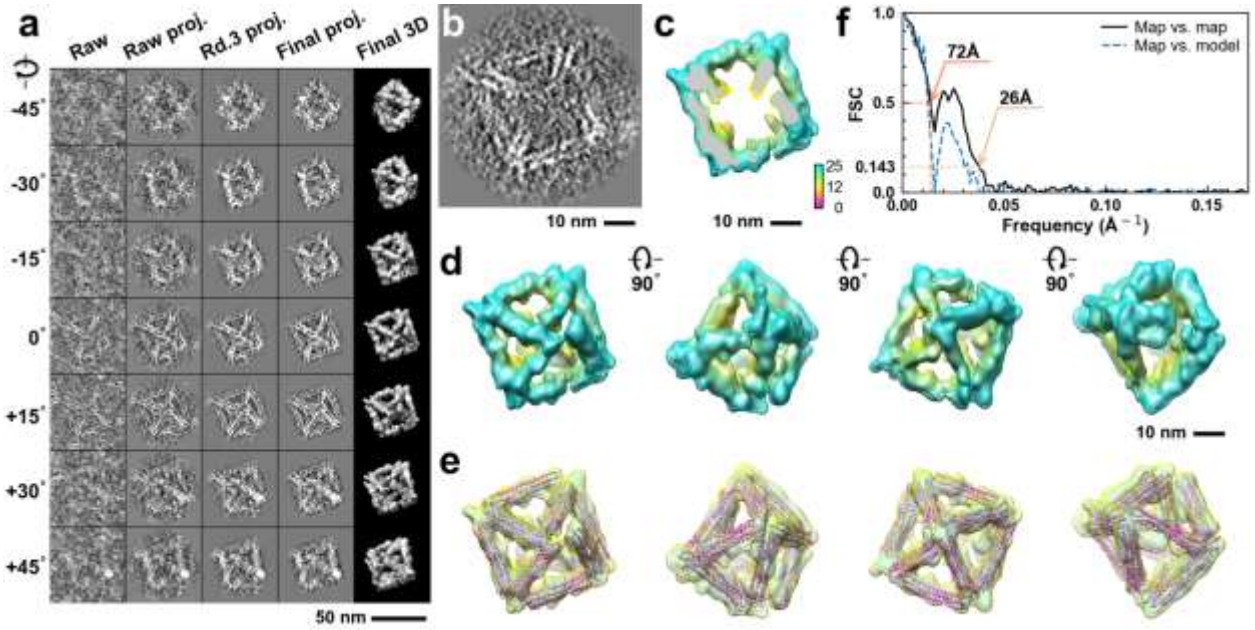

Supplementary Fig. 306: IPET 3D reconstruction and model fitting of an individual unit-cell particle (Index: 298) within a 2D lattice with 0% ferritin loading. a, Seven representative tilt images of a single unit-cell particle are shown in the first column (from left). The tilt images are aligned to a common center using IPET through iterative refinement. The projections of the raw, intermediate, and final 3D reconstruction at the corresponding angles are displayed in the subsequent four columns. **b**, A central cross-section (~23 nm thick) of the final reconstruction before masking is applied. **c**, 3D views of the central cross-section. **d**, Final 3D density map of this particle, viewed from four perpendicular directions. **e**, Final 3D reconstruction superimposed with the fitted model, viewed from four perpendicular directions. **f**, FSC analyses of the final map resolution using two methods: map-map FSC, where each map is reconstructed from one half of the images (even vs. odd tilt angle indices), and map-model FSC, where the model map is generated from the fitted model. Resolution assessments are provided based on tilt-based map-map and map-model FSC analyses at thresholds of FSC=0.5 and 0.143, respectively.

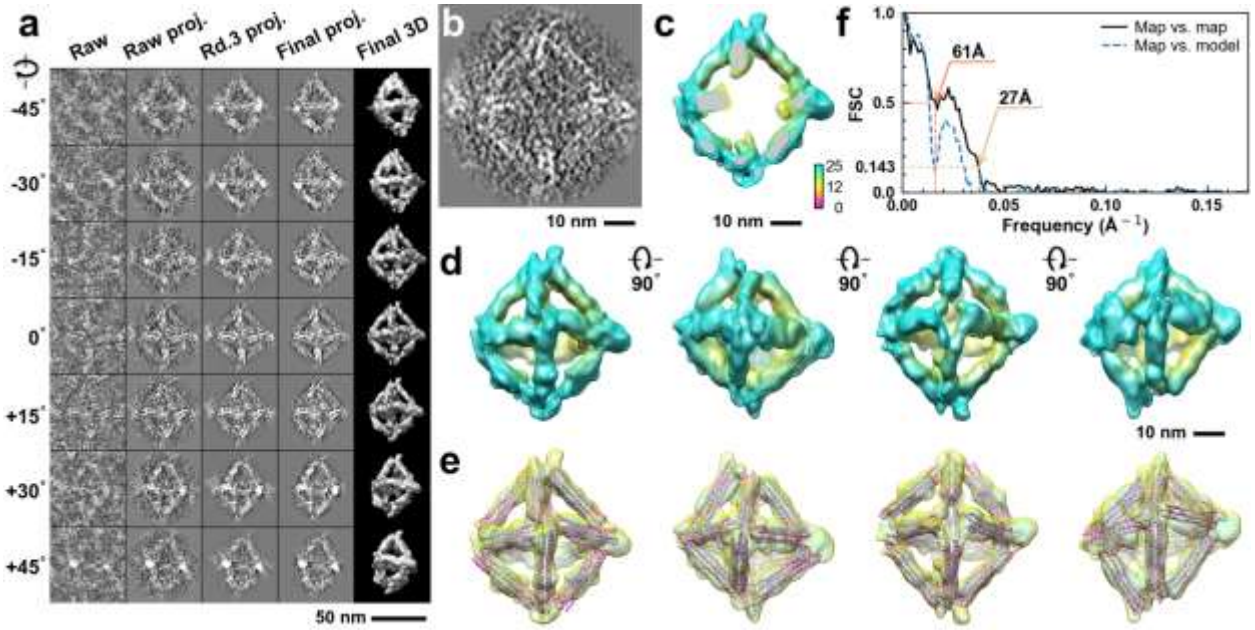

Supplementary Fig. 307: IPET 3D reconstruction and model fitting of an individual unit-cell particle (Index: 299) within a 2D lattice with 0% ferritin loading. a, Seven representative tilt images of a single unit-cell particle are shown in the first column (from left). The tilt images are aligned to a common center using IPET through iterative refinement. The projections of the raw, intermediate, and final 3D reconstruction at the corresponding angles are displayed in the subsequent four columns. **b**, A central cross-section (~23 nm thick) of the final reconstruction before masking is applied. **c**, 3D views of the central cross-section. **d**, Final 3D density map of this particle, viewed from four perpendicular directions. **e**, Final 3D reconstruction superimposed with the fitted model, viewed from four perpendicular directions. **f**, FSC analyses of the final map resolution using two methods: map-map FSC, where each map is reconstructed from one half of the images (even vs. odd tilt angle indices), and map-model FSC, where the model map is generated from the fitted model. Resolution assessments are provided based on tilt-based map-map and map-model FSC analyses at thresholds of FSC=0.5 and 0.143, respectively.

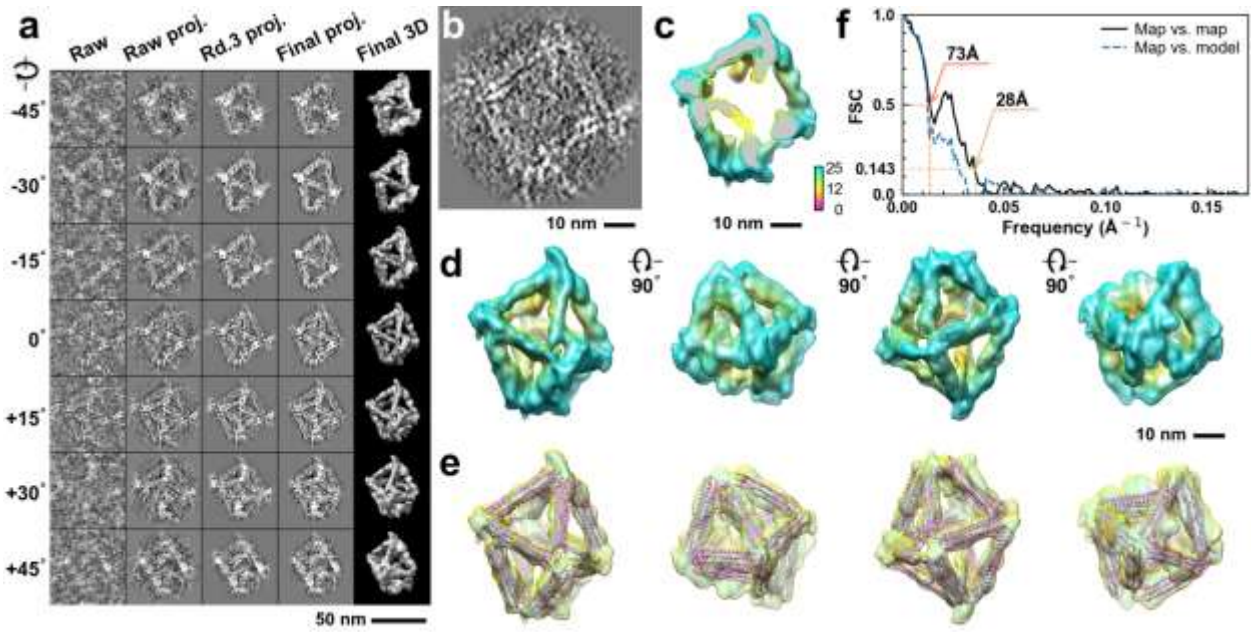

Supplementary Fig. 308: IPET 3D reconstruction and model fitting of an individual unit-cell particle (Index: 300) within a 2D lattice with 0% ferritin loading. a, Seven representative tilt images of a single unit-cell particle are shown in the first column (from left). The tilt images are aligned to a common center using IPET through iterative refinement. The projections of the raw, intermediate, and final 3D reconstruction at the corresponding angles are displayed in the subsequent four columns. **b**, A central cross-section (~23 nm thick) of the final reconstruction before masking is applied. **c**, 3D views of the central cross-section. **d**, Final 3D density map of this particle, viewed from four perpendicular directions. **e**, Final 3D reconstruction superimposed with the fitted model, viewed from four perpendicular directions. **f**, FSC analyses of the final map resolution using two methods: map-map FSC, where each map is reconstructed from one half of the images (even vs. odd tilt angle indices), and map-model FSC, where the model map is generated from the fitted model. Resolution assessments are provided based on tilt-based map-map and map-model FSC analyses at thresholds of FSC=0.5 and 0.143, respectively.

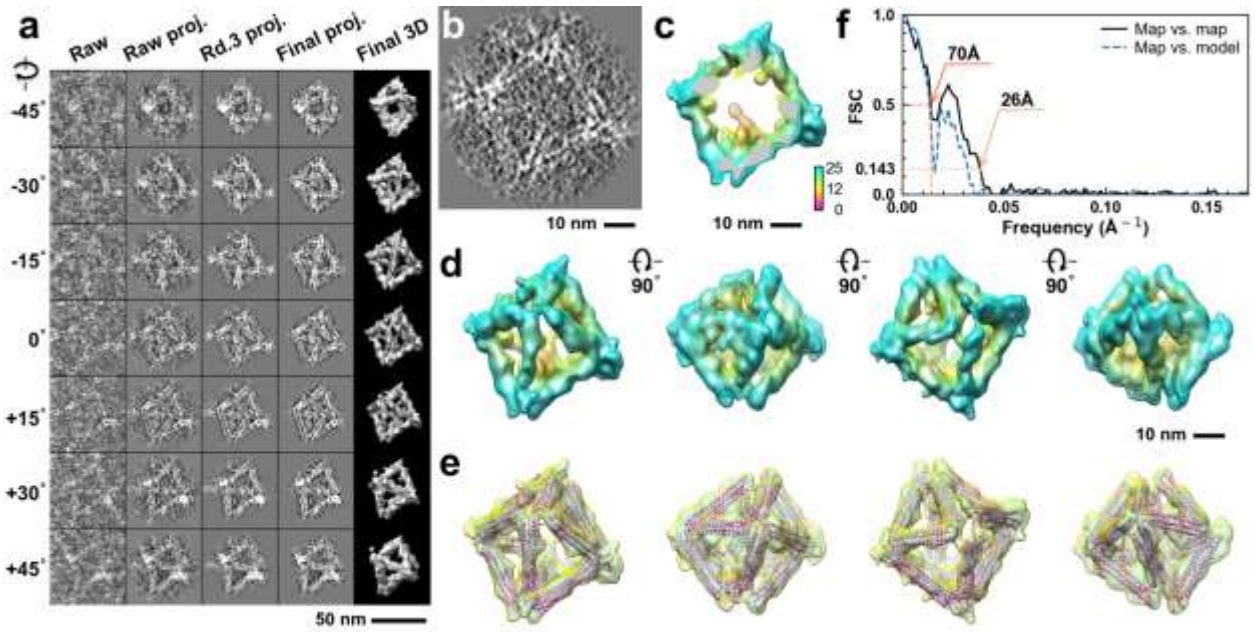

Supplementary Fig. 309: IPET 3D reconstruction and model fitting of an individual unit-cell particle (Index: 301) within a 2D lattice with 0% ferritin loading. a, Seven representative tilt images of a single unit-cell particle are shown in the first column (from left). The tilt images are aligned to a common center using IPET through iterative refinement. The projections of the raw, intermediate, and final 3D reconstruction at the corresponding angles are displayed in the subsequent four columns. **b**, A central cross-section (~23 nm thick) of the final reconstruction before masking is applied. **c**, 3D views of the central cross-section. **d**, Final 3D density map of this particle, viewed from four perpendicular directions. **e**, Final 3D reconstruction superimposed with the fitted model, viewed from four perpendicular directions. **f**, FSC analyses of the final map resolution using two methods: map-map FSC, where each map is reconstructed from one half of the images (even vs. odd tilt angle indices), and map-model FSC, where the model map is generated from the fitted model. Resolution assessments are provided based on tilt-based map-map and map-model FSC analyses at thresholds of FSC=0.5 and 0.143, respectively.

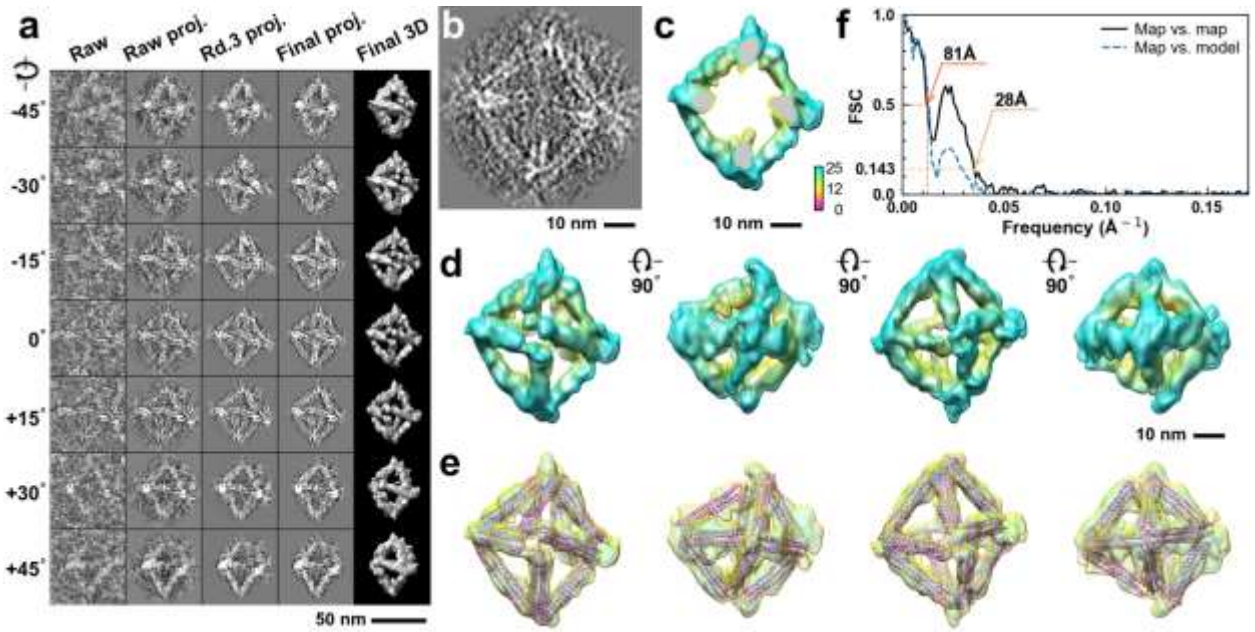

Supplementary Fig. 310: IPET 3D reconstruction and model fitting of an individual unit-cell particle (Index: 302) within a 2D lattice with 0% ferritin loading. a, Seven representative tilt images of a single unit-cell particle are shown in the first column (from left). The tilt images are aligned to a common center using IPET through iterative refinement. The projections of the raw, intermediate, and final 3D reconstruction at the corresponding angles are displayed in the subsequent four columns. **b**, A central cross-section (~23 nm thick) of the final reconstruction before masking is applied. **c**, 3D views of the central cross-section. **d**, Final 3D density map of this particle, viewed from four perpendicular directions. **e**, Final 3D reconstruction superimposed with the fitted model, viewed from four perpendicular directions. **f**, FSC analyses of the final map resolution using two methods: map-map FSC, where each map is reconstructed from one half of the images (even vs. odd tilt angle indices), and map-model FSC, where the model map is generated from the fitted model. Resolution assessments are provided based on tilt-based map-map and map-model FSC analyses at thresholds of FSC=0.5 and 0.143, respectively.

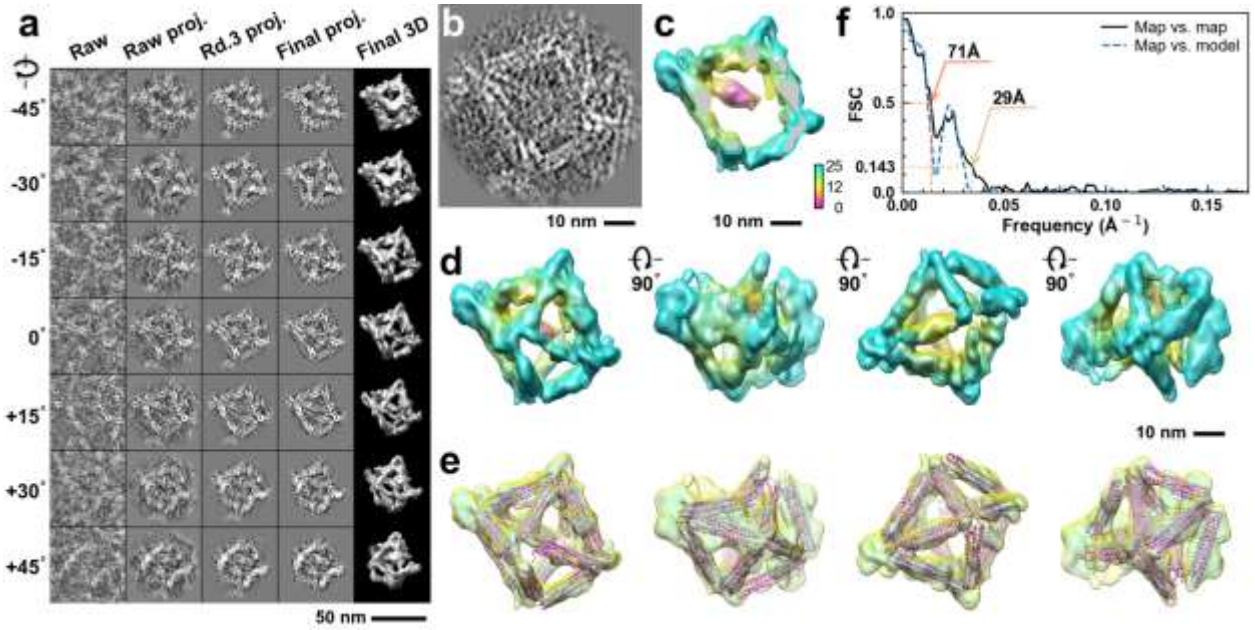

Supplementary Fig. 311: IPET 3D reconstruction and model fitting of an individual unit-cell particle (Index: 303) within a 2D lattice with 0% ferritin loading. a, Seven representative tilt images of a single unit-cell particle are shown in the first column (from left). The tilt images are aligned to a common center using IPET through iterative refinement. The projections of the raw, intermediate, and final 3D reconstruction at the corresponding angles are displayed in the subsequent four columns. **b**, A central cross-section (~23 nm thick) of the final reconstruction before masking is applied. **c**, 3D views of the central cross-section. **d**, Final 3D density map of this particle, viewed from four perpendicular directions. **e**, Final 3D reconstruction superimposed with the fitted model, viewed from four perpendicular directions. **f**, FSC analyses of the final map resolution using two methods: map-map FSC, where each map is reconstructed from one half of the images (even vs. odd tilt angle indices), and map-model FSC, where the model map is generated from the fitted model. Resolution assessments are provided based on tilt-based map-map and map-model FSC analyses at thresholds of FSC=0.5 and 0.143, respectively.

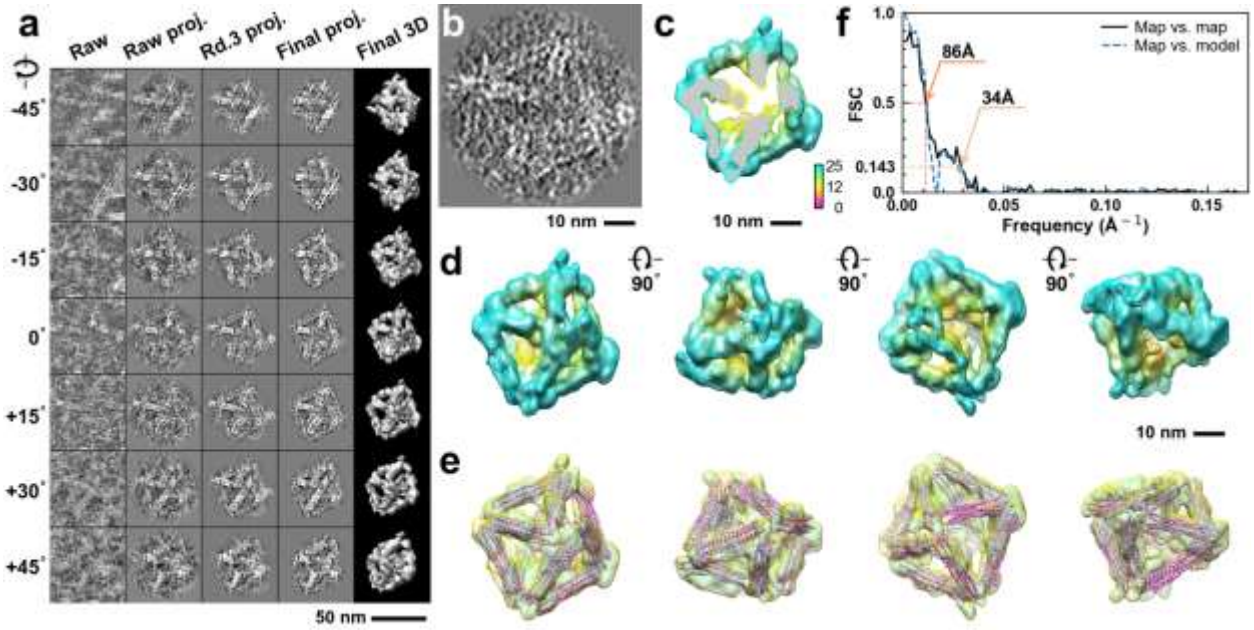

Supplementary Fig. 312: IPET 3D reconstruction and model fitting of an individual unit-cell particle (Index: 304) within a 2D lattice with 0% ferritin loading. a, Seven representative tilt images of a single unit-cell particle are shown in the first column (from left). The tilt images are aligned to a common center using IPET through iterative refinement. The projections of the raw, intermediate, and final 3D reconstruction at the corresponding angles are displayed in the subsequent four columns. **b**, A central cross-section (~23 nm thick) of the final reconstruction before masking is applied. **c**, 3D views of the central cross-section. **d**, Final 3D density map of this particle, viewed from four perpendicular directions. **e**, Final 3D reconstruction superimposed with the fitted model, viewed from four perpendicular directions. **f**, FSC analyses of the final map resolution using two methods: map-map FSC, where each map is reconstructed from one half of the images (even vs. odd tilt angle indices), and map-model FSC, where the model map is generated from the fitted model. Resolution assessments are provided based on tilt-based map-map and map-model FSC analyses at thresholds of FSC=0.5 and 0.143, respectively.

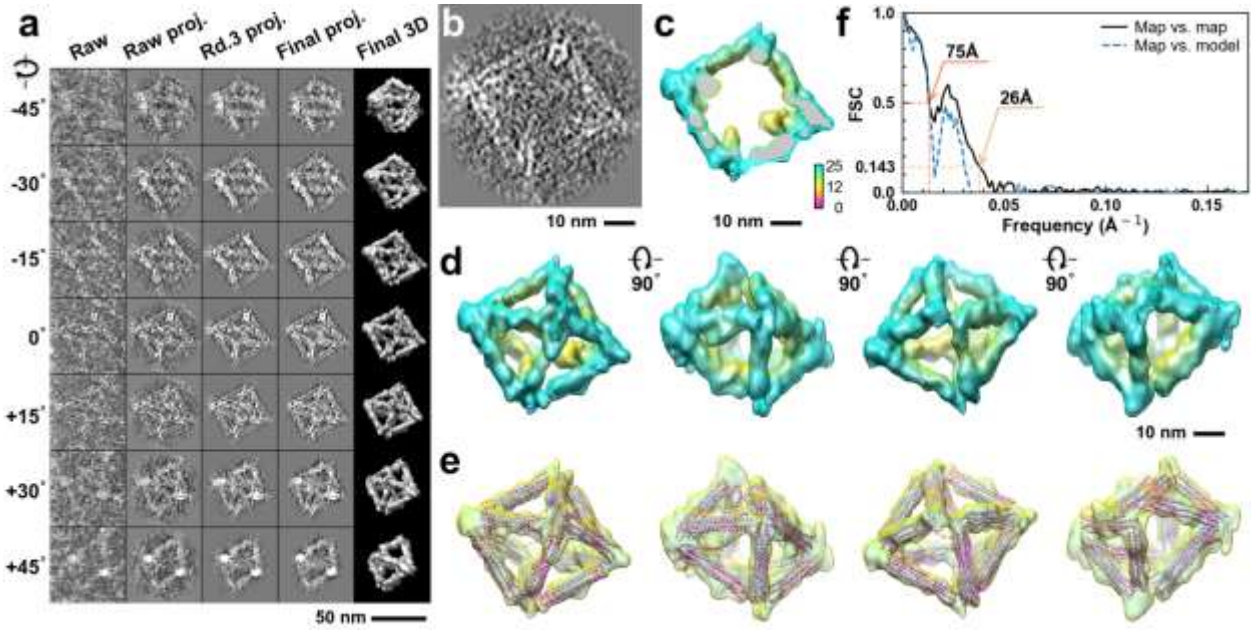

Supplementary Fig. 313: IPET 3D reconstruction and model fitting of an individual unit-cell particle (Index: 305) within a 2D lattice with 0% ferritin loading. a, Seven representative tilt images of a single unit-cell particle are shown in the first column (from left). The tilt images are aligned to a common center using IPET through iterative refinement. The projections of the raw, intermediate, and final 3D reconstruction at the corresponding angles are displayed in the subsequent four columns. **b**, A central cross-section (~23 nm thick) of the final reconstruction before masking is applied. **c**, 3D views of the central cross-section. **d**, Final 3D density map of this particle, viewed from four perpendicular directions. **e**, Final 3D reconstruction superimposed with the fitted model, viewed from four perpendicular directions. **f**, FSC analyses of the final map resolution using two methods: map-map FSC, where each map is reconstructed from one half of the images (even vs. odd tilt angle indices), and map-model FSC, where the model map is generated from the fitted model. Resolution assessments are provided based on tilt-based map-map and map-model FSC analyses at thresholds of FSC=0.5 and 0.143, respectively.

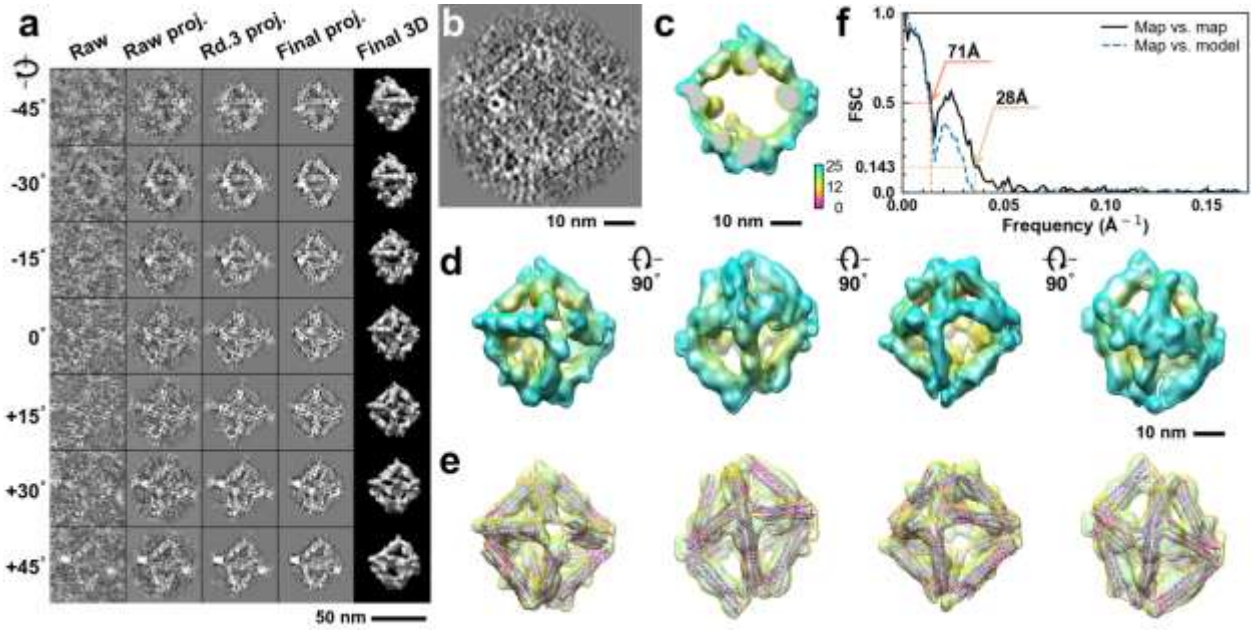

Supplementary Fig. 314: IPET 3D reconstruction and model fitting of an individual unit-cell particle (Index: 306) within a 2D lattice with 0% ferritin loading. a, Seven representative tilt images of a single unit-cell particle are shown in the first column (from left). The tilt images are aligned to a common center using IPET through iterative refinement. The projections of the raw, intermediate, and final 3D reconstruction at the corresponding angles are displayed in the subsequent four columns. **b**, A central cross-section (~23 nm thick) of the final reconstruction before masking is applied. **c**, 3D views of the central cross-section. **d**, Final 3D density map of this particle, viewed from four perpendicular directions. **e**, Final 3D reconstruction superimposed with the fitted model, viewed from four perpendicular directions. **f**, FSC analyses of the final map resolution using two methods: map-map FSC, where each map is reconstructed from one half of the images (even vs. odd tilt angle indices), and map-model FSC, where the model map is generated from the fitted model. Resolution assessments are provided based on tilt-based map-map and map-model FSC analyses at thresholds of FSC=0.5 and 0.143, respectively.

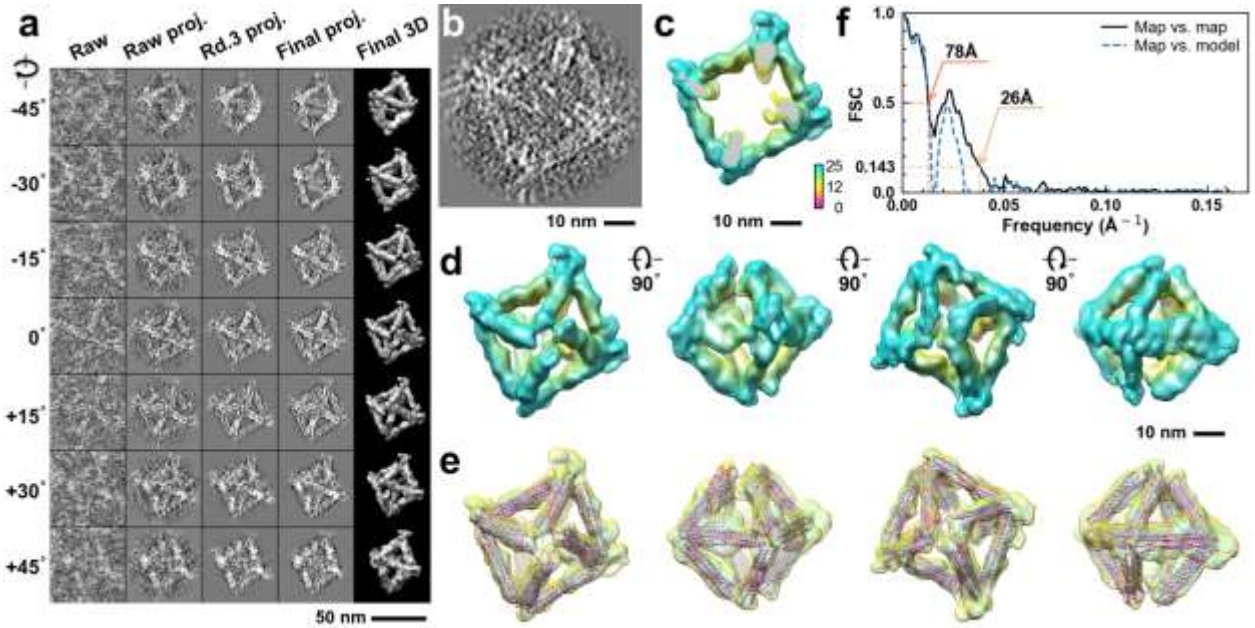

Supplementary Fig. 315: IPET 3D reconstruction and model fitting of an individual unit-cell particle (Index: 307) within a 2D lattice with 0% ferritin loading. a, Seven representative tilt images of a single unit-cell particle are shown in the first column (from left). The tilt images are aligned to a common center using IPET through iterative refinement. The projections of the raw, intermediate, and final 3D reconstruction at the corresponding angles are displayed in the subsequent four columns. **b**, A central cross-section (~23 nm thick) of the final reconstruction before masking is applied. **c**, 3D views of the central cross-section. **d**, Final 3D density map of this particle, viewed from four perpendicular directions. **e**, Final 3D reconstruction superimposed with the fitted model, viewed from four perpendicular directions. **f**, FSC analyses of the final map resolution using two methods: map-map FSC, where each map is reconstructed from one half of the images (even vs. odd tilt angle indices), and map-model FSC, where the model map is generated from the fitted model. Resolution assessments are provided based on tilt-based map-map and map-model FSC analyses at thresholds of FSC=0.5 and 0.143, respectively.

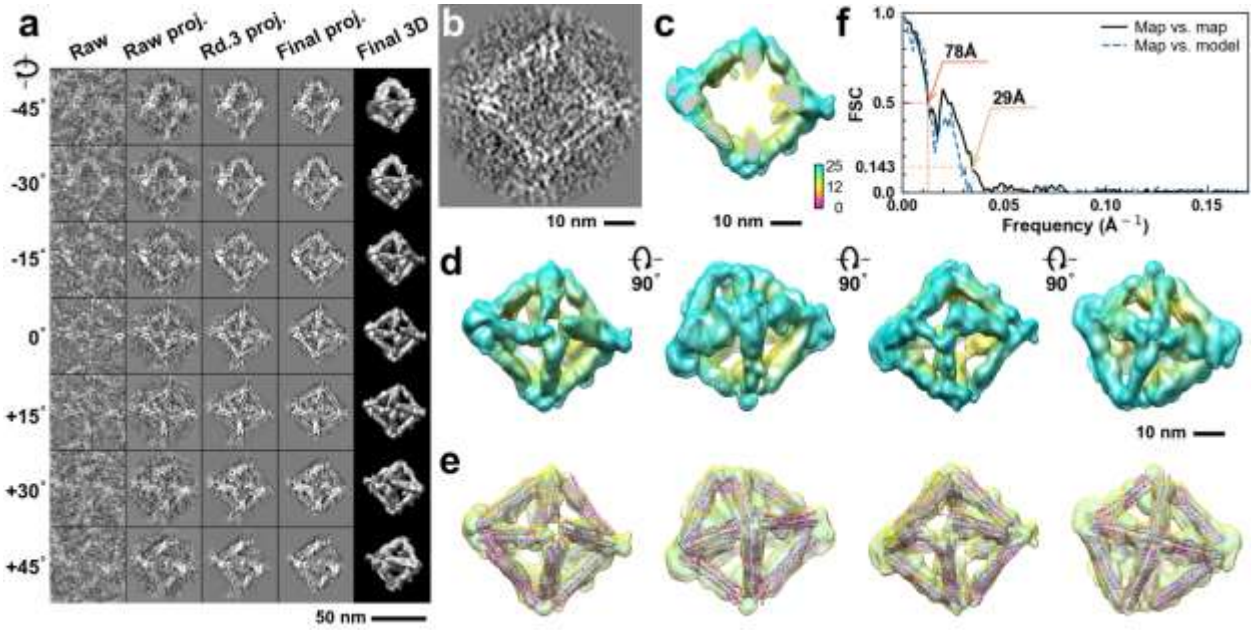

Supplementary Fig. 316: IPET 3D reconstruction and model fitting of an individual unit-cell particle (Index: 308) within a 2D lattice with 0% ferritin loading. a, Seven representative tilt images of a single unit-cell particle are shown in the first column (from left). The tilt images are aligned to a common center using IPET through iterative refinement. The projections of the raw, intermediate, and final 3D reconstruction at the corresponding angles are displayed in the subsequent four columns. **b**, A central cross-section (~23 nm thick) of the final reconstruction before masking is applied. **c**, 3D views of the central cross-section. **d**, Final 3D density map of this particle, viewed from four perpendicular directions. **e**, Final 3D reconstruction superimposed with the fitted model, viewed from four perpendicular directions. **f**, FSC analyses of the final map resolution using two methods: map-map FSC, where each map is reconstructed from one half of the images (even vs. odd tilt angle indices), and map-model FSC, where the model map is generated from the fitted model. Resolution assessments are provided based on tilt-based map-map and map-model FSC analyses at thresholds of FSC=0.5 and 0.143, respectively.

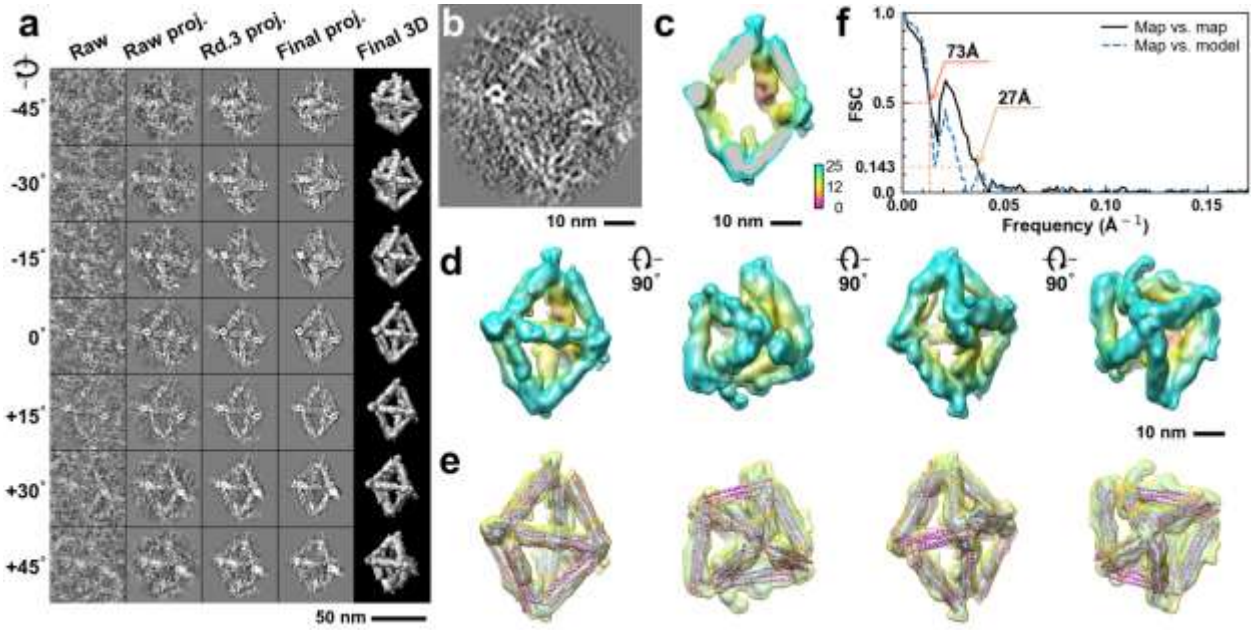

Supplementary Fig. 317: IPET 3D reconstruction and model fitting of an individual unit-cell particle (Index: 309) within a 2D lattice with 0% ferritin loading. a, Seven representative tilt images of a single unit-cell particle are shown in the first column (from left). The tilt images are aligned to a common center using IPET through iterative refinement. The projections of the raw, intermediate, and final 3D reconstruction at the corresponding angles are displayed in the subsequent four columns. **b**, A central cross-section (~23 nm thick) of the final reconstruction before masking is applied. **c**, 3D views of the central cross-section. **d**, Final 3D density map of this particle, viewed from four perpendicular directions. **e**, Final 3D reconstruction superimposed with the fitted model, viewed from four perpendicular directions. **f**, FSC analyses of the final map resolution using two methods: map-map FSC, where each map is reconstructed from one half of the images (even vs. odd tilt angle indices), and map-model FSC, where the model map is generated from the fitted model. Resolution assessments are provided based on tilt-based map-map and map-model FSC analyses at thresholds of FSC=0.5 and 0.143, respectively.

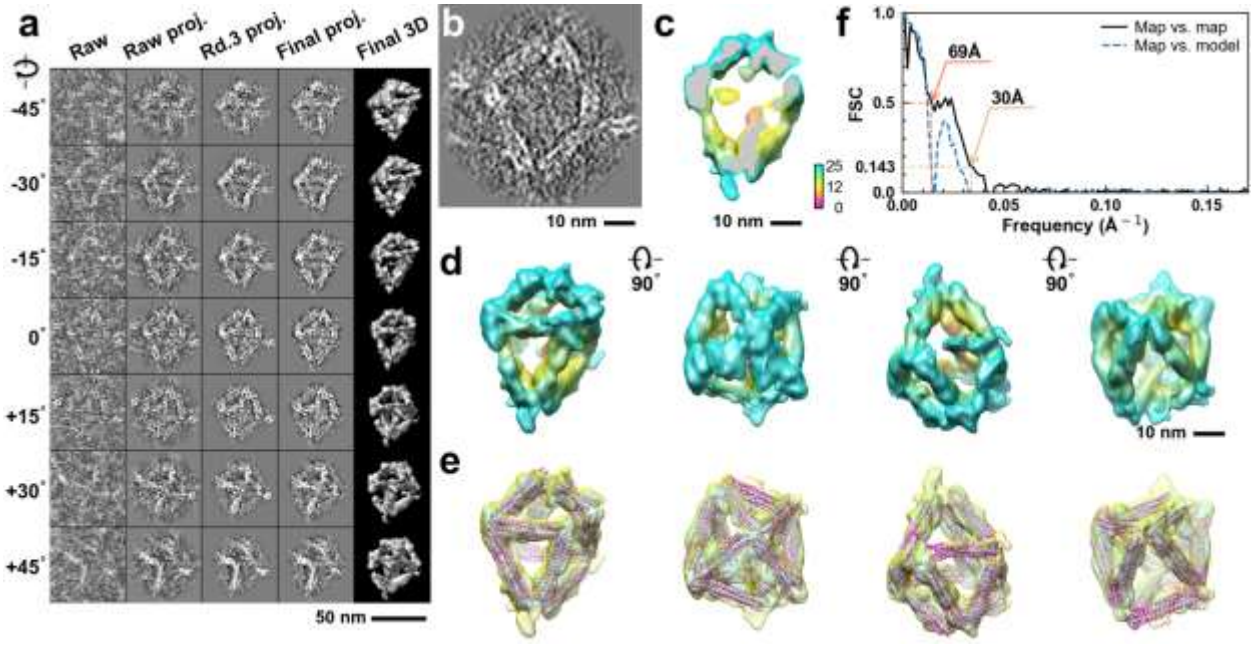

Supplementary Fig. 318: IPET 3D reconstruction and model fitting of an individual unit-cell particle (Index: 310) within a 2D lattice with 0% ferritin loading. a, Seven representative tilt images of a single unit-cell particle are shown in the first column (from left). The tilt images are aligned to a common center using IPET through iterative refinement. The projections of the raw, intermediate, and final 3D reconstruction at the corresponding angles are displayed in the subsequent four columns. **b**, A central cross-section (~23 nm thick) of the final reconstruction before masking is applied. **c**, 3D views of the central cross-section. **d**, Final 3D density map of this particle, viewed from four perpendicular directions. **e**, Final 3D reconstruction superimposed with the fitted model, viewed from four perpendicular directions. **f**, FSC analyses of the final map resolution using two methods: map-map FSC, where each map is reconstructed from one half of the images (even vs. odd tilt angle indices), and map-model FSC, where the model map is generated from the fitted model. Resolution assessments are provided based on tilt-based map-map and map-model FSC analyses at thresholds of FSC=0.5 and 0.143, respectively.

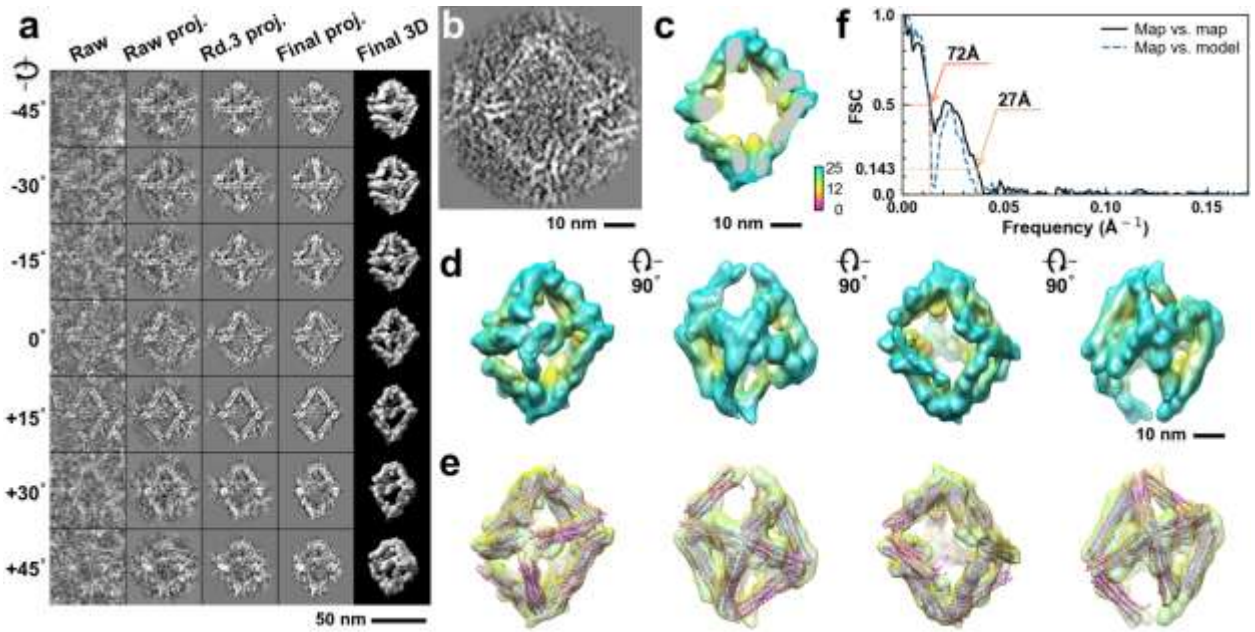

Supplementary Fig. 319: IPET 3D reconstruction and model fitting of an individual unit-cell particle (Index: 311) within a 2D lattice with 0% ferritin loading. a, Seven representative tilt images of a single unit-cell particle are shown in the first column (from left). The tilt images are aligned to a common center using IPET through iterative refinement. The projections of the raw, intermediate, and final 3D reconstruction at the corresponding angles are displayed in the subsequent four columns. **b**, A central cross-section (~23 nm thick) of the final reconstruction before masking is applied. **c**, 3D views of the central cross-section. **d**, Final 3D density map of this particle, viewed from four perpendicular directions. **e**, Final 3D reconstruction superimposed with the fitted model, viewed from four perpendicular directions. **f**, FSC analyses of the final map resolution using two methods: map-map FSC, where each map is reconstructed from one half of the images (even vs. odd tilt angle indices), and map-model FSC, where the model map is generated from the fitted model. Resolution assessments are provided based on tilt-based map-map and map-model FSC analyses at thresholds of FSC=0.5 and 0.143, respectively.

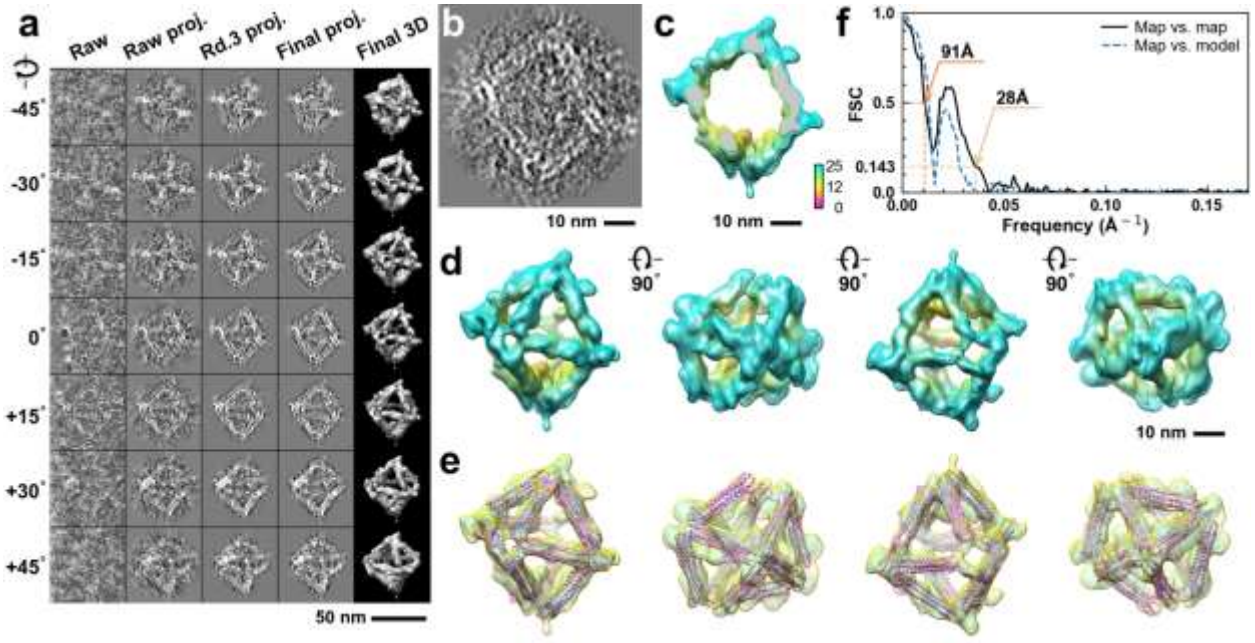

Supplementary Fig. 320: IPET 3D reconstruction and model fitting of an individual unit-cell particle (Index: 312) within a 2D lattice with 0% ferritin loading. a, Seven representative tilt images of a single unit-cell particle are shown in the first column (from left). The tilt images are aligned to a common center using IPET through iterative refinement. The projections of the raw, intermediate, and final 3D reconstruction at the corresponding angles are displayed in the subsequent four columns. **b**, A central cross-section (~23 nm thick) of the final reconstruction before masking is applied. **c**, 3D views of the central cross-section. **d**, Final 3D density map of this particle, viewed from four perpendicular directions. **e**, Final 3D reconstruction superimposed with the fitted model, viewed from four perpendicular directions. **f**, FSC analyses of the final map resolution using two methods: map-map FSC, where each map is reconstructed from one half of the images (even vs. odd tilt angle indices), and map-model FSC, where the model map is generated from the fitted model. Resolution assessments are provided based on tilt-based map-map and map-model FSC analyses at thresholds of FSC=0.5 and 0.143, respectively.

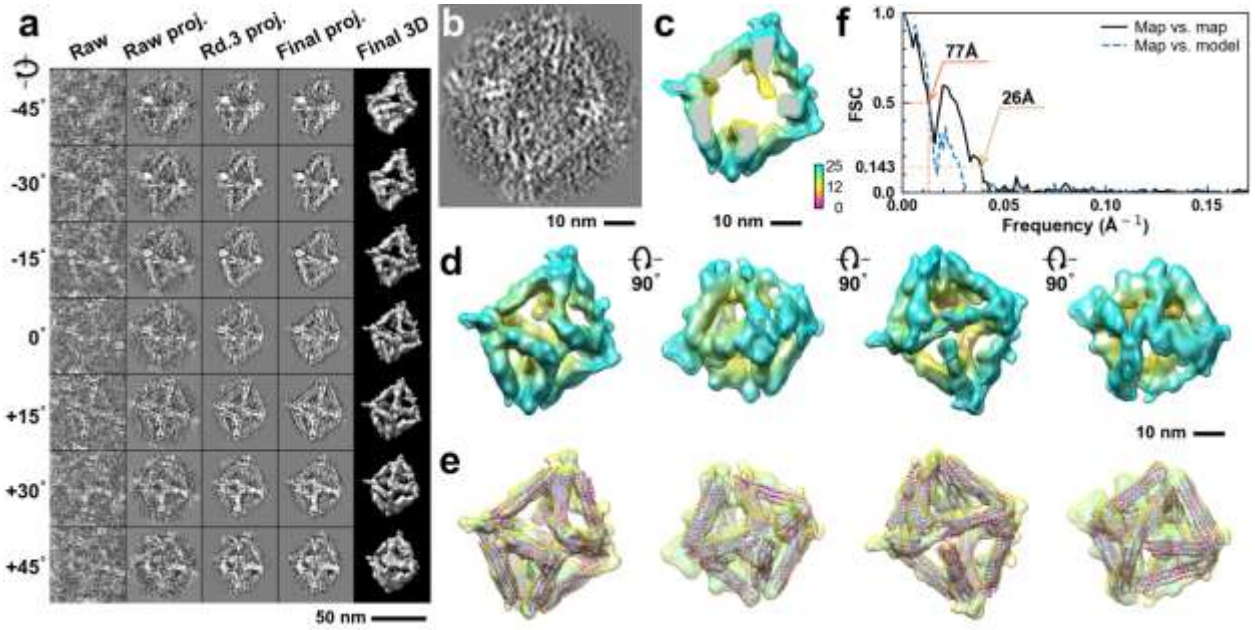

Supplementary Fig. 321: IPET 3D reconstruction and model fitting of an individual unit-cell particle (Index: 313) within a 2D lattice with 0% ferritin loading. a, Seven representative tilt images of a single unit-cell particle are shown in the first column (from left). The tilt images are aligned to a common center using IPET through iterative refinement. The projections of the raw, intermediate, and final 3D reconstruction at the corresponding angles are displayed in the subsequent four columns. **b**, A central cross-section (~23 nm thick) of the final reconstruction before masking is applied. **c**, 3D views of the central cross-section. **d**, Final 3D density map of this particle, viewed from four perpendicular directions. **e**, Final 3D reconstruction superimposed with the fitted model, viewed from four perpendicular directions. **f**, FSC analyses of the final map resolution using two methods: map-map FSC, where each map is reconstructed from one half of the images (even vs. odd tilt angle indices), and map-model FSC, where the model map is generated from the fitted model. Resolution assessments are provided based on tilt-based map-map and map-model FSC analyses at thresholds of FSC=0.5 and 0.143, respectively.

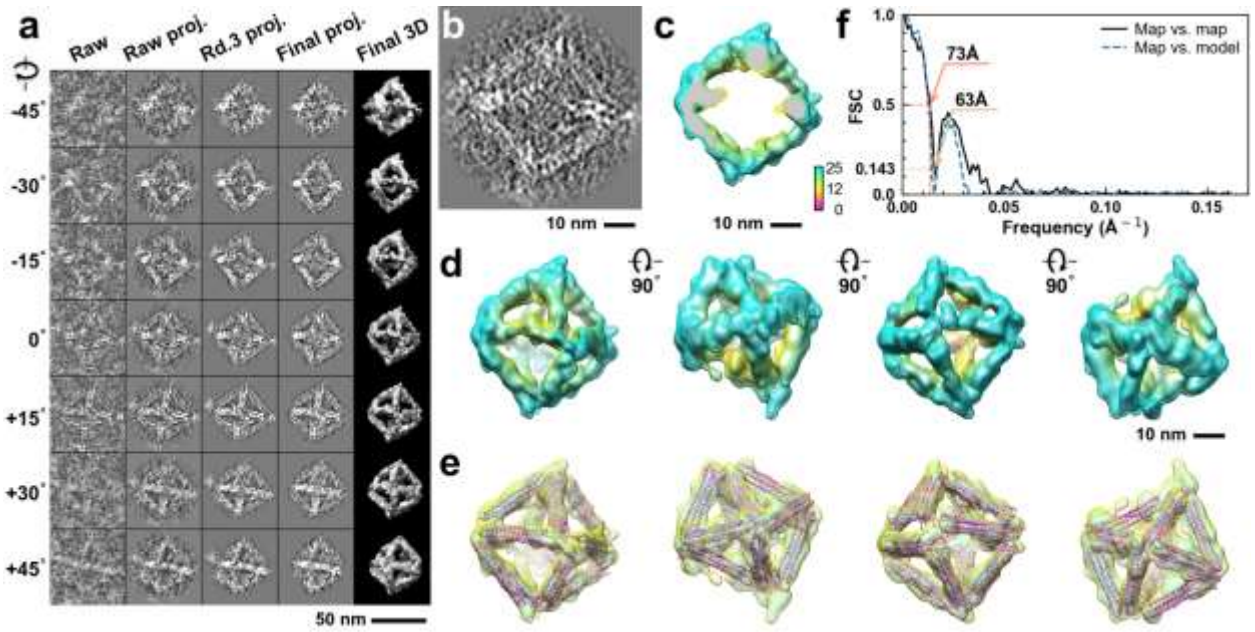

Supplementary Fig. 322: IPET 3D reconstruction and model fitting of an individual unit-cell particle (Index: 314) within a 2D lattice with 0% ferritin loading. a, Seven representative tilt images of a single unit-cell particle are shown in the first column (from left). The tilt images are aligned to a common center using IPET through iterative refinement. The projections of the raw, intermediate, and final 3D reconstruction at the corresponding angles are displayed in the subsequent four columns. **b**, A central cross-section (~23 nm thick) of the final reconstruction before masking is applied. **c**, 3D views of the central cross-section. **d**, Final 3D density map of this particle, viewed from four perpendicular directions. **e**, Final 3D reconstruction superimposed with the fitted model, viewed from four perpendicular directions. **f**, FSC analyses of the final map resolution using two methods: map-map FSC, where each map is reconstructed from one half of the images (even vs. odd tilt angle indices), and map-model FSC, where the model map is generated from the fitted model. Resolution assessments are provided based on tilt-based map-map and map-model FSC analyses at thresholds of FSC=0.5 and 0.143, respectively.

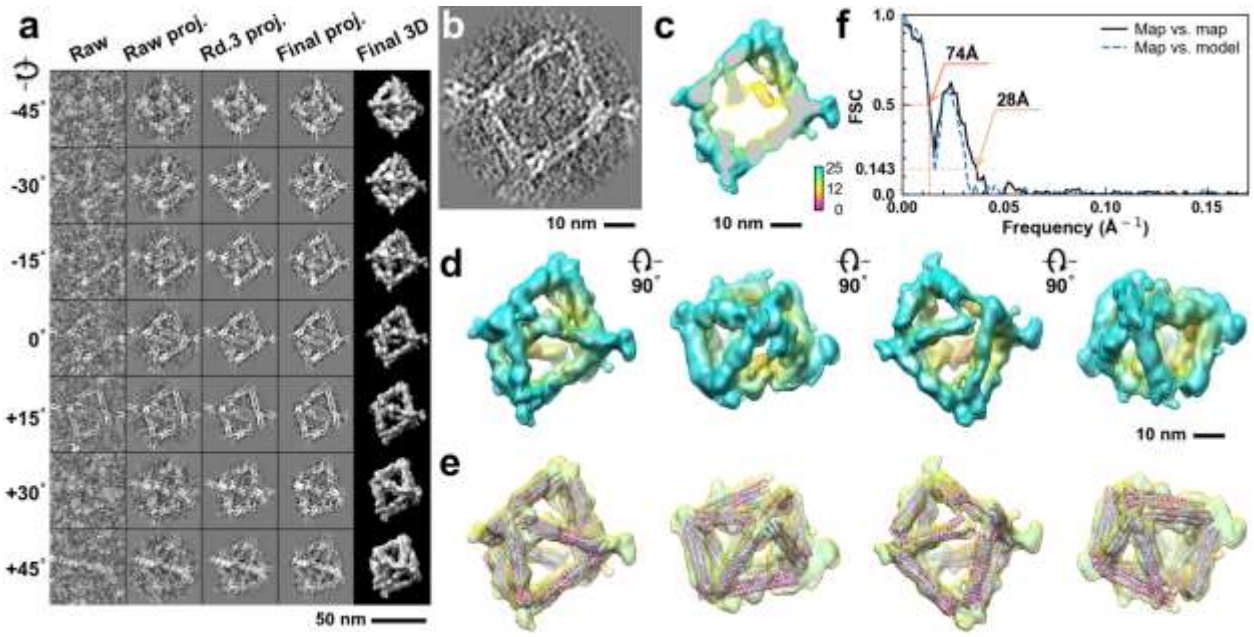

Supplementary Fig. 323: IPET 3D reconstruction and model fitting of an individual unit-cell particle (Index: 315) within a 2D lattice with 0% ferritin loading. a, Seven representative tilt images of a single unit-cell particle are shown in the first column (from left). The tilt images are aligned to a common center using IPET through iterative refinement. The projections of the raw, intermediate, and final 3D reconstruction at the corresponding angles are displayed in the subsequent four columns. **b**, A central cross-section (~23 nm thick) of the final reconstruction before masking is applied. **c**, 3D views of the central cross-section. **d**, Final 3D density map of this particle, viewed from four perpendicular directions. **e**, Final 3D reconstruction superimposed with the fitted model, viewed from four perpendicular directions. **f**, FSC analyses of the final map resolution using two methods: map-map FSC, where each map is reconstructed from one half of the images (even vs. odd tilt angle indices), and map-model FSC, where the model map is generated from the fitted model. Resolution assessments are provided based on tilt-based map-map and map-model FSC analyses at thresholds of FSC=0.5 and 0.143, respectively.

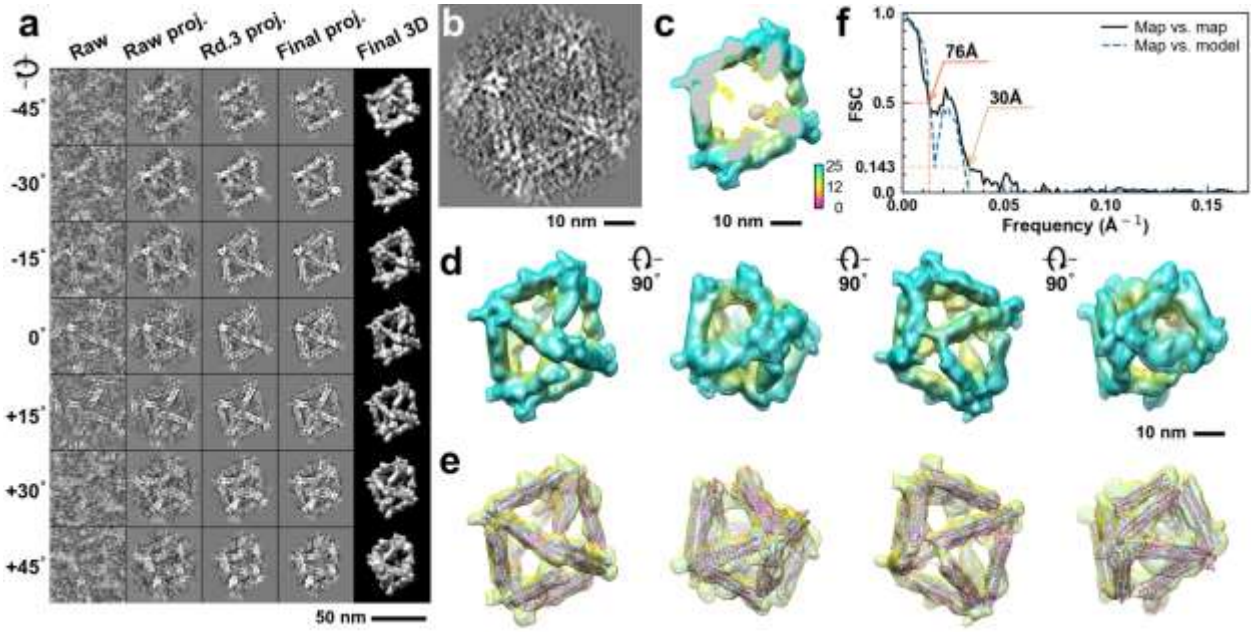

Supplementary Fig. 324: IPET 3D reconstruction and model fitting of an individual unit-cell particle (Index: 316) within a 2D lattice with 0% ferritin loading. a, Seven representative tilt images of a single unit-cell particle are shown in the first column (from left). The tilt images are aligned to a common center using IPET through iterative refinement. The projections of the raw, intermediate, and final 3D reconstruction at the corresponding angles are displayed in the subsequent four columns. **b**, A central cross-section (~23 nm thick) of the final reconstruction before masking is applied. **c**, 3D views of the central cross-section. **d**, Final 3D density map of this particle, viewed from four perpendicular directions. **e**, Final 3D reconstruction superimposed with the fitted model, viewed from four perpendicular directions. **f**, FSC analyses of the final map resolution using two methods: map-map FSC, where each map is reconstructed from one half of the images (even vs. odd tilt angle indices), and map-model FSC, where the model map is generated from the fitted model. Resolution assessments are provided based on tilt-based map-map and map-model FSC analyses at thresholds of FSC=0.5 and 0.143, respectively.

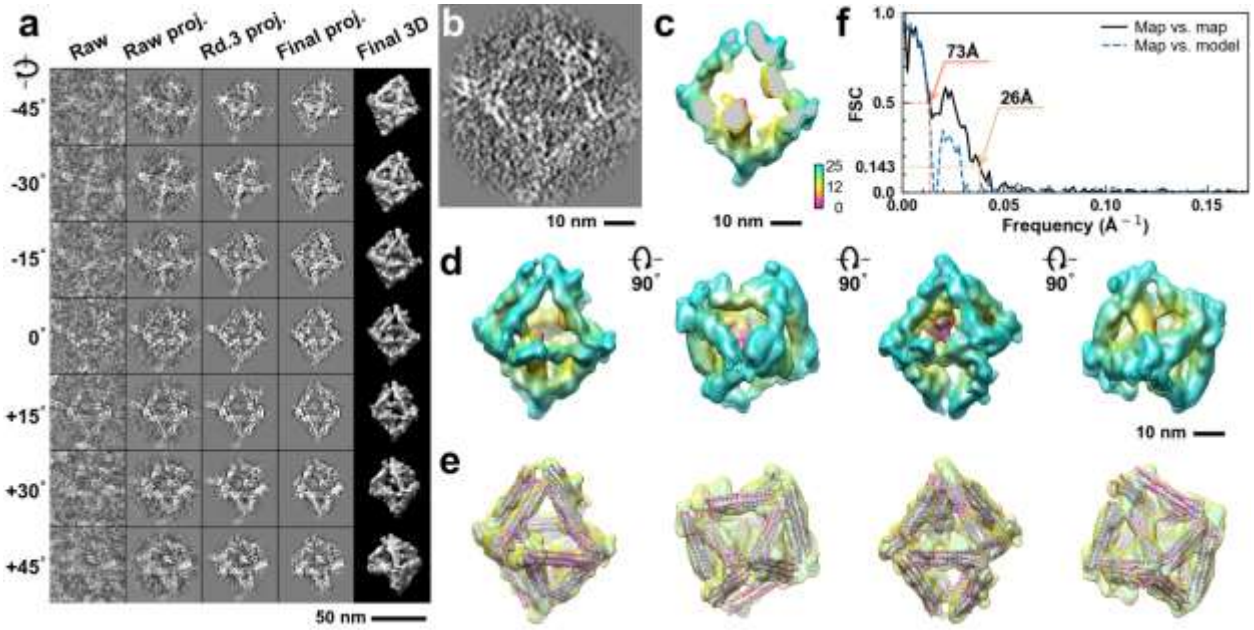

Supplementary Fig. 325: IPET 3D reconstruction and model fitting of an individual unit-cell particle (Index: 317) within a 2D lattice with 0% ferritin loading. a, Seven representative tilt images of a single unit-cell particle are shown in the first column (from left). The tilt images are aligned to a common center using IPET through iterative refinement. The projections of the raw, intermediate, and final 3D reconstruction at the corresponding angles are displayed in the subsequent four columns. **b**, A central cross-section (~23 nm thick) of the final reconstruction before masking is applied. **c**, 3D views of the central cross-section. **d**, Final 3D density map of this particle, viewed from four perpendicular directions. **e**, Final 3D reconstruction superimposed with the fitted model, viewed from four perpendicular directions. **f**, FSC analyses of the final map resolution using two methods: map-map FSC, where each map is reconstructed from one half of the images (even vs. odd tilt angle indices), and map-model FSC, where the model map is generated from the fitted model. Resolution assessments are provided based on tilt-based map-map and map-model FSC analyses at thresholds of FSC=0.5 and 0.143, respectively.

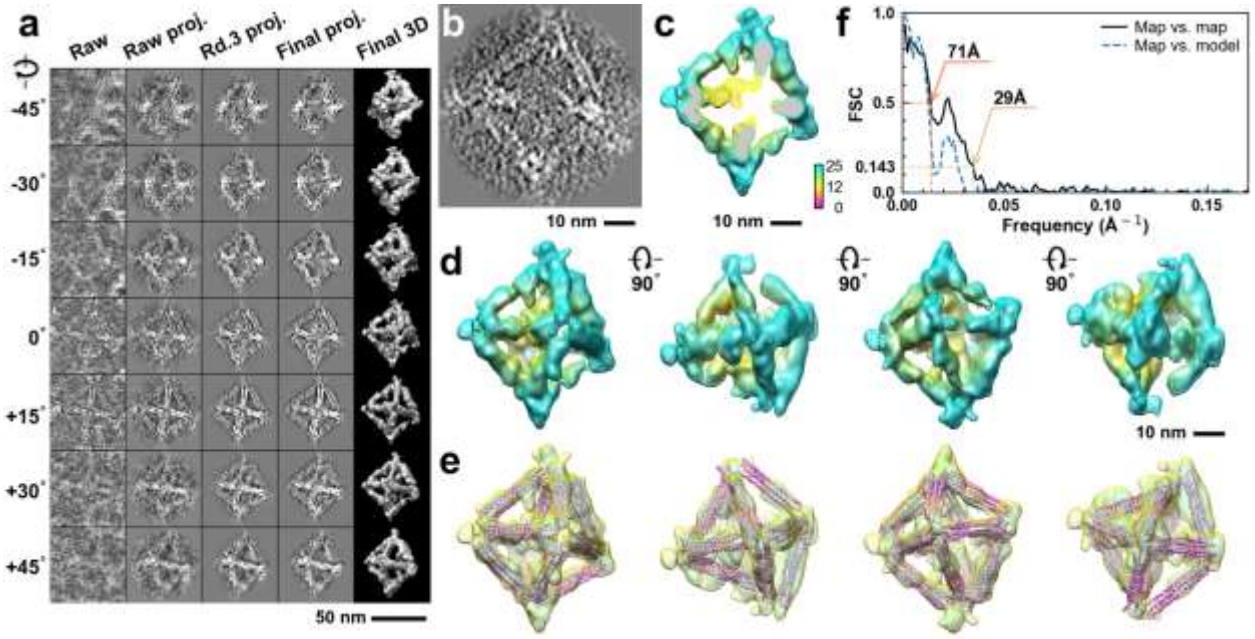

Supplementary Fig. 326: IPET 3D reconstruction and model fitting of an individual unit-cell particle (Index: 318) within a 2D lattice with 0% ferritin loading. a, Seven representative tilt images of a single unit-cell particle are shown in the first column (from left). The tilt images are aligned to a common center using IPET through iterative refinement. The projections of the raw, intermediate, and final 3D reconstruction at the corresponding angles are displayed in the subsequent four columns. **b**, A central cross-section (~23 nm thick) of the final reconstruction before masking is applied. **c**, 3D views of the central cross-section. **d**, Final 3D density map of this particle, viewed from four perpendicular directions. **e**, Final 3D reconstruction superimposed with the fitted model, viewed from four perpendicular directions. **f**, FSC analyses of the final map resolution using two methods: map-map FSC, where each map is reconstructed from one half of the images (even vs. odd tilt angle indices), and map-model FSC, where the model map is generated from the fitted model. Resolution assessments are provided based on tilt-based map-map and map-model FSC analyses at thresholds of FSC=0.5 and 0.143, respectively.

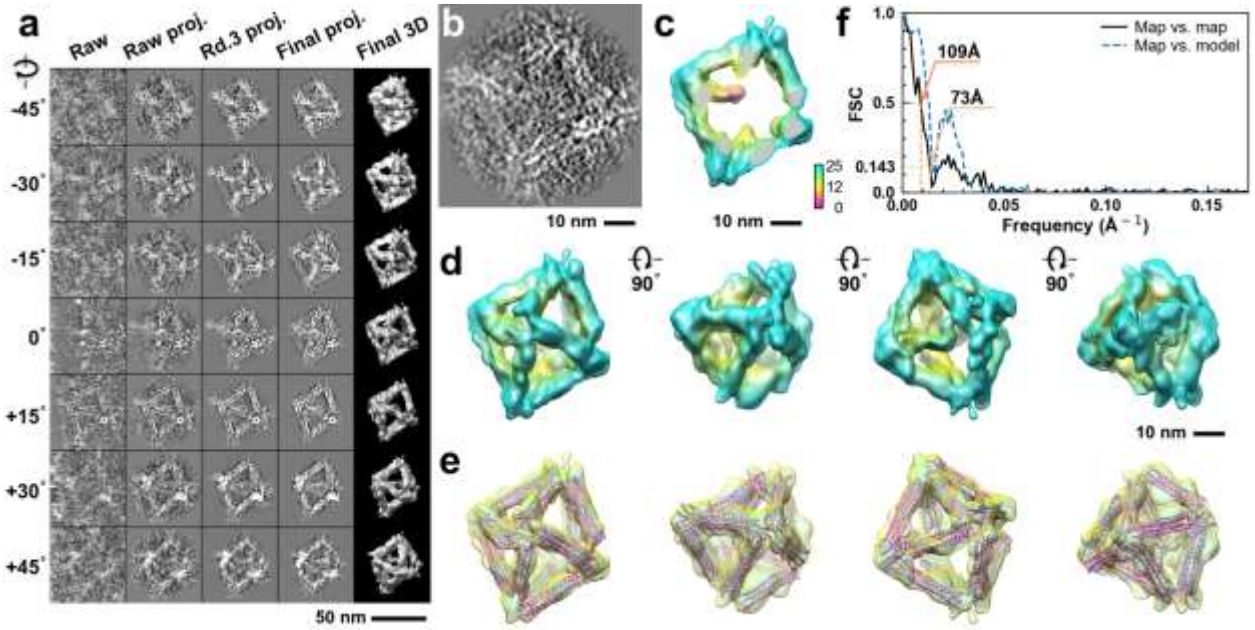

Supplementary Fig. 327: IPET 3D reconstruction and model fitting of an individual unit-cell particle (Index: 319) within a 2D lattice with 0% ferritin loading. a, Seven representative tilt images of a single unit-cell particle are shown in the first column (from left). The tilt images are aligned to a common center using IPET through iterative refinement. The projections of the raw, intermediate, and final 3D reconstruction at the corresponding angles are displayed in the subsequent four columns. **b**, A central cross-section (~23 nm thick) of the final reconstruction before masking is applied. **c**, 3D views of the central cross-section. **d**, Final 3D density map of this particle, viewed from four perpendicular directions. **e**, Final 3D reconstruction superimposed with the fitted model, viewed from four perpendicular directions. **f**, FSC analyses of the final map resolution using two methods: map-map FSC, where each map is reconstructed from one half of the images (even vs. odd tilt angle indices), and map-model FSC, where the model map is generated from the fitted model. Resolution assessments are provided based on tilt-based map-map and map-model FSC analyses at thresholds of FSC=0.5 and 0.143, respectively.

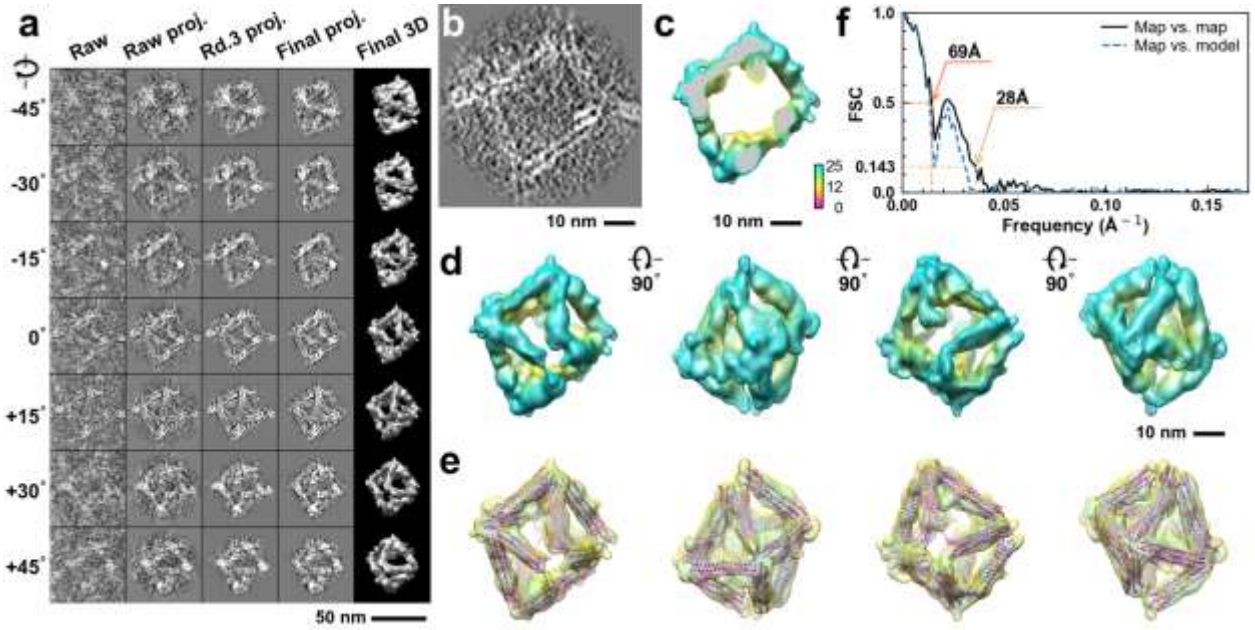

Supplementary Fig. 328: IPET 3D reconstruction and model fitting of an individual unit-cell particle (Index: 320) within a 2D lattice with 0% ferritin loading. a, Seven representative tilt images of a single unit-cell particle are shown in the first column (from left). The tilt images are aligned to a common center using IPET through iterative refinement. The projections of the raw, intermediate, and final 3D reconstruction at the corresponding angles are displayed in the subsequent four columns. **b**, A central cross-section (~23 nm thick) of the final reconstruction before masking is applied. **c**, 3D views of the central cross-section. **d**, Final 3D density map of this particle, viewed from four perpendicular directions. **e**, Final 3D reconstruction superimposed with the fitted model, viewed from four perpendicular directions. **f**, FSC analyses of the final map resolution using two methods: map-map FSC, where each map is reconstructed from one half of the images (even vs. odd tilt angle indices), and map-model FSC, where the model map is generated from the fitted model. Resolution assessments are provided based on tilt-based map-map and map-model FSC analyses at thresholds of FSC=0.5 and 0.143, respectively.

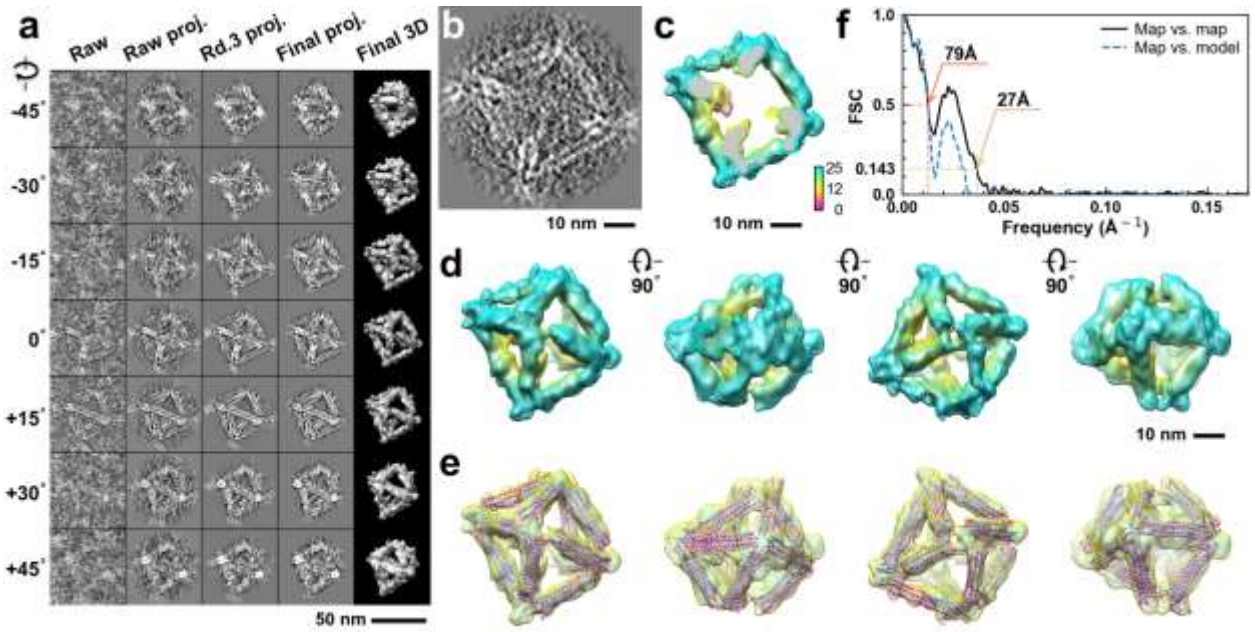

Supplementary Fig. 329: IPET 3D reconstruction and model fitting of an individual unit-cell particle (Index: 321) within a 2D lattice with 0% ferritin loading. a, Seven representative tilt images of a single unit-cell particle are shown in the first column (from left). The tilt images are aligned to a common center using IPET through iterative refinement. The projections of the raw, intermediate, and final 3D reconstruction at the corresponding angles are displayed in the subsequent four columns. **b**, A central cross-section (~23 nm thick) of the final reconstruction before masking is applied. **c**, 3D views of the central cross-section. **d**, Final 3D density map of this particle, viewed from four perpendicular directions. **e**, Final 3D reconstruction superimposed with the fitted model, viewed from four perpendicular directions. **f**, FSC analyses of the final map resolution using two methods: map-map FSC, where each map is reconstructed from one half of the images (even vs. odd tilt angle indices), and map-model FSC, where the model map is generated from the fitted model. Resolution assessments are provided based on tilt-based map-map and map-model FSC analyses at thresholds of FSC=0.5 and 0.143, respectively.

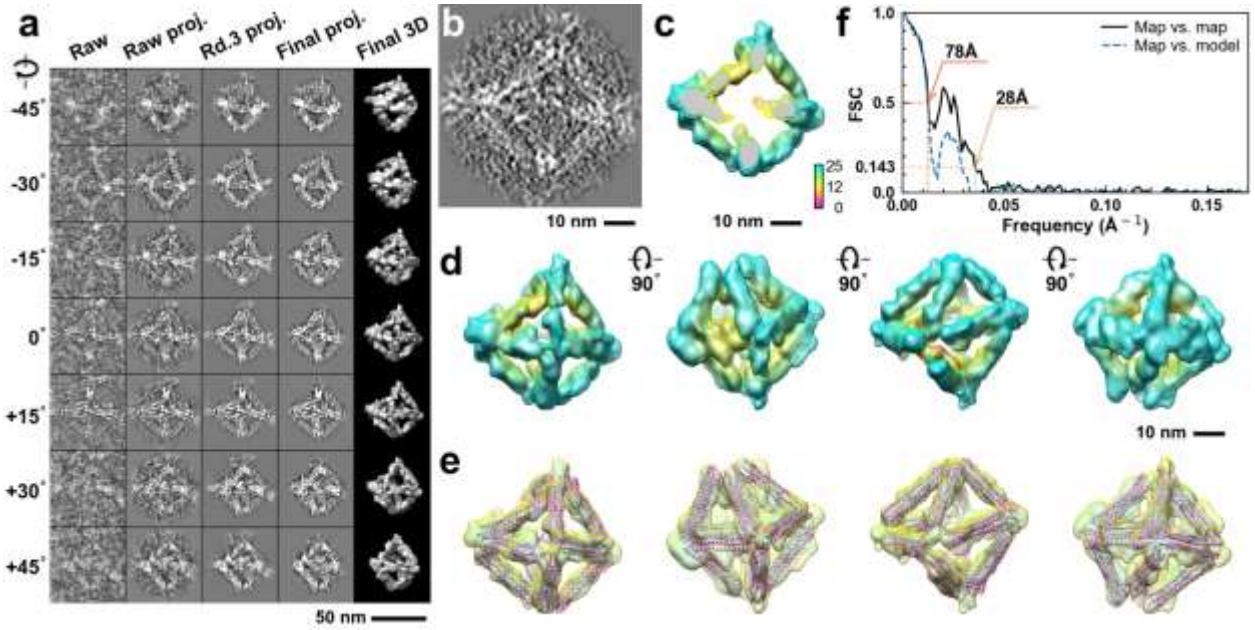

Supplementary Fig. 330: IPET 3D reconstruction and model fitting of an individual unit-cell particle (Index: 322) within a 2D lattice with 0% ferritin loading. a, Seven representative tilt images of a single unit-cell particle are shown in the first column (from left). The tilt images are aligned to a common center using IPET through iterative refinement. The projections of the raw, intermediate, and final 3D reconstruction at the corresponding angles are displayed in the subsequent four columns. **b**, A central cross-section (~23 nm thick) of the final reconstruction before masking is applied. **c**, 3D views of the central cross-section. **d**, Final 3D density map of this particle, viewed from four perpendicular directions. **e**, Final 3D reconstruction superimposed with the fitted model, viewed from four perpendicular directions. **f**, FSC analyses of the final map resolution using two methods: map-map FSC, where each map is reconstructed from one half of the images (even vs. odd tilt angle indices), and map-model FSC, where the model map is generated from the fitted model. Resolution assessments are provided based on tilt-based map-map and map-model FSC analyses at thresholds of FSC=0.5 and 0.143, respectively.

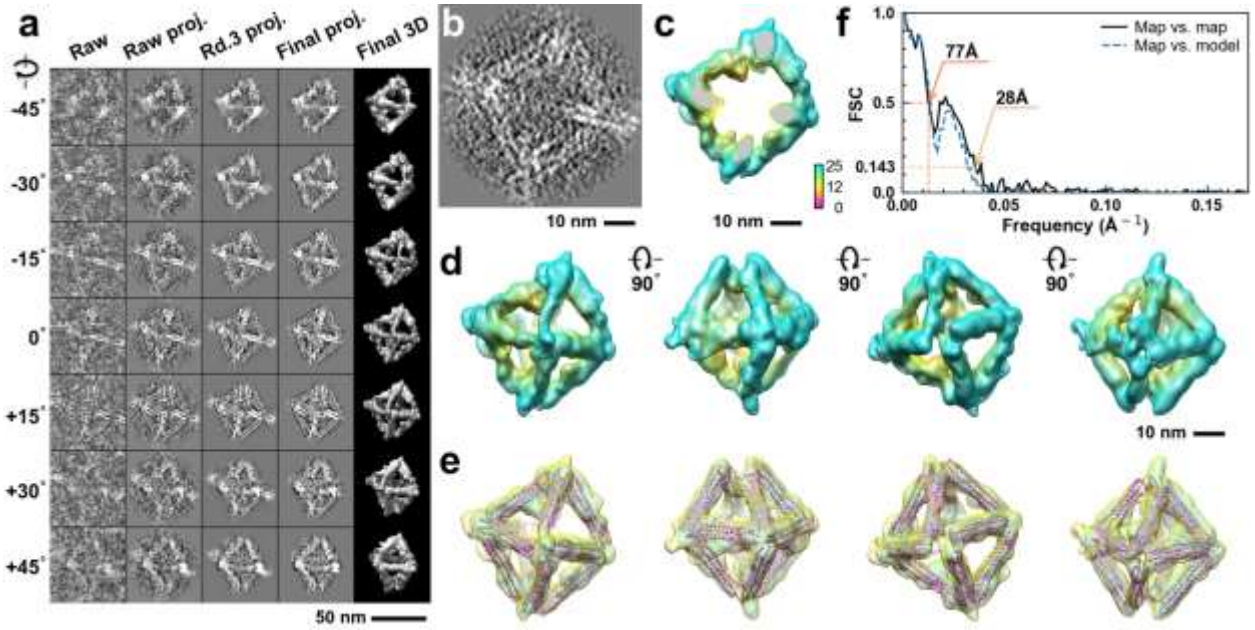

Supplementary Fig. 331: IPET 3D reconstruction and model fitting of an individual unit-cell particle (Index: 323) within a 2D lattice with 0% ferritin loading. a, Seven representative tilt images of a single unit-cell particle are shown in the first column (from left). The tilt images are aligned to a common center using IPET through iterative refinement. The projections of the raw, intermediate, and final 3D reconstruction at the corresponding angles are displayed in the subsequent four columns. **b**, A central cross-section (~23 nm thick) of the final reconstruction before masking is applied. **c**, 3D views of the central cross-section. **d**, Final 3D density map of this particle, viewed from four perpendicular directions. **e**, Final 3D reconstruction superimposed with the fitted model, viewed from four perpendicular directions. **f**, FSC analyses of the final map resolution using two methods: map-map FSC, where each map is reconstructed from one half of the images (even vs. odd tilt angle indices), and map-model FSC, where the model map is generated from the fitted model. Resolution assessments are provided based on tilt-based map-map and map-model FSC analyses at thresholds of FSC=0.5 and 0.143, respectively.

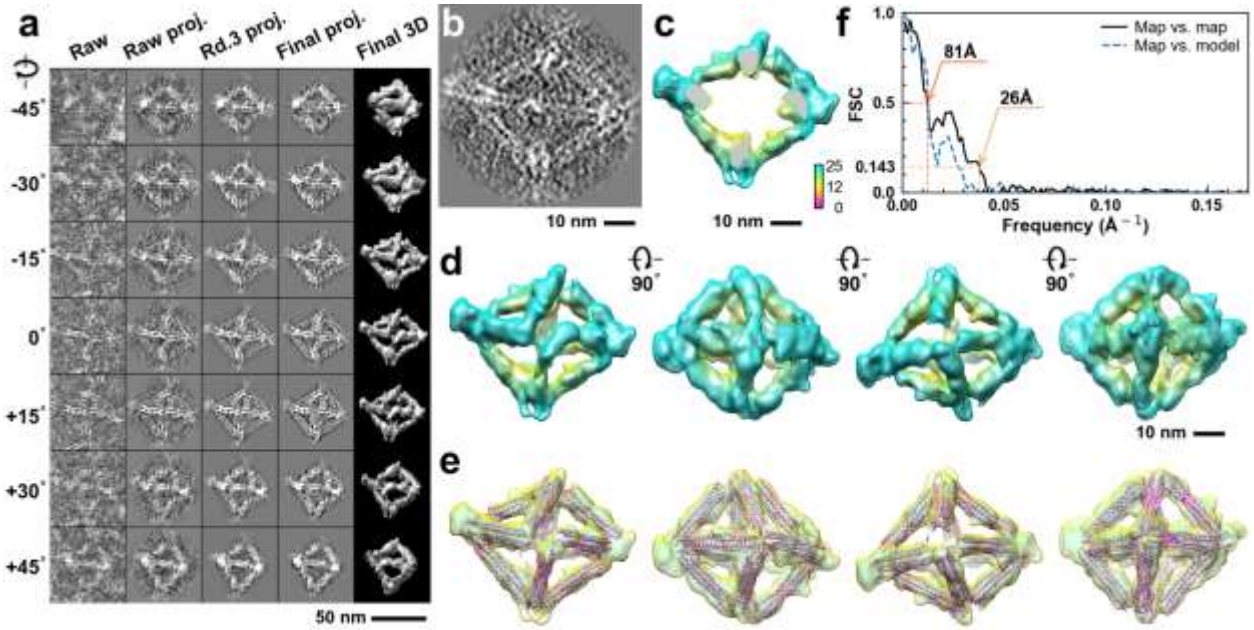

Supplementary Fig. 332: IPET 3D reconstruction and model fitting of an individual unit-cell particle (Index: 324) within a 2D lattice with 0% ferritin loading. a, Seven representative tilt images of a single unit-cell particle are shown in the first column (from left). The tilt images are aligned to a common center using IPET through iterative refinement. The projections of the raw, intermediate, and final 3D reconstruction at the corresponding angles are displayed in the subsequent four columns. **b**, A central cross-section (~23 nm thick) of the final reconstruction before masking is applied. **c**, 3D views of the central cross-section. **d**, Final 3D density map of this particle, viewed from four perpendicular directions. **e**, Final 3D reconstruction superimposed with the fitted model, viewed from four perpendicular directions. **f**, FSC analyses of the final map resolution using two methods: map-map FSC, where each map is reconstructed from one half of the images (even vs. odd tilt angle indices), and map-model FSC, where the model map is generated from the fitted model. Resolution assessments are provided based on tilt-based map-map and map-model FSC analyses at thresholds of FSC=0.5 and 0.143, respectively.

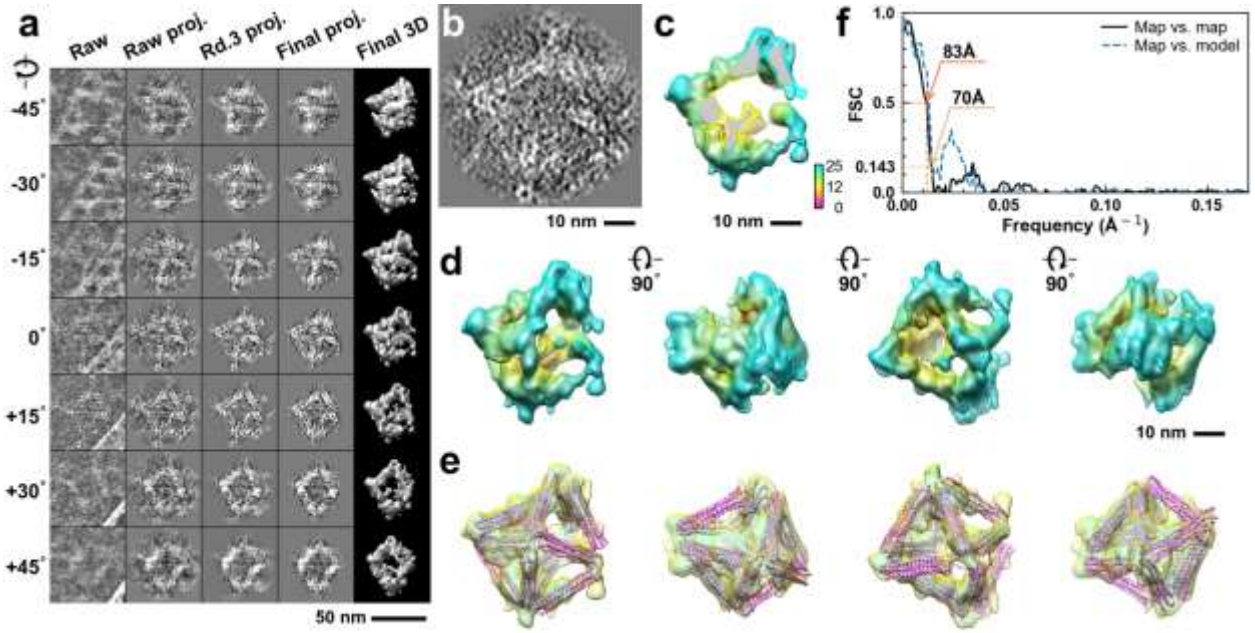

Supplementary Fig. 333: IPET 3D reconstruction and model fitting of an individual unit-cell particle (Index: 325) within a 2D lattice with 0% ferritin loading. a, Seven representative tilt images of a single unit-cell particle are shown in the first column (from left). The tilt images are aligned to a common center using IPET through iterative refinement. The projections of the raw, intermediate, and final 3D reconstruction at the corresponding angles are displayed in the subsequent four columns. **b**, A central cross-section (~23 nm thick) of the final reconstruction before masking is applied. **c**, 3D views of the central cross-section. **d**, Final 3D density map of this particle, viewed from four perpendicular directions. **e**, Final 3D reconstruction superimposed with the fitted model, viewed from four perpendicular directions. **f**, FSC analyses of the final map resolution using two methods: map-map FSC, where each map is reconstructed from one half of the images (even vs. odd tilt angle indices), and map-model FSC, where the model map is generated from the fitted model. Resolution assessments are provided based on tilt-based map-map and map-model FSC analyses at thresholds of FSC=0.5 and 0.143, respectively.

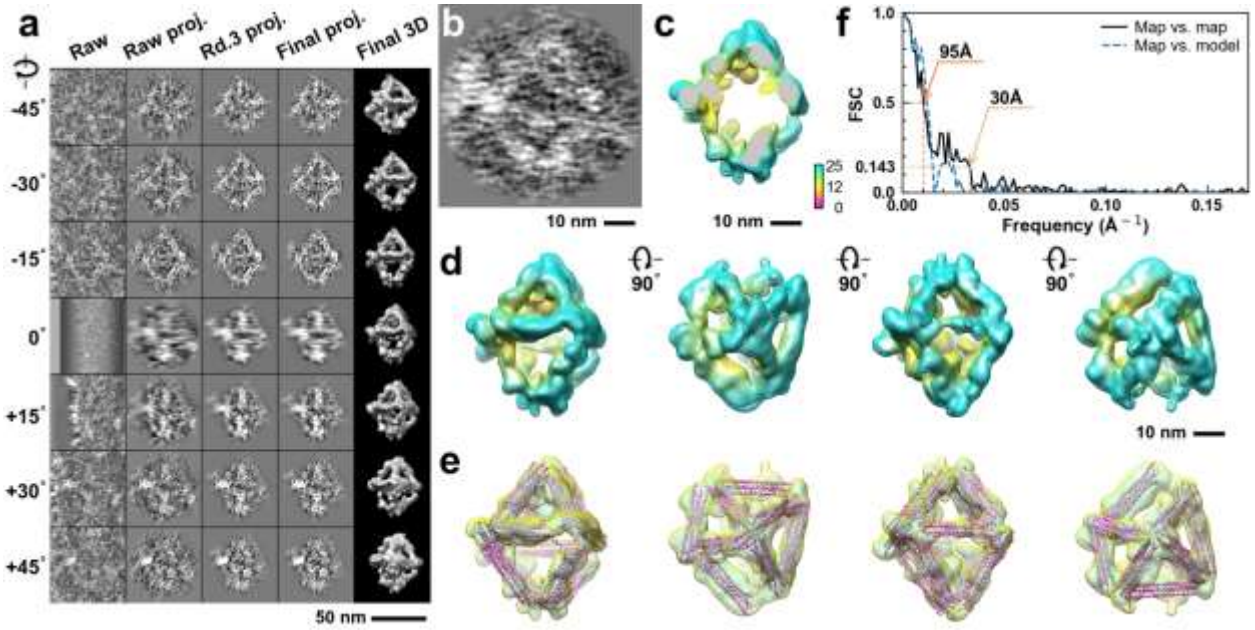

Supplementary Fig. 334: IPET 3D reconstruction and model fitting of an individual unit-cell particle (Index: 326) within a 2D lattice with 0% ferritin loading. a, Seven representative tilt images of a single unit-cell particle are shown in the first column (from left). The tilt images are aligned to a common center using IPET through iterative refinement. The projections of the raw, intermediate, and final 3D reconstruction at the corresponding angles are displayed in the subsequent four columns. **b**, A central cross-section (~23 nm thick) of the final reconstruction before masking is applied. **c**, 3D views of the central cross-section. **d**, Final 3D density map of this particle, viewed from four perpendicular directions. **e**, Final 3D reconstruction superimposed with the fitted model, viewed from four perpendicular directions. **f**, FSC analyses of the final map resolution using two methods: map-map FSC, where each map is reconstructed from one half of the images (even vs. odd tilt angle indices), and map-model FSC, where the model map is generated from the fitted model. Resolution assessments are provided based on tilt-based map-map and map-model FSC analyses at thresholds of FSC=0.5 and 0.143, respectively.

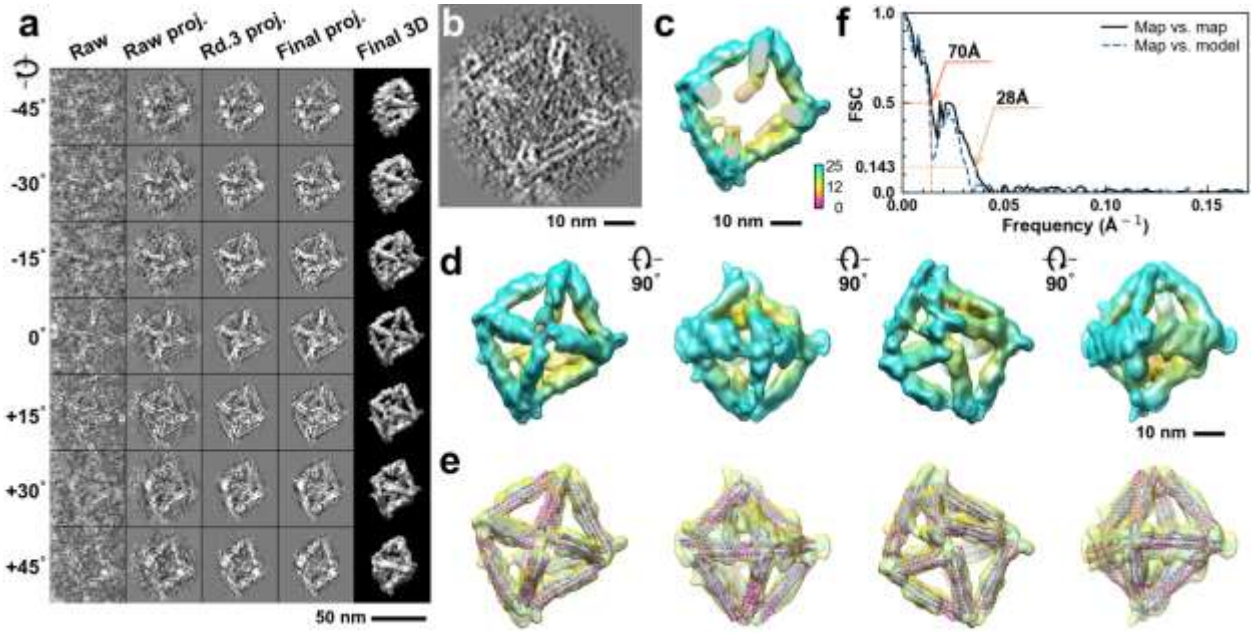

Supplementary Fig. 335: IPET 3D reconstruction and model fitting of an individual unit-cell particle (Index: 327) within a 2D lattice with 0% ferritin loading. a, Seven representative tilt images of a single unit-cell particle are shown in the first column (from left). The tilt images are aligned to a common center using IPET through iterative refinement. The projections of the raw, intermediate, and final 3D reconstruction at the corresponding angles are displayed in the subsequent four columns. **b**, A central cross-section (~23 nm thick) of the final reconstruction before masking is applied. **c**, 3D views of the central cross-section. **d**, Final 3D density map of this particle, viewed from four perpendicular directions. **e**, Final 3D reconstruction superimposed with the fitted model, viewed from four perpendicular directions. **f**, FSC analyses of the final map resolution using two methods: map-map FSC, where each map is reconstructed from one half of the images (even vs. odd tilt angle indices), and map-model FSC, where the model map is generated from the fitted model. Resolution assessments are provided based on tilt-based map-map and map-model FSC analyses at thresholds of FSC=0.5 and 0.143, respectively.

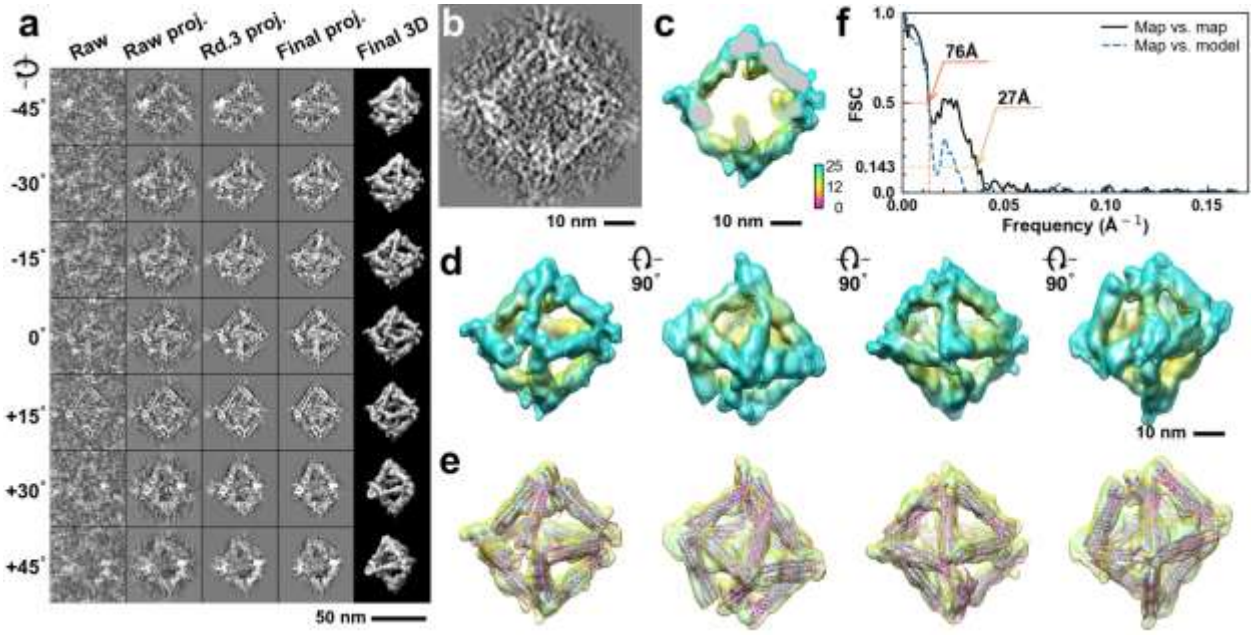

Supplementary Fig. 336: IPET 3D reconstruction and model fitting of an individual unit-cell particle (Index: 328) within a 2D lattice with 0% ferritin loading. a, Seven representative tilt images of a single unit-cell particle are shown in the first column (from left). The tilt images are aligned to a common center using IPET through iterative refinement. The projections of the raw, intermediate, and final 3D reconstruction at the corresponding angles are displayed in the subsequent four columns. **b**, A central cross-section (~23 nm thick) of the final reconstruction before masking is applied. **c**, 3D views of the central cross-section. **d**, Final 3D density map of this particle, viewed from four perpendicular directions. **e**, Final 3D reconstruction superimposed with the fitted model, viewed from four perpendicular directions. **f**, FSC analyses of the final map resolution using two methods: map-map FSC, where each map is reconstructed from one half of the images (even vs. odd tilt angle indices), and map-model FSC, where the model map is generated from the fitted model. Resolution assessments are provided based on tilt-based map-map and map-model FSC analyses at thresholds of FSC=0.5 and 0.143, respectively.

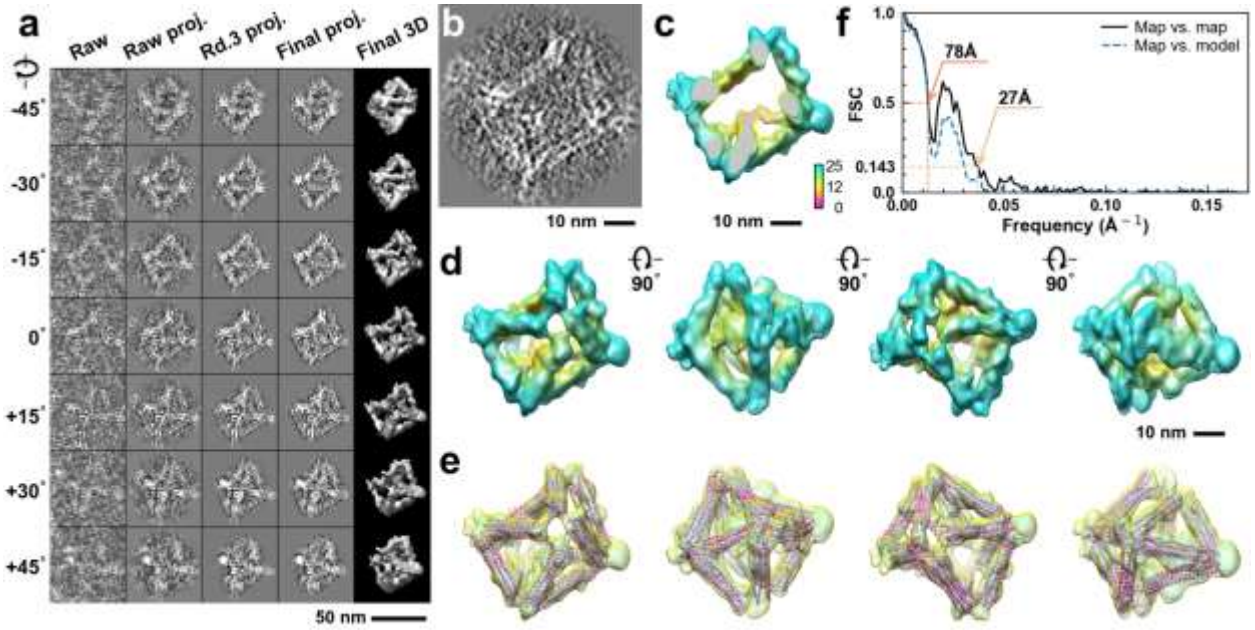

Supplementary Fig. 337: IPET 3D reconstruction and model fitting of an individual unit-cell particle (Index: 329) within a 2D lattice with 0% ferritin loading. a, Seven representative tilt images of a single unit-cell particle are shown in the first column (from left). The tilt images are aligned to a common center using IPET through iterative refinement. The projections of the raw, intermediate, and final 3D reconstruction at the corresponding angles are displayed in the subsequent four columns. **b**, A central cross-section (~23 nm thick) of the final reconstruction before masking is applied. **c**, 3D views of the central cross-section. **d**, Final 3D density map of this particle, viewed from four perpendicular directions. **e**, Final 3D reconstruction superimposed with the fitted model, viewed from four perpendicular directions. **f**, FSC analyses of the final map resolution using two methods: map-map FSC, where each map is reconstructed from one half of the images (even vs. odd tilt angle indices), and map-model FSC, where the model map is generated from the fitted model. Resolution assessments are provided based on tilt-based map-map and map-model FSC analyses at thresholds of FSC=0.5 and 0.143, respectively.

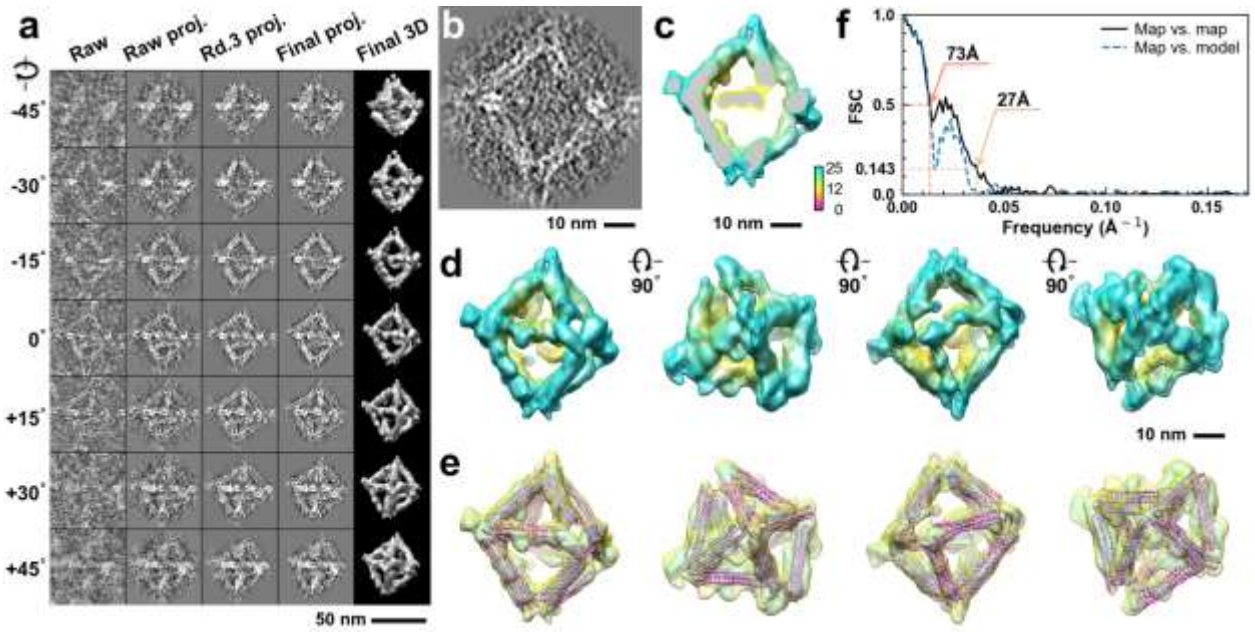

Supplementary Fig. 338: IPET 3D reconstruction and model fitting of an individual unit-cell particle (Index: 330) within a 2D lattice with 0% ferritin loading. a, Seven representative tilt images of a single unit-cell particle are shown in the first column (from left). The tilt images are aligned to a common center using IPET through iterative refinement. The projections of the raw, intermediate, and final 3D reconstruction at the corresponding angles are displayed in the subsequent four columns. **b**, A central cross-section (~23 nm thick) of the final reconstruction before masking is applied. **c**, 3D views of the central cross-section. **d**, Final 3D density map of this particle, viewed from four perpendicular directions. **e**, Final 3D reconstruction superimposed with the fitted model, viewed from four perpendicular directions. **f**, FSC analyses of the final map resolution using two methods: map-map FSC, where each map is reconstructed from one half of the images (even vs. odd tilt angle indices), and map-model FSC, where the model map is generated from the fitted model. Resolution assessments are provided based on tilt-based map-map and map-model FSC analyses at thresholds of FSC=0.5 and 0.143, respectively.

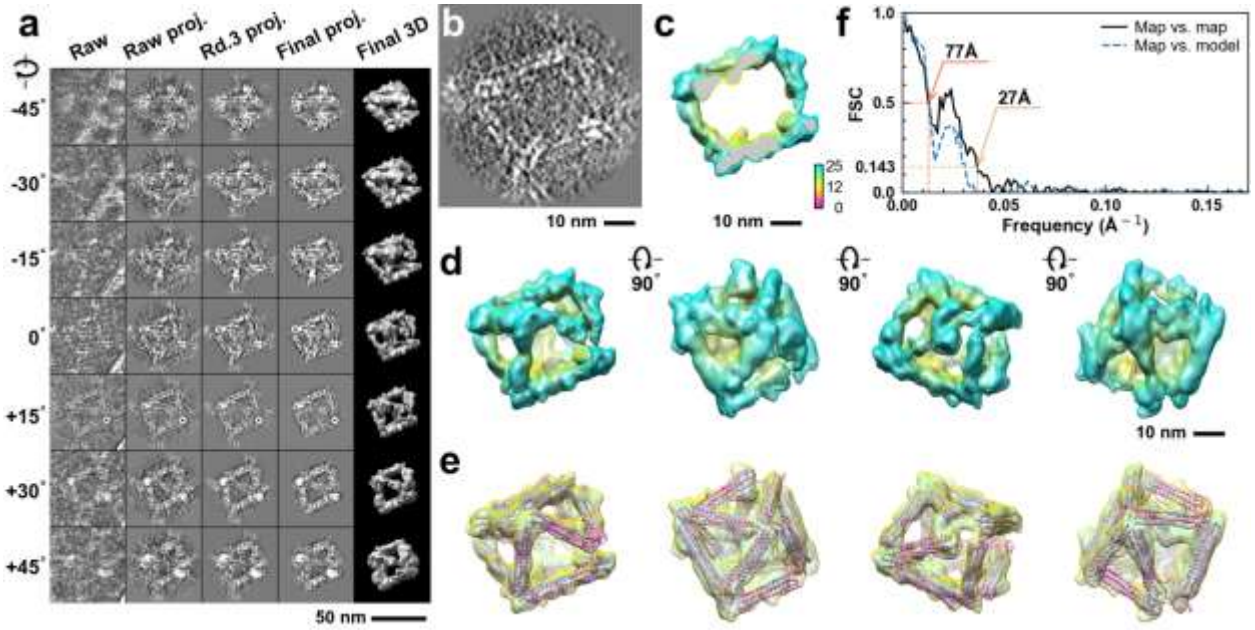

Supplementary Fig. 339: IPET 3D reconstruction and model fitting of an individual unit-cell particle (Index: 331) within a 2D lattice with 0% ferritin loading. a, Seven representative tilt images of a single unit-cell particle are shown in the first column (from left). The tilt images are aligned to a common center using IPET through iterative refinement. The projections of the raw, intermediate, and final 3D reconstruction at the corresponding angles are displayed in the subsequent four columns. **b**, A central cross-section (~23 nm thick) of the final reconstruction before masking is applied. **c**, 3D views of the central cross-section. **d**, Final 3D density map of this particle, viewed from four perpendicular directions. **e**, Final 3D reconstruction superimposed with the fitted model, viewed from four perpendicular directions. **f**, FSC analyses of the final map resolution using two methods: map-map FSC, where each map is reconstructed from one half of the images (even vs. odd tilt angle indices), and map-model FSC, where the model map is generated from the fitted model. Resolution assessments are provided based on tilt-based map-map and map-model FSC analyses at thresholds of FSC=0.5 and 0.143, respectively.

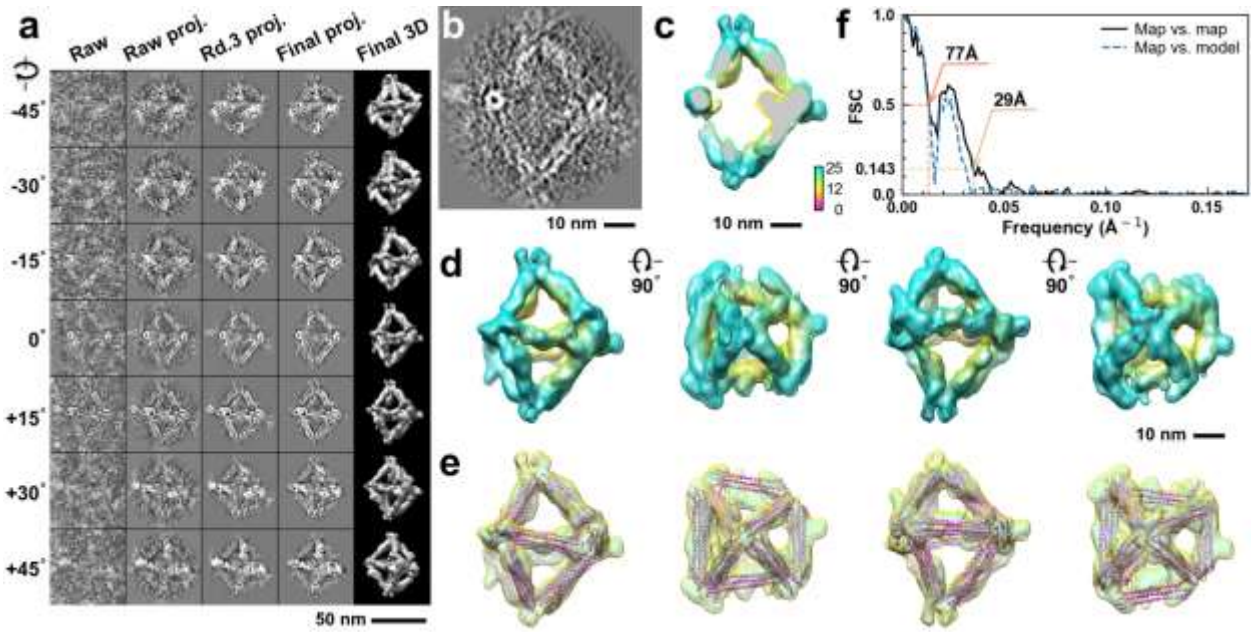

Supplementary Fig. 340: IPET 3D reconstruction and model fitting of an individual unit-cell particle (Index: 332) within a 2D lattice with 0% ferritin loading. a, Seven representative tilt images of a single unit-cell particle are shown in the first column (from left). The tilt images are aligned to a common center using IPET through iterative refinement. The projections of the raw, intermediate, and final 3D reconstruction at the corresponding angles are displayed in the subsequent four columns. **b**, A central cross-section (~23 nm thick) of the final reconstruction before masking is applied. **c**, 3D views of the central cross-section. **d**, Final 3D density map of this particle, viewed from four perpendicular directions. **e**, Final 3D reconstruction superimposed with the fitted model, viewed from four perpendicular directions. **f**, FSC analyses of the final map resolution using two methods: map-map FSC, where each map is reconstructed from one half of the images (even vs. odd tilt angle indices), and map-model FSC, where the model map is generated from the fitted model. Resolution assessments are provided based on tilt-based map-map and map-model FSC analyses at thresholds of FSC=0.5 and 0.143, respectively.

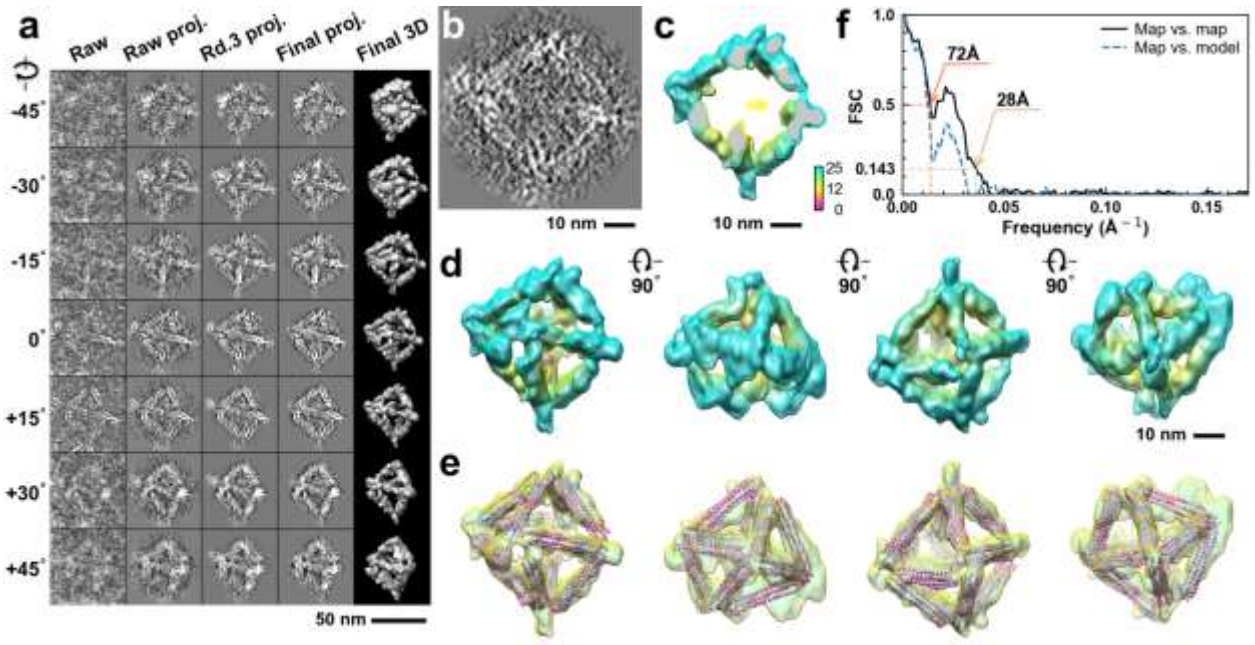

Supplementary Fig. 341: IPET 3D reconstruction and model fitting of an individual unit-cell particle (Index: 333) within a 2D lattice with 0% ferritin loading. a, Seven representative tilt images of a single unit-cell particle are shown in the first column (from left). The tilt images are aligned to a common center using IPET through iterative refinement. The projections of the raw, intermediate, and final 3D reconstruction at the corresponding angles are displayed in the subsequent four columns. **b**, A central cross-section (~23 nm thick) of the final reconstruction before masking is applied. **c**, 3D views of the central cross-section. **d**, Final 3D density map of this particle, viewed from four perpendicular directions. **e**, Final 3D reconstruction superimposed with the fitted model, viewed from four perpendicular directions. **f**, FSC analyses of the final map resolution using two methods: map-map FSC, where each map is reconstructed from one half of the images (even vs. odd tilt angle indices), and map-model FSC, where the model map is generated from the fitted model. Resolution assessments are provided based on tilt-based map-map and map-model FSC analyses at thresholds of FSC=0.5 and 0.143, respectively.

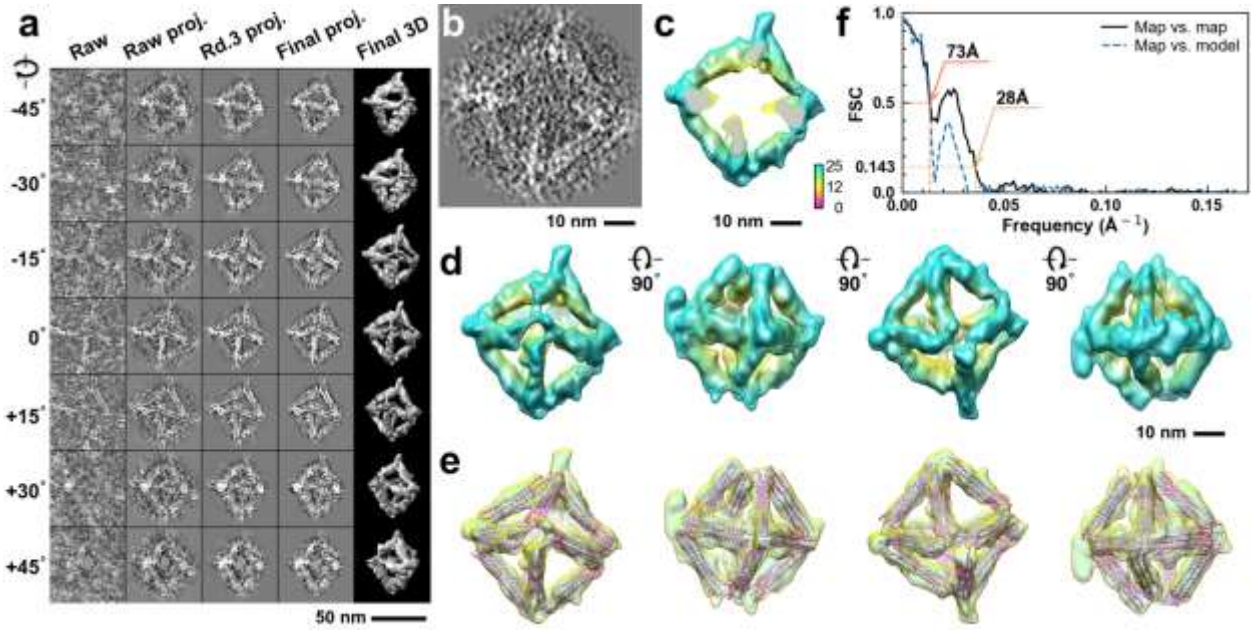

Supplementary Fig. 342: IPET 3D reconstruction and model fitting of an individual unit-cell particle (Index: 334) within a 2D lattice with 0% ferritin loading. a, Seven representative tilt images of a single unit-cell particle are shown in the first column (from left). The tilt images are aligned to a common center using IPET through iterative refinement. The projections of the raw, intermediate, and final 3D reconstruction at the corresponding angles are displayed in the subsequent four columns. **b**, A central cross-section (~23 nm thick) of the final reconstruction before masking is applied. **c**, 3D views of the central cross-section. **d**, Final 3D density map of this particle, viewed from four perpendicular directions. **e**, Final 3D reconstruction superimposed with the fitted model, viewed from four perpendicular directions. **f**, FSC analyses of the final map resolution using two methods: map-map FSC, where each map is reconstructed from one half of the images (even vs. odd tilt angle indices), and map-model FSC, where the model map is generated from the fitted model. Resolution assessments are provided based on tilt-based map-map and map-model FSC analyses at thresholds of FSC=0.5 and 0.143, respectively.

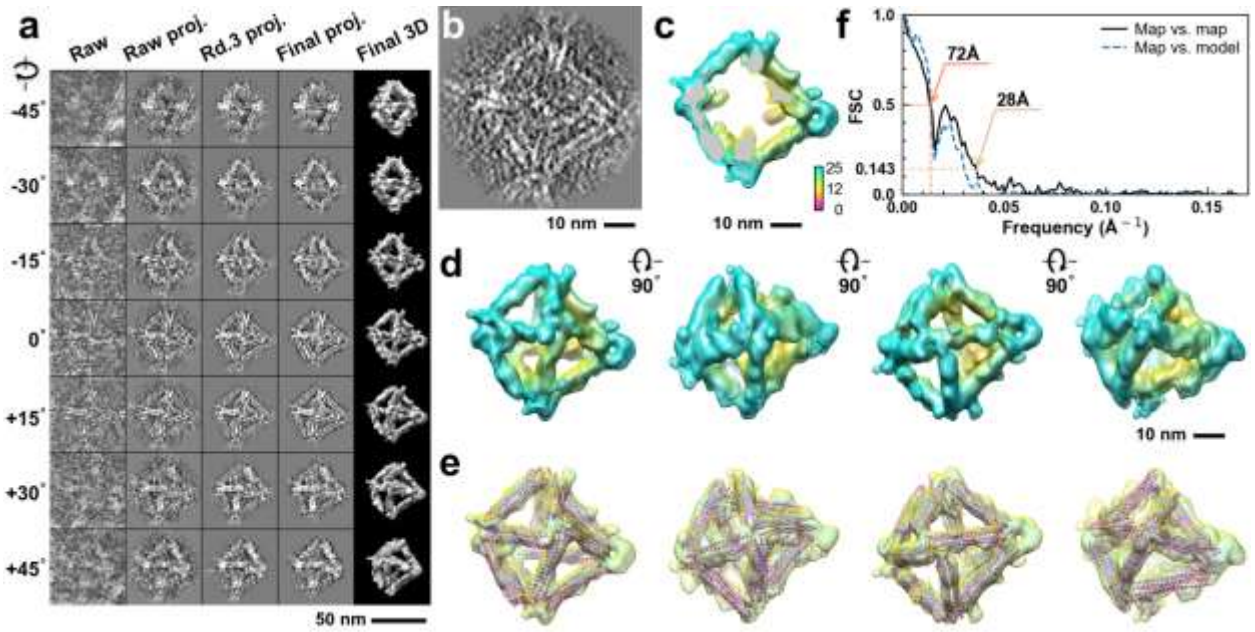

Supplementary Fig. 343: IPET 3D reconstruction and model fitting of an individual unit-cell particle (Index: 335) within a 2D lattice with 0% ferritin loading. a, Seven representative tilt images of a single unit-cell particle are shown in the first column (from left). The tilt images are aligned to a common center using IPET through iterative refinement. The projections of the raw, intermediate, and final 3D reconstruction at the corresponding angles are displayed in the subsequent four columns. **b**, A central cross-section (~23 nm thick) of the final reconstruction before masking is applied. **c**, 3D views of the central cross-section. **d**, Final 3D density map of this particle, viewed from four perpendicular directions. **e**, Final 3D reconstruction superimposed with the fitted model, viewed from four perpendicular directions. **f**, FSC analyses of the final map resolution using two methods: map-map FSC, where each map is reconstructed from one half of the images (even vs. odd tilt angle indices), and map-model FSC, where the model map is generated from the fitted model. Resolution assessments are provided based on tilt-based map-map and map-model FSC analyses at thresholds of FSC=0.5 and 0.143, respectively.

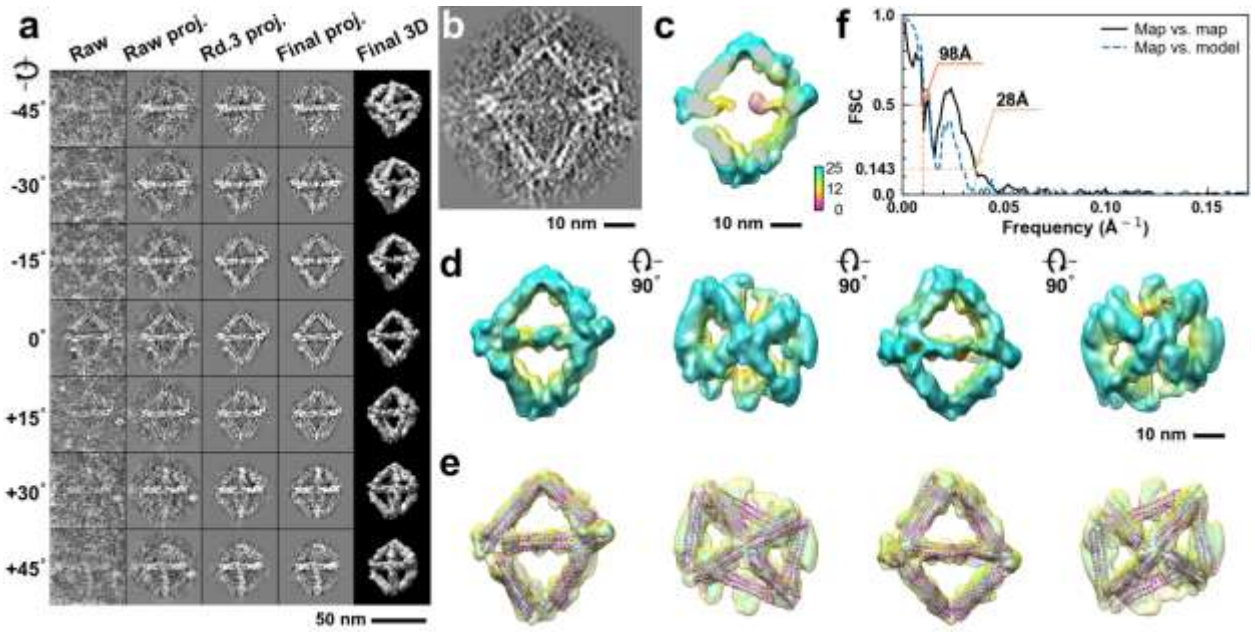

Supplementary Fig. 344: IPET 3D reconstruction and model fitting of an individual unit-cell particle (Index: 336) within a 2D lattice with 0% ferritin loading. a, Seven representative tilt images of a single unit-cell particle are shown in the first column (from left). The tilt images are aligned to a common center using IPET through iterative refinement. The projections of the raw, intermediate, and final 3D reconstruction at the corresponding angles are displayed in the subsequent four columns. **b**, A central cross-section (~23 nm thick) of the final reconstruction before masking is applied. **c**, 3D views of the central cross-section. **d**, Final 3D density map of this particle, viewed from four perpendicular directions. **e**, Final 3D reconstruction superimposed with the fitted model, viewed from four perpendicular directions. **f**, FSC analyses of the final map resolution using two methods: map-map FSC, where each map is reconstructed from one half of the images (even vs. odd tilt angle indices), and map-model FSC, where the model map is generated from the fitted model. Resolution assessments are provided based on tilt-based map-map and map-model FSC analyses at thresholds of FSC=0.5 and 0.143, respectively.

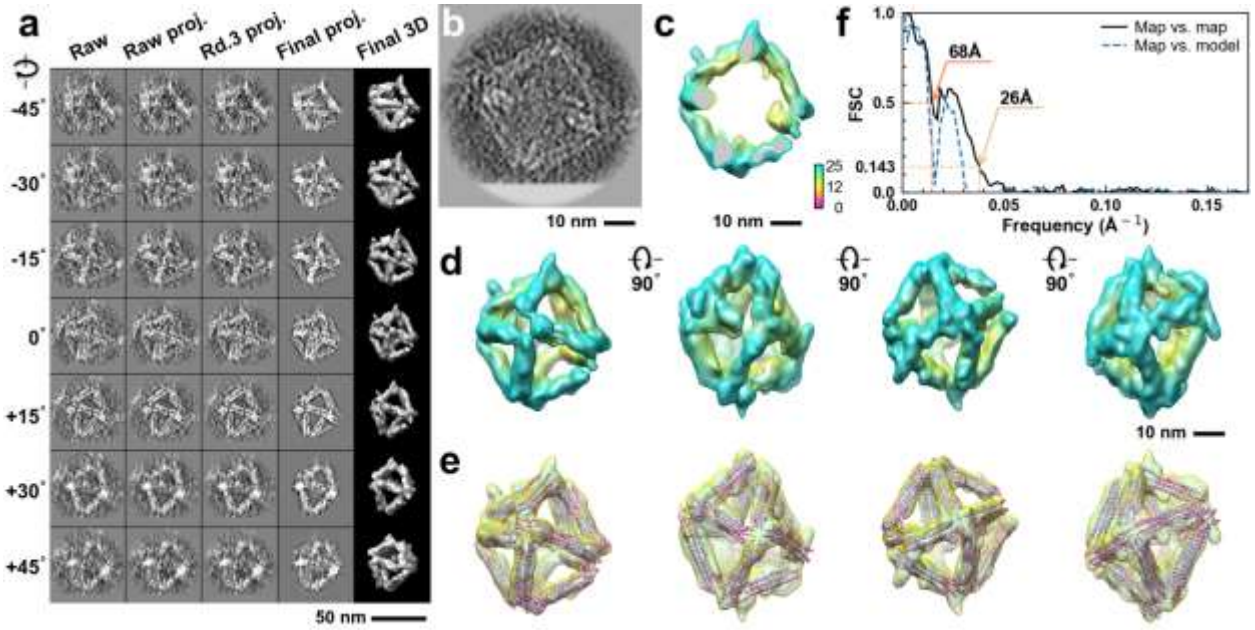

Supplementary Fig. 345: IPET 3D reconstruction and model fitting of an individual unit-cell particle (Index: 337) within a 2D lattice with 0% ferritin loading. a, Seven representative tilt images of a single unit-cell particle are shown in the first column (from left). The tilt images are aligned to a common center using IPET through iterative refinement. The projections of the raw, intermediate, and final 3D reconstruction at the corresponding angles are displayed in the subsequent four columns. **b**, A central cross-section (~23 nm thick) of the final reconstruction before masking is applied. **c**, 3D views of the central cross-section. **d**, Final 3D density map of this particle, viewed from four perpendicular directions. **e**, Final 3D reconstruction superimposed with the fitted model, viewed from four perpendicular directions. **f**, FSC analyses of the final map resolution using two methods: map-map FSC, where each map is reconstructed from one half of the images (even vs. odd tilt angle indices), and map-model FSC, where the model map is generated from the fitted model. Resolution assessments are provided based on tilt-based map-map and map-model FSC analyses at thresholds of FSC=0.5 and 0.143, respectively.